OCTAHEDRAL RUTHENIUM COMPLEXES AS PROTEIN KINASE INHIBITORS

A DISSERTATION

in

Chemistry

Presented to the Faculties of Philipps-Universität Marburg in Partial Fulfillment of

the Requirements for the Degree of Doctor of Science

(Dr. rer. nat.)

Li Feng

Jilin Province, China

Marburg/Lahn 2010

Department of Chemistry of Philipps-Universität Marburg, accepted as a dissertation on

Supervisor: Prof. Dr. Eric Meggers

Second revisor:

Date of defence:

Acknowledgement

My deepest gratitude goes first and foremost to Professor Eric Meggers, my supervisor, for his constant guidance and encouragement. Without his illuminating and selfless instruction, I would not have this thesis to present. His unbelievable source of scientific enthusiasm and inspiration are truly impressive, and his attitude towards the work is respectable. I feel very fortunate to be able to work in his group, and personally, I'm appreciated of Prof. Meggers' patience and understanding over the past years. I wish him and his family all the best.

I would like to express my heartfelt gratitude to my master research advisor, Professor Haiping Xia in Xiamen University, who led me into the world of organometallic chemistry. I wish him continued success in his research area. I also would like to thank Prof. Lilu Zhang and Prof. Xumin He for introducing me to work with Prof. Meggers in Germany. And to lecturer Hong Zhang in Xiamen University, my former lab colleague and my friend, I wish her and her family all the best.

During my time at the Philipps-Universität Marburg, I have been so luky to be surrounded by great people, especially our secretary Ina Pinnschmidt and lab technician Katja Kräling. I'm deeply indebted for their endless assistance and kindness. It was a great time to cooperate with Katja on the DAPK1 project. Thanks for her hard work on the cocrystallization of DAPK1 with my compounds sincerely. I also would like to express my appreciation to Dr. Xiulan Xie of the NMR facility and Dr. Klaus Harms in the X-ray crystallography department, without their help, it would be more difficult in my research.

In Meggers' group, it has been an honor to do my research with lab colleagues past and present. First and foremost, I would like to thank Nicholas Pagano for his help all the time and proofread my thesis patiently, who helped me to get familiar with the project of organometallics as protein kinase inhibitors. It was an honor to work next to and closely with him, although it was only one and half years. I wish him and his fiancé Amanda all the best and happy all the time. I also would like to thank Mark Schlegel

and wish him all the best in his new position. Thanks for them talking with me patiently. Jasna Maksimoska and Ekin Atilla-Gokcumen, with whom I have had the chance to work together have been important parts of my research and I would like to thank them for their input. Also I would like to thank Seann Mulcahy for his help during the time we worked together.

In addition, I'm truly thankful to all of my colleagues in Meggers group, especially to Alexander Wilbur for his proofreading of my thesis carefully and Matthias Bischof, Sebastian Blanck, Stefan Mollin and Marianne Wenzel. I'm appreciated of their friendship and help in my 'tough' life in Germany. I also would like to thank Dong Sun, Nan Zhao, Xianzhi Wang and Jie hou for friendship over the past years. It's fortunate to meet them in Marburg, and I wish them all the best.

Finally my thanks would go to my beloved family for their considerations and great confidience in me all through these years in my life. Thank you for believing in me.

And to my wife, Tianhua. Your support and understanding over the past years have been invaluable and great encouragement to me. No words can express how happy and lucky I am to spend my life with you. I'm looking forward to our next adventure.

List of Abbreviations

[9]aneS_3: 1,4,7-trithiacyclononane

Abl: abelson leukaemia

APE: alanine-aroline-alutamate

Arg: arginine

Asp: aspartate

ATP: adenosine-5'-triphosphate

bpy: 2,2'-bipyridine

CD: circular dichroism

$CHCl_3$: chloroform

CHK2: checkpoint kinase 2

c-Kit: CD117 or C-kit receptor

Cp: cyclopentadienyl

DAPK1: death-associated protein kinase 1

DCM: dichloromethane

DFG: aspartate-phenylalanine-glycine

DFT: density functional theory

DME: 1,2-dimethoxyethane

DMF: dimethylformamide

DMSO: dimethyl sulfoxide

DNA: deoxyribonucleic acid

EGFR: epidermal growth factor receptor

EtOAc: ethyl acetate

EtOH: ethanol

Flt4: fms-related tyrosine kinase 4

Glu: glutamate

GSK3: glycogen synthase kinase 3

HDAC: histone deacetylase

Her-2: human epidermal growth factor receptor

hGR: human glutathione reductase

HPLC: high-performance liquid chroma-tography

hTrxR: human thioredoxin reductase

IC_{50}: concentration of the compound at which 50% of the kinase is inhibited

Ile: isoleucine

IR spectra: infrared spectra

Leu: leucine

LiHMDS: lithium bis-trimethylsilylamide

mCPBA: 3-chloroperoxybenzoic acid

MEK1: mitogen-activated protein kinase kinase-1

MEK2: mitogen-activated protein kinase kinase-2

MeOH: methanol

MLCK: myosin light chain kinase

MSK1: mitogen- and stress-activated protein kinase

PAK1: p21-activated kinase 1

PDGFR: platelet-derived growth factor receptor

Pim1: proto-oncogene serine/threonine-protein kinase

PKC: protein kinase C

PMe_3: trimethyl phosphine

Ret: receptor tyrosine kinase

Rsk: ribosomal S6 kinase

Src: rous sarcoma oncogene cellular homolog

TBAF: tetrabutylammonium fluoride

TBS: tert-butyldimethylsilyl

THF: tetrahydrofuran

TIPS: triisopropylsilyl

TrkA : tropomyosin-related kinase

Val: valine

VEGFR: vascular endothelial growth factor receptor

ZIPK: death-associated protein kinase 3

Table of Contents

Acknowledgement ..... *III*

List of Abbreviations ..... *V*

Table of Contents ..... *VII*

Chapter 1: Introduction *1*

Chapter 1.1: Protein kinases as targets for inhibitor design **1**

Chapter 1.1.1 Kinase inhibitor binding sites 1

Chapter 1.1.2 Kinase inhibitors as potential drugs 4

Chapter 1.2: Organometallic scaffolds for enzyme inhibition **6**

Chapter 1.2.1 Metal complexes as enzyme inhibitors through ligand-substitution 7

Chapter 1.2.2 Substitutionally inert metal complexes as enzyme inhibitors 8

Chapter 1.3: Aim of the work **11**

Chapter 1.4: References **12**

Chapter 2: Targeting Large Kinase Active Site with Rigid, Bulky Octahedral Ruthenium Complexes *15*

Chapter 2.1: Initial screening of an organometallic library for PAK1 inhibition **15**

Chapter 2.2: Designing a precursor for combinatorial coordination chemistry **16**

Chapter 2.3: Evaluation of the diastereoselectivity of coordination chemistry with precursor 2.3 ..... **18**

Chapter 2.4: Synthesis and screening of octahedral ruthenium complexes with different bidentate ligands **21**

Chapter 2.5: Inhibitory property and selectivity of FL172 as PAK1 inhibitor **25**

Chapter 2.6: Cocrystal structure of Λ-FL172 with PAK1 ..... **28**

Chapter 2.7: Derivatives of FL172 as improved selective PAK1 inhibitors **29**

Chapter 2.8: Crystallographic data of FL327 and FL389 for the determination of the relative configurations of FL172 and FL411 ..... **33**

Chapter 2.9: The importance of the carbon monoxide ligand in PAK1 inhibitors FL172 ..... **34**

Chapter 2.10: Replacing chloride of FL172 by other monodentate ligands **35**

Chapter 2.11: An improved PAK1 inhibitor generated by modification of the pyridocarbazole **38**

Chapter 2.12: Discussion and conclusion **45**

Chapter 2.13: References **47**

Chapter 3: Ruthenium Scaffold with Cyclic Tridentate Ligands as Potential Protein Kinase Inhibitors *48*

Chapter 3.1: Development of MLCK inhibitors **48**

Chapter 3.1.1: Scaffold synthesis of MLCK inhibitors 48

Chapter 3.1.2: Identification of suitable monodentate ligands in the scaffold 50

Chapter 3.1.3: Modification of the pyridocarbazole moiety 52

Chapter 3.1.4: Modification of the tridentate ligand moiety 57

Chapter 3.2: Development of DAPK1 inhibitors **64**

Chapter 3.2.1 Scaffold synthesis of DAPK1 inhibitors 64

Chapter 3.2.2: Preliminary structure-affinity relationship study 65

Chapter 3.2.3: Affinity effect of different monodentate ligand on the axial position 66

Chapter 3.2.4: Improved DAPK1 inhibitor by modification on the pyridocarbazole moiety 68

Chapter 3.2.5: Determination of the relative configuration of FL1353-1 72

Chapter 3.2.6: Isomerization of Ru-N and Ru-S of Complex FL1353 monitored by ^{1}H NMR spectra 74

Chapter 3.2.7: Cocrystal structure of (*R*)-FL1353-1 with DAPK1 75

Chapter 3.3: Improved inhibitor for Pim1 kinase **77**

Charpter 3.4: Discussion and conclusion **79**

Chapter 3.6: References **82**

Chapter 4: Ruthenium Scaffold with Acyclic Tridentate Ligands as Potential Protein Kinase Inhibitors *85*

Chapter 4.1: Design of TrkA inhibitors with octahedral ruthenium scaffold **85**

Chapter 4.2: Discovery of octahedral lead structure for protein kinase TrkA **86**

Chapter 4.3: Modification on the pyridocarbazole moiety to improve the potency of TrkA inhibitors **87**

Chapter 4.4: Applying different tridentate ligands to improve the potency for TrkA inhibitors **90**

Chapter 4.5: Conclusion and Outlook **92**

Chapter 4.6: References **93**

Chapter 5: Summary and Outlook *94*

References **100**

Chapter 6: Experimental Section *101*

Chapter 6.1: Synthesis **101**

Chapter 6.1.1: Synthesis of PAK1 inhibitors 101

Chapter 6.1.2: Synthesis of MLCK inhibitors 145

Chapter 6.1.3: Synthesis of DAPK1 inhibitors 183

Chapter 6.1.4: Synthesis of Pim1 inhibitors 192

Chapter 6.1.5: Synthesis of TrkA inhibitors 195

Chapter 6.2: Resolution of racemic mixtures and determination of absolute configurations **202**

Chapter 6.3: Kinase assays **203**

Chapter 6.4: References **208**

Appendix ***209***

A. Crystallographic Data **209**

B. ^{1}H NMR, ^{13}C NMR Spectra **288**

C. Kinase Screening Data **375**

List of Figures ***388***

List of Tables ***394***

Chapter 1: Introduction

Chapter 1.1: Protein kinases as targets for inhibitor design

Protein kinases constitute one of the largest protein families in human[1,2] and play an important role in the regulation of a diverse range of cellular functions. Protein kinases are defined by their ability to catalyze the transfer of the terminal phosphate of ATP to substrates that usually contain serine, threonine or tyrosine residues, and mediate many of signal transduction pathways in eukaryotic cells.[3] Protein kinases are very important in cell growth, metabolism, cell cycle progression, apoptosis, and differentiation. The majority of these targets are being investigated for the treatment of cancer. However, deregulation of protein kinases function has been implicated in other disorders, including immunological, neurological, metabolic, and infectious diseases.[4-6] Therefore, the discovery and development of selective and potent protein kinase inhibitors to treat diseases caused by the deregulation of signaling pathways has become an extremely promising and widespread approach for drug discovery.[7,8]

Chapter 1.1.1 Kinase inhibitor binding sites

So far approximately 518 protein kinases are identified in the human genome that share a catalytic domain highly conserved in sequence and structure but which are significantly different in how their catalysis is regulated.[1] They normally share a conserved arrangement of secondary structure elements which are arranged into twelve subdomains that fold into a bi-lobed catalytic core structure.[5] Between N-terminal lobe and C-terminal lobe of the kinase fold is the ATP-binding pocket (Figure 1.1). ATP binds in the cleft with the adenine ring forming hydrogen bonds with the hinge region, which connects the N-terminus and C-terminus. The ribose and triphosphate groups of ATP bind in a hydrophilic channel extending to the substrate binding site. This active site together with surrounding less conserved pockets have been the focus of kinase inhibitors design.

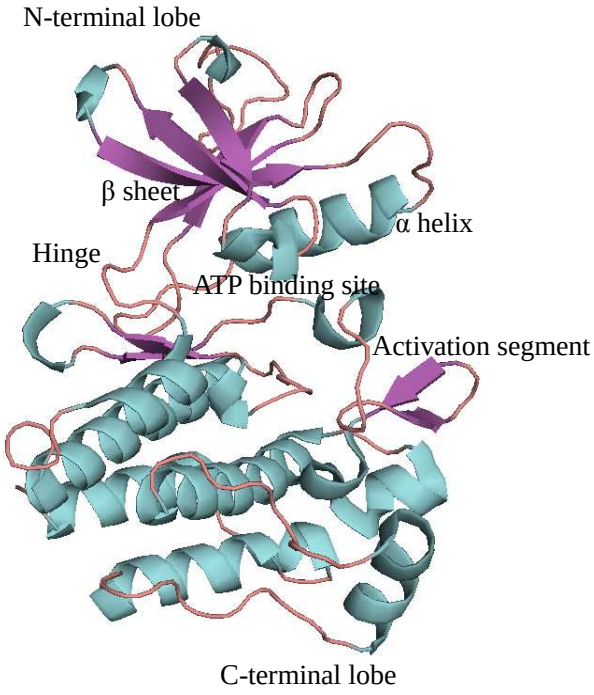

Figure 1.1. Structure of the catalytic domain of cAbl according to ref. 10. The N-terminal lobe consists of a β sheet and one conserved α helix (helix C). The C-terminal lobe is largely helical and contains the activation segment which includes residues that are phosphorylated for activity in many kinases. The hinge region connects these two lobes. The residues close to N-terminus are purple, and those close to C-terminus are blue (PDB: 1IEP). The picture was adopted from ref. 5.

All kinases have a conserved activation loop that is marked by DFG (Asp-Phe-Gly) and APE (Ala-Pro-Glu) motifs at the start and end of the loop, respectively. Most kinase inhibitors discovered are ATP competitive and present hydrogen bonds to the hinge region in the target kinase active site, mimicking the hydrogen bonds formed by the adenine ring of ATP. Four different types of kinase inhibitors can be classified: type I inhibitors, type II inhibitors, allosteric inhibitors, and covalent inhibitors.[33]

Most of the ATP-competitive inhibitors belong to type I inhibitors targeting the active conformation of kinases (Figure 1.2a), a conformation conductive to phosphotransfer. Type I inhibitors normally hold a heterocyclic ring occupying the purine binding site and side chains on this scaffold occupy the adjacent hydrophobic pockets. Correspondingly, type II inhibitors target the inactive conformation of kinases, which is referred to DFG-out due to the rearrangement of this motif. An additional hydrophobic

pocket is exposed due to the arrangement of the activation loop (Figure 1.2b). The active site of type II kinase is highly flexible and can rearrange to accommodate a variety of inhibitors.[34]

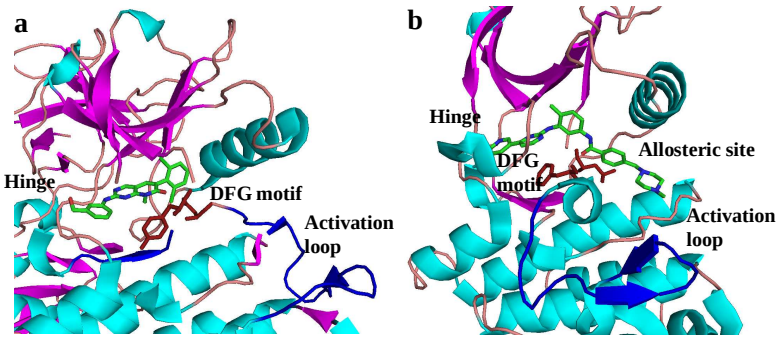

Figure 1.2. Kinase inhibitor binding modes. **a**) ABL1 in complex with the type I ATP-competitive inhibitor PD166326 (PDB: 1OPK). Shown here is the DFG-in conformation of the activation loop (dark blue). **b**) The DFG-out conformation of the activation loop of ABL1 (dark blue) with the type II inhibitor imatinib (PDB: 1IEP). The picture was adopted from ref. 33.

The inhibitor binding at an allosteric site which is adjacent to the ATP-binding site is the third class of kinase inhibitors. The allosteric inhibitors are prone to exhibit high selectivity due to the unique binding site and regulatory mechanisms. The well characterized example is PD318088 and its derivatives, the inhibitors for protein kinase MEK1 and MEK2 (Figure 1.3).[35]

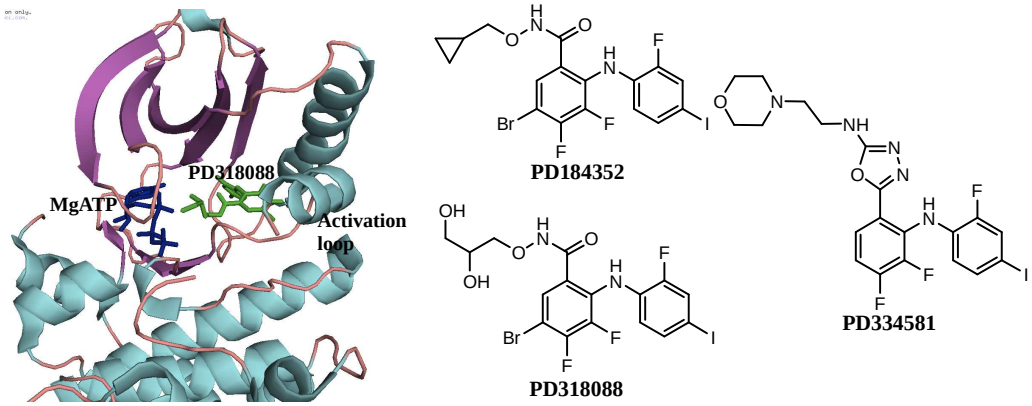

Figure 1.3. MEK1 protein kinase structure and the active site are occupied by MgATP and inhibitor PD318088, and the structure of other derivatives according to ref. 35. ATP is dark blue, and PD318088 is green. (PDB: 1CDK)

The forth class of kinase inhibitors is capable of forming irreversible, covalent bonds to the kinase active site, most by reacting with a nucleophilic cysteine residue.[36] The analysis of human kinome shows that there are 46 kinases which have the particular cysteine residue and about 200 kinases that have a cysteine located adjacent to ATP pocket. This means a large number of protein kinases might be probably targeted with this approach.

Chapter 1.1.2 Kinase inhibitors as potential drugs

The first protein kinase inhibitors were developed by Hiroyoshi Hidaka in the early 1980s.[4,9] Naphthalene sulphonamides, such as *N*-(6-amino-hexyl)-5-chloro-1-naphthalenesulphonamide had already been developed as antagonists of the calcium-binding protein calmodulin, which also acted upon several protein kinases at higher concentration.

The discovery of staurosporine which is produced by bacteria of the genus streptomyces and was found to be a nanomolar inhibitor of PKC[12] led several companies to make and test many derivatives of this bisindolyl maleimide. However, staurosporine and several derivatives were later proven to lack selectivity and inhibited some other protein kinases *in vitro*.[13,14]

By the end of the 1980s, no protein kinase inhibitors had entered human clinical trials.[4] It is a challenge to develop ATP-competitive inhibitors with sufficient potency and selectivity to compete with ATP in the intracellular environment due to its relative high concentration of 2-10 mM. In addition to the 518 kinases encoded in the human genome, there are over 2000 other nucleotide-dependent enzymes, including polymerases, chaperones, motor proteins, reductases, and methyltransferases, which possess potential binding sites.[33]

The identification of cyclosporine as cellular target in 1991 was a turning point for the development of kinase inhibitors.[4] Cyclosporin A (Figure 1.4) was approved for clinical use in 1983 and has revolutionized organ transplantation by its ability to prevent graft rejection. Schreiber and his colleagues showed that the complex that was formed

between cyclosporine and cyclophilin was a potent inhibitor of calcineurin, which is a Ca^{2+}-calmodulin-dependent protein phosphatase. Modulation of the phosphorylation of one or more intracellular proteins plays an important role in the effects of cyclosporin.

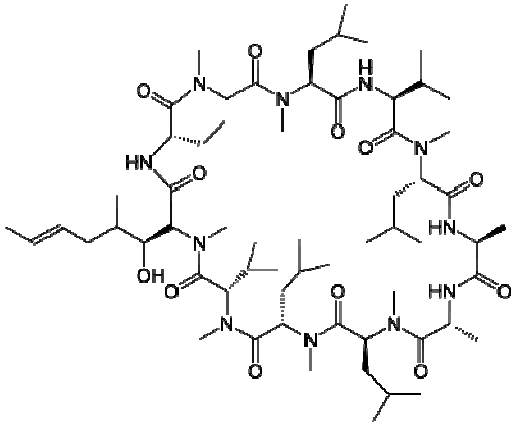

Figure 1.4. Structure of cyclosporin.

At present, some of the most promising drugs as anticancer agents in development are inhibitors of protein kinases. Until 2009, 11 kinase inhibitors have received US Food and Drug Administration approval as cancer treaments and a further more kinase inhibitors are known to be undergoing human clinical trials.[33] The structures of some of these inhibitors are shown in Figure 1.5. The first important drug to be developed by targeting a protein kinase is Gleevec which is developed as an inhibitor of Abelson tyrosine kinase (Abl) and approved for clinical use in 2001. Gleevec is marketed by Novartis[15] for the treatment of chronic myelogenous leukaemia (CML). The structure of Abl with Gleevec displayed that the drug extends much further into the catalytic site.[16] Later, some other protein kinases inhibitors were approved for clinical use such as Iressa[17] (in 2003), Tarceva[18] (in 2005), and Tykerb[19] (in 2007).

Protein kinases are already the second largest group of drug targets after G-protein-coupled receptors and they account for 30-35% of the drug discovery programs of many companies.[4,7] Protein kinase inhibitors are important not only for the treatment of diseases, but also as reagents to help us to understand more about the physiological roles of protein kinases.

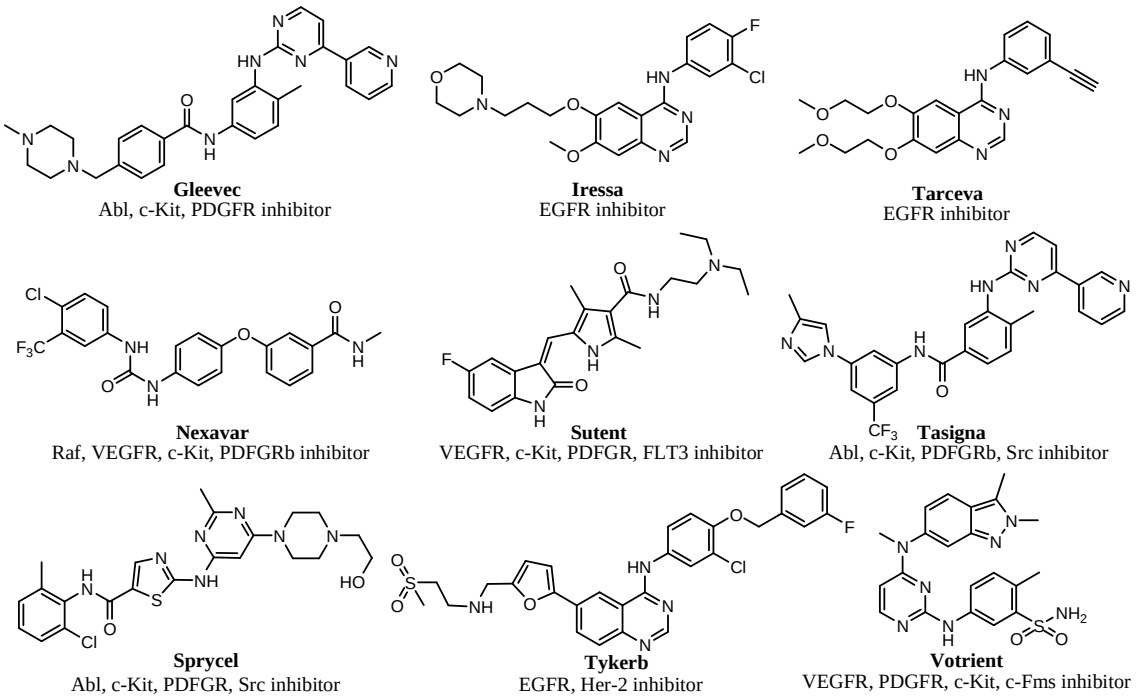

Figure 1.5. Structures of some kinase inhibitors marketed in the U.S. as of 2009 according to ref. 33.

Chapter 1.2: Organometallic scaffolds for enzyme inhibition

The pharmaceutical industry and chemical biology are dominated by organic chemistry, with inorganic compounds playing only a minor role.[20] Metals have potential advantageous properties over the common organic-based drugs, such as the wide range of coordination numbers and geometries, accessible redox states, thermodynamic and kinetic characteristics, and a wide structural diversity. Although metals have long been used for medicinal purpose more or less, the potential of metal-based anticancer agents has been realized and explored since the discovery of the biological activity of cisplatin in the late 1970s. Cisplatin is classified as classical chemotherapeutics which refers to the drugs that target DNA in the field of metal-based anticancer drug design.[31] The cytotoxicity of cisplatin has been studied extensively and is known to originate mainly from the formation of covalent cross-links that result from the binding of cisplatin to two purines of DNA. Such a substitution product is able to inhibit DNA and RNA synthesis and thereby induce cell death. However, cisplatin shows insufficient efficiency against some of the most frequent human cancers, moreover, patients treated with

cisplatin often undergo acquired resistance and heavy side effects.[37] Both the advantages and drawbacks of cisplatin have motivated scientists to search for other metal-based drugs with better therapeutic properties.

Nonclassical chemotherapeutics which refers to the drugs that target cellular signaling pathways overexpressed in cancer cells has emerged recently, such as with proteins and enzymes as targets for anticancer drug design.[31]

Chapter 1.2.1 Metal complexes as enzyme inhibitors through ligand-substitution

Metal complexes with labile ligands have long been known to undergo ligands substitution reactions with biomolecular targets. Metal ions can bind to nitrogen, sulfur or selenium of the histidine, cysteine or seleno cysteine residues in proteins.

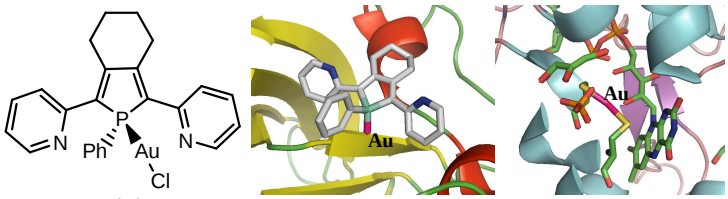

1.1

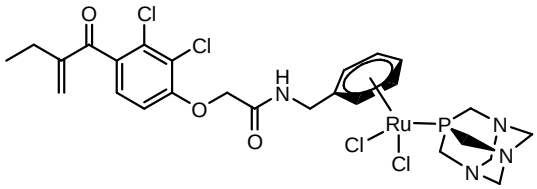

1.2

Figure 1.6. Structures of inhibitor **1.1** and **1.2**. The crystal structure shows the binding sites of gold according to ref. 39 (gold atoms as pink stick, PDB: 2AAQ).

Human thioredoxin reductase (hTrxR) is an interesting target for anticancer drugs due to its association with many cellular processes and tumour proliferation.[38] Gold(I) is highly electrophilic and shows high affinity to the selenocysteine residue of hTrxR. As a result, gold(I) complexes constitute one of the most potent inhibitors of hTrxR. Becker *et al.* presented the gold(I) complex **1.1** (Figure 1.6) as an inhibitor of hTrxR and the related human glutathione reductase (hGR) in nanomolar range.[39] They proved that the

gold unit bound to an exposed cysteine and an additional gold atom which lost both chloride and phosphole ligand formed a linear S-Au-S adduct in the active site by the cocrystal structure of **1.1** with hGR.

Dyson *et al*. developed a new series of glutathione transferase inhibitors in 2009.[40] To study the nature of the interactions of inhibitor **1.2** (Figure 1.6) with the enzyme, crystallographic analysis and mass spectrometry were used. These data suggested that ruthenium complex **1.2** originally binds to glutathione transferase by loss of the two chloride ligands and is then further cleaved, releasing the ruthenium fragment. The potential drawback of this kind of inhibition with metal complexes is the lack of selectivity.[41] The metals may bind to other proteins having metal binding sites which makes the delivery of inhibitors to specific targets difficult.

Chapter 1.2.2 Substitutionally inert metal complexes as enzyme inhibitors

Metals have been attractive and included in anticancer agents because of the wide range of reactivities. On the other hand, metals can also be used as scaffold with well defined, three dimensional structures. Substitutionally inert metal complexes serve as enzyme inhibitors providing a promising scaffold due to the stability of the complexes in cells and the possibility to design the scaffold for specific biomolecular target by mimicking known inhibitors.[41]

In contrast to the complexes which easily undergo ligands exchange in solution, the Che group explored the anticancer activity of gold(III) inhibitors containing multi-anionic chelating ligands.[41] In 2003, gold-**1a** (Figure 1.7) was discovered and had a series of advantages compared to Cisplatin. For example, it is substitutionally inert under physiological conditions and 240-fold more potent than Cisplatin. Further *in vitro* and *in vivo* studies revealed that gold-**1a** is a promising anticancer agent for the treatment of colon and liver cancer. A derivative with a hydroxyl group on porphyrin of gold-**2a** was developed with improved lipophilicity and aqueous stability with IC_{50} values in the nanomolar range in a panel of human breast cancer cell lines. Gold-**2a** was

found to regulate the association of class I histone deacetylase (HDAC) and histone acetylation at the promoter of Wnt/β-catenin signaling molecules and may represent a promising class of anticancer HDAC inhibitors targeting tumor cells with aberrant Wnt/β-catenin signaling.[42]

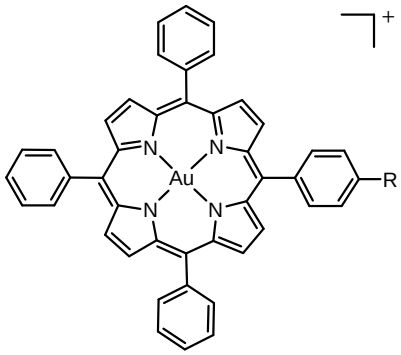

Gold(III) porphyrin
Gold-**1a** (R=H)/-**2a** (R=OH)

Figure 1.7. Structure of gold(III) porphyrin complexes.

Professor Meggers' group recently demonstrated a strategy of exploring the versatility of organometallic complexes as structural scaffold for the design of selective protein kinase inhibitors. The natural product staurosporine (Figure 1.8) was used as lead structure to design bioactive organometallic complexes.

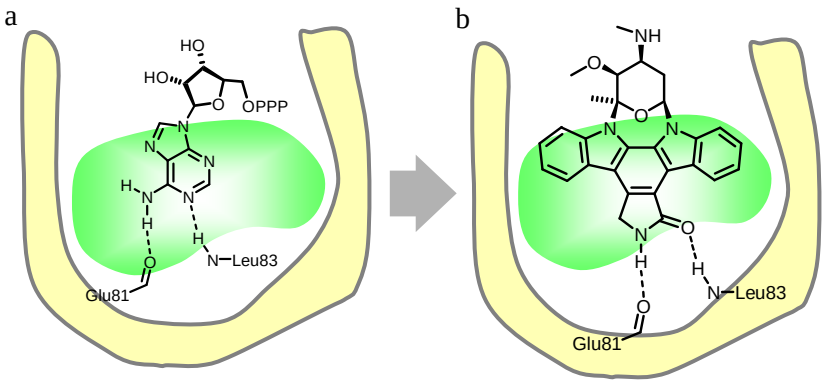

Figure 1.8. a) ATP in the ATP-binding site of CDK-2. b) Staurosporine in the ATP binding site of CDK-2. Adopted from ref. 21.

Staurosporine is a member of the class of indolocarbazole alkaloids and adopts a defined globular structure with the carbohydrate moiety being oriented perpendicular to the plane of the indolocarbazole heterocycle. The indolocarbazole moiety occupies the hydrophobic adenine binding cleft with the lactam group mimicking the hydrogen

bonding pattern of the adenine base, and the carbohydrate moiety forming hydrophobic contacts and hydrogen bonds within the globular ribose binding site. Thus, staurosporine closely matches the shape of the ATP-binding site which makes it a highly potent inhibitor for many protein kinases.[21-23]

In order to match the overall shape of the ATP-binding site of protein kinases similar to staurosporine, the metal-chelating pyridocarbazole was designed as scaffold in which the main features of the indolocarbazole heterocycle are retained and the pyridocarbazole serves as bidentate ligand for metal complexes (Figure 1.9) targeting to the ATP binding site. This gives the opportunity to build defined globular shapes by the ligands coordinated to the metal center.

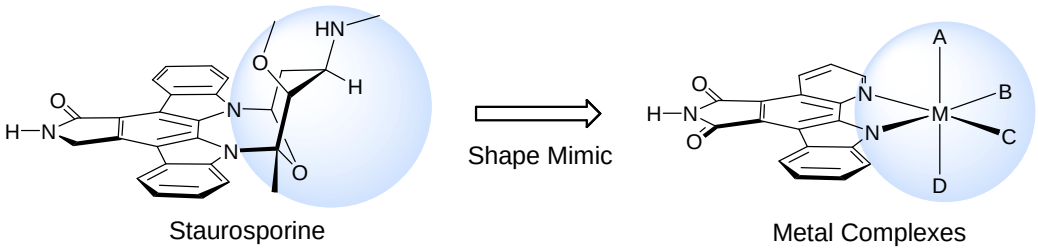

Figure 1.9. Design of ruthenium complexes as protein kinase inhibitors by using staurosporine as lead structure. A, B, C and D represent the organic ligands coordinated to the metal center.

Based on this scaffold, several organometallic inhibitors for the protein kinases of GSK3[24-29], Pim1[26,28,30], MSK1[26] and TrkA[32] were reported over the last 6 years. Some of the published inhibitors belong to the most potent and selective compounds known for their respective protein kinases.

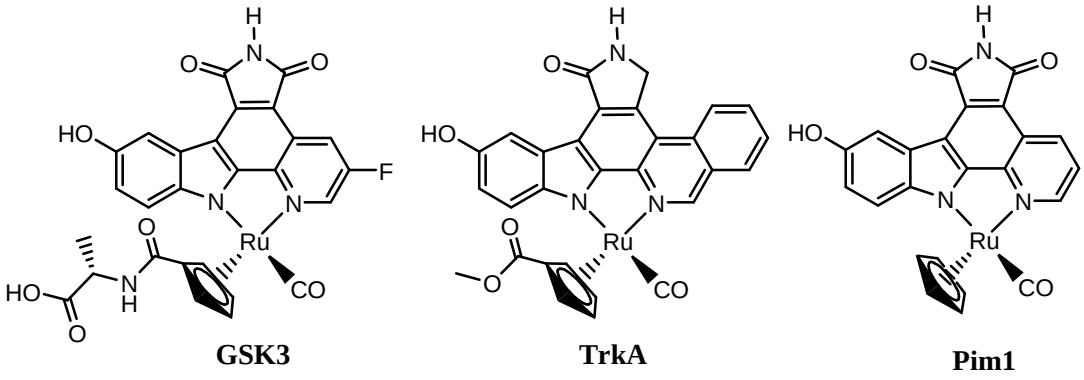

Figure 1.10. Structures of some organoruthenium inhibitors for their respective protein kinases.

Some published organoruthenium kinase inhibitors are shown in Figure 1.10. With different pyridocarbazoles and modifications on the coordinated moiety, these organoruthenium complexes can target different protein kinases potently and selectively, respectively. In the kinase active site, the metal center only exerts a purely structural role, without any interaction with the residues. Besides, such complexes are air-stable, stable in water, and in buffer solutions containing millimolar concentrations of thiols. The stability of the complexes is due to the inert character of typical coordinative bonds to ruthenium. This, together with its relative low price of the starting material $RuCl_3$, its low toxicity, and predictable and established synthetic chemistry,[31] makes ruthenium a very attractive transition metal for establishing the scaffold of protein kinase inhibitors. Overall, these results demonstrate the generality of the design strategy.

Chapter 1.3: Aim of the work

Most of the published organoruthenium inhibitors over the last few years were half-sandwich complexes. Based on previous work in our group, the focus of this thesis is the development of potent and selective protein kinase inhibitors with well defined three-dimensional octahedral ruthenium scaffolds (Figure 1.11). It was envisioned that the octahedral scaffolds can further improve the selectivity of inhibitors based on the bulky and rigid configuration.

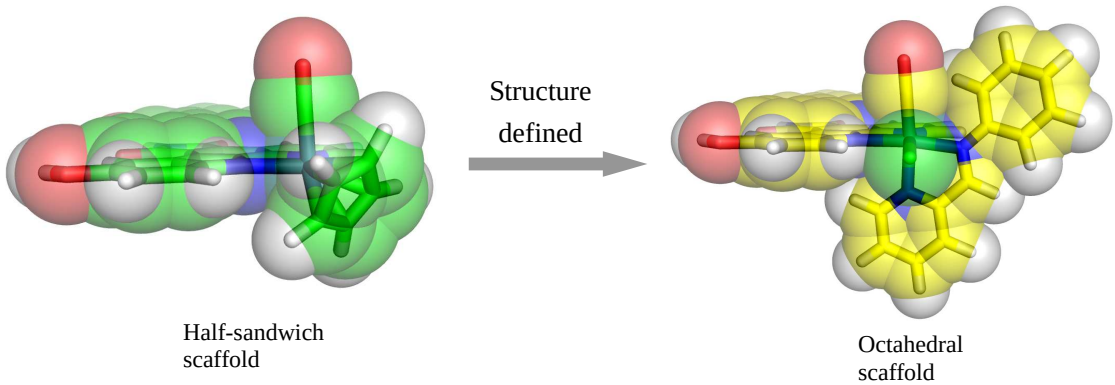

Figure 1.11. Octahedral scaffold with well defined three-dimensional structure compare with half-sandwich geometry.

With well defined three-dimensional structures, octahedral scaffolds can possiblely explore all areas of the biologically relevant chemical space in the protein kinase active site, and another advantage is that octahedral scaffolds are usually more chemically inert than half-sandwich scaffold which is attractive for the investigation of their biological functions. However, with 6 different substituents, an octahedral center is capable of forming 30 different stereoisomers compared to just 2 for a half-sandwich scaffold, which provides more opportunities to achieve inhibitors for protein kinases with high affinity and selectivity. On the other hand, it is also a challenge to find a way to control the stereochemistry of the metal complexes. One possible solution is using symmetrical multidentate ligand instead of monodentate ligand.

Chapter 1.4: References

(1) Manning, G.; Whyte, D. B.; Martinz, R.; Hunter, T.; Sudarsanam, S. *Science* **2002**, *298*, 1912-1916.

(2) Hanks, S. K.; Hunter, T. *FASEB J.* **1995**, *9*, 576-596.

(3) Blume, J. P.; Hunter, T. *Drug Discovery Today* **2001**, *10*, 839-846.

(4) Cohen, P. *Nat. Rev. Drug Discovery* **2002**, 1, 309-315.

(5) Noble, M. E. M.; Endicott, J. A.; Johnson, L. N. *Science* **2004**, *303*, 1800-1805.

(6) Keri, G.; Orfi, L.; Eros, D.; Hegymegi, B. B.; Klebl, B.; Ullrich, A. *Curr. Signal Transduction Ther.* **2006**, *1*, 67-95.

(7) Weinmann, H.; Metternich, R. *ChemBioChem* **2005**, *6*, 455-459.

(8) Stadler, W. M. *J. Clin. Oncol.* **2006**, *24*, 4-5.

(9) Hidaka, H.; Kawamoto, S.; Sasaki, Y. *Biochemistry* **1984**, *23*, 5036-5041.

(10) Nagar, B.; Bornmann, W. G.; Pellicena, P.; Schindler, T.; Veach, D. R.; Miller, W. T.; Clarkson, B.; Kuriyan, J. *Cancer Res.* **2002**, *62*, 4236-4243.

(11) Johnson, L. N.; Noble, M. E. M.; Owen, D. J. *Cell* **1996**, *85*, 149-158.

(12) Tamaoki, T.; Nomoto, H.; Takahashi, I.; Kato, Y.; Morimoto, M.; Tomita, F. *Biochem. Biophys. Res. Commun.* **1986**, *135*, 397-402.

(13) Alessi, D. R. *FEBS Lett.* **1997**, *402*, 121-123.

(14) Davies, S. P.; Reddy, H.; Caivano, M. Cohen, P. *Biochem. J.* **2000**, *351*, 95-105.

(15) Buchdunger, E.; Zimmermann, J.; Mett, H.; Meyer, T.; Druker, B. J.; Lydon, N. B. *Cancer Res*. **1996**, *56*, 100-104.

(16) Schindler, T.; Pellicena, P.; Kuriyan, J. *Science* **2000**, *289*, 1938-1942.

(17) Cohen, M. H.; Williams, G. A.; Pazdur, R. *The Oncologist* **2003**, *8*, 303-306.

(18) Cohen, M. H.; Johnson, J. R.; Chen, Y.; Sridhara, R.; Pazdur, R. *The Oncologist* **2005**, *10*, 461-466.

(19) Ryan, Q.; Ibrahim, A.; Cohen, M. H.; Johnson, J.; Ko, C.; Sridhara, R.; Justice, R.; Pazdur, R. *The Oncologist* **2008**, *13*, 1114-1119.

(20) Hughes, B. *Nat. Rev. Drug Discovery* **2008**, *7*, 107-109.

(21) Huwe, A.; Giannis, A. *Angew. Chem., Int. Ed.* **2003**, *42*, 2122-2138.

(22) Jacobs, M. D.; Fleming, M.; Saxena, K. *J. Biol. Chem.* **2005**, *280*, 13728-13734.

(23) Meggers, E.; Atilla-Gokcumen, G. E.; Bregman, H.; Maksimoska, J.; Mulcahy, S. P.; Pagano, N.; Williams, D. S. *Synlett* **2007**, *8*, 1177-1189.

(24) Bregman, H.; Williams, D. S.; Atilla, G. E.; Carroll, P. J.; Meggers, E. *J. Am. Chem. Soc.* **2004**, *126*, 13594-13595.

(25) Williams, D. S.; Atilla, G. E.; Bregman, H.; Arzoumanian, A.; Klein, P. S.; Meggers, E. *Angew. Chem., Int. Ed.* **2005**, *44*, 1984-1987.

(26) Bregman, H.; Carroll, P. J.; Meggers, E. *J. Am. Chem. Soc.* **2006**, *128*, 877-884.

(27) Atilla-Gokcumen, G. E.; Williams, D. S.; Bregman, H.; Pagano, N.; Meggers, E. *ChemBioChem* **2006**, *7*, 1443-1450.

(28) Bregman, H.; Meggers, E. *Org. Lett.* **2006**, *8*, 5465-5468.

(29) Atilla-Gokcumen, G. E.; Pagano, N.; Streu, C.; Maksimoska, J.; Filippakopoulos, P.; Knapp, S.; Meggers, E. *ChemBioChem* **2008**, *9*, 2933-2936.

(30) Debreczeni, J. E.; Bullock, A. N.; Atilla, G. E.; Williams, D. S.; Bregman, H.; Knapp, S.; Meggers, E. *Angew. Chem., Int. Ed.* **2006**, *45*, 1580-1585.

(31) Rijt, S. H.; Sadler, P. J. *Drug Discovery Today* **2009**, *14*, 1089-1097.

(32) Pagano, N.; Wong, E. Y.; Breiding, T.; Liu, H.; Wilbuer, A.; Bregman, H.; Shen, Q.; Diamond, S. L.; Meggers, E. *J. Org. Chem.* **2009**, *74*, 8997-9009.

(33) Zhang, J. M.; Yang, P. L.; Gray, N. S. *Nature Reviews Cancer* **2009**, *9*, 28-39.

(34) Liu, Y.; Gray, N. S. *Nature Chem. Biol.* **2006**, *2*, 358-364.

(35) Ohren, J. F. *et al*. *Nature Struct. Mol. Biol*. **2004**, *11*, 1192-1197.

(36) Cohen, M. S.; Taunton, J. *Science* **2005**, *308*, 1318-1321.

(37) Wong, E.; Giandomenico, C. M. *Chem. Rev*. **1999**, *99*, 2451-2466.

(38) Bruijnincx, P.; Sadler, P. J. *Curr. Opin. Chem. Biol*. **2008**, *12*, 197-206.

(39) Urig, S.; Reau, R.; Becker, K. *Angew. Chem., Int. Ed.* **2006**, *45*, 1881-1886.

(40) Ang, W. H.; Parker, L. J.; Dyson, P. J. *Angew. Chem., Int. Ed.* **2009**, *48*, 3854-3857.

(41) Che, C. M.; Siu, F. M. *Curr. Opin. Chem. Biol*. **2010**, *14*, 255-261.

(42) Chow, K. H. M.; Sun, R. W. Y.; Che, C. M. *Cancer Res.* **2010**, *70*, 329-337.

Chapter 2: Targeting Large Kinase Active Site with Rigid, Bulky Octahedral Ruthenium Complexes

This chapter discusses a new strategy for the design of selective protein kinase inhibitors that uses rigid, bulky octahedral ruthenium complexes to discriminate between kinase active sites based on the size of the ATP binding pocket. It was envisioned that octahedral complexes would be uniquely suited to selectively target large active sites by establishing rigid shapes which are easily modified by assembling a structure from a single center and changing the character of the coordinating ligands. The p21-activated kinase 1 (PAK1) which is known to contain a relatively open ATP binding site[3] was selected as a model system.

Chapter 2.1: Initial screening of an organometallic library for PAK1 inhibition

An initial screening of a library of 48 organoruthenium complexes (done by former lab colleague Jasna Maksimoska and see appendix for details) led to the identification of the GSK3 and Pim1 half-sandwich inhibitors **NP309** and **DW12** (Figure 2.1) as the most potent complexes for PAK1. These inhibitors, screened as racemic mixtures, have IC_{50} values of ~1 μM in the presence of 1 μM ATP.[4]

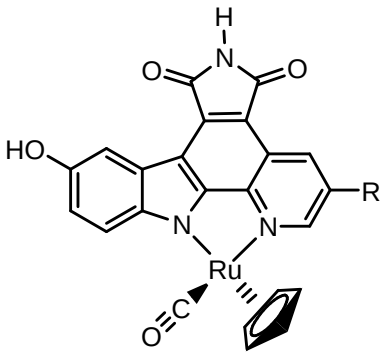

NP309 (R=F), **DW12** (R=H)
GSK3 & Pim1 inhibitors

Figure 2.1. The structures of racemic **NP309** and **DW12**.

A subsequent cocrystal structure obtained by Jasna Maksimoska of (*R*)-**DW12** with the kinase domain of PAK1 (amino acids 249-545, inactivating mutation Lys299Arg) at 2.35 Å resolution (Figure 2.2) revealed the important determinants for this affinity: the maleimide moiety and the indole -OH group account for four hydrogen bonds to the backbone of the hinge region. In addition, the monodentate carbonyl ligand interacts with the residues of the glycine-rich loop. Most interestingly, the η^5-cyclopentadienyl moiety is not in close contact with any amino acid side chains of the protein. Thus, this cocrystal structure highlights the large amount of vacant space accessible in the PAK1 active site which is not available in many other kinases such as Pim1 and GSK3.[4]

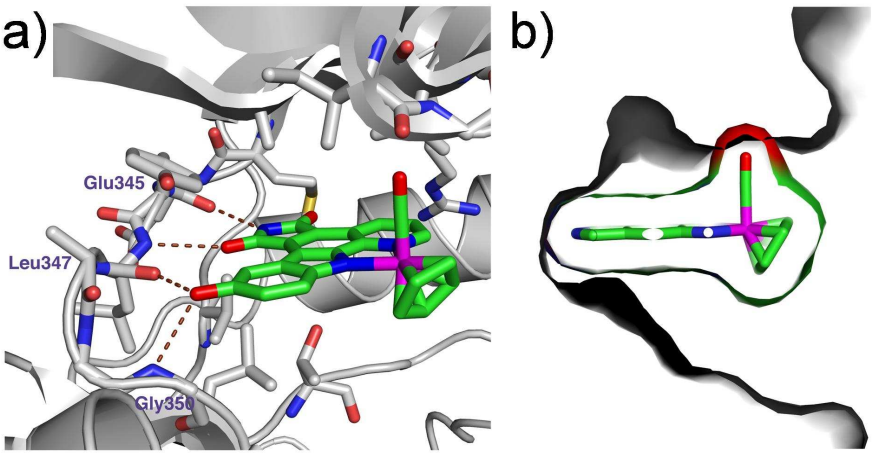

Figure 2.2. Cocrystal structure at 2.35 Å of (*R*)-**DW12** with PAK1 (249-545, mutation Lys299Arg). a) Important H-bonding interactions between (*R*)-**DW12** and PAK1. b) Surface view through the active site to demonstrate the open ATP-binding site of PAK1. Adopted from ref. 4.

Chapter 2.2: Designing a precursor for combinatorial coordination chemistry

To quickly scan for the most suitable ligand combination to fill up the coordination sphere around the ruthenium center, it would be desirable to have a compound which can serve as a common precursor for a large and diverse set of metal containing complexes. The synthesis of such a ruthenium complex **2.3**, shown in Scheme 2.1, has four leaving groups in addition to the pyridocarbazole ligand, thus allowing for rapid

access to a diversity of novel structures by simple ligands replacement chemistry. To elaborate compounds to fill the vacant chemical space in the ATP binding site of PAK1, octahedral ruthenium complexes **2.4** that contained the pyridocarbazole moiety and CO ligand of **NP309** were prepared.

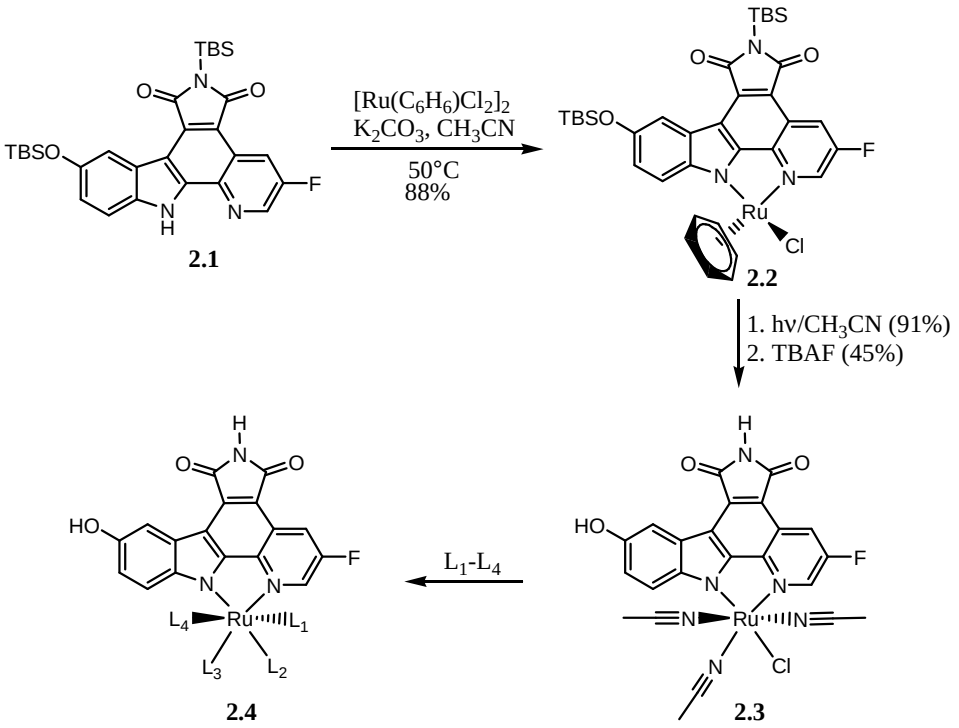

Scheme 2.1. Synthesis of racemic octahedral ruthenium complexes **2.4**.

Accordingly, pyridocarbazole **2.1** was cyclometallated with 0.75 equiv of $[(\eta^6\text{-benzene})RuCl_2]_2$ in the presence of 1.1 equiv of potassium carbonate in acetonitrile at 50 °C affording the racemic η^6-half-sandwich complex **2.2** in 88% yield. The benzene ring was next replaced by three acetonitrile molecules upon UV-photolysis in acetonitrile at room temperature, followed by TBS-deprotection using TBAF (tetrabutylammonium fluoride, 1 M in THF) at 0 °C, which afforded the ruthenium precursor **2.3** in 41% yield over two steps. The complex **2.3** shown in Scheme 2.1 was the major diastereoisomer obtained in which chloride was *trans* to the indole nitrogen.[5] Another diastereomer was also obtained in 25% yield in which chloride was *cis* to the indole nitrogen. Although difficult, these two diastereomers were separated by silica gel chromatography. The use of these individual diastereomers to synthesize octahedral ruthenium complexes demonstrated that both diastereomers had the same reactivity and

provided the same product. Thus, the mixture of these two isomers was subsequently used as a general precursor for the synthesis of a variety of octahedral complexes **2.4**.

Chapter 2.3: Evaluation of the diastereoselectivity of coordination chemistry with precursor 2.3

In order to evaluate the diastereoselectivity of coordination chemistry with a ruthenium precursor containing four replaceable ligands, the imide of precursor **2.3** was protected with a benzyl group to yield precursor **2.5** used for this model system. Precursor **2.5** was first reacted with CO gas, followed by 2,2'-bipyridine (bpy) (Scheme 2.2).

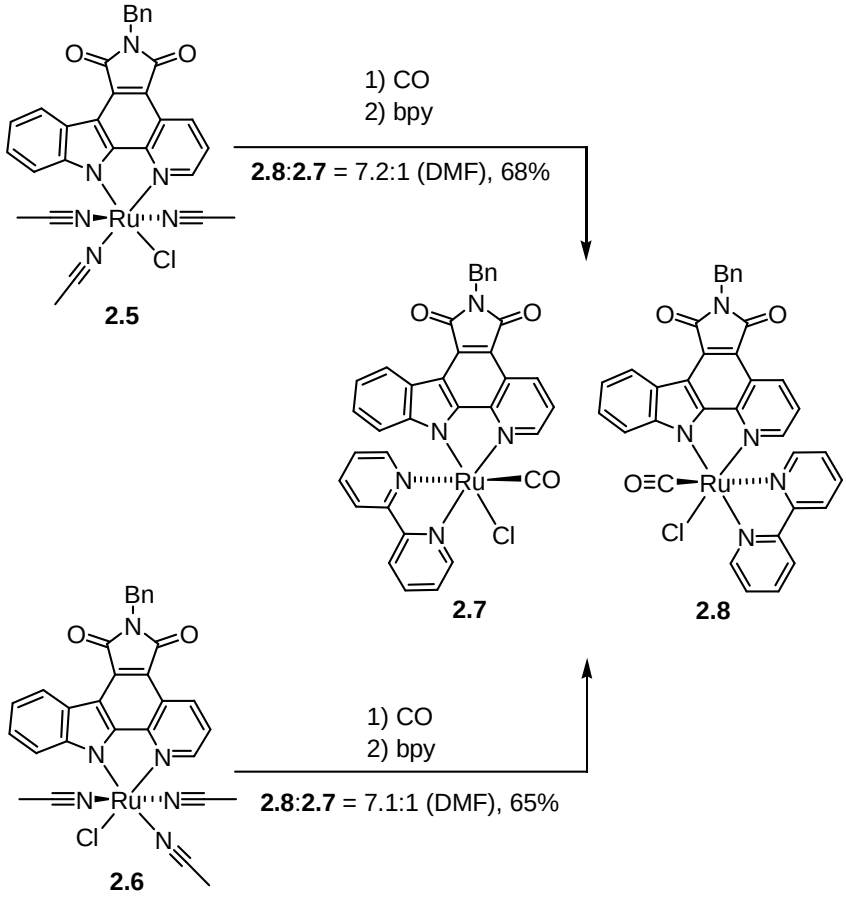

Scheme 2.2. Synthesis of complexes **2.7** and **2.8** starting from precursor **2.5** and **2.6** as a model system to evaluate the diastereoselectivity of coordination chemistry with precursor **2.3**. All the complexes are racemic.

Accordingly, a solution of **2.5** in DMF was first purged with CO gas for 5 min and stirred at 75 °C for 1 hour. Subsequently, the addition of 1 equiv of bpy and increasing the temperature to 95 °C for 1.5 hours afforded the diastereomer **2.8** as the main product along with the diastereomer **2.7** as the single side product (**2.8**:**2.7** = 7.2:1). The diastereoselectivity was solvent dependent. In an aprotic solvent mixture of toluene:$CHCl_3$ (4:1) the selectivity decreased to 2.4:1, whereas in a mixture of EtOH:$CHCl_3$ (4:1) the diastereoselectivity was higher with **2.8**:**2.7** = 20:1. Interestingly, the other three possible diastereomers were not observed in this reaction. Also, curiously, the reaction of the diastereomeric precursor **2.6** with CO and bpy under the same conditions afforded the same main product **2.8** with almost an identical diastereoselectivity (**2.8**:**2.7** = 7.1:1) (Scheme 2.2). The relative configuration of the predominant diastereomer **2.8** was determined via X-ray crystallography. As shown in Figure 2.3, the CO is placed in a position perpendicular to the pyridocarbazole and the chloride ligand *trans* to the pyridine moiety of the pyridocarbazole.

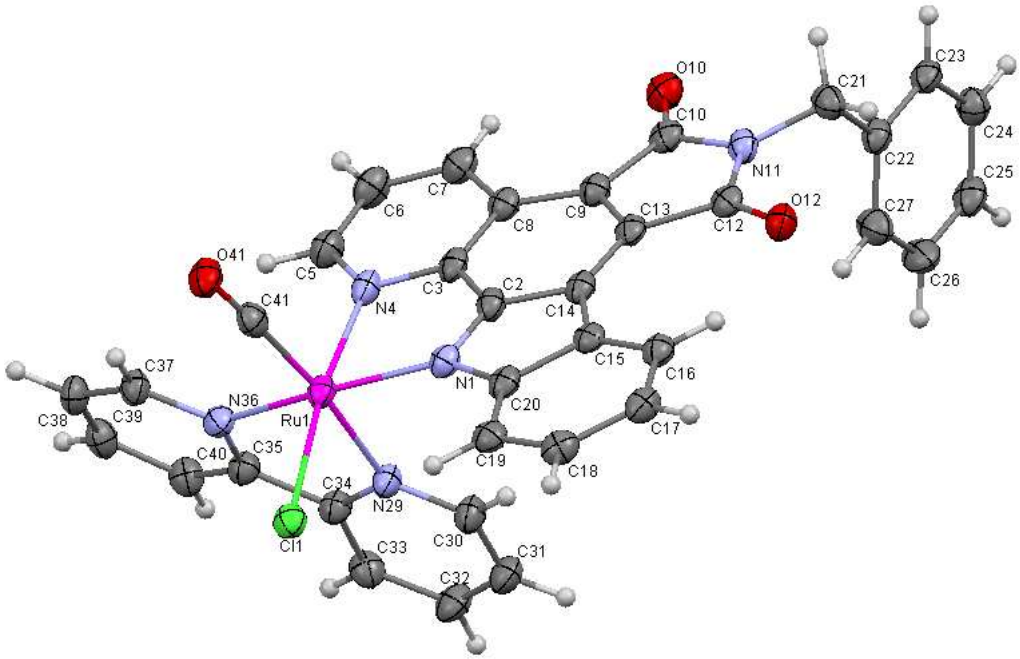

Figure 2.3. Crystal structure of complex **2.8**. ORTEP drawing with 50% probability thermal ellipsoids. All the single crystal structures in this thesis were obtained by Dr. Klaus Harms.

Quantum chemical calculations were carried out by Deepa Devarajan from the group of Prof. Dr. G. Frenking using density functional theory (DFT) employing the BP86 and

B3LYP functionals in conjunction with various basis sets, as well as ab initio calculations at the MP2 level in order to elucidate the mechanism of the reaction of **2.5** and **2.6** with CO and bpy yielding selectively **2.8** with formation of **2.7** as a minor diastereoisomer. The calculations were carried out for the model complexes where the benzyl groups in **2.5** and **2.6** were replaced by hydrogen. All five possible diastereomers of the product molecules **2.9** - **2.13** were calculated and the calculated relatived energies are listed in Scheme 2.3.

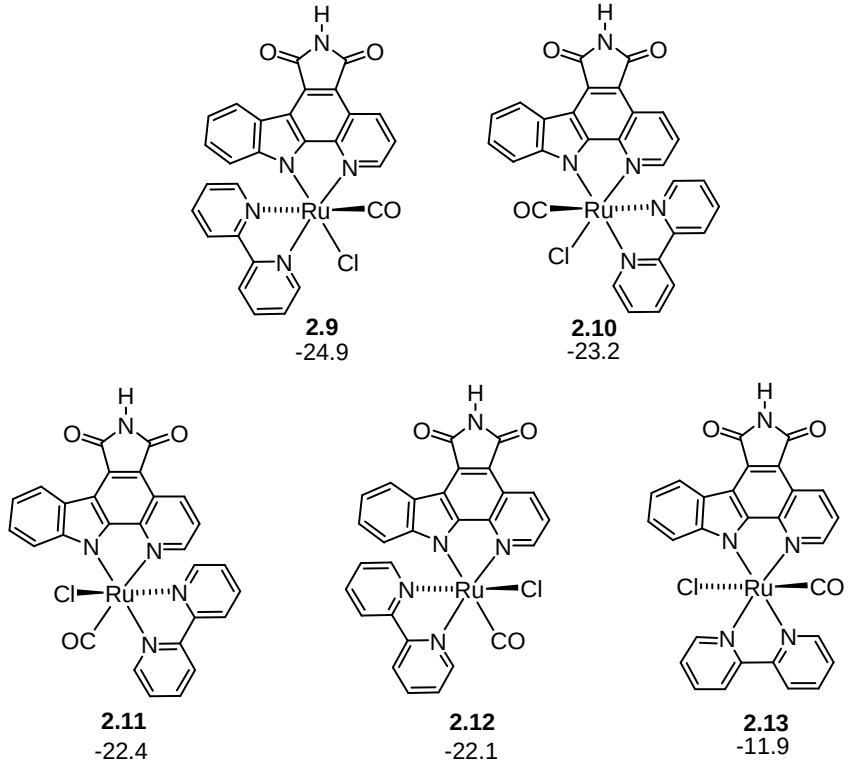

Scheme 2.3. Calculated relative energies in kcal/mol of five possible diastereoisomers **2.9** - **2.13**.

The results showed that the diastereomers **2.9** and **2.10** were the two most stable isomers, explaining why only the former two species were experimentally observed. Structure **2.9** was slightly lower in energy than **2.10** at all levels of theory which were employed when solvent effects were not considered.

Chapter 2.4: Synthesis and screening of octahedral ruthenium complexes with different bidentate ligands

To identify the most interesting scaffold for the development of PAK1 inhibitors, different bidentate ligands were investigated and a library of octahedral ruthenium complexes was synthesized under the conditions shown in Scheme 2.4.

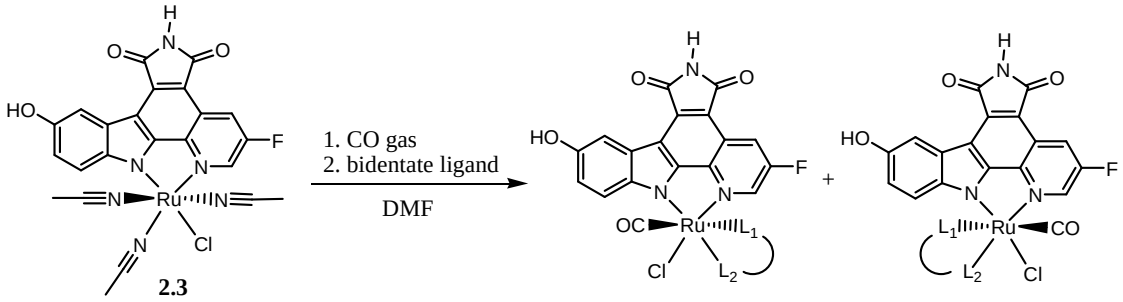

Scheme 2.4. Synthesis of library complexes containing different bidentate ligands.

Reactions were performed starting from the ruthenium precursor **2.3**. Accordingly, a solution of precursor **2.3** in DMF was purged with CO gas for 5 minutes, followed by stirring at 75 °C under the atmosphere of CO for 1 hour. To the resulting solution was added the respective bidentate ligand and the mixture stirred at 95 °C under an atmosphere of nitrogen for 1-3 hours, which depended on the characteristic of the bidentate ligands, affording the crude products. The final products were obtained by the purification through silica gel chromatography. The structures of the complexes synthesized using this method are displayed in Figure 2.4. All the complexes were synthesized as a racemic mixture.

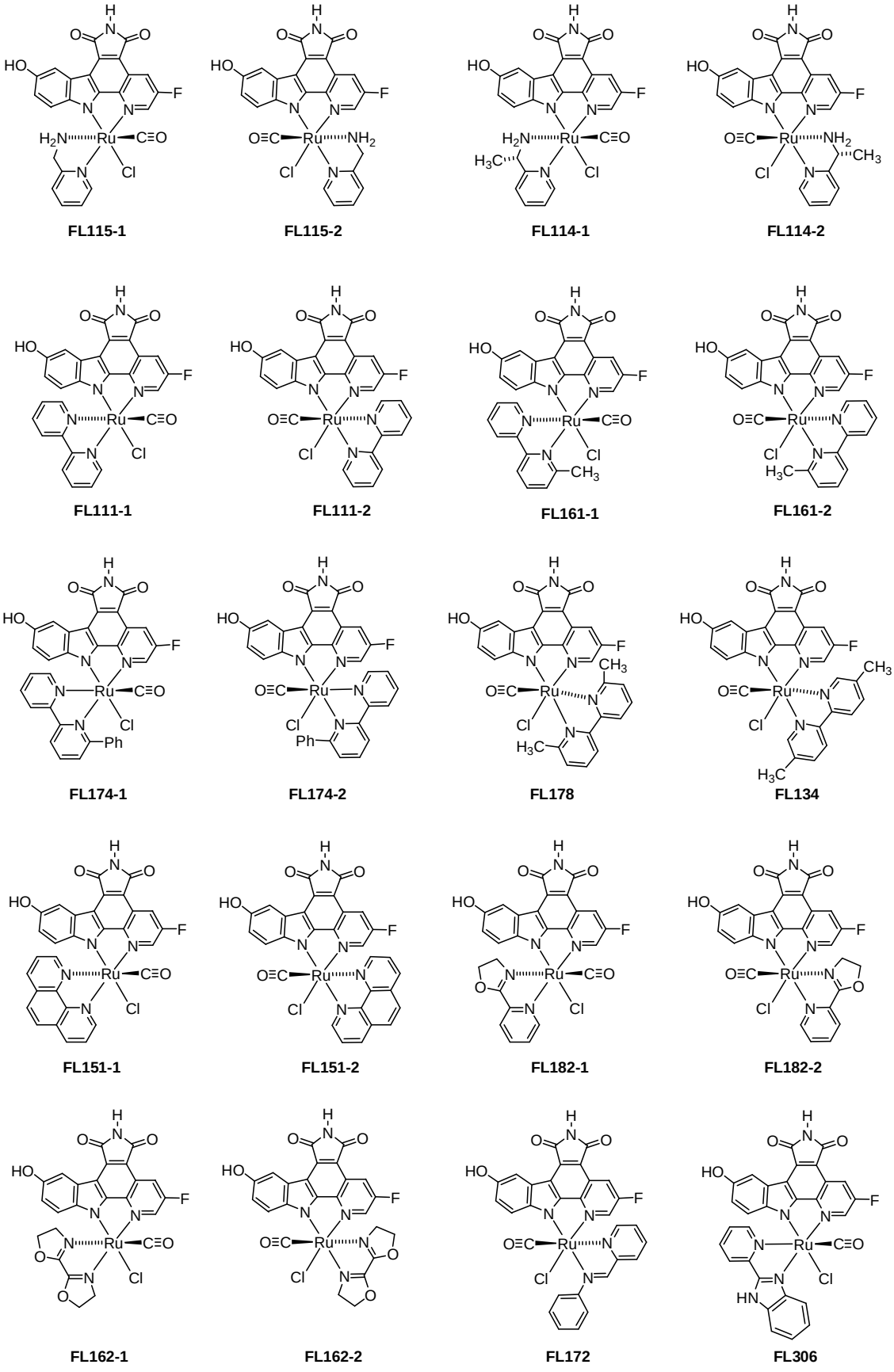

Figure 2.4. Racemic complexes synthesized for screening against PAK1 with different bidentate ligands. The relative configurations of **FL182** and **FL306** were tentatively assigned by ^{1}H NMR.

The two diastereoisomers that were formed for the complexes in Figure 2.4 were able to be separated in most of the cases. The relative configurations were assigned by ^{1}H NMR spectroscopy based on the presence or absence of an upfield shifted indole H-7 proton caused by the ring-current of the adjacent conjugated aromatic π-systems. As shown in Figure 2.5, an upfield shift of the H-7 proton correlates to a *cis* configuration between the indole and the bidentate ligand.

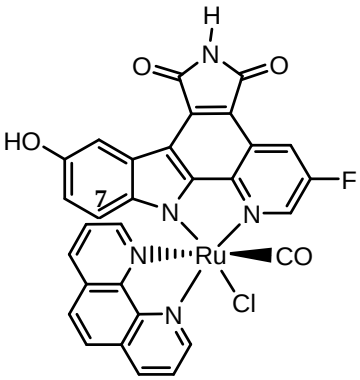

FL151-1

1,10-phenanthroline *cis* to the indole
upfield-shifted H-7 due to ring-current effect

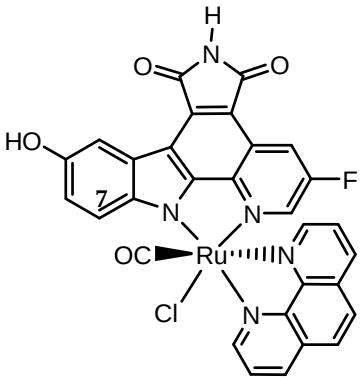

FL151-2

1,10-phenanthroline *trans* to the indole
no ring-current effect

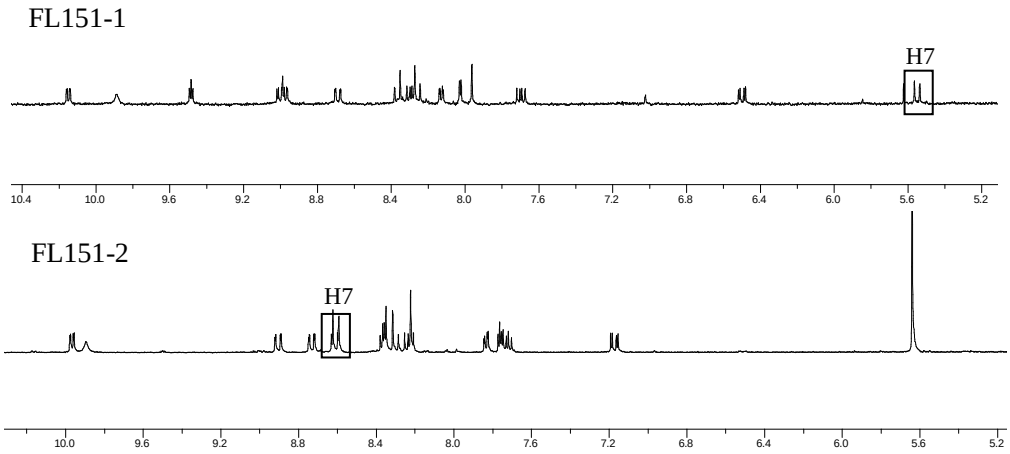

Figure 2.5. Example of the assignment of the relative stereochemistry of racemic octahedral complexes in Figure 2.4 by ^{1}H NMR spectroscopy.

In addition, the relative configuration was further proven by the crystal structure of complex **FL151-1**. X-ray quality crystals of the complex **FL151-1** suitable for single crystal diffraction were obtained from acetone by slow evaporation. The molecular structure of **FL151-1** shown in Figure 2.6 confirms the earlier assignment by ^{1}H NMR

spectroscopy in which the 1,10-phenanthroline bidentate ligand is positioned *cis* to the indole moiety.

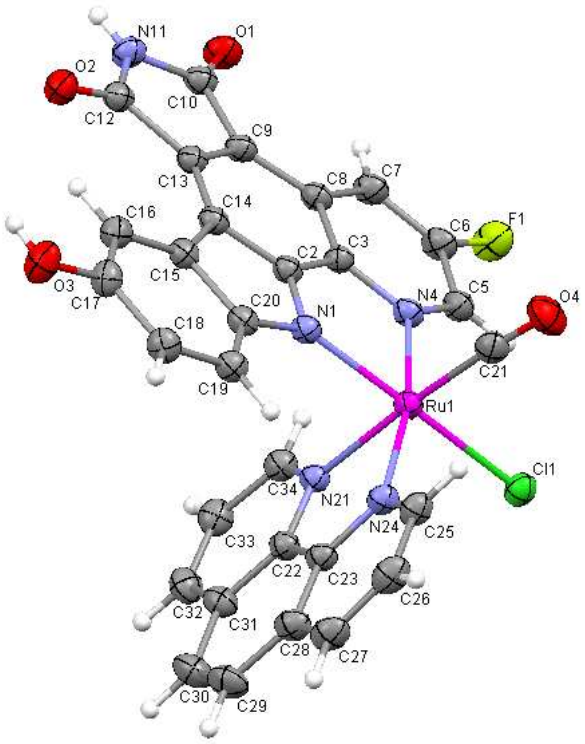

Figure 2.6. Crystal structure of complex **FL151-1**. ORTEP drawing with 50% probability thermal ellipsoids.

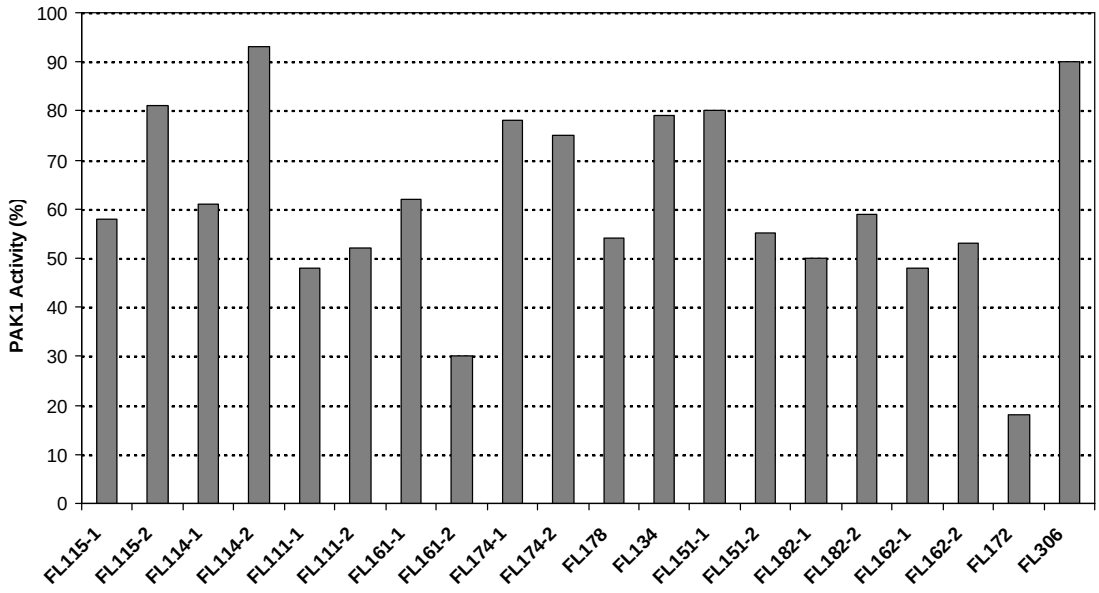

Figure 2.7. Remaining activities of PAK1 with 20 ruthenium complexes (see Figure 2.4 for the structures). Measured at a single inhibitor concentration of 1 μM and in the presence of 1 μM ATP. All the complexes measured above are racemic.

Initial inhibitory activities of this library were measured against PAK1 at a single concentration of the ruthenium complexes of 1 μM in the presence of 1 μM ATP, and the data are shown in Figure 2.7. These data demonstrate that overall the potency of these ruthenium complexes is improved by switching from half-sandwich scaffold to octahedral scaffold. Out of the 20 complexes, **FL172** was the most promising scaffold for PAK1, with only 18% activity remaining at 1 μM of **FL172** with 1 μM ATP (IC_{50} value was around 300 nM). Interestingly, it was found that the reaction of **2.3** with CO gas, and then with 2-(*N*-phenylaminomethyl)pyridine without any prior workup yielded the racemic complex **FL172** under complete diastereoselectivity and oxidation of the amine to imine. The mechanism of the diastereoselectivity in the reaction is still not well understood. However, the bidentate ligand 2-(*N*-phenyliminomethyl)pyridine was tried as a reference in the coordination chemistry to validate the importance of this bidentate ligand in the diastereoselectivity. Surprisingly, totally four diastereoisomers were formed and proven by ^{1}H NMR spectroscopy. Therefore, it can be concluded that one crucial step for the diastereoselectivity is the oxidation of the amine to imine of the bidentate ligand.

Chapter 2.5: Inhibitory property and selectivity of FL172 as PAK1 inhibitor

To investigate the selectivity profile of this scaffold, the racemic complex **FL172** was tested against a panel of 264 protein kinases (Millipore UK Ltd). PAK1, which was not available in the Kinase Profiler panel, was measured with a separate assay. The results revealed that **FL172** showed impressive selectivity over other protein kinases, whereas, at a concentration of 3 μM of **FL172** in the presence of 10 μM ATP, only 15 kinases (5.7% of total) displayed an activity of less than 20%, including PAK1, GSK3, and Pim1 (see appendix for details).

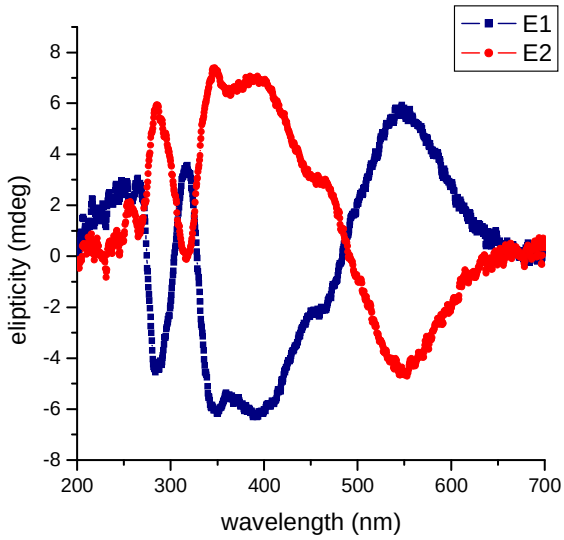

Figure 2.8. Circular dichroism spectra of the two enantiomers of **FL172**, measured at 1 μM of the two enantiomers in DMSO.

To further investigate the inhibitory properties of **FL172**, the complex was resolved into individual enantiomers (Figure 2.8) using a chiral HPLC column (see Experimental Section for details). The structures of Δ- and Λ- enantiomers are shown in Figure 2.9. The absolute configurations of both enantiomers were established from the cocrystal structure with PAK1 (Jasna Maksimoska, Department of Chemistry at the University of Pennsylvania and The Wistar Institute, Philadelphia, USA).[4]

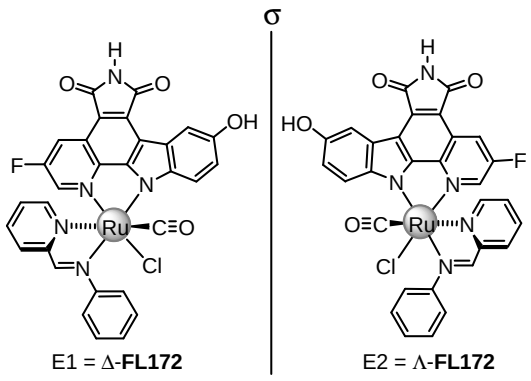

Figure 2.9. Individual enantiomers of **FL172**. The absolute configurations were established from the cocrystal structure with PAK1 (Jasna Maksimoska).

Subsequently, the individual enantiomers of **FL172** were tested against PAK1, GSK3β, and Pim1 with an ATP concentration of 1 μM, and the IC_{50} values are summarized in Table 2.1 combined with the results of **DW12** and **NP309**.

Table 2.1. IC_{50} values in nM of **DW12**, **NP309** and **FL172** against GSK3β, Pim1 and PAK1 in the presence of 1 μM ATP.

	GSK3β	**Pim1**	**PAK1**
rac-**DW12**	0.32	0.14	1090
rac-**NP309**	0.28	0.17	770
Δ-**FL172**	440	140	3480
Λ-**FL172**	1480	440	130

The IC_{50} values revealed a strong modulation in selectivity with the Λ-enantiomer of **FL172** (130 nM) being 27-fold more potent for PAK1 compared to Δ-**FL172**. Λ-**FL172** showed relatively low binding affinity to GSK3β and Pim1, and the IC_{50} values were 1.48 μM and 440 nM, respectively. Comparing with **NP309**, by just replacing the cyclopentadienyl moiety for a chloride and a bulky bidentate phenyliminopyridine ligand in Λ-**FL172** (Figure 2.10), the initial picomolar affinities for Pim1 and GSK3β dropped by factors of 2588 and 5285, respectively, whereas the affinity for PAK1 was improved by a factor of 6 at the same time.

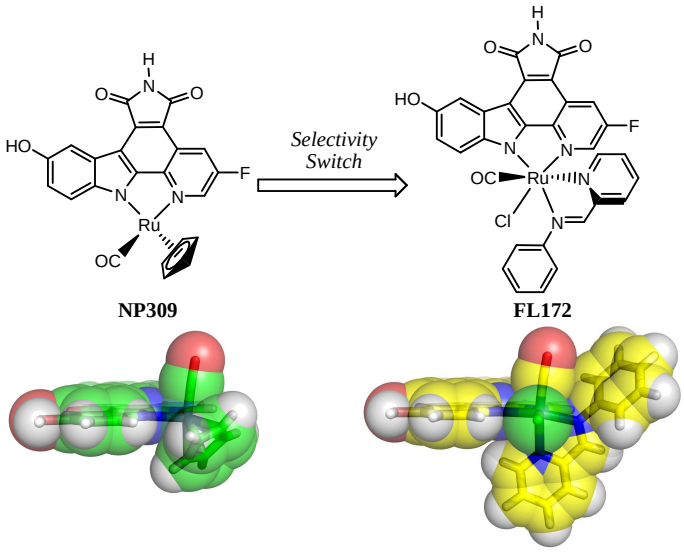

Figure 2.10. Kinase selectivity switched by the transformation of a small half-sandwich scaffold into rigid and bulky octahedral ruthenium complex.

Chapter 2.6: Cocrystal structure of Λ-FL172 with PAK1

A 1.65 Å resolution cocrystal structure of Λ-**FL172** bound to PAK1 was obtained by Jasna Maksimoska (University of Pennsylvania and The Wistar Institute, Philadelphia, USA) revealed the molecular details of the binding of this octahedral scaffold in PAK1 active site.[4] Whereas the pyridocarbazole moiety and CO ligand bind analogously to (*R*)-**DW12**. The maleimide moiety and the indole -OH group account for four canonical hydrogen bonds to the backbone of the hinge region. In addition, the monodentate carbonyl ligand establishes interactions to the residues of the glycine-rich loop and the bulky bidentate phenyliminopyridine ligand now stretches the entire distance from the N-terminal glycine-rich loop to the C-terminal domain (Figure 2.11). In this bulky octahedral complex the distance between the oxygen atom of the CO ligand and the *para*-carbon of the pyridine in *trans* serves as a rigid yardstick of about 8 Å which can only be well accommodated in the active site of PAK1, but not in most other protein kinases.

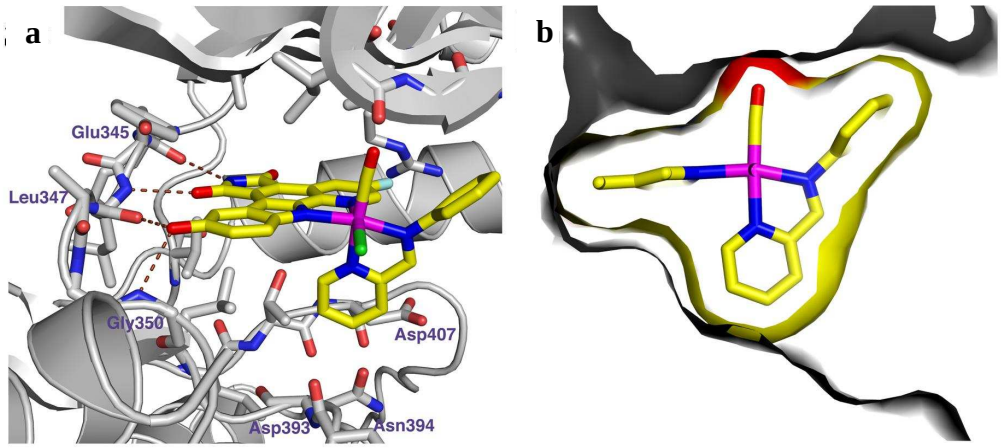

Figure 2.11. Cocrystal structure of Λ-**FL172** with PAK1 (amino acids 249-545, mutation Lys299Arg) at 1.65 Å (by Jasna Maksimoska, University of Pennsylvania and The Wistar Institute, Philadelphia, USA). a) Some important interactions. b) Surface view to visualize the shape complementarity of PAK1 and Λ-**FL172**.

Chapter 2.7: Derivatives of FL172 as improved selective PAK1 inhibitors

Although the binding affinity of Λ-**FL172** for kinase Pim1 was dramatically reduced by a factor of 2588 compared to **NP309**, the selectivity of Λ-**FL172** for PAK1 over Pim1 was only 3-fold. Thus, improving the selectivity over Pim1 is a crucial issue for the development of PAK1 inhibitors.

The cocrystal structure of Λ-**FL172** with PAK1 (Figure 2.8) showed that the phenyl ring and the pyridine in the 2-(*N*-phenyliminomethyl)pyridine bidentate ligand were close to the backbone in the active site. It is possible that modifications of the bidentate ligand may allow the inhibitor to form an increased number of positive interactions with the backbone of the kinase. The 2-(*N*-phenylaminomethyl)pyridine ligand of **FL172** was synthesized by reductive amination from 2-pyridinecarboxaldehyde and aniline to form Schiff base, then reduced by sodium borohydride (Scheme 2.5). Interestingly, a large number of aniline and 2-pyridinecarboxaldehyde derivatives are commercially available, which could be used to synthesize a modified bidentate ligands to perform a structure-activity study.

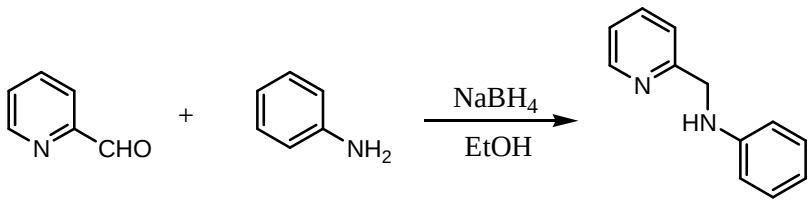

Scheme 2.5. The synthesis of 2-(*N*-phenylaminomethyl)pyridine.

The derivatives of 2-(*N*-phenylaminomethyl)pyridine used as the bidentate ligands in the synthesis of derivatives of **FL172** are shown in Figure 2.12. A methyl group was first used to modify the *ortho*-, *meta*-, and *para*- position of aniline, respectively, to identify whether there is enough space to accommodate these functional groups in the active site of PAK1. These three complexes were tested against PAK1 at a concentration of 100 nM in the presence of 1 μM ATP. It was found that PAK1 showed 97%

remaining activity with complex **FL224** (Figure 2.13). Thus, it turned out that the *para*-position of aniline might be already too close to the backbone of PAK1 to accommodate any modifications.

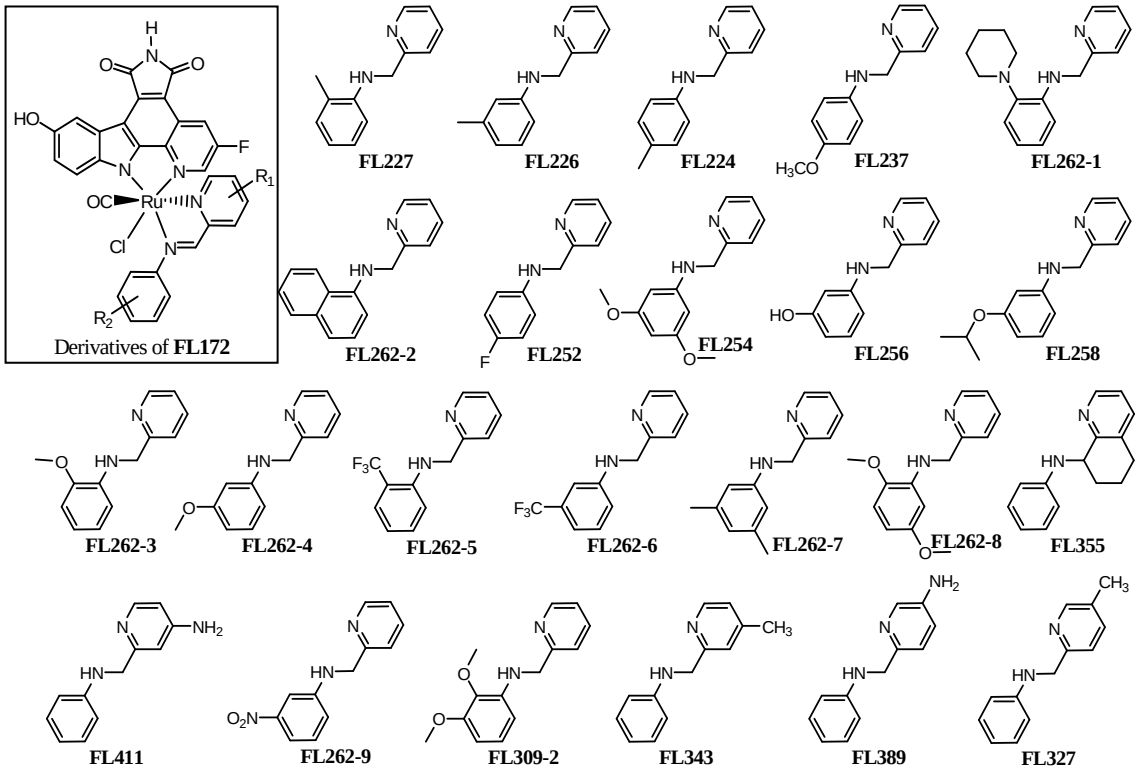

Figure 2.12. The derivatives of **FL172** with series of phenylaminopyridine ligands. The secondary amine in the ligands was oxidized to imine during the synthesis of theruthenium complex. All the derivatives were synthesized as racemic mixtures.

The derivatives of **FL172** were synthesized in analogy to **FL172** first by reacting precursor **2.3** with CO gas, and then the corresponding bidentate ligands. Most of these complexes were purified by silica gel chromatography (see Experimental Section for details). The racemic derivatives were tested against PAK1 at a concentration of 100 nM in the presence of 1 μM ATP and the results are shown in Figure 2.13. The data displayed that **FL256** and **FL411** could be promising complexes out of 23 derivatives, which have a hydroxyl group on the *meta*-position of phenyl ring and an amino group on the *para*-position of pyridine, respectively. PAK1 showed 58% remaining activity with complexes **FL256** and **FL411** compared to 62% with **FL172**.

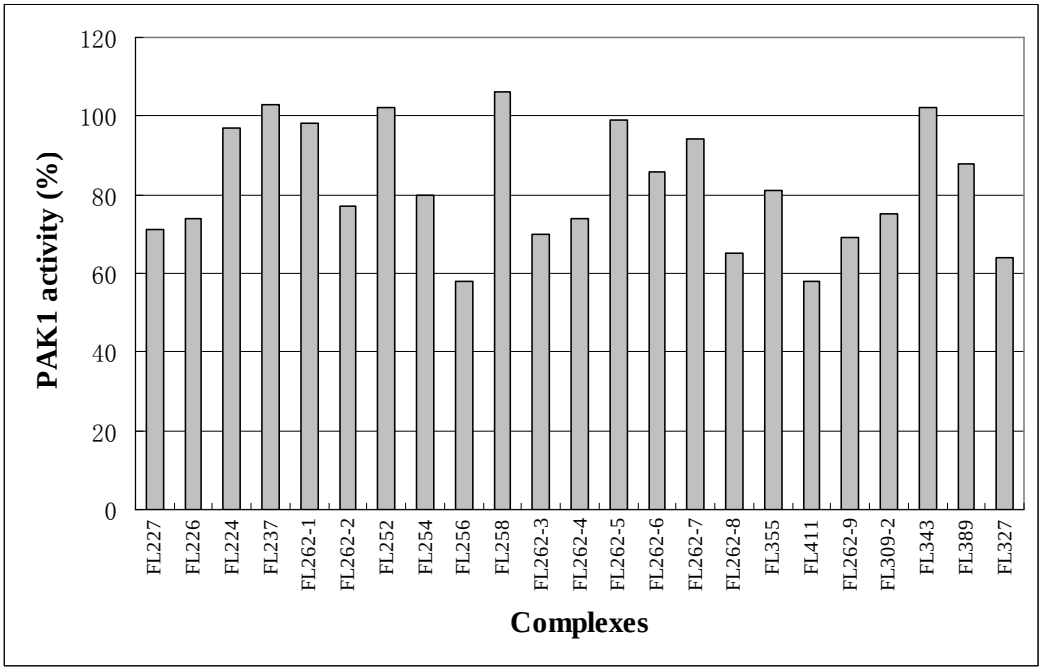

Figure 2.13. Inhibition of PAK1 by racemic derivatives of **FL172** at a single inhibitor concentration of 100 nM and in the presence of 1 μM ATP.

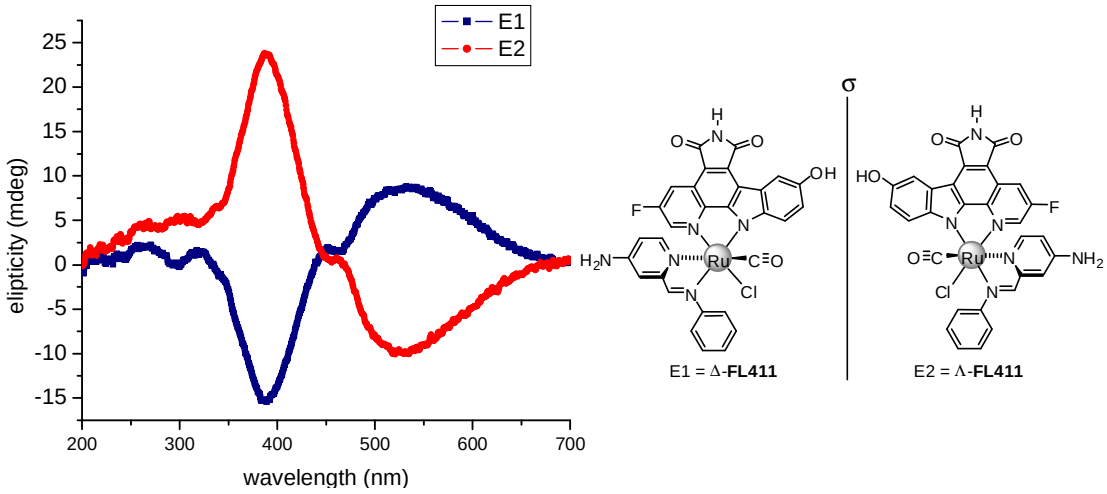

Figure 2.14. Circular dichroism spectra of the two enantiomers of **FL411**, measured at 1 μM of the two enantiomers in DMSO. The absolute configurations were assigned by correlation with the CD spectra of **FL172**.

Complexes **FL256** and **FL411** were later resolved into their individual enantiomers (Δ-**FL256**, Λ-**FL256**, Δ-**FL411**, and Λ-**FL411**, respectively) using a chiral HPLC column (see Experimental Section for details). The CD spectra of the two enantiomers of **FL411** with their corresponding structures are shown in Figure 2.14. The absolute

configurations were assigned by correlation with the CD spectra of **FL172**.[15]

Next, these complexes were measured against PAK1 and Pim1 at a concentration of 100 nM of each enantiomer in the presence of 1 μM ATP. The results are shown in Table 2.2 along with the result of **FL172**.

Table 2.2. Activities in % of PAK1 and Pim1 with individual enantiomers of **FL256**, **FL411** and **FL172** at a concentration of 100 nM and in the presence of 1 μM ATP.

	Δ-FL256	**Λ-FL256**	**Δ-FL411**	**Λ-FL411**	**Δ-FL172**	**Λ-FL172**
PAK1	95	41	102	52	76	50
Pim1	40	57	78	87	68	76

The data demonstrate that the Λ-enantiomers of **FL256** and **FL411** were more potent for PAK1 compared to Δ-enantiomers as **FL172**. The introduction of a hydroxyl group on the *meta*-position of the phenyl ring improved the binding affinity of **Λ-FL256** for PAK1 as well as Pim1 without influence on the selectivity. **Λ-FL411** displayed the same potency with **Λ-FL172** for PAK1. However, the remaining activity of Pim1 with **Λ-FL411** was slightly higher compared to **Λ-FL172** under the same conditions. Thus, **Λ-FL411** might be the potential PAK1 inhibitor as potent as **Λ-FL172**, but more selective over Pim1.

To further investigate the selectivity of **FL411**, individual enantiomers were measured against PAK1, GSK3β, and Pim1 with an ATP concentration of 1 μM, and the IC_{50} values are summarized in Table 2.3.

Table 2.3. IC_{50} values in nM of individual enantiomers of **FL411** against GSK3β, Pim1 and PAK1 in the presence of 1 μM ATP.

	GSK3β	**Pim1**	**PAK1**
Δ-FL411	1930	470	5200
Λ-FL411	14400	2840	110

The data demonstrate that the additional amino group on the *para*-position of pyridine in phenyliminomethylpyridine improved the potency of Λ-**FL411** for PAK1 slightly with an IC_{50} value of 110 nM, but the affinity of Λ-**FL411** for Pim1 (2.84 µM) and GSK3β (14.4 µM) was decreased significantly. The selectivity of Λ-**FL411** over Pim1 and GSK3β was 25-fold and 130-fold, respectively, which was further improved compared to Λ-**FL172** by the introduction of an amino group.

Chapter 2.8: Crystallographic data of FL327 and FL389 for the determination of the relative configurations of FL172 and FL411

Crystal structures of **FL327** and **FL389** shown in Figure 2.15 verified the relative configurations of the related complexes **FL172** and **FL411** indirectly.

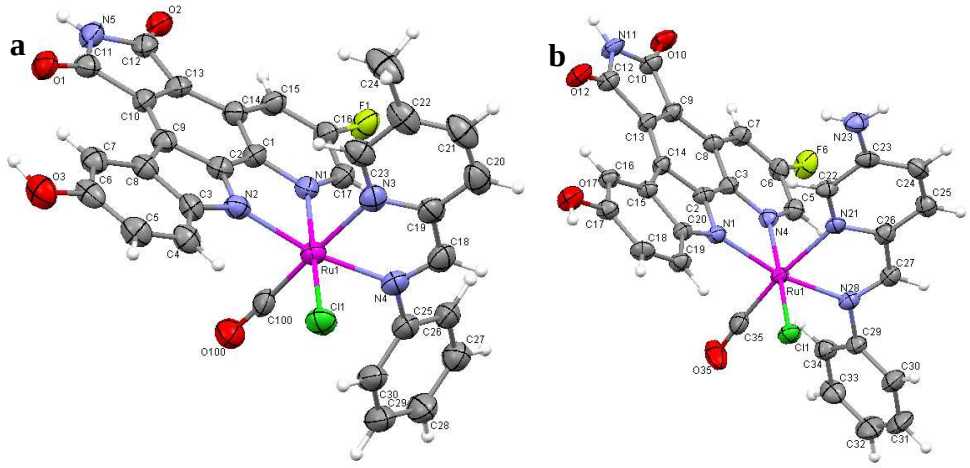

Figure 2.15. a) Crystal structure of complex **FL327**. b) Crystal structure of complex **FL389**. ORTEP drawing with 50% probability thermal ellipsoids.

FL327 and **FL389** were synthesized in analogy to **FL172** and **FL411** by reacting ruthenium precursor **2.3** first with CO gas, and then with the bidentate ligands 2-(phenylaminomethyl)-5-methylpyridine or 2-(phenylaminomethyl)-5-aminopyridine, respectively. X-ray quality crystals of the complexes **FL327** and **FL389** suitable for single crystal diffraction were obtained in acetone by slow evaporation. In the molecular structures, pyridine was on the axial position *trans* to the carbonyl ligand as in the cocrystal structure with PAK1 of Λ-**FL172**. The imino nitrogen in the bidentate ligand

was within the pyridocarbazole plane and *trans* to the indole nitrogen.

Chapter 2.9: The importance of the carbon monoxide ligand in PAK1 inhibitors FL172

The CO ligand on the axial position was beneficial for the potency against Pim1.[5] To investigate the possibility of using other monodentate ligands in the PAK1 inhibitor scaffold **FL172** to improve the selectivity over Pim1, complex **FL637** was synthesized in which the CO ligand was changed to PMe_3. The synthesis of **FL637** was performed in analogy to **FL172** through the reaction of ruthenium precursor **2.3** with PMe_3 instead of CO at 45 °C in DMF, then the addition of 2-(*N*-phenylaminomethyl)pyridine at 95 °C for 2 hours, affording the product in 26% yield (Scheme 2.6). Accordingly, the isomer shown was obtained as the major product in the reaction, along with small amounts of uncharacterizable other diastereomers. On the other hand, it proved the importance of carbonyl ligand in the control of diastereoselectivity in the reaction.

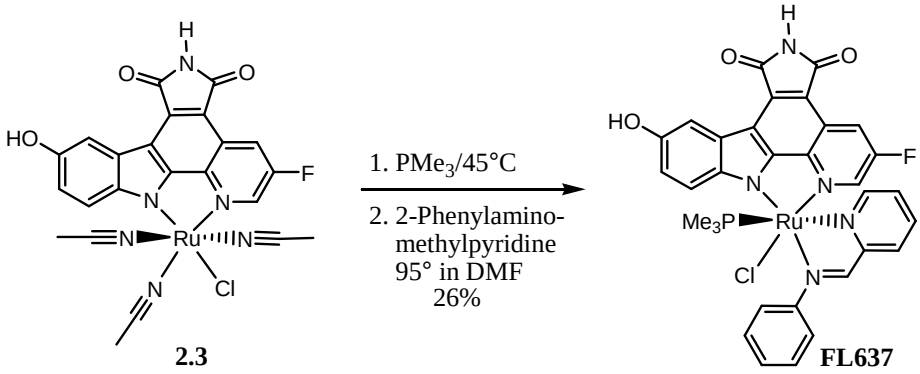

2.3 **FL637**

Scheme 2.6. Synthesis of racemic **FL637**.

FL637 was tested against PAK1 at concentrations of 3 µM, 1 µM, and 0.3 µM in the presence of 1µM ATP. The results combining **FL172** are shown in Table 2.4. The data demonstrate that by changing the CO ligand to PMe_3, the binding affinity for PAK1 was significantly decreased. In comparison to the CO ligand establishing interactions to the residues of the glycine-rich loop (Figure 2.10), the PMe_3 ligand might have a steric clash with the N-terminal domain in the PAK1 active site. With the PMe_3 ligand, the active site needs to open even more to accommodate all the changes.

Table 2.4. Activities in % of PAK1 with racemic **FL637** and **FL172**. Measured at concentrations of 3 µM, 1 µM and 0.3 µM of the inhibitors and in thepresence of 1 µM ATP.

	FL637	**FL172**
3 µM	66	24
1 µM	86	28
0.3 µM	95	51

Chapter 2.10: Replacing chloride of FL172 by other monodentate ligands

In the cocrystal structure of **FL172** with PAK1 (Figure 2.10), the chloride ligand points towards the solvent without any interactions with the backbone of the kinase active site. Thus, it was envisioned that using a bigger monodentate ligand to replace the chloride might be suitable to occupy the extended vacant chemical space. This might further improve the potency of the inhibitors for PAK1, as well as the selectivity over Pim1.

It turned out that the chloride in this octahedral scaffold was very unreactive after trying to replace the chloride under a series of different conditions without forming any new species except recovering the starting material **FL172**. The suitable reaction condition is shown in Scheme 2.7. Accordingly, the reaction was performed in DMSO at a concentration of 30 mM of racemic **FL172** in the presence of 12 equiv of AgOTf (silver trifluoromethanesulfonate), heating at 95 °C under an atmosphere of nitrogen for 7 hours. The mono cationic racemic product **FL866** was obtained by silica gel chromatography in 54% yield.

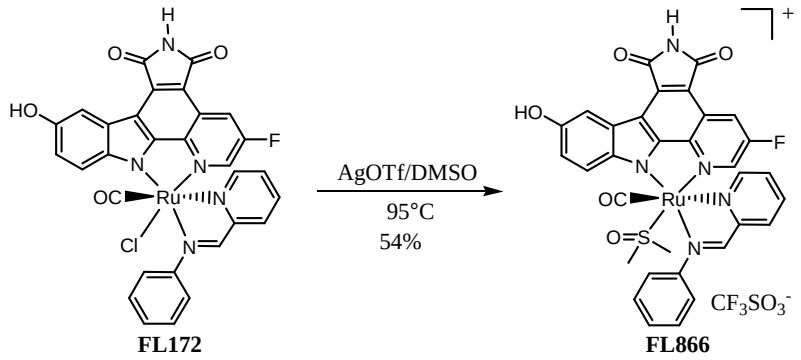

Scheme 2.7. Replacing chloride in racemic **FL172** with DMSO.

The acetonitrile derivative **FL862** was produced under the reaction conditions described in Scheme 2.7 by using acetonitrile instead of DMSO as solvent, but longer reaction time (overnight) was needed. **FL862** and **FL866** were further used as reaction intermediates to produce new derivatives with other monodentate ligands (Scheme 2.8).

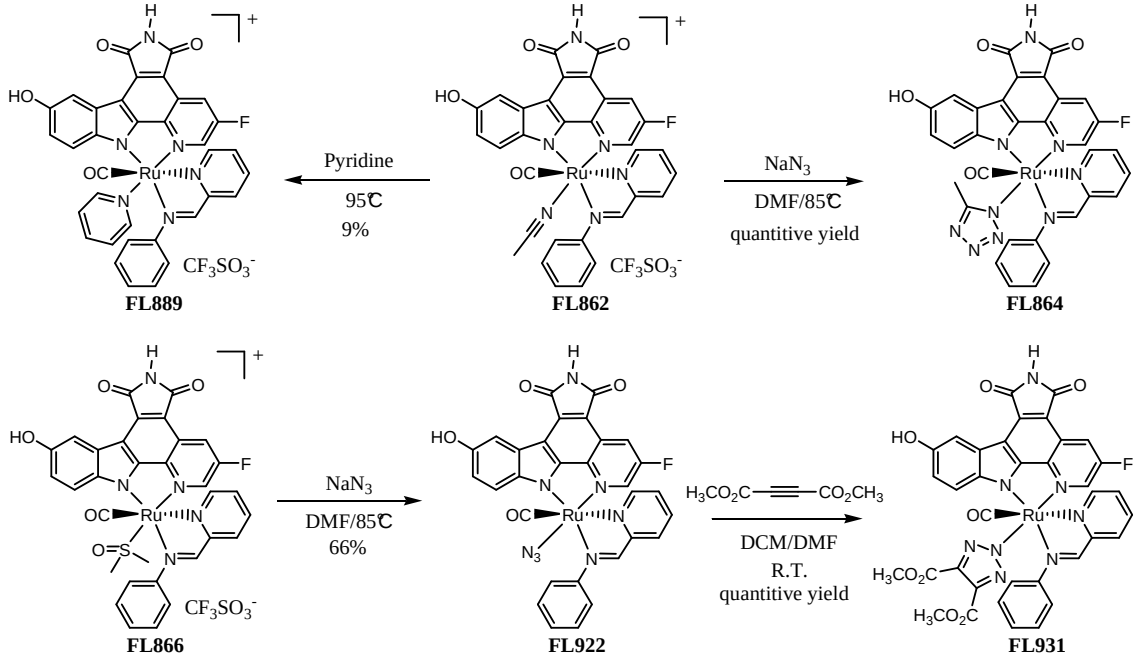

Scheme 2.8. Synthesis of derivatives of **FL172** with other monodentate ligands instead of chloride. All the derivatives were racemic.

FL862 and **FL866** could be further used as reaction intermediates to produce new complexes with other monodentate ligands (Scheme 2.8). Interestingly, the reaction of **FL862** with sodium azide in DMF at 85 °C for 1 hour did not furnish the azido complex, but rather yielded the cyclized tetrazole product **FL864** in a quantitive yield. The azido

complex **FL922** was obtained in 66% yield from the reaction of **FL866** with 5 equiv of sodium azide in DMF at 85 °C for 1 hour. **FL922** could be further used in 'Click' chemistry with alkynes. For example, stirring **FL922** with an excess of dimethyl acetylenedicarboxylate in a solvent mixture of DCM and DMF at room temperature for 1 hour afforded the cyclized triazole product **FL931** in a quantitive yield. Heating **FL862** in pyridine at 95 °C overnight afforded **FL889** in 9% yield, in which a pyridine replaced the acetonitrile ligand. These racemic derivatives were measured against PAK1 with an ATP concentration of 1 μM, and the IC_{50} values are listed in Table 2.5.

Table 2.5. IC_{50} values of the racmic derivatives of **FL172** with 1 μM ATP.

	FL864	**FL866**	**FL889**	**FL922**	**FL931**
PAK1	1.2 μM	1 μM	150 nM	300 nM	> 3 μM

The data demonstrate that with different monodentate ligands, the derivatives showed remarkable differences in affinity for PAK1. The potency of **FL889** was improved by a factor of 2 compared to **FL172** with an IC_{50} value of 150 nM. In contrast, replacing the chloride with a tetrazole, DMSO, or triazole in complexes **FL864**, **FL866**, and **FL931**, respectively, significantly decreased the potency. The IC_{50} values of these derivatives were 1.2 μM, 1 μM, and more than 3 μM, respectively. The azido complex **FL889** showed the same potency as **FL172**, probably because the azide doesn't form any contacts in the PAK1 active site. The affinity of tetrazole complex (**FL864**) compared to pyridine complex (**FL889**) was 8-fold difference, probably due to the electronic effects of the monodentate ligand. However, since the synthesis of **FL889** is very sluggish and only results in a 9% yield starting from **FL172**, it is not practical to use this scaffold to develop PAK1 inhibitors.

Chapter 2.11: An improved PAK1 inhibitor generated by modification of the pyridocarbazole

The pharmacophore pyridocarbazole ligand in the scaffold of **FL172** playes an important role in the inhibition of PAK1. The maleimide moiety and the indole hydroxyl group together account for four hydrogen bonds to the backbone of the hinge region, therefore these two moieties must be kept in this scaffold. Looking into the cocrystal structure of **FL172** with PAK1, the fluorine is close to the residue of Arg299, but does not have any interactions with the backbone. Furthermore, the pyridocarbazole can be easily modified by using differently substituted 2-bromopyridines in the cross coupling during synthesis of the pyridocarbazoles.[6]

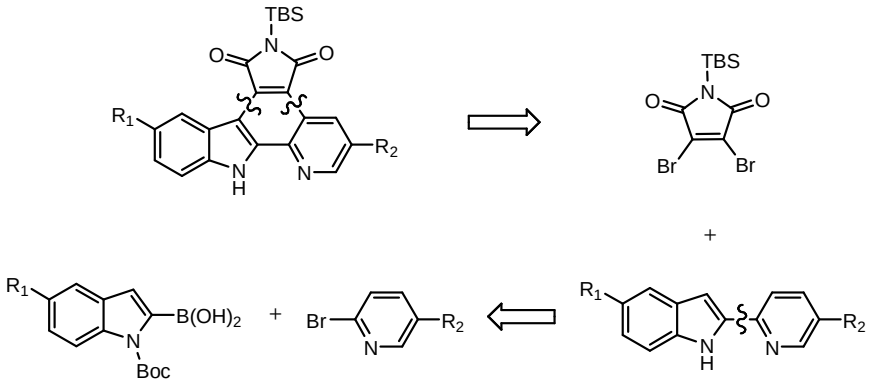

Scheme 2.9. Retrosynthetic analysis of pyridocarbazoles.

A total retrosynthetic analysis of pyridocarbazoles is shown in Scheme 2.9. As described in the literature,[6] pyridocarbazoles were synthesized from the reaction of pyridylindoles with TBS-protected dibromomaleimide by a sequence of substitution and photocyclization. Pyridylindoles were accessible by Suzuki cross-coupling of indole boronic acids with bromopyridines. Thus, it was envisioned that introducing certain functional groups on the pyridocarbazole might provide an opportunity to improve the potency and selectivity of PAK1 inhibitors.

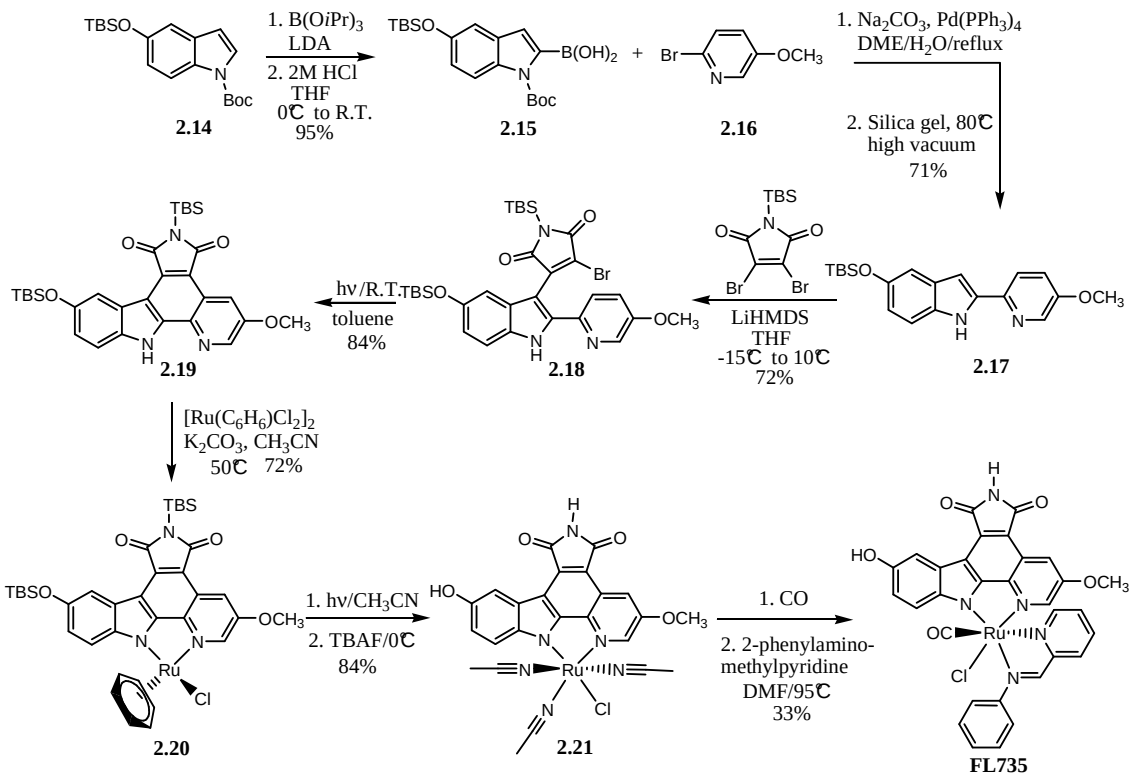

Scheme 2.10. Synthesis of complex **FL735**. All the ruthenium complexes are racemic. **2.21** is shown as the major diastereomer.

The synthesis of one such inhibitor, **FL735**, is shown in Scheme **2.10**. Accordingly, boronic acid **2.15** was prepared from Boc-protected indole **2.14** in 95% yield and used without further purification in the subsequent Suzuki cross-coupling reaction with bromopyridine **2.16**. A mixture of boronic acid **2.15** and bromopyridine **2.16** was refluxed in DME/H_2O (8:1) in the presence of 2.75 equiv of Na_2CO_3 and 0.075 equiv of $Pd(PPh_3)_4$ under nitrogen overnight affording pyridylindoles with the Boc-protection group partially removed. Unable to easily separate these two compounds, the purified mixture was adsorbed onto silica gel and heated under high vacuum to provide pyridylindole **2.17** in 71% yield over two steps. Pyridylindole **2.17** was treated with 3 equiv of LiHMDS at -15 °C in anhydrous THF for 1 hour, quenched with 1.05 equiv of TBS-protected dibromomaleimide, and the mixture was stirred at 10 °C overnight to furnish the relatively unstable monobromide intermediate **2.18** in 72% yield. This was carried forward after purification via flush chromatography through a short bed of silica gel. Cyclization of the monobromide intermediate by an anaerobic photocyclization

using a medium pressure Hg lamp with a pyrex filter afforded the pyridocarbazole **2.19** in 84% yield. **FL735** was produced in analogy to **FL172** first by reacting pyridocarbazole **2.19** with $[(\eta^6\text{-benzene})RuCl_2]_2$ in the presence of potassium carbonate in acetonitrile, affording the racemic η^6-half-sandwich complex **2.20** in 72% yield. Ruthenium precursor **2.21** was produced by UV-photolysis of **2.20** in MeCN to replace the benzene ring, followed by TBS-deprotection using TBAF at 0 °C to yield a mixture of two diastereomers in 84% over two steps. Precursor **2.21** was used to synthesize complex **FL735** by stirring it with CO in DMF, followed by the addition of 2-(phenylaminomethyl)pyridine to afford the product in 33% yield.

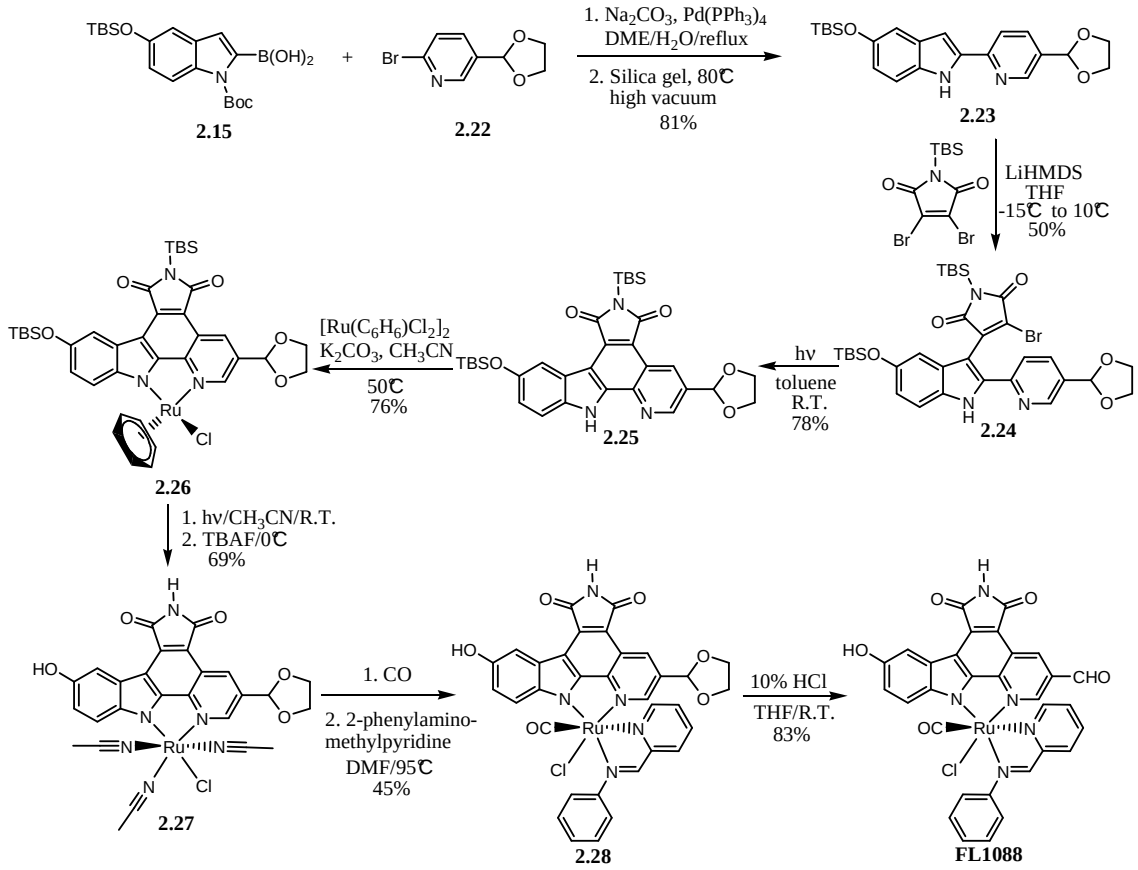

Scheme 2.11. Synthesis of complex **FL1088**. All the ruthenium complexes are racemic. Complex **2.27** is shown as the major diastereomer.

The synthesis of complex **FL1088** is shown in Scheme 2.11. Accordingly, pyridylindole **2.23** was produced in 81% yield by Suzuki cross-coupling of boronic acid **2.15** and bromopyridine **2.22** prepared according to the literature using toluene as

solvent instead of benzene.[11] Pyridocarbazole **2.25** was constructed in 39% yield over two steps by condensation of pyridylindole **2.23** with TBS-protected dibromomaleimide, and then photocyclization with a UV-lamp. The half-sandwich complex **2.26** was produced in good yield (76%), which could then be converted to the precursor **2.27** in 69% yield by photolysis and deprotection of TBS groups, yielding a mixture of two diastereomers. Precursor **2.27** was first reacted with CO, and then 2-(phenylaminomethyl)pyridine to afford complex **2.28** in moderate yield (45%). The deprotection was performed in THF with 10% HCl to provide the aldehyde-complex **FL1088** in 83% yield.

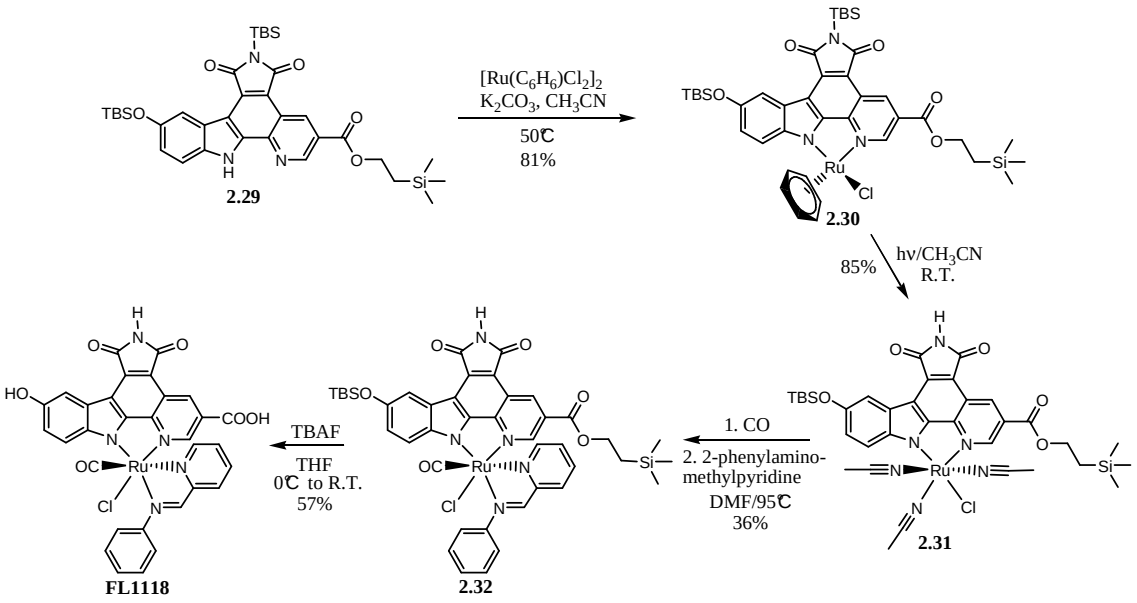

Scheme 2.12. Synthesis of complex **FL1118**. All the ruthenium complexes are racemic. Complex **2.31** is shown as the major diastereomer.

The synthesis of complex **FL1118** is shown in Scheme 2.12. Accordingly, pyridocarbazole **2.29**[12] was cyclometallated with $[(\eta^6\text{-benzene})RuCl_2]_2$ in the presence of potassium carbonate affording the racemic η^6-half-sandwich complex **2.30** in 81% yield. Precursor **2.31** was furnished in 85% yield by replacing the benzene ring with three acetonitrile groups through photolysis as a mixture of two diastereomers. This was then first reacted with CO, followed by the addition of 2-(phenylaminomethyl)pyridine to afford complex **2.32** in 36% yield in which TBS group on the imide was removed

during the reaction. Finally, deprotection of **2.32** was performed in THF with TBAF to provide complex **FL1088** in 57% yield.

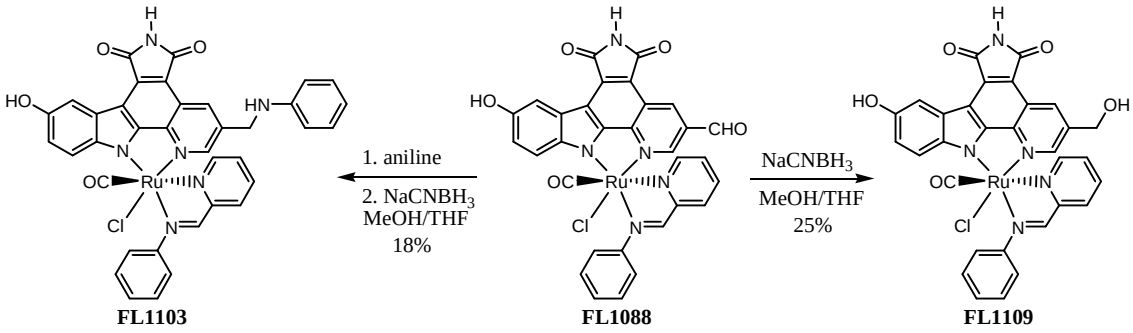

FL1103 **FL1088** **FL1109**

Scheme 2.13. Synthesis of racemic complexes **FL1103** and **FL1109**.

With complex **FL1088** in hand, the reactivity of the aldehyde group could be utilized to produce more derivatives. Reductive amination with aniline and sodium cyanoborohydride in MeOH/THF at 50 °C produced **FL1103** in 18% yield. Using sodium cyanoborohydride to reduce the aldehyde group afforded complex **FL1109** in 25% yield. These derivatives described above were tested against PAK1 in the presence of 1 μM ATP and the IC_{50} values are listed in Table 2.6.

Table 2.6. IC_{50} values of the racemic derivatives of **FL172** with modified pyridocarbazole in the presence of 1 μM ATP.

	FL735	**FL1088**	**FL1103**	**FL1109**	**FL1118**
PAK1	145 nM	93 nM	> 3 μM	2 μM	560 nM

The data demonstrate that the affinity of **FL1103**, **FL1109**, and **FL1118** for PAK1 was decreased when compared to **FL172**. Additionally, the potency of **FL735** (145 nM) and **FL1088** (93 nM) for PAK1 was improved by factors of 2 and 3 compared to **FL172**, respectively. **FL1088** was 3-fold more potent than **FL172**, perhaps due to the reactivity of the aldehyde group which could react with certain residue in the PAK1 active site. Overall, the pyridocarbazole in **FL735** with a hydroxyl group on the 5-position of indole and a methoxy group on the 3-position of pyridine could be the most promising pharmacophore ligand of the PAK1 inhibitors in the following study.

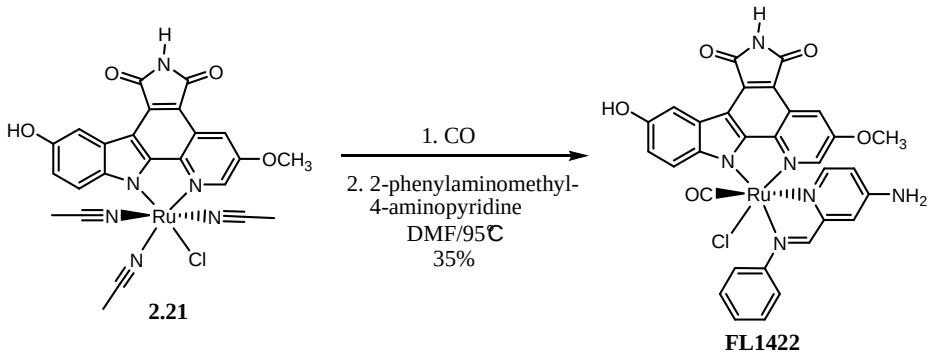

Scheme 2.14. Synthesis of racemic complex **FL1422**.

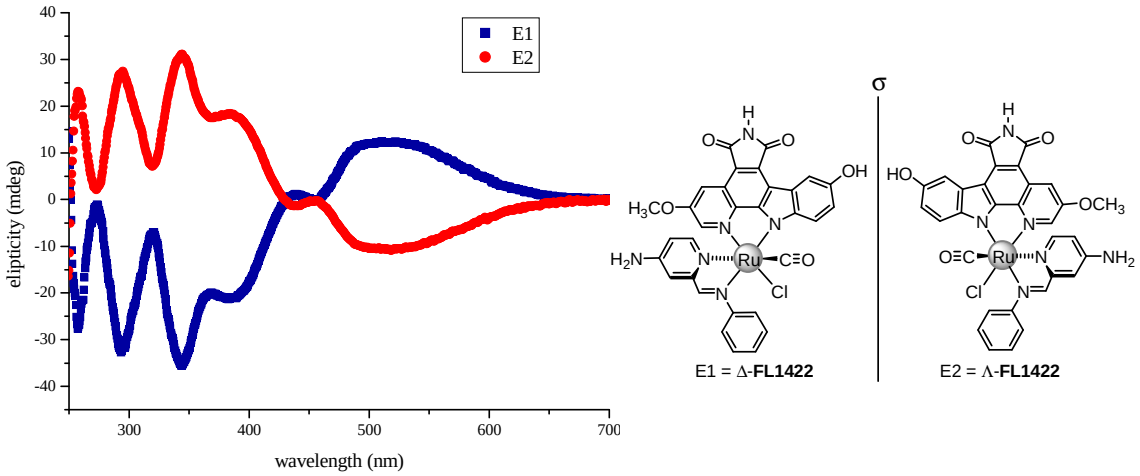

Figure 2.16. Circular dichroism spectra of the two enantiomers of **FL1422**, measured at 1 μM of two enantiomers in DMSO. The absolute configurations were assigned by correlation with the CD spectra of **FL172**.

The synthesis of complex **FL1422** is shown in Scheme 2.14. Complex **FL1422** was synthesized in analogy to **FL735** by reacting the ruthenium precursor **2.21** first with CO, and then with the bidentate ligand 2-(phenylaminomethyl)-4-aminopyridine to give the product in 35% yield. For the resolution of the racemic mixture of **FL1422**, the amino group at the 4-position of the pyridine was Boc-protected and removed after the separation of individual enantiomers Δ-**FL1422** and Λ-**FL1422** (see Experimental Section for details) using a chiral HPLC column. The CD spectra together with the structures of Δ- and Λ- enantiomers are shown in Figure 2.16 and the absolute configurations were assigned by correlation with the CD spectra of **FL172**.[15]

Table 2.7. IC_{50} values of Λ-**FL1422** against GSK3β, Pim1 and PAK1 in the presence of 1 μM ATP.

	GSK3β	**Pim1**	**PAK1**
Λ-**FL1422**	7 μM	2 μM	23 nM

The Λ-enantiomer of **FL1422** was measured against PAK1, Pim1, and GSK3β with an ATP concentration of 1 μM and the IC_{50} values are listed in Table 2.7. The data demonstrate that the potency of inhibitor Λ-**FL1422** (23 nM) for PAK1 was improved almost 5-fold compared to Λ-**FL411** (110 nM) by replacing the fluorine on the pyridocarbazole for a methoxy group. The selectivity over GSK3β (300-fold) and Pim1 (87-fold) was also improved by factors of 2.3 and 3.3, respectively. A possible explanation for this improved selectivity could be that the methoxy group in Λ-**FL1422** forms interactions with the residue Arg299 as hydrogen bond acceptor in the PAK1 active site. In contrast, in the Pim1 active site, the methoxy group might be too close to the isopropyl group of Val126.[10] As a result, the selectivity of Λ-**FL1422** over Pim1 was significantly improved. Thus, it can be concluded that the bulky organoruthenium complex Λ-**FL1422** constitutes a promising scaffold for the generation of improved PAK1 inhibitors by functionalizing the associated ligands in a combinatorial and structural-based fashion.

Chapter 2.12: Discussion and conclusion

PAK1 is implicated in tumorigenesis and metastasis, thus pharmacological inhibitors of PAK1 are promising candidates for cancer therapy.[7,8] However, to the best of our knowledge, there are no selective organic inhibitors with IC_{50} values in the nanomolar range known for PAK1 or other group-I PAK kinases.[4,7,9] In this chapter a strategy for the design of selective organometallic inhibitors for the open and thus difficult to target ATP-binding site of the protein kinase PAK1 using rigid and bulky octahedral ruthenium complexes as structural scaffolds was applied successfully. The octahedral ruthenium complex Λ-**FL1422** was developed as a potent inhibitor for PAK1 with an IC_{50} value of 23 nM in the presence of 1 µM ATP. This inhibitor is very selective over GSK3β (300-fold), Pim1 (87-fold), and other kinases. Octahedral ruthenium complexes with the ability to construct globular, rigid structures with defined shapes in a straightforward fashion provide opportunities for the generation of inhibitors with unprecedented target selectivities.

2-(*N*-phenylaminomethyl)pyridine was discovered as the most promising bidentate ligand in the scaffold of PAK1 inhibitors based on a screening of different bidentate ligands. This scaffold displayed high affinity for PAK1. Interestingly, the synthesis of this scaffold was quite diastereoselective, which made the screening relatively simple using this ligand. However, the mechanism of the diastereoselectivity needs to be further investigated.

A cocrystal structure of Λ-**FL172** bound to PAK1 revealed the molecular details of the binding of this octahedral scaffold to PAK1. The maleimide moiety and the indole -OH group together mediate four canonical hydrogen bonds to the backbone of the hinge region. In addition, the monodentate carbonyl ligand establishes interactions with the residues of the glycine-rich loop. The bulky bidentate iminopyridine ligand stretches the entire distance from the N-terminal glycine-rich loop to C-terminal domain which can be well accommodated by the active site of PAK1.

Λ-**FL172** showed an IC_{50} value of 130 nM for PAK1 in the presence of 1 µM ATP

but only 3-fold selectivity over Pim1. Comparatively, by the modification with an amino group on the *para*-position of pyridine in the phenylaminomethylpyridine bidentate ligand (Λ-**FL411**), the selectivity over Pim1 was improved by a factor of 7 compared to Λ-**FL172**. Furthermore, by the introduction of a methoxy group on the pyridocarbazole ligand instead of the fluorine, the affinity of Λ-**FL1422** for PAK1 was improved by a factor of 5.6 with an IC_{50} value of 23 nM in the presence of 1 μM ATP compared to Λ-**FL172**. At the same time, the selectivity over Pim1 was improved by a factor of 25 to 87-fold overall compared to Λ-**FL172**.

Compared to the published ATP-competitive PAK1 inhibitors with small organic molecules such as CEP-1347[9] and OSU-03012[13] which have been developed with IC_{50} values in the single digit micromolar range, Λ-**FL1422** displays better affinity for PAK1 and impressive selectivity over the other protein kinases. Recently, the organic compound 2,2'-dihydroxy-1,10-dinaphthyldisulfide was discovered as a PAK1 inhibitor binding at an allosteric site.[14] This allosteric inhibitor displays poor potency, albeit with a favorable selectivity profile. However, the lability of the disulfide bond under physiological conditions significantly limits its effectiveness in cellular systems. Overall, the bulky organoruthenium complex Λ-**FL1422** constitutes a promising scaffold for the generation of improved PAK1 inhibitors by functionalizing the associated ligands in a combinatorial and structural-based fashion.

Chapter 2.13: References

(1) Cohen, M. S.; Zhang, C.; Shokat, K. M.; Taunton, J. *Science* **2005**, *308*, 1318-1321.

(2) Manning, G.; Whyte, D. B.; Martinez, R.; Hunter, T.; Sudarsanam, S. *Science* **2002**, *298*, 1912-1934.

(3) Lei, M.; Lu, W. G.; Meng, W. Y.; Parrini, M. C.; Eck, M. J.; Mayer, B. J.; Harrison, S. C. *Cell* **2000**, *102*, 387-397.

(4) Maksimoska, J.; Feng, L.; Harms, K.; Yi, C.; Kissil, J.; Marmorstein, R.; Meggers, E. *J. Am. Chem. Soc.* **2008**, *130*, 15764-15765.

(5) Bregman, H.; Carroll, P. J.; Meggers, E. *J. Am. Chem. Soc.* **2006**, *128*, 877-884.

(6) Pagano, N.; Maksimoska, J.; Bregman, H.; Williams, D. S.; Richard D.; Webster, R. D.; Meggers, E. *Org. Biomol. Chem.* **2007**, *5*, 1218-1227.

(7) Kumar, R.; Gururaj, A. E.; Barnes, C. J. *Nature Rev. Cancer* **2006**, *6*, 459-471.

(8) Bright, M. D.; Garner, A. P.; Ridley, A. J. *Cellular Signalling* **2009**, *21*, 1738-1747.

(9) Nheu, T. V.; Hirokawa, Y.; Tamaki, K.; Florin, L.; Schmitz, M. L. *The Cancer Journal* **2002**, *8*, 328-336.

(10) Debreczeni, J. E.; Bullock, A. N.; Atilla, G. E.; Williams, D. S.; Bregman, H.; Knapp, S.; Meggers, E. *Angew. Chem., Int. Ed.* **2006**, *45*, 1580-1585.

(11) Zoppellaro, G.; Ivanova, A.; Enkelmann, V.; Geies, A.; Baumgarten, M. *Polyhedron* **2003**, *22*, 2099-2110.

(12) Ph.D. thesis of Bregman, H. University of Pennsylvania **2007**.

(13) Porchia, L. M.; Guerra, M.; Wang, Y. C.; Shinohara, M. *Mol. Pharmacol.* **2007**, *72*, 1124-1131.

(14) Bokoch, G. M. *Chem. Biol.* **2008**, *15*, 305-306.

(15) Lo, L. C.; Berova, N.; Nakanishi, K.; Schlingmann, G.; Carter, G. T.; Borders, D. B. *J. Am. Chem. Soc.* **1992**, *114*, 7371-7374.

Chapter 3: Ruthenium Scaffold with Cyclic Tridentate Ligands as Potential Protein Kinase Inhibitors

Transition metal complexes with thioether ligands are of much interest due to their similarities to biological systems and their kinetic and thermodynamic properties. Crown thioether ligands are effective π-acid ligands for metal ions and also tend to stabilize first-, second-, and third-row metals in low oxidation states.[11]

One essential feature of the crown thioether is the exodentate position of the sulfur donor atoms in most compounds (the sulfur atoms are directed out of the cavity). One exception is the 1,4,7-trithiacyclononane in which the sulfur atoms are preorganized in an endodentate fashion (the sulfur atoms are directed toward the center of the ring) prone to metal complexation due to the sterical constrain in the 9-member ring.[12] Therefore, this preorganization makes the complexation of 1,4,7-trithiacyclononane more stable in contrast to other flexible crown thioethers.[11,13]

In this chapter, the development of potent and selective inhibitors for MLCK, DAPK1 and Pim1 kinases is discussed, respectively. All the developed octahedral ruthenium inhibitors contain the cyclic tridentate ligand: 1,4,7-trithiacyclononane, and the selectivity of these inhibitors is achieved by using different pyridocarbazoles and monodentate ligands in the complex.

Chapter 3.1: Development of MLCK inhibitors

Chapter 3.1.1: Scaffold synthesis of MLCK inhibitors

The scaffold of MLCK inhibitors was initially identified by screening racemic ruthenium complex **FL475** (Figure 3.1) against a panel of 232 human wild-type protein kinases (Millipore KinaseProfiler and see appendix for details). The screening result demonstrated that there was only 2% remaining activity for MLCK at a concentration of 100 nM of **FL475** in the presence of 10 μM ATP. The IC_{50} value against MLCK was

further determined which was only 13 nM in the presence of 100 μM ATP. Thus, complex **FL475** could be the potential lead structure for the development of MLCK inhibitors, which includes the pharmacophore ligand pyridocarbazole, tridentate ligand 1,4,7-trithiacyclononane, and anionic monodentate ligand three moieties around the ruthenium center.

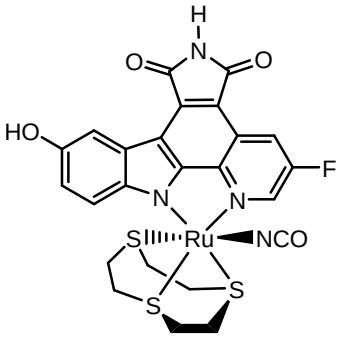

FL475

Figure 3.1. Structure of racemic ruthenium complex **FL475**.

The scaffold can be constructed as shown in Scheme 3.1. The synthsis of pyridocarbazoles was already described in chapter 2. The ruthenium fragment was introduced by reacting TBS-protected pyridocarbazoles **3** with ruthenium precursor **2**[5] in the presence of potassium carbonate in DMF under microwave irradiation without need to exclude water and air, followed by using an anionic monodentate ligand to replace the one remaining acetonitrile group in the same pot. The TBS protection group on the imide was removed simultaneously during the reaction due to the basic condition under heating.

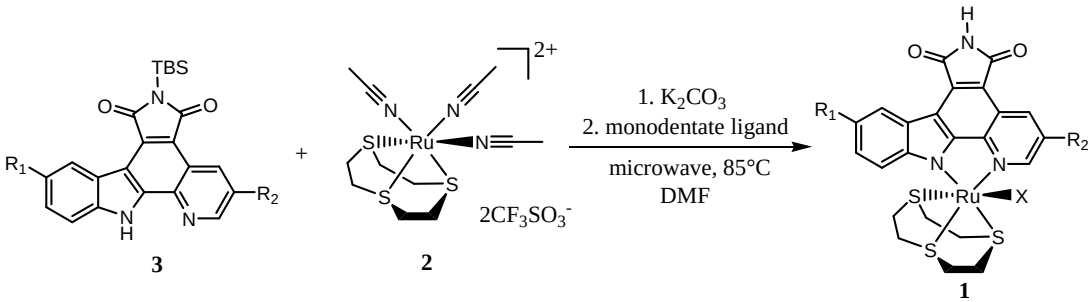

Scheme 3.1. Synthesis of racemic ruthenium complexes using microwave irradiation. R_1, R_2: different substituents on pyridocarbazole, X: different monodentate ligands.

Chapter 3.1.2: Identification of suitable monodentate ligands in the scaffold

Three different moieties can be investigated in this scaffold: pyridocarbazole, 1,4,7-trithiacyclononane ring, and monodentate ligand. To identify the most suitable monodentate ligand in the scaffold, a library of ruthenium complexes with different monodentate ligands was synthesized (Scheme 3.2).

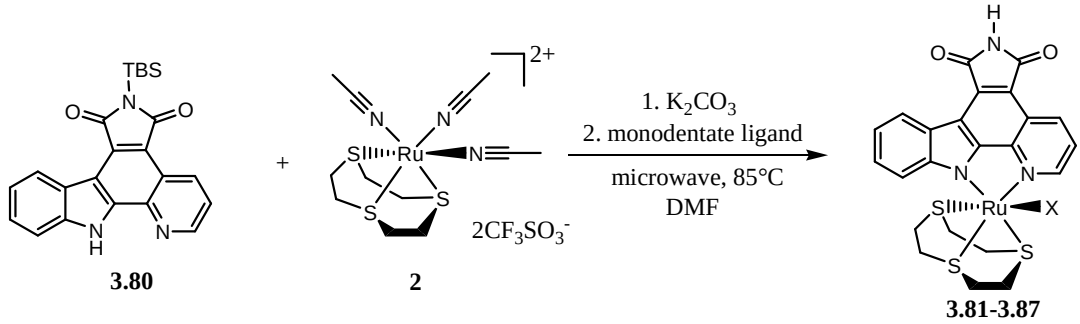

Scheme 3.2. Synthesis of a library of ruthenium complexes with different monodentate ligands. **3.81**: X=N_3 yield: 48%, **3.82**: X=NO_2 yield: 65%, **3.83**: X=NCSe yield: 33%, **3.84**: X=NCO yield: 46%, **3.85**: X=CN yield: 42%, **3.86**: X=NCS yield: 52%, **3.87**: X=CO yield: 52%. All the complexes were synthesized as racemic mixtures. **3.87** was monocationic complex with PF_6^- as counterion.

Here the plain pyridocarbazole and 1,4,7-trithiacyclononane scaffold was used as starting point. Anionic ligands such as -N_3, -NO_2, -NCSe, -NCO, -CN, -NCS, and -CO were tried in this library. All the complexes were synthesized under microwave irradiation and purified by silica gel chromatography. -NCS and -NCSe usually behave as ambidentate ligand.[20,23] In **3.86** the Ru-N bonding linkage isomer was observed (see subchapter 3.2). Complex **3.83** was assigned as Ru-N bonding isomer according to the IR bands of the -NCSe group. In the IR spectrum of **3.83**, the absorption frequency of the -NCSe group is at 2101 cm^{-1} as two bands which is consistent with the literature[33] and the Lange's handbook of chemistry (15^{th} Edition, Spectroscopy, Table 7.22) in which the absorption frequency of -NCSe is in the range of 2000-2200 cm^{-1} as two bands. The racemic complexes were tested against protein kinases MLCK, Pim1, and GSK3α with 100 μM ATP and the IC_{50} values are shown in Table 3.1.

Table 3.1. IC_{50} values of the racemic ruthenium complexes for MLCK, Pim1 and GSK3α in the presence of 100 μM ATP.

IC_{50}	**3.81**	**3.82**	**3.83**	**3.84**	**3.85**	**3.86**	**3.87**
MLCK	57 nM	120 nM	15 nM	101 nM	330 nM	74 nM	3 nM
Pim1	58 nM	33 nM	6.4 nM	93 nM	90 nM	50 nM	450 pM
GSK3α	7.4 μM	> 30 μM	1.8 μM	3.8 μM	> 30 μM	3.2 μM	14 nM

The data demonstrate that the monodentate ligand causes notable influence on the binding affinity of the inhibitors in the kinase active site. The most potent inhibitor for MLCK was complex **3.87** with an IC_{50} value of 3 nM, but it also displayed high affinity for Pim1 and GSK3α,[7] which meant **3.87** was not ideal to be used as the lead structure to develop selective MLCK inhibitors. The binding affinity for MLCK was decreased by a factor of 22 when -NCSe (**3.83**) was changed to -CN (**3.85**) in the complex. Complex **3.83** showed high binding affinity against MLCK of which the IC_{50} value was 15 nM. However, it also had strong effect on Pim1 and the IC_{50} value was only 6 nM. **3.81** and **3.86** also showed relatively high potency for MLCK and the IC_{50} values were 57 nM and 74 nM, respectively. Especially, the IC_{50} value of **3.81** for Pim1 was 58 nM which showed better selectivity than **3.86**. The selectivity for MLCK over Pim1 was improved slightly by switching -NCSe to $-N_3$, which could be further improved by the modification of the pyridocarbazole moiety. Overall, this scaffold showed very low affinity with kinase GSK3α except **3.87**. With the ambidentate ligand -NCS or -NCSe in the complex, the linkage isomerizes under certain conditions which makes the synthesis and purification of the complexes more complicated. Correspondingly, $-N_3$ has only one mode of binding to the ruthenium center. Thus, considering the potency, selectivity, and stability of the complex, azide can be the potential anionic monodentate ligand in the development of selective inhibitors for MLCK.

Chapter 3.1.3: Modification of the pyridocarbazole moiety

Since our lab colleague Nicholas Pagano developed a very successful synthetic route to pyridocarbazoles,[6] functionalized pyridocarbazoles can be easily constructed by using substituted indoles and pyridines. Thus it could be a very powerful tool to modify the MLCK inhibitors to improve the potency and selectivity by using pyridocarbazoles with different substituents. The synthesis of a series of pyridocarbazoles with different substituents and ruthenium complexes with respective pyridocarbazole is summarized below.

Table 3.2. Pyridylindole synthesis by Suzuki coupling.

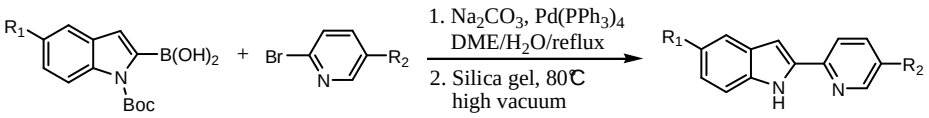

Indole (R_1)		Pyridine (R_2)	Pyridylindole	Yield (%)
3.34	OCH_3	H	**3.54**	87
3.14	SCH_3	F	**3.15**	87
3.14	SCH_3	H	**3.19**	76
3.14	SCH_3	$N(Allyl)_2$	**3.24**	73
3.34	OCH_3	F	**3.35**	84
3.34	OCH_3	OCH_3	**3.39**	80
3.3	O*i*Pr	F	**3.8**	97
3.3	O*i*Pr	H	**3.4**	87

The synthesis of pyridylindoles by Suzuki cross-coupling is shown above (Table 3.2). Derivatives of the indole boronic acids were prepared in two synthetic steps from the appropriate commercially available or published indoles by Boc-protection, followed by introducing boronic acid.[34] These boronic acids were yielded quantitively and used in

the subsequent Suzuki cross-coupling reaction with bromopyridines as crude. The mixture of boronic acids and bromopyridines was refluxed in DME/H_2O (8:1) in the presence of 2.75 equiv of Na_2CO_3 and 0.075 equiv of $Pd(PPh_3)_4$ under nitrogen overnight affording pyridylindoles with the Boc-protection group partially removed. Unable to easily separate the two compounds in these cases, the purified mixture in each case was adsorbed onto silica gel and heated at 80 °C under high vacuum to provide pyridylindoles in the range of 76-97% yield over two steps which were used to produce corresponding pyridocarbazoles.

Table 3.3. Synthesis of pyridocarbazoles from pyridylindoles.

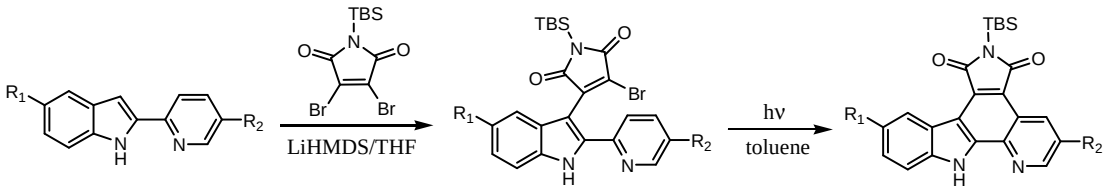

Pyridylindole (R_1, R_2)		Intermediate	Pyridocarbazole	Yield (%)
3.54	OCH_3, H	**3.55**	**3.56**	56
3.15	SCH_3, F	**3.16**	**3.17**	18
3.19	SCH_3, H	**3.20**	**3.21**	42
3.24	SCH_3, $N(Allyl)_2$	**3.25**	**3.26**	39[a]
3.35	OCH_3, F	**3.36**	**3.37**	45
3.39	OCH_3, OCH_3	**3.40**	**3.41**	51
3.8	O*i*Pr, F	**3.9**	**3.10**	57
3.4	O*i*Pr, H	**3.5**	**3.6**	58

a) monoallyl-protected product obtained in 11% yield during photocyclization.

The synthesis of pyridocarbazoles from pyridylindoles is shown above (Table 3.3). Accordingly, pyridylindoles were treated carefully with 3 equiv of LiHMDS at -15 °C

in anhydrous THF for 1 hour and quenched with 1.05 equiv of TBS-protected dibromomaleimide, after stirring the mixture at 10 °C overnight, furnishing the relatively unstable monobromide intermediates which were carried forward after purified through a short flash silica gel chromatography. Cyclization of the monobromide intermediates by an anaerobic photocyclization with a medium pressure Hg lamp with a pyrex filter afforded the corresponding pyridocarbazoles in the range of 18-58% yield over two steps. The allyl-deprotection of **3.26** was performed in DCM in the presence of 6 equiv of 1,3-dimethylbarbituric acid and 0.2 equiv of $Pd(PPh_3)_4$ under reflux for 7 hours to provide deprotected pyridocarbazole. The key step for the synthesis of pyridocarbazoles is the condensation of pyridylindoles with dibromomaleimide which significantly influences the synthetic yield. Electron-withdrawing groups on the pyridylindole decreases the yield of the reaction probably as a result of the decreased nucleophilicity of the joined heterocycles and the quality of LiHMDS also influences this reaction.

Table 3.4. Racemic ruthenium complexes synthesized with microwave irradiation.

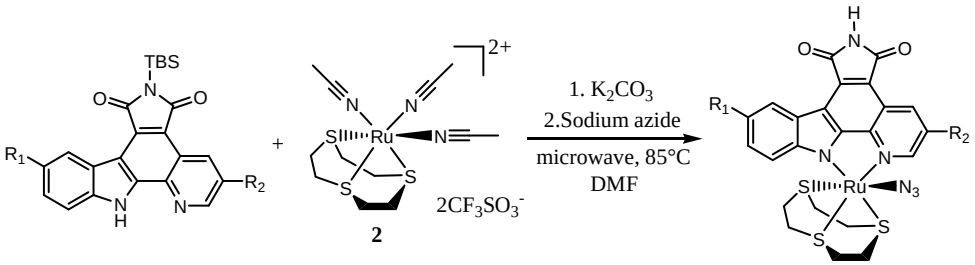

	R_1	R_2	Yield (%)
FL123	OH	F	42
FL1381	OCH_3	H	62
FL1288	SCH_3	F	45
FL1343	SCH_3	H	48
FL1358	SCH_3	NH_2	49

FL1055	OCH_3	F	68
FL1229	OCH_3	OCH_3	57
FL1335	O*i*Pr	F	48
FL1359	O*i*Pr	H	53

With pyridocarbazoles and ruthenium precursor **2** in hand, the synthesis of metal complexes was quite convenient which was conducted as described in chapter 3.1.1. The reactions were mostly clean and the products were easy to be purified by silica gel chromatography. The yield of these reactions in this library was in the range of 42-68% (Table 3.4).

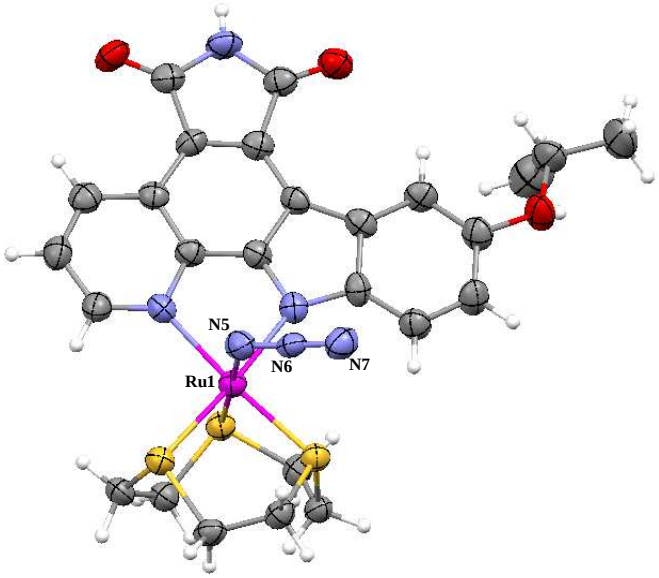

Figure 3.2. Crystal structure of complex **FL1359**. ORTEP drawing with 50% probability thermal ellipsoids.

X-ray quality crystals of the complex **FL1359** suitable for single crystal diffraction were obtained from acetone by slow evaporation. The molecular structure of **FL1359** is shown in Figure 3.2 which confirmed the relative configuration of the ruthenium scaffold. Because of the cyclic nature of the tridentate ligand and the sp^3 hybridization at the coordinating sulfur atoms, 1,4,7-trithiacyclononane has to occupy both coordination sites within the plane of the pyridocarbazole ligand, thus leaving a position

perpendicular to the pyridocarbazole plane for the coordination of the azide ligand. The bond angle of Ru1-N5-N6 is 119.4˚ due to the sp^2 hybridization of the N5 and the bond of N5-N6-N7 is almost linear (176.7˚).

Next, the library of these ruthenium complexes was measured against protein kinases MLCK and Pim1 in the presence of 100 μM ATP and the IC_{50} values are displayed in Table 3.5. The first derivative inhibitor made for MLCK was complex **FL123**. Introduction of a hydroxyl group on the 5-position of the indole and a fluorine on the 3-position of the pyridine improved the binding affinity for MLCK by a factor of 3 compared to **3.81** with an IC_{50} value of 19 nM. As expected, **FL123** also showed high potency against Pim1 and the IC_{50} value was 18 nM. Same with **3.81**, there was no selectivity for MLCK over Pim1. The hydroxyl group on the indole moiety can possibly form hydrogen bonds in the Pim1 active site.[21,22]

Table 3.5. IC_{50} values in nM of racemic complexes against MLCK and Pim1 in the presence of 100 μM ATP.

	FL123	**FL1381**	**FL1055**	**FL1288**	**FL1343**	**FL1358**	**FL1229**	**FL1359**	**FL1335**
MLCK	19	15	10	84	18	22	40	27	21
Pim1	18	52	44	982	154	609	161	847	520

To improve the selectivity of the inhibitors for MLCK over Pim1, hydrophobic group was introduced instead of the hydroxyl group on the 5-position of indole and modifications on the 3-position of pyridine were tested. The data demonstrate that a profound influence on the potency and selectivity of the ruthenium complexes is achieved by the modification on the 5-position of indole and/or 3-position of pyridine. The introduction of a big hydrophobic group on the 5-position of indole decreases the binding affinity for Pim1 dramatically. Replacing the hydroxyl group of **FL123** by a methoxy group (**FL1055**) reduced the binding affinity for Pim1 by a factor of 2.4 compared to **FL123**. Modification with a methoxy group both on the 5-position of indole and 3-position of pyridine (**FL1229**) decreased the potency of the inhibitor for

Pim1, but the selectivity for MLCK (40 nM) over Pim1 (161 nM) was only 4-fold. However, using a methylthio group (**FL1288**) or an isopropyloxy group (**FL1335**) instead of the hydroxyl group, the binding affinity for Pim1 was reduced by factors of 54 and 29 compared to **FL123**, respectively. But the binding affinity of **FL1288** for MLCK (84 nM) was decreased by a factor of 4.4 when compared to **FL123**. The data showed the modification of a fluorine on the 3-position of pyridine also influenced the potency and selectivity of the inhibitors, but there was no consistent effect found in this screening data, which probably depends on the binding mode of the inhibitors in the kinase active site. Although complex **FL1358** displayed high affinity for MLCK (22 nM) and selectivity over Pim1 (27-fold), the synthesis of the pyridocarbazole pharmacophore ligand was more complicated than other inhibitors. Considering the factors of potency, selectivity and simplicity of the inhibitors, complex **FL1359** was supposed to be the most promising lead structure for the development of MLCK inhibitors. With an IC_{50} value of 27 nM for MLCK, **FL1359** displayed a significant selectivity over Pim1 (31-fold).

Chapter 3.1.4: Modification of the tridentate ligand moiety

In order to verify the obtained ruthenium complexes were indeed promising lead structures for the design of organometallic complexes as inhibitors for the protein kinases different from Pim1, complex **FL1359** was used as a starting point for the proof-of-principle design of the more potent and selective inhibitors for MLCK. It was envisioned that the modification on the 1,4,7-trithiacyclononane ring should influence the binding affinity for MLCK and Pim1. But due to the low reactivity of the 1,4,7-trithiacyclononane, there are not too many options for functionalizing this 9-member ring directly. Once the ligand turns unsymmetric, more diastereoisomers will be formed in the coordination reactions, which makes the reaction more complicated and the separation of these diastereoisomers more difficult. On the other hand, it will give more opportunities to design the potent and selective inhibitors for protein kinases, as long as the chemistry is under control.

The different tridentate ligands shown in Figure 3.3 were used to modify the MLCK inhibitors. Three diastereoisomers can be formed when using these tridentate ligands in the coordination chemistry.

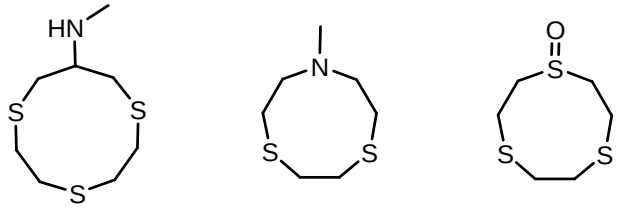

Figure 3.3. Tridentate ligands for modification of MLCK inhibitors.

As using ruthenium precursor **2** as the starting point to synthesize the metal complexes, ruthenium precursors were first made containing respective tridentate ligands. The synthesis of complex **FL1392** is shown in Scheme 3.3. Compound 1,4,7-trithiacyclodecan-9-one was used as starting point. After reductive amination with 1.2 equiv of methyl amine in the presence of 2 equiv of sodium borohydride as reductive reagent, the secondary amine in compound **3.62** was protected with Alloc group using 1.5 equiv of allyl chloroformate as reagent in the presence of 1 equiv of pyridine and catalytic amount of DMAP in dichloromethane in 76% yield. Ruthenium species **3.64** was provided from the reaction of compound **3.63** with $RuCl_2(dmso)_4$ by refluxing in chloroform for 5 hours. Followed by refluxing **3.64** in acetonitrile with 2 equiv of silver trifluoromethanesulfonate for 6 hours to furnish the ruthenium precursor **3.65** in 72% yield over two steps, which was reacted with pyridocarbazole **3.6** in DMF in the presence of 1.1 equiv of potassium carbonate under microwave irradiation, followed by using sodium azide to replace the one remaining acetonitrile group to afford the Alloc protected complex **FL1392**. Three diastereomers were formed in this reaction, but only the first isomer can be obtained purely by silica gel chromatography as the major product. The Alloc-deprotection of the complex was performed in dichloromethane with 8 equiv of N,N-dimethylbarbituric acid and $Pd(PPh_3)_4$ as catalyst at room temperature to afford the final racemic complex **FL1392** in 22% yield over two steps.

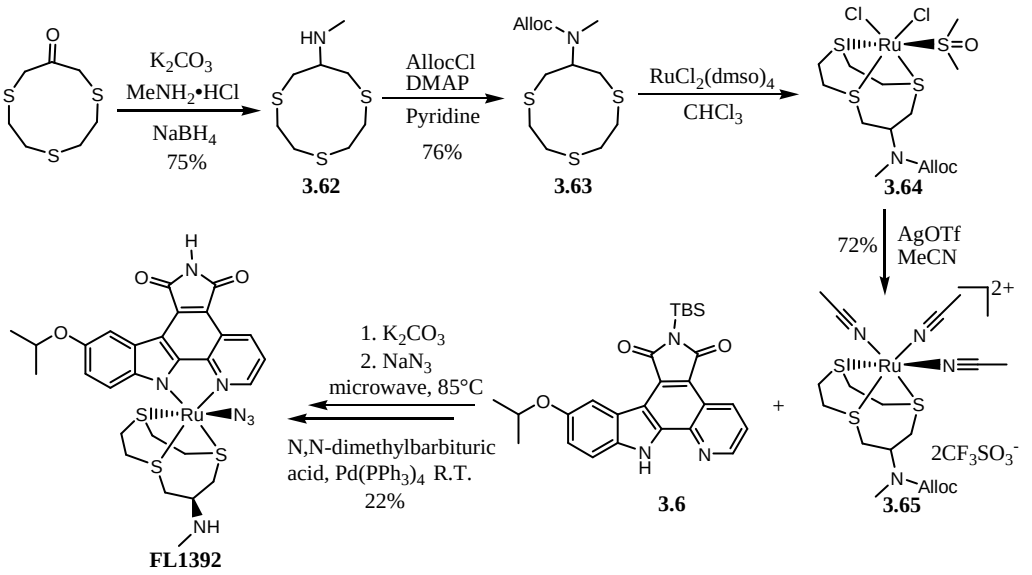

Scheme 3.3. Synthesis of racemic complexes **FL1392**.

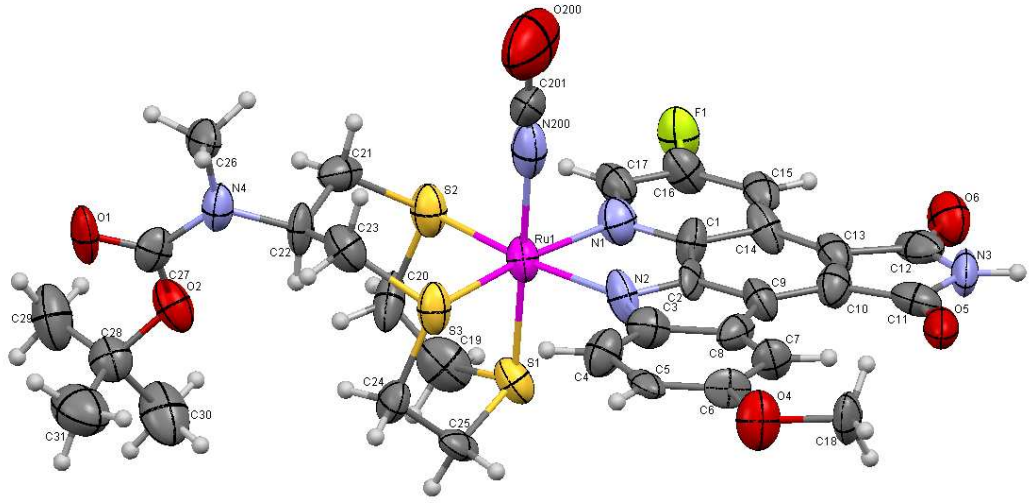

Figure 3.4. Crystal structure of complex **FL626-1**. ORTEP drawing with 50% probability thermal ellipsoids.

The relative configuration of **FL1392** was proven indirectly by the crystal structure of **FL626-1** (Figure 3.4). **FL626-1** was synthesized in analogy to **FL1392** by reacting **3.37** with precursor **3.74** in which Boc group was on the secondary amine under microwave irradiation, and then sodium cyanate was used to replace the remaining acetonitrile (Scheme 3.4). The crystals of **FL626-1** were obtained from chloroform by slow evaporation. In the molecular structure, C22 was within the plane of pyridocarbazole and far away from it, probably due to the steric hindrance effect of the substitution on the C22.

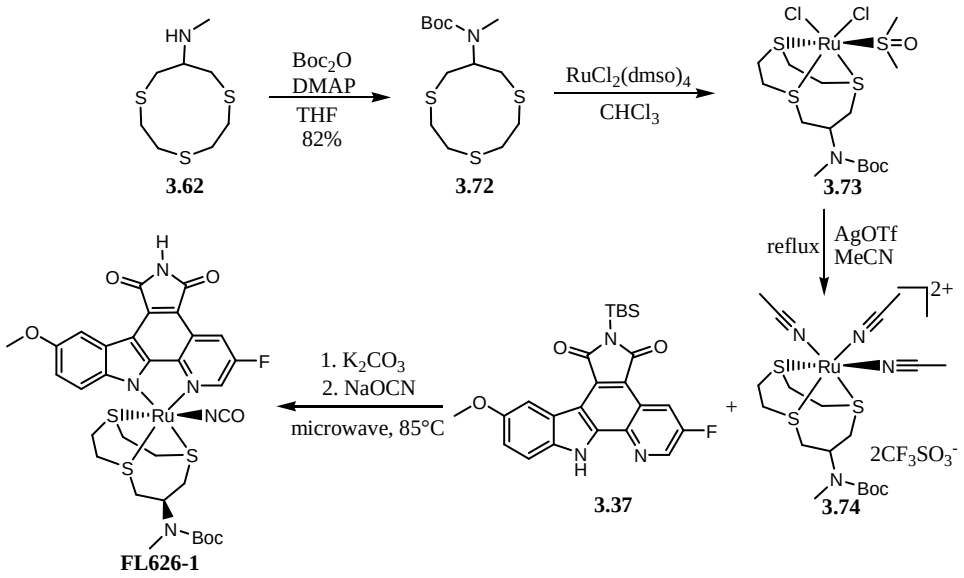

Scheme 3.4. Synthesis of racemic complex **FL626-1**.

Complex **FL1473** was synthesized (Scheme 3.5) starting with the tridentate ligand **3.66**, and the ruthenium precursor **3.68** was produced in the similar route using $[RuCl_2(\eta^6\text{-}C_6H_6)]_2$ instead of $RuCl_2(dmso)_4$ and acetonitrile/ethanol mixture (1:2) as solvent. Three diastereomers were formed during the synthesis of **FL1473**, which can not be separated by silica gel chromatography. Fortunately, the major product can be purified by crystallization of the mixture in acetone, but the yield of the reaction was only around 10%.

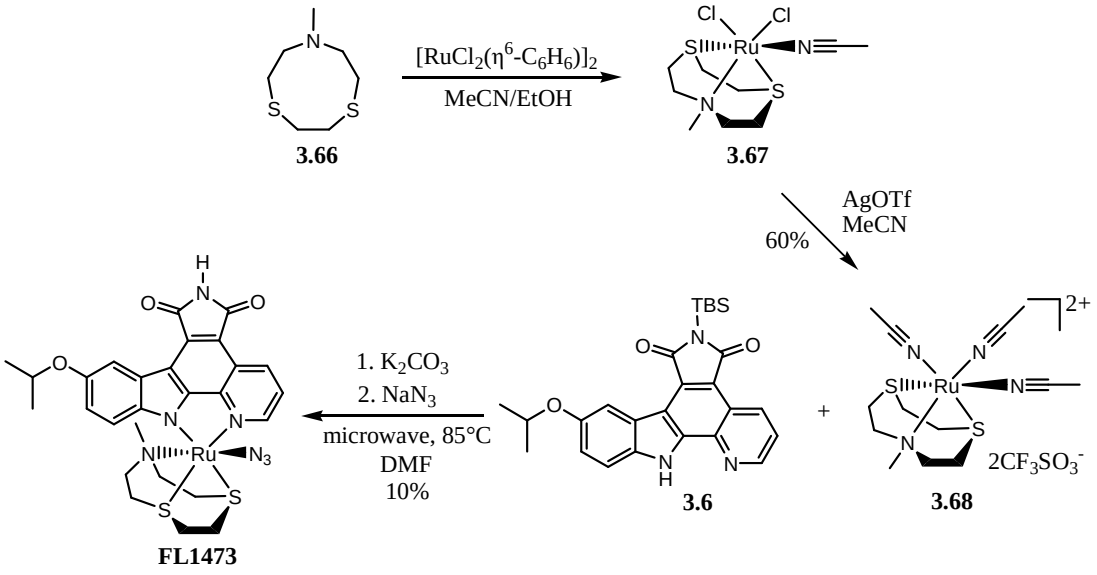

Scheme 3.5. Synthesis of racemic complex **FL1473**.

The crystal structure of **FL1473** shown in Figure 3.5 displays that N28 is on the axial position *trans* to the azide, due to the steric hindrance of the methyl group on the N28. In complex **FL1473**, the bond length of Ru-S1, Ru-S2, and Ru-N28 is 2.28 Å, 2.28 Å, and 2.18 Å, respectively. Ru-N28 is slightly shorter than Ru-S bond. The nitrogen makes the 9-member ring more strained, which probably results in the low yield of this reaction.

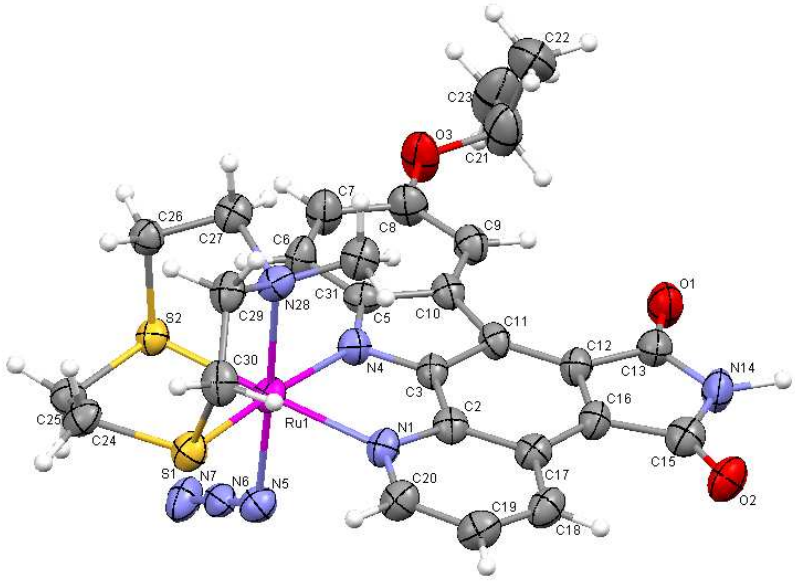

Figure 3.5. Crystal structure of the complex **FL1473**. ORTEP drawing with 50% probability thermal ellipsoids.

To verify whether the modifications improved the potency of the resulting inhibitors or not, racemic complexes **FL1392** and **FL1473** were measured against MLCK and the IC_{50} values were 110 nM and 230 nM in the presence of 100 μM ATP, respectively. The binding affinity was decreased by factors of 4 and 8.5 for MLCK compared to **FL1359**, respectively, probably due to the hydrophobic effect of the methyl group on the nitrogen in the tridentate ligand in both complexes. Thus, introduction of a hydrophilic group on the 9-member ring might be a promising opportunity.

The synthesis of racemic complex **FL1528-1** is summarized in Scheme 3.6. Starting with 1,4,7-trithiocyclononane, oxidization with 0.9 equiv of mCPBA in chloroform afforded mono-sulfoxide compound **3.60** in 64% yield, which was subsequently coordinated with the ruthenium precursor $RuCl_2(dmso)_4$ to yield the intermediate of

ruthenium species. Ruthenium precursor **3.61** was produced in the same way with **3.65** in 80% yield over two steps, which was used to furnish **FL1528-1** with the pyridocarbazole **3.6** under microwave irradiation. Similarly, three diastereomers were formed in the reaction and **FL1528-1** was obtained purely by silica gel chromatography as the first fraction in 12% yield and the other two isomers were obtained as a mixture in 34% yield.

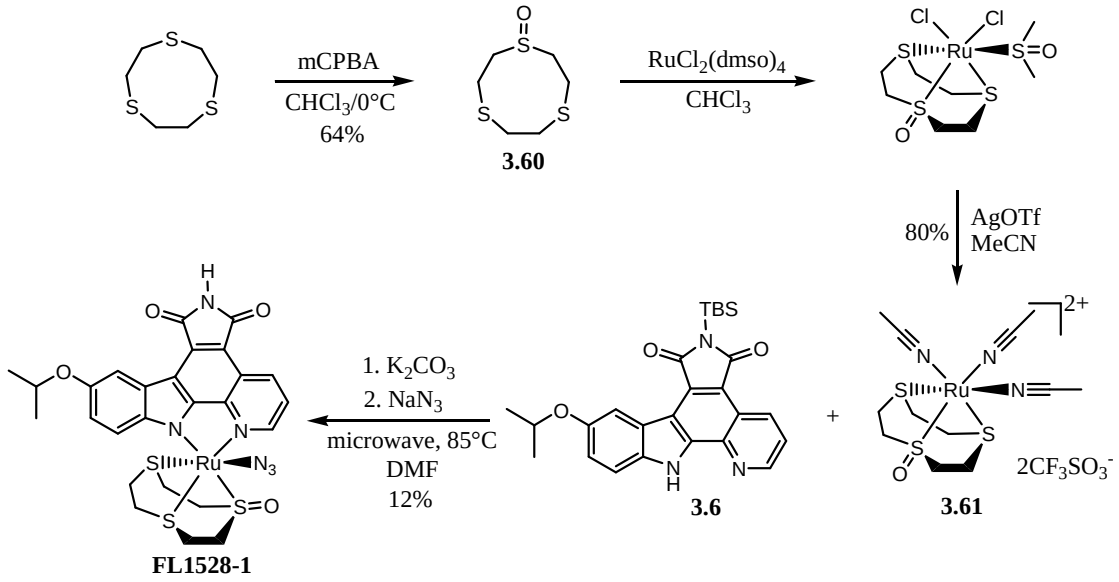

Scheme 3.6. Synthesis of racemic MLCK inhibitor **FL1528-1**.

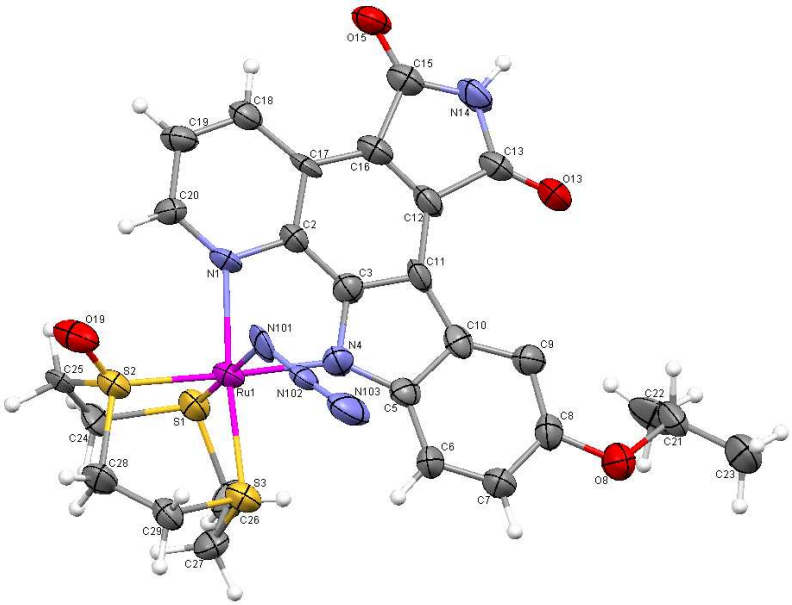

Figure 3.6. Crystal structure of complex **FL1528-1**. ORTEP drawing with 50% probability thermal ellipsoids.

X-ray quality crystals of complex **FL1528-1** suitable for single crystal diffraction were obtained from DMF/diethyl ether by slow diffusion. The molecular structure shown in Figure 3.6 confirms the relative configuration of **FL1528-1**, in which the sulfoxide group is within the plane of pyridocarbazole ligand and positioned *trans* to the indole moiety.

IC_{50} values of **FL1528-1** against MLCK, PAK1, DAPK1, GSK3α, Flt4, and Pim1 in the presence of 100 µM ATP are shown in Table 3.6. Excitingly, **FL1528-1** displayes an improved potency and selectivity significantly compared to the lead structure **FL1359**. With an IC_{50} value of 4.4 nM for MLCK, **FL1528-1** showed at least 10-fold selectivity over the other five protein kinases on which our group is working (Pim1: 98-fold).

Table 3.6. IC_{50} values of racemic **FL1528-1** against MLCK, PAK1, DAPK1, GSK3α, Flt4 and Pim1 in the presence of 100 µM ATP.

IC_{50}	**MLCK**	**PAK1**	**DAPK1**	**GSK3α**	**Flt4**	**Pim1**
FL1528-1	4.4 nM	> 100 µM	113 nM	31 µM	48 nM	435 nM

Furthermore, a screening result shown in Figure 3.7 of complex **FL1528-1** against a panel of 230 human wild-type protein kinases (Millipore UK Ltd) demonstrates the excellent selectivity profile of **FL1528-1**. In 230 tested human protein kinases, with a concentration of 30 nM of **FL1528-1** (10 µM ATP) there were 205 kinases remained more than 50% activity. Impressively, only 7 kinases (MLCK: 2%, ZIPK: 5%, DAPK2: 12%, Ret: 13%, DAPK1: 15%, Rsk2: 19% and Rsk1: 20%) displayed activity below 20% under these conditions (see appendix for details). It was verified that the IC_{50} values of **FL1528-1** for ZIPK and Ret were 18 nM and 70 nM in the presence of 100 µM ATP, respectively. **FL1528-1** showed 4-fold selectivity for MLCK over ZIPK. Therefore, it can be concluded that organoruthenium complex **FL1528-1** constitutes a highly selective molecular probe for the protein kinase MLCK.

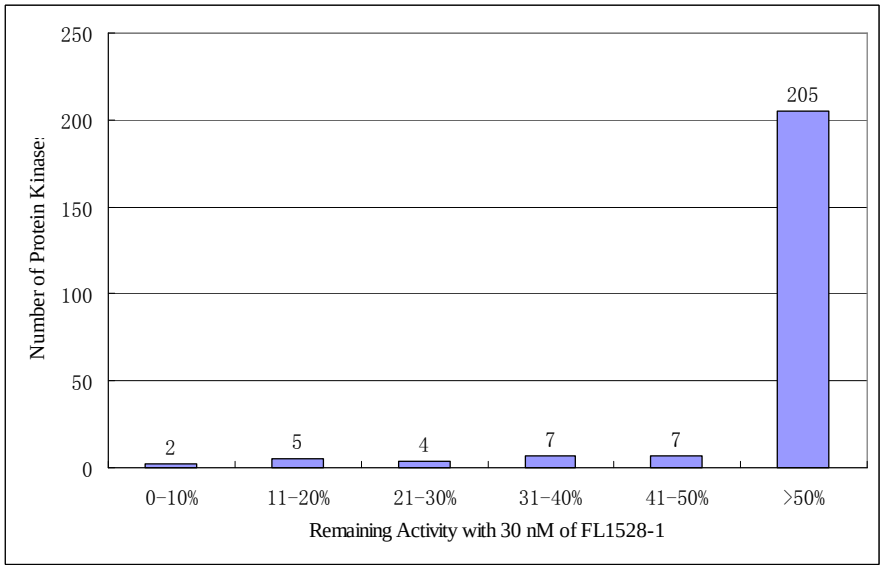

Figure 3.7. Selectivity profile of racemic **FL1528-1** tested against a panel of 230 human wild-type protein kinases at a single concentration of 30 nM and an ATP concentration of 10 μM. The most inhibited kinases in this panel were MLCK (2%), ZIPK (5%), DAPK2 (12%), Ret (13%), DAPK1 (15%), Rsk2 (19%) and Rsk1 (20%). Duplicate measurements were performed and the average was taken. See appendix for more details.

Chapter 3.2: Development of DAPK1 inhibitors

Chapter 3.2.1 Scaffold synthesis of DAPK1 inhibitors

The scaffold of DAPK1 inhibitors was initially identified from a screening of organoruthenium complexes including half-sandwich complexes and octahedral complexes against different kinases performed by former lab members. It was found that the potency for DAPK1 was improved almost 500-fold by changing half-sandwich complex to octahedral complex (Figure 3.8). Complex **3.86** was the only scaffold preferred by DAPK1 in this screening. Thus, scaffold **3.86** was used as the starting point to develop DAPK1 inhibitors.

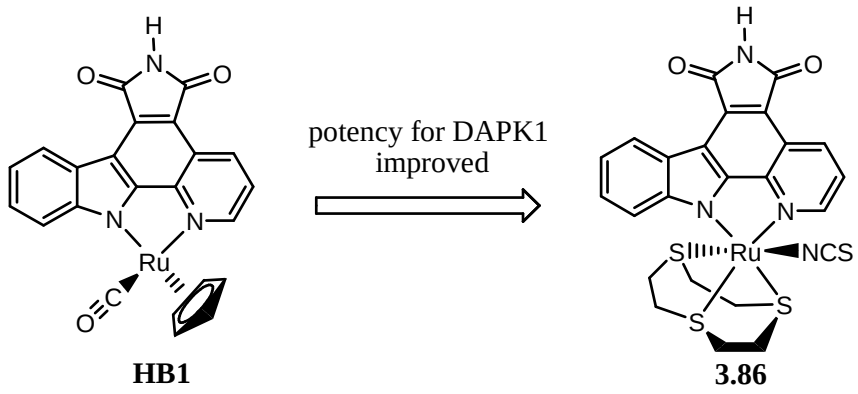

Figure 3.8. Racemic complex **3.86** was identified as initial DAPK1 inhibitor.

The scaffold of DAPK1 inhibitors was constructed in analogy to the MLCK inhibitors just using thiocyanate as monodentate ligand. In the same way, synthesis of the ruthenium scaffold was performed under microwave irradiation (Scheme 3.7). Thiocyanate is known to be an ambidentate ligand in the coordination chemistry,[20,23] and it can form Ru-N bond and Ru-S bond with the ruthenium center in this reaction which can be separated by silica gel chromatography. It was identified that the first fraction was always the Ru-N bonding linkage isomer, which will be proven in chapter 3.2.5 by crystallography and ^{15}N NMR spectra.

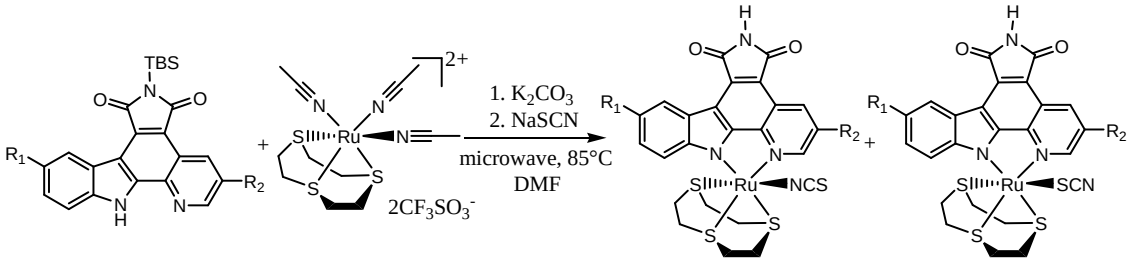

Scheme 3.7. Synthesis of racemic ruthenium complexes with microwave irradiation. R_1, R_2: different substituents on pyridocarbazole

Chapter 3.2.2: Preliminary structure-affinity relationship study

To verify complex **3.86** suitable as the lead structure of DAPK1 inhibitors, the racemic derivative complex **FL823-1** was synthesized as starting point (Figure 3.9), in which a hydroxyl group was on the 5-position of indole and a fluorine on the 3-position of pyridine on the pyridocarbazole.

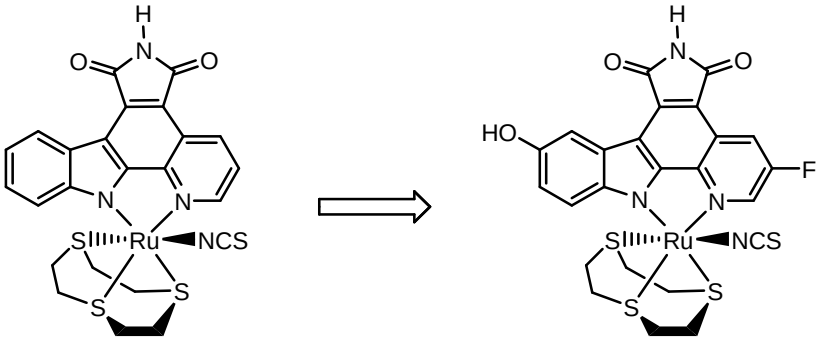

3.86
IC50 = 200 nM

FL823-1
IC50 = 20 nM

Figure 3.9. IC_{50} values of racemic **3.86** and **FL823-1** for DAPK1 with 100 μM ATP.

FL823-1 was tested against DAPK1 in the presence of 100 μM ATP and the IC_{50} value was 20 nM which was improved by a factor of 10 compared to **3.86** (200 nM) by introducing a hydroxyl group and a fluorine on the pyridocarbazole. To investigate the selectivity profile of this scaffold, **FL823-1** was measured against protein kinases GSK3α, GSK3β, and Pim1, and the IC_{50} values were 500 nM, 600 nM, and 3 nM, respectively, in the presence of 100 μM ATP (measured by G. Ekin Atilla-Gokcumen). The scaffold displayed high selectivity over both isoforms of GSK3, but very high affinity for Pim1. Thus, developing potent DAPK1 inhibitors but selective over Pim1 is of great interest.

Chapter 3.2.3: Affinity effect of different monodentate ligand on the axial position

To investigate the influence on the binding affinity to DAPK1 of the monodentate ligand in the scaffold, a series of ruthenium complexes with different monodentate ligands were synthesized by reacting ruthenium precursor **2.3** first with 1 equiv of 1,4,7-trithiacyclononane in DMF, and then different monodentate ligands (Figure 3.10). All the complexes were obtained by silica gel chromatography.

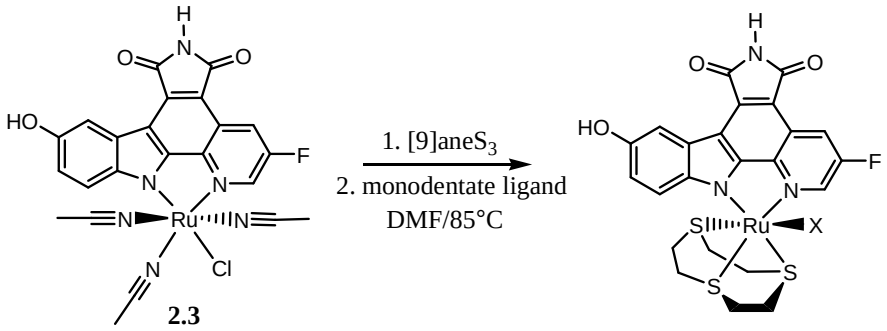

Figure 3.10. Synthesis of ruthenium complexes with different monodentate ligands. **FL253**: X=CN yield: 17%, **FL475**: X=NCO yield: 27%, **FL528**: X=NCSe yield: 45%, **FL576**: X=CO yield: 50%, **FL823-2**: X=SCN yield: 34%. All the complexes were racemic. **FL528** was assigned as Ru-N bonding isomer according to complex **3.83** by IR spectra. **FL576** was monocationic complex with PF_6^- as counterion.

Next, these complexes were tested against DAPK1 as racemic mixture in the presence of 100 μM ATP and the IC_{50} values are listed in Table 3.7.

Table 3.7. IC_{50} values of racemic ruthenium complexes with different monodentate ligands on the axial position in the presence of 100 μM ATP. (measured by G. Ekin Atilla-Gokcumen)

	FL823-1	**FL253**	**FL475**	**FL528**	**FL576**	**FL823-2**
DAPK1	20 nM	> 10 μM	500 nM	3 nM	250 nM	30 nM

The data demonstrate that there is significant influence on the affinity of the scaffold for DAPK1 with different monodentate ligands on the axial position. Complex **FL253** was completely inactive when using a cyanide instead of the isothiocyanate and the IC_{50} value was more than 10 μM. The binding affinity was also decreased by factors of 25 and 12.5 compared to **FL823-1**, respectively, when using -NCO (**FL475**) or -CO (**FL576**) on the axial position. The big difference of the affinity for DAPK1 between -CN and -CO is due to the difference of hydrophobicity of these two ligands. Although they are isoelectronic, the coordinated carbonyl group is more hydrophobic compared to cyanide which tends to form hydrogen bonds with the lone pair of nitrogen. Therefore, cyanide is more disfavored in the hydrophobic pocket in DAPK1 active site.[24,25] The

affinity of the -SCN complex (**FL823-2**) was slightly higher than the -NCS complex (**FL823-1**), probablely due to the different angle of the coordinated monodentate ligands. However, when using a more hydrophobic ligand -NCSe instead of -NCS, the potency of **FL528** for DAPK1 was increased significantly by a factor of 7 compared to **FL823-1**. Therefore, the data demonstrated that a hydrophobic group on the axial position is more favorable in the active site of DAPK1.

Chapter 3.2.4: Improved DAPK1 inhibitor by modification on the pyridocarbazole moiety

Although **FL528** showed high affinity for DAPK1 with an IC_{50} value of 3 nM in the presence of 100 μM ATP, it was much more potent for Pim1 with an IC_{50} value of lower than 0.3 nM. Thus, it was still promising to use the isothiocyanate as monodentate ligand to develop the more potent and selective DAPK1 inhibitors. It was envisioned that the same strategy of the development of MLCK inhibitors might be suitable for DAPK1 project. Especially, both catalytic domains of DAPK1 and MLCK have very high sequence similarity. With a series of pyridocarbazoles in hand, it can be very convenient to identify the promising pharmacophore ligand for the scaffold of DAPK1 inhibitors.

All the derivatives of inhibitors for DAPK1 are shown in Table 3.8. These racemic derivatives were synthesized in analogy to MLCK inhibitors by first reacting corresponding pyridocarbazoles with the ruthenium precursor **2** under microwave irradiation, followed by the addition of sodium thiocyanate to replace the remaining acetonitrile group. The isothiocyanato complexes were abtained by silica gel chromatography except **FL1334**, which was a mixture of isothiocyanato and thiocyanato complexes with the ratio of around 1 : 1.

Table 3.8. Ruthenium complexes with different substituents on the pyridocarbazole. All the complexes were synthesized as racemic mixtures.

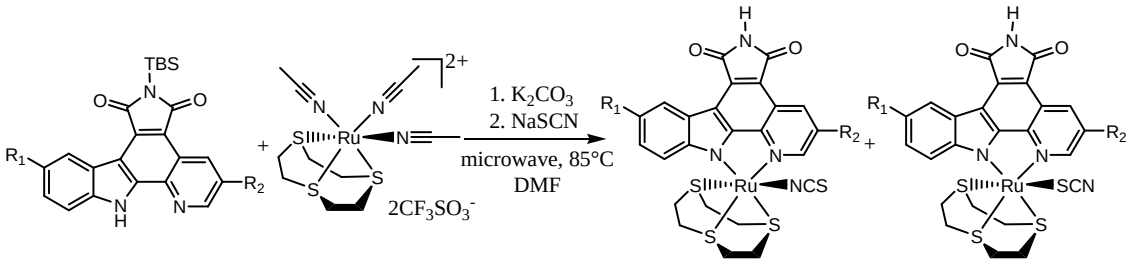

	R_1	R_2	Yield (%)
FL812-1	OCH_3	F	33
FL1289-1	SCH_3	F	17
FL1334	SCH_3	NH_2	43
FL1352-1	SCH_3	H	23
FL1353-1	O*i*Pr	F	37
FL1370-1	O*i*Pr	H	40

Derivative **FL812-1** was first synthesized and tested against DAPK1 and Pim1. The IC_{50} values against DAPK1 and Pim1 in the presence of 100 μM ATP were 6 nM and 7 nM, respectively. The potency of **FL812-1** for DAPK1 was improved by a factor of 3, and for Pim1 was decreased by a factor of 2 compared to **FL823-1** by changing the hydroxyl group on the indole to a methoxy group. But **FL812-1** still had no selectivity over Pim1. Interestingly, the modification with a hydrophobic group on the 5-position of indole improved the potency of inhibitors for DAPK1. As discussed in the MLCK inhibitors subchapter, introduction of a big hydrophobic group on the 5-position of indole disfavores Pim1 kinase significantly. Thus, to further improve the potency and selectivity of DAPK1 inhibitors, the modification of pyridocarbazole with hydrophobic substituents was tried in this scaffold. These derivatives were tested against DAPK1 and Pim1 in the presence of 100 μM ATP and the results are shown in Table 3.9.

Table3.9. IC_{50} values in nM of racemic derivatives with different pyridocarbazoles for DAPK1 and Pim1 in the presence of 100 μM ATP.

	FL812-1	**FL1289-1**	**FL1334**	**FL1352-1**	**FL1353-1**	**FL1370-1**
DAPK1	6	12.5	3.7	4.2	2	3.9
Pim1	7	172	72	100	169	434

The data demonstrate that a profound influence on the potency and selectivity of the ruthenium complexes is achieved by the modification on the 5-position of indole with a hydrophobic group and/or 3-position of pyridine. A big hydrophobic group on the 5-position of indole significantly improved the selectivity of inhibitors over Pim1. Using a methylthio group (**FL1289-1**) instead of the methoxy group, the potency for DAPK1 (12.5 nM) was decreased by a factor of 2 compared to **FL812-1**. At the same time, the affinity for Pim1 (172 nM) was decreased by a factor of 24. Using an amino group instead of the fluorine (**FL1334**) or just removing the fluorine (**FL1352-1**) on the pyridine moiety, both increased the affinity for DAPK1 and Pim1, and the IC_{50} values were 3.7 nM and 4.2 nM for DAPK1, and 72 nM and 100 nM for Pim1, respectively. However, the selectivity over Pim1 was further improved. **FL1334** and **FL1352-1** showed 19-fold and 24-fold selectivity over Pim1, respectively. In addition, the potency and selectivity of **FL1353-1** was further improved with an isopropyloxy group on the 5-position of indole and a fluorine on the 3-position of pyridine in the scaffold. The IC_{50} value for DAPK1 was 2 nM and for Pim1 was 169 nM which was improved by factors of 3 and 24 compared to **FL812-1**, respectively, and the selectivity over Pim1 of **FL1353-1** was around 85-fold. After removing the fluorine on the pyridine in complex **FL1370-1**, the selectivity over Pim1 was further improved (111-fold), but the potency for DAPK1 was decreased to 3.9 nM. Thus, overall, complex **FL1353-1** was the most promising inhibitor for DAPK1 in the library. By the modification of the pyridocarbazole, the potency of **FL1353-1** for DAPK1 was improved by a factor of 100 compared to complex **3.86**.

Complex **FL1353-1** was further tested against PAK1, MLCK, GSK3α, and Flt4 to investigate the selectivity profile of this scaffold. The IC_{50} values are listed in Table 3.10. With an IC_{50} value of 2 nM for DAPK1, **FL1353-1** showed at least 12-fold selectivity over the other five kinases (MLCK: 12-fold, Pim1: 84-fold).

Table 3.10. IC_{50} values of racemic **FL1353-1** against DAPK1, Pim1, PAK1, MLCK, GSK3α and Flt4 in the presence of 100 μM ATP.

	DAPK1	**Pim1**	**PAK1**	**MLCK**	**GSK3α**	**Flt4**
FL1353-1	2 nM	169 nM	> 100 μM	25.3 nM	> 100 μM	163 nM

Furthermore, a screening result shown in Figure 3.11 of complex **FL1353-1** against a panel of 102 human wild-type protein kinases (Millipore UK Ltd) demonstrates the excellent selectivity profile of **FL1353-1**.

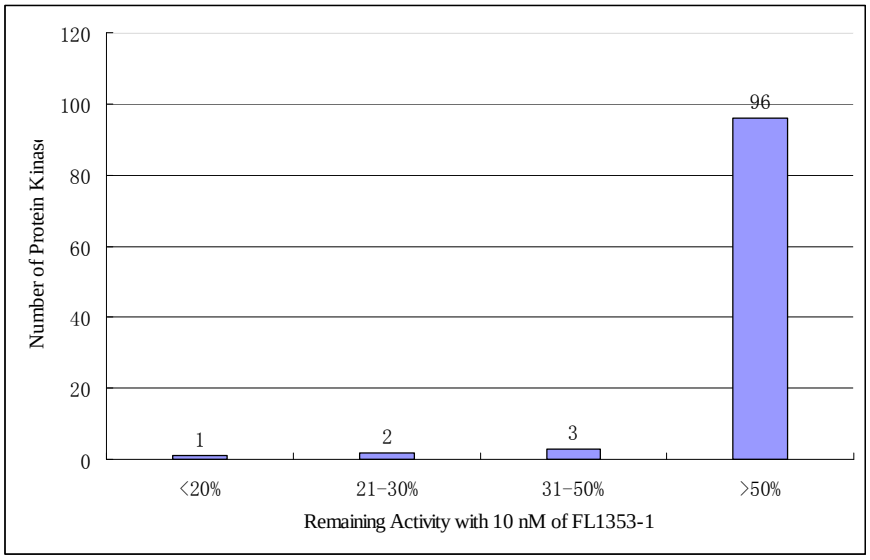

Figure 3.11. Selectivity profile of racemic **FL1353-1** tested against a panel of 102 human wild-type protein kinases at a single concentration of 10 nM and an ATP concentration of 10 μM, with DAPK1 displaying a remaining activity of 12% under these conditions and the remaining kinases below 50% activity being ZIPK (22%), Rsk2 (27%), Rsk1 (31%), MELK (37%) and Pim1 (38%). Duplicate measurements were performed and the average was taken. See appendix for more details.

In 102 tested human protein kinases, with a concentration of 10 nM of racemic **FL1353-1** (10 μM ATP) there were 96 kinases remained more than 50% activity. Impressively, only DAPK1 (12% activity) displayed activity below 20% under these conditions (see appendix for details), and the other kinases showed lower than 50% activity were ZIPK (22%), Rsk2 (27%), Rsk1 (31%), MELK (37%), and Pim1 (38%). It was verified that the IC_{50} value of **FL1353-1** for ZIPK was 8.8 nM in the presence of 100 μM ATP. **FL1353-1** showed 4-fold selectivity over ZIPK. Therefore, it can be concluded that organoruthenium complex **FL1353-1** was developed as a highly potent and selective inhibitor for protein kinase DAPK1.

Chapter 3.2.5: Determination of the relative configuration of FL1353-1

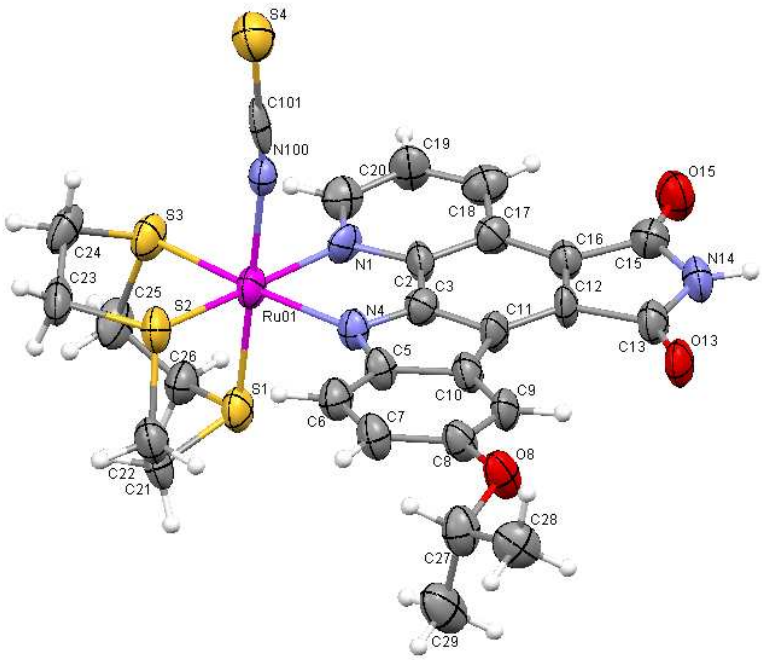

Figure 3.12. Crystal structure of complex **FL1370-1**. ORTEP drawing with 50% probability thermal ellipsoids.

The crystal structure of **FL1370-1** shown in Figure 3.12 verified the relative configuration of the related complex **FL1353-1** indirectly. Crystallization of **FL1353-1** didn't succeed. X-ray quality crystals of the complex **FL1370-1** suitable for single

crystal diffraction were obtained in acetone and methanol mixture solvent by slow evaporation. In the molecular structure, the isothiocyanate ligand is on the axial position perpendicular to the pyridocarbazole and the angle of Ru01-N100-C101 bond is almost linear (171.8˚) which is consistent with the literature.[26,27]

In complex **FL1353-1**, the ruthenium center binding with the isothiocyanate binding mode (Ru-N bond) was also proven by ^{15}N NMR measurements, which was performed with complexes **FL534-1** and **FL534-2** (Figure 3.13). It was synthesized in analogy to **FL823** just using potassium thiocyanate-^{15}N instead of sodium thiocyanate as the monodentate ligand.

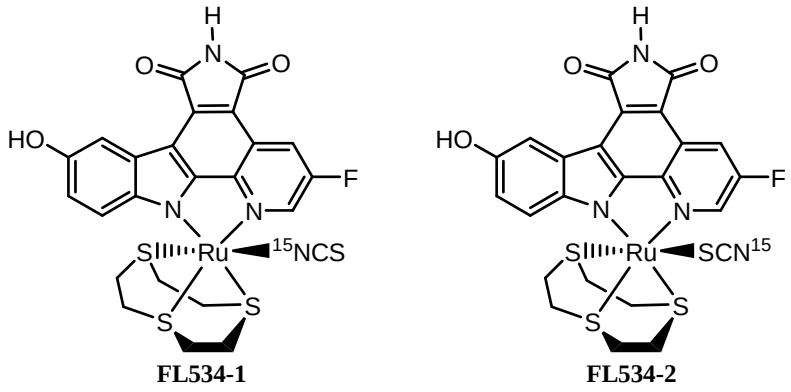

Figure 3.13. Structure of racemic complexes **FL534-1** and **FL534-2**.

The ^{15}N NMR spectra of **FL534-1** and **FL534-2** shown in Figure 3.14 were recorded in anhydrous DMSO-d_6. **FL534-2** was measured as a mixture of both linkage isomers and NH_3 liquid was used as standard in the measurement. The chemical shift of isothiocyanate in **FL534-1** was 125.5 ppm, more up-field shifted than thiocyanate in **FL534-2** which was 236.5 ppm. The result was consistent with the data in Lange's Handbook of Chemistry (15th Edition, Spectroscopy, Table 7.63), in which the chemical shift of isothiocyanates is in the range of 95-120 ppm and the chemical shift of thiocyanates is in the range of 265-280 ppm with liquid NH_3 as standard, more downfield-shifted than isothiocyanates. Thus, it further proved the relative configuration of **FL1353-1** which is the Ru-N linkage isomer.

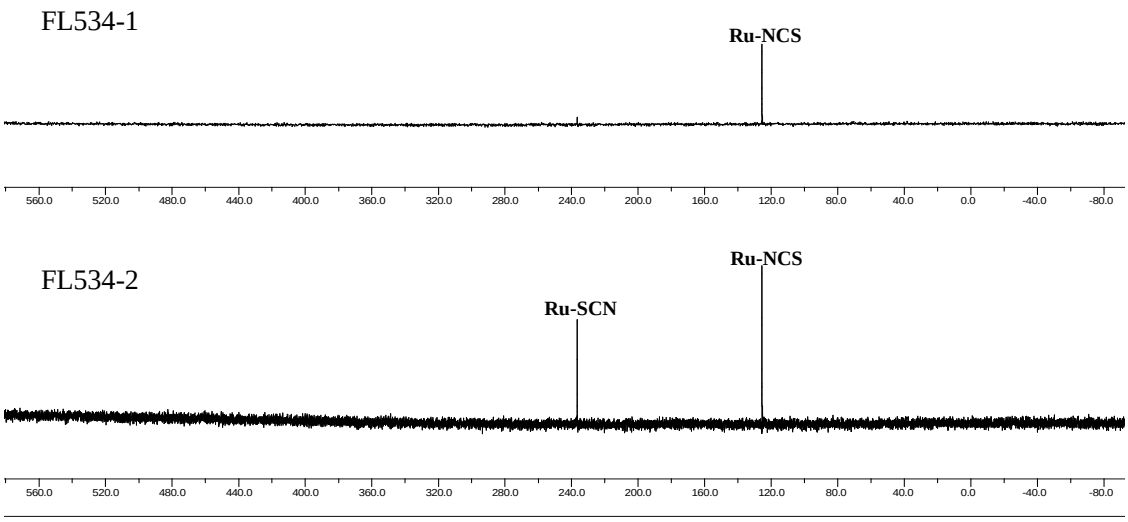

Figure 3.14. ^{15}N NMR spectra of **FL534-1** and **FL534-2**. NH_3 liquid was used as standard, and **FL534-2** was measured as a mixture of both linkage isomers.

Chapter 3.2.6: Isomerization of Ru-N and Ru-S of Complex FL1353 monitored by ^1H NMR spectra

Thiocyanate is well known as ambidentate ligand and linkage isomers of cobalt[28] and platinum[29] complexes for example containing thiocyanate have been studied. However, very little work has been reported on ruthenium thiocyanate linkage isomers.[30] The linkage isomerization was performed in DMSO-d_6/D_2O (9:1) at room temperature and monitored by ^1H NMR spectra starting from these two pure racemic isomers **FL1353-1** (Ru-N bonding) and **FL1353-2** (Ru-S bonding). The ratios of these two linkage isomers (Ru-N bonding and Ru-S bonding) are listed in Table 3.11 as a function of time.

Table 3.11. Ratio of Ru-N bonding isomer and Ru-S bonding isomer.

	FL1353-1 (Ru-N isomer)	**FL1353-2 (Ru-S isomer)**
1 hour	1 : 0	0.05 :1
2 hours	1 : 0	0.11 : 1
4 hours	1 : 0.05	0.2 : 1

21 hours	1 : 0.15	0.8 : 1
45 hours	1 : 0.25	2 : 1
70 hours	1 : 0.28	2.9 : 1
4 days	1 : 0.28	3.3 : 1
5 days	1 : 0.29	1 : 0.29
7 days	1 : 0.29	1 : 0.29
10 days	1 : 0.29	1 : 0.29

The data demonstrate that **FL1353-1** isomerized more slowly compared to **FL1353-2** and Ru-N bonding was more favorable in this equilibrium. After 3 days, they both reached equilibrium with the ratio of 1:0.29 of two linkage isomers (Ru-N:Ru-S), in which the Ru-N bonding isomer was the major one. The ^{1}H NMR spectra only showed the isomerization of these two linkage isomers without any decomposition of the complexes which meant that the linkage isomerized without dissociation from ruthenium center.

Chapter 3.2.7: Cocrystal structure of (*R*)-FL1353-1 with DAPK1

To understand the molecular details of the binding of the octahedral scaffold to DAPK1, cocrystallization of racemic **FL1353-1** (Ru-N) and **FL1353-2** (Ru-S) with DAPK1 was carried out, respectively, by lab colleague Katja Kräling. A cocrystal structure was obtained by Yann Geisselbrecht from the group of Prof. Dr. Lars-Oliver Essen and is shown in Figure 3.15. The cocrystal was initially executed with Ru-S isomer, but it isomerized to Ru-N isomer during the cocrystallization. The angle of Ru-N-C (linkage) is 142.9˚ in the cocrystal structure, slightly bendier than in the single crystal of 171.8˚ (Figure 3.12), probably due to the steric clash of the linkage with the glycine-rich loop.

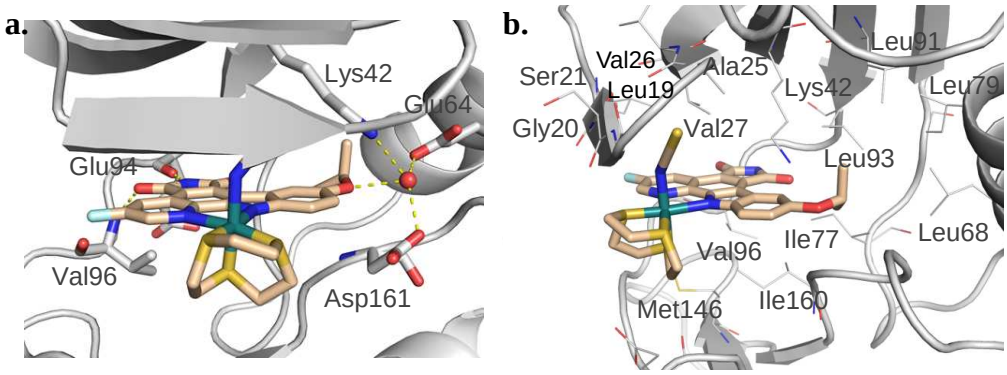

Figure 3.15. Cocrystal structure of (*R*)-**FL1353-1** with DAPK1 at the resolution of 2.2 Å. a) Hydrogen bonding interactions between the hinge region and (*R*)-**FL1353-1**. b) Hydrophobic interactions of (*R*)-**FL1353-1** in the active site. The absolute configuration at the ruthenium was assigned according to the Cahn-Ingold-Prelog rules treating the complex as being pseudo-tetrahedral with the 1,4,7-trithiacyclononane being formally regarded as a single substituent, with the priority order of the substituents being 1,4,7-trithiacyclononane > pyridine [N(C,C,C)] > NCS > indole [N(C,C,lone pair)].

The structure reveals that the (*R*)-enantiomer of **FL1353-1** occupies the ATP-binding site. Whereas the maleimide moiety forms two canonical hydrogen bonds with the hinge region of DAPK1 (Val96 and Glu94) (Figure 3.15a). Furthermore, the isopropyl ether oxygen at the indole moiety forms a water-mediated contact to the amino acids Lys42 (2.7 Å), Glu64 (2.8 Å), and Asp161 (2.5 Å), and the isopropyl substituent reaches into a small hydrophobic pocket composed out of Lys42, Ile77, Leu93, Leu91, and Leu68 (Figure 3.15b). The pyridocarbazole heterocycle is sandwiched by key hydrophobic contacts from amino acids of the N-terminal (Leu19, Val27, and Leu93) and C-terminal (Ile77, Val96, Met146, and Ile160) domains. The 1,4,7-trithiacyclononane ligand points towards the more hydrophilic entrance of the ATP-binding site and occupies the extended chemical space in the domain. The isothiocyanate ligand on the axial position points towards the hydrophobic pocket of glycin-rich loop forming close contact with the side chain residues of Val27, Ala25, and Lys42, as well as the backbone residues of Gly20, Val26, and Ser21 in the active site.

Chapter 3.3: Improved inhibitor for Pim1 kinase

Our group published **3.87** (Scheme 3.2) as Pim1 kinase inhibitor in 2006 with an IC_{50} value of 450 pM in the presence of 100 μM ATP.[7] Based on the structure-affinity relationship study of half-sandwich ruthenium inhibitors,[17,21] it was envisioned that the potency of this inhibitor might be improved by introducing the hydrophilic hydroxyl groups both on the indole and pyridine of the pyridocarbazole.

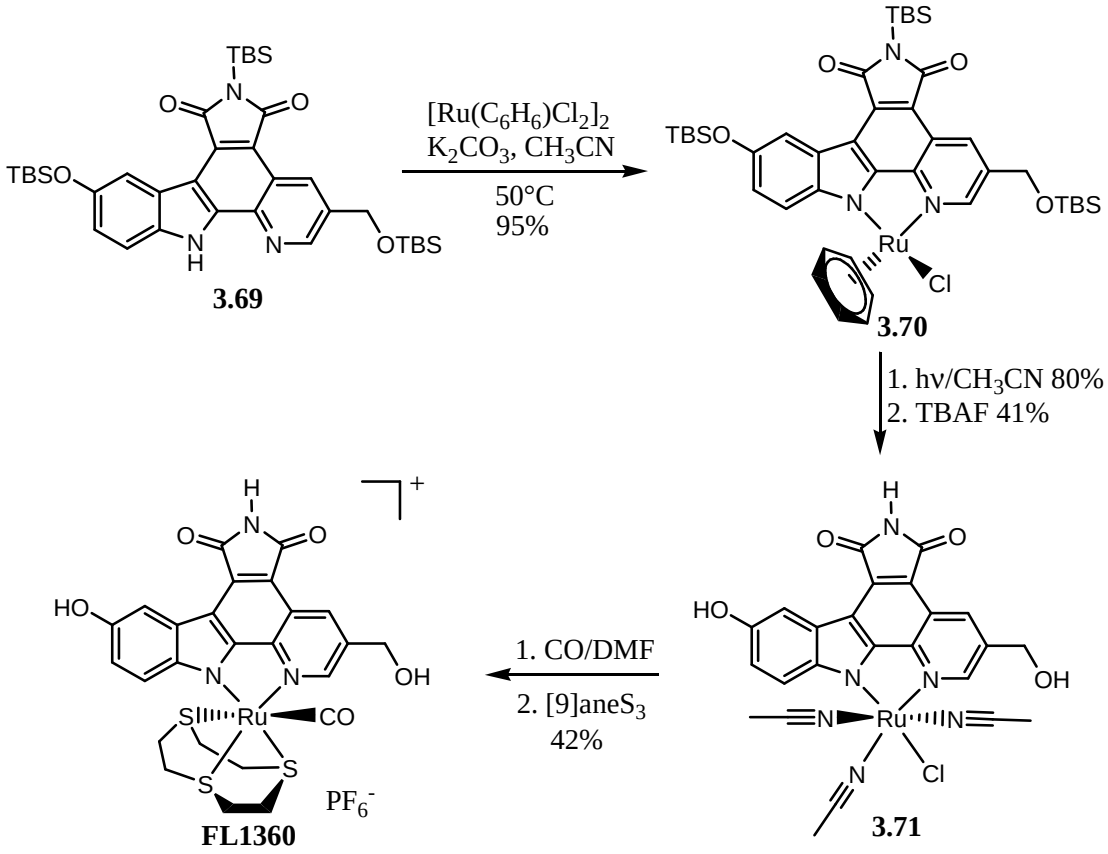

Scheme 3.8. Synthesis of racemic **FL1360** starting from pyridocarbazole **3.69**.

The synthesis of racemic **FL1360** starting from pyridocarbazole **3.69**[35] is shown in Scheme 3.8. Accordingly, pyridocarbazole **3.69** was cyclometallated with 0.75 equiv of $[(\eta^6\text{-benzene})RuCl_2]_2$ in the presence of 1.1 equiv of potassium carbonate in acetonitrile at 50 °C affording the η^6-half-sandwich complex **3.70** in 95% yield. The benzene ring was replaced by three acetonitrile molecules upon UV-photolysis in acetonitrile at room temperature, followed by TBS-deprotection using TBAF (1 M in THF) at 0 °C, which

afforded the ruthenium precursor **3.71**. The complex **3.71** shown in Scheme 3.7 is the major diastereoisomer obtained in 33% yield over two steps, which was subsequently used as a precursor for the synthesis of octahedral complex **FL1360**. The solution of **3.71** in DMF was first reacted with CO gas at 75 °C, and then with 1 equiv of 1,4,7-trithiacyclononane at 95 °C to provide the racemic cationic complex **FL1360** in 42% yield, in which the counter ion was exchanged to PF_6^-.

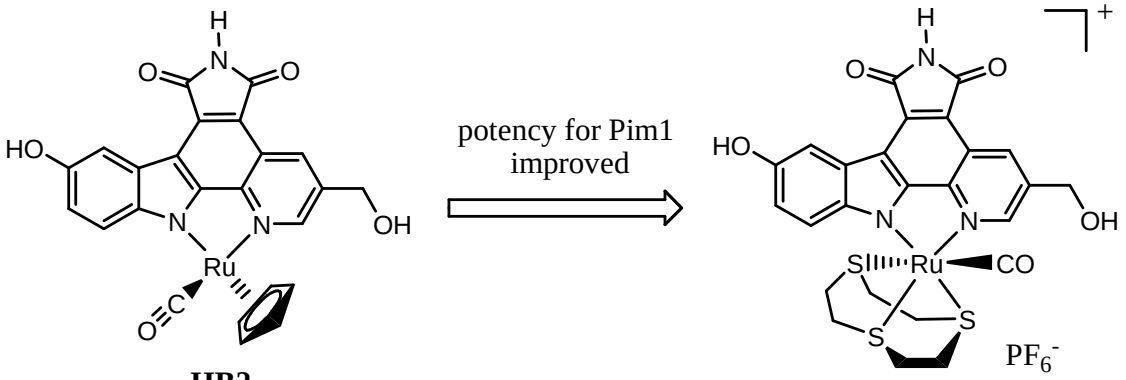

HB2
IC_{50}: 250 pM

FL1360
IC_{50}: 75 pM

Figure 3.16. Potency for Pim1 was improved by the transformation of half-sandwich scaffold into octahedral scaffold.

Complex **FL1360** was measured as racemic mixture against Pim1 and GSK3α in the presence of 100 μM ATP and the IC_{50} values were 75 pM and 20 nM, respectively. Correspondingly, lab colleague Howard Bregman synthesized the half-sandwich complex **HB2** (Figure 3.16) with the bis-hydroxyl pyridocarbazole and the IC_{50} value of **HB2** for Pim1 was 250 pM and for GSK3α was 500 pM in the presence of 100 μM ATP. The potency of this scaffold for Pim1 was improved by a factor of 3.3 by switching the cyclopentadienyl ligand into 1,4,7-trithiacyclononane ligand. At the same time, the potency for GSK3α was decreased by a factor of 16 compared to **HB2**.

According to the previous study of MLCK and DAPK1 inhibitors discussed above, 1,4,7-trithiacyclononane scaffold disfavors GSK3α kinase. Here, the selectivity over GSK3α of **FL1360** was also significantly improved. Compared to **3.87** (450 pM for Pim1), the potency of **FL1360** for Pim1 was improved by a factor of 6, probably because both hydroxyl groups form hydrogen bonding interactions with the backbone in

the Pim1 active site.

Table 3.12. IC_{50} values of racemic **FL1360** against protein kinases of Pim1, DAPK1, PAK1, MLCK, GSK3α, and Flt4 in the presence of 100 μM ATP.

	Pim1	**DAPK1**	**PAK1**	**MLCK**	**GSK3α**	**Flt4**
FL1360	75 pM	315 nM	82 nM	2.2 nM	8 nM	29 nM

Complex **FL1360** was also tested against protein kinases of PAK1, MLCK, DAPK1, GSK3α, and Flt4 in the presence of 100 μM ATP and the results are listed in Table 3.12. The data demonstrat that **FL1360** showed high affinity to the other five different protein kinases and the IC_{50} values were all in nanomolar range. But the Pim1 inhibitor of **FL1360** still displays at least 29-fold selectivity over the other five kinases.

Charpter 3.4: Discussion and conclusion

Potent and selective organoruthenium inhibitors for MLCK, DAPK1, and Pim1 were developed with the trithiacyclononane scaffold containing different pyridocarbazoles and monodentate ligands.

MLCK is a serine/threonine specific protein kinase and one of the key regulatory enzymes in Ca^{2+}-dependent responses.[8,9] Recent research demonstrated that increased MLCK activity might be involved in the bronchoconstriction in asthma attacks.[14,15] A nanomolar inhibitor **FL1528-1** for MLCK was developed. The MLCK inhibitor scaffold was identified by screening several potential organoruthenium inhibitors against a panel of human protein kinases, which turned out to be a very useful method for the discovery of new inhibitors for certain kinases.

The potency and selectivity over the other kinases especially for Pim1 of the MLCK inhibitors can be improved by modifying the three moieties in the scaffold. First, using azide as the monodentate ligand gave the inhibitor relatively high potency for MLCK and stability compared to other monodentate ligands such as: -NCO, -NCS, -NO_2, and -CN. Second, the selectivity of the inhibitors for MLCK over Pim1 was improved easily

by the modification of pyridocarbazole. It was found that the introduction of a big hydrophobic group on the 5-position of indole disfavored Pim1 dramatically. For example, using an isopropyloxyl group (**FL1359**) instead of the methoxyl group (**FL1381**) on the pyridocarbazole, the binding affinity for Pim1 was reduced from 52 nM to 847 nM in the presence of 100 μM ATP by a factor of 16. Lastly, the potency of the lead structure of MLCK inhibitors (**FL1359**) was further improved by the modification of the tridentate ligand trithiacyclononane. The results demonstrated that a hydrophobic group modified on the tridentate ligand decreased the potency of the MLCK inhibitors. Contrarily, the introduction of a small sulfoxide group increased the binding affinity for MLCK from 27 nM (**FL1359**) to 4.4 nM (**FL1528-1**) in the presence of 100 μM ATP by a factor of 6. **FL1528-1** displayed high potency for MLCK and impressive selectivity over the other kinases. **FL1528-1** was measured against a panel of human protein kinases. In 230 tested protein kinases, with a concentration of 30 nM of **FL1528-1** (10 μM ATP) there were 205 kinases remained more than 50% activity. Impressively, only 2 kinases displayed activity below 10% under these conditions including MLCK.

DAPK is a novel cytoskeletal-associated cell death serine/threonine kinase whose activation by Ca^{2+}/calmodulin may be linked to the biochemical mechanism underlying the cytoskeletal alterations that occur during cell death.[31] The role of the kinase activity of DAPK in eukaryotic cell apoptosis has made it a drug discovery target for neurodegenerative disorders.[32] Octahedral ruthenium complex **FL1353-1** was developed as a very potent and selective inhibitor for protein kinase DAPK1. With an IC_{50} value of 2 nM for DAPK1 in the presence of 100 μM ATP, **FL1353-1** showed 84-fold selectivity over Pim1 and completely inactive for GSK3α.

The DAPK1 inhibitor scaffold was identified from a screen of organoruthenium complexes against a panel of protein kinases. Complex **FL823-1** showed improved binding affinity to DAPK1 by the introduction of a hydroxyl group on the 5-position of indole and a fluorine on the 3-position of pyridine with an IC_{50} value of 20 nM in the presence of 100 μM ATP, but more potent for Pim1. The affinity influence of different

monodentate ligands in the scaffold was investigated. It was identified that a hydrophobic monodentate ligand was more favorable in the DAPK1 active site and the isothiocyanate was used as the monodentate ligand in the scaffold to develop more potent and selective DAPK1 inhibitors.

The potency and selectivity of DAPK1 inhibitors was improved by the modification of the pyridocarbazole. It was found that a profound influence on the potency and selectivity of the ruthenium complexes was achieved by the modification on the 5-position of indole with a hydrophobic group and/or 3-position of pyridine. With a big hydrophobic group such as isopropyloxy group (**FL1353-1**) on the 5-position of indole, the IC_{50} value for DAPK1 was improved from 20 nM to 2 nM in the presence of 100 μM ATP by a factor of 10 compared to **FL823-1**. At the same time, the IC_{50} value for Pim1 was decreased from 3 nM to 169 nM by a factor of 53. It turned out that **FL1353-1** displayed high kinase selectivity after testing it against a panel of 102 human protein kinases. With a concentration of 10 nM of **FL1353-1**, only DAPK1 displayed activity below 20% in the presence of 10 μM ATP. The relative configuration of **FL1353-1** was verified by the X-ray single crystal diffraction and ^{15}N NMR spectra.

A cocrystal structure of (*R*)-**FL1353-1** with DAPK1 revealed the details of interactions of the inhibitor in DAPK1 active site. Whereas the maleimide moiety forms two canonical hydrogen bonds with the hinge region of DAPK1 (Val96 and Glu94). Furthermore, the isopropyl ether oxygn at the indole moiety forms a water-mediated contact to the amino acids Lys42, Glu64, and Asp161, and the isopropyl substituent reaches into a small hydrophobic pocket composed out of Lys42, Ile77, Leu93, Leu91, and Leu68. The 1,4,7-trithiacyclononane ligand points towards the more hydrophilic entrance of the ATP-binding site and occupies the extended chemical space in the domain. The isothiocyanate ligand on the axial position points towards the hydrophobic pocket of glycin-rich loop forming close contact with the side chain residues of Val27, Ala25, and Lys42, as well as the backbone residues of Gly20, Val26, and Ser21 in the active site.

A picomolar range organoruthenium inhibitor **FL1360** for Pim1 was obtained. The

potency for Pim1 was improved by a factor of 6 by the introduction of a hydroxyl group on the 5-position of indole and a hydroxylmethy group on the 3-position of pyridine compared to complex **3.87**. The selectivity of **FL1360** over GSK3α was 106-fold, improved significantly by switching the cyclopentadienyl group to a trithiacyclononane compared to the half-sandwich complex **HB2** (2-fold). **FL1360** also showed high selectivity over PAK1, MLCK, DAPK1, and Flt4.

In addition, the microwave irradiation methodology was used in the synthesis of the organoruthenium inhibitors. Starting from the ruthenium complex **2** which is proven to be a novel precursor to synthesize kinase inhibitors, it is very convenient to construct metal complexes with different pyridocarbazoles with relatively short reaction time and high yield under microwave irradiation. The microwave irradiation is proven to be very efficient in this kind of reactions.

Chapter 3.6: References

(1) Arnold, J.; Artis, D. R.; Hurt, C.; Ibrahim, P. N.; Krupka, H.; Lin, J.; Milburn, M. V.; Wang, W. R.; Zhang, C. *PCT Int. Appl.* 2005009958, 03 Feb 2005.

(2) Petit, S.; Curoc, Y.; Larue, V.; Dardel, F. *Chem Med Chem* **2009**, *4*, 261-275.

(3) Bailey, W. F.; Salgaonkar, P. D.; Brubaker, J. D.; Sharma, V. *Organic Letters* **2008**, *10(6)*, 1071-1074.

(4) Edema, J. H.; Buter, J.; Kellogg, R. M.; Spek, A. L.; Bolhuis, F. *J. Chem. Soc., Chem. Commun.* **1992**, 1558-60.

(5) Landgrafe, C.; Sheldrick, W. S. *J. Chem. Soc. Dalton Trans.* **1996**, 989-998.

(6) Pagano, N.; Maksimoska, J.; Bregman, H.; Williams, D. S.; Richard D. Webster, R. D.; Meggers, E. *Org. Biomol. Chem.* **2007**, *5*, 1218-1227.

(7) Bregman, H.; Carroll, P. J.; Meggers, E. *J. Am. Chem. Soc.* **2006**, *128*, 877-884.

(8) Bylund, D. B. *Trends Pharmacol. Sci.* **1988**, *9*, 356-361.

(9) Kobilka, B. K.; Matsui, H.; Kobilka, T. S.; Lefkowitz, R. J.; Regan, J. W. *Science* **1987**, *238*, 650-656.

(10) Krueger, J. K.; Zhi, G.; Stull, J. T.; Trewhella, J. *Biochemistry* **1998**, *37*,

13997-14004.

(11) Cooper, S. R.; Rawle, S. C. *Structure and Bonding* **1990**, *72*, 1-72.

(12) Glass, R. S.; Wilson, G. S.; Setzer, W. N. *J. Am. Chem. Soc.* **1980**, *102*, 5068-5069.

(13) Cooper, S. R. *Acc. Chem. Res.* **1988**, *21*, 141-146.

(14) Ammit, A. J.; Armour, C. L.; Black, J. L. *Am. J. Respir. Crit. Care Med.* **2000**, *161*, 257-263.

(15) Ma, X.; Chen, Z.; Kong, H., Wang, Y.; Unruh, H.; Stephens, N. L.; Laviolette, M. *Am. J. Physiol.* **2002**, *283*, 1181-1189.

(16) Pagano, N.; Wong, E. Y.; Breiding, T.; Liu, H.; Wilbuer, A.; Bregman, H.; Shen, Q.; Diamond, S. L.; Meggers, E. *J. Org. Chem.* **2009**, *74*, 8997-9009**.**

(17) Pagano, N.; Maksimoska, J.; Bregman, H.; Williams, D. S.; Richard D. Webster, R. D.; Meggers, E. *Org. Biomol. Chem.* **2007**, *5*, 1218-1227.

(18) Koning, C. B.; Michael, J. P.; Rousseau, A. L. *J. Chem. Soc., Perkin Trans.* **2000**, *1*, 1705-1713.

(19) Nagao, H. *Inorganica Chimica Acta* **2001**, *320*, 60-66.

(20) Burmeister, J. L. *Coord. Chem. Rev.* **1990**, *105*, 77-133.

(21) Debreczeni, J. E.; Bullock, A. N.; Atilla, G. E.; Williams, D. S.; Bregman, H.; Knapp, S.; Meggers, E. *Angew. Chem., Int. Ed.* **2006**, *45*, 1580-1585.

(22) Meggers, E.; Atilla-Gokcumen, G. E.; Bregman, H.; Maksimoska, J.; Mulcahy, S. P.; Pagano, N.; Williams, D. S. *Synlett* **2007**, *8*, 1177-1189.

(23) Buckingham, D. A. *Coord. Chem. Rev.* **1994**, *135/136*, 587-621.

(24) Paulini, R.; Muller, K.; Diederich, F. *Angew. Chem., Int. Ed.* **2005**, *44*, 1788-1805.

(25) Youn, H.; Kerby, R. L.; Roberts, G. P. *J. Biol. Chem.* **2003**, *278*, 2333-2340.

(26) Kumar, P.; Singh, A. K.; Sharma, S.; Pandey, D. S. *J. Organometallic Chem.* **2009**, *694*, 3643-3652.

(27) Lazarides, T.; Adams, H.; Sykes, D.; Faulkner, S.; Calogero, G.; Ward, M. D. *Dalton Trans.* **2008**, 691-698.

(28) Buckingham, D. A. *Coordination Chemistry*, Chapter 21, **1994**, 256-274.

(29) Kishi, S.; Kato, M. *Inorg. Chem.* **2003**, *42*, 8728-8734.

(30) Vandenburgh, L.; Buck, M. R.; Freedman, D. A. *Inorg. Chem.* **2008**, *47*, 9134-9136.

(31) Cohen, O.; Feinstein, E.; Kimchi, A. *The EMBO Journal* **1997**, *15*, 998-1008.

(32) McNamara, L. K.; Watterson, D. M.; Brunzelle, J. S. *Acta Cryst.* **2009**, *65*, 241-248.

(33) Broomhead, J. A. *Journal of Inorganic and Nuclear Chemistry* **1981**, *43*, 3181-3182.

(34) Vazquez, E.; Davies, W.; Payack, F. *J. Org. Chem.* **2000**, *67*, 7551-7552.

(35) Ph.D. thesis of Bregman, H. University of Pennsylvania **2007**.

Chapter 4: Ruthenium Scaffold with Acyclic Tridentate Ligands as Potential Protein Kinase Inhibitors

Chapter 4.1: Design of TrkA inhibitors with octahedral ruthenium scaffold

Lab colleague Nicholas Pagano published a low nanomolar half-sandwich lactam metallo-pyridocarbazole inhibitor (Figure 4.1) for protein kinase TrkA, which displayed high potency (IC_{50}: 6 nM with 100 μM ATP) and impressive selectivity out of 229 tested human protein kinases.[1]

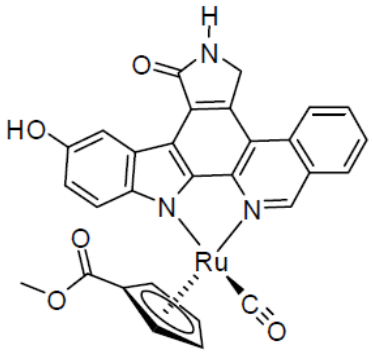

Figure 4.1. Structure of TrkA inhibitor **NP**.

In this scaffold the lactam pharmacophore was developed instead of maleimide to achieve the selectivity of the inhibitor over the other kinases, especially for Pim1.[1] But synthesis of the lactam pharmacophore was a little more complicated than pyridocarbazole synthesis. The strategy of exploring potent, selective protein kinase inhibitors with octahedral ruthenium scaffold has been applied successfully in the previous chapters either containing bidentate ligands or cyclic tridentate ligands. Here a new organoruthenium scaffold containing pyridocarbazole as the hinge-binder plus acyclic tridentate ligands is designed.

Chapter 4.2: Discovery of octahedral lead structure for protein kinase TrkA

2,6-Bis(methyliminomethyl)pyridine was used as starting point. Synthesis of the scaffold is shown in Scheme 4.1. Accordingly, the scaffold was constructed by reacting ruthenium precursor **4.1**[7] with tridentate ligand **4.2**[8] in DMF at 70 °C for 1 hour. Two diastereomers were formed in the reaction in which pyridine of **4.2** was at the position *cis* (**FL792-1**) or *trans* (**FL792-2**) to the indole moiety of pyridocarbazole in 26% and 24% yield, respectively. These two diastereomers can be assigned by ^{1}H NMR spectroscopy as discussed in chapter 2.4. The scaffold is simple and the synthesis is easy to control.

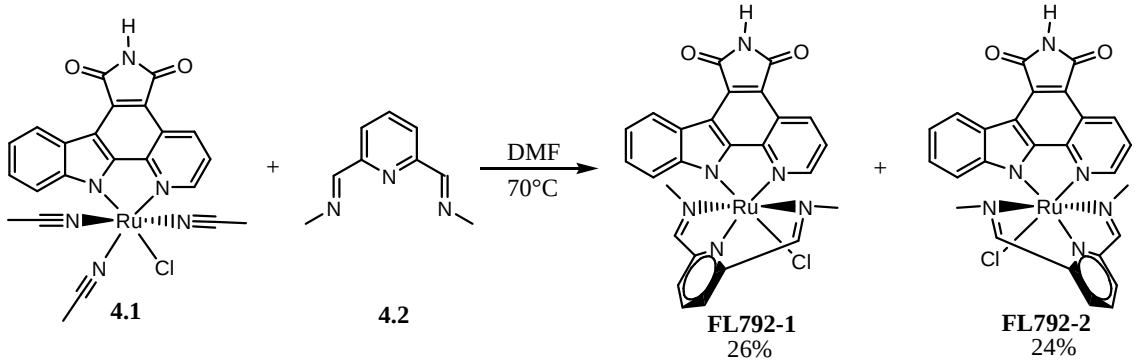

Scheme 4.1. Synthesis of **FL792-1** and **FL792-2**.

Next, **FL792-1** and **FL792-2** were screened against a panel of 227 human protein kinases at the concentration of 1 μM in the presence of 10 μM ATP. The result (see appendix for details) demonstrate that out of 227 tested human protein kinases, this scaffold displayed impressive selectivity profile, with only four kinases (CHK2: 3% with **FL792-2**, GSK3α: 9% with **FL792-1**, Pim1: 6% with **FL792-1** and 8% with **FL792-2**, and TrkA: 4% with **FL792-1**) displaying less than 10% activity under these conditions. It was verified that the IC_{50} value of complex **FL792-1** for TrkA was 480 nM in the presence of 100 μM ATP. Thus, in principle, it might be the lead structure to develop potent and selective TrkA inhibitors with less synthetic effort.

Chapter 4.3: Modification on the pyridocarbazole moiety to improve the potency of TrkA inhibitors

To improve the potency of the TrkA inhibitors, different pyridocarbazoles were used to modify this scaffold. The synthesis of some derivatives is shown in Scheme 4.2.

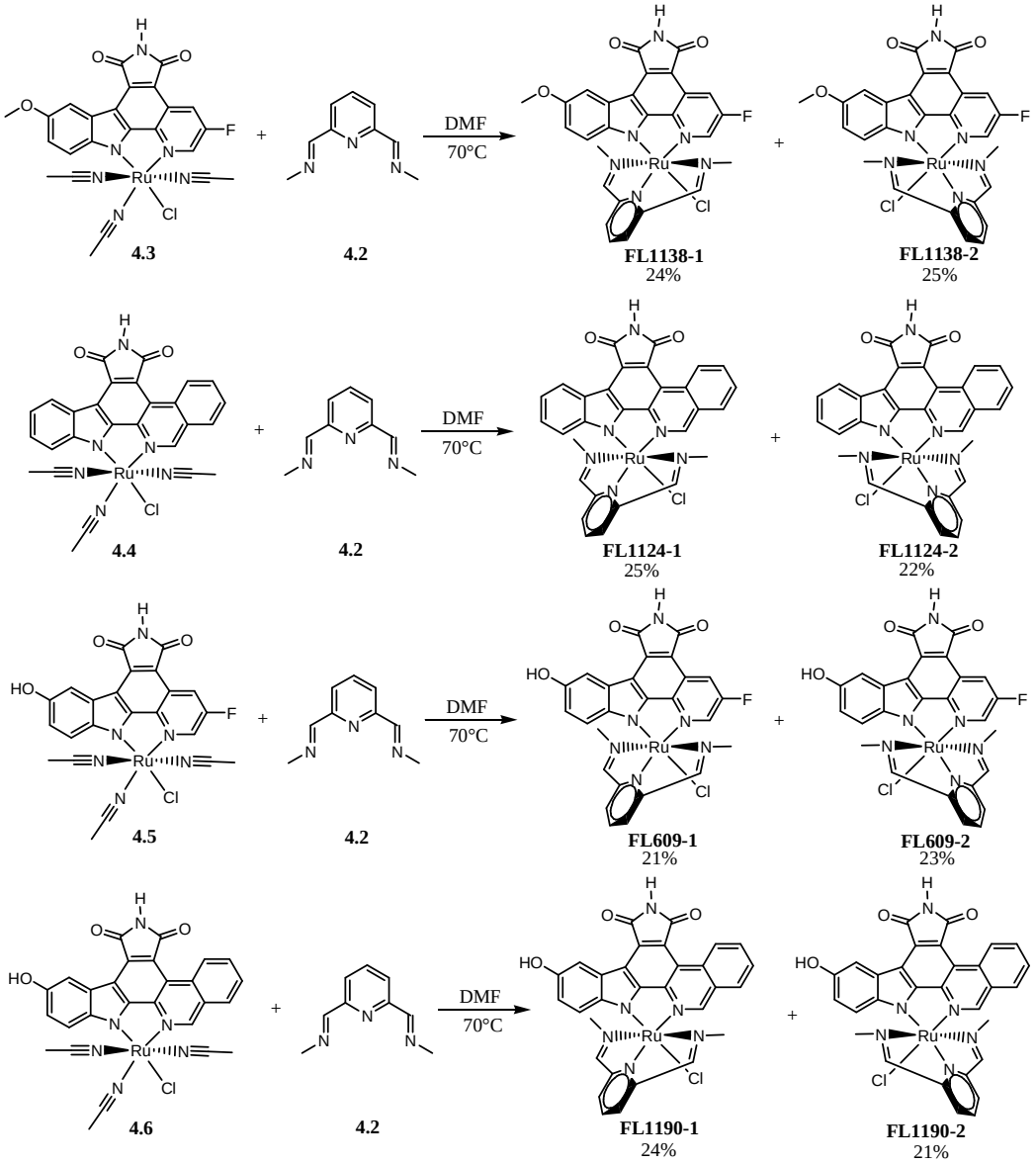

Scheme 4.2. Synthesis of derivatives of TrkA inhibitors. All precursors **4.3-4.6** were used as a mixture of two diastereomers and only one isomer is shown.

Accordingly, ruthenium precursors **4.3-4.6** were synthesized in analogy to precursor **2.3** (chapter 2.2) by first reacting corresponding pyridocarbazole ligand with $[(\eta^6\text{-benzene})RuCl_2]_2$ in the presence of potassium carbonate in acetonitrile affording

the η^6-half-sandwich complex, and then the benzene ring was replaced by three acetonitrile molecules upon UV-photolysis in acetonitrile, followed by TBS-deprotection using TBAF, which afforded the ruthenium precursor complex as a mixture of two diastereomers in each case which was used in the subsequent reaction without separation. Following, the precursors **4.3**-**4.6** were reacted with 1 equiv of tridentate ligand **4.2** in DMF at 70 °C to afford the corresponding ruthenium complexes as a mixture of two diastereomers with the ratio of around 1:1 in each case, which were separated by silica gel chromatography. Complexes **FL1138-1**, **FL1124-1**, **FL609-1**, and **FL1190-1** were tested against TrkA in the presence of 100 μM ATP and the IC_{50} values are listed in Table 4.1.

Table 4.1. IC_{50} values of the derivatives for TrkA in the presence of 100 μM ATP.

	FL1138-1	**FL1124-1**	**FL609-1**	**FL1190-1**
TrkA	>3 μM	360 nM	110 nM	41 nM

The data demonstrate that substitution with a hydrophobic group on the 5-position of indole disfavored TrkA. The IC_{50} value of **FL1138-1** was more than 3 μM, completely inactive for TrkA by modifying pyridocarbazole with a methoxy group on the 5-position of indole and a fluorine on the 3-position of pyridine. The potency of **FL1124-1** (360 nM) was improved slightly by changing the pyridine moiety into an isoquinoline compared to **FL792-1**. Introduction of a hydroxyl group on the 5-position of indole significantly improved the potency. The affinity of **FL609-1** (110 nM) and **FL1190-1** (41 nM) was improved by factors of 4 and 12 compared to **FL792-1**, respectively.

To investigate the selectivity of this scaffold over Pim1, **FL1190-1** was measured against Pim1 and it turned out that this scaffold displayed very high potency for Pim1 as well, with an IC_{50} value of 10 nM in the presence of 100 μM ATP. The key to achieve the selectivity for TrkA inhibitor **NP** over Pim1 is using lactam as pharmacophore ligand instead of pyridocarbazole.[1] Thus, it was envisioned that introducing the lactam ligand in the scaffold (Figure 4.2) might improve the potency for TrkA and selectivity

over Pim1.

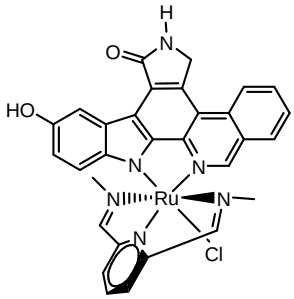

FL1220

Figure 4.2. Structure of complex **FL1220**.

To synthesize complex **FL1220**, a new synthetic route needs to be developed different from the synthesis of **FL792**, as the synthesis of analogous tris-acetonitrile precursor with lactam ligand never succeeded so far due to its lability of the lactam. Ruthenium precursor **4.7**[2,3] similar to 1,4,7-trithiacyclononane precursor (chapter 3) was prepared by refluxing the tridentate ligand **4.2** and $[(\eta^6\text{-benzene})RuCl_2]_2$ in acetonitrile/ethanol (1:2) over 24 hours under nitrogen (Scheme 4.3).

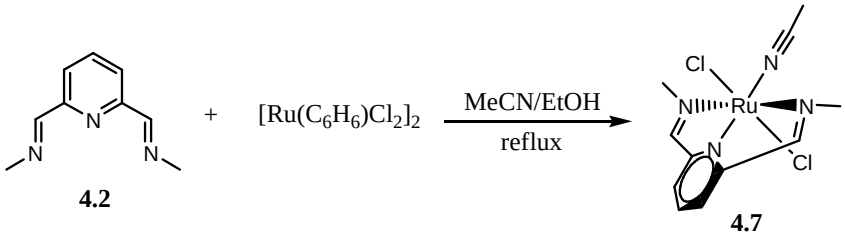

Scheme 4.3. Synthesis of ruthenium precursor **4.7**.

To discover the ideal reaction condition for the synthesis of **FL1220**, pyridocarbazole **3.37** was used as model system. The best condition ever tried is shown in Scheme 4.4. Correspondingly, ligand **3.37** and 1.1 equiv of precursor **4.7** with 1.1 equiv of potassium carbonate as base in ethanol were refluxed for 1.5 hours yielding a mixture of two diastereoisomers which had TBS group on the imide. Interestingly, TBS protected **FL1138-1** was the major isomer and the ratio of these two diastereomers was 1:0.15. Deprection of TBS group was following performed with TBAF in MeCN, after which **FL1138-1** was obtained by silica gel chromatography easily in 49% yield over the two steps.

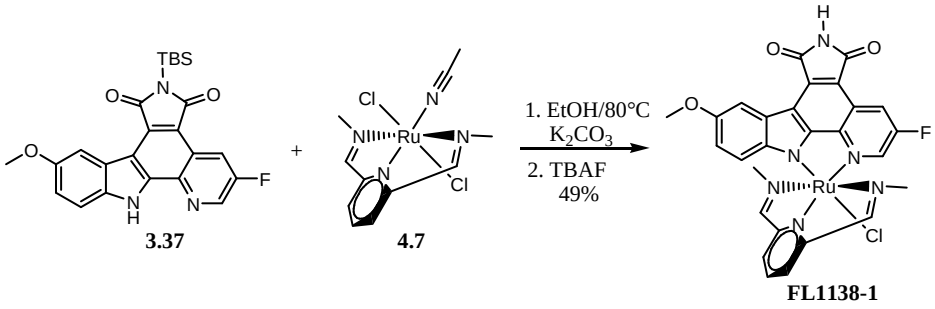

Scheme 4.4. Model system to discovery the reaction condition of pyridocarbazole with ruthenium precursor **4.7**.

Next, synthesis of complex **FL1220** was performed in a similar way (Scheme 4.5) by reacting lactam ligand **4.8**[1] with 1.1 equiv of precursor **4.7** in the presence of 1.1 equiv of potassium carbonate in ethanol, refluxing for 6 hours, followed by TIPS-deprotection with TBAF in MeCN to yield **FL1220** in 18% over two steps. Complex **FL1220** was measured against TrkA. Unfortunately, the IC_{50} value was only 83 nM in the presence of 100 μM ATP, which was decreased by a factor of 14 compared to the published inhibitor **NP**, by replacing the Cp and CO moiety for the tridentate ligand scaffold. Thus, it was decided to not further investigate the scaffold with lactam.

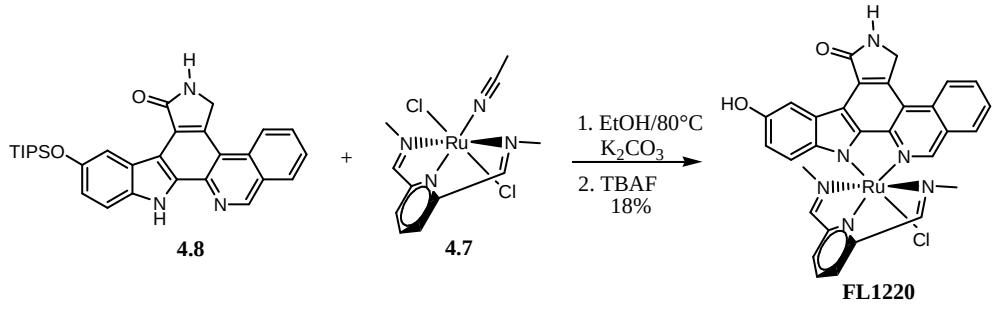

Scheme 4.5. Synthesis of complex **FL1220**.

Chapter 4.4: Applying different tridentate ligands to improve the potency for TrkA inhibitors

Complex **FL1190-1** is a promising scaffold to develop potent TrkA inhibitors but one needs to overcome the lack of selectivity over the Pim1 kinase. It was envisioned that it was possible to improve the potency and selectivity of inhibitors by modifying the tridentate ligand moiety.

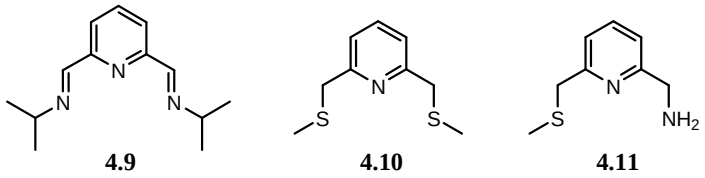

Figure 4.3. Structures of tridentate ligands used to modify TrkA inhibitors.

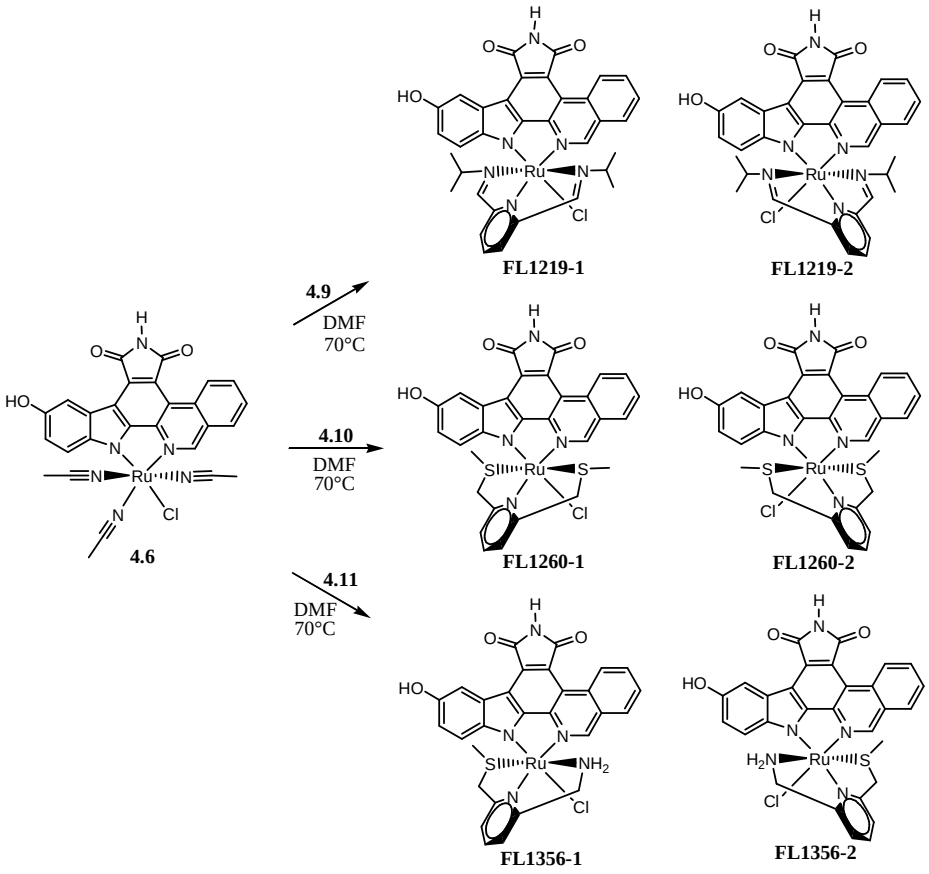

Scheme 4.6. Synthesis of ruthenium complexes with different tridentate ligands from precursor **4.6**. **4.6** was used as a mixture of two diastereomers and only one isomer is shown. **FL1356** was racemic mixture.

The tridentate ligands used to modify the TrkA inhibitors are shown in Figure 4.3 and the synthesis of ruthenium complexes with these ligands from precursor **4.6** is summarized in Scheme 4.6. The coordination reactions were performed in analogy to **FL1190** by stirring equivalent precursor **4.6** and corresponding tridentate ligand in DMF at 70 °C. Two diastereoisomers were obtained in each reaction and all the complexes were tested against TrkA in the presence of 100 μM ATP. The IC_{50} values are listed in Table 4.2.

Table 4.2. IC_{50} values of ruthenium complexes with different tridentate ligands for TrkA in the presence of 100 μM ATP.

	FL1219-1	**FL1219-2**	**FL1260-1**	**FL1260-2**	**FL1356-1**	**FL1356-2**
TrkA	240 nM	300 nM	60 nM	20 nM	102 nM	56 nM

The data demonstrate that the potency of complex **FL1219** for TrkA was decreased significantly compared to **FL1190**, due to the steric clash of the isopropyl group in the ATP binding site and the active site needs to open even more to accommodate the change. The best ligand in the library was **4.10** which improved the affinity of **FL1260-2** for TrkA by a factor of 2 compared to **FL1190-1** with an IC_{50} value of 20 nM. It was in the following measured against Pim1. Unfortunately, it still displayd high affinity for Pim1 with an IC_{50} value of 8 nM in the presence of 100 μM ATP.

Chapter 4.5: Conclusion and Outlook

Scaffold **FL792** was discovered to be very selective by screening it against a panel of 227 human protein kinases. With tridentate ligand 2,6-bis(methyliminomethyl)pyridine, only two diastereoisomers formed in the synthesis. It was a good starting point to develop inhibitors for certain protein kinases due to the simplicity and selectivity of this scaffold.

TrkA was used as the target of complex **FL792-1**. With the modification of the pyridocarbazole, **FL1190-1** was verified to be the most promising scaffold for TrkA with an IC_{50} value of 41 nM in the presence of 100 μM ATP, with a hydroxyl group on the 5-position of indole, and isoquinoline instead of the pyridine. Unfortunately, it also showed high affinity for Pim1 kinase. Following, a series of tridentate ligands were tried to modify the scaffold. It turned out that the potency for TrkA of **FL1260-2** was improved by a factor of 2 compared to **FL1190-1** by using the tridentate ligand of 2,6-bis(methylthiomethyl)pyridine, but still no improvement on the selectivity over Pim1.

Overall, this octahedral scaffold doesn't behave well for TrkA as initially designed so far, and the affinity for TrkA and selectivity over Pim1 of this scaffold need to be improved further. First, a right pharmacophore ligand needs to be developed which disfavors Pim1 but not TrkA. For example, amino group on the 5-position of indole might be an option, and a methoxy group on the 3-position of pyridine instead of isoquinoline moiety. Second, modification of the tridentate ligand moiety might be still interesting. Such as introduction of an ester group on the 4-position of pyridine in the tridentate ligand might form interactions with the backbone of TrkA in the active site, without influence on the symmetry of the tridentate ligand. Last, the chloride ligand in this scaffold can possibly be replaced by other monodentate ligands such as -NO_2, triazole or tetrazole as modifications in PAK1 inhibitors to utilize the extended space to develop more potent and selective TrkA inhibitors. Our group is also trying to use tetradentate ligands to develop octahedral ruthenium inhibitors for TrkA.

Chapter 4.6: References

(1) Pagano, N.; Wong, E. Y.; Breiding, T.; Bregman, H.; Shen, Q.; Diamond, S. L.; Meggers, E. *J. Org. Chem.* **2009**, *74*, 8997-9009.

(2) Britovsek, G. J. P.; England, J.; Spitzmesser, S. K.; White, A. J. P.; Williams, D. J. *Dalton Trans.* **2005**, 945-955.

(3) Cetinkaya, B.; Cetinkaya, E.; Brookhart, M.; White, P. S. *Journal of Molecular Catalysis A: Chemical* **1999**, *142*, 101-112.

(4) Seitz, M.; Kaiser, A.; Tereshchenko, A.; Geiger, C.; Uematsu, Y.; Reiser, O. *Tetrahedron* **2006**, *62*, 9973-9980.

(5) Lai, W.; Berry, S. M.; Bebout, D. C. *Inorg. Chem.* **2006**, *45*, 571-581.

(6) Gergely, J.; Shinya, H.; Katsuya, I.; Yonezo, M. *Chemistry Letters* **2003**, *32*, 882-883.

(7) Bregman, H.; Carroll, P. J.; Meggers, E. *J. Am. Chem. Soc.* **2006**, *128*, 877-884.

(8) Seitz, M.; Kaiser, A.; Tereshchenko, A.; Uematsu, Y.; Reiser, O. *Tetrahedron* **2006**, *62*, 9973-9980.

Chapter 5: Summary and Outlook

A new strategy for the design of selective protein kinase inhibitors has been initiated with chemically inert metallo-pyridocarbazoles scaffold by the group of Prof. Meggers since 2004. The natural product staurosporine was used as lead structure, in which the indolocarbazole alkaloid structure was replaced with simple metal complex to match the shape of the ATP-binding site of protein kinases (Figure 5.1). Whereas previous work was focused mainly on half-sandwich complexes, this thesis had the goal to develop octahedral ruthenium complexes as protein kinase inhibitors.

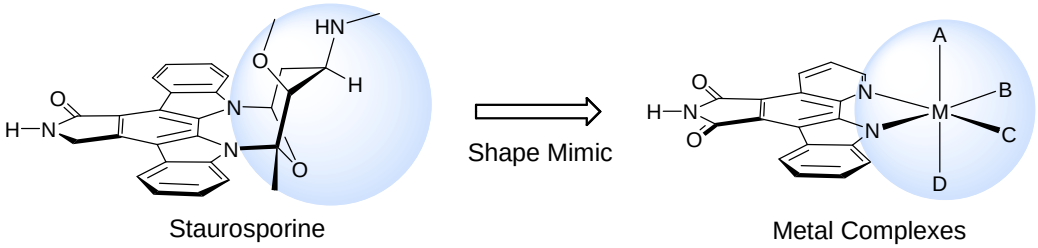

Figure 5.1. Design of ruthenium complexes as protein kinase inhibitors by using staurosporine as lead structure. A, B, C and D represent the organic ligands coordinated to the metal center.

In chapter 2, a new strategy for the design of selective protein kinase inhibitors that makes use of a discrimination between the sizes of ATP-binding sites through the use of rigid, bulky octahedral ruthenium complexes was developed. Protein kinase PAK1 which contains an open ATP-binding site was chosen as a model system and the organoruthenium complex Λ-**FL1422** (Figure 5.2) was developed as an inhibitor for PAK1 with an IC_{50} value of 23 nM in the presence of 1 μM ATP which is the only selective inhibitor with IC_{50} value in the low nanomolar range for PAK1 or other group-I PAK kinases known to date.[1-3]

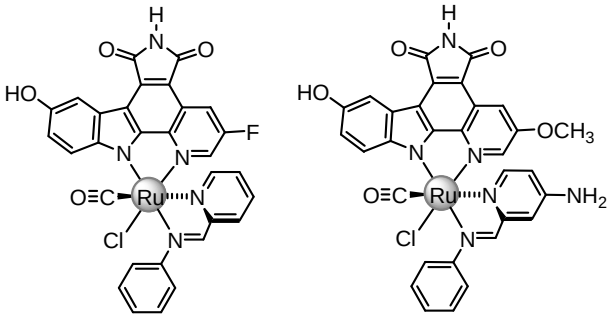

Figure 5.2. Structures of Λ-**FL172** and Λ-**FL1422**.

In addition, a cocrystal structure of Λ-**FL172** bound to PAK1 revealed the molecular details of the binding of this octahedral scaffold to PAK1 (Figure 5.3).[4] Whereas, the maleimide moiety and the indole -OH group together mediate four canonical hydrogen bonds to the backbone of the hinge region. In addition, the monodentate carbonyl ligand establishes interactions to the residues of the glycine-rich loop and the bulky bidentate phenyliminopyridine ligand stretches the entire distance from the N-terminal glycine rich loop to the C-terminal domain. In this bulky octahedral scaffold, the distance between the oxygen atom of the CO ligand and the *para*-carbon of the pyridine in *trans* serves as a rigid yardstick of about 8 Å which can only be well accommodated in the active site of PAK1, but not in most other protein kinases.

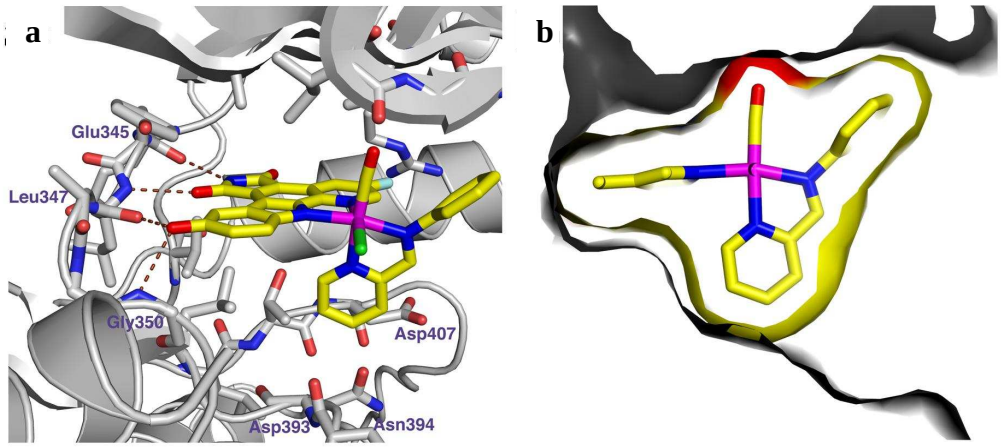

Figure 5.3. Cocrystal structure of Λ-**FL172** with PAK1 (amino acids 249-545, mutation Lys299Arg) at 1.65 Å (by Jasna Maksimoska, Universit of Pennsylvania and The Wistar Institute, Philadelphia, USA). a) Some important interactions. b) Surface view to visualize the shape complementarity of PAK1 and Λ-**FL172**.

In chapter 3, a novel scaffold containing 1,4,7-trithiacyclononane, pyridocarbazole, and monodentate ligand was used to develop protein kinase inhibitors. With the modifications of the ligands coordinated to the ruthenium center, potent and selective octahedral organoruthenium inhibitors for MLCK, DAPK1, and Pim1 were developed, respectively. The inhibitor **FL1528-1** (Figure 5.4) for protein kinase MLCK with an IC_{50} value of 4.4 nM in the presence of 100 μM ATP was discovered based on the screening of the 1,4,7-trithiacyclononane scaffold with different pyridocarbazoles modified with a series of substituents on the indole and/or pyridine. The selectivity profile of **FL1528-1** was verified by screening it against a panel of 230 human protein kinases. The relative configuration of **FL1528-1** was further confirmed by single crystal X-ray diffraction.

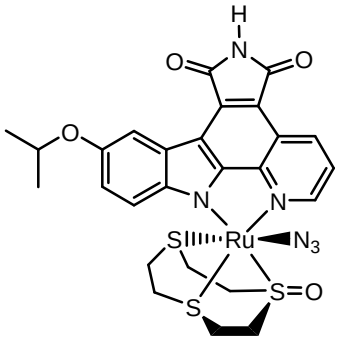

Figure 5.4. Structure of racemic complex **FL1528-1**.

Using a similar scaffold, the ruthenium complex **FL1353-1** (Figure 5.5) was developed and verified to be a very potent and selective inhibitor for DAPK1 with an IC_{50} value of 2 nM in the presence of 100 μM ATP. It showed 84-fold selectivity over Pim1 and was completely inactive for GSK3α.

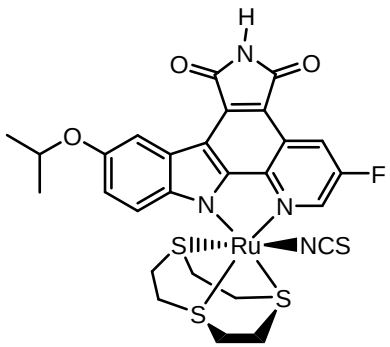

Figure 5.5. Structure of racemic complex **FL1353-1**.

Furthermore, a cocrystal structure of (*R*)-**FL1353-1** bound to DAPK1 obtained by Katja Kräling in collaboration with Yann Geisselbrecht and Prof. Dr. L.-O. Essen revealed the details of interactions of the inhibitor in the DAPK1 active site (Figure 5.6). The structure reveals that the maleimide moiety forms two canonical hydrogen bonds with the hinge region of DAPK1 (Val96 and Glu94) (Figure 5.6a). In addition, the isopropyl ether oxygen at the indole moiety forms a water-mediated contact to the amino acids Lys42, Glu64, and Asp161, and the isopropyl substituent reaches into a small hydrophobic pocket composed out of Lys42, Ile77, Leu93, Leu91, and Leu68 (Figure 5.6b). The 1,4,7-trithiacyclononane ligand points towards the more hydrophilic entrance of the ATP-binding site and occupies the extended chemical space in the domain. The isothiocyanate ligand on the axial position points towards the hydrophobic pocket of the glycin-rich loop forming close contact with the side chain residues of Val27, Ala25, and Lys42, as well as the backbone residues of Gly20, Val26, and Ser21 in the active site.

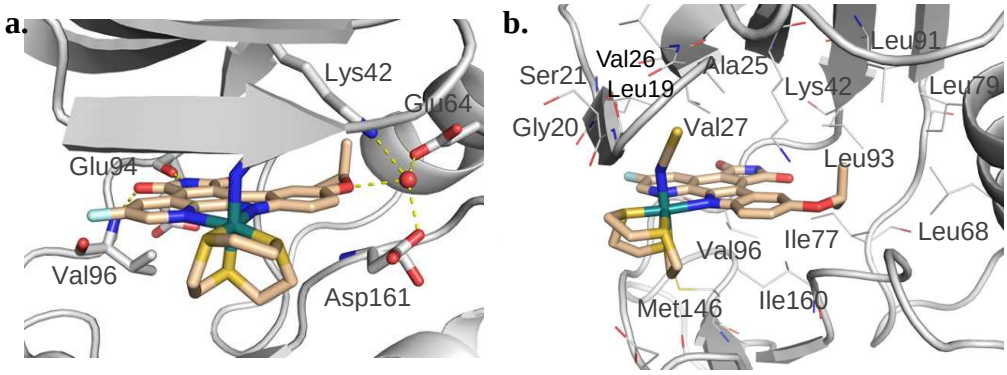

Figure 5.6. Cocrystal structure of (*R*)-**FL1353-1** with DAPK1 at the resolution of 2.2 Å. a) Hydrogen bonding interactions between the hinge region and (*R*)-**FL1353-1**. b) Hydrophobic interactions of (*R*)-**FL1353-1** in the active site. (cocrystallized by Katja Kräling and the cocrystal structure was obtained by Yann Geisselbrecht from the group of Prof. Dr. Lars-Oliver Essen)

The potency and selectivity of metal-containing Pim1 inhibitors was further improved by using an octahedral ruthenium scaffold (Figure 5.7). **FL1360** was discovered to be a very potent inhibitor for Pim1 with an IC_{50} value of 75 pM in the presence of 100 µM ATP. The selectivity of **FL1360** over GSK3α was 106-fold,

significantly improved by switching the cyclopentadienyl group to a 1,4,7-trithiacyclononane compared to the half-sandwich complex **HB2** (2-fold).

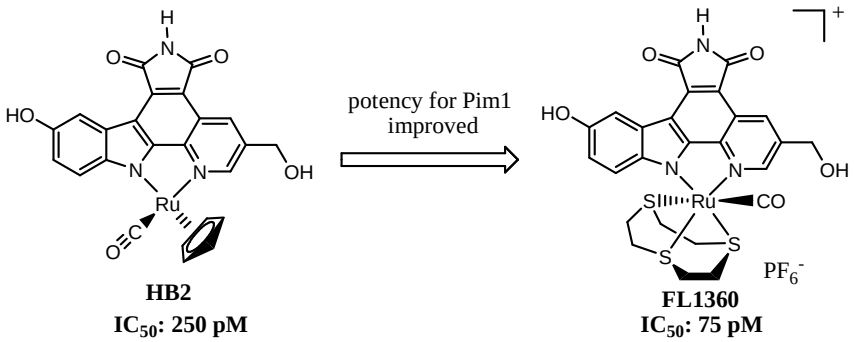

Figure 5.7. Potency for Pim1 was improved by the transformation of half-sandwich scaffold into octahedral scaffold.

In chapter 4, a ruthenium scaffold containing an acyclic tridentate ligand was explored. Complex **FL792** was discovered to be a very selective scaffold by screening it against a panel of 227 human kinases, which was used as a lead structure to develop the TrkA inhibitors. Based on the modifications of pyridocarbazole and tridentate ligand, **FL1260-2** (Figure 5.8) showed high potency for TrkA with an IC_{50} value of 20 nM in the presence of 100 μM ATP, but lacking selectivity over Pim1. The potency and selectivity of TrkA inhibitors with this scaffold need to be further improved.

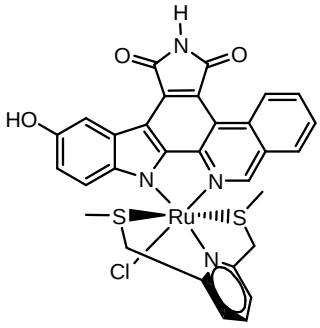

Figure 5.8. Structure of complex **FL1260-2**.

Organoruthenium inhibitors for MLCK, DAPK1, and Pim1 were developed with a same scaffold. The potency and selectivity of the inhibitors were achieved by modifying the surrounding ligands of ruthenium center, which further proved that the metal center only exerts a purely structural role in the kinase active site and controls the orientation

of the organic ligands. The success of the development of potent and selective octahedral organoruthenium inhibitors verified the versatility of the approach initiated by our group to the design of protein kinase inhibitors with metal complexes as structural scaffolds.

Recently, notable progress has been made in the field of medicinal bioinorganic chemistry and many new approaches to the design of novel metal-based anticancer drugs are emerging as some examples mentioned previously.[5] Therefore, it will be very interesting to evaluate whether these organoruthenium inhibitors can be utilized as potential therapeutic agents.

Although ruthenium has low toxicity,[6,7] it is of great interest to explore protein kinase inhibitors with stable iron complexes. Iron is a necessary trace element found in nearly all living organisms and participates in many biological oxidations and transportations. The potential drawback of iron complexes is that they are usually not as stable as ruthenium complexes. However, multidentate ligands (tridentate or tetradentate ligands) can be used to stabilize the iron complexes, such as 2,6-bis(methyliminomethyl)-pyridine or its derivatives.[8,9] It might be also possible to extend the strategy to other transition metals, as long as the metal complexes formed are stable under physiological conditions. Our group already published metal complexes containing osmium or iridium as protein kinase inhibitors.[10,11]

The here developed methodology might be also applicable to other classes of targets. Large target sites are beneficial because our approach has an advantage to design three-dimensional structures from a metal center in a very convenient fashion.

References

(1) Nheu, T. V.; Hirokawa, Y.; Tamaki, K.; Florin, L.; Schmitz, M. L. *The Cancer Journal* **2002**, *8*, 328-336.

(2) Porchia, L. M.; Guerra, M.; Wang, Y. C.; Shinohara, M. *Mol. Pharmacol.* **2007**, *72*, 1124-1131.

(3) Bokoch, G. M. *Chem. Biol.* **2008**, *15*, 305-306.

(4) Maksimoska, J.; Feng, L.; Harms, K.; Yi, C.; Kissil, J.; Marmorstein, R.; Meggers, E. *J. Am. Chem. Soc.* **2008**, *130*, 15764-15765.

(5) Rijt, S. H.; Sadler, P. J. *Drug Discovery Today* **2009**, *14*, 1089-1097.

(6) Hartinger, C. G.; Zorbas-Seifried, S.; Jakupec, M. A.; Kynast, B.; Zorbas, H.; Keppler, B. K. *J. Inorg. Biochem.* **2006**, *100*, 891-904.

(7) Dyson, P. J.; Sava, G. *Dalton Trans.* **2006**, *16*, 1929-1933.

(8) Kendall, A. J.; Zakharov, L. N.; Gillbertson, J. D. *Inorganic Chemistry* **2010**, *49*, 8656-8658.

(9) Campora, J.; Cartes, M. A.; Rodriguez-Delgado, A. Naz, A. M.; Palma, P.; Perez, C. M.; del Rio, D. *Inorganic Chemistry* **2009**, *48*, 3679-3691.

(10) Maksimoska, J.; Williams, D. S.; Atilla-Gokcumen, G. E.; Smalley, K. S. M.; Meggers, E. *Chem. Eur. J.* **2008**, *14*, 4816-4822.

(11) Wilbuer, A.; Vlecken, D. H.; Schmitz, D. J.; Kräling, K.; Harms, K.; Bagowski, C. P.; Meggers, E. *Angew. Chem., Int. Ed.* **2010**, *49*, 3839-3842.

Chapter 6: Experimental Section

Chapter 6.1: Synthesis

General Procedures. NMR spectra were recorded on a Bruker AM-400 (400 MHz) AM-500 (500 MHz), or AV-300 (300 MHz) spectrometer. Low-resolution mass spectra were obtained on an LC platform from Micromass using the ESI technique. High-resolution mass spectra were obtained on a Micromass Autospec instrument using either CI or ES ionization or a Thermo Finnigan LTQ FT instrument using ES ionization. Infrared spectra were recorded on a Bruker IFS 88 or Perkin Elmer 1600 series FTIR spectrometer. Photolysis was performed with a medium pressure Hg lamp (150 W or 700 W). Microwave reactions were conducted using a CEM Discover reactor. CD spectra were recorded on a JASCO J-810 spectropolarimeter. Solvents and reagents were supplied from Aldrich, Acros, or Strem. Reactions were performed under an atmosphere of nitrogen unless otherwise specified. Compound **2.1**,[6] 5-isopropyloxyindole **3.1**[1], 1,4,7-trithiacyclodecan-9-one[4], 5-methylthioindole **3.12**[2], bis-allyl-2-bromo-5-aminopyridine **3.23**[3], TBS-protected pyridocarbazole **3.69**[6], **3.81**, **3.85**, **3.87**[5], **4.1**[7], **4.4**[8], and **4.5**[9] were synthesized as published. NMR standards used are as follows: (^{1}H NMR) $CDCl_3$: 7.26 ppm, CD_3CN: 1.94 ppm, DMSO-d_6: 2.50 ppm, $(CD_3)_2CO$: 2.05 ppm, DMF-d_7: 8.03, 2.92, 2.75 ppm. (^{13}C NMR) $CDCl_3$: 77.23 ppm, DMSO-d_6: 39.51 ppm, DMF-d_7: 163.15, 34.89, 29.76 ppm.

Chapter 6.1.1: Synthesis of PAK1 inhibitors

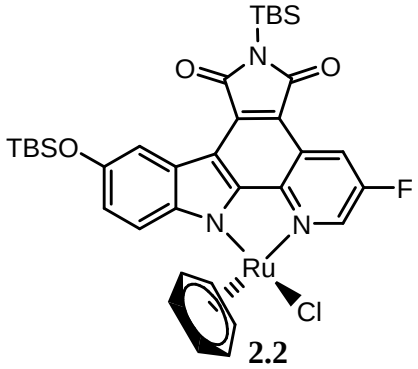

2.2

Complex 2.2. A suspension of the ligand **2.1** (180 mg, 0.33 mmol), K_2CO_3 (50 mg, 0.36

mmol), and $[RuCl_2(\eta^6\text{-}C_6H_6)]_2$ (123 mg, 0.25 mmol) in CH_3CN (50 mL) was purged with nitrogen and stirred at 50 °C for 3 h. The resulting dark red suspension was dried *in vacuo* and the crude material was adsorbed onto silica gel and subjected to silica gel chromatography with dichloromethane : methanol (first 50:1, then 35:1) as the eluting solvent. The half-sandwich complex **2.2** was isolated as a dark red solid (220 mg, 88%). ^{1}H NMR (300 MHz, CD_3CN): δ (ppm) 9.46 (t, J = 2.6 Hz, 1H), 8.86 (dd, J = 9.4, 2.3 Hz, 1H), 8.25 (d, J = 2.5 Hz, 1H), 7.88 (d, J = 9.1 Hz, 1H), 7.23 (dd, J = 8.8, 2.6 Hz, 1H), 6.08 (s, 6H), 1.07 (s, 9H), 1.01 (s, 9H), 0.55 (s, 6H), 0.30 (s, 6H). ^{13}C NMR (75.5 MHz, $CDCl_3$): δ (ppm) 175.1, 173.9, 157.1 (d, $J_{C\text{-}F}$ = 251.4 Hz), 153.0, 150.2, 146.5, 140.9, 140.4, 140.2, 133.9, 125.0, 121.5 (d, $J_{C\text{-}F}$ = 8.4 Hz), 120.7, 119.9 (d, $J_{C\text{-}F}$ = 19.9 Hz), 115.0, 114.6, 113.9 (d, $J_{C\text{-}F}$ = 4.9 Hz), 83.4, 26.5, 26.0, 19.1, 18.4, -4.0, -4.2. IR (film): ν (cm^{-1}) 2955, 2930, 2857, 1746, 1688, 1562, 1462, 1335, 1310, 1296, 1258, 1238, 829. HRMS calculated for $C_{35}H_{41}FN_3O_3Si_2Ru$ $(M - Cl)^+$ 728.1708, found $(M - Cl)^+$ 728.1701.

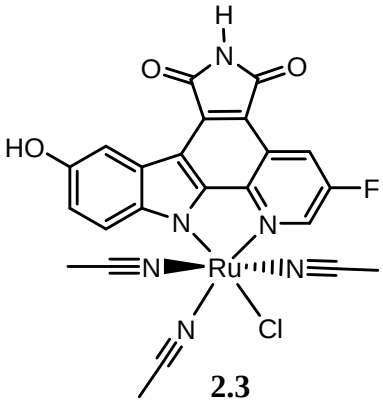

2.3

Complex 2.3. A red solution of **2.2** (180 mg, 0.24 mmol) in CH_3CN (220 mL) was purged with nitrogen for 10 min and then irradiated with a mercury medium pressure lamp (150W, pyrex filter) for 3 hours while nitrogen was bubbled through the solution. The resulting dark green solution was dried *in vacuo* and the crude material was adsorbed onto silica gel and subjected to silica gel chromatography with dichloromethane : methanol (first 75:1, then 35:1). The combined product eluents were isolated as a mixture of two diastereoisomers (175 mg, 91%). To the stirred green solution of the mixture (175 mg, 0.22 mmol) in CH_3CN was added tetrabutylammonium

fluoride (660 µL, 1 M in THF, 0.66 mmol) at 0 °C, and the solution was stirred at 0 °C for 5 min. To the resulting green solution was added glacial acetic acid (38 µL, 0.66 mmol) and it was stirred for 2 min at 0 °C. The solution was dried *in vacuo* and the crude material was adsorbed onto silica gel and subjected to silica gel chromatography with dichloromethane : methanol (first 50:1, then 20:1) to yield the precursor complex **2.3** (57 mg, 45%) and a second diastereoisomer in lower amounts (31 mg, 25%). Analytical data for the main diastereomer **2.3**: ^{1}H NMR (400 MHz, DMF-d_7): δ (ppm) 10.88 (s, 1H), 9.53 (t, J = 2.9 Hz, 1H), 9.27 (s, 1H), 8.65 (dd, J = 9.5, 2.5 Hz, 1H), 8.28 (d, J = 2.4 Hz, 1H), 7.81 (d, J = 8.7 Hz, 1H), 7.17 (dd, J = 8.7, 2.5 Hz, 1H), 3.04 (s, 3H), 2.27(s, 6H). ^{13}C NMR (100.6 MHz, DMF-d_7): δ (ppm) 171.4, 171.1, 157.1 (d, $J_{C\text{-}F}$ = 246.0 Hz), 156.3, 152.2, 148.0, 144.1, 141.2, 140.9, 131.6, 127.4, 125.1, 122.8, 121.1 (d, $J_{C\text{-}F}$ = 8.5 Hz), 116.3 (d, $J_{C\text{-}F}$ = 13.6 Hz), 115.5 (d, $J_{C\text{-}F}$ = 20.6 Hz), 115.1, 110.1 (d, $J_{C\text{-}F}$ = 4.6 Hz), 109.0 (the methyl group peaks were hidden by the solvent peak). IR (film): v (cm^{-1}) 2277, 1721, 1649, 1529, 1497, 1469, 1437, 1384, 1083, 1028, 774. HRMS calculated for $C_{23}H_{16}FN_6O_3Ru$ (M - Cl)$^+$ 545.0306, found (M - Cl)$^+$ 545.0307.

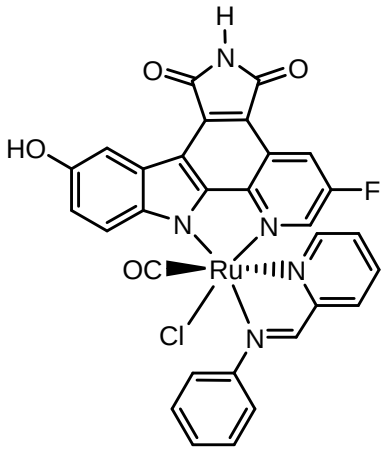

FL172

Complex FL172. A solution of precursor complex **2.3** (7 mg, 0.012 mmol) in DMF (2 mL) was purged with CO gas for 5 min, then stirred at 75 °C under an atmosphere of CO for 1 hour. To the resulting solution was added 2-(phenylaminomethyl)pyridine (120 µL, 100 mM in DMF), then the solution was stirred at 95 °C under an atmosphere of nitrogen for 1.5 hours, after which the purple solution was dried under high vacuum. The crude material was adsorbed onto silica gel and subjected to silica gel

chromatography with dichloromethane : methanol (50:1) to yield compound **FL172** as a single diastereomer (3.5 mg, 44%). ^{1}H NMR (300 MHz, acetone-d_6): δ (ppm) 9.89 (s, 1H), 9.22 (s, 1H), 8.69 (dd, J = 9.4, 2.4 Hz, 1H), 8.59 (d, J = 8.9 Hz, 1H), 8.38 (dt, J = 7.7, 0.9 Hz, 1H), 8.36 (t, J = 2.6 Hz, 1H), 8.31 (dd, J = 2.5, 0.4 Hz, 1H), 8.21 (s, 1H), 8.16 (td, J = 7.6, 1.9 Hz, 1H), 8.13 (m, 2H), 7.69 (m, 2H), 7.59 (m, 1H), 7.48 (m, 1H), 7.44 (td, J = 5.4, 1.3 Hz, 1H), 7.15 (dd, J = 8.9, 2.6 Hz, 1H). ^{13}C NMR (100.6 MHz, DMSO-d_6): δ (ppm) 200.7, 170.4 (d, $J_{C\text{-}F}$ = 16.9 Hz), 169.7, 157.6, 155.1, 154.4, 153.1, 151.8, 147.5 (d, $J_{C\text{-}F}$ = 217.4 Hz), 141.3 (d, $J_{C\text{-}F}$ = 33.8 Hz), 140.5, 139.7, 131.7, 129.5, 129.1 (d, $J_{C\text{-}F}$ = 23.9 Hz), 128.3, 124.3, 122.4, 120.3 (d, $J_{C\text{-}F}$ = 8.3 Hz), 117.9, 117.6 (d, $J_{C\text{-}F}$ = 19.6 Hz), 116.5, 114.4, 111.0, 108.1. IR (film): ν (cm^{-1}) 3199, 2919, 1962, 1687, 1650, 1499, 1469, 1428, 1405, 1384, 1335, 1028. HRMS calculated for $C_{30}H_{17}ClFN_5O_4RuNa$ $(M + Na)^+$ 689.9889, found $(M + Na)^+$ 689.9906.

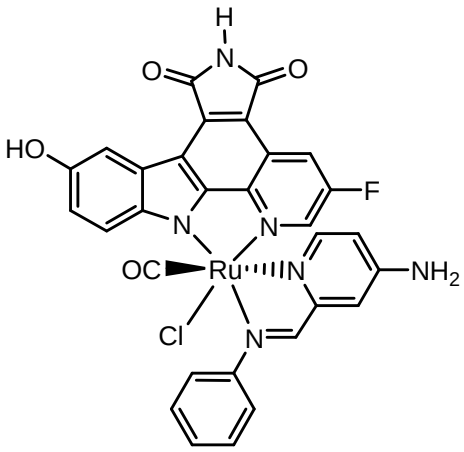

FL411

Complex FL411. A solution of precursor complex **2.3** (7 mg, 0.012 mmol) in DMF (2 mL) was purged with CO gas for 5 min, then stirred at 75 °C under an atmosphere of CO for 1 hour. To the resulting solution was added 2-(phenylaminomethyl)-4-aminopyridine (120 µL, 100 mM in DMF), then the solution was stirred at 95 °C under an atmosphere of nitrogen for 3 hours, after which the purple solution was dried under high vacuum. The crude material was adsorbed onto silica gel and subjected to silica gel chromatography with dichloromethane : methanol (35:1) to obtain complex **FL411** (2.5 mg, 30%). ^{1}H NMR (300 MHz, acetone-d_6): δ (ppm) 9.86 (s, 1H), 8.90(s, 1H), 8.70 (dd, J = 9.4, 2.4 Hz, 1H), 8.60 (d, J = 8.9 Hz, 1H), 8.32 (t, J = 2.6 Hz, 1H),

8.29 (d, J = 2.3 Hz, 1H), 8.18 (s, 1H), 8.09 (m, 2H), 7.65 (m, 2H), 7.54 (m, 1H), 7.45 (d, J = 2.5 Hz, 1H), 7.14 (dd, J = 8.9, 2.6 Hz, 1H), 6.78 (d, J = 6.3 Hz, 1H), 6.53 (s, 2H), 6.43 (dd, J = 6.3, 2.5 Hz, 1H). ^{13}C NMR (100.6 MHz, DMSO-d_6): δ (ppm) 200.6, 170.6, 170.4 (d, $J_{C\text{-}F}$ = 13.4 Hz), 157.6, 155.3 (d, $J_{C\text{-}F}$ = 211.5 Hz), 155.1, 153.2 (d, $J_{C\text{-}F}$ = 5.3 Hz), 151.7, 147.3, 146.5, 140.6, 140.5 (d, $J_{C\text{-}F}$ = 33.4 Hz), 131.7, 129.3, 128.6, 124.1, 122.4, 120.2 (d, $J_{C\text{-}F}$ = 8.5 Hz), 118.0, 117.3 (d, $J_{C\text{-}F}$ = 20.1 Hz), 116.3, 114.3, 114.2, 110.6 (d, $J_{C\text{-}F}$ = 4.9 Hz), 110.4, 108.0. IR (film): ν (cm^{-1}) 3312, 3204, 1960, 1715, 1470, 1454, 1385, 1335, 1099, 1024, 403. HRMS calculated for $C_{30}H_{18}ClFN_6O_4RuNa$ $(M + Na)^+$ 704.9998, found $(M + Na)^+$ 704.9991.

Complexes 2.7 and 2.8. A solution of precursor complex **2.5** or **2.6** (10 mg, 0.016 mmol) in 2.5 ml solvent was purged with CO gas for 5 min, then stirred at 75 °C under an atmosphere of CO for 1 hour. To the resulting solution was added bipyridine (160 μL, 100 mM in toluene), then the solution was stirred at 95 °C under an atmosphere of nitrogen for 1.5 hours, after which the solution was dried under high vacuum. The crude material was adsorbed onto silica gel and subjected to silica gel chromatography with toluene : acetone (3:1) to yield complexes **2.7** and **2.8.** Yields and diastereoselectivities depend on the used solvent. Toluene/$CHCl_3$ (4:1): 67% overall yield, **2.8**:**2.7** = 2.4:1; DMF: 62% overall yield, **2.8**:**2.7** = 7:1; EtOH/$CHCl_3$ (4:1): 55% overall yield, **2.8**:**2.7** = 20:1.

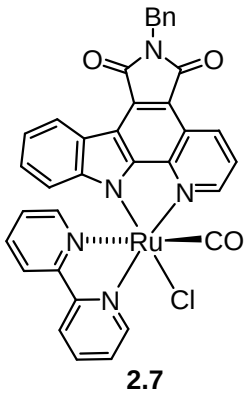

2.7

Complex 2.7: ^{1}H NMR (300 MHz, $CDCl_3$): δ (ppm) 9.78 (d, J = 8.9 Hz, 1H), 9.52 (dd, J = 5.1, 1.1 Hz, 1H), 9.39 (dd, J = 8.4, 1.1 Hz, 1H), 8.75 (d, J = 7.2 Hz, 1H), 8.25 (d, J = 8.1 Hz, 1H), 8.15-8.09 (m, 2H), 7.86-7.77 (m, 2H), 7.69 (m, 1H), 7.53-7.50 (m, 2H),

7.46 (d, *J* = 4.4 Hz, 1H), 7.35-7.30 (m, 2H), 7.25-7.06 (m, 4H), 5.88 (d, *J* = 8.1 Hz, 1H), 4.96 (s, 2H). ^{13}C NMR (100.6 MHz, $CDCl_3$): δ (ppm) 200.8, 169.9, 169.5, 157.5, 157.2, 154.9, 151.2, 148.3, 143.9, 138.7, 137.4, 137.3, 134.8, 128.8, 128.6, 127.7, 126.8, 126.7, 126.2, 125.2, 124.2, 123.2, 122.8, 122.2, 121.9, 119.5, 116.2, 115.5, 113.4, 113.1, 112.5, 41.6. IR (film): ν (cm^{-1}) 2924, 2853, 1957, 1749, 1696, 1495, 1471, 1420, 1387, 1341, 1229, 739. HRMS calculated for $C_{35}H_{22}ClN_5O_3RuNa$ $(M + Na)^+$ 720.0347, found $(M + Na)^+$ 720.0351.

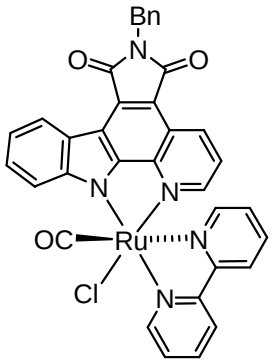

2.8

Complex 2.8: ^{1}H NMR (300 MHz, DMSO-d_6): δ (ppm) 9.49 (d, *J* = 4.7 Hz, 1H), 8.97 (dd, *J* = 8.4, 1.0 Hz, 1H), 8.82 (d, *J* = 8.1 Hz, 1H), 8.77 (d, *J* = 5.0 Hz, 1H), 8.74 (d, *J* = 5.4 Hz, 1H), 8.51 (d, *J* = 5.4 Hz, 1H), 8.31 (td, *J* = 8.0, 1.3 Hz, 1H), 8.11 (m, 1H), 7.85 (m, 1H), 7.73 (dd, *J* = 5.2, 1.0 Hz, 1H), 7.56-7.47 (m, 2H), 7.42-7.24 (m, 8H), 4.87 (s, 2H). ^{13}C NMR (100.6 MHz, DMSO-d_6): δ (ppm) 201.9, 169.01, 168.96, 156.4, 156.0, 154.6, 153.6, 152.4, 150.1, 148.1, 142.9, 139.7, 138.3, 137.3, 133.3, 129.8, 128.6, 127.7, 127.4, 127.3, 127.1, 126.2, 124.3, 123.7, 123.6, 123.5, 123.4, 120.7, 119.7, 117.5, 115.1, 111.6, 40.7. IR (film): ν (cm^{-1}) 2923, 2853, 1955, 1749, 1696, 1495, 1468, 1419, 1387, 1351, 1231, 760. HRMS calculated for $C_{35}H_{22}ClN_5O_3RuNa$ $(M + Na)^+$ 720.0347, found $(M + Na)^+$ 720.0347.

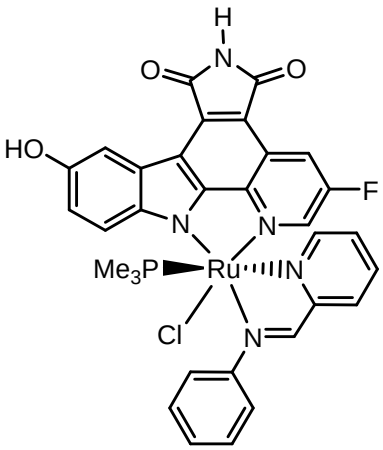

FL637

Complex FL637. To a solution of precursor complex **2.3** (7 mg, 0.012 mmol) in DMF (2 mL) was added PMe_3 (12 µL, 1 M in THF), then stirred at 45 °C under nitrogen for 1 hour. To the resulting solution was added 2-(phenylaminomethyl)pyridine (120 µL, 100 mM in DMF), then the solution was stirred at 95 °C under an atmosphere of nitrogen for 2 hours, after which the solution was dried under high vacuum. The crude material was adsorbed onto silica gel and subjected to silica gel chromatography with dichloromethane : methanol (50:1) to obtain complex **FL637** (2.2 mg, 26%). ^{1}H NMR (300 MHz, acetone-d_6): δ (ppm) 9.75 (s, 1H), 9.18(s, 1H), 8.69 (d, J = 8.8 Hz, 1H), 8.50-8.47 (m, 2H), 8.31 (d, J = 2.5 Hz, 1H), 8.24 (d, J = 7.8 Hz, 1H), 8.15 (s, 1H), 7.91-7.83 (m, 3H), 7.64-7.59 (m, 2H), 7.52 (m, 1H), 7.37 (m, 1H), 7.21 (m, 1H), 7.13 (dd, J = 8.8, 2.6 Hz, 1H), 0.48 (d, J = 9.1 Hz, 9H).

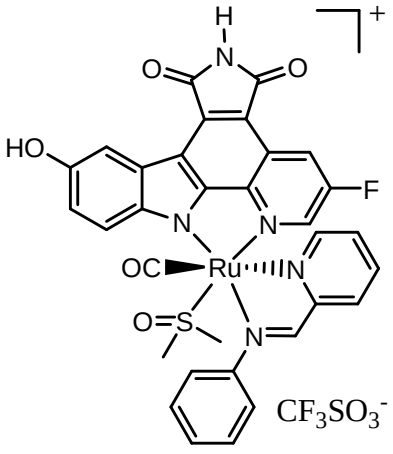

FL866

Complex FL866. To a solution of complex **FL172** (7 mg, 0.01 mmol) in DMSO (0.35 mL) was added silver trifluoromethanesulfonate (32.3 mg, 0.126 mmol), then stirred at

95 °C under nitrogen for 7 hours, after which the solution was dried under high vacuum. The crude material was adsorbed onto silica gel and subjected to silica gel chromatography with dichloromethane : methanol (10:1) to obtain complex **FL866** (4.9 mg, 54%). ^{1}H NMR (300 MHz, acetone-d_6): δ (ppm) 10.07 (s, 1H), 9.62(s, 1H), 8.90 (dd, *J* = 9.1, 2.4 Hz, 1H), 8.69 (t, *J* = 2.5 Hz, 1H), 8.58 (d, *J* = 7.3 Hz, 1H), 8.47 (d, *J* = 2.5 Hz, 1H), 8.41-8.37 (m, 2H), 8.33 (td, *J* = 7.8, 1.5 Hz, 1H), 8.29-8.26 (m, 2H), 7.81-7.72 (m, 4H), 7.63 (m, 1H), 7.22 (dd, *J* = 9.0, 2.7 Hz, 1H), 3.59 (s, 3H), 3.26 (s, 3H). HRMS calculated for $C_{32}H_{23}FN_5O_5SRu$ $(M)^+$ 710.0442, found $(M)^+$ 709.6657.

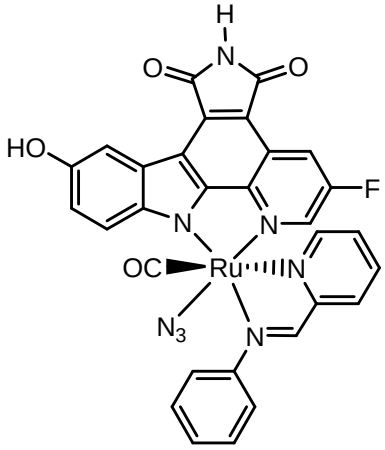

FL922

Complex FL922. To a solution of complex **FL172** (7 mg, 0.01 mmol) in DMSO (0.35 mL) was added silver trifluoromethanesulfonate (32.3 mg, 0.126 mmol), then stirred at 95 °C under nitrogen for 7 hours, after which the solution was dried under high vacuum. The residue was dissolved in DMF (1.5 mL), then sodium azide (11.6 mg, 0.178 mmol) was added. The mixture was stirred at 85 °C under nitrogen for 1 hour, after which the solution was dried under high vacuum. The crude material was adsorbed onto silica gel and subjected to silica gel chromatography with dichloromethane : methanol (first 20:1, then 15:1) to obtain complex **FL922** (4.7 mg, 66%). ^{1}H NMR (300 MHz, acetone-d_6): δ (ppm) 9.92 (s, 1H), 9.35(s, 1H), 8.70 (dd, *J* = 9.4, 2.4 Hz, 1H), 8.45 (t, *J* = 2.5 Hz, 1H), 8.41 (m, 1H), 8.32 (d, *J* = 2.3 Hz, 1H), 8.19 (td, *J* = 7.7, 1.6 Hz, 1H), 8.12-8.05 (m, 4H), 7.75-7.70 (m, 2H), 7.63 (m, 1H), 7.48 (m, 1H), 7.37 (m, 1H), 7.21 (dd, *J* = 8.8, 2.5 Hz, 1H).

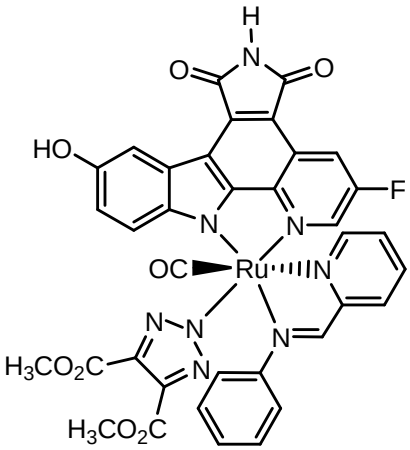

FL931

Complex FL931. To a solution of complex **FL922** (4.2 mg, 0.006 mmol) in DCM/DMF (2.5 mL/0.5 mL) was added dimethyl acetylenedicarboxylate (13.3 mg, 0.094 mmol), then stirred at room temperature under nitrogen for 2 hours, after which the solution was dried under high vacuum. The crude material was adsorbed onto silica gel and subjected to silica gel chromatography with dichloromethane : methanol (first 20:1, then 10:1) to obtain complex **FL931** in quantitive yield. ^{1}H NMR (300 MHz, acetone-d_6): δ (ppm) 9.94 (s, 1H), 9.26 (s, 1H), 8.76 (dd, J = 9.4, 2.4 Hz, 1H), 8.46 (t, J = 2.5 Hz, 1H), 8.37 (m, 1H), 8.30 (m, 1H), 8.22-8.16 (m, 2H), 8.02-7.99 (m, 2H), 7.68-7.63 (m, 2H), 7.57 (m, 1H), 7.46-7.44 (m, 2H), 6.92 (dd, J = 8.9, 2.5 Hz, 1H), 6.39 (d, J = 8.9 Hz, 1H), 3.77 (s, 6H). HRMS calculated for $C_{36}H_{23}FN_8O_8RuNa$ $(M + Na)^+$ 839.0559, found $(M + Na)^+$ 839.0565.

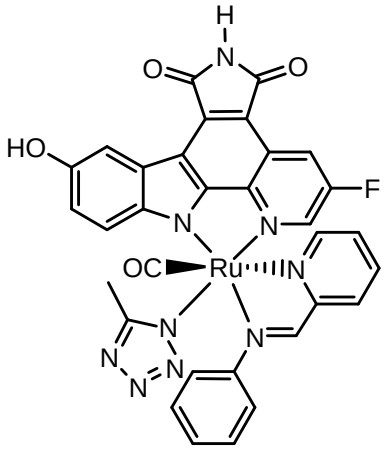

FL864

Complex FL864. To a solution of complex **FL172** (8.5 mg, 0.013 mmol) in acetonitrile (1 mL) was added silver trifluoromethanesulfonate (90 mg, 0.35 mmol), then refluxed

under nitrogen overnight, after which the solution was dried under high vacuum. The residue was dissolved in DMF (1.5 mL), then sodium azide (23.2 mg, 0.357 mmol) was added. The mixture was stirred at 85 °C under nitrogen for 0.5 hour, after which the solution was dried under high vacuum. The crude material was adsorbed onto silica gel and subjected to silica gel chromatography with dichloromethane : methanol (10:1) to obtain complex **FL864** (3 mg, 32%). ^{1}H NMR (300 MHz, acetone-d_6): δ (ppm) 9.90 (s, 1H), 9.21 (s, 1H), 8.76 (dd, *J* = 9.4, 2.4 Hz, 1H), 8.44 (t, *J* = 2.5 Hz, 1H), 8.37 (dt, *J* = 7.7, 1.0 Hz, 1H), 8.29 (dd, *J* = 2.6, 0.3 Hz, 1H), 8.22-8.16 (m, 2H), 8.02-7.99 (m, 2H), 7.68-7.63 (m, 2H), 7.56 (m, 1H), 7.47-7.45 (m, 2H), 6.89 (dd, *J* = 8.9, 2.5 Hz, 1H), 6.16 (d, *J* = 8.9 Hz, 1H), 2.35 (s, 3H). HRMS calculated for $C_{32}H_{21}FN_9O_4Ru$ $(M + H)^+$ 716.0739, found $(M + H)^+$ 716.0734.

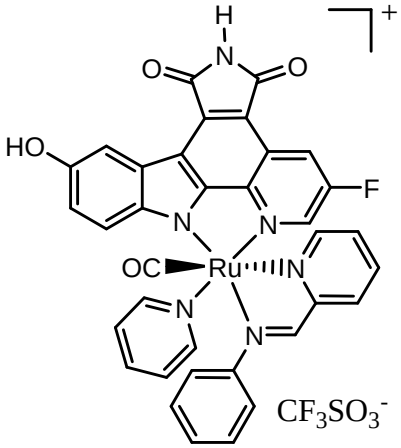

FL889

Complex FL889. To a solution of complex **FL172** (8.5 mg, 0.013 mmol) in acetonitrile (1 mL) was added silver trifluoromethanesulfonate (90 mg, 0.35 mmol), then refluxed under nitrogen overnight, after which the solution was dried under high vacuum. The residue was dissolved in pyridine (0.9 mL), then stirred at 95 °C under nitrogen overnight, after which the solution was dried under high vacuum. The crude material was adsorbed onto silica gel and subjected to silica gel chromatography with dichloromethane : methanol (10:1) to obtain complex **FL889** (1.2 mg, 9%). ^{1}H NMR (300 MHz, acetone-d_6): δ (ppm) 10.07 (s, 1H), 9.44 (s, 1H), 8.84 (dd, *J* = 9.2, 2.3 Hz, 1H), 8.77 (t, *J* = 2.5 Hz, 1H), 8.68-8.66 (m, 2H), 8.53 (m, 1H), 8.39-8.31 (m, 3H), 8.21 (m, 1H), 7.97-7.93 (m, 2H), 7.79-7.63 (m, 6H), 6.91 (dd, *J* = 8.9, 2.5 Hz, 1H), 6.38 (d, *J*

= 8.8 Hz, 1H). HRMS calculated for $C_{35}H_{22}FN_6O_4Ru$ $(M)^+$ 711.0725, found $(M)^+$ 711.0719.

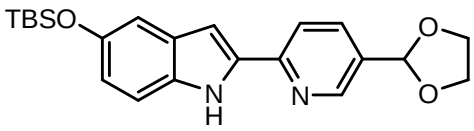

2.23

Compound 2.23. A biphasic suspension of **2.15** (1.2 g, 3.06 mmol), **2.22** (644 mg, 2.80 mmol), tetrakis(triphenylphosphine)palladium(0) (226 mg, 0.19 mmol) and Na_2CO_3 (816 mg, 7.70 mmol) in 1,2-dimethoxyethane (12.3 mL) and water (3.2 mL) was purged with nitrogen and refluxed overnight. The resulting reaction mixture was cooled to room temperature, diluted with water and extracted with EtOAc for three times. The combined organic layers were washed with brine, dried using Na_2SO_4, filtered and concentrated to dryness *in vacuo*. The crude material was adsorbed onto silica gel and subjected to silica gel chromatography with hexane : EtOAc (first 6:1, then 3:1) as the eluting solvent. The combined product eluents were isolated as a mixture of Boc-protected pyridylindole and **2.23**. The resulting solid was dissolved into DCM and adsorbed onto silica gel (10 g) using rotary evaporation. The white powder was heated to 80 °C overnight under high vacuum. The silica gel was cooled to room temperature, filtered through celite with EtOAc and the filtrate was dried *in vacuo* to provide **2.23** (898 mg, 81% over two steps) as a solid. ^{1}H NMR (300 MHz, $CDCl_3$): δ (ppm) 9.39 (s, 1H), 8.63 (s, 1H), 7.83-7.75 (m, 2H), 7.26 (d, *J* = 8.5 Hz, 1H), 7.06 (d, *J* = 2.1 Hz, 1H), 6.92 (d, *J* = 1.9 Hz, 1H), 6.80 (dd, *J* = 8.7, 2.2 Hz, 1H), 5.87 (s, 1H), 4.19-4.05 (m, 4H), 1.01 (s, 9H), 0.21 (s, 6H).

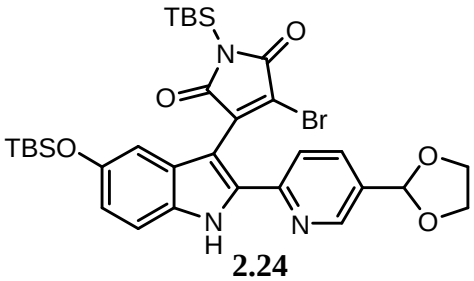

2.24

Compound 2.24. A solution of **2.23** (750 mg, 1.89 mmol) in anhydrous THF (5 mL) was prepared after drying **2.23** under high vacuum overnight. After cooling the solution

to -15 °C, lithium bis(trimethylsilyl)amide (1 M solution in hexanes) (5.7 mL, 5.70 mmol) was added dropwise over 15 minutes and the resulting suspension was stirred at -15 °C for an additional 1 hour. A solution of TBS-protected dibromomaleimide (734 mg, 1.99 mmol) in THF (5 mL) cooled to 0 °C was added and the reaction mixture was stirred at -15 °C for 20 minutes and 10 °C overnight. The resulting dark purple reaction mixture was carefully poured into stirring ice cold 10% HCl (35 mL) and extracted with EtOAc twice. The combined organic layers were washed with saturated $NaHCO_3$ followed by brine, dried using Na_2SO_4, filtered and concentrated to dryness *in vacuo*. The crude material was adsorbed onto silica gel and subjected to silica gel chromatography with hexane : EtOAc (first 6:1, then 3:1 to 1:1) as the eluting solvent. The combined product eluents were dried *in vacuo* to provide **2.24** (650 mg, 50%) as a solid which was carried forward without characterization.

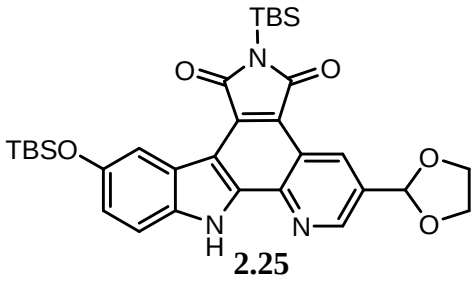

2.25

Compound 2.25. A solution of **2.24** (650 mg, 0.95 mmol) in toluene (220 mL) was irradiated with a medium pressure Hg lamp (150 W) with pyrex filter for 3 hours with constant nitrogen flow through the solution. The resulting red solution was concentrated to dryness *in vacuo*. The crude material was adsorbed onto silica gel and subjected to silica gel chromatography with hexane : EtOAc (1:1) as the eluting solvent. The combined product eluents were dried *in vacuo* to provide **2.25** (500 mg, 84%) as a yellow solid. ^{1}H NMR (300 MHz, $CDCl_3$): δ (ppm) 9.94 (s, 1H), 9.48 (d, *J* = 2.0 Hz, 1H), 9.09 (d, *J* = 2.1 Hz, 1H), 8.62 (d, *J* = 2.5 Hz, 1H), 7.50 (d, *J* = 8.7 Hz, 1H), 7.15 (dd, *J* = 8.7, 2.5 Hz, 1H), 6.08 (s, 1H), 4.28-4.11 (m, 4H), 1.06 (s, 18H), 0.62 (s, 6H), 0.32 (s, 6H).

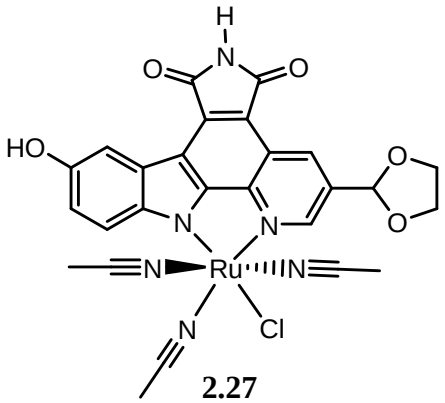

2.27

Complex 2.27. A suspension of the ligand **2.25** (200 mg, 0.33 mmol), K_2CO_3 (50 mg, 0.36 mmol), and $[RuCl_2(\eta^6\text{-}C_6H_6)]_2$ (124 mg, 0.25 mmol) in CH_3CN (30 mL) was purged with nitrogen for 5 minutes and stirred at 55 °C under nitrogen for 1.5 h. The resulting dark red soulution was dried *in vacuo* and the crude material was adsorbed onto silica gel and subjected to silica gel chromatography with dichloromethane : methanol (20:1) as the eluting solvent. The half-sandwich complex **2.26** was isolated as a dark red solid (206 mg, 76%). A red solution of **2.26** (200 mg, 0.24 mmol) in CH_3CN (900 mL) was purged with nitrogen for 5 min and then irradiated with a mercury medium pressure lamp (700W) for 1.5 hours while nitrogen was bubbled through the solution. The resulting dark green solution was dried *in vacuo* and the crude material was adsorbed onto silica gel and subjected to silica gel chromatography with dichloromethane : methanol (15:1). The combined product eluents were isolated as a mixture of two diastereoisomers. To the stirred green solution of the mixture (170 mg, 0.20 mmol) in CH_3CN (5 mL) was added tetrabutylammonium fluoride (600 μL, 1 M in THF, 0.60 mmol) at 0 °C, and the solution was stirred at 0 °C for 3 min. To the resulting green solution was added glacial acetic acid (34.7 μL, 0.60 mmol), and it was stirred for 1 min at 0 °C. The solution was dried *in vacuo* and the crude material was adsorbed onto silica gel and subjected to silica gel chromatography with dichloromethane : methanol (10:1) to yield the mixture precursor complex **2.27** (107 mg, 69%) over two steps.

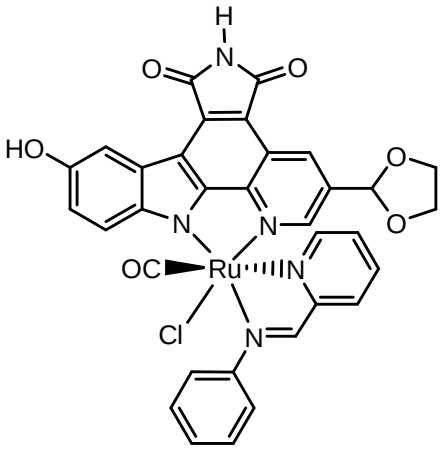

2.28

Complex 2.28. A solution of precursor complex **2.27** (10 mg, 0.016 mmol) in DMF (1.8 mL) was purged with CO gas for 5 min, then stirred at 75 °C under an atmosphere of CO for 1 hour. To the resulting solution was added 2-(phenylaminomethyl)pyridine (160 μL, 100 mM in DMF), then the solution was stirred at 95 °C under an atmosphere of nitrogen for 4 hours, after which the solution was dried under high vacuum. The crude material was adsorbed onto silica gel and subjected to silica gel chromatography with dichloromethane : methanol (50:1) to obtain complex **2.28** (5.1 mg, 45%). ^{1}H NMR (300 MHz, acetone-d_6): δ (ppm) 9.86 (s, 1H), 9.21 (s, 1H), 9.09 (d, J = 1.4 Hz, 1H), 8.59 (d, J = 8.9 Hz, 1H), 8.43 (d, J = 1.5 Hz, 1H), 8.35 (d, J = 7.8 Hz, 1H), 8.32 (d, J = 2.6 Hz, 1H), 8.21 (s, 1H), 8.14 (td, J = 7.5, 2.0 Hz, 1H), 8.09-8.06 (m, 2H), 7.73-7.68 (m, 2H), 7.59 (m, 1H), 7.48-7.41 (m, 2H), 7.16 (dd, J = 8.9, 2.6 Hz, 1H), 4.17-4.03 (m, 4H).

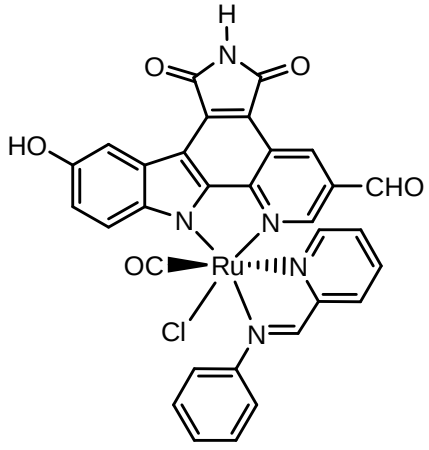

FL1088

Complex FL1088. To a solution of **2.28** (6.4 mg, 0.009 mmol) in THF (1 mL) was

added 10% HCl solution (1 mL) under nitrogen at room temperature carefully. The resulting solution was stirred for additional 1 hour, followed by quenching with saturated $NaHCO_3$ solution (2.5 mL). The mixture was extracted with DCM twice, and the combined organic layers were concentrated. The crude material was adsorbed onto silica gel and subjected to silica gel chromatography with dichloromethane : methanol (15:1) to yield complex **FL1088** (5 mg, 83%). ^{1}H NMR (300 MHz, acetone-d_6): δ (ppm) 10.20 (s, 1H), 9.99 (s, 1H), 9.24 (s, 1H), 8.82 (d, *J* = 1.5 Hz, 1H), 8.65 (dd, *J* = 9.0 Hz, 1H), 8.38-8.34 (m, 3H), 8.18-8.10 (m, 3H), 7.74-7.69 (m, 2H), 7.60 (m, 1H), 7.46-7.41 (m, 2H), 7.28 (dd, *J* = 9.0, 2.6 Hz, 1H).

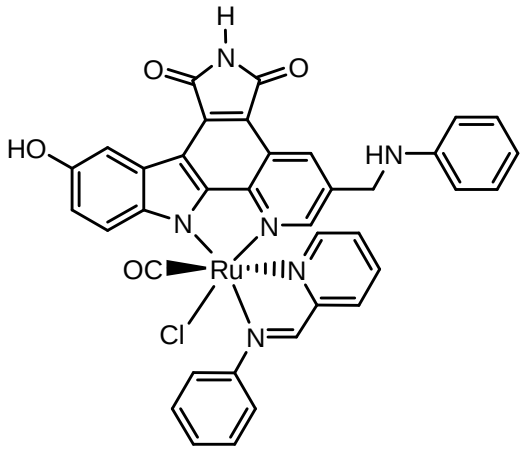

FL1103

Complex FL1103. To a solution of complex **FL1088** (5.4 mg, 0.008 mmol) in MeOH/THF (0.7 mL/0.2 mL) was added aniline (0.8 μL, 0.009 mmol) and *p*-toluenesulfonic acid (0.15 mg, 0.001 mmol), then stirred under nitrogen at 50 °C for 3 hours, followed by quenching with saturated $NaHCO_3$ solution, after which the solution was dried under high vacuum. The crude material was adsorbed onto silica gel and subjected to silica gel chromatography with dichloromethane : methanol (35:1) to obtain complex **FL1103** (1.3 mg, 18%). ^{1}H NMR (300 MHz, acetone-d_6): δ (ppm) 9.80 (s, 1H), 8.97 (m, 1H), 8.77 (s, 1H), 8.56 (d, *J* = 8.9 Hz, 1H), 8.30 (d, *J* = 2.2 Hz, 1H), 8.27-8.23 (m, 2H), 8.17 (s, 1H), 8.14 (td, *J* = 7.7, 2.0 Hz, 1H), 7.77-7.74 (m, 2H), 7.63-7.53 (m, 3H), 7.43-7.37 (m, 2H), 7.15-7.10 (m, 3H), 6.72 (m, 1H), 6.64-6.61 (m, 2H), 5.96 (t, *J* = 6.3 Hz, 1H), 4.75-4.55 (m, 2H).

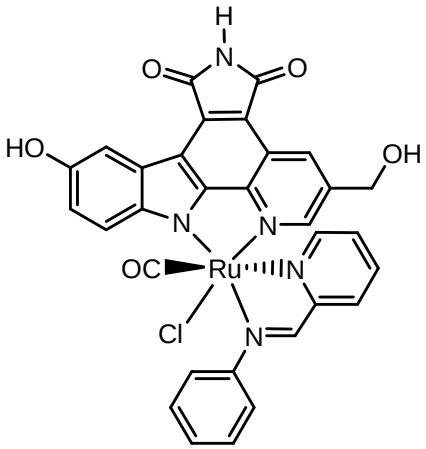

FL1109

Complex FL1109. To a solution of complex **FL1088** (4.7 mg, 0.007 mmol) in MeOH/THF (1 mL/0.5 mL) was added sodium cyanoborohydride (0.9 mg, 0.014 mmol), then stirred under nitrogen at 50 °C for 3 hours, followed by quenching with saturated $NaHCO_3$ solution, after which the solution was dried under high vacuum. The crude material was adsorbed onto silica gel and subjected to silica gel chromatography with dichloromethane : methanol (first 15:1, then 10:1) to obtain complex **FL1109** (1.2 mg, 25%). ^{1}H NMR (300 MHz, acetone-d_6): δ (ppm) 9.80 (s, 1H), 9.19 (s, 1H), 8.98 (m, 1H), 8.58 (d, J = 8.9 Hz, 1H), 8.42 (d, J = 1.6 Hz, 1H), 8.36 (m, 1H), 8.31 (m, 1H), 8.18-8.08 (m, 3H), 8.71-7.65 (m, 2H), 7.58 (m, 1H), 7.49-7.42 (m, 2H), 7.13 (dd, J = 8.9, 2.6 Hz, 1H), 4.82-4.72 (m, 3H). HRMS calculated for $C_{31}H_{21}ClN_5O_5Ru$ $(M + H)^+$ 680.0269, found $(M + H)^+$ 680.0278.

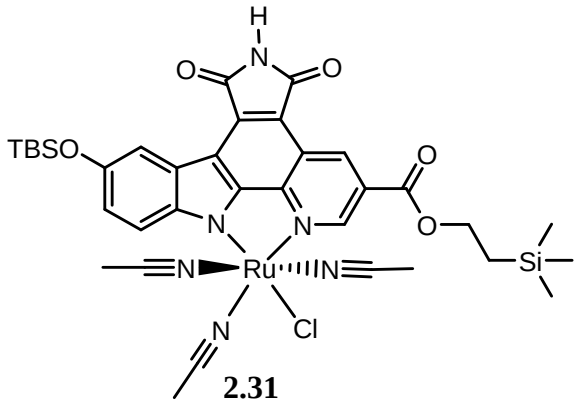

2.31

Complex 2.31. A suspension of the ligand **2.29** (71 mg, 0.11 mmol), K_2CO_3 (16 mg, 0.12 mmol), and $[RuCl_2(\eta^6\text{-}C_6H_6)]_2$ (40 mg, 0.08 mmol) in CH_3CN (10 mL) was purged with nitrogen for 5 minutes and stirred at 50 °C under nitrogen for 6 h. The resulting

dark red soulution was dried *in vacuo* and the crude material was adsorbed onto silica gel and subjected to silica gel chromatography with dichloromethane : methanol (20:1) as the eluting solvent. The half-sandwich complex **2.30** was isolated as a dark red solid (76 mg, 81%). A red solution of **2.30** (80 mg, 0.09 mmol) in CH_3CN (220 mL) was purged with nitrogen for 5 min, then irradiated with a mercury medium pressure lamp (150W, pyrex filter) for 3 hours while nitrogen was bubbled through the solution. The resulting dark green solution was dried *in vacuo* and the crude material was adsorbed onto silica gel and subjected to silica gel chromatography with dichloromethane : methanol (10:1). The combined product eluents were isolated as a mixture of two diastereoisomers (71 mg, 85%).

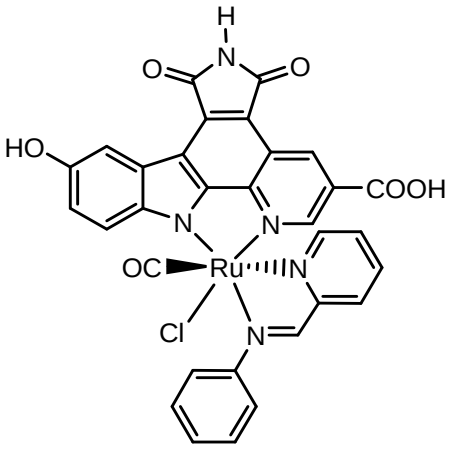

FL1118

Complex FL1118. A solution of precursor complex **2.31** (15.3 mg, 0.016 mmol) in DMF (1.8 mL) was purged with CO gas for 5 min, then stirred at 75 °C under an atmosphere of CO for 1 hour. To the resulting solution was added 2-(phenylaminomethyl)pyridine (160 μL, 100 mM in DMF), then the solution was stirred at 95 °C under an atmosphere of nitrogen for 5 hours, after which the solution was dried under high vacuum. The crude material was adsorbed onto silica gel and subjected to silica gel chromatography with dichloromethane : methanol (100:1) to obtain complex **2.32** (5.4 mg, 36%). To the stirred solution of **2.32** (5.4 mg, 0.006 mmol) in THF (1 mL) was added tetrabutylammonium fluoride (24 μL, 1 M in THF, 0.024 mmol) at 0 °C and the solution was stirred at 0 °C for 2 min, then 10 min at room temperature. To the resulting suspension was added glacial acetic acid (1.4 μL, 0.60

mmol), then the crude material was adsorbed onto silica gel and subjected to silica gel chromatography with dichloromethane : methanol (first 10:1, then 5:1) to yield complex **FL1118** (2.3 mg, 57%). ^{1}H NMR (300 MHz, DMSO-d_6): δ (ppm) 11.0 (s, 1H), 9.32 (s, 1H), 9.30 (d, *J* = 1.2 Hz, 1H), 9.20 (s, 1H), 8.72 (d, *J* = 1.3 Hz, 1H), 8.35-8.30 (m, 2H), 8.17-8.11 (m, 2H), 7.93-7.91 (m, 2H), 7.73-7.68 (m, 3H), 7.59 (m, 1H), 7.45 (m, 1H), 7.26 (m, 1H), 7.03 (dd, *J* = 8.9, 2.5 Hz, 1H). HRMS calculated for $C_{31}H_{17}ClN_5O_6Ru$ (M - H)$^-$ 691.9916, found (M - H)$^-$ 691.9902.

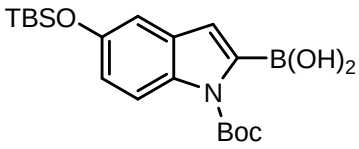

2.15

Compound 2.15. To a solution of 5-[(*tert*-butyldimethylsilyl)oxy]-1-(*tert*-butoxy-carbonyl)-indole (600 mg, 1.73 mmol) in anhydrous THF (4 mL) was added triisopropyl borate (0.60 mL, 2.60 mmol). The reaction mixture was cooled to 0 °C and lithium diisopropylamide (2.0 M solution in heptane-tetrahydrofuran-ethylbenzene) (1.3 mL, 2.60 mmol) was added dropwise over 15 minutes. After stirring for an additional 45 minutes at 0 °C, 2 M HCl (4.3 mL) was carefully added and stirred at 0 °C for 5 minutes. The resulting organic layer was separated and the aqueous layer was extracted using EtOAc twice. The combined organic layers were dried using Na_2SO_4, filtered and concentrated to dryness *in vacuo* to provide **2.15** (642 mg, 95%) which was carried forward without characterization.

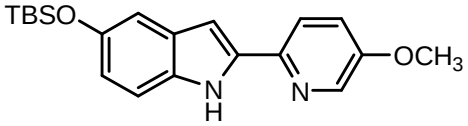

2.17

Compound 2.17. A biphasic suspension of 5-(*tert*-butyldimethylsilyl)indole-2-boronic acid (755 mg, 1.93 mmol), 2-bromo-5-methoxypyridine (330 mg, 1.75 mmol), tetrakis(triphenylphosphine)palladium(0) (142 mg, 0.12 mmol) and Na_2CO_3 (512 mg, 4.83 mmol) in 1,2-dimethoxyethane (17.5 mL) and water (2.0 mL) was purged with nitrogen and refluxed overnight. The resulting reaction mixture was cooled to room

temperature, diluted with water and extracted with EtOAc for three times. The combined organic layers were washed with brine, dried using Na_2SO_4, filtered and concentrated to dryness *in vacuo*. The crude material was adsorbed onto silica gel and subjected to silica gel chromatography with hexane : EtOAc (8:1) as the eluting solvent. The combined product eluents were isolated as a mixture of Boc-protected pyridylindole and **2.17**. The resulting solid was dissolved into DCM and adsorbed onto silica gel (7 g) using rotary evaporation. The white powder was heated to 80 °C overnight under high vacuum. The silica gel was cooled to room temperature, filtered through celite with EtOAc and the filtrate was dried *in vacuo* to provide **2.17** (440 mg, 71% over two steps) as a solid. ^{1}H NMR (300 MHz, $CDCl_3$): δ (ppm) 9.43 (s, 1H), 8.28 (d, *J* = 2.8 Hz, 1H), 7.73 (d, *J* = 8.8 Hz, 1H), 7.28 (m, 1H), 7.23 (d, *J* = 8.4 Hz, 1H), 7.07 (d, *J* = 2.0 Hz, 1H), 6.80-6.76 (m, 2H), 3.91 (s, 3H), 1.04 (s, 9H), 0.23 (s, 6H). ^{13}C NMR (75.5 MHz, $CDCl_3$): δ (ppm) 154.9, 149.7, 143.6, 137.6, 136.4, 132.3, 130.1, 121.8, 120.4, 117.2, 111.6, 110.2, 98.7, 55.9, 26.0, 18.4, -4.2. IR (film): *v* (cm^{-1}) 3054, 2956, 1592, 1563, 1464, 1263, 1150, 1028, 965, 888, 834, 781, 731. HRMS calculated for $C_{20}H_{27}N_2O_2Si$ $(M + H)^+$ 355.1836, found $(M + H)^+$ 355.1835.

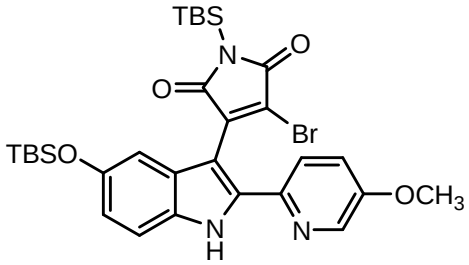

2.18

Compound 2.18. A solution of **2.17** (520 mg, 1.47 mmol) in anhydrous THF (4.4 mL) was prepared after drying **2.17** under high vacuum overnight. After cooling the solution to -15 °C, lithium bis(trimethylsilyl)amide (1 M solution in hexanes) (4.4 mL, 4.40 mmol) was added dropwise over 15 minutes and the resulting suspension was stirred at -15 °C for an additional 1 hour. A solution of TBS-protected dibromomaleimide (569 mg, 1.54 mmol) in THF (4.4 mL) cooled to 0 °C was added and the reaction mixture was stirred at -15 °C for 20 minutes and 10 °C overnight. The resulting dark purple

reaction mixture was carefully poured into stirring ice cold 10% HCl (30 mL) and extracted with EtOAc twice. The combined organic layers were washed with saturated $NaHCO_3$ solution followed by brine, dried using Na_2SO_4, filtered and concentrated to dryness *in vacuo*. The crude material was adsorbed onto silica gel and subjected to silica gel chromatography with hexane : EtOAc (first 6:1, then 3:1) as the eluting solvent. The combined product eluents were dried *in vacuo* to provide **2.18** (680 mg, 72%) as a solid which was carried forward without characterization.

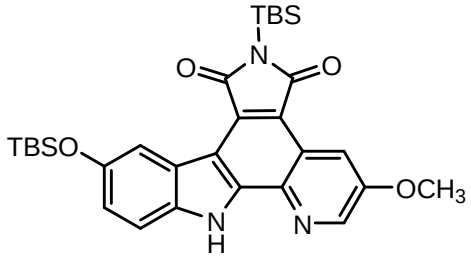

2.19

Compound 2.19. A solution of **2.18** (680 mg, 1.06 mmol) in toluene (220 mL) was irradiated with a medium pressure Hg lamp (150 W) with pyrex filter for 3 hours with constant nitrogen flow through the solution. The resulting red solution was concentrated to dryness *in vacuo*. The crude material was adsorbed onto silica gel and subjected to silica gel chromatography with hexane : EtOAc (first 6:1, then 3:1) as the eluting solvent. The combined product eluents were dried *in vacuo* to provide **2.19** (500 mg, 84%) as a yellow solid. ^{1}H NMR (300 MHz, $CDCl_3$): δ (ppm) 10.14 (s, 1H), 8.68 (d, *J* = 2.9 Hz, 1H), 8.64 (d, *J* = 2.9 Hz, 1H), 8.57 (d, *J* = 2.5 Hz, 1H), 7.36 (d, *J* = 8.7 Hz, 1H), 7.08 (dd, *J* = 8.7, 2.5 Hz, 1H), 4.02 (s, 3H), 1.08 (s, 9H), 1.06 (s, 9H), 0.64 (s, 6H), 0.33 (s, 6H). ^{13}C NMR (75.5 MHz, $CDCl_3$): δ (ppm) 175.9, 174.1, 155.1, 150.9, 144.5, 141.4, 134.8, 133.1, 131.0, 123.3, 123.1, 120.9, 119.2, 114.8, 114.0, 111.7, 110.9, 56.0, 26.7, 26.1, 19.3, 18.6, -3.8, -4.2. IR (film): *v* (cm^{-1}) 2934, 2858, 1746, 1691, 1628, 1603, 1568, 1468, 1408, 1371, 1341, 1310, 1261, 1220, 1043, 964, 887, 830, 775. HRMS calculated for $C_{30}H_{39}N_3O_4Si_2Na$ $(M + Na)^+$ 584.2371, found $(M + Na)^+$ 584.2372.

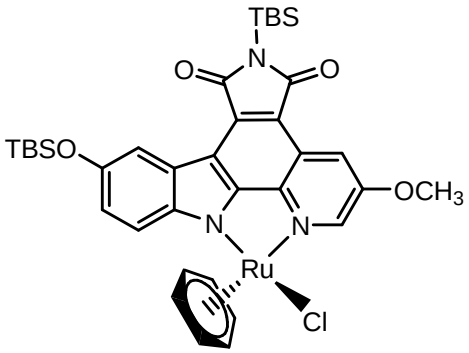

2.20

Complex 2.20. A suspension of the ligand **2.19** (100 mg, 0.18 mmol), K_2CO_3 (27 mg, 0.19 mmol), and $[RuCl_2(\eta^6\text{-}C_6H_6)]_2$ (89 mg, 0.18 mmol) in CH_3CN/MeOH/DCM (3.5 mL/3.5 mL/2 mL) was purged with nitrogen for 5 minutes and stirred at 55 °C under nitrogen for 3 h. The resulting dark red suspension was dried *in vacuo* and the crude material was adsorbed onto silica gel and subjected to silica gel chromatography with dichloromethane : methanol (20:1) as the eluting solvent. The half-sandwich complex **2.20** was isolated as a dark red solid (100 mg, 72%). ^{1}H NMR (300 MHz, $CDCl_3$): δ (ppm) 8.96 (d, *J* = 2.2 Hz, 1H), 8.61 (d, *J* = 2.2 Hz, 1H), 8.34 (d, *J* = 2.4 Hz, 1H), 7.60 (d, *J* = 8.7 Hz, 1H), 7.12 (dd, *J* = 8.7, 2.4 Hz, 1H), 5.87 (s, 6H), 4.07 (s, 3H), 1.06 (s, 9H), 1.02 (s, 9H), 0.59 (s, 6H), 0.30 (s, 3H), 0.28 (s, 3H). ^{13}C NMR (75.5 MHz, $CDCl_3$): δ (ppm) 175.8, 174.4, 155.2, 154.0, 150.0, 146.6, 144.1, 137.9, 133.4, 125.2, 122.3, 120.2, 115.1, 114.4, 114.0, 113.6, 83.4, 56.6, 26.7, 26.1, 19.3, 18.6, -3.7, -4.1. IR (film): *v* (cm^{-1}) 2930, 2892, 2857, 1741, 1685, 1564, 1460, 1421, 1342, 1306, 1256, 1213, 1045, 905, 831, 778, 694, 666. HRMS calculated for $C_{36}H_{44}N_3O_4Si_2Ru$ $(M - Cl)^+$ 740.1908, found $(M - Cl)^+$ 740.1909.

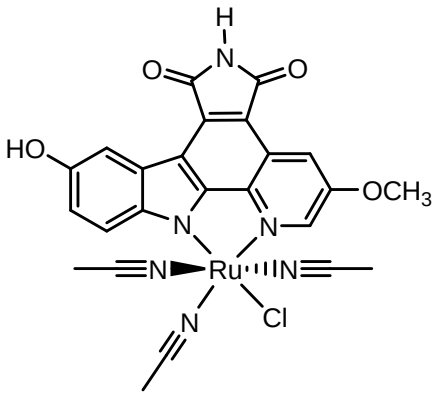

2.21

Complex 2.21. A red solution of **2.20** (60 mg, 0.08 mmol) in CH_3CN (220 mL) was purged with nitrogen for 10 min, then irradiated with a mercury medium pressure lamp (150W, pyrex filter) for 2 hours while nitrogen was bubbled through the solution. The resulting dark green solution was dried *in vacuo* and the crude material was adsorbed onto silica gel and subjected to silica gel chromatography with dichloromethane : methanol (15:1). The combined product eluents were isolated as a mixture of two diastereoisomers (53 mg, 84%). To the stirred green solution of the mixture (121 mg, 0.15 mmol) in CH_3CN (6 mL) was added tetrabutylammonium fluoride (445 μL, 1 M in THF, 0.45 mmol) at 0 °C, and the solution was stirred at 0 °C for 3 min. To the resulting green solution was added glacial acetic acid (26 μL, 0.45 mmol), and it was stirred for 2 min at 0 °C. The solution was dried *in vacuo* and the crude material was adsorbed onto silica gel and subjected to silica gel chromatography with dichloromethane : methanol (first 35:1, then 15:1) to yield the precursor complex **2.21** (43 mg, 49%) and a second diastereoisomer in lower amounts (31 mg, 35%). Analytical data for the main diastereomer **2.21**: ^{1}H NMR (300 MHz, DMSO-d_6): δ (ppm) 10.82 (s, 1H), 9.18 (br, 1H), 9.03 (s, 1H), 8.34 (br, 1H), 8.04 (br, 1H), 7.59 (d, J = 8.7 Hz, 1H), 7.00 (d, J = 8.7 Hz, 1H), 4.04 (s, 3H), 2.94 (s, 3H), 2.22 (s, 6H). IR (film): ν (cm^{-1}) 3245, 2925, 2278, 1741, 1702, 1565, 1465, 1424, 1398, 1348, 1325, 1215, 1061, 1014, 863, 700, 640, 487. HRMS calculated for $C_{24}H_{19}N_6O_4ClRu$ (M) 592.0195, found (M) 592.0194.

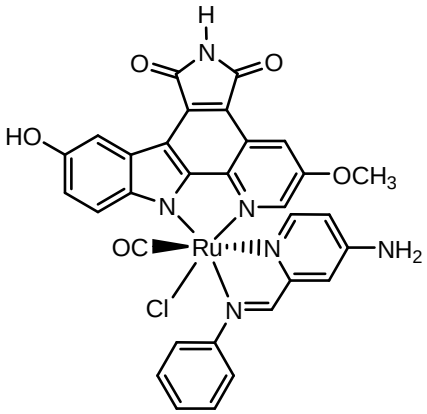

FL1422

Complex FL1422. A solution of precursor complex **2.21** (6 mg, 0.010 mmol) in DMF (1.8 mL) was purged with CO gas for 5 min, then stirred at 75 °C under an atmosphere

of CO for 1 hour. To the resulting solution was added 2-(phenylaminomethyl)-4-aminopyridine (100 μL, 100 mM in DMF), then the solution was stirred at 95 °C under an atmosphere of nitrogen for 4 hours, after which the solution was dried under high vacuum. The crude material was adsorbed onto silica gel and subjected to silica gel chromatography with dichloromethane : methanol (first 50:1, then 35:1) to obtain complex **FL1422** (2.5 mg, 35%). ^{1}H NMR (500 MHz, DMSO-d_6): δ (ppm) 10.95 (s, 1H), 9.09 (s, 1H), 8.89 (s, 1H), 8.34 (d, *J* = 2.3 Hz, 1H), 8.27 (d, *J* = 8.7 Hz, 1H), 8.11 (d, *J* = 2.4 Hz, 1H), 7.94 (d, *J* = 7.7 Hz, 2H), 7.89 (d, *J* = 2.3 Hz, 1H), 7.64 (t, *J* = 7.9 Hz, 2H), 7.51 (t, *J* = 7.4 Hz, 1H), 7.29 (d, *J* = 2.3 Hz, 1H), 7.03 (br, 2H), 6.98 (dd, *J* = 8.8, 2.5 Hz, 1H), 6.63 (d, *J* = 6.3 Hz, 1H), 6.32 (dd, *J* = 6.3, 2.5 Hz, 1H). ^{13}C NMR (100.6 MHz, DMSO-d_6): δ (ppm) 201.1, 170.9, 170.6, 170.3, 156.3, 154.3, 154.2, 153.9, 153.1, 151.3, 147.3, 146.5, 142.3, 138.0, 131.2, 129.4, 128.6, 124.2, 122.4, 121.1, 117.6, 115.7, 114.3, 113.4, 111.6, 110.4, 110.1, 108.0, 69.8. IR (film): *v* (cm^{-1}) 3351, 3216, 1960, 1747, 1711, 1631, 1567, 1493, 1468, 1341, 1218, 1023, 766, 702. HRMS calculated for $C_{31}H_{22}ClN_6O_5Ru$ $(M + H)^+$ 695.0379, found $(M + H)^+$ 695.0385.

Synthesis of an initial library of octahedral ruthenium complexes from precursor complex 2.3.

Reactions were performed starting from the ruthenium precursor **2.3**. A solution of **2.3** in DMF (9 mM, 2.5 mL) was purged with CO gas for 5 minutes, followed by stirring at 75 °C under an atmosphere of CO for 1 hour. To the resulting solution was added 1 equiv of different bidentate ligands, then the mixture was stirred at 95 °C under an atmosphere of nitrogen for 1-3 hours, which depended on the characteristic of the bidentate ligands, affording the products, which were purified by the silica gel chromatography with dichloromethane and methanol. The constitutions each were confirmed by mass spectrometry and ^{1}H-NMR analysis.

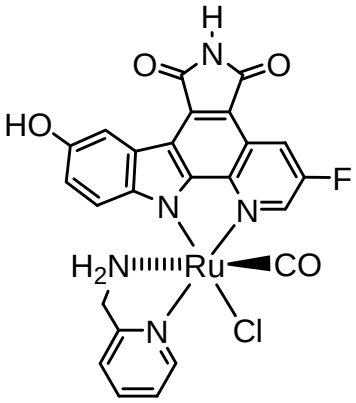

FL115-1

Complex FL115-1. The crude material was adsorbed onto silica gel and subjected to silica gel chromatography with dichloromethane : methanol (first 50:1, then 35:1) to obtain complex **FL115-1** (3 mg, 29%). ^{1}H NMR (300 MHz, acetone-d_6): δ (ppm) 9.86 (s, 1H), 9.36 (d, *J* = 8.9 Hz, 1H), 9.20 (t, *J* = 2.6 Hz, 1H), 8.81 (dd, *J* = 9.4, 2.6 Hz, 1H), 8.20 (d, *J* = 2.2 Hz, 1H), 8.12 (s, 1H), 8.08 (td, *J* = 7.8, 1.5 Hz, 1H), 7.67 (m, 2H), 6.78 (dd, *J* = 8.8, 2.6 Hz, 1H), 5.96 (d, *J* = 8.9 Hz, 1H), 4.82 (m, 3H), 4.22 (m, 1H). HRMS calculated for $C_{24}H_{16}ClFN_5O_4Ru$ $(M + H)^+$ 593.9913, found $(M + H)^+$ 593.9949.

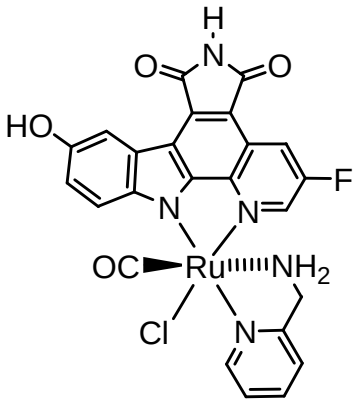

FL115-2

Complex FL115-2. The crude material was adsorbed onto silica gel and subjected to silica gel chromatography with dichloromethane : methanol (first 50:1, then 35:1) to obtain complex **FL115-2** (2.5 mg, 25%). ^{1}H NMR (300 MHz, acetone-d_6): δ (ppm) 9.82 (s, 1H), 9.25 (d, *J* = 5.2 Hz, 1H), 8.74 (dd, *J* = 9.5, 2.4 Hz, 1H), 8.45 (d, *J* = 8.9 Hz, 1H), 8.21 (d, *J* = 2.4 Hz, 1H), 8.10 (s, 1H), 8.02 (td, *J* = 7.7, 1.5 Hz, 1H), 7.90 (m, 1H), 7.69 (d, *J* = 7.8 Hz, 1H), 7.60 (m, 1H), 7.09 (dd, *J* = 8.9, 2.6 Hz, 1H), 4.92 (m, 3H), 4.51 (m, 1H). HRMS calculated for $C_{24}H_{16}ClFN_5O_4Ru$ $(M + H)^+$ 593.9913, found $(M + H)^+$

593.9934.

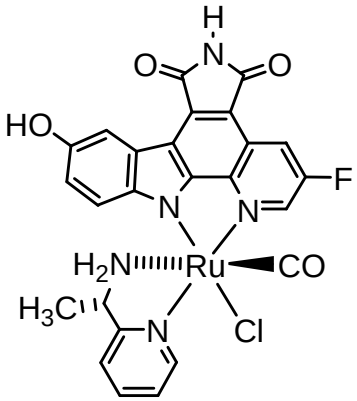

FL114-1

Complex FL114-1. The crude material was adsorbed onto silica gel and subjected to silica gel chromatography with dichloromethane : methanol (first 50:1, then 40:1) to obtain complex **FL114-1** (3.5 mg, 33%). Including two diastereoisomers with the ratio of around 1:1. ^{1}H NMR (300 MHz, acetone-d_6): δ (ppm) 9.86 (s, 2H), 9.48 (m, 1H), 9.37 (m, 1H), 9.23 (t, J = 2.7 Hz, 1H), 9.17 (t, J = 2.6 Hz, 1H), 8.82 (dd, J = 9.4, 2.5 Hz, 2H), 8.20-8.08 (m, 6H), 7.69-7.65 (m, 4H), 6.78 (m, 2H), 6.07 (d, J = 8.8 Hz, 1H), 5.89 (d, J = 8.7 Hz, 1H), 5.31 (m, 2H), 5.16 (m, 1H), 4.55 (m, 1H), 4.30 (m, 2H), 1.71 (d, J = 6.3 Hz, 3H), 1.42 (d, J = 7.0 Hz, 3H). HRMS calculated for $C_{25}H_{18}ClFN_5O_4Ru$ (M + H)$^+$ 608.0069, found (M + H)$^+$ 608.0057.

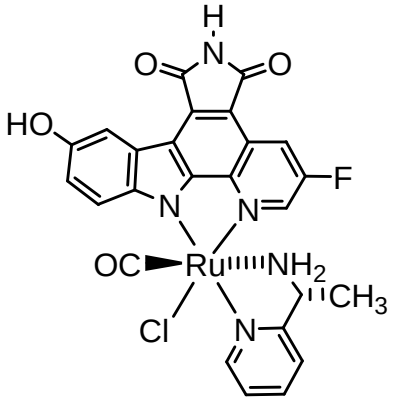

FL114-2

Complex FL114-2. The crude material was adsorbed onto silica gel and subjected to silica gel chromatography with dichloromethane : methanol (first 50:1, then 35:1) to obtain complex **FL114-2** (3 mg, 29%). Including two diastereoisomers with the ratio of around 1:1. ^{1}H NMR (300 MHz, acetone-d_6): δ (ppm) 9.81 (s, 2H), 9.36 (m, 1H), 9.24

(m, 1H), 8.76-8.69 (m, 2H), 8.49 (d, *J* = 8.8 Hz, 1H), 8.41 (d, *J* = 8.9 Hz, 1H), 8.21 (d, *J* = 2.5 Hz, 2H), 8.11-8.04 (m, 4H), 7.91 (t, *J* = 2.5 Hz, 1H), 7.85 (t, *J* = 2.5 Hz, 1H), 7.69-7.57 (m, 4H), 7.10 (dd, *J* = 2.5, 1.5 Hz, 1H), 7.07 (dd, *J* = 2.5, 1.5 Hz, 1H), 5.29 (m, 3H), 4.60 (m, 2H), 4.45 (m, 1H), 1.78 (d, *J* = 6.6 Hz, 3H), 1.64 (d, *J* = 6.7 Hz, 3H). HRMS calculated for $C_{25}H_{18}ClFN_5O_4Ru$ $(M + H)^+$ 608.0069, found $(M + H)^+$ 608.0059.

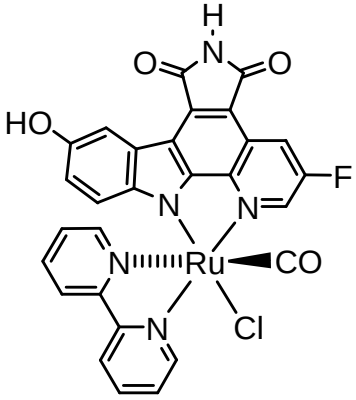

FL111-1

Complex FL111-1. The crude material was adsorbed onto silica gel and subjected to silica gel chromatography with dichloromethane : methanol (first 50:1, then 35:1) to obtain complex **FL111-1** (1 mg, 9%). ^{1}H NMR (300 MHz, acetone-d_6): δ (ppm) 9.88 (s, 1H), 9.79 (d, *J* = 5.8 Hz, 1H), 9.40 (t, *J* = 2.8 Hz, 1H), 8.96 (dd, *J* = 9.3, 2.5 Hz, 1H), 8.77 (d, *J* = 8.1 Hz, 1H), 8.63 (d, *J* = 8.4 Hz, 1H), 8.38 (td, *J* = 8.0, 1.5 Hz, 1H), 8.11-8.01 (m, 3H), 7.93 (m, 1H), 7.76 (d, *J* = 5.5 Hz, 1H), 7.35 (m, 1H), 6.69 (dd, *J* = 8.8, 2.6 Hz, 1H), 5.84 (d, *J* = 8.8 Hz, 1H). HRMS calculated for $C_{28}H_{15}Cl_2FN_5O_4Ru$ $(M + Cl)^-$ 675.9529, found $(M + Cl)^-$ 675.9471.

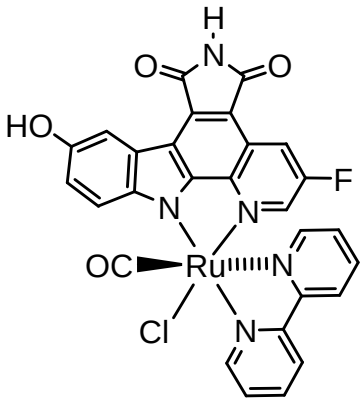

FL111-2

Complex FL111-2. The crude material was adsorbed onto silica gel and subjected to

silica gel chromatography with dichloromethane : methanol (35:1) to obtain complex **FL111-2** (5.5 mg, 50%). ^{1}H NMR (300 MHz, acetone-d_6): δ (ppm) 9.87 (s, 1H), 9.61 (d, J = 5.6 Hz, 1H), 8.74 (d, J = 7.9 Hz, 1H), 8.68-8.64 (m, 2H), 8.55 (d, J = 8.9 Hz, 1H), 8.32-8.27 (m, 2H), 8.19 (s, 1H), 8.11 (td, J = 8.1, 1.6 Hz, 1H), 7.87 (m, 1H), 7.80 (t, J = 2.6 Hz, 1H), 7.52 (d, J = 5.4 Hz, 1H), 7.35 (m, 1H), 7.15 (dd, J = 8.9, 2.6 Hz, 1H). HRMS calculated for $C_{28}H_{16}ClFN_5O_4Ru$ $(M + H)^+$ 641.9913, found $(M + H)^+$ 641.9898.

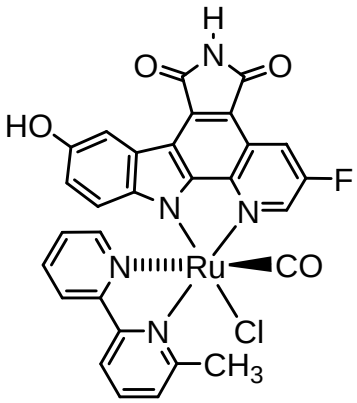

FL161-1

Complex FL161-1. The crude material was adsorbed onto silica gel and subjected to silica gel chromatography with dichloromethane : methanol (first 50:1, then 35:1) to obtain complex **FL161-1** (1.1 mg, 10%). ^{1}H NMR (300 MHz, acetone-d_6): δ (ppm) 9.89 (s, 1H), 9.38 (t, J = 2.6 Hz, 1H), 8.96 (dd, J = 9.3, 2.5 Hz, 1H), 8.56 (t, J = 8.3 Hz, 2H), 8.23 (t, J = 7.9 Hz, 1H), 8.10-7.94 (m, 4H), 7.71 (d, J = 5.5 Hz, 1H), 7.31 (m, 1H), 6.70 (dd, J = 8.8, 2.6 Hz, 1H), 5.78 (d, J = 8.9 Hz, 1H), 3.46 (s, 3H). HRMS calculated for $C_{29}H_{18}ClFN_5O_4Ru$ $(M + H)^+$ 656.0069, found $(M + H)^+$ 656.0052.

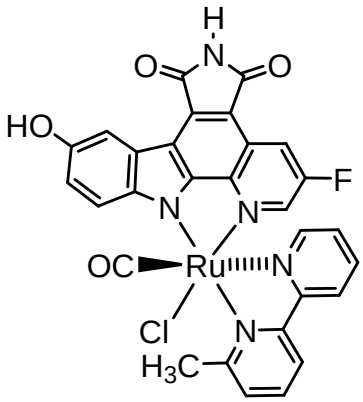

FL161-2

Complex FL161-2. The crude material was adsorbed onto silica gel and subjected to

silica gel chromatography with dichloromethane : methanol (first 50:1, then 35:1) to obtain complex **FL161-2** (2.6 mg, 24%). ^{1}H NMR (300 MHz, acetone-d_6): δ (ppm) 9.88 (s, 1H), 8.66-8.53 (m, 4H), 8.31 (d, *J* = 2.6 Hz, 1H), 8.21 (s, 1H), 8.16 (t, *J* = 7.9 Hz, 1H), 8.07 (td, *J* = 8.2, 1.7 Hz, 1H), 7.88 (d, *J* = 7.8 Hz, 1H), 7.71 (t, *J* = 2.2 Hz, 1H), 7.49 (d, *J* = 5.5 Hz, 1H), 7.30 (m, 1H), 7.16 (dd, *J* = 8.9, 2.6 Hz, 1H), 3.41 (s, 3H). HRMS calculated for $C_{29}H_{18}Cl_2FN_5O_4Ru$ $(M + Cl)^-$ 689.9685, found $(M + Cl)^-$ 689.9655.

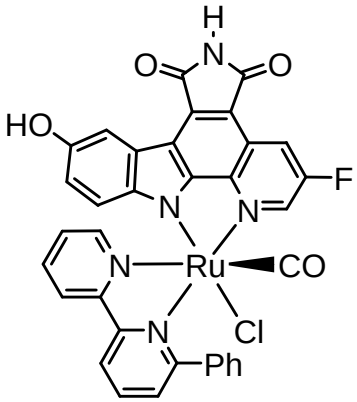

FL174-1

Complex FL174-1. HRMS calculated for $C_{34}H_{19}ClFN_5O_4Ru$ $(M)^+$ 717.0153, found $(M)^+$ 717.0350.

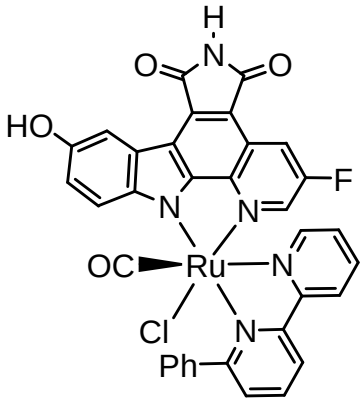

FL174-2

Complex FL174-2. The crude material was adsorbed onto silica gel and subjected to silica gel chromatography with dichloromethane : methanol (first 50:1, then 35:1) to obtain complex **FL174-2** (3 mg, 37%). ^{1}H NMR (300 MHz, acetone-d_6): δ (ppm) 9.83 (s, 1H), 8.77 (dd, *J* = 8.2, 1.3 Hz, 1H), 8.67 (d, *J* = 8.2 Hz, 1H), 8.62-8.56 (m, 2H), 8.33 (t, *J* = 7.9 Hz, 1H), 8.26 (d, *J* = 2.6 Hz, 1H), 8.17 (s, 1H), 8.15-7.81 (m, 4H), 7.61-7.48

(m, 5H), 7.35 (m, 1H), 7.12 (dd, *J* = 8.8, 2.6 Hz, 1H). HRMS calculated for $C_{34}H_{20}ClFN_5O_4Ru$ $(M + H)^+$ 718.0226, found $(M + H)^+$ 718.0204.

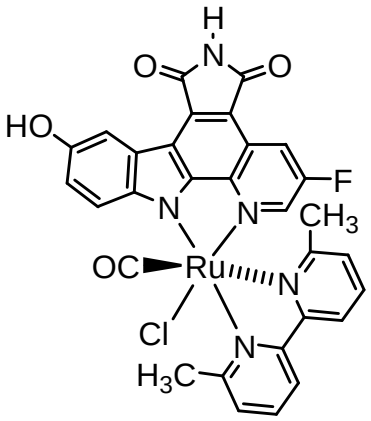

FL178

Complex FL178. The crude material was adsorbed onto silica gel and subjected to silica gel chromatography with dichloromethane : methanol (first 50:1, then 35:1) to obtain complex **FL178** (1.2 mg, 15%). ^{1}H NMR (300 MHz, acetone-d_6): δ (ppm) 9.85 (s, 1H), 8.64-8.60 (m, 2H), 8.55 (d, *J* = 8.2 Hz, 1H), 8.40 (d, *J* = 8.0 Hz, 1H), 8.28 (d, *J* = 2.6 Hz, 1H), 8.19-8.14 (m, 2H), 7.87 (t, *J* = 7.9 Hz, 1H), 7.80 (d, *J* = 7.8 Hz, 1H), 7.29 (m, 1H), 7.20 (dd, *J* = 8.9, 2.6 Hz, 1H), 7.15 (d, *J* = 7.9 Hz, 1H), 3.45 (s, 3H), 1.93 (s, 3H). HRMS calculated for $C_{30}H_{20}ClFN_5O_4Ru$ $(M + H)^+$ 670.0226, found $(M + H)^+$ 670.0225.

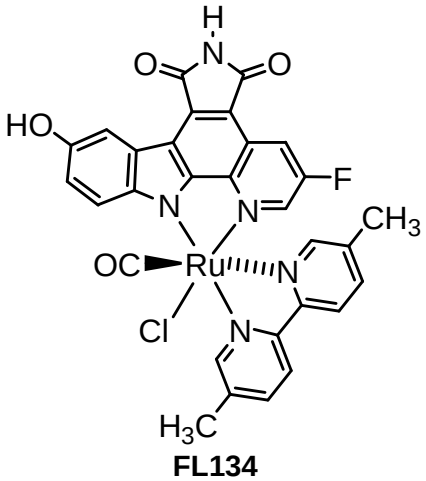

FL134

Complex FL134. The crude material was adsorbed onto silica gel and subjected to silica gel chromatography with dichloromethane : methanol (first 50:1, then 35:1) to obtain complex **FL134** (4 mg, 43%). ^{1}H NMR (300 MHz, acetone-d_6): δ (ppm) 9.87 (s,

1H), 9.41 (s, 1H), 8.65 (dd, *J* = 9.5, 2.4 Hz, 1H), 8.55 (d, *J* = 8.7 Hz, 2H), 8.48 (d, *J* = 8.3 Hz, 1H), 8.32 (d, *J* = 2.6 Hz, 1H), 8.18 (s, 1H), 8.08 (d, *J* = 8.3 Hz, 1H), 7.89 (d, *J* = 8.4 Hz, 1H), 7.77 (t, *J* = 2.5 Hz, 1H), 7.36 (m, 1H), 7.15 (dd, *J* = 8.9, 2.6 Hz, 1H), 2.64 (s, 3H), 1.92 (s, 3H). HRMS calculated for $C_{30}H_{20}ClFN_5O_4Ru$ $(M + H)^+$ 670.0226, found $(M + H)^+$ 670.0203.

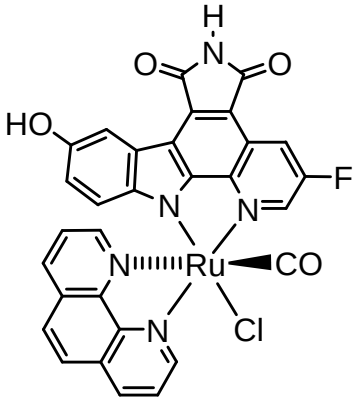

FL151-1

Complex FL151-1. The crude material was adsorbed onto silica gel and subjected to silica gel chromatography with dichloromethane : methanol (first 50:1, then 35:1) to obtain complex **FL151-1** (2.5 mg, 22%). ^{1}H NMR (300 MHz, DMSO-d_6): δ (ppm) 11.13 (s, 1H), 10.05 (dd, *J* = 5.3, 1.1 Hz, 1H), 9.27 (t, *J* = 2.6 Hz, 1H), 9.04 (s, 1H), 9.00 (dd, *J* = 8.3, 1.1 Hz, 1H), 8.95 (dd, *J* = 9.2, 2.5 Hz, 1H), 8.74 (dd, *J* = 8.3, 1.2 Hz, 1H), 8.40-8.22 (m, 3H), 8.01 (dd, *J* = 5.1, 1.2 Hz, 1H), 7.88 (d, *J* = 2.4 Hz, 1H), 7.71 (dd, *J* = 8.2, 5.1 Hz, 1H), 6.40 (dd, *J* = 8.8, 2.5 Hz, 1H), 5.31 (d, *J* = 8.8 Hz, 1H). HRMS calculated for $C_{30}H_{16}ClFN_5O_4Ru$ $(M + H)^+$ 665.9913, found $(M + H)^+$ 665.9923.

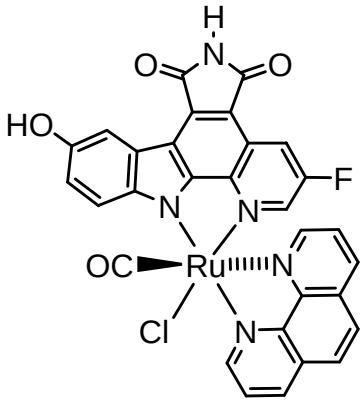

FL151-2

Complex FL151-2. The crude material was adsorbed onto silica gel and subjected to

silica gel chromatography with dichloromethane : methanol (first 50:1, then 35:1) to obtain complex **FL151-2** (3 mg, 26%). ^{1}H NMR (300 MHz, acetone-d_6): δ (ppm) 9.97 (dd, *J* = 5.2, 1.3 Hz, 1H), 9.89 (s, 1H), 8.91 (dd, *J* = 8.3, 1.3 Hz, 1H), 8.73 (dd, *J* = 8.2, 1.4 Hz, 1H), 8.63-8.59 (m, 2H), 8.38-8.21 (m, 5H), 7.83 (dd, *J* = 5.1, 1.5 Hz, 1H), 7.77-7.70 (m, 2H), 7.17 (dd, *J* = 8.8, 2.6 Hz, 1H). HRMS calculated for $C_{30}H_{16}ClFN_5O_4Ru$ $(M + H)^+$ 665.9913, found $(M + H)^+$ 665.9906.

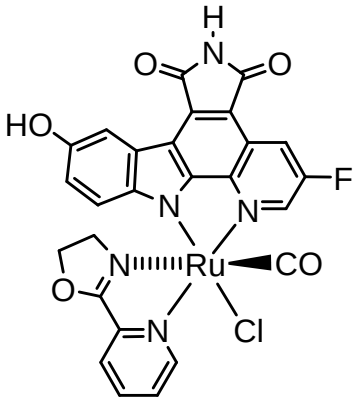

FL182-1

Complex FL182-1. The crude material was adsorbed onto silica gel and subjected to silica gel chromatography with dichloromethane : methanol (first 50:1, then 40:1) to obtain complex **FL182-1** (3.1 mg, 40%). ^{1}H NMR (300 MHz, acetone-d_6): δ (ppm) 9.89 (s, 1H), 9.74 (m, 1H), 9.31 (t, *J* = 2.6 Hz, 1H), 8.90 (dd, *J* = 9.3, 2.6 Hz, 1H), 8.39 (td, *J* = 7.8, 1.4 Hz, 1H), 8.21-8.17 (m, 2H), 8.11 (s, 1H), 8.06 (m, 1H), 6.74 (dd, *J* = 8.8, 2.6 Hz, 1H), 5.92 (d, *J* = 8.8 Hz, 1H), 4.92 (m, 1H), 4.68 (m, 1H), 3.89 (m, 1H), 3.17 (m, 1H). HRMS calculated for $C_{26}H_{16}ClFN_5O_5Ru$ $(M + H)^+$ 633.9862, found $(M + H)^+$ 633.9844.

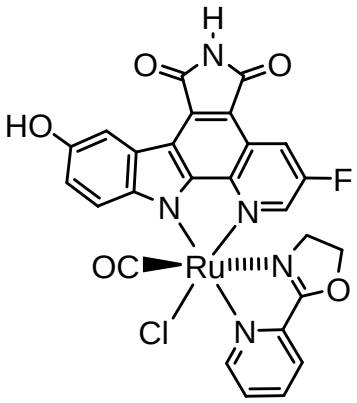

FL182-2

Complex FL182-2. The crude material was adsorbed onto silica gel and subjected to silica gel chromatography with dichloromethane : methanol (first 50:1, then 35:1) to obtain complex **FL182-2** (3.6 mg, 47%). ^{1}H NMR (300 MHz, acetone-d_6): δ (ppm) 9.85 (s, 1H), 9.53 (m, 1H), 8.71 (dd, *J* = 9.5, 2.4 Hz, 1H), 8.51 (d, *J* = 8.9 Hz, 1H), 8.31 (td, *J* = 7.8, 1.4 Hz, 1H), 8.25 (d, *J* = 2.6 Hz, 1H), 8.16 (m, 1H), 8.12 (s, 1H), 7.97 (m, 1H), 7.93 (t, *J* = 2.5 Hz, 1H), 7.11 (dd, *J* = 8.9, 2.6 Hz, 1H), 4.91 (m, 1H), 4.64 (m, 1H), 3.66 (m, 1H), 3.12 (m, 1H). HRMS calculated for $C_{26}H_{16}ClFN_5O_5Ru$ $(M + H)^+$ 633.9862, found $(M + H)^+$ 633.9841.

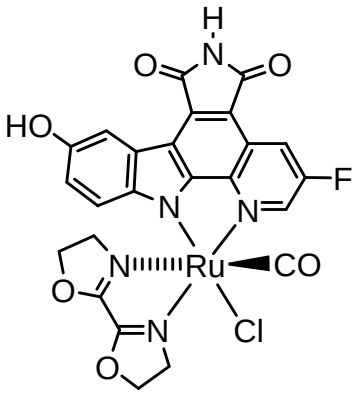

FL162-1

Complex FL162-1. The crude material was adsorbed onto silica gel and subjected to silica gel chromatography with dichloromethane : methanol (50:1) to obtain complex **FL162-1** (3 mg, 40%). ^{1}H NMR (300 MHz, acetone-d_6): δ (ppm) 9.89 (s, 1H), 9.26 (m, 1H), 8.88 (dd, *J* = 9.3, 2.5 Hz, 1H), 8.21 (dd, *J* = 2.3, 0.8 Hz, 1H), 8.17 (s, 1H), 7.10-7.02 (m, 2H), 5.44 (m, 2H), 4.95 (m, 2H), 4.71 (m, 1H), 4.49 (m, 1H), 3.84 (m, 1H), 3.16 (m, 1H). HRMS calculated for $C_{24}H_{16}ClFN_5O_6Ru$ $(M + H)^+$ 625.9811, found $(M + H)^+$ 625.9795.

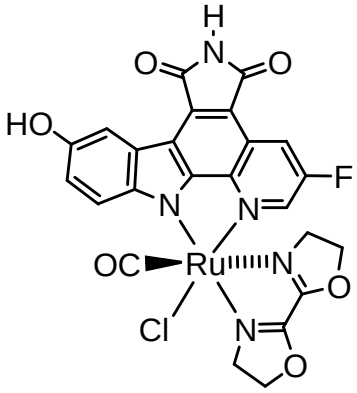

FL162-2

Complex FL162-2. The crude material was adsorbed onto silica gel and subjected to silica gel chromatography with dichloromethane : methanol (50:1) to obtain complex **FL162-2** (3.6 mg, 47%). ^{1}H NMR (300 MHz, acetone-d_6): δ (ppm) 9.84 (s, 1H), 8.74 (dd, *J* = 9.6, 2.4 Hz, 1H), 8.56 (t, *J* = 2.5 Hz, 1H), 8.46 (d, *J* = 8.9 Hz, 1H), 8.23 (d, *J* = 2.6 Hz, 1H), 8.09 (s, 1H), 7.09 (dd, *J* = 8.9, 2.6 Hz, 1H), 5.27 (m, 2H), 4.91 (m, 2H), 4.65 (m, 1H), 4.33 (m, 1H), 3.60 (m, 1H), 3.11 (m, 1H). HRMS calculated for $C_{24}H_{16}ClFN_5O_6Ru$ $(M + H)^+$ 625.9811, found $(M + H)^+$ 625.9799.

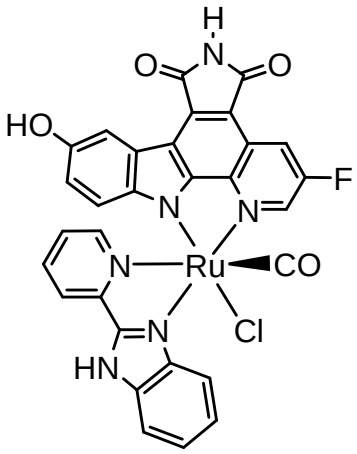

FL306

Complex FL306. The crude material was adsorbed onto silica gel and subjected to silica gel chromatography with dichloromethane : methanol (first 50:1, then 30:1) to obtain complex **FL306** (4.7 mg, 57%). ^{1}H NMR (300 MHz, acetone-d_6): δ (ppm) 9.85 (s, 1H), 9.59 (dd, *J* = 5.6, 1.1 Hz, 1H), 8.65-8.58 (m, 2H), 8.50 (d, *J* = 7.9 Hz, 1H), 8.41-8.33 (m, 2H), 8.22 (t, *J* = 7.7 Hz, 1H), 7.86-7.82 (m, 2H), 7.63 (m, 1H), 7.42 (d, *J* = 8.2 Hz, 1H), 7.17 (dd, *J* = 8.9, 2.6 Hz, 1H), 7.07 (m, 1H), 6.61 (m, 1H), 5.50 (d, *J* =

8.4 Hz, 1H). HRMS calculated for $C_{30}H_{16}ClFN_6O_4RuNa$ $(M + Na)^+$ 702.9841, found $(M + Na)^+$ 702.9857.

Synthesis of the modified FL172 with derivatized 2-(phenylaminomethyl)pyridines.

The synthesis was performed in analogy to **FL172** by reacting ruthenium precursor **2.3** in DMF (9 mM, 2.5 mL) first with CO gas stirring at 75 °C for 1 hour, then by addition of 1 equiv of derivatized 2-(phenylaminomethyl)pyridine stirring at 95 °C under nitrogen for 3 hours. Some derivatives were just used as crude in the measurement of PAK1 assays.

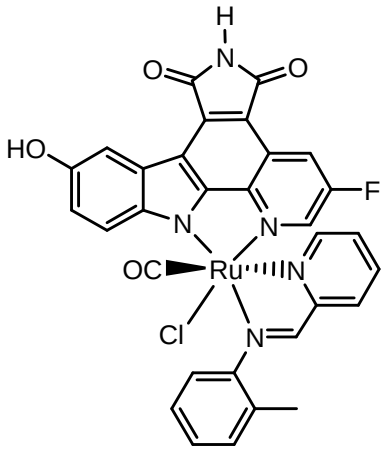

FL227

Complex FL227. The crude material was adsorbed onto silica gel and subjected to silica gel chromatography with dichloromethane : methanol (50:1) to obtain complex **FL227** (4.2 mg, 51%). ^{1}H NMR (300 MHz, acetone-d_6): δ (ppm) 9.89 (s, 1H), 9.18 (s, 1H), 8.73 (dd, *J* = 9.3, 2.4 Hz, 1H), 8.63 (m, 1H), 8.59 (d, *J* = 8.9 Hz, 1H), 8.42 (m, 1H), 8.31 (d, *J* = 2.5 Hz, 1H), 8.184 (s, 1H), 8.180 (td, *J* = 7.8, 1.6 Hz, 1H), 8.05 (d, *J* = 7.7 Hz, 1H), 7.57-7.35 (m, 5H), 7.12 (dd, *J* = 8.9, 2.6 Hz, 1H), 2.64 (s, 3H). HRMS calculated for $C_{31}H_{19}ClFN_5O_4RuNa$ $(M + Na)^+$ 704.0045, found $(M + Na)^+$ 704.0043.

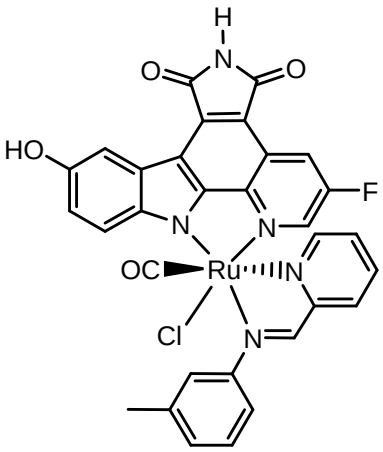

FL226

Complex FL226. The crude material was adsorbed onto silica gel and subjected to silica gel chromatography with dichloromethane : methanol (50:1) to obtain complex **FL226** (3.2 mg, 39%). ^{1}H NMR (300 MHz, acetone-d_6): δ (ppm) 9.88 (s, 1H), 9.21 (s, 1H), 8.69 (dd, *J* = 9.4, 2.4 Hz, 1H), 8.59 (d, *J* = 8.9 Hz, 1H), 8.37 (m, 1H), 8.34 (t, *J* = 2.5 Hz, 1H), 8.31 (d, *J* = 2.6 Hz, 1H), 8.19 (s, 1H), 8.16 (td, *J* = 7.7, 1.8 Hz, 1H), 7.95-7.92 (m, 2H), 7.56 (t, *J* = 7.7 Hz, 1H), 7.49-7.39 (m, 3H), 7.15 (dd, *J* = 8.9, 2.6 Hz, 1H), 2.52 (s, 3H). HRMS calculated for $C_{31}H_{19}ClFN_5O_4RuNa$ $(M + Na)^+$ 704.0045, found $(M + Na)^+$ 704.0055.

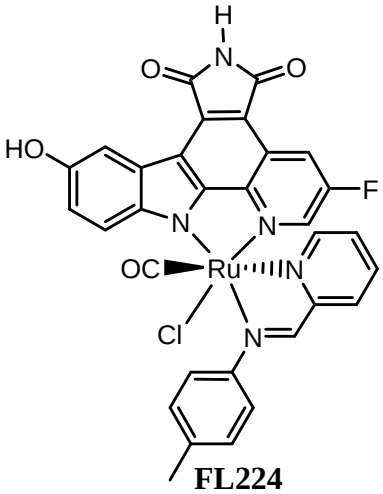

FL224

Complex FL224. The crude material was adsorbed onto silica gel and subjected to silica gel chromatography with dichloromethane : methanol (50:1) to obtain complex **FL224** (5.1 mg, 61%). ^{1}H NMR (300 MHz, acetone-d_6): δ (ppm) 9.88 (s, 1H), 9.18 (s, 1H), 8.69 (dd, *J* = 9.4, 2.4 Hz, 1H), 8.59 (d, *J* = 8.9 Hz, 1H), 8.36 (m, 1H), 8.33-8.31 (m, 2H), 8.20 (s, 1H), 8.15 (td, *J* = 7.7, 1.8 Hz, 1H), 8.03-8.00 (m, 2H), 7.50-7.40 (m, 4H),

7.15 (dd, *J* = 8.9, 2.6 Hz, 1H), 2.47 (s, 3H). HRMS calculated for $C_{31}H_{20}ClFN_5O_4Ru$ (M + H)$^+$ 682.0226, found (M + H)$^+$ 682.0231.

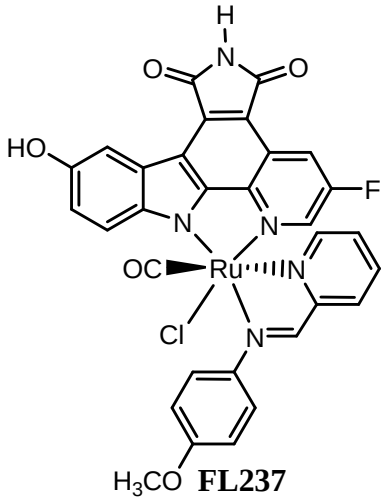

FL237

Complex FL237. The crude material was adsorbed onto silica gel and subjected to silica gel chromatography with dichloromethane : methanol (50:1) to obtain complex **FL237** (4.2 mg, 53%). ^{1}H NMR (300 MHz, acetone-d_6): δ (ppm) 9.88 (s, 1H), 9.15 (s, 1H), 8.68 (dd, *J* = 9.4, 2.3 Hz, 1H), 8.59 (d, *J* = 8.9 Hz, 1H), 8.35-8.30 (m, 3H), 8.19 (s, 1H), 8.16-8.07 (m, 3H), 7.48-7.39 (m, 2H), 7.24-7.19 (m, 2H), 7.15 (dd, *J* = 8.9, 2.6 Hz, 1H), 3.94 (s, 3H). HRMS calculated for $C_{31}H_{19}ClFN_5O_6RuNa$ (M + Na)$^+$ 719.9994, found (M + Na)$^+$ 719.9999.

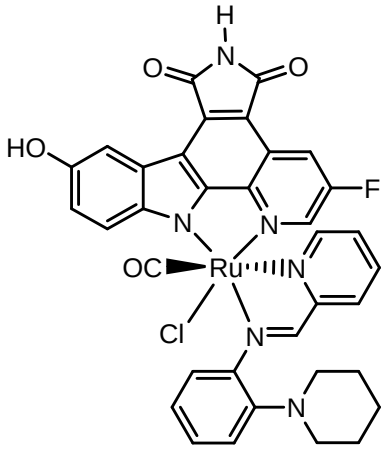

FL262-1

Complex FL262-1. Used as crude. HRMS calculated for $C_{35}H_{27}ClFN_6O_4Ru$ (M + H)$^+$ 751.0810, found (M + H)$^+$ 751.0784.

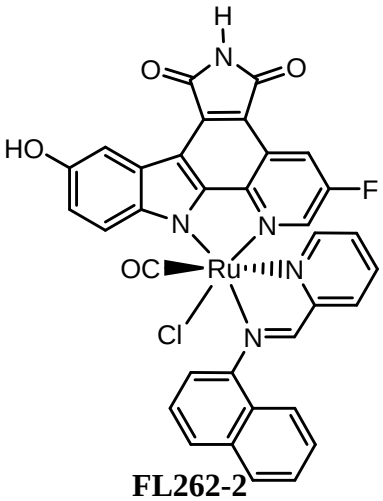

FL262-2

Complex FL262-2. Used as crude. HRMS calculated for $C_{36}H_{22}FN_6O_4Ru$ (M - Cl + $CH_3CN)^+$ 723.0730, found (M - Cl + $CH_3CN)^+$ 723.0787.

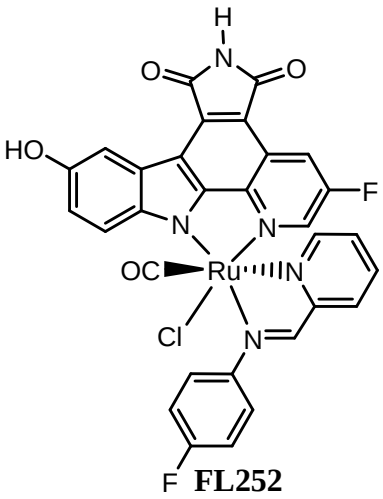

FL252

Complex FL252. The crude material was adsorbed onto silica gel and subjected to silica gel chromatography with dichloromethane : methanol (first 50:1, then 45:1) to obtain complex **FL252** (3.5 mg, 49%). ^{1}H NMR (300 MHz, acetone-d_6): δ (ppm) 9.89 (s, 1H), 9.23 (s, 1H), 8.69 (dd, *J* = 9.4, 2.4 Hz, 1H), 8.57 (d, *J* = 8.9 Hz, 1H), 8.38 (m, 1H), 8.36 (t, *J* = 2.5 Hz, 1H), 8.31 (d, *J* = 2.3 Hz, 1H), 8.23-8.14 (m, 4H), 7.51-7.43 (m, 4H), 7.15 (dd, *J* = 8.9, 2.6 Hz, 1H). HRMS calculated for $C_{30}H_{17}ClF_2N_5O_4Ru$ (M + H)$^+$ 685.9975, found (M + H)$^+$ 685.9981.

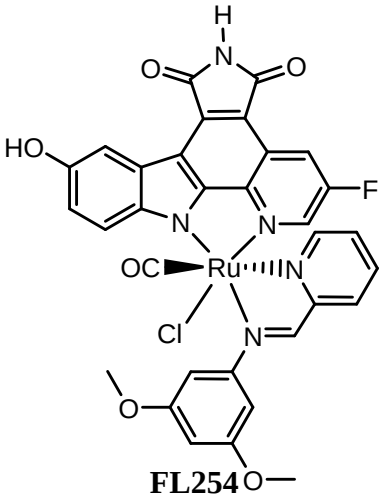

FL254

Complex FL254. The crude material was adsorbed onto silica gel and subjected to silica gel chromatography with dichloromethane : methanol (50:1) to obtain complex **FL254** (3.8 mg, 46%). ^{1}H NMR (300 MHz, acetone-d_6): δ (ppm) 9.89 (s, 1H), 9.23 (s, 1H), 8.68 (dd, *J* = 9.4, 2.4 Hz, 1H), 8.59 (d, *J* = 8.9 Hz, 1H), 8.38-8.34 (m, 2H), 8.31 (d, *J* = 2.6 Hz, 1H), 8.21 (s, 1H), 8.16 (td, *J* = 7.6, 1.8 Hz, 1H), 7.50-7.42 (m, 2H), 7.39 (d, *J* = 2.3 Hz, 2H), 7.15 (dd, *J* = 8.9, 2.6 Hz, 1H), 6.67 (t, *J* = 2.2 Hz, 1H), 3.94 (s, 6H). HRMS calculated for $C_{32}H_{22}ClFN_5O_6Ru$ $(M + H)^+$ 728.0281, found $(M + H)^+$ 728.0286.

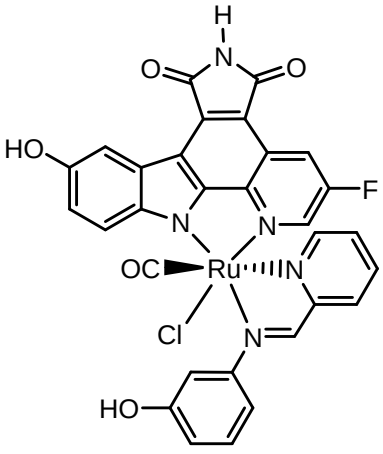

FL256

Complex FL256. The crude material was adsorbed onto silica gel and subjected to silica gel chromatography with dichloromethane : methanol (first 50:1, then 45:1) to obtain complex **FL256** (3.3 mg, 42%). ^{1}H NMR (300 MHz, acetone-d_6): δ (ppm) 9.89 (s, 1H), 9.18 (s, 1H), 9.10 (br, 1H), 8.69 (dd, *J* = 9.4, 2.4 Hz, 1H), 8.59 (d, *J* = 9.2 Hz, 1H), 8.37 (m, 1H), 8.34 (t, *J* = 2.5 Hz, 1H), 8.31 (d, *J* = 2.5 Hz, 1H), 8.21 (s, 1H), 8.15 (td, *J* = 7.7, 1.8 Hz, 1H), 7.62 (t, *J* = 2.1 Hz, 1H), 7.57-7.41 (m, 4H), 7.15 (dd, *J* = 8.9,

2.6 Hz, 1H), 7.04 (m, 1H). HRMS calculated for $C_{30}H_{17}ClFN_5O_5RuNa$ $(M + Na)^+$ 7005.9838, found $(M + Na)^+$ 705.9897.

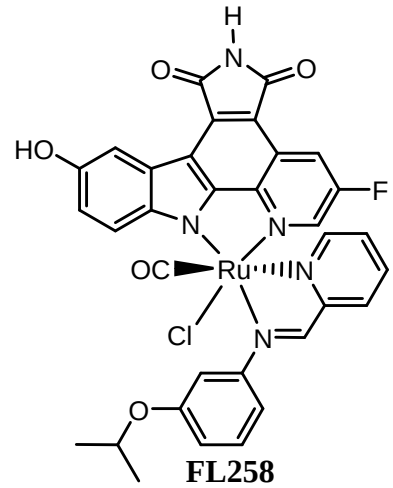

FL258

Complex FL258. The crude material was adsorbed onto silica gel and subjected to silica gel chromatography with dichloromethane : methanol (50:1) to obtain complex **FL258** (2.7 mg, 33%). ^{1}H NMR (300 MHz, acetone-d_6): δ (ppm) 9.88 (s, 1H), 9.21 (s, 1H), 8.69 (dd, J = 9.4, 2.3 Hz, 1H), 8.59 (d, J = 8.9 Hz, 1H), 8.37 (m, 1H), 8.34 (t, J = 2.5 Hz, 1H), 8.31 (d, J = 2.6 Hz, 1H), 8.21 (s, 1H), 8.16 (td, J = 7.7, 1.8 Hz, 1H), 7.78 (t, J = 2.2 Hz, 1H), 7.66 (m, 1H), 7.55 (t, J = 8.0 Hz, 1H), 7.50-7.42 (m, 2H), 7.15 (dd, J = 8.9, 2.6 Hz, 1H), 7.11 (m, 1H), 4.81 (m, 1H), 1.41 (m, 6H). HRMS calculated for $C_{33}H_{24}ClFN_5O_5Ru$ $(M + H)^+$ 726.0488, found $(M + H)^+$ 726.0508.

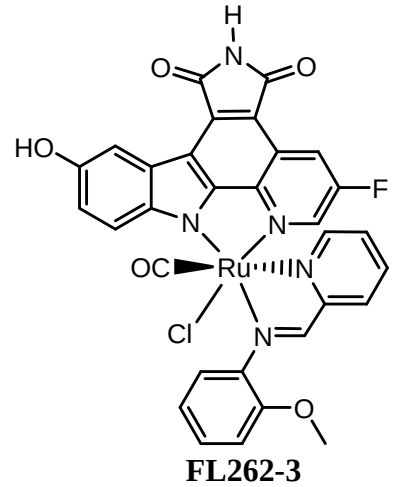

FL262-3

Complex FL262-3. The crude material was adsorbed onto silica gel and subjected to silica gel chromatography with dichloromethane : methanol (first 50:1, then 45:1) to obtain complex **FL262-3** (1.3 mg, 15%). ^{1}H NMR (300 MHz, acetone-d_6): δ (ppm) 9.87

(s, 1H), 9.19 (s, 1H), 8.82 (dd, *J* = 3.4, 2.4 Hz, 1H), 8.70 (dd, *J* = 9.2, 2.4 Hz, 1H), 8.58 (d, *J* = 8.9 Hz, 1H), 8.38 (m, 1H), 8.31 (d, *J* = 2.6 Hz, 1H), 8.17 (s, 1H), 8.16 (td, *J* = 7.7, 1.7 Hz, 1H), 8.03 (dd, *J* = 7.9, 1.6 Hz, 1H), 7.53-7.39 (m, 4H), 7.21 (m, 1H), 7.13 (dd, *J* = 8.9, 2.6 Hz, 1H), 4.14 (s, 3H). HRMS calculated for $C_{31}H_{19}ClFN_5O_6RuNa$ $(M + Na)^+$ 719.9994, found $(M + Na)^+$ 720.0002. The amino-complex is also isolated in the reaction: ^1H NMR (300 MHz, acetone-d_6): δ (ppm) 9.87 (s, 1H), 9.24 (dd, *J* = 3.9, 2.4 Hz, 1H), 8.81 (dd, *J* = 9.2, 2.4 Hz, 1H), 8.58 (d, *J* = 8.9 Hz, 1H), 8.27 (d, *J* = 2.5 Hz, 1H), 8.16 (m, 1H), 8.11 (s, 1H), 7.89 (td, *J* = 7.3, 2.0 Hz, 1H), 7.79-7.72 (m, 2H), 7.32-7.23 (m, 2H), 7.14-7.03 (m, 4H), 5.81 (dd, *J* = 14.1, 10.9 Hz, 1H), 4.54 (dd, *J* = 14.4, 3.9 Hz, 1H), 4.13 (s, 3H).

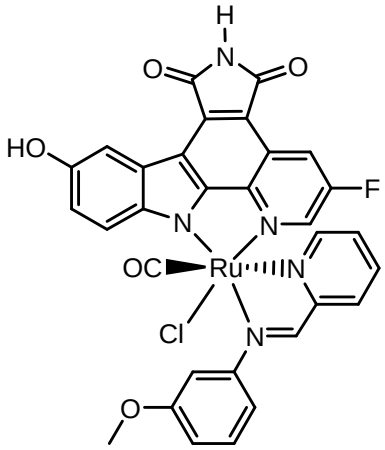

FL262-4

Complex FL262-4. Used as crude. HRMS calculated for $C_{31}H_{19}ClFN_5O_6Ru$ $(M + Na)^+$ 719.9994, found $(M + Na)^+$ 719.9998.

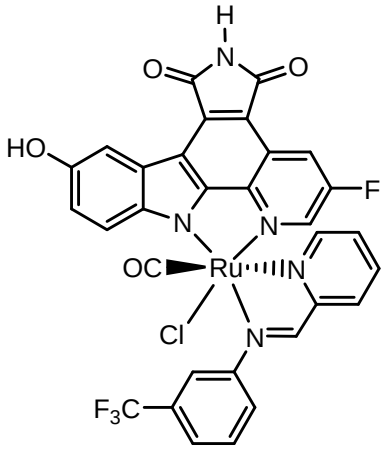

FL262-6

Complex FL262-6. Used as crude. HRMS calculated for $C_{31}H_{16}Cl_2F_4N_5O_4Ru$ $(M + Cl)^-$

769.9559, found $(M + Cl)^-$ 769.9484.

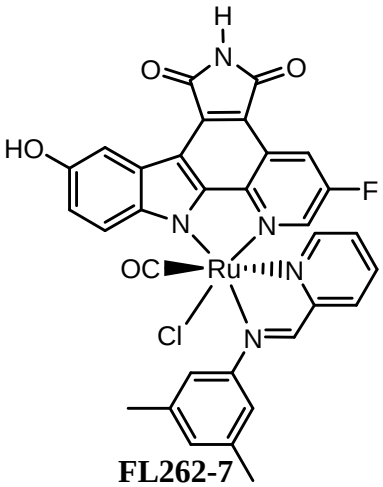

FL262-7

Complex FL262-7. Used as crude. HRMS calculated for $C_{34}H_{24}FN_6O_4Ru$ $(M - Cl + CH_3CN)^+$ 701.0887, found $(M - Cl + CH_3CN)^+$ 701.0856.

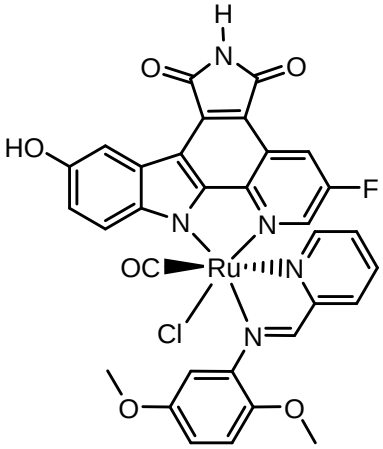

FL262-8

Complex FL262-8. Used as crude. HRMS calculated for $C_{32}H_{22}ClFN_5O_6Ru$ $(M + H)^+$ 728.0281, found $(M + H)^+$ 728.0287.

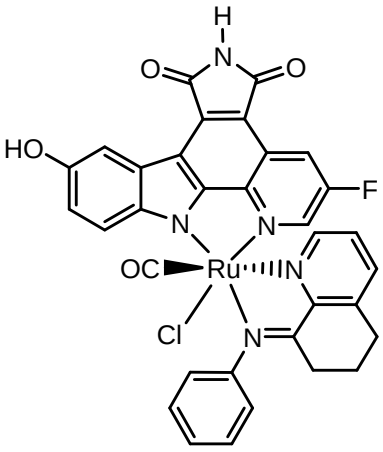

FL355

Complex FL355. The crude material was adsorbed onto silica gel and subjected to silica gel chromatography with dichloromethane : methanol (50:1) to obtain complex **FL355** (2.7 mg, 32%). ^{1}H NMR (300 MHz, acetone-d_6): δ (ppm) 9.86 (s, 1H), 8.69 (dd, *J* = 9.4, 2.3 Hz, 1H), 8.58-8.55 (m, 2H), 8.29 (d, d, *J* = 2.6 Hz, 1H), 8.17 (s, 1H), 7.97-7.34 (m, 8H), 7.12 (dd, *J* = 8.9, 2.6 Hz, 1H), 3.39-2.99 (m, 4H), 2.18 (m, 1H), 1.90 (m, 1H). HRMS calculated for $C_{33}H_{22}ClFN_5O_4Ru$ $(M + H)^+$ 708.0382, found $(M + H)^+$ 708.0386.

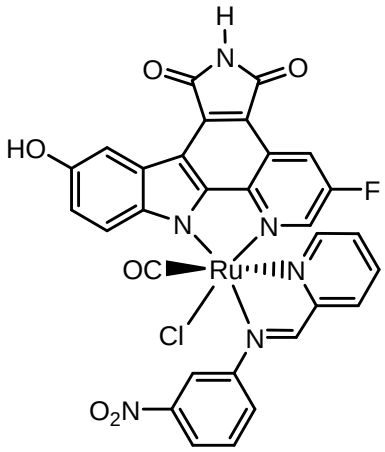

FL262-9

Complex FL262-9. The crude material was adsorbed onto silica gel and subjected to silica gel chromatography with dichloromethane : methanol (first 50:1, then 40:1) to obtain complex **FL262-9** (2.3 mg, 27%). ^{1}H NMR (300 MHz, acetone-d_6): δ (ppm) 9.90 (s, 1H), 9.42 (s, 1H), 9.00 (t, *J* = 2.1 Hz, 1H), 8.71-8.65 (m, 2H), 8.58 (d, *J* = 8.9 Hz, 1H), 8.48-8.45 (m, 3H), 8.31 (d, *J* = 2.6 Hz, 1H), 8.21 (s, 1H), 8.21 (td, *J* = 6.9, 2.5 Hz, 1H), 8.03 (t, *J* = 8.2 Hz, 1H), 7.54-7.48 (m, 2H), 7.16 (dd, *J* = 8.9, 2.6 Hz, 1H). HRMS calculated for $C_{30}H_{17}ClFN_6O_6Ru$ $(M + H)^+$ 712.9920, found $(M + H)^+$ 712.9949.

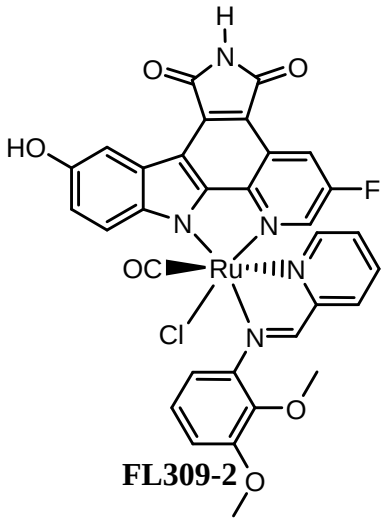

FL309-2

Complex FL309-2. Used as crude. HRMS calculated for $C_{32}H_{22}ClFN_5O_6Ru$ $(M + H)^+$ 728.0281, found $(M + H)^+$ 728.0291.

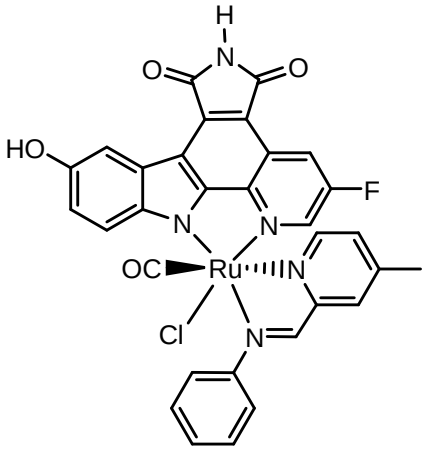

FL343

Complex FL343. The crude material was adsorbed onto silica gel and subjected to silica gel chromatography with dichloromethane : methanol (50:1) to obtain complex **FL343** (2.9 mg, 35%). ^{1}H NMR (300 MHz, acetone-d_6): δ (ppm) 9.88 (s, 1H), 9.13 (s, 1H), 8.69 (dd, *J* = 9.4, 2.4 Hz, 1H), 8.58 (d, *J* = 8.9 Hz, 1H), 8.34 (t, *J* = 2.5 Hz, 1H), 8.31 (d, *J* = 2.5 Hz, 1H), 8.20 (s, 1H), 8.18 (m, 1H), 8.13-8.09 (m, 2H), 7.72-7.65 (m, 2H), 7.58 (m, 1H), 7.31-7.24 (m, 2H), 7.15 (dd, *J* = 8.9, 2.6 Hz, 1H), 2.47 (s, 3H). HRMS calculated for $C_{31}H_{19}ClFN_5O_4RuNa$ $(M + Na)^+$ 704.0045, found $(M + Na)^+$ 704.0047.

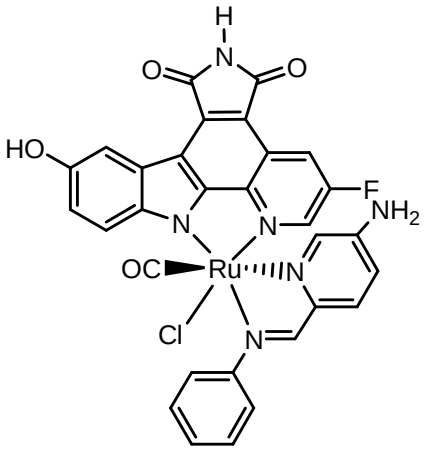

FL389

Complex FL389. The crude material was adsorbed onto silica gel and subjected to silica gel chromatography with dichloromethane : methanol (35:1) to obtain complex **FL389** (2.5 mg, 30%). ^{1}H NMR (300 MHz, acetone-d_6): δ (ppm) 9.87 (s, 1H), 8.83 (s, 1H), 8.70 (dd, *J* = 9.4, 2.4 Hz, 1H), 8.59 (d, *J* = 8.9 Hz, 1H), 8.31 (t, *J* = 2.5 Hz, 1H), 8.27 (d, *J* = 2.5 Hz, 1H), 8.19 (s, 1H), 8.07-8.02 (m, 2H), 7.98 (d, *J* = 8.6 Hz, 1H), 7.64-7.58 (m, 2H), 7.49 (m, 1H), 7.19-7.11 (m, 2H), 7.05 (d, *J* = 2.6 Hz, 1H), 6.06 (s, 2H). HRMS calculated for $C_{30}H_{18}ClFN_6O_4RuNa$ $(M + Na)^+$ 704.9998, found $(M + Na)^+$ 704.9999.

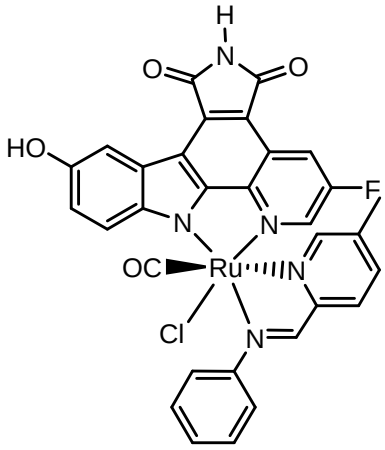

FL327

Complex FL327. The crude material was adsorbed onto silica gel and subjected to silica gel chromatography with dichloromethane : methanol (45:1) to obtain complex **FL327** (3.1 mg, 37%). ^{1}H NMR (300 MHz, acetone-d_6): δ (ppm) 9.88 (s, 1H), 9.12 (s, 1H), 9.06 (s, 1H), 8.69 (dd, *J* = 9.5, 2.4 Hz, 1H), 8.59 (d, *J* = 8.9 Hz, 1H), 8.33 (t, *J* = 2.5 Hz, 1H), 8.31 (d, *J* = 2.6 Hz, 1H), 8.26 (d, *J* = 8.0 Hz, 1H), 8.20 (s, 1H), 7.96 (m,

1H), 7.59 (m, 1H), 7.53 (m, 1H), 7.47 (t, *J* = 7.9 Hz, 1H), 7.39 (m, 1H), 7.15 (dd, *J* = 8.9, 2.6 Hz, 1H), 7.02 (m, 1H), 2.01 (s, 3H). HRMS calculated for $C_{31}H_{20}ClFN_5O_5Ru$ $(M + H)^+$ 698.0175, found $(M + H)^+$ 698.0178.

Chapter 6.1.2: Synthesis of MLCK inhibitors

General procedure for the synthesis of 3.81-3.86:

A suspension of the plain pyridocarbazole (10 mM), K_2CO_3 (1.1 equiv), and $[Ru(MeCN)_3([9]aneS_3)](CF_3SO_3)_2$ (1.1 equiv) in DMF (1.2 mL) was stirred at 85 °C under microwave irradiation for 30 minutes, followed by adding the monodentate ligand salt (2 equiv), then the mixture was stirred at 85 °C for an additional 30 minutes. The resulting suspension was dried *in vacuo* and the crude material was adsorbed onto silica gel and subjected to silica gel chromatography with dichloromethane : methanol (15:1) as the eluting solvent.

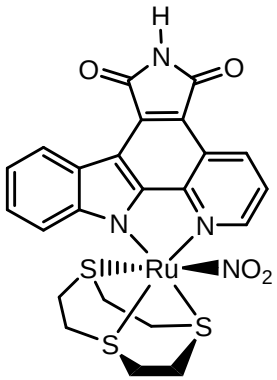

3.82

Complex 3.82. Yield: 65%. ^{1}H NMR (300 MHz, DMSO-d_6): δ (ppm) 11.04 (s, 1H), 9.13 (dd, *J* = 8.4, 1.1 Hz, 1H), 9.05 (dd, *J* = 5.0, 1.1 Hz, 1H), 8.73 (d, *J* = 7.5 Hz, 1H), 7.80-7.75 (m, 2H), 7.51 (m, 1H), 7.30 (m, 1H), 3.13-2.20 (m, 12H). ^{13}C NMR (125.8 MHz, DMSO-d_6): δ (ppm) 170.9, 170.8, 154.3, 151.9, 150.8, 143.7, 132.3, 130.3, 125.7, 124.1, 123.8, 123.3, 121.1, 118.7, 114.8, 114.7, 111.9, 34.8, 33.4, 33.3, 32.1, 31.1, 29.7. IR (film): *v* (cm^{-1}) 3012, 2930, 2154, 1747, 1702, 1582, 1481, 1412, 1345, 1288, 1230, 1027, 816, 754, 638, 493.

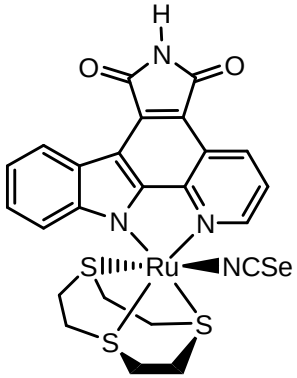

3.83

Complex 3.83. Yield: 33%. ^{1}H NMR (300 MHz, DMSO-d_6): δ (ppm) 11.05 (s, 1H), 9.09 (dd, J = 8.4, 1.1 Hz, 1H), 9.05 (dd, J = 5.1, 1.1 Hz, 1H), 8.73 (d, J = 7.5 Hz, 1H), 7.79 (dd, J = 8.4, 5.1 Hz, 1H), 7.68 (d, J = 8.3 Hz, 1H), 7.51 (m, 1H), 7.31 (m, 1H), 3.05-2.27 (m, 12H). ^{13}C NMR (100.6 MHz, DMSO-d_6): δ (ppm) 170.9, 170.8, 153.5, 151.9, 150.8, 143.2, 132.0, 130.2, 125.8, 124.1, 123.9, 123.5, 121.1, 118.8, 114.9, 114.7, 112.1, 106.7, 35.3, 34.7, 33.3, 33.1, 32.4, 30.3. IR (film): v (cm^{-1}) 3143, 3150, 2101, 1742, 1701, 1582, 1490, 1413, 1342, 1289, 1263, 1226, 1013, 819, 744, 638.

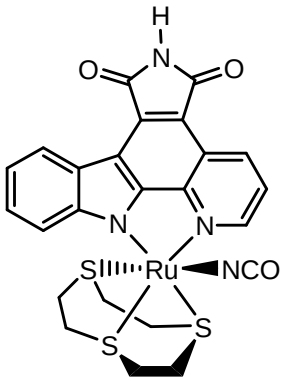

3.84

Complex 3.84. Yield: 46%. ^{1}H NMR (300 MHz, DMSO-d_6): δ (ppm) 11.03 (s, 1H), 9.13-9.08 (m, 2H), 8.75 (d, J = 7.4 Hz, 1H), 7.80-7.74 (m, 2H), 7.53 (m, 1H), 7.31 (m, 1H), 3.08-2.22 (m, 12H). ^{13}C NMR (125.8 MHz, DMSO-d_6): δ (ppm) 171.0, 170.9, 153.8, 151.9, 150.5, 143.4, 132.1, 130.3, 125.7, 124.1, 123.8, 123.3, 121.1, 118.7, 114.9, 114.6, 111.7, 34.8, 34.1, 33.5, 32.9, 32.0, 29.4. IR (film): v (cm^{-1}) 3052, 2978, 2226, 1749, 1701, 1547, 1412, 1342, 1291, 1226, 1011, 819, 794, 749, 703, 635, 492, 436.

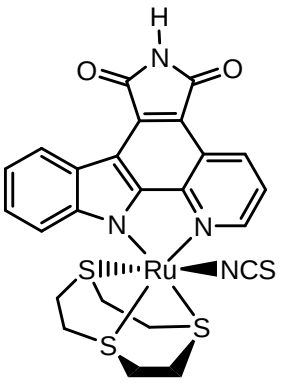

3.86

Complex 3.86. Yield: 52%. ^{1}H NMR (300 MHz, DMSO-d_6): δ (ppm) 11.07 (s, 1H), 9.15 (dd, J = 8.4, 1.0 Hz, 1H), 9.05 (dd, J = 5.1, 1.0 Hz, 1H), 8.76 (d, J = 7.8 Hz, 1H), 7.81 (dd, J = 8.4, 5.1 Hz, 1H), 7.74 (d, J = 8.3 Hz, 1H), 7.54 (m, 1H), 7.33 (m, 1H), 3.31-2.24 (m, 12H). ^{13}C NMR (125.8 MHz, DMSO-d_6): δ (ppm) 170.9, 170.7, 153.7, 151.8, 150.9, 143.2, 132.64, 132.58, 130.4, 125.9, 124.2, 123.8, 123.5, 121.0, 118.8, 114.75, 114.70, 112.1, 34.35, 34.28, 33.7, 32.6, 32.1, 29.7. IR (film): v (cm^{-1}) 2952, 2913, 2101, 1746, 1708, 1481, 1441, 1413, 1345, 1290, 1265, 1229, 1018, 820, 794, 748, 704, 637, 493, 440.

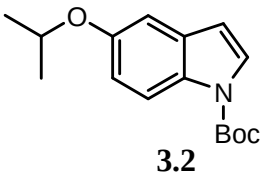

3.2

Compound 3.2. A solution of **3.1** (750 mg, 4.29 mmol) in THF (5 mL) was purged with nitrogen while cooling to 0 °C. To the solution was added di-*tert*-butyl dicarbonate (981 mg, 4.50 mmol), followed by the careful addition of solid 4-dimethylaminopyridine (621 mg, 4.50 mmol). The resulting suspension was warmed to room temperature naturally and stirred overnight. The reaction mixture was cooled to 0 °C and 1 M HCl (3 mL) was added carefully. After stirring at 0 °C for 5 minutes, the organic layer was separated and the aqueous layer was extracted with EtOAc twice. The combined organic layers were washed with brine, dried using Na_2SO_4, filtered and concentrated to dryness *in vacuo*. The crude material was adsorbed onto silica gel and subjected to silica gel chromatography with hexane : EtOAc (10:1) as the eluting solvent. The combined product eluents were dried *in vacuo* to provide **3.2** (1.16 g, 98%) as a solid. ^{1}H NMR

(300 MHz, $CDCl_3$): δ (ppm) 7.99 (d, *J* = 8.8 Hz, 1H), 7.55 (d, *J* = 3.4 Hz, 1H), 7.04 (d, *J* = 2.3 Hz, 1H), 6.91 (dd, *J* = 8.9, 2.3 Hz, 1H), 6.47 (d, *J* = 3.6 Hz, 1H), 4.55 (septet, *J* = 6.1 Hz, 1H), 1.66 (s, 9H), 1.34 (d, *J* = 6.1 Hz, 6H). ^{13}C NMR (100.6 MHz, $CDCl_3$): δ (ppm) 154.1, 126.6, 115.9, 115.2, 107.2, 107.1, 77.4, 71.0, 28.4, 22.3. IR (film): *v* (cm^{-1}) 2977, 1730, 1614, 1583, 1466, 1373, 1263, 1163, 1116, 1023, 974, 849, 763, 722. HRMS calculated for $C_{16}H_{22}NO_3$ $(M + H)^+$ 276.1594, found $(M + H)^+$ 276.1603.

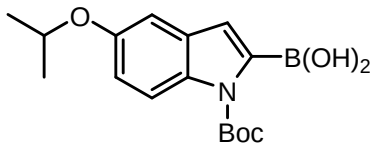

3.3

Compound 3.3. A solution of **3.2** (600 mg, 2.18 mmol) in anhydrous THF (4 mL) was prepared after drying **3.2** overnight under high vacuum. Following the addition of triisopropyl borate (0.76 mL, 3.28 mmol), the reaction mixture was cooled to 0 °C and lithium diisopropylamide (2.0 M solution in heptane-tetrahydrofuran-ethylbenzene) (1.64 mL, 3.28 mmol) was added dropwise over 15 minutes. After stirring for an additional 45 minutes at 0 °C, 2 M HCl (5.4 mL) was carefully added and stirred at 0 °C for 5 minutes. The resulting organic layer was separated and the aqueous layer was extracted using EtOAc twice. The combined organic layers were dried using Na_2SO_4, filtered and concentrated to dryness *in vacuo* to provide **3.3** (668 mg, 96%) which was carried forward without characterization.

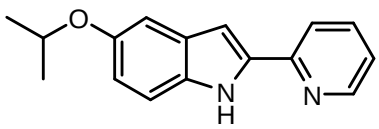

3.4

Compound 3.4. A biphasic suspension of **3.3** (624 mg, 1.96 mmol), 2-bromopyridine (281 mg, 1.78 mmol), tetrakis(triphenylphosphine)palladium(0) (144 mg, 0.12 mmol) and Na_2CO_3 (518 mg, 4.89 mmol) in 1,2-dimethoxyethane (18 mL) and water (2.1 mL) was purged with nitrogen and refluxed overnight. The resulting reaction mixture was cooled to room temperature, diluted with water and extracted with EtOAc for three times. The combined organic layers were washed with brine, dried using Na_2SO_4,

filtered and concentrated to dryness *in vacuo*. The crude material was adsorbed onto silica gel and subjected to silica gel chromatography with hexane : EtOAc (first 6:1, then 3:1) as the eluting solvent. The combined product eluents were isolated as a mixture of Boc-protected pyridylindole and **3.4**. The resulting solid was dissolved into DCM and adsorbed onto silica gel (8 g) using rotary evaporation. The white powder was heated to 80 °C overnight under high vacuum. The silica gel was cooled to room temperature, filtered through celite with EtOAc and the filtrate was dried *in vacuo* to provide **3.4** (390 mg, 87% over two steps) as a solid. ^{1}H NMR (300 MHz, $CDCl_3$): δ (ppm) 9.55 (s, 1H), 8.56 (d, *J* = 4.5 Hz, 1H), 7.78-7.68 (m, 2H), 7.28 (d, *J* = 8.8 Hz, 1H), 7.17-7.12 (m, 2H), 6.93 (s, 1H), 6.88 (dd, *J* = 8.8, 2.0 Hz, 1H), 4.53 (septet, *J* = 6.1 Hz, 1H), 1.36 (d, *J* = 6.1 Hz, 6H). ^{13}C NMR (100.6 MHz, $CDCl_3$): δ (ppm) 152.5, 150.5, 149.3, 137.4, 136.7, 132.2, 129.7, 122.0, 119.9, 116.0, 112.1, 106.5, 100.3, 71.3, 22.4. IR (film): *v* (cm^{-1}) 3189, 2973, 1592, 1543, 1443, 1381, 1369, 1211, 1134, 1113, 1070, 969, 774, 742. HRMS calculated for $C_{16}H_{17}N_2O$ $(M + H)^+$ 253.1335, found $(M + H)^+$ 253.1341.

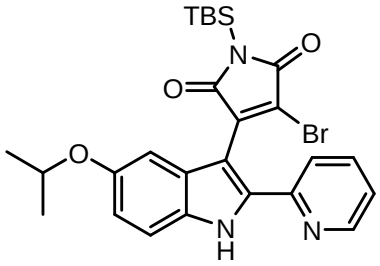

3.5

Compound 3.5. A solution of **3.4** (380 mg, 1.51 mmol) in anhydrous THF (4.5 mL) was prepared after drying **3.4** under high vacuum overnight. After cooling the solution to -15 °C, lithium bis(trimethylsilyl)amide (1 M solution in hexanes) (4.5 mL, 4.50 mmol) was added dropwise over 15 minutes and the resulting suspension was stirred at -15 °C for an additional 1 hour. A solution of TBS-protected dibromomaleimide (584 mg, 1.58 mmol) in THF (4.5 mL) cooled to 0 °C was added and the reaction mixture was stirred at -15 °C for 20 minutes and 10 °C overnight. The resulting dark purple reaction mixture was carefully poured into stirring ice cold 10% HCl (50 mL) and extracted with

EtOAc twice. The combined organic layers were washed with saturated $NaHCO_3$ followed by brine, dried using Na_2SO_4, filtered and concentrated to dryness *in vacuo*. The crude material was adsorbed onto silica gel and subjected to silica gel chromatography with hexane : EtOAc (first 6:1, then 3:1) as the eluting solvent. The combined product eluents were dried *in vacuo* to provide **3.5** as a solid which was carried forward without characterization.

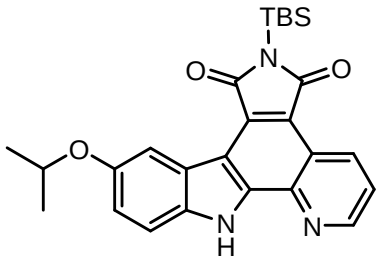

3.6

Compound 3.6. A solution of **3.5** in toluene (950 mL) was irradiated with a medium pressure Hg lamp (700 W) for 1 hour with constant nitrogen flow through the solution. The resulting red solution was concentrated to dryness *in vacuo*. The crude material was adsorbed onto silica gel and subjected to silica gel chromatography with hexane : EtOAc (3:1) as the eluting solvent. The combined product eluents were dried *in vacuo* to provide **3.6** (400 mg, 58% over two steps) as a yellow solid. ^{1}H NMR (300 MHz, $CDCl_3$): δ (ppm) 10.25 (br, 1H), 9.42 (dd, *J* = 8.5, 1.7 Hz, 1H), 8.99 (dd, *J* = 4.3, 1.7 Hz, 1H), 8.64 (d, *J* = 2.4 Hz, 1H), 7.63 (dd, *J* = 8.5, 4.3 Hz, 1H), 7.50 (d, *J* = 8.8, 1H), 7.20 (dd, *J* = 8.8, 2.4 Hz, 1H), 4.79 (septet, *J* = 6.1 Hz, 1H), 1.44 (d, *J* = 6.1 Hz, 6H), 1.07 (s, 9H), 0.63 (s, 6H). ^{13}C NMR (75.5 MHz, $CDCl_3$): δ (ppm) 175.7, 174.2, 153.5, 150.5, 140.7, 138.6, 134.6, 134.4, 130.9, 123.2, 122.9, 121.9, 120.3, 119.1, 115.2, 112.1, 110.8, 71.3, 26.7, 22.3, 19.3, -3.8. IR (film): *v* (cm^{-1}) 2956, 2930, 1748, 1690, 1469, 1333, 1313, 1282, 1216, 1114, 1066, 1041, 847, 826, 799. HRMS calculated for $C_{26}H_{30}N_3O_3Si$ $(M + H)^+$ 460.2051, found $(M + H)^+$ 460.2062.

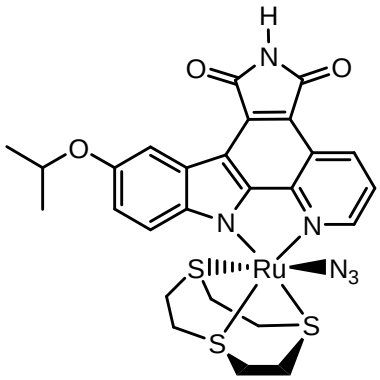

FL1359

Complex FL1359. A suspension of the ligand **3.6** (6 mg, 0.013 mmol), K_2CO_3 (2 mg, 0.014 mmol), and $[Ru(MeCN)_3([9]aneS_3)](CF_3SO_3)_2$ (10.1 mg, 0.014 mmol) in DMF (0.5 mL) was stirred at 85 °C under microwave irradiation for 30 minutes, followed by adding sodium azide (1.7 mg, 0.026 mmol), the mixture was stirred at 85 °C for an additional 30 minutes. The resulting suspension was dried *in vacuo* and the crude material was adsorbed onto silica gel and subjected to silica gel chromatography with dichloromethane : methanol (15:1) as the eluting solvent. The metal complex **FL1359** was isolated as a green solid (4.6 mg, 53%). ^{1}H NMR (300 MHz, DMSO-d_6): δ (ppm) 10.99 (s, 1H), 9.06-9.03 (m, 2H), 8.28 (d, J = 2.5 Hz, 1H), 7.74 (dd, J = 8.3, 5.1 Hz, 1H), 7.64 (d, J = 8.9 Hz, 1H), 7.17 (dd, J = 8.9, 2.5 Hz, 1H), 4.66 (septet, J = 6.0 Hz, 1H), 3.05-2.18 (m, 12H), 1.36 (d, J = 6.0 Hz, 6H). ^{13}C NMR (125.8 MHz, DMSO-d_6): δ (ppm) 171.0, 153.9, 151.0, 150.2, 147.1, 143.7, 132.0, 130.4, 124.1, 123.1, 121.1, 117.2, 115.5, 114.5, 110.9, 109.6, 70.5, 34.5, 33.9, 33.3, 32.7, 31.7, 29.4, 22.11, 22.08. IR (film): v (cm^{-1}) 3198, 2967, 2929, 2033, 1746, 1703, 1600, 1461, 1419, 1339, 1211, 1117, 699. HRMS calculated for $C_{26}H_{26}N_6O_3S_3Ru$ (M) 668.0267, found (M) 668.0259.

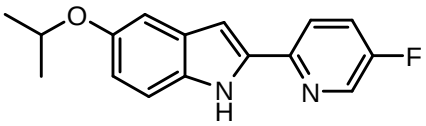

3.8

Compound 3.8. A biphasic suspension of **3.3** (668 mg, 2.09 mmol), 2-bromo-5-fluoropyridine (333 mg, 1.90 mmol), tetrakis(triphenylphosphine)palladium(0) (154 mg, 0.13 mmol) and Na_2CO_3 (555 mg, 5.23 mmol) in 1,2-dimethoxyethane (19 mL) and water (2.3 mL) was purged with nitrogen and refluxed overnight. The resulting reaction

mixture was cooled to room temperature, diluted with water and extracted with EtOAc for three times. The combined organic layers were washed with brine, dried using Na_2SO_4, filtered and concentrated to dryness *in vacuo*. The crude material was adsorbed onto silica gel and subjected to silica gel chromatography with hexane : EtOAc (8:1) as the eluting solvent. The combined product eluents were isolated as a mixture of Boc-protected pyridylindole and **3.8**. The resulting solid was dissolved into DCM and adsorbed onto silica gel (10 g) using rotary evaporation. The white powder was heated to 80 °C overnight under high vacuum. The silica gel was cooled to room temperature, filtered through celite with EtOAc and the filtrate was dried *in vacuo* to provide **3.8** (500 mg, 97% over two steps) as a solid. ^{1}H NMR (300 MHz, $CDCl_3$): δ (ppm) 9.27 (s, 1H), 8.41 (d, *J* = 2.8 Hz, 1H), 7.75 (dd, *J* = 8.8, 4.3 Hz, 1H), 7.44 (td, *J* = 8.6, 2.9 Hz, 1H), 7.29 (d, *J* = 8.8 Hz, 1H), 7.11 (d, *J* = 2.2 Hz, 1H), 6.88 (dd, *J* = 8.8, 2.3 Hz, 1H), 6.85 (d, *J* = 1.8 Hz, 1H), 4.53 (septet, *J* = 6.1 Hz, 1H), 1.36 (d, *J* = 6.1 Hz, 6H). ^{13}C NMR (75.5 MHz, $CDCl_3$): δ (ppm) 160.3, 156.9, 152.6, 147.0, 137.5, 137.1, 136.6, 132.2, 129.7, 124.0, 123.8, 120.7, 120.6, 116.0, 112.1, 106.5, 100.10, 100.09, 71.3, 22.4. IR (film): *v* (cm^{-1}) 3428, 3411, 2977, 1548, 1454, 1427, 1381, 1228, 1205, 1150, 1114, 968, 918, 835, 792, 532. HRMS calculated for $C_{16}H_{16}FN_2O$ $(M + H)^+$ 271.1241, found $(M + H)^+$ 271.1245.

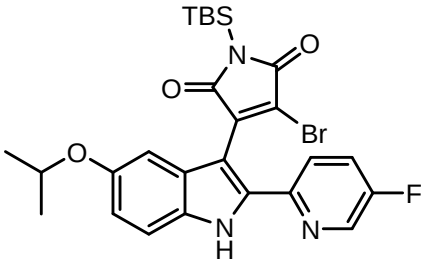

3.9

Compound 3.9. A solution of **3.8** (500 mg, 1.85 mmol) in anhydrous THF (5.6 mL) was prepared after drying **3.8** under high vacuum overnight. After cooling the solution to -15 °C, lithium bis(trimethylsilyl)amide (1 M solution in hexanes) (5.6 mL, 5.60 mmol) was added dropwise over 15 minutes and the resulting suspension was stirred at -15 °C for an additional 1 hour. A solution of TBS-protected dibromomaleimide (718 mg, 1.94

mmol) in THF (5.6 mL) cooled to 0 °C was added and the reaction mixture was stirred at -15 °C for 20 minutes and 10 °C overnight. The resulting dark purple reaction mixture was carefully poured into stirring ice cold 10% HCl (50 mL) and extracted with EtOAc twice. The combined organic layers were washed with saturated $NaHCO_3$ followed by brine, dried using Na_2SO_4, filtered and concentrated to dryness *in vacuo*. The crude material was adsorbed onto silica gel and subjected to silica gel chromatography with hexane : EtOAc (first 6:1, then 3:1) as the eluting solvent. The combined product eluents were dried *in vacuo* to provide **3.9** (710 mg, 68%) as a solid which was carried forward without characterization.

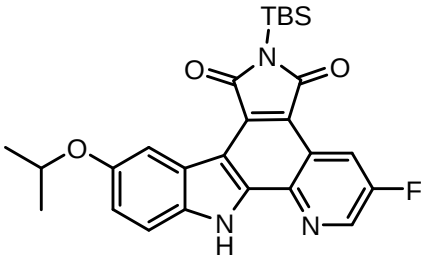

3.10

Compound 3.10. A solution of **3.9** (300 mg, 0.54 mmol) in toluene (950 mL) was irradiated with a medium pressure Hg lamp (700 W) for 20 minutes with constant nitrogen flow through the solution. The resulting red solution was concentrated to dryness *in vacuo*. The crude material was adsorbed onto silica gel and subjected to silica gel chromatography with hexane : EtOAc (8:1) as the eluting solvent. The combined product eluents were dried *in vacuo* to provide **3.10** (215 mg, 84%) as a yellow solid. ^{1}H NMR (300 MHz, $CDCl_3$): δ (ppm) 10.05 (s, 1H), 8.96 (dd, *J* = 9.4, 2.8 Hz, 1H), 8.78 (d, *J* = 2.8 Hz, 1H), 8.53 (d, *J* = 2.4 Hz, 1H), 7.42 (d, *J* = 8.8 Hz, 1H), 7.17 (dd, *J* = 8.8, 2.5 Hz, 1H), 4.75 (septet, *J* = 6.1 Hz, 1H), 1.44 (d, *J* = 6.1 Hz, 6H), 1.07 (s, 9H), 0.65 (s, 6H). ^{13}C NMR (75.5 MHz, $CDCl_3$): δ (ppm) 175.3, 173.8, 159.6, 156.2, 153.6, 141.4, 141.1, 140.5, 135.24, 135.22, 134.3, 131.7, 122.9, 122.2, 122.1, 119.6, 119.5, 119.1, 117.9, 117.6, 114.7, 112.1, 110.7, 71.2, 26.6, 22.3, 19.3, -3.8. IR (film): *v* (cm^{-1}) 3464, 2930, 1748, 1692, 1468, 1310, 1288, 1252, 1215, 1058, 1039, 827, 763, 478, 451. HRMS calculated for $C_{26}H_{29}FN_3O_3Si$ $(M + H)^+$ 478.1957, found $(M + H)^+$ 478.1957.

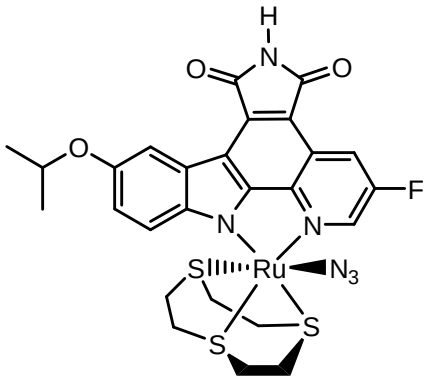

FL1335

Complex FL1335. A suspension of the ligand **3.10** (7 mg, 0.015 mmol), K_2CO_3 (2 mg, 0.016 mmol), and $[Ru(MeCN)_3([9]aneS_3)](CF_3SO_3)_2$ (11.3 mg, 0.016 mmol) in DMF (0.6 mL) was stirred at 85 °C under microwave irradiation for 30 minutes, followed by adding sodium azide (1.9 mg, 0.029 mmol), then the mixture was stirred at 85 °C for an additional 30 minutes. The resulting suspension was dried *in vacuo* and the crude material was adsorbed onto silica gel and subjected to silica gel chromatography with dichloromethane : methanol (15:1) as the eluting solvent. The metal complex **FL1335** was isolated as a solid (4.8 mg, 48%). ^{1}H NMR (300 MHz, DMSO-d_6): δ (ppm) 11.1 (s, 1H), 9.06 (t, *J* = 2.3 Hz, 1H), 8.74 (dd, *J* = 9.4, 2.1 Hz, 1H), 8.28 (d, *J* = 2.5 Hz, 1H), 7.63 (d, *J* = 8.9 Hz, 1H), 7.19 (dd, *J* = 8.9, 2.5 Hz, 1H), 4.67 (septet, *J* = 6.0 Hz, 1H), 3.02-2.27 (m, 12H), 1.36 (d, *J* = 6.0 Hz, 6H). ^{13}C NMR (125.8 MHz, DMSO-d_6): δ (ppm) 170.7, 170.6, 158.2, 155.7, 153.9, 151.3, 147.1, 140.9, 140.1, 139.8, 131.1, 124.1, 120.8, 120.7, 117.3, 116.1, 115.9, 115.5, 114.5, 110.22, 110.17, 109.7, 70.4, 33.9, 33.4, 33.3, 32.9, 32.5, 30.0, 22.09, 22.06. IR (film): *ν* (cm^{-1}) 2030, 1744, 1711, 1559, 1458, 1411, 1336, 1261, 1224, 1197, 1111, 966, 818, 756. HRMS calculated for $C_{26}H_{25}FN_6O_3S_3RuNa$ $(M + Na)^+$ 709.0070, found $(M + Na)^+$ 709.0076.

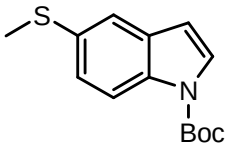

3.13

Compound 3.13. A solution of **3.12** (830 mg, 5.09 mmol) in THF (5 mL) was purged with nitrogen while cooling to 0 °C. To the solution was added di-*tert*-butyl dicarbonate (1.17 g, 5.37 mmol), followed by the careful addition of solid 4-dimethylaminopyridine

(738 mg, 5.37 mmol). The resulting suspension was warmed to room temperature naturally and stirred overnight. The reaction mixture was cooled to 0 °C and 1 M HCl (3.6 mL) was added carefully. After stirring at 0 °C for 5 minutes, the organic layer was separated and the aqueous layer was extracted with EtOAc twice. The combined organic layers were washed with brine, dried using Na_2SO_4, filtered and concentrated to dryness *in vacuo*. The crude material was adsorbed onto silica gel and subjected to silica gel chromatography with hexane : EtOAc (15:1) as the eluting solvent. The combined product eluents were dried *in vacuo* to provide **3.13** (1.09 g, 81%) as a solid. ^{1}H NMR (300 MHz, $CDCl_3$): δ (ppm) 8.05 (d, *J* = 8.5 Hz, 1H), 7.58 (d, *J* = 3.6 Hz, 1H), 7.49 (d, *J* = 1.8 Hz, 1H), 7.27 (dd, *J* = 8.5, 1.9 Hz, 1H), 6.51 (d, *J* = 3.7 Hz, 1H), 2.52 (s, 3H), 1.67 (s, 9H). ^{13}C NMR (100.6 MHz, $CDCl_3$): δ (ppm) 131.9, 131.5, 126.7, 124.9, 120.3, 115.7, 106.9, 84.1, 28.3, 17.7. IR (film): *v* (cm^{-1}) 2978, 1734, 1451, 1369, 1340, 1280, 1248, 1202, 1161, 1136, 1085, 1023, 764, 723. HRMS calculated for $C_{14}H_{17}NO_2SNa$ $(M + Na)^+$ 286.0872, found $(M + Na)^+$ 286.0872.

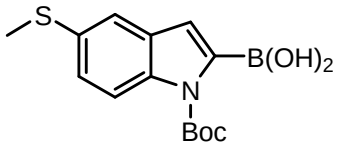

3.14

Compound 3.14. A solution of **3.13** (500 mg, 1.90 mmol) in anhydrous THF (3 mL) was prepared after drying **3.13** overnight under high vacuum. Following the addition of triisopropyl borate (0.66 mL, 2.85 mmol), the reaction mixture was cooled to 0 °C and lithium diisopropylamide (2.0 M solution in heptane-tetrahydrofuran-ethylbenzene) (1.43 mL, 2.86 mmol) was added dropwise over 15 minutes. After stirring for an additional 45 minutes at 0 °C, 2 M HCl (4.7 mL) was carefully added and stirred at 0 °C for 5 minutes. The resulting organic layer was separated and the aqueous layer was extracted using EtOAc twice. The combined organic layers were dried using Na_2SO_4, filtered and concentrated to dryness *in vacuo* to provide **3.14** (572 mg, 98%) which was carried forward without characterization.

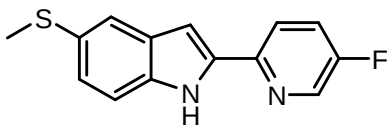

3.15

Compound 3.15. A biphasic suspension of **3.14** (572 mg, 1.86 mmol), 2-bromo-5-fluoropyridine (298 mg, 1.69 mmol), tetrakis(triphenylphosphine)palladium(0) (137 mg, 0.12 mmol) and Na_2CO_3 (493 mg, 4.65 mmol) in 1,2-dimethoxyethane (17 mL) and water (2.0 mL) was purged with nitrogen and refluxed overnight. The resulting reaction mixture was cooled to room temperature, diluted with water and extracted with EtOAc for three times. The combined organic layers were washed with brine, dried using Na_2SO_4, filtered and concentrated to dryness *in vacuo*. The crude material was adsorbed onto silica gel and subjected to silica gel chromatography with hexane : EtOAc (8:1) as the eluting solvent. The combined product eluents were isolated as a mixture of Boc-protected pyridylindole and **3.15**. The resulting solid was dissolved into DCM and adsorbed onto silica gel (8 g) using rotary evaporation. The white powder was heated to 80 °C overnight under high vacuum. The silica gel was cooled to room temperature, filtered through celite with EtOAc and the filtrate was dried *in vacuo* to provide **3.15** (380 mg, 87% over two steps) as a solid. ^{1}H NMR (300 MHz, $CDCl_3$): δ (ppm) 9.44 (s, 1H), 8.43 (d, *J* = 2.8 Hz, 1H), 7.77 (dd, *J* = 8.8, 4.3 Hz, 1H), 7.63 (br, 1H), 7.45 (td, *J* = 8.5, 2.8 Hz, 1H), 7.34 (d, *J* = 8.5 Hz, 1H), 7.24 (dd, *J* = 8.5, 1.7 Hz, 1H), 6.88 (d, *J* = 1.7 Hz, 1H), 2.53 (s, 3H). ^{13}C NMR (75.5 MHz, $CDCl_3$): δ (ppm) 160.4, 157.1, 146.74, 146.69, 137.5, 137.2, 136.6, 135.4, 130.0, 128.7, 125.3, 124.1, 123.9, 121.6, 120.93, 120.87, 112.0, 99.90, 99.89, 18.7. IR (film): *v* (cm^{-1}) 3427, 1730, 1547, 1469, 1451, 1422, 1311, 1266, 1230, 837, 796, 735, 535. HRMS calculated for $C_{14}H_{12}FN_2S$ $(M + H)^+$ 259.0700, found $(M + H)^+$ 259.0698.

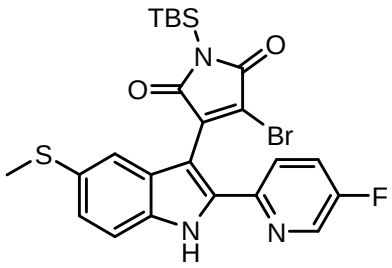

3.16

Compound 3.16. A solution of **3.15** (380 mg, 1.47 mmol) in anhydrous THF (4.0 mL) was prepared after drying **3.15** under high vacuum overnight. After cooling the solution to -15 °C, lithium bis(trimethylsilyl)amide (1 M solution in hexanes) (4.4 mL, 4.40 mmol) was added dropwise over 15 minutes and the resulting suspension was stirred at -15 °C for an additional 1 hour. A solution of TBS-protected dibromomaleimide (571 mg, 1.55 mmol) in THF (4.0 mL) cooled to 0 °C was added and the reaction mixture was stirred at -15 °C for 20 minutes and 10 °C overnight. The resulting dark purple reaction mixture was carefully poured into stirring ice cold 10% HCl (50 mL) and extracted with EtOAc twice. The combined organic layers were washed with saturated $NaHCO_3$ followed by brine, dried using Na_2SO_4, filtered and concentrated to dryness *in vacuo*. The crude material was adsorbed onto silica gel and subjected to silica gel chromatography with hexane : EtOAc (first 6:1, then 3:1) as the eluting solvent. The combined product eluents were dried *in vacuo* to provide **3.16** as a solid which was carried forward without characterization.

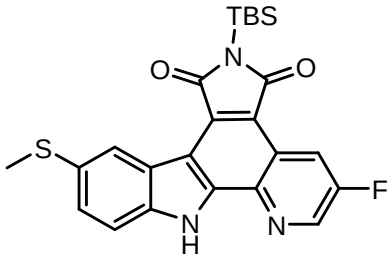

3.17

Compound 3.17. A solution of **3.16** in toluene (220 mL) was irradiated with a medium pressure Hg lamp (150 W) using a pyrex filter for 2.5 hours with constant nitrogen flow through the solution. The resulting red solution was concentrated to dryness *in vacuo*. The crude material was adsorbed onto silica gel and subjected to silica gel

chromatography with hexane : EtOAc (3:1) as the eluting solvent. The combined product eluents were dried *in vacuo* to provide **3.17** (123 mg, 18% over two steps) as a yellow solid. ^{1}H NMR (300 MHz, $CDCl_3$): δ (ppm) 9.85 (s, 1H), 9.07-9.03 (m, 2H), 8.88 (d, *J* = 2.8 Hz, 1H), 7.57 (m, 2H), 2.67 (s, 3H), 1.06 (s, 9H), 0.63 (s, 6H). ^{13}C NMR (125.8 MHz, $CDCl_3$): δ (ppm) 175.3, 173.7, 159.2, 157.1, 141.9, 141.7, 140.4, 137.8, 135.4, 131.7, 131.3, 128.5, 124.8, 123.1, 122.6, 122.5, 120.55, 120.52, 117.9, 117.8, 114.2, 112.0, 26.6, 19.3, 18.2, -3.9. IR (film): *v* (cm^{-1}) 2930, 2859, 1750, 1692, 1561, 1461, 1414, 1336, 1304, 1282, 1257, 1057, 846, 826, 768. HRMS calculated for $C_{24}H_{24}FN_3O_2SSiNa$ $(M + Na)^+$ 488.1235, found $(M + Na)^+$ 488.1237.

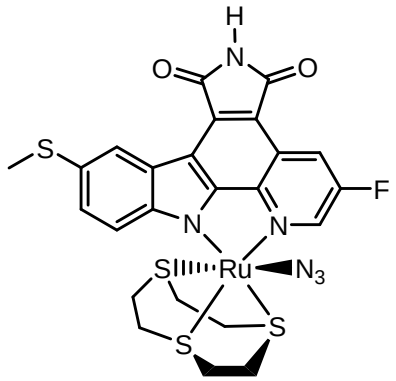

FL1288

Complex FL1288. A suspension of the ligand **3.17** (7 mg, 0.015 mmol), K_2CO_3 (2.3 mg, 0.017 mmol), and $[Ru(MeCN)_3([9]aneS_3)](CF_3SO_3)_2$ (11.6 mg, 0.017 mmol) in DMF (0.6 mL) was stirred at 85 °C under microwave irradiation for 30 minutes, followed by adding sodium azide (2 mg, 0.031 mmol), then the mixture was stirred at 85 °C for an additional 40 minutes. The resulting suspension was dried *in vacuo* and the crude material was adsorbed onto silica gel and subjected to silica gel chromatography with dichloromethane : methanol (15:1) as the eluting solvent. The metal complex **FL1288** was isolated as a solid (4.5 mg, 45%). ^{1}H NMR (300 MHz, DMSO-d_6): δ (ppm) 11.17 (s, 1H), 9.11 (t, *J* = 2.5 Hz, 1H), 8.77 (dd, *J* = 9.4, 2.3 Hz, 1H), 8.71 (d, *J* = 1.9 Hz, 1H), 7.70 (d, *J* = 8.6 Hz, 1H), 7.54 (dd, *J* = 8.7, 1.9 Hz, 1H), 3.02-2.26 (m, 12H), 2.57 (s, 3H). ^{13}C NMR (100.6 MHz, DMSO-d_6): δ (ppm) 170.7, 170.5, 158.4, 155.9, 154.0, 150.6, 140.9, 140.5, 131.0, 127.1, 126.7, 124.3, 123.9, 120.9, 120.8, 116.3, 116.1, 115.6, 113.9, 111.62, 111.57, 33.9, 33.5, 33.3, 33.0, 32.6, 30.0, 17.9. IR (film): *v* (cm^{-1}) 2033, 1736,

1700, 1609, 1555, 1488, 1405, 1333, 1252, 1222, 1199, 1025, 1001, 820, 802, 635.

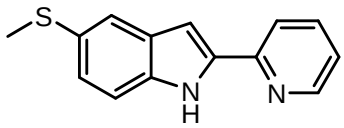

3.19

Compound 3.19. A biphasic suspension of **3.14** (572 mg, 1.86 mmol), 2-bromo pyridine (268 mg, 1.70 mmol), tetrakis(triphenylphosphine)palladium(0) (137 mg, 0.12 mmol) and Na_2CO_3 (493 mg, 4.65 mmol) in 1,2-dimethoxyethane (17 mL) and water (2.0 mL) was purged with nitrogen and refluxed overnight. The resulting reaction mixture was cooled to room temperature, diluted with water and extracted with EtOAc for three times. The combined organic layers were washed with brine, dried using Na_2SO_4, filtered and concentrated to dryness *in vacuo*. The crude material was adsorbed onto silica gel and subjected to silica gel chromatography with hexane : EtOAc (first 8:1, then 6:1) as the eluting solvent. The combined product eluents were isolated as a mixture of Boc-protected pyridylindole and **3.19**. The resulting solid was dissolved into DCM and adsorbed onto silica gel (6 g) using rotary evaporation. The white powder was heated to 80 °C overnight under high vacuum. The silica gel was cooled to room temperature, filtered through celite with EtOAc and the filtrate was dried *in vacuo* to provide **3.19** (310 mg, 76% over two steps) as a solid. ^{1}H NMR (300 MHz, $CDCl_3$): δ (ppm) 9.57 (s, 1H), 8.57 (d, *J* = 4.7 Hz, 1H), 7.79 (d, *J* = 8.0 Hz, 1H), 7.72 (td, *J* = 8.0, 1.7 Hz, 1H), 7.64 (br, 1H), 7.34 (d, *J* = 8.5 Hz, 1H), 7.24 (dd, *J* = 8.5, 1.7 Hz, 1H), 7.18 (m, 1H), 6.95 (br, 1H), 2.53 (s, 3H). ^{13}C NMR (100.6 MHz, $CDCl_3$): δ (ppm) 150.2, 149.3, 137.5, 136.8, 135.3, 130.1, 128.5, 125.3, 122.3, 121.7, 120.0, 112.0, 100.1, 18.8. IR (film): *v* (cm^{-1}) 3138, 2916, 1592, 1563, 1542, 1440, 1408, 1310, 1185, 1152, 775, 743, 5973, 527. HRMS calculated for $C_{14}H_{13}N_2S$ $(M + H)^+$ 241.0794, found $(M + H)^+$ 241.0796.

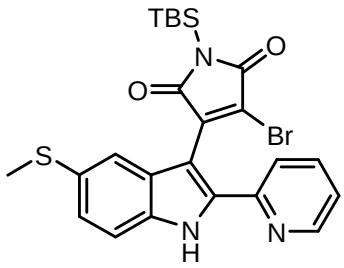

3.20

Compound 3.20. A solution of **3.19** (310 mg, 1.29 mmol) in anhydrous THF (3.9 mL) was prepared after drying **3.19** under high vacuum overnight. After cooling the solution to -15 °C, lithium bis(trimethylsilyl)amide (1 M solution in hexanes) (3.9 mL, 3.90 mmol) was added dropwise over 15 minutes and the resulting suspension was stirred at -15 °C for an additional 1 hour. A solution of TBS-protected dibromomaleimide (500 mg, 1.35 mmol) in THF (3.9 mL) cooled to 0 °C was added and the reaction mixture was stirred at -15 °C for 20 minutes and 10 °C overnight. The resulting dark purple reaction mixture was carefully poured into stirring ice cold 10% HCl (50 mL) and extracted with EtOAc twice. The combined organic layers were washed with saturated $NaHCO_3$ followed by brine, dried using Na_2SO_4, filtered and concentrated to dryness *in vacuo*. The crude material was adsorbed onto silica gel and subjected to silica gel chromatography with hexane : EtOAc (3:1) as the eluting solvent. The combined product eluents were dried *in vacuo* to provide **3.20** as a solid which was carried forward without characterization.

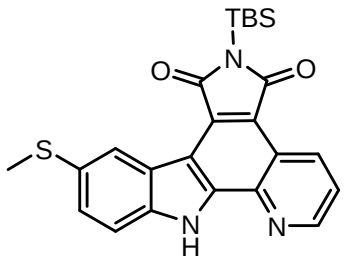

3.21

Compound 3.21. A solution of **3.20** in toluene (950 mL) was irradiated with a medium pressure Hg lamp (700 W) for 30 minutes with constant nitrogen flow through the solution. The resulting red solution was concentrated to dryness *in vacuo*. The crude material was adsorbed onto silica gel and subjected to silica gel chromatography with

hexane : EtOAc (6:1) as the eluting solvent. The combined product eluents were dried *in vacuo* to provide **3.21** (242 mg, 42% over two steps) as a yellow solid. ^{1}H NMR (300 MHz, $CDCl_3$): δ (ppm) 10.57 (s, 1H), 9.42 (dd, *J* = 8.5, 1.6 Hz, 1H), 9.05 (br, 1H), 9.0 (dd, *J* = 4.3, 1.7 Hz, 1H), 7.65 (dd, *J* = 8.5, 4.3 Hz, 1H), 7.55-7.47 (m, 2H), 2.66 (s, 3H), 1.07 (s, 9H), 0.64 (s, 6H). ^{13}C NMR (75.5 MHz, $CDCl_3$): δ (ppm) 175.5, 174.0, 150.7, 140.3, 138.5, 138.0, 134.5, 130.9, 130.8, 128.5, 124.9, 123.2, 123.1, 122.1, 114.6, 112.0, 26.7, 19.3, 18.3, -3.8. IR (film): *v* (cm^{-1}) 2927, 2854, 1685, 1594, 1332, 1303, 1276, 1258, 1056, 1039, 823, 793, 736, 694, 524, 478. HRMS calculated for $C_{24}H_{25}N_3O_2SSiNa$ $(M + Na)^+$ 470.1329, found $(M + Na)^+$ 470.1331.

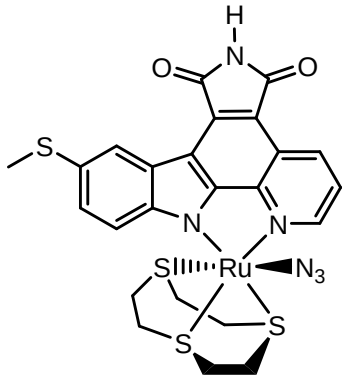

FL1343

Complex FL1343. A suspension of the ligand **3.21** (7 mg, 0.016 mmol), K_2CO_3 (2.4 mg, 0.017 mmol), and $[Ru(MeCN)_3([9]aneS_3)](CF_3SO_3)_2$ (12.1 mg, 0.017 mmol) in DMF (0.6 mL) was stirred at 85 °C under microwave irradiation for 30 minutes, followed by adding sodium azide (2 mg, 0.031 mmol), then the mixture was stirred at 85 °C for an additional 30 minutes. The resulting suspension was dried *in vacuo* and the crude material was adsorbed onto silica gel and subjected to silica gel chromatography with dichloromethane : methanol (10:1) as the eluting solvent. The metal complex **FL1343** was isolated as a solid (5 mg, 48%). ^{1}H NMR (400 MHz, DMSO-d_6): δ (ppm) 11.05 (s, 1H), 9.11-9.08 (m, 2H), 8.74 (d, *J* = 1.8 Hz, 1H), 7.79 (dd, *J* = 8.3, 5.1 Hz, 1H), 7.73 (d, *J* = 8.6 Hz, 1H), 7.53 (dd, *J* = 8.6, 2.0 Hz, 1H), 3.07-2.21 (m, 12H), 2.58 (s, 3H). ^{13}C NMR (125.8 MHz, DMSO-d_6): δ (ppm) 170.9, 170.8, 154.0, 150.7, 150.6, 143.5, 132.2, 130.3, 126.9, 126.1, 124.4, 124.1, 123.4, 121.2, 115.6, 113.9, 112.2, 34.5, 33.8, 33.4, 32.7, 31.7, 29.5, 18.0. IR (film): *v* (cm^{-1}) 2032, 1738, 1701, 1595, 1527, 1486, 1418,

1339, 1225, 1131, 1093, 820, 792, 671, 638. HRMS calculated for $C_{24}H_{22}N_6O_2S_4RuNa$ $(M + Na)^+$ 678.9623, found $(M + Na)^+$ 678.9629.

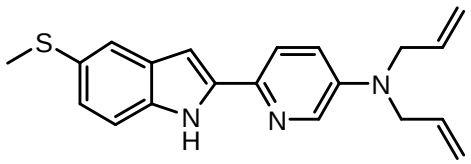

3.24

Compound 3.24. A biphasic suspension of **3.14** (675 mg, 2.20 mmol), **3.23** (504 mg, 2.0 mmol), tetrakis(triphenylphosphine)palladium(0) (162 mg, 0.14 mmol) and Na_2CO_3 (583 mg, 5.50 mmol) in 1,2-dimethoxyethane (20 mL) and water (2.4 mL) was purged with nitrogen and refluxed overnight. The resulting reaction mixture was cooled to room temperature, diluted with water and extracted with EtOAc for three times. The combined organic layers were washed with brine, dried using Na_2SO_4, filtered and concentrated to dryness *in vacuo*. The crude material was adsorbed onto silica gel and subjected to silica gel chromatography with hexane : EtOAc (first 8:1, then 6:1) as the eluting solvent. The combined product eluents were isolated as a mixture of Boc-protected pyridylindole and **3.24**. The resulting solid was dissolved into DCM and adsorbed onto silica gel (10 g) using rotary evaporation. The white powder was heated to 80 °C overnight under high vacuum. The silica gel was cooled to room temperature, filtered through celite with EtOAc and the filtrate was dried *in vacuo* to provide **3.24** (490 mg, 73% over two steps) as a solid. ^{1}H NMR (300 MHz, $CDCl_3$): δ (ppm) 9.49 (s, 1H), 8.06 (d, *J* = 2.9 Hz, 1H), 7.61 (d, *J* = 8.9 Hz, 1H), 7.60 (br, 1H), 7.28 (d, *J* = 8.5 Hz, 1H), 7.17 (dd, *J* = 8.4, 1.7 Hz, 1H), 7.01 (dd, *J* = 8.9, 3.0 Hz, 1H), 6.72 (m, 1H), 5.92-5.80 (m, 2H), 5.23-5.17 (m, 4H), 3.98 (m, 4H), 2.52 (s, 3H). ^{13}C NMR (100.6 MHz, $CDCl_3$): δ (ppm) 143.7, 138.7, 138.5, 135.1, 133.7, 133.0, 130.5, 127.9, 124.2, 121.4, 120.5, 119.6, 116.9, 111.6, 97.1, 52.9, 19.0. IR (film): *v* (cm^{-1}) 3080, 2915, 1590, 1554, 1485, 1458, 1439, 1418, 1393, 1304, 1234, 1176, 917, 823, 791, 734, 546. HRMS calculated for $C_{20}H_{22}N_3S$ $(M + H)^+$ 336.1529, found $(M + H)^+$ 336.1530.

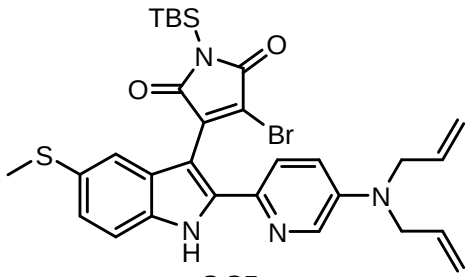

3.25

Compound 3.25. A solution of **3.24** (480 mg, 1.43 mmol) in anhydrous THF (4.3 mL) was prepared after drying **3.24** under high vacuum overnight. After cooling the solution to -15 °C, lithium bis(trimethylsilyl)amide (1 M solution in hexanes) (4.3 mL, 4.30 mmol) was added dropwise over 15 minutes and the resulting suspension was stirred at -15 °C for an additional 1 hour. A solution of TBS-protected dibromomaleimide (555 mg, 1.50 mmol) in THF (4.3 mL) cooled to 0 °C was added and the reaction mixture was stirred at -15 °C for 20 minutes and 10 °C overnight. The resulting dark purple reaction mixture was carefully poured into stirring ice cold 10% HCl (50 mL) and extracted with EtOAc twice. The combined organic layers were washed with saturated $NaHCO_3$ followed by brine, dried using Na_2SO_4, filtered and concentrated to dryness *in vacuo*. The crude material was adsorbed onto silica gel and subjected to flush silica gel chromatography with CH_2Cl_2 : MeOH (10:1) as the eluting solvent. The combined product eluents were dried *in vacuo* to provide **3.25** as a solid which was carried forward without characterization.

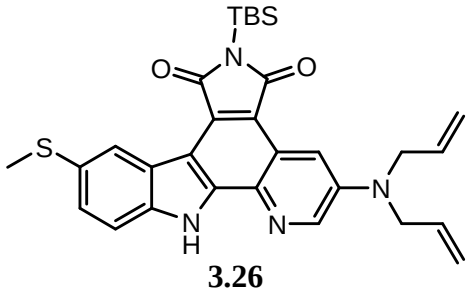

3.26

Compound 3.26. A solution of **3.25** in toluene (950 mL) was irradiated with a medium pressure Hg lamp (700 W) for 1 hour with constant nitrogen flow through the solution. The resulting red solution was concentrated to dryness *in vacuo*. The crude material was adsorbed onto silica gel and subjected to silica gel chromatography with hexane : EtOAc (first 2:1, then 1:2) as the eluting solvent. The combined product eluents were

dried *in vacuo* to provide **3.26** (300 mg, 39% over two steps) as a yellow solid and mono allyl protected product (83 mg, 11%). ^{1}H NMR (300 MHz, $CDCl_3$): δ (ppm) 10.08 (s, 1H), 9.03 (br, 1H), 8.63 (d, *J* = 3.0 Hz, 1H), 8.47 (d, *J* = 3.0 Hz, 1H), 7.51-7.44 (m, 2H), 6.0-5.88 (m, 2H), 5.31-5.25 (m, 4H), 4.15 (d, *J* = 3.0 Hz, 4H), 2.64 (s, 3H), 1.06 (s, 9H), 0.61 (s, 6H). ^{13}C NMR (100.6 MHz, $CDCl_3$): δ (ppm) 175.8, 174.5, 143.9, 141.2, 140.5, 138.0, 132.5, 131.1, 130.7, 130.2, 127.7, 124.9, 123.9, 123.7, 119.4, 117.5, 112.0, 111.7, 110.6, 52.9, 26.7, 19.3, 18.6, -3.7. IR (film): *v* (cm^{-1}) 2953, 2927, 2856, 1743, 1686, 1589, 1562, 1447, 1408, 1311, 1277, 1250, 1053, 929, 846, 824, 677. HRMS calculated for $C_{30}H_{34}N_4O_2SSiNa$ $(M + Na)^+$ 565.2064, found $(M + Na)^+$ 565.2076.

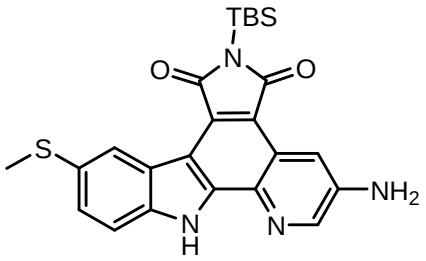

3.27

Compound 3.27. A mixture solution of **3.26** (56 mg, 0.103 mmol), 1,3-dimethylbarbituric acid (96.8 mg, 0.620 mmol), and tetrakis(triphenylphosphine)-palladium(0) (23.9 mg, 0.021 mmol) in dichloromethane (5 mL) was purged with nitrogen and refluxed for 7 hours. The resulting reaction mixture was cooled to room temperature, diluted with dichloromethane and washed with saturated $NaHCO_3$. The organic layer was separated, and the aqueous phase was extracted with dichloromethane for three times. The combined organic layers were washed with brine, dried using Na_2SO_4, filtered and concentrated to dryness *in vacuo*. The crude material was adsorbed onto silica gel and subjected to silica gel chromatography with hexane : EtOAc (1:1) as the eluting solvent. The combined product eluents were dried *in vacuo* to provide **3.27** (33 mg, 69%) as a yellow solid. ^{1}H NMR (300 MHz, $CDCl_3$): δ (ppm) 10.47 (s, 1H), 8.93 (d, *J* = 1.4 Hz, 1H), 8.45-8.39 (m, 2H), 7.43 (dd, *J* = 8.5, 1.8 Hz, 1H), 7.33 (d, *J* = 8.5 Hz, 1H), 4.19 (s, 2H), 2.62 (s, 3H), 1.06 (s, 9H), 0.63 (s, 6H). ^{13}C NMR (75.5 MHz,

$CDCl_3$): δ (ppm) 176.0, 174.1, 142.3, 142.2, 141.1, 137.9, 132.0, 131.0, 130.3, 127.7, 124.7, 123.43, 123.37, 119.1, 113.2, 112.4, 111.7, 26.7, 19.3, 18.4, -3.8. IR (film): *v* (cm^{-1}) 3368, 2952, 2927, 1743, 1683, 1619, 1563, 1432, 1415, 1346, 1311, 1291, 1277, 1057, 846, 824, 695, 678. HRMS calculated for $C_{24}H_{27}N_4O_2SSi$ $(M + H)^+$ 463.1618, found $(M + H)^+$ 463.1666.

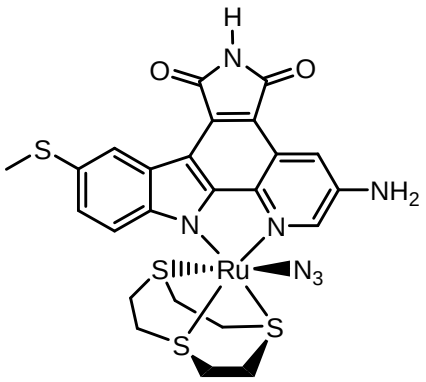

FL1358

Complex FL1358. A suspension of the ligand **3.27** (6 mg, 0.013 mmol), K_2CO_3 (2 mg, 0.014 mmol), and $[Ru(MeCN)_3([9]aneS_3)](CF_3SO_3)_2$ (10 mg, 0.014 mmol) in DMF (0.5 mL) was stirred at 85 °C under microwave irradiation for 30 minutes, followed by adding sodium azide (1.7 mg, 0.026 mmol), then the mixture was stirred at 85 °C for an additional 30 minutes. The resulting suspension was dried *in vacuo* and the crude material was adsorbed onto silica gel and subjected to silica gel chromatography with dichloromethane : methanol (10:1) as the eluting solvent. The metal complex **FL1358** was isolated as a solid (4.3 mg, 49%). ^{1}H NMR (300 MHz, DMSO-d_6): δ (ppm) 10.83 (s, 1H), 8.62-8.60 (m, 2H), 8.12 (d, *J* = 1.9 Hz, 1H), 7.59 (d, *J* = 8.5 Hz, 1H), 7.42 (dd, *J* = 8.5, 1.7 Hz, 1H), 6.21 (br, 2H), 3.11-2.04 (m, 12H), 2.54 (s, 3H). ^{13}C NMR (100.6 MHz, DMSO-d_6): δ (ppm) 171.7, 171.5, 156.0, 151.2, 145.9, 142.1, 136.5, 130.8, 126.9, 125.5, 125.4, 124.6, 123.6, 122.8, 119.6, 115.4, 112.0, 110.8, 110.4, 35.7, 35.3, 34.6, 32.3, 31.3, 29.1, 18.9. IR (film): *v* (cm^{-1}) 2030, 1742, 1703, 1621, 1566, 1487, 1415, 1349, 1269, 12304, 1168, 1034, 821, 762, 639. HRMS calculated for $C_{24}H_{23}N_7O_2S_4RuNa$ $(M + Na)^+$ 693.9735, found $(M + Na)^+$ 693.9718.

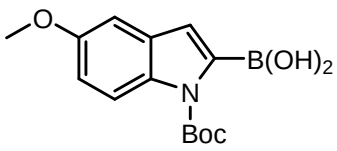

3.34

Compound 3.34. To a solution of Boc-protected 5-methoxyindole (948 mg, 3.83 mmol) in anhydrous THF (5 mL) was added triisopropyl borate (1.36 mL, 5.75 mmol), the reaction mixture was cooled to 0 °C and lithium diisopropylamide (2.0 M solution in heptane-tetrahydrofuran-ethylbenzene) (2.87 mL, 5.74 mmol) was added dropwise over 15 minutes. After stirring for an additional 45 minutes at 0 °C, 2 M HCl (10.5 mL) was carefully added and stirred at 0 °C for 5 minutes. The resulting organic layer was separated and the aqueous layer was extracted using EtOAc twice. The combined organic layers were dried using Na_2SO_4, filtered and concentrated to dryness *in vacuo* to provide **3.34** (1.08 g, 97%) which was carried forward without characterization.

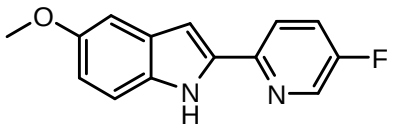

3.35

Compound 3.35. A biphasic suspension of **3.34** (1.08 g, 3.71 mmol), 2-bromo-5-fluoropyridine (594 mg, 3.37 mmol), tetrakis(triphenylphosphine)palladium(0) (390 mg, 0.34 mmol) and Na_2CO_3 (984 mg, 9.28 mmol) in 1,2-dimethoxyethane (34 mL) and water (4.0 mL) was purged with nitrogen and refluxed overnight. The resulting reaction mixture was cooled to room temperature, diluted with water and extracted with EtOAc for three times. The combined organic layers were washed with brine, dried using Na_2SO_4, filtered and concentrated to dryness *in vacuo*. The crude material was adsorbed onto silica gel and subjected to silica gel chromatography with hexane : EtOAc (8:1) as the eluting solvent. The combined product eluents were isolated as a mixture of Boc-protected pyridylindole and **3.35**. The resulting solid was dissolved into DCM and adsorbed onto silica gel (12 g) using rotary evaporation. The white powder was heated to 80 °C overnight under high vacuum. The silica gel was cooled to room temperature, filtered through celite with EtOAc and the filtrate was dried *in vacuo* to provide **3.35** (760 mg, 84% over two steps) as a solid. ^{1}H NMR (300 MHz, DMSO-d_6): δ (ppm)

11.51 (s, 1H), 8.61 (d, *J* = 2.9 Hz, 1H), 8.02 (dd, *J* = 8.8, 4.3 Hz, 1H), 7.81 (td, *J* = 8.8, 2.8 Hz, 1H), 7.34 (d, *J* = 8.8 Hz, 1H), 7.05 (d, *J* = 2.3 Hz, 1H), 7.03 (d, *J* = 1.5 Hz, 1H), 6.78 (dd, *J* = 8.8, 2.3 Hz, 1H), 3.76 (s, 3H). ^{13}C NMR (75.5 MHz, DMSO-d_6): δ (ppm) 159.7, 156.3, 153.7, 147.3, 147.2, 137.1, 136.8, 136.6, 132.4, 128.7, 124.3, 124.1, 121.1, 121.0, 113.0, 112.7, 101.7, 100.4, 55.2. IR (film): *v* (cm^{-1}) 3449, 1547, 1461, 1445, 1214, 1149, 1113, 1029, 828, 785, 748, 732, 517, 443. HRMS calculated for $C_{14}H_{12}FN_2O$ (M + H)$^+$ 243.0928, found (M + H)$^+$ 243.0934.

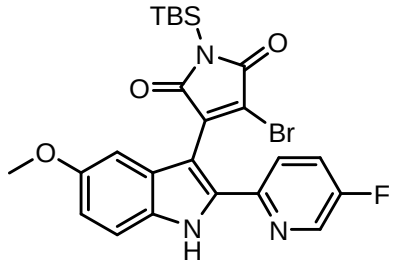

3.36

Compound 3.36. A solution of **3.35** (526 mg, 2.17 mmol) in anhydrous THF (6.0 mL) was prepared after drying **3.35** under high vacuum overnight. After cooling the solution to -15 °C, lithium bis(trimethylsilyl)amide (1 M solution in hexanes) (6.5 mL, 6.50 mmol) was added dropwise over 15 minutes and the resulting suspension was stirred at -15 °C for an additional 1 hour. A solution of TBS-protected dibromomaleimide (841 mg, 2.28 mmol) in THF (6.0 mL) cooled to 0 °C was added and the reaction mixture was stirred at -15 °C for 20 minutes and 10 °C overnight. The resulting dark purple reaction mixture was carefully poured into stirring ice cold 10% HCl (50 mL) and extracted with EtOAc twice. The combined organic layers were washed with saturated $NaHCO_3$ followed by brine, dried using Na_2SO_4, filtered and concentrated to dryness *in vacuo*. The crude material was adsorbed onto silica gel and subjected to silica gel chromatography with hexane : EtOAc (first 6:1, then 3:1) as the eluting solvent. The combined product eluents were dried *in vacuo* to provide **3.36** (600 mg, 52%) as a solid which was carried forward without characterization.

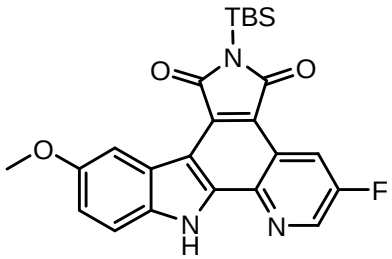

3.37

Compound 3.37. A solution of **3.36** (585 mg, 1.10 mmol) in toluene (220 mL) was irradiated with a medium pressure Hg lamp (150 W) using a pyrex filter for 3.5 hours with constant nitrogen flow through the solution. The resulting red solution was concentrated to dryness *in vacuo*. The crude material was adsorbed onto silica gel and subjected to silica gel chromatography with hexane : EtOAc (first 6:1, then 3:1) as the eluting solvent. The combined product eluents were dried *in vacuo* to provide **3.37** (430 mg, 86%) as a yellow solid. ^{1}H NMR (300 MHz, DMSO-d_6): δ (ppm) 12.95 (s, 1H), 9.06 (d, J = 2.9 Hz, 1H), 8.80 (dd, J = 9.7, 2.9 Hz, 1H), 8.30 (d, J = 2.5 Hz, 1H), 7.59 (d, J = 8.9 Hz, 1H), 7.21 (dd, J = 8.9, 2.5 Hz, 1H), 3.89 (s, 3H), 0.98 (s, 9H), 0.57 (s, 6H). ^{13}C NMR (75.5 MHz, DMSO-d_6): δ (ppm) 174.3, 173.7, 158.9, 155.5, 154.4, 141.4, 141.0, 140.4, 135.0, 130.9, 121.4, 121.3, 121.2, 117.9, 117.8, 116.4, 116.1, 113.3, 113.1, 106.3, 55.6, 26.2, 18.7, -4.3. IR (film): ν (cm^{-1}) 3445, 2953, 2928, 1745, 1688, 1472, 1445, 1308, 1288, 1254, 1214, 1040, 847, 828, 804, 762, 473. HRMS calculated for $C_{24}H_{25}FN_3O_3Si$ $(M + H)^+$ 450.1644, found $(M + H)^+$ 450.1655.

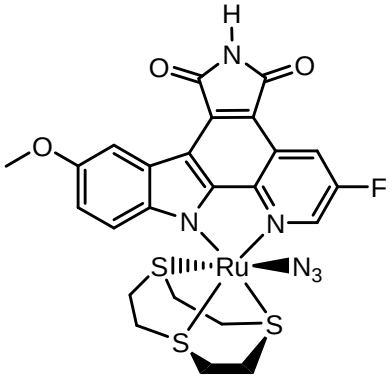

FL1055

Complex FL1055. A suspension of the ligand **3.37** (10 mg, 0.022 mmol), K_2CO_3 (3.4 mg, 0.025 mmol), and $[Ru(MeCN)_3([9]aneS_3)](CF_3SO_3)_2$ (17.2 mg, 0.024 mmol) in DMF (0.7 mL) was stirred at 85 °C under microwave irradiation for 30 minutes,

followed by adding sodium azide (2.9 mg, 0.045 mmol), then the mixture was stirred at 85 °C for an additional 30 minutes. The resulting suspension was dried *in vacuo* and the crude material was adsorbed onto silica gel and subjected to silica gel chromatography with dichloromethane : methanol (10:1) as the eluting solvent. The metal complex **FL1055** was isolated as a solid (10 mg, 68%). ^{1}H NMR (300 MHz, DMSO-d_6): δ (ppm) 11.09 (s, 1H), 9.06 (t, *J* = 2.4 Hz, 1H), 8.74 (dd, *J* = 9.5, 2.4 Hz, 1H), 8.28 (d, *J* = 2.6 Hz, 1H), 7.65 (d, *J* = 8.9 Hz, 1H), 7.21 (dd, *J* = 8.9, 2.7 Hz, 1H), 3.90 (s, 3H), 3.03-2.26 (m, 12H). ^{13}C NMR (100.6 MHz, DMSO-d_6): δ (ppm) 170.8, 170.7, 158.3, 155.8, 153.9, 153.5, 147.1, 141.1, 140.2, 139.9, 131.1, 124.0, 120.9, 120.8, 116.2, 116.0, 115.7, 114.6, 110.34, 110.29, 106.3, 55.7, 34.1, 33.5, 33.4, 33.1, 32.5, 30.0. IR (film): *v* (cm^{-1}) 2021, 17354, 1690, 1554, 1404, 1332, 1223, 1196, 1025, 1000, 814, 756, 693, 633, 518, 480.

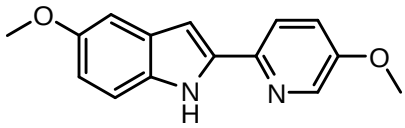

3.39

Compound 3.39. A biphasic suspension of **3.34** (409 mg, 1.41 mmol), 2-bromo-5-methoxypyridine (240 mg, 1.28 mmol), tetrakis(triphenylphosphine)palladium(0) (147 mg, 0.13 mmol) and Na_2CO_3 (372 mg, 3.51 mmol) in 1,2-dimethoxyethane (13.5 mL) and water (2.0 mL) was purged with nitrogen and refluxed overnight. The resulting reaction mixture was cooled to room temperature, diluted with water and extracted with EtOAc for three times. The combined organic layers were washed with brine, dried using Na_2SO_4, filtered and concentrated to dryness *in vacuo*. The crude material was adsorbed onto silica gel and subjected to silica gel chromatography with hexane : EtOAc (first 6:1, then 3:1) as the eluting solvent. The combined product eluents were isolated as a mixture of Boc-protected pyridylindole and **3.39**. The resulting solid was dissolved into DCM and adsorbed onto silica gel (5 g) using rotary evaporation. The white powder was heated to 80 °C overnight under high vacuum. The silica gel was cooled to room temperature, filtered through celite with EtOAc and the filtrate was dried *in vacuo* to provide **3.39** (260 mg, 80% over two steps) as a solid. ^{1}H NMR (300

MHz, $CDCl_3$): δ (ppm) 9.43 (s, 1H), 8.26 (d, *J* = 2.8 Hz, 1H), 7.71 (d, *J* = 8.8 Hz, 1H), 7.28-7.23 (m, 2H), 7.08 (d, *J* = 2.3 Hz, 1H), 6.86 (dd, *J* = 8.8, 2.4 Hz, 1H), 6.81 (m, 1H), 3.89 (s, 3H), 3.86 (s, 3H). ^{13}C NMR (75.5 MHz, $CDCl_3$): δ (ppm) 155.6, 137.1, 132.3, 128.2, 125.0, 124.5, 112.5, 111.8, 102.5, 56.1.

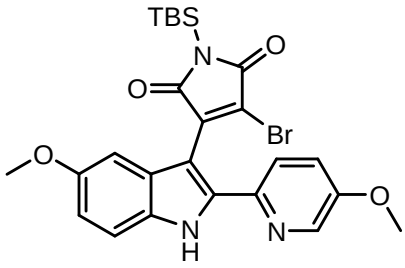

3.40

Compound 3.40. A solution of **3.39** (260 mg, 1.02 mmol) in anhydrous THF (5.0 mL) was prepared after drying **3.39** under high vacuum overnight. After cooling the solution to -15 °C, lithium bis(trimethylsilyl)amide (1 M solution in hexanes) (3.1 mL, 3.10 mmol) was added dropwise over 15 minutes and the resulting suspension was stirred at -15 °C for an additional 1 hour. A solution of TBS-protected dibromomaleimide (397 mg, 1.07 mmol) in THF (3.5 mL) cooled to 0 °C was added and the reaction mixture was stirred at -15 °C for 20 minutes and 10 °C overnight. The resulting dark purple reaction mixture was carefully poured into stirring ice cold 10% HCl (50 mL) and extracted with EtOAc twice. The combined organic layers were washed with saturated $NaHCO_3$ followed by brine, dried using Na_2SO_4, filtered and concentrated to dryness *in vacuo*. The crude material was adsorbed onto silica gel and subjected to silica gel chromatography with hexane : EtOAc (first 6:1, then 3:1) as the eluting solvent. The combined product eluents were dried *in vacuo* to provide **3.40** (320 mg, 58%) as a solid which was carried forward without characterization.

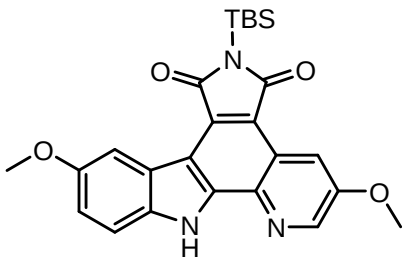

3.41

Compound 3.41. A solution of **3.40** (320 mg, 0.59 mmol) in toluene (220 mL) was

irradiated with a medium pressure Hg lamp (150 W) using a pyrex filter for 3 hours with constant nitrogen flow through the solution. The resulting solution was concentrated to dryness *in vacuo*. The crude material was adsorbed onto silica gel and subjected to silica gel chromatography with hexane : EtOAc (first 6:1, then 3:1) as the eluting solvent. The combined product eluents were dried *in vacuo* to provide **3.41** (240 mg, 88%) as a yellow solid. ^{1}H NMR (300 MHz, $CDCl_3$): δ (ppm) 9.81 (s, 1H), 8.70 (d, *J* = 2.9 Hz, 1H), 8.64 (d, *J* = 2.9 Hz, 1H), 8.57 (d, *J* = 2.5 Hz, 1H), 7.48 (d, *J* = 8.8 Hz, 1H), 7.18 (dd, *J* = 8.8, 2.6 Hz, 1H), 4.03 (s, 3H), 4.02 (s, 3H), 1.07 (s, 9H), 0.63 (s, 6H). IR (film): *v* (cm^{-1}) 3462, 2929, 1744, 1689, 1600, 1565, 1470, 1446, 1310, 1291, 1218, 1026, 830, 799, 761, 470. HRMS calculated for $C_{25}H_{28}N_3O_4Si$ $(M + H)^+$ 462.1844, found $(M + H)^+$ 462.1853.

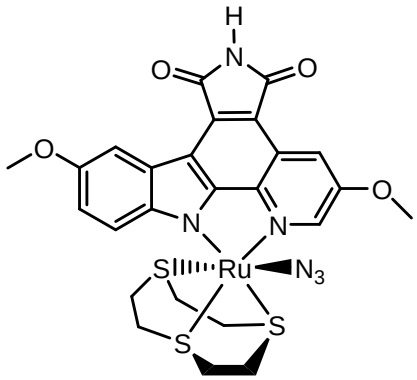

FL1229

Complex FL1229. A suspension of the ligand **3.41** (8 mg, 0.017 mmol), K_2CO_3 (2.6 mg, 0.019 mmol), and $[Ru(MeCN)_3([9]aneS_3)](CF_3SO_3)_2$ (13.4 mg, 0.019 mmol) in DMF (0.6 mL) was stirred at 85 °C under microwave irradiation for 30 minutes, followed by adding sodium azide (2.3 mg, 0.035 mmol), then the mixture was stirred at 85 °C for an additional 30 minutes. The resulting suspension was dried *in vacuo* and the crude material was adsorbed onto silica gel and subjected to silica gel chromatography with dichloromethane : methanol (10:1) as the eluting solvent. The metal complex **FL1229** was isolated as a solid (6.6 mg, 57%). ^{1}H NMR (300 MHz, DMSO-d_6): δ (ppm) 10.98 (s, 1H), 8.70 (d, *J* = 2.4 Hz, 1H), 8.47 (d, *J* = 2.4 Hz, 1H), 8.25 (d, *J* = 2.6 Hz, 1H), 7.58 (d, *J* = 8.9 Hz, 1H), 7.15 (dd, *J* = 8.9, 2.7 Hz, 1H), 4.05 (s, 3H), 3.89 (s, 3H), 3.01-2.26 (m, 12H). IR (film): *v* (cm^{-1}) 2029, 1740, 1712, 1564, 1468, 1427, 1399, 1345, 1235,

1214, 1048, 1025, 858, 805, 756, 695.

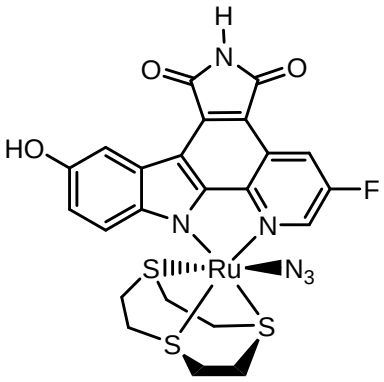

FL123

Complex FL123. A suspension of the ligand **3.69** (15 mg, 0.027 mmol), K_2CO_3 (4.2 mg, 0.030 mmol), and $[Ru(MeCN)_3([9]aneS_3)](CF_3SO_3)_2$ (21.6 mg, 0.030 mmol) in DMF (0.8 mL) was stirred at 85 °C under microwave irradiation for 30 minutes, followed by adding sodium azide (3.5 mg, 0.054 mmol), then the mixture was stirred at 85 °C for an additional 30 minutes. The resulting suspension was dried *in vacuo* and the crude material was adsorbed onto silica gel and subjected to silica gel chromatography with dichloromethane : methanol (15:1) as the eluting solvent. The main fraction was isolated as a solid which was carried forward without characterization. To a solution of the solid product in acetone (5 mL) at 0 °C was added TBAF (1 M in THF, 81 μL, 0.081 mmol) under nitrogen, the resulting purple solution was stirred at 0 °C for 5 minutes, followed by adding glacial acetic acid (3.7 μL, 0.081 mmol). The resulting solution was dried *in vacuo* and the crude material was adsorbed onto silica gel and subjected to silica gel chromatography with dichloromethane : methanol (first 20:1, then 10:1) as the eluting solvent. The metal complex **FL123** was isolated as a green solid (7.4 mg, 42%). ^{1}H NMR (300 MHz, DMSO-d_6): δ (ppm) 11.01 (s, 1H), 9.18 (s, 1H), 9.02 (t, J = 2.4 Hz, 1H), 8.72 (dd, J = 9.5, 2.3 Hz, 1H), 8.16 (d, J = 2.4 Hz, 1H), 7.56 (d, J = 8.8 Hz, 1H), 7.05 (dd, J = 8.8, 2.5 Hz, 1H), 3.03-2.56 (m, 12H). ^{13}C NMR (100.6 MHz, DMSO-d_6): δ (ppm) 170.8, 170.6, 158.2, 155.7, 153.7, 151.3, 146.3, 141.0, 139.8, 139.5, 131.1, 124.4, 120.9, 120.8, 116.1, 115.9, 115.4, 114.5, 109.54, 109.50, 108.6, 34.1, 33.5, 33.3, 33.1, 32.4, 29.9. IR (film): ν (cm^{-1}) 2029, 1744, 1708, 1557, 1493, 1468, 1411, 1332, 1223, 1196, 1021, 996, 818, 765, 698, 635. HRMS calculated for $C_{23}H_{19}FN_6O_3S_3RuNa$

$(M + Na)^+$ 666.9604, found $(M + Na)^+$ 666.9595.

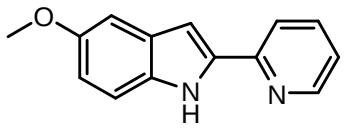

3.54

Compound 3.54. A biphasic suspension of **3.34** (692 mg, 2.38 mmol), 2-bromo-pyridine (341 mg, 2.16 mmol), tetrakis(triphenylphosphine)palladium(0) (174 mg, 0.15 mmol) and Na_2CO_3 (629 mg, 5.93 mmol) in 1,2-dimethoxyethane (22 mL) and water (2.5 mL) was purged with nitrogen and refluxed overnight. The resulting reaction mixture was cooled to room temperature, diluted with water and extracted with EtOAc for three times. The combined organic layers were washed with brine, dried using Na_2SO_4, filtered and concentrated to dryness *in vacuo*. The crude material was adsorbed onto silica gel and subjected to silica gel chromatography with hexane : EtOAc (first 6:1, then 3:1) as the eluting solvent. The combined product eluents were isolated as a mixture of Boc-protected pyridylindole and **3.54**. The resulting solid was dissolved into DCM and adsorbed onto silica gel (10 g) using rotary evaporation. The white powder was heated to 80 °C overnight under high vacuum. The silica gel was cooled to room temperature, filtered through celite with EtOAc and the filtrate was dried *in vacuo* to provide **3.54** (420 mg, 87% over two steps) as a solid. ^{1}H NMR (300 MHz, $CDCl_3$): δ (ppm) 9.55 (s, 1H), 8.56 (d, *J* = 4.8 Hz, 1H), 7.77 (d, *J* = 8.0 Hz, 1H), 7.71 (td, *J* = 8.0, 1.7 Hz, 1H), 7.29 (d, *J* = 8.8 Hz, 1H), 7.16 (ddd, *J* = 7.1, 4.9, 1.3 Hz, 1H), 7.09 (d, *J* = 2.3 Hz, 1H), 6.94 (d, *J* = 1.9 Hz, 1H), 6.89 (dd, *J* = 8.8, 2.4 Hz, 1H), 3.87 (s, 3H). ^{13}C NMR (75.5 MHz, $CDCl_3$): δ (ppm) 154.6, 150.5, 149.3, 137.4, 136.7, 132.0, 129.7, 122.0, 119.9, 114.0, 112.3, 102.5, 100.4, 56.0. IR (film): *ν* (cm^{-1}) 3434, 2993, 2941, 1622, 1591, 1543, 1444, 1300, 1219, 1149, 1118, 1030, 839, 775, 740. HRMS calculated for $C_{14}H_{13}N_2O$ $(M + H)^+$ 225.1022, found $(M + H)^+$ 225.1027.

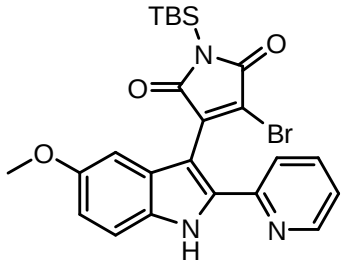

3.55

Compound 3.55. A solution of **3.54** (420 mg, 1.87 mmol) in anhydrous THF (5.6 mL) was prepared after drying **3.54** under high vacuum overnight. After cooling the solution to -15 °C, lithium bis(trimethylsilyl)amide (1 M solution in hexanes) (5.6 mL, 5.60 mmol) was added dropwise over 15 minutes and the resulting suspension was stirred at -15 °C for an additional 1 hour. A solution of TBS-protected dibromomaleimide (726 mg, 1.97 mmol) in THF (5.6 mL) cooled to 0 °C was added and the reaction mixture was stirred at -15 °C for 20 minutes and 10 °C overnight. The resulting dark purple reaction mixture was carefully poured into stirring ice cold 10% HCl (50 mL) and extracted with EtOAc twice. The combined organic layers were washed with saturated $NaHCO_3$ followed by brine, dried using Na_2SO_4, filtered and concentrated to dryness *in vacuo*. The crude material was adsorbed onto silica gel and subjected to silica gel chromatography with hexane : EtOAc (first 3:1, then 1:1) as the eluting solvent. The combined product eluents were dried *in vacuo* to provide **3.55** as a solid which was carried forward without characterization.

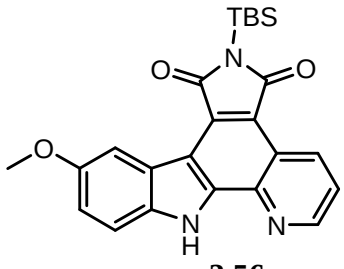

3.56

Compound 3.56. A solution of **3.55** in toluene (900 mL) was irradiated with a medium pressure Hg lamp (700 W) for 1 hour with constant nitrogen flow through the solution. The resulting solution was concentrated to dryness *in vacuo*. The crude material was adsorbed onto silica gel and subjected to silica gel chromatography with dichloromethane : methanol (first 75:1, then 50:1) as the eluting solvent. The combined

product eluents were dried *in vacuo* to provide **3.56** (455 mg, 56% over two steps) as a yellow solid. ^{1}H NMR (300 MHz, $CDCl_3$): δ (ppm) 10.50 (s, 1H), 9.42 (dd, *J* = 8.5, 1.6 Hz, 1H), 8.99 (dd, *J* = 4.3, 1.6 Hz, 1H), 8.60 (d, *J* = 2.3 Hz, 1H), 7.63 (dd, *J* = 8.5, 4.3 Hz, 1H), 7.45 (d, *J* = 8.8 Hz, 1H), 7.19 (dd, *J* = 8.8, 2.3 Hz, 1H), 4.03 (s, 3H), 1.07 (s, 9H), 0.64 (s, 6H). ^{13}C NMR (75.5 MHz, $CDCl_3$): δ (ppm) 175.7, 174.3, 155.4, 150.5, 140.6, 138.6, 134.5, 134.4, 130.9, 123.0, 122.9, 121.9, 120.4, 117.6, 115.2, 112.3, 107.2, 101.5, 56.3, 26.7, 19.3, -3.8. IR (film): *v* (cm^{-1}) 2926, 2855, 1749, 1689, 1475, 1436, 1333, 1316, 1282, 1216, 1044, 845, 826, 799, 696. HRMS calculated for $C_{24}H_{26}N_3O_3Si$ $(M + H)^+$ 432.1738, found $(M + H)^+$ 432.1742.

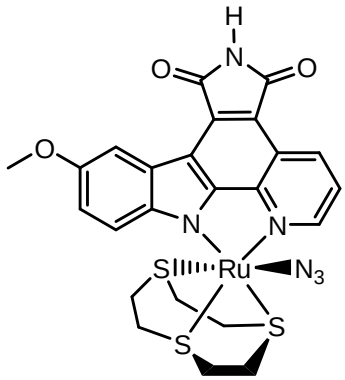

FL1381

Complex FL1381. A suspension of the ligand **3.56** (6 mg, 0.014 mmol), K_2CO_3 (2.1 mg, 0.015 mmol), and $[Ru(MeCN)_3([9]aneS_3)](CF_3SO_3)_2$ (10.8 mg, 0.015 mmol) in DMF (0.5 mL) was stirred at 85 °C under microwave irradiation for 30 minutes, followed by adding sodium azide (1.8 mg, 0.028 mmol), the mixture was stirred at 85 °C for an additional 30 minutes. The resulting suspension was dried *in vacuo* and the crude material was adsorbed onto silica gel and subjected to silica gel chromatography with dichloromethane : methanol (15:1) as the eluting solvent. The metal complex **FL1381** was isolated as a solid (5.5 mg, 62%). ^{1}H NMR (300 MHz, DMSO-d_6): δ (ppm) 11.0 (s, 1H), 9.07-9.03 (m, 2H), 8.29 (d, *J* = 2.6 Hz, 1H), 7.75 (dd, *J* = 8.3, 5.1 Hz, 1H), 7.67 (d, *J* = 8.9 Hz, 1H), 7.19 (dd, *J* = 8.9, 2.7 Hz, 1H), 3.90 (s, 3H), 3.05-2.19 (m, 12H). ^{13}C NMR (125.8 MHz, DMSO-d_6): δ (ppm) 171.01, 170.99, 153.8, 153.2, 150.2, 147.1, 143.7, 132.0, 130.5, 124.0, 123.1, 121.1, 115.6, 115.5, 114.6, 110.9, 106.1, 55.6, 34.6, 34.0, 33.5, 32.6, 31.6, 29.4. IR (film): *v* (cm^{-1}) 2025, 1738, 1698, 1587, 1492, 1418,

1339, 1235, 1212, 1028, 817, 794, 695, 637, 493. HRMS calculated for $C_{24}H_{22}N_6O_3S_3RuNa$ $(M + Na)^+$ 662.9855, found $(M + Na)^+$ 662.9840.

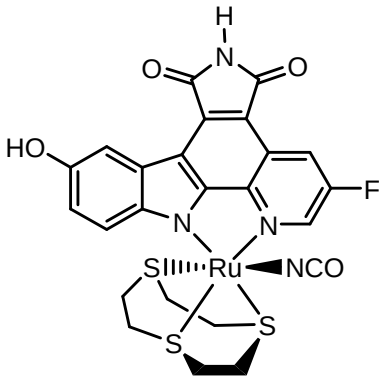

FL475

Complex FL475. To a solution of precursor **2.3** (7 mg, 0.012 mmol) in DMF (2 mL) was added [9]aneS_3 (2.2 mg, 0.012 mmol) under nitrogen, the mixture was stirred at 85 °C for 1 hour, followed by adding sodium cyanate (0.8 mg, 0.012 mmol), then the mixture was kept at 85 °C for an additional 1.5 hours. The resulting solution was dried *in vacuo* and the crude material was adsorbed onto silica gel and subjected to silica gel chromatography with dichloromethane : methanol (first 20:1, then 10:1) as the eluting solvent. The metal complex **FL475** was isolated as a green solid (2.1 mg, 27%). ^{1}H NMR (300 MHz, DMSO-d_6): δ (ppm) 11.0 (s, 1H), 9.18 (s, 1H), 9.02 (t, J = 2.4 Hz, 1H), 8.72 (dd, J = 9.5, 2.4 Hz, 1H), 8.17 (d, J = 2.5 Hz, 1H), 7.55 (d, J = 8.8 Hz, 1H), 7.05 (dd, J = 8.8, 2.5 Hz, 1H), 3.01-2.27 (m, 12H). IR (film): ν (cm^{-1}) 2237, 1738, 1707, 1553, 1495, 1410, 1332, 1304, 1196, 1167, 1024, 999, 820, 766, 699, 637.

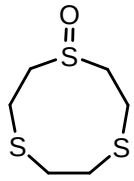

3.60

Compound 3.60. To a solution of [9]aneS_3 (150 mg, 0.83 mmol) in DCM (10 mL) at 0 °C was added the DCM solution (10 mL) of mCPBA dropwise in 10 minutes. The resulting mixture solution was stirred at 0 °C for additional 1 hour, followed by adding 10 mL saturated $NaHCO_3$ solution, then the organic layer was separated, and the aqueous layer was extracted with DCM twice. The combined organic layers were dried

using Na_2SO_4, filtered and concentrated to dryness *in vacuo*. The crude material was adsorbed onto silica gel and subjected to silica gel chromatography with DCM : MeOH (15:1) as the eluting solvent. The combined product eluents were dried *in vacuo* to provide **3.60** (105 mg, 64%) as white solid. ^{1}H NMR (300 MHz, $CDCl_3$): δ (ppm) 4.05-3.97 (m, 2H), 3.47-3.39 (m, 2H), 3.35-3.26 (m, 2H), 3.07-2.89 (m, 4H), 2.84-2.75 (m, 2H). ^{13}C NMR (75.5 MHz, $CDCl_3$): δ (ppm) 52.9, 35.5, 26.1. IR (film): *v* (cm^{-1}) 3419, 2905, 1645, 1408, 1272, 1206, 1141, 1020, 925, 833, 625. HRMS calculated for $C_6H_{12}OS_3Na$ $(M + Na)^+$ 218.9942, found $(M + Na)^+$ 218.9939.

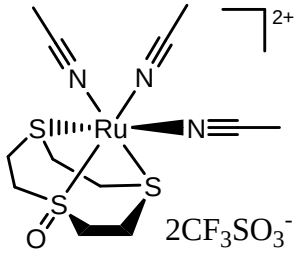

3.61

Compound 3.61. A solution of **3.60** (97 mg, 0.49 mmol) and $RuCl_2(dmso)_4$ (240 mg, 0.49 mmol) in chloroform (6 mL) was refluxed under nitrogen for 4 hours, the resulting yellow solid was collected and washed with chloroform for three times and dried *in vacuo* to provide the ruthenium intermediate which was carried forward without characterization. To the solution of ruthenium intermediate (210 mg, 0.47 mmol) in MeCN (10 mL) was added AgOTf (242 mg, 0.94 mmol) under nitrogen, the mixture was refluxed for 8 hours. The resulting suspension was cooled to room temperature and filtered through celite. The yellow filtrate was reduced in volume to 2 mL and precipitated by the addition of Et_2O to provide **3.61** (284 mg, 80% over two steps). ^{1}H NMR (300 MHz, CD_3CN): δ (ppm) 3.89-3.82 (m, 2H), 3.62-3.55 (m, 2H), 3.28-3.19 (m, 2H), 2.82-2.61 (m, 6H). IR (film): *v* (cm^{-1}) 3554, 2995, 2936, 2296, 1636, 1417, 1253, 1149, 1104, 1026, 946, 913, 843, 634, 572, 516. HRMS calculated for $C_{13}H_{21}F_3N_3O_4S_4Ru$ $(M)^+$ 569.9405, found $(M)^+$ 569.9418.

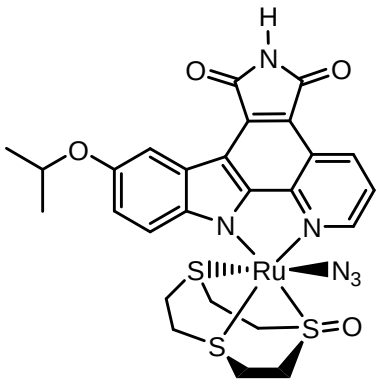

FL1528-1

Complex FL1528-1. A suspension of the ligand **3.6** (10 mg, 0.022 mmol), K_2CO_3 (3.3 mg, 0.024 mmol), and **3.61** (17.2 mg, 0.024 mmol) in DMF (0.7 mL) was stirred at 85 °C under microwave irradiation for 30 minutes, followed by adding sodium azide (2.8 mg, 0.043 mmol), then the mixture was stirred at 85 °C for an additional 30 minutes. The resulting suspension was dried *in vacuo* and the crude material was adsorbed onto silica gel and subjected to silica gel chromatography with dichloromethane : methanol (10:1) as the eluting solvent. The metal complex **FL1528-1** was isolated as a solid (1.8 mg, 12%), and the mixture of other two diastereoisomers (5.0 mg, 34%). ^{1}H NMR (300 MHz, DMSO-d_6): δ (ppm) 11.06 (s, 1H), 9.26 (dd, J = 5.2, 1.2 Hz, 1H), 9.12 (dd, J = 8.4, 1.2 Hz, 1H), 8.32 (d, J = 2.5 Hz, 1H), 7.85 (dd, J = 8.4, 5.1 Hz, 1H), 7.57 (d, J = 8.9 Hz, 1H), 7.17 (dd, J = 8.9, 2.6 Hz, 1H), 4.66 (septet, J = 6.0 Hz, 1H), 4.07-3.95 (m, 2H), 3.57-3.41 (m, 2H), 3.27-3.02 (m, 3H), 2.80-2.54 (m, 4H), 2.18 (m, 1H), 1.36 (d, J = 6.0 Hz, 6H). ^{13}C NMR (100.6 MHz, DMSO-d_6): δ (ppm) 171.0, 170.8, 153.3, 151.2, 151.0, 146.6, 143.0, 132.8, 130.7, 124.3, 123.2, 121.1, 117.5, 115.3, 114.9, 111.7, 109.7, 70.4, 60.5, 56.4, 35.3, 32.4, 31.7, 30.2, 22.12, 22.09. IR (film): ν (cm^{-1}) 2033, 1744, 1705, 1490, 1461, 1416, 1336, 1271, 1159, 1118, 1035, 952, 699, 636, 519, 494. HRMS calculated for $C_{26}H_{26}N_6O_4S_3RuNa$ $(M + Na)^+$ 707.0118, found $(M + Na)^+$ 707.0117.

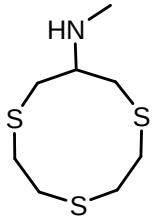

3.62

Compound 3.62. To a solution of $MeNH_2 \cdot HCl$ (58.4 mg, 0.87 mmol) in methanol (1 mL) at 0 °C was added potassium carbonate (119.4 mg, 0.87 mmol) under nitrogen. The resulting mixture was stirred at 0 °C for an additional 1 hour, followed by adding 1,4,7-trithiacyclodecan-9-one (150 mg, 0.72 mmol) in 10 mL methanol, then the suspension was stirred at room temperature for 3 hours. Water was added and extracted with DCM twice, the combined organic layers were dried using Na_2SO_4, filtered and concentrated to dryness *in vacuo*. The residue was dissolved in methanol (6 mL) and $NaBH_4$ (54.8 mg, 1.44 mmol) was added. The resulting solution was stirred at room temperature for 1 hour, followed by adding 5 mL saturated $NaHCO_3$ solution, the aqueous layer was extracted with DCM twice. The combined organic layers were dried using Na_2SO_4, filtered and concentrated to dryness *in vacuo*. The crude material was adsorbed onto silica gel and subjected to silica gel chromatography with DCM : methanol (first 35:1, then 20:1) as the eluting solvent. The combined product eluents were dried *in vacuo* to provide **3.62** (120 mg, 75%). ^{1}H NMR (300 MHz, $CDCl_3$): δ (ppm) 3.24-2.79 (m, 13H), 2.38 (s, 3H), 1.40 (br, 1H). ^{13}C NMR (75.5 MHz, $CDCl_3$): δ (ppm) 59.4, 34.3, 34.1, 34.0, 33.8. IR (film): *v* (cm^{-1}) 2904, 2848, 2787, 1476, 1411, 1268, 1103, 820, 742. HRMS calculated for $C_8H_{18}NS_3$ $(M + H)^+$ 224.0596, found $(M + H)^+$ 224.0594.

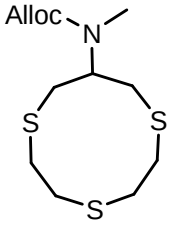

3.63

Compound 3.63. To a solution of **3.62** (90 mg, 0.40 mmol) in DCM (3 mL) at 0 °C was added allyl chloroformate (72.8 mg, 0.60 mmol), pyridine (31.8 mg, 0.40 mmol), and DMAP (2 mg, 0.016 mmol) under nitrogen, then the resulting mixture solution was allowed to warm to room temperature slowly and stirred overnight. The solution was diluted with DCM and washed with brine and water twice. The organic layer was separated and dried using Na_2SO_4, filtered and concentrated to dryness *in vacuo*. The

crude material **3.63** (90 mg, 76%) was used in the next step without any purification. ^{1}H NMR (300 MHz, $CDCl_3$): δ (ppm) 5.93 (m, 1H), 5.32-5.18 (m, 2H), 4.59 (d, *J* = 5.5 Hz, 2H), 3.33-2.90 (m, 13H), 2.86 (s, 3H). IR (film): *v* (cm^{-1}) 2910, 1692, 1448, 1399, 1321, 1266, 1231, 1198, 1145, 992, 928, 768. HRMS calculated for $C_{12}H_{21}NO_2S_3Na$ $(M + Na)^+$ 330.0627, found $(M + Na)^+$ 330.0622.

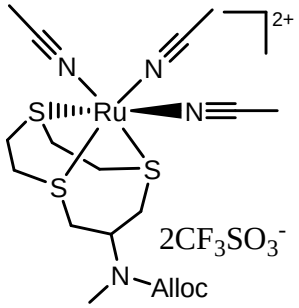

3.65

Compound 3.65. A solution of **3.63** (54 mg, 0.17 mmol) and $RuCl_2(dmso)_4$ (85 mg, 0.17 mmol) in chloroform (5 mL) was refluxed under nitrogen for 5 hours, then the resulting solution was concentrated and precipitated with diethyl ether. The solid was collected and washed with diethyl ether for three times and dried *in vacuo* to provide **3.64** which was carried forward without characterization. To the solution of **3.64** (89 mg, 0.16 mmol) in MeCN (5 mL) was added AgOTf (82 mg, 0.32 mmol) under nitrogen, the mixture was refluxed for 6 hours. The resulting suspension was cooled to room temperature and filtered through celite. The yellow filtrate was reduced in volume to 1 mL and precipitated by the addition of Et_2O to provide **3.65** (106 mg, 72% over two steps). ^{1}H NMR (300 MHz, CD_3CN): δ (ppm) 5.95 (m, 1H), 5.30 (m, 1H), 5.21 (m, 1H), 4.57-4.55 (m, 2H), 3.31-2.61 (m, 16H), 2.53 (s, 3H), 2.41 (s, 6H). IR (film): *v* (cm^{-1}) 3509, 2993, 2936, 2293, 1691, 1404, 1369, 1327, 1250, 1148, 1024, 954, 833, 761, 632, 571, 514. HRMS calculated for $C_{19}H_{30}F_3N_4O_5S_4Ru$ $(M)^+$ 681.0089, found $(M)^+$ 681.0085.

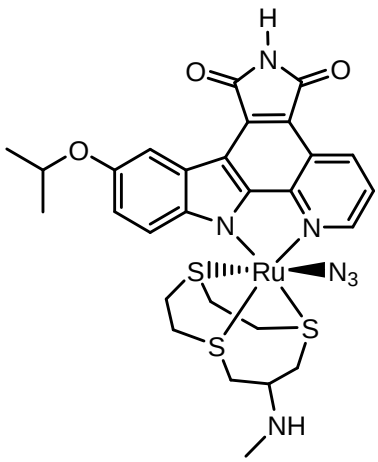

FL1392

Complex FL1392. A suspension of the ligand **3.6** (15 mg, 0.033 mmol), K_2CO_3 (5 mg, 0.036 mmol), and ruthenium precursor **3.65** (30 mg, 0.036 mmol) in DMF (0.9 mL) was stirred at 85 °C under microwave irradiation for 40 minutes, followed by adding sodium azide (4.2 mg, 0.065 mmol), then the mixture was stirred at 85 °C for an additional 40 minutes. The resulting suspension was dried *in vacuo* and the crude material was adsorbed onto silica gel and subjected to silica gel chromatography with dichloromethane : methanol (35:1) as the eluting solvent. The first main fraction was isolated as a solid (10 mg, 38%) which was carried forward without characterization. To a solution of the solid product (6 mg, 0.0075 mmol) in DCM (2.5 mL) was added 1,3-dimethylbarbituric acid (9.4 mg, 0.06 mmol) and $Pd(PPh_3)_4$ (1.3 mg, 0.0011 mmol) under nitrogen. The resulting mixture was stirred at room temperature for 5 minutes, followed by adding 0.5 mL saturated $NaHCO_3$ solution to quench the reaction. The resulting suspension was dried *in vacuo* and the crude material was adsorbed onto silica gel and subjected to silica gel chromatography with dichloromethane : methanol (first 10:1, then 5:1) as the eluting solvent to get the metal complex **FL1392** (3.2 mg, 59%). **FL1392:** ^{1}H NMR (300 MHz, DMSO-d_6): δ (ppm) 10.99 (s, 1H), 9.07 (d, J = 8.3 Hz, 1H), 9.01 (d, J = 5.3 Hz, 1H), 8.29 (d, J = 2.5 Hz, 1H), 7.99 (d, J = 8.9 Hz, 1H), 7.80 (dd, J = 8.3, 5.2 Hz, 1H), 4.65 (septet, J = 6.1 Hz, 1H), 3.71-2.16 (m, 17H), 1.35 (d, J = 6.1 Hz, 6H). ^{13}C NMR (125.8 MHz, DMSO-d_6): δ (ppm) 171.01, 170.99, 153.8, 150.9, 148.0, 147.2, 143.9, 132.1, 130.3, 124.5, 122.5, 121.1, 117.1, 115.9, 114.7, 110.9, 109.3, 70.3, 55.9, 35.8, 33.3, 31.5, 30.7, 29.6, 28.2, 26.2, 22.14, 22.08. IR (film): ν (cm^{-1}) 2033,

1747, 1701, 1596, 1460, 1424, 1338, 1234, 1209, 1112, 1020, 823, 793, 698, 638, 500. HRMS calculated for $C_{28}H_{31}N_7O_3S_3RuNa$ $(M + Na)^+$ 734.0592, found $(M + Na)^+$ 734.0573.

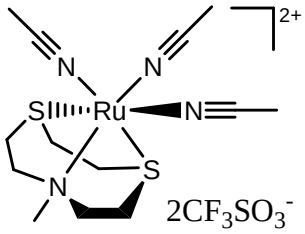

3.68

Compound 3.68. A suspension of **3.66** (78 mg, 0.44 mmol) and $[RuCl_2(\eta^6\text{-}C_6H_6)]_2$ (104 mg, 0.21 mmol) in acetonitrile/ethanol (2.6 mL/5.2 mL) was refluxed under nitrogen for 24 hours. The resulting solution was concentrated and precipitated with diethyl ether, then the solid was collected and washed with diethyl ether for three times and dried *in vacuo* to provide **3.67** which was carried forward without characterization. To the solution of **3.67** (70 mg, 0.18 mmol) in MeCN (6 mL) was added AgOTf (92 mg, 0.36 mmol) under nitrogen, the mixture was refluxed for 7 hours. The resulting suspension was cooled to room temperature and filtered through celite. The yellow filtrate was reduced in volume to 1 mL and precipitated by the addition of Et_2O to provide **3.68** (83 mg, 60% over two steps). ^1H NMR (300 MHz, CD_3CN): δ (ppm) 3.04-2.95 (m, 2H), 2.81 (s, 3H), 2.78-2.59 (m, 10H), 2.48 (s, 6H), 2.33 (s, 3H). IR (film): *v* (cm^{-1}) 2994, 2941, 2290, 1469, 1422, 1258, 1221, 1147, 1024, 821, 752, 631, 572, 515. HRMS calculated for $C_{14}H_{24}F_3N_4O_3S_3Ru$ $(M)^+$ 551.0000, found $(M)^+$ 550.9995.

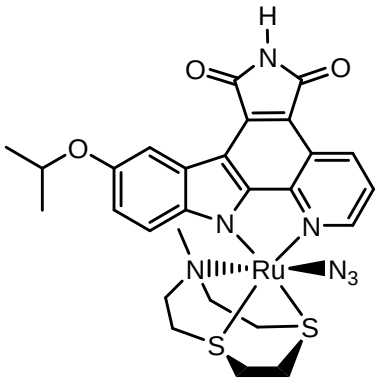

FL1473

Complex FL1473. A suspension of the ligand **3.6** (12 mg, 0.026 mmol), K_2CO_3 (3.9 mg,

0.028 mmol), and ruthenium precursor **3.68** (20 mg, 0.028 mmol) in DMF (0.7 mL) was stirred at 85 °C under microwave irradiation for 40 minutes, followed by adding sodium azide (3.4 mg, 0.052 mmol), then the mixture was stirred at 85 °C for an additional 30 minutes. The resulting suspension was dried *in vacuo* and the crude material was adsorbed onto silica gel and subjected to silica gel chromatography with dichloromethane : methanol (15:1 with 0.5% concentrated ammonium hydroxide) as the eluting solvent. The metal complex **FL1473** was isolated as a mixture with the other two diastereoisomers (1.7 mg, 10%) which were separated by crystallization in acetone. ^{1}H NMR (300 MHz, DMSO-d_6): δ (ppm) 10.94 (s, 1H), 9.33 (dd, *J* = 5.1, 1.1 Hz, 1H), 9.05 (dd, *J* = 8.4, 1.1 Hz, 1H), 8.34 (d, *J* = 2.5 Hz, 1H), 7.87 (d, *J* = 8.9 Hz, 1H), 7.81 (dd, *J* = 8.3, 5.1 Hz, 1H), 7.23 (dd, *J* = 8.9, 2.6 Hz, 1H), 4.69 (septet, *J* = 6.0 Hz, 1H), 3.21-2.03 (m, 12H), 1.38 (d, *J* = 6.0 Hz, 6H), 1.35 (s, 3H). IR (film): *v* (cm^{-1}) 2972, 2926, 2023, 1742, 1709, 1591, 1490, 1460, 1420, 1341, 1280, 1235, 1213, 1023, 952, 700, 639, 498.

Chapter 6.1.3: Synthesis of DAPK1 inhibitors

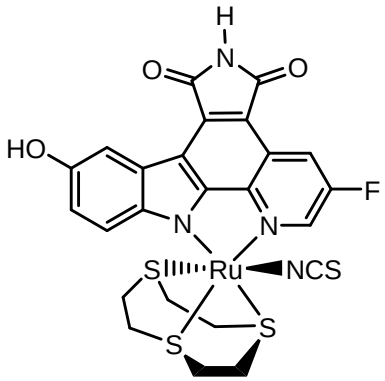

FL823-1

Complex FL823-1. A suspension of the ligand **2.1** (32 mg, 0.058 mmol), K_2CO_3 (8.8 mg, 0.064 mmol), and $[Ru(MeCN)_3([9]aneS_3)](CF_3SO_3)_2$ (45.1 mg, 0.064 mmol) in DMF (2 mL) was stirred at 85 °C under microwave irradiation for 40 minutes, followed by adding sodium thiocyanate (9.4 mg, 0.116 mmol), then the mixture was stirred at 85 °C for an additional 30 minutes. The resulting suspension was dried *in vacuo* and the crude material was adsorbed onto silica gel and subjected to silica gel chromatography

with dichloromethane : methanol (10:1) as the eluting solvent. These two linkage isomers were collected together (28 mg, 62%), which was carried forward without characterization. To a solution of the product (28 mg, 0.036 mmol) in acetone (20 mL) at 0 °C was added TBAF (1 M in THF, 72.7 μL, 0.073 mmol) under nitrogen, the resulting mixture was stirred at 0 °C for 2 minutes, followed by adding glacial acetic acid (4.3 μL, 0.072 mmol). The reaction mixture was dried *in vacuo* and the crude material was adsorbed onto silica gel and subjected to silica gel chromatography with dichloromethane : methanol (first 20:1, then 15:1) as the eluting solvent. The metal complex **FL823-1** was isolated as a solid (10 mg, 42%) and the other linkage isomer **FL823-2** was also obtained (8 mg, 34%). **FL823-1:** ^{1}H NMR (300 MHz, DMSO-d_6): δ (ppm) 11.0 (s, 1H), 9.23 (s, 1H), 9.06 (t, *J* = 2.4 Hz, 1H), 8.76 (dd, *J* = 9.4, 2.3 Hz, 1H), 8.18 (d, *J* = 2.5 Hz, 1H), 7.55 (d, *J* = 8.8 Hz, 1H), 7.07 (dd, *J* = 8.8, 2.5 Hz, 1H), 3.06-2.27 (m, 12H). IR (film): *v* (cm^{-1}) 2105, 1739, 1706, 1556, 1494, 1468, 1410, 1332, 1229, 1196, 1167, 1022, 998, 819, 699, 636. **FL823-2:** ^{1}H NMR (300 MHz, DMSO-d_6): δ (ppm) 11.0 (s, 1H), 9.20 (s, 1H), 8.94 (t, *J* = 2.5 Hz, 1H), 8.72 (dd, *J* = 9.5, 2.4 Hz, 1H), 8.15 (d, *J* = 2.5 Hz, 1H), 7.47 (d, *J* = 8.8 Hz, 1H), 7.03 (dd, *J* = 8.8, 2.5 Hz, 1H), 3.07-2.37 (m, 12H). IR (film): *v* (cm^{-1}) 2111, 1738, 1704, 1555, 1493, 1468, 1409, 1330, 1288, 1256, 1194, 1167, 1022, 998, 818, 699, 635.

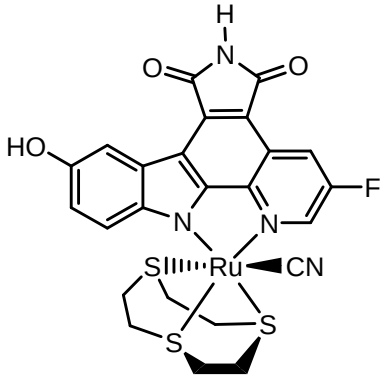

FL253

Complex FL253. A solution of precursor complex **2.3** (7 mg, 0.012 mmol) and 1,4,7-trithiacyclononane (2.2 mg, 0.012 mmol) in DMF (1.5 mL) was stirred at 85 °C under nitrogen for 1 hour. To the resulting solution was added sodium cyanide (0.6 mg, 0.012 mmol), then the solution was stirred at 85 °C for an additional 30 minuts, after

which the solution was dried under high vacuum. The crude material was adsorbed onto silica gel and subjected to silica gel chromatography with dichloromethane : methanol (first 20:1, then 10:1) as the eluting solvent. The metal complex **FL253** was isolated as a solid (1.4 mg, 17%). ^{1}H NMR (300 MHz, DMSO-d_6): δ (ppm) 11.03 (s, 1H), 9.20 (s, 1H), 8.91 (t, J = 2.4 Hz, 1H), 8.71 (dd, J = 9.5, 2.3 Hz, 1H), 8.15 (d, J = 2.5 Hz, 1H), 7.49 (d, J = 8.8 Hz, 1H), 7.05 (dd, J = 8.8, 2.5 Hz, 1H), 3.05-2.27 (m, 12H). IR (film): ν (cm^{-1}) 2922, 2852, 2068, 1744, 1700, 1543, 1523, 1454, 1287, 1263, 1228, 668.

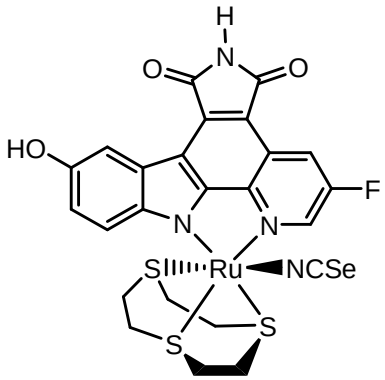

FL528

Complex FL528. A solution of precursor complex **2.3** (7 mg, 0.012 mmol) and 1,4,7-trithiacyclononane (2.2 mg, 0.012 mmol) in DMF (1.5 mL) was stirred at 85 °C under nitrogen for 1 hour. To the resulting solution was added potassium selenocyanate (1.7 mg, 0.012 mmol), then the solution was stirred at 85 °C for an additional 40 minuts, after which the solution was dried under high vacuum. The crude material was adsorbed onto silica gel and subjected to silica gel chromatography with dichloromethane : methanol (first 20:1, then 15:1) as the eluting solvent. The metal complex **FL528** was isolated as a solid (3.8 mg, 45%). ^{1}H NMR (300 MHz, DMSO-d_6): δ (ppm) 11.02 (s, 1H), 9.20 (s, 1H), 8.94 (t, *J* = 2.5 Hz, 1H), 8.71 (dd, *J* = 9.5, 2.3 Hz, 1H), 8.15 (d, *J* = 2.5 Hz, 1H), 7.47 (d, *J* = 8.8 Hz, 1H), 7.03 (dd, *J* = 8.8, 2.5 Hz, 1H), 3.07-2.34 (m, 12H). IR (film): *v* (cm^{-1}) 3143, 3150, 2101, 1742, 1701, 1582, 1490, 1413, 1342, 1289, 1263, 1226, 1013, 819, 744, 638.

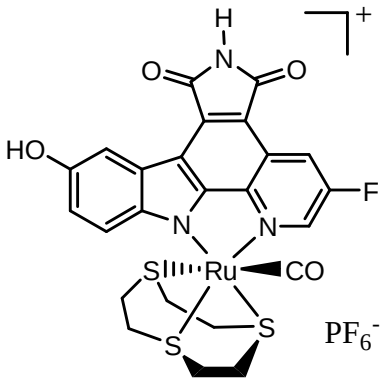

FL576

Complex FL576. A solution of precursor complex **2.3** (27 mg, 0.047 mmol) in DMF (3 mL) was purged with CO gas for 5 min, then stirred at 75 °C under an atmosphere of CO for 1.5 hours. To the resulting solution was added 1,4,7-trithiacyclononane (8.5 mg, 0.047 mmol), then the solution was stirred at 95 °C under an atmosphere of nitrogen for 2.5 hours, after which the purple solution was dried under high vacuum. The crude material was adsorbed onto silica gel and subjected to silica gel chromatography with MeCN : H_2O : KNO_3 (100:3:1) to obtain purple solid. The resulting material was dissolved in minimal acetonitrile/water. The product was precipitated by the addition of excess solid NH_4PF_6. The precipitate was centrifuged and washed twice with water. The material was then dried under high vacuum to yield **FL576** (18 mg, 50%). ^{1}H NMR (500 MHz, DMSO-d_6): δ (ppm) 11.1 (s, 1H), 9.36 (s, 1H), 9.05 (t, J = 2.3 Hz, 1H), 8.92 (dd, J = 9.1, 2.3 Hz, 1H), 8.21 (d, J = 2.5 Hz, 1H), 7.45 (d, J = 8.7 Hz, 1H), 7.13 (dd, J = 8.8, 2.5 Hz, 1H), 3.50-2.57 (m, 12H). ^{13}C NMR (125.8 MHz, DMSO-d_6): δ (ppm) 191.8, 170.5, 170.0, 158.2, 156.2, 152.7, 151.9, 144.6, 143.1, 142.9, 140.1, 131.8, 124.5, 121.04, 120.97, 118.9, 118.7, 117.1, 114.8, 114.3, 112.09, 112.06, 108.9, 37.9, 37.2, 35.6, 32.5, 31.5, 31.1. IR (film): ν (cm^{-1}) 2011, 1750, 1713, 1564, 1495, 1413, 1335, 1228, 1203, 1026, 1000, 840, 760, 700, 638, 557, 488. HRMS calculated for $C_{24}H_{19}FN_3O_4S_3Ru$ $(M)^+$ 629.9560, found $(M)^+$ 629.9572.

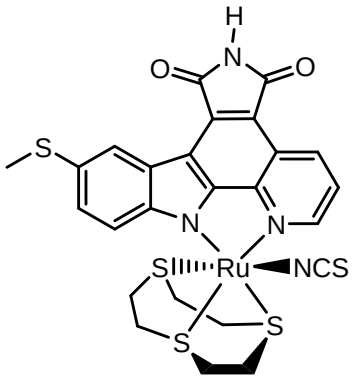

FL1352-1

Complex FL1352-1. A suspension of the ligand **3.21** (7 mg, 0.016 mmol), K_2CO_3 (2.4 mg, 0.017 mmol), and $[Ru(MeCN)_3([9]aneS_3)](CF_3SO_3)_2$ (12.1 mg, 0.017 mmol) in DMF (0.6 mL) was stirred at 85 °C under microwave irradiation for 30 minutes, followed by adding sodium thiocyanate (2.5 mg, 0.031 mmol), then the mixture was stirred at 85 °C for an additional 30 minutes. The resulting suspension was dried *in vacuo* and the crude material was adsorbed onto silica gel and subjected to silica gel chromatography with dichloromethane : methanol (first 20:1, then 15:1) as the eluting solvent. The metal complex **FL1352-1** was isolated as a solid (2.4 mg, 23%) and the other linkage isomer was also obtained (2 mg, 19%). **FL1352-1:** ^{1}H NMR (300 MHz, DMSO-d_6): δ (ppm) 11.1 (s, 1H), 9.14 (d, J = 8.5 Hz, 1H), 9.11 (d, J = 5.1 Hz, 1H), 8.75 (d, J = 1.8 Hz, 1H), 7.81 (dd, J = 8.4, 5.2 Hz, 1H), 7.70 (d, J = 8.7 Hz, 1H), 7.55 (dd, J = 8.6, 1.8 Hz, 1H), 3.10-2.63 (m, 12H), 2.58 (s, 3H). IR (film): ν (cm^{-1}) 2098, 1741, 1704, 1597, 1526, 1486, 1417, 1338, 1269, 1225, 1131, 1018, 817, 796, 670, 638, 494.

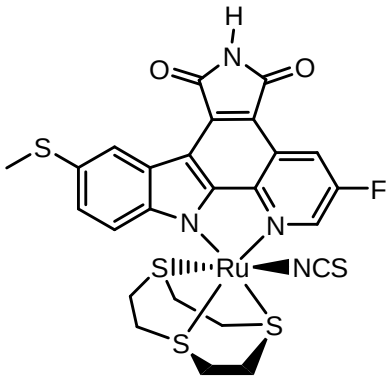

FL1289-1

Complex FL1289-1. A suspension of the ligand **3.17** (7 mg, 0.015 mmol), K_2CO_3 (2.3 mg, 0.017 mmol), and $[Ru(MeCN)_3([9]aneS_3)](CF_3SO_3)_2$ (11.6 mg, 0.017 mmol) in

DMF (0.6 mL) was stirred at 85 °C under microwave irradiation for 30 minutes, followed by adding sodium thiocyanate (2.5 mg, 0.031 mmol), then the mixture was stirred at 85 °C for an additional 40 minutes. The resulting suspension was dried *in vacuo* and the crude material was adsorbed onto silica gel and subjected to silica gel chromatography with dichloromethane : methanol (first 20:1, then 15:1) as the eluting solvent. The metal complex **FL1289-1** was isolated as a solid (1.8 mg, 17%) and the other linkage isomer **FL1289-2** was also obtained (0.8 mg, 8%). **FL1289-1:** ^{1}H NMR (300 MHz, DMSO-d_6): δ (ppm) 11.2 (s, 1H), 9.15 (t, *J* = 2.3 Hz, 1H), 8.81 (dd, *J* = 9.3, 2.3 Hz, 1H), 8.73 (d, *J* = 1.9 Hz, 1H), 7.69 (d, *J* = 8.6 Hz, 1H), 7.56 (dd, *J* = 8.5, 1.8 Hz, 1H), 3.04-2.33 (m, 12H), 2.58 (s, 3H). IR (film): *v* (cm^{-1}) 2105, 1735, 1698, 1556, 1490, 1404, 1334, 1253, 1223, 1199, 1024, 1000, 803, 635, 521, 475. **FL1289-2:** ^{1}H NMR (300 MHz, DMSO-d_6): δ (ppm) 11.2 (s, 1H), 9.03 (t, *J* = 2.5 Hz, 1H), 8.77 (dd, *J* = 9.4, 2.3 Hz, 1H), 8.70 (d, *J* = 1.9 Hz, 1H), 7.62 (d, *J* = 8.5 Hz, 1H), 7.52 (dd, *J* = 8.7, 1.9 Hz, 1H), 3.10-2.40 (m, 12H), 2.57 (s, 3H). IR (film): *v* (cm^{-1}) 2103, 1739, 1704, 1611, 1558, 1489, 1405, 1334, 1254, 1224, 1200, 1025, 997, 911, 893, 821, 804, 676, 638, 475.

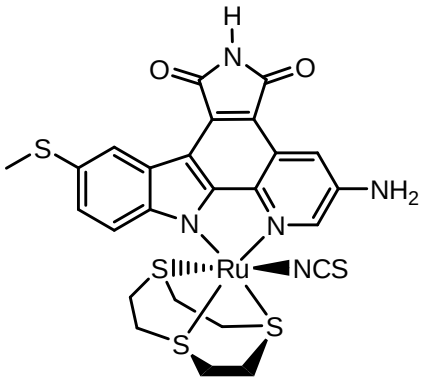

FL1334

Complex FL1334. A suspension of the ligand **3.27** (10 mg, 0.022 mmol), K_2CO_3 (3.3 mg, 0.024 mmol), and $[Ru(MeCN)_3([9]aneS_3)](CF_3SO_3)_2$ (16.7 mg, 0.024 mmol) in DMF (0.7 mL) was stirred at 85 °C under microwave irradiation for 30 minutes, followed by adding sodium thiocyanate (3.5 mg, 0.043 mmol), then the mixture was stirred at 85 °C for an additional 30 minutes. The resulting suspension was dried *in vacuo* and the crude material was adsorbed onto silica gel and subjected to silica gel chromatography with dichloromethane : methanol (first 10:1, then 5:1) as the eluting

solvent. The metal complex **FL1334** was isolated as a mixture of two linkage isomers. (6.4 mg, 43%). IR (film): *v* (cm^{-1}) 3344, 3213, 2102, 1741, 1702, 620, 1565, 1414, 1348, 1293, 1268, 1228, 1048, 1023, 1003, 816, 679, 638, 472. HRMS calculated for $C_{25}H_{23}N_5O_2S_5RuNa$ $(M + Na)^+$ 709.9391, found $(M + Na)^+$ 709.9403.

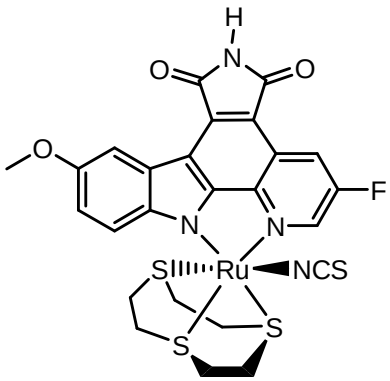

FL812-1

Complex FL812-1. A suspension of the ligand **3.37** (20 mg, 0.045 mmol), K_2CO_3 (6.8 mg, 0.049 mmol), and $[Ru(MeCN)_3([9]aneS_3)](CF_3SO_3)_2$ (34.4 mg, 0.049 mmol) in DMF (1.4 mL) was stirred at 85 °C under microwave irradiation for 30 minutes, followed by adding sodium thiocyanate (7.2 mg, 0.089 mmol), then the mixture was stirred at 85 °C for an additional 30 minutes. The resulting suspension was dried *in vacuo* and the crude material was adsorbed onto silica gel and subjected to silica gel chromatography with dichloromethane : methanol (first 35:1, then 10:1) as the eluting solvent. The metal complex **FL812-1** was isolated as a solid (9.8 mg, 33%) and the other linkage isomer **FL812-2** was also obtained (7 mg, 23%). **FL812-1:** ^{1}H NMR (400 MHz, DMSO-d_6): δ (ppm) 11.1 (s, 1H), 9.09 (t, *J* = 2.4 Hz, 1H), 8.79 (dd, *J* = 9.4, 2.3 Hz, 1H), 8.30 (d, *J* = 2.6 Hz, 1H), 7.65 (d, *J* = 8.9 Hz, 1H), 7.23 (dd, *J* = 8.9, 2.7 Hz, 1H), 3.91 (s, 3H), 3.06-2.30 (m, 12H). ^{13}C NMR (100.6 MHz, DMSO-d_6): δ (ppm) 170.7, 170.5, 158.2, 155.7, 153.6, 153.5, 146.8, 140.9, 140.89, 140.7, 140.4, 132.8, 131.3, 124.0, 120.8, 120.7, 116.8, 116.6, 115.9, 115.4, 114.5, 110.69, 110.64, 106.4, 55.6, 33.8, 33.3, 33.2, 33.0, 30.3. IR (film): *v* (cm^{-1}) 2103, 1739, 1702, 1558, 1496, 1421, 1405, 13326, 1281, 1256, 1231, 1196, 1028, 996, 816, 634. **FL812-2:** ^{1}H NMR (300 MHz, DMSO-d_6): δ (ppm) 11.1 (s, 1H), 8.98 (t, *J* = 2.5 Hz, 1H), 8.75 (dd, *J* = 9.5, 2.4 Hz, 1H), 8.27 (d, *J* = 2.6 Hz, 1H), 7.57 (d, *J* = 8.9 Hz, 1H), 7.19 (dd, *J* = 8.9, 2.7 Hz,

1H), 3.89 (s, 3H), 3.09-2.36 (m, 12H).

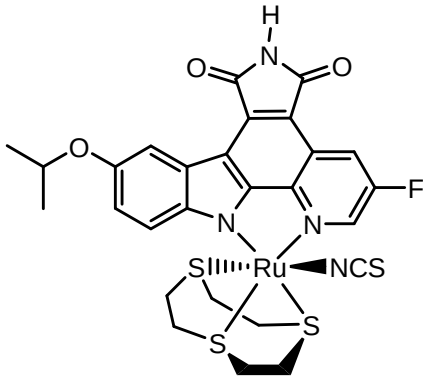

FL1353-1

Complex FL1353-1. A suspension of the ligand **3.10** (10 mg, 0.021 mmol), K_2CO_3 (3.2 mg, 0.023 mmol), and $[Ru(MeCN)_3([9]aneS_3)](CF_3SO_3)_2$ (16.2 mg, 0.023 mmol) in DMF (0.7 mL) was stirred at 85 °C under microwave irradiation for 30 minutes, followed by adding sodium thiocyanate (3.4 mg, 0.042 mmol), then the mixture was stirred at 85 °C for an additional 40 minutes. The resulting suspension was dried *in vacuo* and the crude material was adsorbed onto silica gel and subjected to silica gel chromatography with dichloromethane : methanol (15:1) as the eluting solvent. The metal complex **FL1353-1** was isolated as a green solid (5.5 mg, 37%)and the other linkage isomer **FL1353-2** was also obtained (3.6 mg, 24%). **FL1353-1:** ^{1}H NMR (300 MHz, DMSO-d_6): δ (ppm) 11.1 (s, 1H), 9.11 (t, *J* = 2.0 Hz, 1H), 8.79 (dd, *J* = 9.3, 2.0 Hz, 1H), 8.30 (d, *J* = 2.5 Hz, 1H), 7.63 (d, *J* = 8.9 Hz, 1H), 7.21 (dd, *J* = 9.0, 2.4 Hz, 1H), 4.67 (septet, *J* = 6.1 Hz, 1H), 3.06-2.32 (m, 12H), 1.37 (d, *J* = 6.1 Hz, 6H). ^{13}C NMR (100.6 MHz, DMSO-d_6): δ (ppm) 170.7, 170.5, 162.3, 158.2, 155.7, 153.7, 151.4, 146.9, 140.9, 140.7, 140.4, 132.8, 131.3, 124.1, 120.8, 120.7, 117.6, 116.8, 116.6, 115.3, 114.5, 110.65, 110.61, 109.8, 70.5, 35.8, 33.7, 33.4, 33.2, 33.1, 30.8, 30.4, 22.11, 22.08. IR (film): *v* (cm^{-1}) 3369, 2969, 2106, 1747, 1713, 1593, 1457, 1410, 1337, 1223, 1196, 1109, 965, 939, 801. HRMS calculated for $C_{27}H_{25}FN_4O_3RuS_4$ (M) 701.9836, found (M) 701.9834. **FL1353-2:** ^{1}H NMR (300 MHz, DMSO-d_6): δ (ppm) 11.09 (s, 1H), 8.98 (t, *J* = 1.9 Hz, 1H), 8.74 (dd, *J* = 9.4, 1.9 Hz, 1H), 8.27 (d, *J* = 2.4 Hz, 1H), 7.55 (d, *J* = 8.9 Hz, 1H), 7.17 (dd, *J* = 9.0, 2.3 Hz, 1H), 4.65 (septet, *J* = 6.0 Hz, 1H), 3.09-2.40 (m, 12H), 1.36 (d, *J* = 6.0 Hz, 6H). IR (film): *v* (cm^{-1}) 3154, 2972, 2100, 1749, 1717, 1560,

1491, 1458, 1410, 1333, 1223, 1200, 1112, 810, 698, 637. HRMS calculated for $C_{27}H_{25}FN_4O_3RuS_4$ (M) 701.9836, found (M) 701.9827.

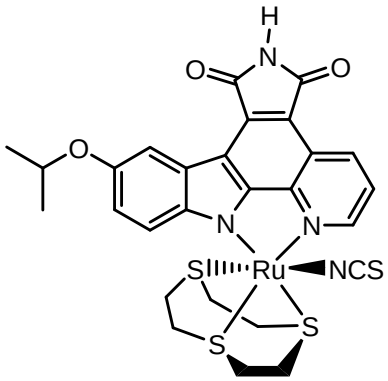

FL1370-1

Complex FL1370-1. A suspension of the ligand **3.6** (10 mg, 0.022 mmol), K_2CO_3 (3.3 mg, 0.024 mmol), and $[Ru(MeCN)_3([9]aneS_3)](CF_3SO_3)_2$ (16.8 mg, 0.024 mmol) in DMF (0.7 mL) was stirred at 85 °C under microwave irradiation for 30 minutes, followed by adding sodium thiocyanate (3.5 mg, 0.043 mmol), then the mixture was stirred at 85 °C for an additional 40 minutes. The resulting suspension was dried *in vacuo* and the crude material was adsorbed onto silica gel and subjected to silica gel chromatography with dichloromethane : methanol (first 20:1, then 15:1) as the eluting solvent. The metal complex **FL1370-1** was isolated as a solid (6 mg, 40%) and the other linkage isomer **FL1370-2** was also obtained (4.4 mg, 29%). **FL1370-1:** ^{1}H NMR (300 MHz, DMSO-d_6): δ (ppm) 11.0 (s, 1H), 9.10 (dd, J = 8.4, 1.0 Hz, 1H), 9.05 (dd, J = 5.1, 1.0 Hz, 1H), 8.30 (d, J = 2.5 Hz, 1H), 7.77 (dd, J = 8.9, 5.1 Hz, 1H), 7.63 (d, J = 8.9 Hz, 1H), 7.19 (dd, J = 8.9, 2.6 Hz, 1H), 4.66 (septet, J = 6.1 Hz, 1H), 3.10-2.20 (m, 12H), 1.37 (d, J = 6.1 Hz, 6H). ^{13}C NMR (100.6 MHz, DMSO-d_6): δ (ppm) 170.9, 170.8, 153.7, 151.1, 150.6, 146.9, 143.5, 132.6, 132.5, 130.7, 124.1, 123.3, 121.1, 117.5, 115.3, 114.6, 111.2, 109.7, 70.5, 34.3, 33.6, 32.6, 32.2, 29.7, 22.11, 22.08. IR (film): ν (cm^{-1}) 2099, 1745, 1698, 1597, 1490, 1461, 1413, 1337, 1232, 1214, 1181, 1118, 1003, 982, 823, 799, 698, 635, 497. HRMS calculated for $C_{27}H_{26}N_4O_3S_4RuNa$ $(M + Na)^+$ 706.9828, found $(M + Na)^+$ 706.9838. **FL1370-2:** ^{1}H NMR (300 MHz, DMSO-d_6): δ (ppm) 11.0 (s, 1H), 9.05 (dd, J = 8.4, 1.1 Hz, 1H), 8.97 (dd, J = 5.1, 1.1 Hz, 1H), 8.27 (d, J = 2.5 Hz, 1H), 7.76 (dd, J = 8.4, 5.1 Hz, 1H), 7.57 (d, J = 8.9 Hz, 1H), 7.16 (dd, J = 8.9, 2.6 Hz,

1H), 4.65 (septet, *J* = 6.1 Hz, 1H), 3.06-2.27 (m, 12H), 1.36 (d, *J* = 6.1 Hz, 6H). IR (film): *v* (cm^{-1}) 2974, 2100, 1745, 1703, 1596, 1493, 1460, 1418, 1338, 1278, 1232, 1208, 1116, 1023, 819, 799, 495. HRMS calculated for $C_{27}H_{26}N_4O_3S_4RuNa$ $(M + Na)^+$ 706.9828, found $(M + Na)^+$ 706.9832.

Chapter 6.1.4: Synthesis of Pim1 inhibitors

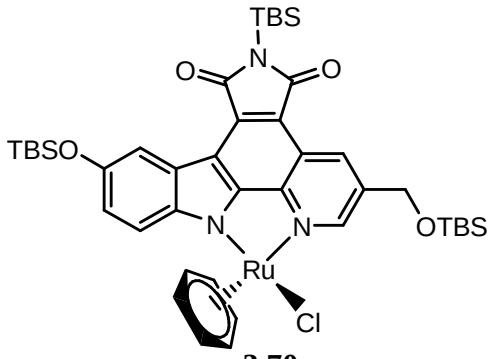

3.70

Complex 3.70. A suspension of the pyridocarbazole ligand **3.69** (160 mg, 0.24 mmol), K_2CO_3 (36 mg, 0.26 mmol), and $[RuCl_2(\eta^6\text{-}C_6H_6)]_2$ (89 mg, 0.18 mmol) in CH_3CN (30 mL) was purged with nitrogen for 5 minutes and stirred at 50 °C under nitrogen overnight. The resulting dark red suspension was dried *in vacuo* and the crude material was adsorbed onto silica gel and subjected to silica gel chromatography with dichloromethane : methanol (35:1) as the eluting solvent. The half-sandwich complex **3.70** was isolated as a dark red solid (200 mg, 95%). ^{1}H NMR (300 MHz, $CDCl_3$): δ (ppm) 9.26 (d, *J* = 1.3 Hz, 1H), 9.05 (d, *J* = 1.3 Hz, 1H), 8.35 (d, *J* = 2.5 Hz, 1H), 7.64 (d, *J* = 8.7 Hz, 1H), 7.14 (dd, *J* = 8.7, 2.5 Hz, 1H), 5.82 (s, 6H), 5.05 (d, *J* = 13.6 Hz, 1H), 4.98 (d, *J* = 13.6 Hz, 1H), 1.07 (s, 9H), 1.04 (s, 9H), 1.03 (s, 9H), 0.60 (s, 6H), 0.31 (s, 3H), 0.30 (s, 3H), 0.22 (s, 3H), 0.20 (s, 3H). ^{13}C NMR (75.5 MHz, $CDCl_3$): δ (ppm) 175.5, 174.4, 153.3, 150.0, 149.9, 146.6, 142.3, 136.4, 133.4, 132.1, 125.1, 121.3, 120.5, 114.9, 114.8, 114.6, 114.3, 83.3, 63.2, 26.6, 26.1, 19.2, 18.5, -3.8, -4.09, -4.12, -4.99, -5.05. IR (film): *v* (cm^{-1}) 2928, 2856, 1744, 1691, 1608, 1555, 1461, 1430, 1305, 1255, 1209, 1148, 1096, 1048, 907, 836, 778. HRMS calculated for $C_{42}H_{58}N_3O_4Si_3Ru$ $(M - Cl)^+$ 854.2784, found $(M - Cl)^+$ 854.2788.

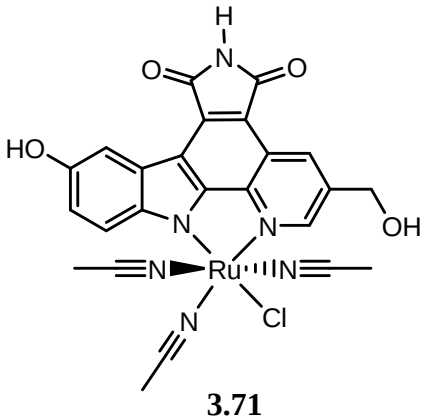

3.71

Complex 3.71. A red solution of **3.70** (200 mg, 0.22 mmol) in CH_3CN (220 mL) was purged with nitrogen for 10 min, then irradiated with a mercury medium pressure lamp (150 W, pyrex filter) for 3 hours while nitrogen was bubbled through the solution. The resulting dark green solution was dried *in vacuo* and the crude material was adsorbed onto silica gel and subjected to silica gel chromatography with dichloromethane : methanol (first 35:1, then 15:1). The combined product eluents were isolated as a mixture of two diastereoisomers (170 mg, 80%). To the stirred green solution of the mixture (170 mg, 0.18 mmol) in CH_3CN (25 mL) was added tetrabutylammonium fluoride (820 μL, 1 M in THF, 0.82 mmol) at 0 °C, then the solution was stirred at 0 °C for 10 min. To the resulting green solution was added glacial acetic acid (47.7 μL, 0.82 mmol) and stirred for 1 min at 0 °C. The solution was dried *in vacuo* and the crude material was adsorbed onto silica gel and subjected to silica gel chromatography with dichloromethane : methanol (first 10:1, then 5:1) to yield the precursor complex **3.71** (44 mg, 41%) and a second diastereoisomer in lower amounts (31 mg, 29%). Analytical data for the main diastereomer **3.71**: ^{1}H NMR (300 MHz, DMSO-d_6): δ (ppm) 10.83 (s, 1H), 9.42 (br, 1H), 9.06 (s, 1H), 8.87 (br, 1H), 8.07 (br, 1H), 7.65 (d, J = 8.7 Hz, 1H), 7.03 (d, J = 8.7 Hz, 1H), 5.69 (t, J = 5.4 Hz, 1H), 4.83 (d, J = 5.4 Hz, 2H), 2.94 (s, 3H), 2.21 (s, 6H). IR (film): ν (cm^{-1}) 3231, 2926, 2274, 1745, 1686, 1556, 1490, 1422, 1337, 1285, 1229, 1192, 1138, 1028, 858, 700, 671, 638, 506, 478. HRMS calculated for $C_{24}H_{19}N_6O_4ClRu$ (M) 592.0198, found (M) 592.0197.

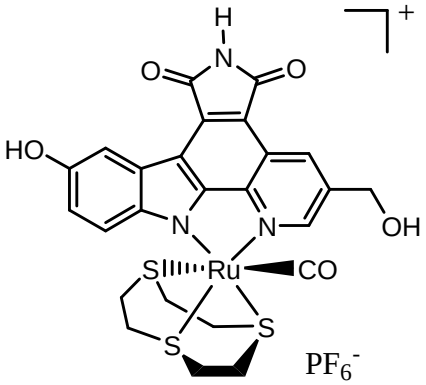

FL1360

Complex FL1360. A solution of precursor complex **3.71** (15 mg, 0.025 mmol) in DMF (2.5 mL) was purged with CO gas for 5 min, then stirred at 75 °C under an atmosphere of CO for 1 hour. To the resulting solution was added [9]aneS_3, then the solution was stirred at 95 °C under an atmosphere of nitrogen for 3 hours, after which the purple solution was dried under high vacuum. The crude material was adsorbed onto silica gel and subjected to silica gel chromatography with MeCN : H_2O : KNO_3 (50:3:1) to obtain purple solid. The resulting material was dissolved in a minimal acetonitrile/water. The product was precipitated by the addition of excess solid NH_4PF_6. The precipitate was centrifuged and washed twice with water. The material was then dried under high vacuum to yield **FL1360** (8.4 mg, 42%). ^{1}H NMR (300 MHz, DMSO-d_6): δ (ppm) 11.18 (s, 1H), 9.35 (s, 1H), 9.21 (s, 1H), 8.81 (s, 1H), 8.20 (d, J = 2.4 Hz, 1H), 7.45 (d, J = 8.8 Hz, 1H), 7.11 (dd, J = 8.8, 2.4 Hz, 1H), 5.79 (br, 1H), 4.89 (br, 2H), 3.52-2.53 (m, 12H). ^{13}C NMR (100.6 MHz, DMSO-d_6): δ (ppm) 192.3, 170.7, 170.3, 152.8, 151.6, 151.0, 144.6, 141.7, 139.0, 131.7, 131.3, 124.6, 121.1, 117.0, 114.7, 114.2, 112.4, 108.8, 60.5, 38.2, 36.6, 36.0, 32.0, 31.6, 31.0. IR (film): ν (cm^{-1}) 3210, 2008, 1751, 1714, 1492, 1470, 1418, 1337, 1026, 999, 842, 704. HRMS calculated for $C_{25}H_{22}N_3O_5S_3Ru$ $(M)^+$ 641.9760, found $(M)^+$ 641.9750.

Chapter 6.1.5: Synthesis of TrkA inhibitors

General procedure for the synthesis of ruthenium complexes with tridentate ligands: To a soulution of ruthenium precursor in DMF (8 mM, 2 mL) was added tridentate ligand (1 equiv), then the mixture was stirred at 70 °C under an atmosphere of nitrogen for 1 hour. The resulting solution was dried *in vacuo* and the crude material was adsorbed onto silica gel and subjected to silica gel chromatography with dichloromethane : methanol as eluting solvent.

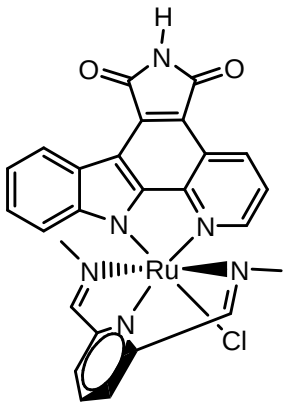

FL792-1

Complex FL792-1. Using dichloromethane : methanol (75:1) as the eluting solvent. (5 mg, 26%). ^{1}H NMR (300 MHz, $CDCl_3$): δ (ppm) 10.02 (dd, *J* = 5.1, 1.2 Hz, 1H), 9.32 (dd, *J* = 8.4, 1.2 Hz, 1H), 8.71 (d, *J* = 7.5 Hz, 1H), 8.27 (s, 1H), 8.26 (s, 1H), 7.92 (dd, *J* = 8.4, 5.1 Hz, 1H), 7.88-7.85 (m, 2H), 7.73 (m, 1H), 7.43 (s, 1H), 7.15 (m, 1H), 7.01 (m, 1H), 5.59 (d, *J* = 8.2 Hz, 1H), 3.17 (s, 3H), 3.16 (s, 3H).

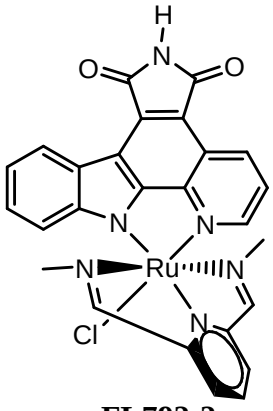

FL792-2

Complex FL792-2. Using dichloromethane : methanol (75:1) as the eluting solvent.

(4.6 mg, 24%). ^{1}H NMR (300 MHz, $CDCl_3$): δ (ppm) 9.05 (d, *J* = 8.0 Hz, 1H), 8.87 (d, *J* = 8.0 Hz, 1H), 8.32 (s, 1H), 8.31 (s, 1H), 7.85-7.83 (m, 2H), 7.73-7.62 (m, 3H), 7.53 (m, 1H), 7.40 (s, 1H), 7.05 (dd, *J* = 8.3, 5.2 Hz, 1H), 6.6 (m, 1H), 3.19 (s, 6H).

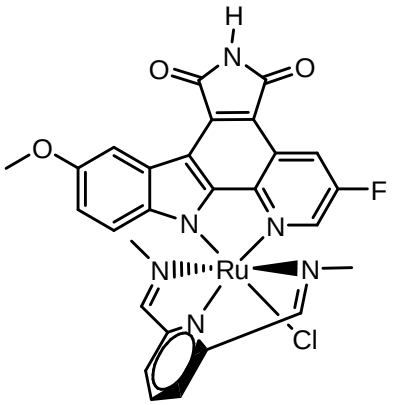

FL1138-1

Complex FL1138-1. Using dichloromethane : methanol (75:1) as the eluting solvent. (2.5 mg, 24%). ^{1}H NMR (300 MHz, acetone-d_6): δ (ppm) 9.90-9.88 (m, 2H), 8.87 (dd, *J* = 9.5, 2.5 Hz, 1H), 8.58 (s, 1H), 8.57 (s, 1H), 8.19 (d, *J* = 2.6 Hz, 1H), 8.17-8.15 (m, 2H), 7.80 (dd, *J* = 8.2, 7.7 Hz, 1H), 6.66 (dd, *J* = 8.9, 2.6 Hz, 1H), 5.60 (d, *J* = 8.9 Hz, 1H), 3.81 (s, 3H), 3.16 (s, 3H), 3.15 (s, 3H).

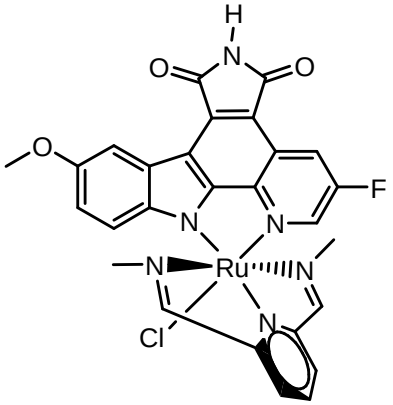

FL1138-2

Complex FL1138-2. Using dichloromethane : methanol (75:1) as the eluting solvent. (2.5 mg, 24%). ^{1}H NMR (300 MHz, DMSO-d_6): δ (ppm) 11.01 (s, 1H), 8.71 (d, *J* = 9.0 Hz, 1H), 8.60 (s, 1H), 8.59 (s, 1H), 8.39-8.34 (m, 2H), 8.11-8.08 (m, 2H), 7.83 (t, *J* = 8.1 Hz, 1H), 7.23 (dd, *J* = 9.0, 2.7 Hz, 1H), 6.87 (t, *J* = 2.5 Hz, 1H), 3.95 (s, 3H), 2.93 (s, 3H), 2.92 (s, 3H).

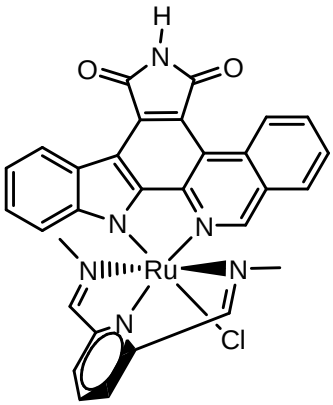

FL1124-1

Complex FL1124-1. Using dichloromethane : methanol (75:1) as the eluting solvent. (2.7 mg, 25%). ^{1}H NMR (300 MHz, DMSO-d_6): δ (ppm) 11.28 (s, 1H), 10.67 (d, J = 8.4 Hz, 1H), 10.48 (s, 1H), 8.70 (d, J = 7.4 Hz, 1H), 8.63 (s, 1H), 8.62 (s, 1H), 8.56 (d, J = 7.8 Hz, 1H), 8.18-8.12 (m, 3H), 8.01 (t, J = 7.4 Hz, 1H), 7.90 (t, J = 8.0 Hz, 1H), 7.07-6.97 (m, 2H), 5.51 (d, J = 7.5 Hz, 1H), 3.05 (s, 6H).

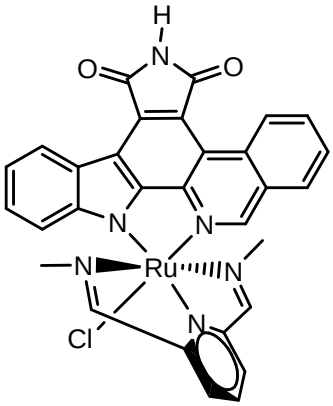

FL1124-2

Complex FL1124-2. Using dichloromethane : methanol (75:1) as the eluting solvent. (2.4 mg, 22%). ^{1}H NMR (300 MHz, $CDCl_3$): δ (ppm) 10.49 (d, J = 8.5 Hz, 1H), 9.24 (d, J = 7.9 Hz, 1H), 8.97 (br, 1H), 8.34 (s, 2H), 7.91-7.83 (m, 3H), 7.76-7.57 (m, 4H), 7.45 (m, 1H), 7.01 (m, 1H), 3.21 (s, 6H).

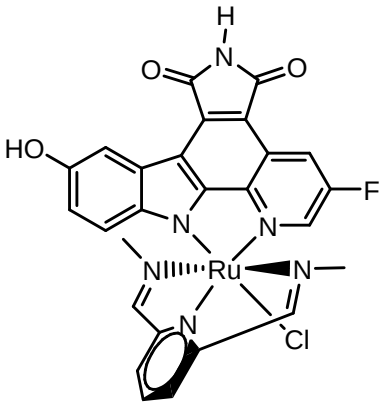

FL609-1

Complex FL609-1. Using dichloromethane : methanol (50:1) as the eluting solvent. (1.5 mg, 21%). ^{1}H NMR (300 MHz, acetone-d_6): δ (ppm) 9.87 (dd, J = 3.4, 2.5 Hz, 1H), 9.79 (br, 1H), 8.84 (dd, J = 9.5, 2.5 Hz, 1H), 8.57 (s, 1H), 8.56 (s, 1H), 8.17-8.14 (m, 2H), 8.07 (d, J = 2.5 Hz, 1H), 7.98 (m, 1H), 7.89 (dd, J = 8.2, 7.6 Hz, 1H), 6.60 (dd, J = 8.8, 2.6 Hz, 1H), 5.54 (d, J = 8.8 Hz, 1H), 3.16 (s, 3H), 3.15 (s, 3H).

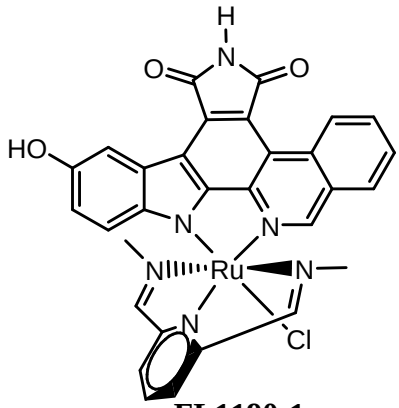

FL1190-1

Complex FL1190-1. Using dichloromethane : methanol (first 35:1, then 20:1) as the eluting solvent. (1.8 mg, 24%). ^{1}H NMR (300 MHz, acetone-d_6): δ (ppm) 10.81 (d, J = 8.6 Hz, 1H), 10.57 (s, 1H), 9.97 (s, 1H), 8.67-8.58 (m, 2H), 8.50 (m, 1H), 8.16-7.95 (m, 4H), 7.90-7.82 (m, 2H), 6.61 (dd, J = 8.8, 2.6 Hz, 1H), 5.51 (d, J = 8.8 Hz, 1H), 3.17 (s, 6H).

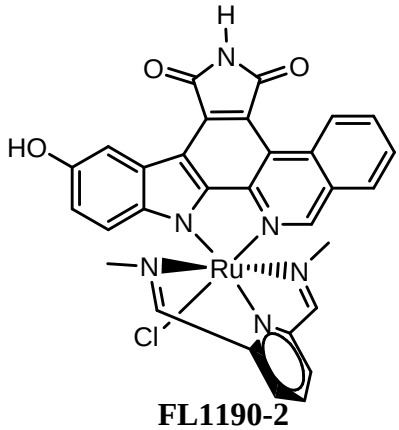

FL1190-2

Complex FL1190-2. Using dichloromethane : methanol (first 35:1, then 20:1) as the eluting solvent. (1.5 mg, 21%). ^{1}H NMR (300 MHz, acetone-d_6): δ (ppm) 10.58 (d, J = 8.6 Hz, 1H), 9.93 (br, 1H), 8.92 (d, J = 8.9 Hz, 1H), 8.65 (d, J = 2.4 Hz, 1H), 8.63 (s, 1H), 8.62 (s, 1H), 8.14-8.11 (m, 2H), 7.96 (s, 1H), 7.85-7.79 (m, 2H), 7.69-7.59 (m, 2H), 7.45 (s, 1H), 7.21 (dd, J = 8.8, 2.6 Hz, 1H), 3.11 (s, 3H), 3.10 (s, 3H).

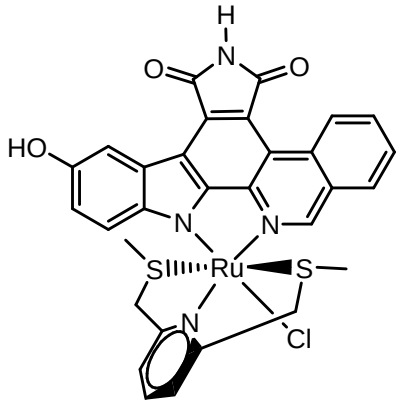

FL1260-1

Complex FL1260-1. Using dichloromethane : methanol (35:1) as the eluting solvent. (1.8 mg, 16%). ^{1}H NMR (300 MHz, acetone-d_6): δ (ppm) 10.70 (d, J = 8.5 Hz, 1H), 10.23 (s, 1H), 9.97 (br, 1H), 8.49 (d, J = 2.5 Hz, 1H), 8.29 (d, J = 8.2 Hz, 1H), 8.0 (m, 1H), 7.92-7.75 (m, 5H), 6.82 (dd, J = 8.7, 2.6 Hz, 1H), 5.96 (d, J = 8.7 Hz, 1H), 5.05-4.90 (m, 2H), 4.31-4.17 (m, 2H), and the methyl group was overlapped by the solvent peak.

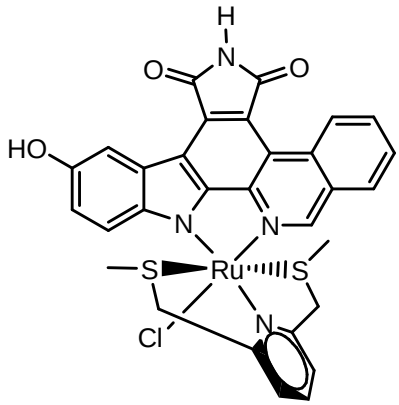

FL1260-2

Complex FL1260-2. Using dichloromethane : methanol (first 35:1) as the eluting solvent. (2.5 mg, 22%). ^{1}H NMR (300 MHz, acetone-d_6): δ (ppm) 10.68 (d, J = 8.6 Hz, 1H), 9.97 (br, 1H), 8.96 (d, J = 8.9 Hz, 1H), 8.57 (d, J = 2.4 Hz, 1H), 8.17-8.14 (m, 2H), 7.92 (s, 1H), 7.82-7.76 (m, 2H), 7.74-7.64 (m, 2H), 7.48 (s, 1H), 7.16 (dd, J = 8.8, 2.6 Hz, 1H), 5.01-4.86 (m, 2H), 4.35-4.21 (m, 2H), and the methyl group was overlapped by the solvent peak. HRMS calculated for $C_{30}H_{24}ClN_4O_3S_2Ru$ $(M + H)^+$ 689.0027, found $(M + H)^+$ 689.0023.

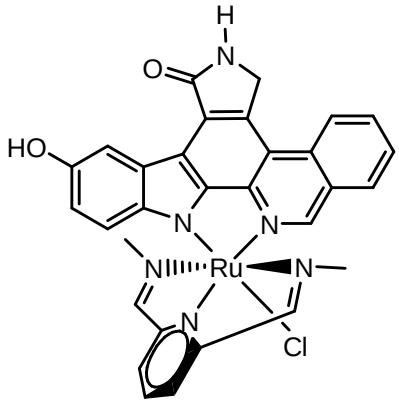

FL1220

Complex FL1220. A mixture solution of compound **4.3** (15 mg, 0.030 mmol), precursor **4.2** (13.6 mg, 0.036 mmol), and K_2CO_3 (5 mg, 0.036 mmol) in ethanol (3 mL) was refluxed under an atmosphere of nitrogen for 6 hours. The resulting solution was dried *in vacuo* and the crude material was filtered by flash silica gel chromatography with dichloromethane : methanol (20:1) as eluting solvent. The resulting solid was dissolved in acetonitrile, followed by adding TBAF (1 M in THF, 60 μL, 0.06 mmol) at 0 °C. After stirring for 3 minutes at 0 °C, the reaction was quenched with saturated

ammonium chloride solution. The resulting solution was dried *in vacuo* and the crude material was adsorbed onto silica gel and subjected to silica gel chromatography with dichloromethane : methanol (15:1) as eluting solvent to yield complex **FL1220** (3.4 mg, 18% over two steps). ^{1}H NMR (300 MHz, DMSO-d_6): δ (ppm) 10.42 (s, 1H), 8.99 (s, 1H), 8.63-8.56 (m, 4H), 8.22 (d, *J* = 2.4 Hz, 1H), 8.15-8.09 (m, 3H), 8.94 (m, 1H), 7.84 (m, 1H), 6.36 (dd, *J* = 8.8, 2.6 Hz, 1H), 5.30 (s, 2H), 5.23 (d, *J* = 8.8 Hz, 1H), 3.03 (s, 6H).

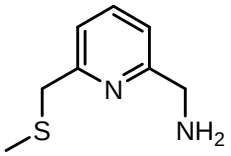

4.6

Compound 4.6. A mixture solution of 2,6-bis(chloromethyl)pyridine (50 mg, 0.286 mmol), sodium methanethiolate (20 mg, 0.286 mmol), and 12-crown-4 (50 mg, 0.284 mmol) in ethanol (1 mL) was stirred at room temperature under an atmosphere of nitrogen overnight. The resulting mixture was diluted with water and extracted with DCM twice. The combined organic layers were concentrated, then dissolved in DMF (1 mL), followed by adding sodium azide (17 mg, 0.254 mmol). After stirring at 50 °C overnight, the resulting mixture was dried *in vacuo* and filtered by flash silica gel chromatography with hexane : EtOAc (3:1) as eluting solvent. The resulting product was dissolved in THF (1 mL), followed by adding triphenylphosphine (150 mg, 0.572 mmol), and water (20.6 mg, 1.14 mmol). After refluxing under nitrogen for 2 hours, the resulting solution was dried *in vacuo* and the crude material was adsorbed onto silica gel and subjected to silica gel chromatography with dichloromethane : methanol (first 35:1, then 20:1 with 0.5% concentrated ammonium) as eluting solvent to yield compound **4.6** (10 mg, 20% over three steps). ^{1}H NMR (300 MHz, $CDCl_3$): δ (ppm) 7.59 (t, *J* = 7.7 Hz, 1H), 7.19 (d, *J* = 7.7 Hz, 1H), 7.13 (d, *J* = 7.7 Hz, 1H), 3.94 (s, 2H), 3.76 (s, 2H), 2.23 (s, 2H), 2.04 (s, 3H). ^{13}C NMR (75.5 MHz, $CDCl_3$): δ (ppm) 159.0, 158.3, 137.5, 121.5, 119.8, 46.6, 40.1, 15.5. HRMS calculated for $C_8H_{13}N_2S$ $(M + H)^+$ 169.0794, found $(M + H)^+$ 169.0794.

Chapter 6.2: Resolution of racemic mixtures and determination of absolute configurations

Complex FL172. The enantiomers were seperated using a CHIRALPAK IB analytical HPLC column (Daicel/Chiral Technologies, 250 x 4.6 mm) using the solvent of ethanol : hexane (1 : 1) in 15 minutes with a flow rate of 0.75 ml/minute. The enantiomers were baseline separated under these conditions with retention times of 12.9 (E1) and 15.3 min (E2). The enantiomers did not show any racemization in an ethanol solution over a time period of 12 hours. The CD spectra of the separated enantiomers were were recorded on a Model J-810 Spectropolarimeter and shown in Figure 2.8. The slower eluting enantiomer E2 showed more potent PAK-1 inhibition and was cocrystallized with PAK1 and based on this cocrystal structure assigned with the Λ-configuration.

Complex FL411: For the resolution of the racemic mixture of **FL411**, the amino group at the 4-position of the pyridine was BOC-protected and removed after the separation with a CHIRALPAK IB analytical HPLC column (Daicel/Chiral Technologies, 250 x 4.6 mm) with the solvent of ethanol : hexane (2 : 3) in 15 minutes with a flow rate of 0.75 ml/minute. The enantiomers were baseline-separated under these conditions with retention times of ca. 10.5 (E1) and 15.7 min (E2). The enantiomers did not show any significant racemization in an ethanol solution over a time period of 12 hours. The CD spectra of the separated enantiomers after BOC-deprotection were shown in Figure 2.14. Absolute configurations were assigned by correlation with the CD spectra of **FL172**.

Complex FL1422: For the resolution of the racemic mixture of **FL1422**, the amino group at the 4-position of the pyridine was BOC-protected and removed after the separation with a CHIRALPAK IB analytical HPLC column (Daicel/Chiral Technologies, 250 x 4.6 mm) with the solvent of ethanol : hexane (45 : 55) in 16 minutes with a flow rate of 0.75 ml/minute. The enantiomers were baseline-separated under these conditions with retention times of ca. 8.7 (E1) and 15.5 min (E2). The enantiomers did not show any significant racemization in an ethanol solution over a

time period of 12 hours. The CD spectra of the separated enantiomers after BOC-deprotection were shown in Figure 2.16. Absolute configurations were assigned by correlation with the CD spectra of **FL172**.

Chapter 6.3: Kinase assays

Protein kinase (human) and substrate were purchased from Upstate Biotechnology USA, Millipore or MoBiTec GmbH, and PAK1 was purified by Jasna Maksimoska (University of Pennsylvania and The Wistar Institute, Philadelphia, USA). [γ-^{33}P]ATP was purchased from PerkinElmer.

Protein Kinase PAK1 Assay Using [γ-^{33}P]ATP. Various concentrations of ruthenium complexes were incubated at room temperature in 20 mM MOPS, 10 mM $Mg(OAc)_2$, 0.8 μg/μL BSA, 5% DMSO (resulting from the inhibitor stock solution), pH 7.0, in the presence of substrate (12.5 μg MBP peptide), and kinase PAK1 (0.2 nM). After 15 min, the reaction was initiated by adding ATP to a final concentration of 100 μM, including approximately 0.06 μCi/μL [γ-^{33}P]ATP. Reactions were performed in a total volume of 25 μL. After 45 minutes, the reaction was terminated by spotting 15 μL on a circular P81 phosphocellulose paper (2.1 cm diameter, Whatman), followed by washing three times (5 minutes each wash) with 0.75% phosphoric acid and once with acetone. The dried P81 papers were transferred to a scintillation vial, 5mL of scintillation cocktail was added and the counts per minute (CPM) were determined with a Beckmann 6500 scintillation counter. IC_{50} values were defined to be the concentration of inhibitor at which the CPM was 50% of the control sample, corrected by the background.

Protein Kinase Pim1 Assay Using [γ-^{33}P]ATP. Various concentrations of ruthenium complexes were incubated at room temperature in 10 mM MOPS, 10 mM $Mg(OAc)_2$, 0.1 μg/μL BSA, 5% DMSO (resulting from the inhibitor stock solution), pH 7.0, in the presence of substrate S6 peptide (50 μM, AKRRRLSSLRA), and kinase Pim1 (1.6 nM). After 15 min, the reaction was initiated by adding ATP to a final concentration of 100 μM, including approximately 0.04 μCi/μL [γ-^{33}P]ATP. Reactions were performed in a

total volume of 25 μL. After 30 minutes, the reaction was terminated by spotting 15 μL on a circular P81 phosphocellulose paper (2.1 cm diameter, Whatman), followed by washing three times (5 minutes each wash) with 0.75% phosphoric acid and once with acetone. The dried P81 papers were transferred to a scintillation vial, 5mL of scintillation cocktail was added and the counts per minute (CPM) were determined with a Beckmann 6500 scintillation counter. IC_{50} values were defined to be the concentration of inhibitor at which the CPM was 50% of the control sample, corrected by the background.

Protein Kinase GSK3β Assay Using [γ-^{33}P]ATP. Various concentrations of ruthenium complexes were incubated at room temperature in 20 mM MOPS, 10 mM $Mg(OAc)_2$, 0.8 μg/μL BSA, 5% DMSO (resulting from the inhibitor stock solution), pH 7.0, in the presence of substrate phosphoglycogen synthase peptide-2 (20 μM, YRRAAVPPSPSLSRHSSPHQ-pS-EDEEE), and kinase GSK3β (1.8 nM). After 15 min, the reaction was initiated by adding ATP to a final concentration of 100 μM, including approximately 0.05 μCi/μL [γ-^{33}P]ATP. Reactions were performed in a total volume of 25 μL. After 45 minutes, the reaction was terminated by spotting 15 μL on a circular P81 phosphocellulose paper (2.1 cm diameter, Whatman), followed by washing three times (5 minutes each wash) with 0.75% phosphoric acid and once with acetone. The dried P81 papers were transferred to a scintillation vial, 5mL of scintillation cocktail was added and the counts per minute (CPM) were determined with a Beckmann 6500 scintillation counter. IC_{50} values were defined to be the concentration of inhibitor at which the CPM was 50% of the control sample, corrected by the background.

Protein Kinase MLCK Assay Using [γ-^{33}P]ATP. Various concentrations of ruthenium complexes were incubated at room temperature in 10 mM MOPS, 10 mM $Mg(OAc)_2$, 0.1 μg/μL BSA, 5% DMSO (resulting from the inhibitor stock solution), pH 7.0, in the presence of substrate ZIP peptide (62.5 μM, KKLNRTLSFAEPG), calmodulin (1 μM), $CaCl_2$ (0.5 mM) and kinase MLCK (4.6 nM). After 15 min, the reaction was initiated by adding ATP to a final concentration of 100 μM, including approximately 0.1 μCi/μL

[γ-^{33}P]ATP. Reactions were performed in a total volume of 25 μL. After 30 minutes, the reaction was terminated by spotting 15 μL on a circular P81 phosphocellulose paper (2.1 cm diameter, Whatman), followed by washing three times (5 minutes each wash) with 0.75% phosphoric acid and once with acetone. The dried P81 papers were transferred to a scintillation vial, 5mL of scintillation cocktail was added and the counts per minute (CPM) were determined with a Beckmann 6500 scintillation counter. IC_{50} values were defined to be the concentration of inhibitor at which the CPM was 50% of the control sample, corrected by the background.

Protein Kinase GSK3α Assay Using [γ-^{33}P]ATP. Various concentrations of ruthenium complexes were incubated at room temperature in 20 mM MOPS, 10 mM $Mg(OAc)_2$, 0.8 μg/μL BSA, 5% DMSO (resulting from the inhibitor stock solution), pH 7.0, in the presence of substrate phosphoglycogen synthase peptide-2 (20 μM, YRRAAVPPSPSLSRHSSPHQ-pS-EDEEE), and kinase GSK3α (1.8 nM). After 15 min, the reaction was initiated by adding ATP to a final concentration of 100 μM, including approximately 0.05 μCi/μL [γ-^{33}P]ATP. Reactions were performed in a total volume of 25 μL. After 45 minutes, the reaction was terminated by spotting 15 μL on a circular P81 phosphocellulose paper (2.1 cm diameter, Whatman), followed by washing three times (5 minutes each wash) with 0.75% phosphoric acid and once with acetone. The dried P81 papers were transferred to a scintillation vial, 5mL of scintillation cocktail was added and the counts per minute (CPM) were determined with a Beckmann 6500 scintillation counter. IC_{50} values were defined to be the concentration of inhibitor at which the CPM was 50% of the control sample, corrected by the background.

Protein Kinase Flt4 Assay Using [γ-^{33}P]ATP. Various concentrations of ruthenium complexes were incubated at room temperature in 20 mM MOPS, 10 mM $Mg(OAc)_2$, 0.8 μg/μL BSA, 5% DMSO (resulting from the inhibitor stock solution), pH 7.0, in the presence of substrate Jak3tide (100 μM, GGEEEEYFELVKKKK), and kinase Flt4 (8.8 nM). After 30 min, the reaction was initiated by adding ATP to a final concentration of 100 μM, including approximately 0.1 μCi/μL [γ-^{33}P]ATP. Reactions were performed in

a total volume of 25 μL. After 120 minutes, the reaction was terminated by spotting 15 μL on a circular P81 phosphocellulose paper (2.1 cm diameter, Whatman), followed by washing three times (5 minutes each wash) with 0.75% phosphoric acid and once with acetone. The dried P81 papers were transferred to a scintillation vial, 5mL of scintillation cocktail was added and the counts per minute (CPM) were determined with a Beckmann 6500 scintillation counter. IC_{50} values were defined to be the concentration of inhibitor at which the CPM was 50% of the control sample, corrected by the background.

Protein Kinase DAPK1 Assay Using [γ-^{33}P]ATP. Various concentrations of ruthenium complexes were incubated at room temperature in 20 mM MOPS, 10 mM $Mg(OAc)_2$, 0.1 μg/μL BSA, 5% DMSO (resulting from the inhibitor stock solution), pH 7.0, in the presence of substrate (62.5 μM ZIP peptide KKLNRTLSFAEPG) and kinase DAPK1 (1 nM). After 15 min, the reaction was initiated by adding ATP to a final concentration of 100 μM, including approximately 0.08 μCi/μL [γ-^{33}P]ATP. Reactions were performed in a total volume of 25 μL. After 30 minutes, the reaction was terminated by spotting 15 μL on a circular P81 phosphocellulose paper (2.1 cm diameter, Whatman), followed by washing three times (5 minutes each wash) with 0.75% phosphoric acid and once with acetone. The dried P81 papers were transferred to a scintillation vial, 5mL of scintillation cocktail was added and the counts per minute (CPM) were determined with a Beckmann 6500 scintillation counter. IC_{50} values were defined to be the concentration of inhibitor at which the CPM was 50% of the control sample, corrected by the background.

Protein Kinase ZIPK Assay Using [γ-^{33}P]ATP. Various concentrations of ruthenium complexes were incubated at room temperature in 20 mM MOPS, 10 mM $Mg(OAc)_2$, 0.1 μg/μL BSA, 5% DMSO (resulting from the inhibitor stock solution), pH 7.0, in the presence of substrate (62.5 μM ZIP peptide KKLNRTLSFAEPG) and kinase ZIPK (10 nM). After 15 min, the reaction was initiated by adding ATP to a final concentration of 100 μM, including approximately 0.1 μCi/μL [γ-^{33}P]ATP. Reactions were performed in

a total volume of 25 µL. After 30 minutes, the reaction was terminated by spotting 15 µL on a circular P81 phosphocellulose paper (2.1 cm diameter, Whatman), followed by washing three times (5 minutes each wash) with 0.75% phosphoric acid and once with acetone. The dried P81 papers were transferred to a scintillation vial, 5mL of scintillation cocktail was added and the counts per minute (CPM) were determined with a Beckmann 6500 scintillation counter. IC_{50} values were defined to be the concentration of inhibitor at which the CPM was 50% of the control sample, corrected by the background.

Protein Kinase TrkA Assay Using [γ-^{33}P]ATP. Various concentrations of ruthenium complexes were incubated at room temperature in 20 mM MOPS, 30 mM $Mg(OAc)_2$, 0.8 µg/µL BSA, 5% DMSO (resulting from the inhibitor stock solution), pH 7.0, in the presence of substrate IGF-IR peptide (150 µM, KKKSPGEYVNIEFG) and kinase TrkA (9.8 nM). After 15 min, the reaction was initiated by adding ATP to a final concentration of 100 µM, including approximately 0.1 µCi/µL [γ-^{33}P]ATP. Reactions were performed in a total volume of 25 µL. After 2 hours, the reaction was terminated by spotting 15 µL on a circular P81 phosphocellulose paper (2.1 cm diameter, Whatman), followed by washing three times (5 minutes each wash) with 0.75% phosphoric acid and once with acetone. The dried P81 papers were transferred to a scintillation vial, 5mL of scintillation cocktail was added and the counts per minute (CPM) were determined with a Beckmann 6500 scintillation counter. IC_{50} values were defined to be the concentration of inhibitor at which the CPM was 50% of the control sample, corrected by the background.

Chapter 6.4: References

(1) Arnold, J.; Artis, D. R.; Hurt, C.; Ibrahim, P. N.; Krupka, H.; Lin, J.; Milburn, M. V.; Wang, W. R.; Zhang, C. *PCT Int. Appl.* 2005009958, 03 Feb 2005.

(2) Petit, S.; Curoc, Y.; Larue, V.; Dardel, F. *Chem Med Chem* **2009**, *4*, 261-275.

(3) Bailey, W. F.; Salgaonkar, P. D.; Brubaker, J. D.; Sharma, V. *Organic Letters* **2008**, *10(6)*, 1071-1074.

(4) Edema, J. H.; Buter, J.; Kellogg, R. M.; Spek, A. L.; Bolhuis, F. *J. Chem. Soc., Chem. Commun.* **1992**, 1558-60.

(5) Bregman, H.; Carroll, P. J.; Meggers, E. *J. Am. Chem. Soc.* **2006**, *128*, 877-884.

(6) Pagano, N.; Maksimoska, J.; Bregman, H.; Williams, D. S.; Richard D. Webster, R. D.; Meggers, E. *Org. Biomol. Chem.* **2007**, *5*, 1218-1227.

(7) Seitz, M.; Kaiser, A.; Tereshchenko, A.; Geiger, C.; Uematsu, Y.; Reiser, O. *Tetrahedron* **2006**, *62*, 9973-9980.

(8) Gergely, J.; Shinya, H.; Katsuya, I.; Yonezo, M. *Chemistry Letters* **2003**, *32*, 882-883.

(9) Lai, W.; Berry, S. M.; Bebout, D. C. *Inorg. Chem*. **2006**, *45*, 571-581.

Appendix

A. Crystallographic Data

Crystal structure of FL151-1.

Table 6.1. Crystal data and structure refinement for **FL151-1**.

Identification code	fl151-1	
Habitus, colour	plate, red	
Crystal size	0.30 x 0.26 x 0.06 mm^3	
Crystal system	Triclinic	
Space group	$P\bar{1}$	Z = 2
Unit cell dimensions	a = 10.6778(4) Å	α= 88.265(3)°.
	b = 13.2390(4) Å	β= 70.059(2)°.
	c = 13.9507(4) Å	γ = 68.259(3)°.
Volume	1711.56(10) $Å^3$	
Cell determination	21187 peaks with Theta 1.5 to 28°.	
Empirical formula	$C_{37.50}$ H_{30} Cl F N_5 $O_{6.50}$ Ru	
Formula weight	810.18	
Density (calculated)	1.572 Mg/m^3	
Absorption coefficient	0.599 mm^{-1}	
F(000)	824	

Data collection:

Diffractometer type	IPDS2
Wavelength	0.71073 Å
Temperature	100(2) K
Theta range for data collection	1.56 to 27.91°.
Index ranges	-14<=h<=13, -17<=k<=17, -18<=l<=18
Data collection software	STOE WinXpose (X-Area)
Cell refinement software	STOE WinCell (X-Area)
Data reduction software	STOE WinIntegrate (X-Area)

Solution and refinement:

Reflections collected	19070
Independent reflections	8134 [R(int) = 0.0334]
Completeness to theta = 25.00°	100.0 %
Observed reflections	6933[I>2sigma(I)]
Reflections used for refinement	8134
Absorption correction	Semi-empirical from equivalents
Max. and min. transmission	0.9838 and 0.8168
Largest diff. peak and hole	0.506 and -0.901 e.$Å^{-3}$
Solution	Direct methods
Refinement	Full-matrix least-squares on F^2
Treatment of hydrogen atoms	C-H geometrical, O-H located, “mixed” refinement
Programs used	SIR2004 (Giacovazzo et al, 2004)
	SHELXL-97 (Sheldrick, 1997)
	Diamond 3.1, STOE IPDS2 software
Data / restraints / parameters	8134 / 6 / 501
Goodness-of-fit on F^2	0.977
R index (all data)	wR2 = 0.0717
R index conventional [I>2sigma(I)]	R1 = 0.0285

Table 6.2. Atomic coordinates and equivalent isotropic displacement parameters ($Å^2$) for **FL151-1**. U(eq) is defined as one third of the trace of the orthogonalized U^{ij} tensor.

	x	y	z	U(eq)	Occupancy
N1	0.21583(17)	0.24244(12)	0.15534(11)	0.0219(3)	1
O1	0.26653(17)	-0.16933(11)	-0.11508(11)	0.0322(3)	1
Cl1	-0.19529(5)	0.32146(4)	0.42267(3)	0.02774(10)	1
Ru1	0.03256(2)	0.28269(1)	0.28516(1)	0.02062(5)	1
F1	-0.13800(14)	-0.05047(10)	0.24125(10)	0.0399(3)	1
C2	0.2323(2)	0.15579(14)	0.09788(13)	0.0218(3)	1
O2	0.56811(16)	0.01599(11)	-0.21740(10)	0.0307(3)	1
C3	0.1398(2)	0.09878(14)	0.13185(13)	0.0217(3)	1
O3	0.67426(18)	0.33568(14)	-0.10060(12)	0.0354(3)	1
N4	0.03425(17)	0.13695(12)	0.22581(12)	0.0226(3)	1
O4	0.1742(2)	0.17242(13)	0.43272(12)	0.0411(4)	1
C5	-0.0572(2)	0.08645(15)	0.26063(15)	0.0261(4)	1
C6	-0.0411(2)	-0.00376(15)	0.20093(16)	0.0285(4)	1
C7	0.0628(2)	-0.04434(15)	0.10669(15)	0.0284(4)	1
C8	0.1590(2)	0.00918(14)	0.06793(14)	0.0239(4)	1
C9	0.2734(2)	-0.01631(14)	-0.02849(14)	0.0236(4)	1
C10	0.3191(2)	-0.10314(15)	-0.11091(14)	0.0255(4)	1
N11	0.43754(19)	-0.09498(13)	-0.18836(13)	0.0277(3)	1
C12	0.4722(2)	-0.01067(15)	-0.16406(14)	0.0250(4)	1
C13	0.3643(2)	0.04054(14)	-0.05924(14)	0.0221(3)	1
C14	0.3480(2)	0.12883(14)	0.00333(13)	0.0223(3)	1
C15	0.4106(2)	0.20816(14)	0.00366(13)	0.0222(3)	1
C16	0.5291(2)	0.22623(15)	-0.06456(14)	0.0253(4)	1
C17	0.5599(2)	0.31183(16)	-0.03877(14)	0.0273(4)	1
C18	0.4743(2)	0.37982(16)	0.05411(14)	0.0269(4)	1
C19	0.3583(2)	0.36262(15)	0.12310(14)	0.0249(4)	1
C20	0.3248(2)	0.27636(14)	0.09890(14)	0.0223(3)	1
C21	0.1255(2)	0.21323(15)	0.37382(15)	0.0290(4)	1
N21	-0.07938(17)	0.37301(12)	0.19026(11)	0.0218(3)	1
C22	-0.0936(2)	0.47950(14)	0.19380(14)	0.0232(3)	1
C23	-0.0364(2)	0.51312(14)	0.26057(14)	0.0232(3)	1
N24	0.02789(17)	0.43583(12)	0.31450(11)	0.0228(3)	1
C25	0.0838(2)	0.46629(16)	0.37513(14)	0.0275(4)	1
C26	0.0780(2)	0.57306(17)	0.38579(15)	0.0321(4)	1
C27	0.0117(2)	0.65088(17)	0.33294(16)	0.0330(4)	1
C28	-0.0468(2)	0.62169(15)	0.26704(16)	0.0293(4)	1
C29	-0.1155(3)	0.69626(16)	0.20695(18)	0.0360(5)	1
C30	-0.1685(3)	0.66454(17)	0.14400(18)	0.0362(5)	1
C31	-0.1589(2)	0.55405(16)	0.13514(15)	0.0281(4)	1
C32	-0.2097(2)	0.51493(17)	0.06948(16)	0.0318(4)	1
C33	-0.1945(2)	0.40772(17)	0.06594(15)	0.0296(4)	1
C34	-0.1294(2)	0.33907(15)	0.12793(14)	0.0252(4)	1
O100	0.5753(3)	-0.25325(18)	-0.36931(15)	0.0760(8)	1
C100	0.5575(2)	-0.33285(18)	-0.39152(17)	0.0371(5)	1
C101	0.4835(3)	-0.3892(2)	-0.31250(18)	0.0426(5)	1
C102	0.6133(3)	-0.3798(2)	-0.50087(18)	0.0478(6)	1
O200	0.81068(18)	0.19712(14)	-0.27848(12)	0.0425(4)	1
C200	0.7503(3)	0.18318(18)	-0.33333(16)	0.0377(5)	1
C201	0.6022(3)	0.2583(2)	-0.3237(2)	0.0517(6)	1
C202	0.8230(4)	0.0873(2)	-0.4128(2)	0.0642(9)	1
O300	0.3741(5)	-0.0971(4)	-0.4630(3)	0.0603(10)	0.50
C300	0.4541(5)	-0.0484(4)	-0.4866(4)	0.0421(10)	0.50
C301	0.4259(19)	0.0530(11)	-0.4247(14)	0.068(4)	0.50
C302	0.5896(14)	-0.0877(11)	-0.5788(12)	0.053(2)	0.50

Table 6.3. Bond lengths [Å] and angles [°] for **FL151-1**.

N1-C2	1.342(2)	C23-C28	1.403(2)
N1-C20	1.384(2)	N24-C25	1.333(2)
N1-Ru1	2.0645(15)	C25-C26	1.402(3)
O1-C10	1.215(2)	C25-H25	0.9500
Cl1-Ru1	2.4112(5)	C26-C27	1.369(3)
Ru1-C21	1.858(2)	C26-H26	0.9500
Ru1-N24	2.0596(15)	C27-C28	1.406(3)
Ru1-N4	2.1141(15)	C27-H27	0.9500
Ru1-N21	2.1299(15)	C28-C29	1.431(3)
F1-C6	1.351(2)	C29-C30	1.344(3)
C2-C3	1.407(2)	C29-H29	0.9500
C2-C14	1.409(2)	C30-C31	1.434(3)
O2-C12	1.208(2)	C30-H30	0.9500
C3-N4	1.362(2)	C31-C32	1.406(3)
C3-C8	1.416(2)	C32-C33	1.368(3)
O3-C17	1.373(2)	C32-H32	0.9500
O3-H3	0.77(3)	C33-C34	1.397(3)
N4-C5	1.333(2)	C33-H33	0.9500
O4-C21	1.137(3)	C34-H34	0.9500
C5-C6	1.400(3)	O100-C100	1.204(3)
C5-H5	0.9500	C100-C101	1.480(3)
C6-C7	1.362(3)	C100-C102	1.494(3)
C7-C8	1.410(3)	C101-H10A	0.9800
C7-H7	0.9500	C101-H10B	0.9800
C8-C9	1.420(3)	C101-H10C	0.9800
C9-C13	1.389(2)	C102-H10D	0.9800
C9-C10	1.471(2)	C102-H10E	0.9800
C10-N11	1.393(3)	C102-H10F	0.9800
N11-C12	1.383(2)	O200-C200	1.212(3)
N11-H11	0.78(3)	C200-C201	1.485(4)
C12-C13	1.503(2)	C200-C202	1.487(3)
C13-C14	1.402(2)	C201-H20A	0.9800
C14-C15	1.439(2)	C201-H20B	0.9800
C15-C16	1.398(2)	C201-H20C	0.9800
C15-C20	1.431(2)	C202-H20D	0.9800
C16-C17	1.380(3)	C202-H20E	0.9800
C16-H16	0.9500	C202-H20F	0.9800
C17-C18	1.406(3)	O300-C300	1.207(6)
C18-C19	1.377(3)	C300-C301	1.493(12)
C18-H18	0.9500	C300-C302	1.494(13)
C19-C20	1.398(2)	C301-H30A	0.9800
C19-H19	0.9500	C301-H30B	0.9800
N21-C34	1.327(2)	C301-H30C	0.9800
N21-C22	1.361(2)	C302-H30D	0.9800
C22-C31	1.400(3)	C302-H30E	0.9800
C22-C23	1.433(3)	C302-H30F	0.9800
C23-N24	1.367(2)		

C2-N1-C20	105.42(14)	N1-Ru1-N21	85.63(6)
C2-N1-Ru1	110.56(12)	N4-Ru1-N21	89.92(6)
C20-N1-Ru1	143.71(12)	C21-Ru1-Cl1	88.82(6)
C21-Ru1-N24	96.95(7)	N24-Ru1-Cl1	91.59(4)
C21-Ru1-N1	96.40(8)	N1-Ru1-Cl1	172.28(4)
N24-Ru1-N1	93.42(6)	N4-Ru1-Cl1	93.44(4)
C21-Ru1-N4	93.93(7)	N21-Ru1-Cl1	89.52(4)
N24-Ru1-N4	168.10(6)	N1-C2-C3	121.39(16)
N1-Ru1-N4	80.55(6)	N1-C2-C14	114.14(15)
C21-Ru1-N21	175.90(7)	C3-C2-C14	124.47(16)
N24-Ru1-N21	79.34(6)	N4-C3-C2	115.90(15)

N4-C3-C8	124.48(16)	N24-C23-C28	123.13(17)
C2-C3-C8	119.61(16)	N24-C23-C22	117.43(15)
C17-O3-H3	110(2)	C28-C23-C22	119.44(17)
C5-N4-C3	118.05(15)	C25-N24-C23	117.58(16)
C5-N4-Ru1	130.52(13)	C25-N24-Ru1	128.27(13)
C3-N4-Ru1	111.05(11)	C23-N24-Ru1	114.09(12)
N4-C5-C6	119.58(17)	N24-C25-C26	122.80(19)
N4-C5-H5	120.2	N24-C25-H25	118.6
C6-C5-H5	120.2	C26-C25-H25	118.6
F1-C6-C7	119.69(17)	C27-C26-C25	119.64(19)
F1-C6-C5	116.13(17)	C27-C26-H26	120.2
C7-C6-C5	124.17(17)	C25-C26-H26	120.2
C6-C7-C8	117.02(17)	C26-C27-C28	119.33(18)
C6-C7-H7	121.5	C26-C27-H27	120.3
C8-C7-H7	121.5	C28-C27-H27	120.3
C7-C8-C3	116.68(17)	C23-C28-C27	117.51(19)
C7-C8-C9	127.38(17)	C23-C28-C29	118.84(19)
C3-C8-C9	115.94(16)	C27-C28-C29	123.64(18)
C13-C9-C8	123.11(16)	C30-C29-C28	121.68(19)
C13-C9-C10	108.21(16)	C30-C29-H29	119.2
C8-C9-C10	128.67(17)	C28-C29-H29	119.2
O1-C10-N11	124.74(18)	C29-C30-C31	120.9(2)
O1-C10-C9	128.97(18)	C29-C30-H30	119.6
N11-C10-C9	106.28(16)	C31-C30-H30	119.6
C12-N11-C10	112.41(16)	C22-C31-C32	117.43(17)
C12-N11-H11	124(2)	C22-C31-C30	118.73(19)
C10-N11-H11	124(2)	C32-C31-C30	123.84(19)
O2-C12-N11	126.58(17)	C33-C32-C31	119.39(19)
O2-C12-C13	128.05(17)	C33-C32-H32	120.3
N11-C12-C13	105.36(16)	C31-C32-H32	120.3
C9-C13-C14	121.84(16)	C32-C33-C34	119.50(18)
C9-C13-C12	107.73(15)	C32-C33-H33	120.2
C14-C13-C12	130.43(16)	C34-C33-H33	120.2
C13-C14-C2	115.01(16)	N21-C34-C33	122.72(17)
C13-C14-C15	140.80(17)	N21-C34-H34	118.6
C2-C14-C15	104.18(15)	C33-C34-H34	118.6
C16-C15-C20	120.36(16)	O100-C100-C101	121.8(2)
C16-C15-C14	134.05(17)	O100-C100-C102	120.6(2)
C20-C15-C14	105.58(15)	C101-C100-C102	117.5(2)
C17-C16-C15	118.62(17)	C100-C101-H10A	109.5
C17-C16-H16	120.7	C100-C101-H10B	109.5
C15-C16-H16	120.7	H10A-C101-H10B	109.5
O3-C17-C16	122.83(17)	C100-C101-H10C	109.5
O3-C17-C18	116.15(17)	H10A-C101-H10C	109.5
C16-C17-C18	121.01(17)	H10B-C101-H10C	109.5
C19-C18-C17	121.37(17)	C100-C102-H10D	109.5
C19-C18-H18	119.3	C100-C102-H10E	109.5
C17-C18-H18	119.3	H10D-C102-H10E	109.5
C18-C19-C20	118.78(17)	C100-C102-H10F	109.5
C18-C19-H19	120.6	H10D-C102-H10F	109.5
C20-C19-H19	120.6	H10E-C102-H10F	109.5
N1-C20-C19	129.47(17)	O200-C200-C201	122.4(2)
N1-C20-C15	110.68(15)	O200-C200-C202	120.3(3)
C19-C20-C15	119.85(17)	C201-C200-C202	117.4(3)
O4-C21-Ru1	175.73(19)	C200-C201-H20A	109.5
C34-N21-C22	118.09(16)	C200-C201-H20B	109.5
C34-N21-Ru1	129.47(13)	H20A-C201-H20B	109.5
C22-N21-Ru1	112.38(12)	C200-C201-H20C	109.5
N21-C22-C31	122.85(17)	H20A-C201-H20C	109.5
N21-C22-C23	116.72(16)	H20B-C201-H20C	109.5
C31-C22-C23	120.42(16)	C200-C202-H20D	109.5

C200-C202-H20E	109.5	H20E-C202-H20F	109.5
H20D-C202-H20E	109.5	O300-C300-C301	122.4(8)
C200-C202-H20F	109.5	O300-C300-C302	121.7(6)
H20D-C202-H20F	109.5	C301-C300-C302	115.9(10)

Symmetry transformations used to generate equivalent atoms:

Table 6.4. Anisotropic displacement parameters ($Å^2$) for **FL151-1**.
The anisotropicdisplacement factor exponent takes the form: $-2\pi^2[h^2a^{*2}U^{11} + ... + 2 h k a^* b^* U^{12}]$

	U^{11}	U^{22}	U^{33}	U^{23}	U^{13}	U^{12}
N1	0.0244(7)	0.0202(7)	0.0237(7)	0.0020(6)	-0.0094(6)	-0.0105(6)
O1	0.0386(8)	0.0255(7)	0.0360(7)	-0.0021(6)	-0.0126(6)	-0.0162(6)
Cl1	0.0303(2)	0.0275(2)	0.0249(2)	-0.00025(16)	-0.00613(17)	-0.01371(18)
Ru1	0.02495(8)	0.01817(7)	0.02108(7)	0.00172(5)	-0.00902(5)	-0.01000(5)
F1	0.0426(7)	0.0320(6)	0.0450(7)	-0.0029(5)	-0.0008(6)	-0.0270(6)
C2	0.0251(9)	0.0184(8)	0.0238(8)	0.0028(6)	-0.0100(7)	-0.0091(7)
O2	0.0314(7)	0.0316(7)	0.0284(7)	0.0004(5)	-0.0071(6)	-0.0145(6)
C3	0.0245(9)	0.0181(8)	0.0226(8)	0.0013(6)	-0.0081(7)	-0.0085(7)
O3	0.0358(8)	0.0425(9)	0.0323(8)	-0.0020(7)	-0.0046(7)	-0.0262(7)
N4	0.0271(8)	0.0175(7)	0.0259(7)	0.0026(6)	-0.0103(6)	-0.0107(6)
O4	0.0549(10)	0.0363(8)	0.0412(8)	0.0113(7)	-0.0296(8)	-0.0166(7)
C5	0.0291(9)	0.0213(8)	0.0286(9)	0.0035(7)	-0.0077(8)	-0.0127(7)
C6	0.0315(10)	0.0213(8)	0.0358(10)	0.0033(7)	-0.0090(8)	-0.0162(8)
C7	0.0323(10)	0.0206(8)	0.0337(10)	0.0015(7)	-0.0101(8)	-0.0129(8)
C8	0.0276(9)	0.0177(8)	0.0287(9)	0.0033(7)	-0.0109(7)	-0.0105(7)
C9	0.0273(9)	0.0170(8)	0.0273(9)	0.0008(6)	-0.0106(7)	-0.0083(7)
C10	0.0289(9)	0.0202(8)	0.0282(9)	0.0009(7)	-0.0122(8)	-0.0081(7)
N11	0.0322(9)	0.0240(8)	0.0262(8)	-0.0032(6)	-0.0087(7)	-0.0110(7)
C12	0.0278(9)	0.0214(8)	0.0261(9)	0.0014(7)	-0.0124(7)	-0.0069(7)
C13	0.0235(8)	0.0187(8)	0.0241(8)	0.0016(6)	-0.0097(7)	-0.0070(7)
C14	0.0247(9)	0.0192(8)	0.0247(8)	0.0026(6)	-0.0110(7)	-0.0084(7)
C15	0.0244(9)	0.0213(8)	0.0243(8)	0.0038(6)	-0.0117(7)	-0.0098(7)
C16	0.0265(9)	0.0263(9)	0.0257(9)	0.0019(7)	-0.0105(7)	-0.0119(7)
C17	0.0276(9)	0.0324(10)	0.0272(9)	0.0046(7)	-0.0104(8)	-0.0166(8)
C18	0.0316(10)	0.0278(9)	0.0295(9)	0.0031(7)	-0.0139(8)	-0.0175(8)
C19	0.0292(9)	0.0235(8)	0.0264(8)	0.0020(7)	-0.0130(7)	-0.0121(7)
C20	0.0255(9)	0.0206(8)	0.0251(8)	0.0037(6)	-0.0129(7)	-0.0099(7)
C21	0.0353(10)	0.0234(9)	0.0297(9)	0.0007(7)	-0.0097(8)	-0.0142(8)
N21	0.0233(7)	0.0200(7)	0.0230(7)	0.0012(5)	-0.0080(6)	-0.0094(6)
C22	0.0241(9)	0.0200(8)	0.0256(8)	0.0020(6)	-0.0073(7)	-0.0097(7)
C23	0.0244(9)	0.0193(8)	0.0253(8)	-0.0003(6)	-0.0063(7)	-0.0099(7)
N24	0.0258(8)	0.0219(7)	0.0234(7)	-0.0005(6)	-0.0088(6)	-0.0115(6)
C25	0.0303(10)	0.0297(9)	0.0252(9)	-0.0015(7)	-0.0090(8)	-0.0148(8)
C26	0.0342(11)	0.0360(11)	0.0311(10)	-0.0056(8)	-0.0094(8)	-0.0203(9)
C27	0.0373(11)	0.0267(9)	0.0360(10)	-0.0048(8)	-0.0080(9)	-0.0173(9)
C28	0.0309(10)	0.0226(9)	0.0346(10)	-0.0007(7)	-0.0081(8)	-0.0133(8)
C29	0.0430(12)	0.0203(9)	0.0468(12)	0.0058(8)	-0.0162(10)	-0.0143(9)
C30	0.0403(12)	0.0240(9)	0.0469(12)	0.0105(9)	-0.0203(10)	-0.0112(9)
C31	0.0292(10)	0.0242(9)	0.0327(10)	0.0052(7)	-0.0125(8)	-0.0109(8)
C32	0.0322(10)	0.0335(10)	0.0325(10)	0.0086(8)	-0.0160(8)	-0.0121(9)
C33	0.0285(10)	0.0350(10)	0.0304(9)	0.0027(8)	-0.0134(8)	-0.0148(8)
C34	0.0264(9)	0.0253(9)	0.0268(9)	0.0008(7)	-0.0102(7)	-0.0122(7)
O100	0.1058(19)	0.0649(13)	0.0474(11)	-0.0209(9)	0.0158(11)	-0.0590(14)
C100	0.0354(11)	0.0332(11)	0.0369(11)	-0.0058(9)	-0.0091(9)	-0.0096(9)
C101	0.0423(13)	0.0505(13)	0.0423(12)	0.0031(10)	-0.0175(10)	-0.0233(11)
C102	0.0542(15)	0.0399(12)	0.0387(12)	-0.0060(10)	-0.0126(11)	-0.0093(11)
O200	0.0386(9)	0.0468(9)	0.0388(8)	0.0002(7)	-0.0039(7)	-0.0215(8)
C200	0.0480(13)	0.0345(11)	0.0297(10)	0.0072(8)	-0.0061(9)	-0.0220(10)
C201	0.0531(15)	0.0646(17)	0.0369(12)	0.0182(11)	-0.0152(11)	-0.0236(13)
C202	0.100(3)	0.0424(14)	0.0381(13)	-0.0011(11)	-0.0171(15)	-0.0207(16)
O300	0.059(2)	0.067(3)	0.060(2)	-0.0007(19)	-0.0099(19)	-0.039(2)
C300	0.045(3)	0.051(3)	0.040(2)	0.008(2)	-0.017(2)	-0.028(2)
C301	0.086(8)	0.075(9)	0.046(4)	-0.001(5)	-0.006(5)	-0.052(7)
C302	0.043(4)	0.074(8)	0.044(4)	0.009(5)	-0.013(3)	-0.028(5)

Table 6.5. Hydrogen coordinates and isotropic displacement parameters ($Å^2$)for **FL151-1**.

	x	y	z	U(eq)	Occupancy
H5	-0.1327	0.1115	0.3255	0.031	1
H7	0.0701	-0.1060	0.0688	0.034	1
H16	0.5872	0.1805	-0.1274	0.030	1
H18	0.4971	0.4388	0.0696	0.032	1
H19	0.3021	0.4085	0.1860	0.030	1
H25	0.1295	0.4134	0.4127	0.033	1
H26	0.1197	0.5913	0.4294	0.038	1
H27	0.0054	0.7239	0.3407	0.040	1
H29	-0.1238	0.7701	0.2117	0.043	1
H30	-0.2129	0.7160	0.1048	0.043	1
H32	-0.2543	0.5625	0.0280	0.038	1
H33	-0.2279	0.3801	0.0217	0.036	1
H34	-0.1205	0.2650	0.1254	0.030	1
H10A	0.4436	-0.3465	-0.2454	0.064	1
H10B	0.5526	-0.4620	-0.3104	0.064	1
H10C	0.4052	-0.3966	-0.3294	0.064	1
H10D	0.6593	-0.3351	-0.5452	0.072	1
H10E	0.5331	-0.3805	-0.5197	0.072	1
H10F	0.6841	-0.4548	-0.5095	0.072	1
H20A	0.5688	0.3203	-0.2722	0.078	1
H20B	0.5371	0.2189	-0.3024	0.078	1
H20C	0.6028	0.2852	-0.3900	0.078	1
H20D	0.9213	0.0467	-0.4140	0.096	1
H20E	0.8267	0.1125	-0.4801	0.096	1
H20F	0.7689	0.0394	-0.3965	0.096	1
H30A	0.4333	0.1103	-0.4698	0.101	0.50
H30B	0.4971	0.0373	-0.3911	0.101	0.50
H30C	0.3288	0.0778	-0.3725	0.101	0.50
H30D	0.6731	-0.1088	-0.5571	0.079	0.50
H30E	0.5900	-0.0290	-0.6233	0.079	0.50
H30F	0.5944	-0.1511	-0.6165	0.079	0.50
H3	0.717(3)	0.294(2)	-0.149(2)	0.046(8)	1
H11	0.480(3)	-0.134(2)	-0.240(2)	0.043(7)	1

Table 6.6. Torsion angles [°] for **FL151-1**.

C2-N1-Ru1-C21	99.04(13)	C10-C9-C13-C12	-0.2(2)
C20-N1-Ru1-C21	-88.8(2)	O2-C12-C13-C9	179.05(19)
C2-N1-Ru1-N24	-163.57(12)	N11-C12-C13-C9	0.0(2)
C20-N1-Ru1-N24	8.6(2)	O2-C12-C13-C14	-1.1(3)
C2-N1-Ru1-N4	6.10(12)	N11-C12-C13-C14	179.78(19)
C20-N1-Ru1-N4	178.2(2)	C9-C13-C14-C2	-0.9(3)
C2-N1-Ru1-N21	-84.54(12)	C12-C13-C14-C2	179.30(18)
C20-N1-Ru1-N21	87.6(2)	C9-C13-C14-C15	-178.9(2)
C2-N1-Ru1-Cl1	-33.2(4)	C12-C13-C14-C15	1.3(4)
C20-N1-Ru1-Cl1	138.9(3)	N1-C2-C14-C13	-178.13(16)
C20-N1-C2-C3	179.46(16)	C3-C2-C14-C13	2.0(3)
Ru1-N1-C2-C3	-5.4(2)	N1-C2-C14-C15	0.6(2)
C20-N1-C2-C14	-0.4(2)	C3-C2-C14-C15	-179.30(17)
Ru1-N1-C2-C14	174.76(12)	C13-C14-C15-C16	-3.8(4)
N1-C2-C3-N4	-0.1(3)	C2-C14-C15-C16	178.1(2)
C14-C2-C3-N4	179.76(17)	C13-C14-C15-C20	177.7(2)
N1-C2-C3-C8	178.67(17)	C2-C14-C15-C20	-0.48(19)
C14-C2-C3-C8	-1.5(3)	C20-C15-C16-C17	-1.0(3)
C2-C3-N4-C5	179.10(17)	C14-C15-C16-C17	-179.4(2)
C8-C3-N4-C5	0.4(3)	C15-C16-C17-O3	179.73(18)
C2-C3-N4-Ru1	5.4(2)	C15-C16-C17-C18	0.0(3)
C8-C3-N4-Ru1	-173.30(15)	O3-C17-C18-C19	-178.83(18)
C21-Ru1-N4-C5	85.18(18)	C16-C17-C18-C19	0.9(3)
N24-Ru1-N4-C5	-118.7(3)	C17-C18-C19-C20	-0.8(3)
N1-Ru1-N4-C5	-178.97(18)	C2-N1-C20-C19	-179.44(19)
N21-Ru1-N4-C5	-93.39(17)	Ru1-N1-C20-C19	8.2(3)
Cl1-Ru1-N4-C5	-3.87(17)	C2-N1-C20-C15	0.1(2)
C21-Ru1-N4-C3	-102.14(14)	Ru1-N1-C20-C15	-172.28(15)
N24-Ru1-N4-C3	54.0(4)	C18-C19-C20-N1	179.34(18)
N1-Ru1-N4-C3	-6.30(12)	C18-C19-C20-C15	-0.1(3)
N21-Ru1-N4-C3	79.28(13)	C16-C15-C20-N1	-178.53(16)
Cl1-Ru1-N4-C3	168.80(12)	C14-C15-C20-N1	0.3(2)
C3-N4-C5-C6	0.7(3)	C16-C15-C20-C19	1.0(3)
Ru1-N4-C5-C6	172.96(14)	C14-C15-C20-C19	179.84(17)
N4-C5-C6-F1	-179.89(17)	N24-Ru1-C21-O4	90(2)
N4-C5-C6-C7	-0.8(3)	N1-Ru1-C21-O4	-176(2)
F1-C6-C7-C8	178.82(18)	N4-Ru1-C21-O4	-95(2)
C5-C6-C7-C8	-0.2(3)	N21-Ru1-C21-O4	65(3)
C6-C7-C8-C3	1.2(3)	Cl1-Ru1-C21-O4	-2(2)
C6-C7-C8-C9	-178.62(19)	C21-Ru1-N21-C34	-155.8(10)
N4-C3-C8-C7	-1.4(3)	N24-Ru1-N21-C34	178.74(17)
C2-C3-C8-C7	179.94(17)	N1-Ru1-N21-C34	84.43(16)
N4-C3-C8-C9	178.48(17)	N4-Ru1-N21-C34	3.90(16)
C2-C3-C8-C9	-0.2(3)	Cl1-Ru1-N21-C34	-89.55(16)
C7-C8-C9-C13	-178.93(19)	C21-Ru1-N21-C22	27.2(11)
C3-C8-C9-C13	1.2(3)	N24-Ru1-N21-C22	1.69(12)
C7-C8-C9-C10	0.3(3)	N1-Ru1-N21-C22	-92.62(12)
C3-C8-C9-C10	-179.56(18)	N4-Ru1-N21-C22	-173.15(12)
C13-C9-C10-O1	-178.5(2)	Cl1-Ru1-N21-C22	93.40(12)
C8-C9-C10-O1	2.1(3)	C34-N21-C22-C31	0.3(3)
C13-C9-C10-N11	0.3(2)	Ru1-N21-C22-C31	177.73(15)
C8-C9-C10-N11	-178.98(18)	C34-N21-C22-C23	-179.01(16)
O1-C10-N11-C12	178.56(19)	Ru1-N21-C22-C23	-1.6(2)
C9-C10-N11-C12	-0.4(2)	N21-C22-C23-N24	0.3(2)
C10-N11-C12-O2	-178.84(19)	C31-C22-C23-N24	-179.03(17)
C10-N11-C12-C13	0.3(2)	N21-C22-C23-C28	179.54(16)
C8-C9-C13-C14	-0.7(3)	C31-C22-C23-C28	0.2(3)
C10-C9-C13-C14	179.98(17)	C28-C23-N24-C25	-0.5(3)
C8-C9-C13-C12	179.17(17)	C22-C23-N24-C25	178.68(16)

C28-C23-N24-Ru1	-178.00(14)	N24-C23-C28-C29	179.63(18)
C22-C23-N24-Ru1	1.2(2)	C22-C23-C28-C29	0.4(3)
C21-Ru1-N24-C25	3.08(17)	C26-C27-C28-C23	1.3(3)
N1-Ru1-N24-C25	-93.80(16)	C26-C27-C28-C29	-178.7(2)
N4-Ru1-N24-C25	-152.9(3)	C23-C28-C29-C30	-0.7(3)
N21-Ru1-N24-C25	-178.70(17)	C27-C28-C29-C30	179.2(2)
Cl1-Ru1-N24-C25	92.09(16)	C28-C29-C30-C31	0.4(4)
C21-Ru1-N24-C23	-179.77(13)	N21-C22-C31-C32	-0.7(3)
N1-Ru1-N24-C23	83.35(13)	C23-C22-C31-C32	178.58(17)
N4-Ru1-N24-C23	24.3(4)	N21-C22-C31-C30	-179.85(18)
N21-Ru1-N24-C23	-1.55(12)	C23-C22-C31-C30	-0.6(3)
Cl1-Ru1-N24-C23	-90.76(12)	C29-C30-C31-C22	0.3(3)
C23-N24-C25-C26	0.5(3)	C29-C30-C31-C32	-178.8(2)
Ru1-N24-C25-C26	177.53(14)	C22-C31-C32-C33	0.4(3)
N24-C25-C26-C27	0.5(3)	C30-C31-C32-C33	179.5(2)
C25-C26-C27-C28	-1.3(3)	C31-C32-C33-C34	0.3(3)
N24-C23-C28-C27	-0.3(3)	C22-N21-C34-C33	0.5(3)
C22-C23-C28-C27	-179.52(18)	Ru1-N21-C34-C33	-176.45(14)
C32-C33-C34-N21	-0.8(3)		

Symmetry transformations used to generate equivalent atoms:

Table 6.7. Hydrogen bonds for **FL151-1** [Å and °].

D-H...A	d(D-H)	d(H...A)	d(D...A)	<(DHA)
O3-H3...O200	0.77(3)	1.97(3)	2.734(2)	173(3)
N11-H11...O100	0.78(3)	2.13(3)	2.904(2)	172(3)

Symmetry transformations used to generate equivalent atoms:

Crystal structure of FL327.

Table 6.8. Crystal data and structure refinement for **FL327**.

Identification code	fl327	
Habitus, colour	plate, dark red	
Crystal size	0.14 x 0.09 x 0.03 mm^3	
Crystal system	Monoclinic	
Space group	P $2_1/n$	Z = 4
Unit cell dimensions	a = 9.7730(5) Å	α= 90°.
	b = 11.8601(6) Å	β= 98.014(4)°.
	c = 29.6398(16) Å	γ = 90°.
Volume	3402.0(3) $Å^3$	
Cell determination	9578 peaks with Theta 1.4 to 25°.	
Empirical formula	C_{37} H_{31} Cl F N_5 O_6 Ru	
Formula weight	797.19	
Density (calculated)	1.556 Mg/m^3	
Absorption coefficient	0.601 mm^{-1}	
F(000)	1624	

Data collection:

Diffractometer type	IPDS2
Wavelength	0.71073 Å
Temperature	100(2) K
Theta range for data collection	1.39 to 25.00°.
Index ranges	-11<=h<=11, -14<=k<=13, -35<=l<=34
Data collection software	STOE WinXpose (X-Area)
Cell refinement software	STOE WinCell (X-Area)
Data reduction software	STOE WinIntegrate (X-Area)

Solution and refinement:

Reflections collected	19119
Independent reflections	5988 [R(int) = 0.0771]
Completeness to theta = 25.00°	100.0 %
Observed reflections	3554[I>2sigma(I)]
Reflections used for refinement	5988
Absorption correction	Semi-empirical from equivalents
Max. and min. transmission	1.1054 and 0.8848
Largest diff. peak and hole	0.480 and -0.610 $e.Å^{-3}$
Solution	Direct methods
Refinement	Full-matrix least-squares on F^2
Treatment of hydrogen atoms	geom, constr
Programs used	SIR92 (Giacovazzo et al, 1993)
	SHELXL-97 (Sheldrick, 1997)
	Diamond 3.1, STOE IPDS2 software
Data / restraints / parameters	5988 / 0 / 473
Goodness-of-fit on F^2	0.797
R index (all data)	wR2 = 0.0776
R index conventional [I>2sigma(I)]	R1 = 0.0396

Table 6.9. Atomic coordinates and equivalent isotropic displacement parameters (Å^2) for **FL327**. U(eq) is defined as one third of the trace of the orthogonalized U^{ij} tensor.

	x	y	z	U(eq)	Occupancy
C1	1.1167(4)	0.1500(4)	0.62114(12)	0.0329(9)	1
C2	1.0168(4)	0.0666(3)	0.60773(13)	0.0328(9)	1
C3	0.8313(4)	-0.0355(3)	0.60474(14)	0.0348(10)	1
C4	0.7042(4)	-0.0811(4)	0.61063(15)	0.0422(11)	1
C5	0.6572(4)	-0.1741(4)	0.58538(14)	0.0450(11)	1
C6	0.7332(4)	-0.2224(4)	0.55398(15)	0.0428(11)	1
C7	0.8585(4)	-0.1773(4)	0.54653(13)	0.0389(10)	1
C8	0.9080(4)	-0.0830(4)	0.57184(13)	0.0350(10)	1
C9	1.0313(4)	-0.0151(3)	0.57378(13)	0.0335(10)	1
C10	1.1535(4)	-0.0085(3)	0.55410(13)	0.0328(9)	1
C11	1.2083(4)	-0.0818(4)	0.51959(13)	0.0356(10)	1
C12	1.3683(4)	0.0573(4)	0.54115(13)	0.0372(10)	1
C13	1.2528(4)	0.0750(4)	0.56642(12)	0.0336(10)	1
C14	1.2375(4)	0.1584(4)	0.60010(12)	0.0334(9)	1
C15	1.3305(4)	0.2464(4)	0.61533(13)	0.0363(10)	1
C16	1.2943(4)	0.3169(4)	0.64794(13)	0.0357(10)	1
C17	1.1756(4)	0.3036(3)	0.66843(13)	0.0368(10)	1
C18	0.8517(4)	0.3863(4)	0.71603(15)	0.0462(11)	1
C19	0.7792(4)	0.3886(4)	0.66985(15)	0.0434(11)	1
C20	0.7079(5)	0.4825(4)	0.65078(17)	0.0526(13)	1
C21	0.6493(5)	0.4773(4)	0.60564(18)	0.0555(13)	1
C22	0.6596(4)	0.3813(4)	0.58026(18)	0.0519(13)	1
C23	0.7321(4)	0.2896(4)	0.60173(15)	0.0436(11)	1
C24	0.6016(5)	0.3732(4)	0.53062(17)	0.0664(16)	1
C25	1.0037(5)	0.2980(4)	0.77380(14)	0.0427(11)	1
C26	1.0833(5)	0.3915(4)	0.78754(15)	0.0449(11)	1
C27	1.1655(5)	0.3917(4)	0.82991(15)	0.0515(13)	1
C28	1.1678(6)	0.2978(4)	0.85746(17)	0.0589(14)	1
C29	1.0890(5)	0.2043(4)	0.84330(15)	0.0585(14)	1
C30	1.0069(5)	0.2048(4)	0.80158(15)	0.0515(12)	1
C100	1.0105(4)	0.0582(4)	0.71679(14)	0.0396(11)	1
C200	1.0455(4)	0.6514(4)	0.69833(14)	0.0448(11)	1
C201	0.9470(5)	0.7353(4)	0.67357(18)	0.0625(15)	1
C202	1.1251(4)	0.6921(4)	0.74181(15)	0.0488(12)	1
N1	1.0873(3)	0.2198(3)	0.65577(10)	0.0327(8)	1
N2	0.9002(3)	0.0566(3)	0.62655(11)	0.0356(8)	1
N3	0.7924(3)	0.2928(3)	0.64566(12)	0.0395(9)	1
N4	0.9219(4)	0.2957(3)	0.72925(11)	0.0416(9)	1
N5	1.3347(4)	-0.0372(3)	0.51418(12)	0.0384(9)	1
O1	1.1549(3)	-0.1652(3)	0.50046(9)	0.0439(7)	1
O2	1.4755(3)	0.1113(2)	0.54306(9)	0.0372(7)	1
O3	0.6772(3)	-0.3169(3)	0.53172(11)	0.0540(9)	1
O100	1.0741(3)	-0.0140(3)	0.73698(10)	0.0523(8)	1
O200	1.0566(3)	0.5558(3)	0.68485(11)	0.0559(9)	1
F1	1.3779(2)	0.4047(2)	0.66251(8)	0.0492(7)	1
Cl1	0.69881(11)	0.10741(10)	0.70823(4)	0.0473(3)	1
Ru1	0.91023(4)	0.16574(3)	0.68281(1)	0.03517(10)	1
C300	0.8842(5)	-0.4731(4)	0.44780(16)	0.0521(13)	1
C302	1.0090(6)	-0.4223(7)	0.4366(2)	0.117(3)	1
C301	0.8489(8)	-0.5867(5)	0.4303(2)	0.105(2)	1
O300	0.8129(5)	-0.4261(4)	0.47119(13)	0.0929(14)	1

Table 6.10. Bond lengths [Å] and angles [°] for **FL327**.

C1-N1	1.380(5)	C23-N3	1.353(5)
C1-C2	1.408(5)	C23-H23	0.9500
C1-C14	1.413(5)	C24-H24A	0.9800
C2-N2	1.342(5)	C24-H24B	0.9800
C2-C9	1.418(5)	C24-H24C	0.9800
C3-C4	1.388(6)	C25-C30	1.376(6)
C3-N2	1.394(5)	C25-C26	1.383(6)
C3-C8	1.426(6)	C25-N4	1.445(5)
C4-C5	1.376(6)	C26-C27	1.394(6)
C4-H4	0.9500	C26-H26	0.9500
C5-C6	1.393(6)	C27-C28	1.380(6)
C5-H5A	0.9500	C27-H27	0.9500
C6-O3	1.375(5)	C28-C29	1.382(7)
C6-C7	1.382(6)	C28-H28	0.9500
C7-C8	1.395(6)	C29-C30	1.377(6)
C7-H7	0.9500	C29-H29	0.9500
C8-C9	1.443(5)	C30-H30	0.9500
C9-C10	1.403(6)	C100-O100	1.173(5)
C10-C13	1.399(5)	C100-Ru1	1.823(5)
C10-C11	1.497(6)	C200-O200	1.211(5)
C11-O1	1.221(5)	C200-C202	1.490(6)
C11-N5	1.374(5)	C200-C201	1.503(6)
C12-O2	1.222(5)	C201-H20A	0.9800
C12-N5	1.389(5)	C201-H20B	0.9800
C12-C13	1.454(6)	C201-H20C	0.9800
C13-C14	1.428(5)	C202-H20D	0.9800
C14-C15	1.416(6)	C202-H20E	0.9800
C15-C16	1.361(5)	C202-H20F	0.9800
C15-H15	0.9500	N1-Ru1	2.106(3)
C16-F1	1.357(4)	N2-Ru1	2.103(3)
C16-C17	1.392(5)	N3-Ru1	2.111(3)
C17-N1	1.334(5)	N4-Ru1	2.059(4)
C17-H17	0.9500	N5-H5	0.82(4)
C18-N4	1.305(5)	O3-H3	0.97(5)
C18-C19	1.451(6)	Cl1-Ru1	2.3979(11)
C18-H18	0.9500	C300-O300	1.189(6)
C19-N3	1.360(5)	C300-C302	1.439(7)
C19-C20	1.391(6)	C300-C301	1.467(7)
C20-C21	1.382(7)	C302-H30A	0.9800
C20-H20	0.9500	C302-H30B	0.9800
C21-C22	1.377(7)	C302-H30C	0.9800
C21-H21	0.9500	C301-H30D	0.9800
C22-C23	1.401(6)	C301-H30E	0.9800
C22-C24	1.504(7)	C301-H30F	0.9800

N1-C1-C2	115.1(3)	C6-C5-H5A	119.2
N1-C1-C14	124.0(4)	O3-C6-C7	122.8(4)
C2-C1-C14	120.9(4)	O3-C6-C5	116.2(4)
N2-C2-C1	122.7(4)	C7-C6-C5	121.0(4)
N2-C2-C9	114.1(4)	C6-C7-C8	118.2(4)
C1-C2-C9	123.1(4)	C6-C7-H7	120.9
C4-C3-N2	129.1(4)	C8-C7-H7	120.9
C4-C3-C8	119.8(4)	C7-C8-C3	120.5(4)
N2-C3-C8	111.1(4)	C7-C8-C9	133.9(4)
C5-C4-C3	118.8(4)	C3-C8-C9	105.5(4)
C5-C4-H4	120.6	C10-C9-C2	115.6(4)
C3-C4-H4	120.6	C10-C9-C8	140.3(4)
C4-C5-C6	121.6(4)	C2-C9-C8	104.1(4)
C4-C5-H5A	119.2	C13-C10-C9	122.1(4)

C13-C10-C11	106.8(4)	C28-C29-H29	120.0
C9-C10-C11	131.1(4)	C25-C30-C29	120.2(5)
O1-C11-N5	126.2(4)	C25-C30-H30	119.9
O1-C11-C10	128.2(4)	C29-C30-H30	119.9
N5-C11-C10	105.6(4)	O100-C100-Ru1	177.0(4)
O2-C12-N5	125.6(4)	O200-C200-C202	121.9(4)
O2-C12-C13	128.5(4)	O200-C200-C201	122.6(4)
N5-C12-C13	105.9(4)	C202-C200-C201	115.4(4)
C10-C13-C14	122.4(4)	C200-C201-H20A	109.5
C10-C13-C12	108.9(4)	C200-C201-H20B	109.5
C14-C13-C12	128.7(4)	H20A-C201-H20B	109.5
C1-C14-C15	116.7(4)	C200-C201-H20C	109.5
C1-C14-C13	115.8(4)	H20A-C201-H20C	109.5
C15-C14-C13	127.4(3)	H20B-C201-H20C	109.5
C16-C15-C14	117.4(4)	C200-C202-H20D	109.5
C16-C15-H15	121.3	C200-C202-H20E	109.5
C14-C15-H15	121.3	H20D-C202-H20E	109.5
F1-C16-C15	119.5(4)	C200-C202-H20F	109.5
F1-C16-C17	116.7(3)	H20D-C202-H20F	109.5
C15-C16-C17	123.7(4)	H20E-C202-H20F	109.5
N1-C17-C16	120.5(4)	C17-N1-C1	117.5(3)
N1-C17-H17	119.8	C17-N1-Ru1	130.7(3)
C16-C17-H17	119.8	C1-N1-Ru1	111.6(2)
N4-C18-C19	117.8(4)	C2-N2-C3	105.1(3)
N4-C18-H18	121.1	C2-N2-Ru1	109.1(3)
C19-C18-H18	121.1	C3-N2-Ru1	144.7(3)
N3-C19-C20	122.3(4)	C23-N3-C19	118.1(4)
N3-C19-C18	114.3(4)	C23-N3-Ru1	128.0(3)
C20-C19-C18	123.3(5)	C19-N3-Ru1	114.0(3)
C21-C20-C19	118.4(5)	C18-N4-C25	117.3(4)
C21-C20-H20	120.8	C18-N4-Ru1	116.0(3)
C19-C20-H20	120.8	C25-N4-Ru1	126.6(3)
C22-C21-C20	120.9(5)	C11-N5-C12	112.8(4)
C22-C21-H21	119.6	C11-N5-H5	120(3)
C20-C21-H21	119.6	C12-N5-H5	126(3)
C21-C22-C23	117.7(4)	C6-O3-H3	109(3)
C21-C22-C24	122.7(5)	C100-Ru1-N4	100.31(16)
C23-C22-C24	119.5(5)	C100-Ru1-N2	88.24(15)
N3-C23-C22	122.7(5)	N4-Ru1-N2	169.49(13)
N3-C23-H23	118.6	C100-Ru1-N1	90.94(16)
C22-C23-H23	118.6	N4-Ru1-N1	93.14(13)
C22-C24-H24A	109.5	N2-Ru1-N1	80.53(13)
C22-C24-H24B	109.5	C100-Ru1-N3	177.95(16)
H24A-C24-H24B	109.5	N4-Ru1-N3	77.87(14)
C22-C24-H24C	109.5	N2-Ru1-N3	93.67(13)
H24A-C24-H24C	109.5	N1-Ru1-N3	90.10(12)
H24B-C24-H24C	109.5	C100-Ru1-Cl1	92.56(14)
C30-C25-C26	120.2(4)	N4-Ru1-Cl1	88.61(10)
C30-C25-N4	119.7(4)	N2-Ru1-Cl1	97.17(9)
C26-C25-N4	120.1(4)	N1-Ru1-Cl1	175.74(9)
C25-C26-C27	119.8(4)	N3-Ru1-Cl1	86.47(9)
C25-C26-H26	120.1	O300-C300-C302	121.5(6)
C27-C26-H26	120.1	O300-C300-C301	120.6(6)
C28-C27-C26	119.4(5)	C302-C300-C301	117.9(6)
C28-C27-H27	120.3	C300-C302-H30A	109.5
C26-C27-H27	120.3	C300-C302-H30B	109.5
C27-C28-C29	120.4(5)	H30A-C302-H30B	109.5
C27-C28-H28	119.8	C300-C302-H30C	109.5
C29-C28-H28	119.8	H30A-C302-H30C	109.5
C30-C29-C28	120.0(5)	H30B-C302-H30C	109.5
C30-C29-H29	120.0	C300-C301-H30D	109.5

C300-C301-H30E	109.5	H30D-C301-H30F	109.5
H30D-C301-H30E	109.5	H30E-C301-H30F	109.5
C300-C301-H30F	109.5		

Symmetry transformations used to generate equivalent atoms:

Table 6.11. Anisotropic displacement parameters ($Å^2$) for **FL327**.
The anisotropicdisplacement factor exponent takes the form: $-2\pi^2[h^2a^{*2}U^{11} + ... + 2 h k a^* b^* U^{12}]$

	U^{11}	U^{22}	U^{33}	U^{23}	U^{13}	U^{12}
C1	0.038(2)	0.033(3)	0.029(2)	-0.0002(19)	0.0094(17)	0.002(2)
C2	0.033(2)	0.034(2)	0.031(2)	0.0047(19)	0.0032(18)	-0.0005(19)
C3	0.035(2)	0.028(2)	0.041(2)	0.0039(19)	0.0028(19)	0.0011(19)
C4	0.036(2)	0.040(3)	0.049(3)	0.006(2)	0.002(2)	0.003(2)
C5	0.035(2)	0.045(3)	0.054(3)	0.004(3)	0.003(2)	-0.007(2)
C6	0.047(3)	0.035(3)	0.042(3)	0.007(2)	-0.012(2)	-0.010(2)
C7	0.041(2)	0.037(3)	0.037(2)	0.003(2)	-0.0012(18)	0.001(2)
C8	0.032(2)	0.034(3)	0.037(2)	0.0046(19)	-0.0008(18)	-0.0021(19)
C9	0.038(2)	0.034(2)	0.027(2)	0.0030(18)	-0.0009(18)	-0.0001(19)
C10	0.038(2)	0.033(2)	0.028(2)	-0.0006(18)	0.0051(18)	0.004(2)
C11	0.041(2)	0.036(3)	0.030(2)	0.005(2)	0.0040(19)	0.000(2)
C12	0.045(3)	0.039(3)	0.027(2)	0.001(2)	0.0026(19)	0.005(2)
C13	0.038(2)	0.039(3)	0.024(2)	0.0029(18)	0.0053(17)	0.000(2)
C14	0.035(2)	0.034(2)	0.032(2)	0.001(2)	0.0059(16)	-0.001(2)
C15	0.037(2)	0.041(3)	0.033(2)	-0.001(2)	0.0123(18)	-0.001(2)
C16	0.043(2)	0.032(3)	0.034(2)	-0.0051(19)	0.0092(18)	-0.014(2)
C17	0.043(2)	0.036(3)	0.032(2)	-0.0032(18)	0.0082(18)	-0.002(2)
C18	0.047(3)	0.048(3)	0.048(3)	-0.005(2)	0.021(2)	0.001(2)
C19	0.041(2)	0.045(3)	0.048(3)	0.005(2)	0.020(2)	0.006(2)
C20	0.049(3)	0.041(3)	0.072(3)	0.004(3)	0.023(3)	0.007(2)
C21	0.041(3)	0.046(3)	0.078(4)	0.016(3)	0.003(3)	0.005(2)
C22	0.035(2)	0.046(3)	0.074(3)	0.014(3)	0.003(2)	-0.003(2)
C23	0.036(2)	0.044(3)	0.051(3)	0.009(2)	0.006(2)	-0.005(2)
C24	0.066(3)	0.056(4)	0.068(3)	0.019(3)	-0.023(3)	-0.008(3)
C25	0.050(3)	0.042(3)	0.039(3)	-0.002(2)	0.016(2)	0.000(2)
C26	0.058(3)	0.038(3)	0.042(3)	-0.004(2)	0.018(2)	-0.003(2)
C27	0.064(3)	0.046(3)	0.046(3)	-0.006(2)	0.013(2)	-0.007(3)
C28	0.082(4)	0.053(4)	0.041(3)	-0.004(2)	0.007(3)	-0.005(3)
C29	0.087(4)	0.052(3)	0.038(3)	0.001(2)	0.017(3)	-0.006(3)
C30	0.068(3)	0.050(3)	0.040(3)	-0.001(2)	0.018(2)	-0.010(2)
C100	0.048(3)	0.034(3)	0.039(2)	-0.012(2)	0.013(2)	-0.002(2)
C200	0.049(2)	0.043(3)	0.043(2)	0.003(2)	0.009(2)	-0.001(3)
C201	0.069(3)	0.045(3)	0.066(3)	0.005(3)	-0.016(3)	0.005(3)
C202	0.045(2)	0.043(3)	0.057(3)	0.007(2)	0.001(2)	-0.003(2)
N1	0.0401(19)	0.0295(19)	0.0290(18)	0.0018(15)	0.0061(15)	0.0012(16)
N2	0.0353(19)	0.036(2)	0.0372(19)	0.0067(16)	0.0100(15)	-0.0002(16)
N3	0.0332(19)	0.041(2)	0.047(2)	-0.0002(18)	0.0146(17)	-0.0017(16)
N4	0.045(2)	0.045(2)	0.038(2)	0.0006(17)	0.0169(17)	0.0007(19)
N5	0.043(2)	0.040(2)	0.034(2)	-0.0076(18)	0.0094(18)	-0.0018(19)
O1	0.0525(16)	0.0404(17)	0.0393(15)	-0.0103(16)	0.0083(13)	-0.0066(17)
O2	0.0392(16)	0.0398(17)	0.0335(15)	-0.0023(13)	0.0080(13)	-0.0030(14)
O3	0.0555(19)	0.043(2)	0.060(2)	-0.0042(17)	-0.0024(17)	-0.0159(17)
O100	0.060(2)	0.048(2)	0.0481(19)	0.0037(17)	0.0037(16)	0.0083(17)
O200	0.067(2)	0.046(2)	0.054(2)	-0.0023(17)	0.0047(17)	0.0023(18)
F1	0.0526(15)	0.0502(17)	0.0486(14)	-0.0154(13)	0.0199(12)	-0.0180(13)
Cl1	0.0446(6)	0.0479(7)	0.0531(7)	0.0074(6)	0.0201(5)	-0.0033(5)
Ru1	0.03740(17)	0.03490(19)	0.03504(17)	0.0019(2)	0.01151(13)	0.0004(2)
C300	0.064(3)	0.054(3)	0.038(3)	0.013(2)	0.005(2)	-0.003(3)
C302	0.084(4)	0.193(9)	0.070(4)	0.059(5)	-0.009(3)	-0.050(5)
C301	0.186(7)	0.066(5)	0.060(4)	-0.005(3)	0.005(4)	-0.021(5)
O300	0.142(4)	0.085(3)	0.056(2)	-0.003(2)	0.027(3)	0.029(3)

Table 6.12. Hydrogen coordinates and isotropic displacement parameters ($Å^2$)for **FL327**.

	x	y	z	U(eq)	Occupancy
H4	0.6507	-0.0486	0.6317	0.051	1
H5A	0.5707	-0.2062	0.5895	0.054	1
H7	0.9095	-0.2097	0.5248	0.047	1
H15	1.4148	0.2559	0.6033	0.044	1
H17	1.1572	0.3545	0.6916	0.044	1
H18	0.8482	0.4486	0.7360	0.055	1
H20	0.6998	0.5485	0.6684	0.063	1
H21	0.6011	0.5410	0.5919	0.067	1
H23	0.7391	0.2224	0.5847	0.052	1
H24A	0.5032	0.3541	0.5277	0.100	1
H24B	0.6509	0.3144	0.5161	0.100	1
H24C	0.6130	0.4457	0.5157	0.100	1
H26	1.0819	0.4554	0.7682	0.054	1
H27	1.2196	0.4560	0.8397	0.062	1
H28	1.2239	0.2974	0.8863	0.071	1
H29	1.0915	0.1396	0.8623	0.070	1
H30	0.9523	0.1406	0.7919	0.062	1
H20A	0.8964	0.6999	0.6464	0.094	1
H20B	0.9989	0.8003	0.6646	0.094	1
H20C	0.8815	0.7605	0.6937	0.094	1
H20D	1.0639	0.6964	0.7653	0.073	1
H20E	1.1630	0.7670	0.7371	0.073	1
H20F	1.2009	0.6396	0.7516	0.073	1
H30A	1.0198	-0.3470	0.4503	0.176	1
H30B	1.0036	-0.4161	0.4035	0.176	1
H30C	1.0884	-0.4692	0.4486	0.176	1
H30D	0.7590	-0.6088	0.4385	0.158	1
H30E	0.9197	-0.6401	0.4436	0.158	1
H30F	0.8443	-0.5869	0.3971	0.158	1
H3	0.734(4)	-0.339(5)	0.5086(15)	0.062(15)	1
H5	1.386(4)	-0.070(3)	0.4990(13)	0.026(12)	1

Table 6.13. Torsion angles [°] for **FL327**.

N1-C1-C2-N2	1.1(5)	C19-C20-C21-C22	0.8(7)
C14-C1-C2-N2	-179.3(4)	C20-C21-C22-C23	-0.3(7)
N1-C1-C2-C9	-177.9(3)	C20-C21-C22-C24	-177.9(5)
C14-C1-C2-C9	1.7(6)	C21-C22-C23-N3	-0.7(7)
N2-C3-C4-C5	-179.2(4)	C24-C22-C23-N3	176.9(4)
C8-C3-C4-C5	2.1(6)	C30-C25-C26-C27	-0.9(7)
C3-C4-C5-C6	-0.6(6)	N4-C25-C26-C27	-177.8(4)
C4-C5-C6-O3	178.3(4)	C25-C26-C27-C28	0.8(7)
C4-C5-C6-C7	-1.0(6)	C26-C27-C28-C29	-0.2(8)
O3-C6-C7-C8	-178.2(4)	C27-C28-C29-C30	-0.4(8)
C5-C6-C7-C8	1.0(6)	C26-C25-C30-C29	0.3(7)
C6-C7-C8-C3	0.5(6)	N4-C25-C30-C29	177.2(4)
C6-C7-C8-C9	179.4(4)	C28-C29-C30-C25	0.4(8)
C4-C3-C8-C7	-2.1(6)	C16-C17-N1-C1	-1.7(5)
N2-C3-C8-C7	179.0(3)	C16-C17-N1-Ru1	173.7(3)
C4-C3-C8-C9	178.8(4)	C2-C1-N1-C17	-177.1(3)
N2-C3-C8-C9	-0.2(4)	C14-C1-N1-C17	3.4(5)
N2-C2-C9-C10	-178.7(3)	C2-C1-N1-Ru1	6.7(4)
C1-C2-C9-C10	0.4(6)	C14-C1-N1-Ru1	-172.8(3)
N2-C2-C9-C8	0.0(4)	C1-C2-N2-C3	-179.2(3)
C1-C2-C9-C8	179.1(3)	C9-C2-N2-C3	-0.1(4)
C7-C8-C9-C10	-0.8(8)	C1-C2-N2-Ru1	-8.2(4)
C3-C8-C9-C10	178.2(5)	C9-C2-N2-Ru1	170.9(3)
C7-C8-C9-C2	-178.9(4)	C4-C3-N2-C2	-178.6(4)
C3-C8-C9-C2	0.1(4)	C8-C3-N2-C2	0.2(4)
C2-C9-C10-C13	-1.6(5)	C4-C3-N2-Ru1	16.2(7)
C8-C9-C10-C13	-179.5(4)	C8-C3-N2-Ru1	-165.0(3)
C2-C9-C10-C11	176.5(4)	C22-C23-N3-C19	1.2(6)
C8-C9-C10-C11	-1.4(8)	C22-C23-N3-Ru1	-177.9(3)
C13-C10-C11-O1	179.0(4)	C20-C19-N3-C23	-0.8(6)
C9-C10-C11-O1	0.7(7)	C18-C19-N3-C23	-177.6(4)
C13-C10-C11-N5	0.2(4)	C20-C19-N3-Ru1	178.5(3)
C9-C10-C11-N5	-178.1(4)	C18-C19-N3-Ru1	1.6(5)
C9-C10-C13-C14	0.7(6)	C19-C18-N4-C25	174.6(4)
C11-C10-C13-C14	-177.8(3)	C19-C18-N4-Ru1	-3.0(5)
C9-C10-C13-C12	178.4(4)	C30-C25-N4-C18	138.8(4)
C11-C10-C13-C12	-0.1(4)	C26-C25-N4-C18	-44.2(6)
O2-C12-C13-C10	-178.7(4)	C30-C25-N4-Ru1	-43.9(6)
N5-C12-C13-C10	0.0(4)	C26-C25-N4-Ru1	133.1(4)
O2-C12-C13-C14	-1.2(7)	O1-C11-N5-C12	-179.1(4)
N5-C12-C13-C14	177.5(4)	C10-C11-N5-C12	-0.2(4)
N1-C1-C14-C15	-1.7(6)	O2-C12-N5-C11	178.9(4)
C2-C1-C14-C15	178.8(4)	C13-C12-N5-C11	0.2(5)
N1-C1-C14-C13	177.0(3)	O100-C100-Ru1-N4	-178(100)
C2-C1-C14-C13	-2.5(5)	O100-C100-Ru1-N2	-4(8)
C10-C13-C14-C1	1.4(6)	O100-C100-Ru1-N1	-84(8)
C12-C13-C14-C1	-175.8(4)	O100-C100-Ru1-N3	155(6)
C10-C13-C14-C15	179.9(4)	O100-C100-Ru1-Cl1	93(8)
C12-C13-C14-C15	2.7(7)	C18-N4-Ru1-C100	-176.1(3)
C1-C14-C15-C16	-1.6(5)	C25-N4-Ru1-C100	6.5(4)
C13-C14-C15-C16	179.8(4)	C18-N4-Ru1-N2	39.8(9)
C14-C15-C16-F1	-177.8(3)	C25-N4-Ru1-N2	-137.5(7)
C14-C15-C16-C17	3.3(6)	C18-N4-Ru1-N1	92.3(3)
F1-C16-C17-N1	179.4(3)	C25-N4-Ru1-N1	-85.0(3)
C15-C16-C17-N1	-1.6(6)	C18-N4-Ru1-N3	2.9(3)
N4-C18-C19-N3	0.9(6)	C25-N4-Ru1-N3	-174.4(4)
N4-C18-C19-C20	-176.0(4)	C18-N4-Ru1-Cl1	-83.8(3)
N3-C19-C20-C21	-0.2(7)	C25-N4-Ru1-Cl1	98.9(3)
C18-C19-C20-C21	176.4(4)	C2-N2-Ru1-C100	-82.7(3)

C3-N2-Ru1-C100	82.2(5)	C1-N1-Ru1-N2	-8.4(2)
C2-N2-Ru1-N4	62.0(8)	C17-N1-Ru1-N3	82.3(3)
C3-N2-Ru1-N4	-133.1(7)	C1-N1-Ru1-N3	-102.1(3)
C2-N2-Ru1-N1	8.6(3)	C17-N1-Ru1-Cl1	118.5(12)
C3-N2-Ru1-N1	173.4(5)	C1-N1-Ru1-Cl1	-65.8(14)
C2-N2-Ru1-N3	98.1(3)	C23-N3-Ru1-C100	-156(5)
C3-N2-Ru1-N3	-97.1(4)	C19-N3-Ru1-C100	25(5)
C2-N2-Ru1-Cl1	-175.0(2)	C23-N3-Ru1-N4	176.8(4)
C3-N2-Ru1-Cl1	-10.2(5)	C19-N3-Ru1-N4	-2.4(3)
C17-N1-Ru1-C100	-95.9(3)	C23-N3-Ru1-N2	3.1(4)
C1-N1-Ru1-C100	79.7(3)	C19-N3-Ru1-N2	-176.1(3)
C17-N1-Ru1-N4	4.4(3)	C23-N3-Ru1-N1	83.6(3)
C1-N1-Ru1-N4	-179.9(3)	C19-N3-Ru1-N1	-95.6(3)
C17-N1-Ru1-N2	176.0(3)	C23-N3-Ru1-Cl1	-93.9(3)
C19-N3-Ru1-Cl1	87.0(3)		

Symmetry transformations used to generate equivalent atoms:

Table 6.14. Hydrogen bonds for **FL327** [Å and °].

D-H...A	d(D-H)	d(H...A)	d(D...A)	<(DHA)
O3-H3...O300	0.97(5)	1.77(5)	2.705(6)	159(5)
N5-H5...O2#1	0.82(4)	2.03(4)	2.823(5)	165(4)

Symmetry transformations used to generate equivalent atoms:
#1 -x+3,-y,-z+1

Crystal structure of FL389.

Table 6.15. Crystal data and structure refinement for **FL389**.

Identification code	fl389	
Habitus, colour	prism, red	
Crystal size	0.27 x 0.09 x 0.02 mm^3	
Crystal system	Triclinic	
Space group	$P\bar{1}$	Z = 2
Unit cell dimensions	a = 7.6625(3) Å	α= 101.764(3)°
	b = 15.8593(6) Å	β= 92.604(3)°
	c = 15.9895(5) Å	γ = 96.270(3)°
Volume	1886.30(12) $Å^3$	
Cell determination	18229 peaks with Theta 4.5 to 25°.	
Empirical formula	C_{39} H_{36} Cl F N_6 O_7 Ru	
Formula weight	856.26	
Density (calculated)	1.508 Mg/m^3	
Absorption coefficient	0.550 mm^{-1}	
F(000)	876	

Data collection:

Diffractometer type	IPDS 2T
Wavelength	0.71073 Å
Temperature	193(2) K
Theta range for data collection	4.64 to 25.00°.
Index ranges	-8<=h<=9, -18<=k<=18, -18<=l<=18
Data collection software	STOE WinXpose (X-Area)
Cell refinement software	STOE WinCell (X-Area)
Data reduction software	STOE WinIntegrate (X-Area)

Solution and refinement:

Reflections collected	16388
Independent reflections	6276 [R(int) = 0.0611]
Completeness to theta = 25.00°	94.7 %
Observed reflections	5215[I>2sigma(I)]
Reflections used for refinement	6276
Absorption correction	Semi-empirical from equivalents
Max. and min. transmission	0.9761 and 0.9054
Largest diff. peak and hole	0.615 and -0.595 e.$Å^{-3}$
Solution	Direct methods
Refinement	Full-matrix least-squares on F^2
Treatment of hydrogen atoms	Calculated positions, riding model
Programs used	SIR92 (Giacovazzo et al, 1993)
	SHELXL-97 (Sheldrick, 1997)
	Diamond 3.1, STOE IPDS2 software
Data / restraints / parameters	6276 / 0 / 503
Goodness-of-fit on F^2	1.066
R index (all data)	wR2 = 0.1015
R index conventional [I>2sigma(I)]	R1 = 0.0454

Table 6.16. Atomic coordinates and equivalent isotropic displacement parameters ($Å^2$) for **FL389**. U(eq) is defined as one third of the trace of the orthogonalized U^{ij} tensor.

	x	y	z	U(eq)	Occupancy
C2	0.9858(5)	0.8349(2)	0.1618(2)	0.0266(7)	1
C3	0.8261(5)	0.8562(2)	0.1302(2)	0.0261(7)	1
C5	0.6536(5)	0.9653(3)	0.1209(2)	0.0302(8)	1
C6	0.5258(5)	0.9026(3)	0.0738(2)	0.0306(8)	1
C7	0.5400(5)	0.8171(3)	0.0544(2)	0.0299(8)	1
C8	0.6975(5)	0.7907(2)	0.0842(2)	0.0269(8)	1
C9	0.7386(5)	0.7042(2)	0.0738(2)	0.0284(8)	1
C10	0.6278(5)	0.6231(3)	0.0361(2)	0.0331(8)	1
C12	0.8913(5)	0.5878(2)	0.0853(2)	0.0301(8)	1
C13	0.8974(5)	0.6840(2)	0.1047(2)	0.0274(8)	1
C14	1.0284(5)	0.7487(2)	0.1489(2)	0.0251(7)	1
C15	1.2021(5)	0.7575(2)	0.1900(2)	0.0250(7)	1
C16	1.3197(5)	0.6976(2)	0.1999(2)	0.0291(8)	1
C17	1.4780(5)	0.7285(3)	0.2461(2)	0.0318(8)	1
C18	1.5214(5)	0.8175(3)	0.2817(2)	0.0336(9)	1
C19	1.4090(5)	0.8778(3)	0.2718(2)	0.0293(8)	1
C20	1.2472(5)	0.8476(2)	0.2250(2)	0.0258(7)	1
C22	0.9090(5)	0.9434(2)	0.3781(2)	0.0273(8)	1
C23	0.8225(5)	0.9435(3)	0.4540(2)	0.0307(8)	1
C24	0.7244(5)	1.0111(3)	0.4832(2)	0.0338(9)	1
C25	0.7137(5)	1.0742(3)	0.4364(2)	0.0335(8)	1
C26	0.8023(5)	1.0716(3)	0.3624(2)	0.0297(8)	1
C27	0.8084(5)	1.1375(2)	0.3121(2)	0.0299(8)	1
C29	0.9124(5)	1.1998(2)	0.2009(2)	0.0299(8)	1
C30	0.9526(6)	1.2837(3)	0.2455(3)	0.0444(10)	1
C31	0.9619(8)	1.3500(3)	0.2001(4)	0.0580(13)	1
C32	0.9351(7)	1.3328(3)	0.1132(4)	0.0544(13)	1
C33	0.8963(6)	1.2492(3)	0.0691(3)	0.0423(10)	1
C34	0.8854(5)	1.1816(3)	0.1125(3)	0.0344(9)	1
C35	1.1277(5)	1.0440(3)	0.1246(3)	0.0364(9)	1
C100	1.0162(5)	0.6820(3)	0.3567(3)	0.0391(9)	1
C101	1.1883(7)	0.7120(5)	0.4063(3)	0.0656(15)	1
C102	0.9732(8)	0.5880(3)	0.3180(4)	0.0597(13)	1
C200	0.7674(8)	0.6397(5)	0.5249(4)	0.0740(18)	1
C201	0.6022(9)	0.6670(6)	0.4963(6)	0.107(3)	1
C202	0.7641(13)	0.5499(7)	0.5341(7)	0.131(4)	1
C300	0.4902(10)	0.3734(6)	0.2514(5)	0.093(2)	1
C301	0.4610(14)	0.4464(6)	0.2101(6)	0.117(3)	1
C302	0.4465(10)	0.2855(5)	0.1952(6)	0.097(2)	1
N1	1.1115(4)	0.89448(19)	0.20618(18)	0.0250(6)	1
N4	0.8050(4)	0.9425(2)	0.14865(19)	0.0268(6)	1
N11	0.7273(4)	0.5566(2)	0.0439(2)	0.0354(7)	1
N21	0.8985(4)	1.0059(2)	0.33386(18)	0.0260(6)	1
N23	0.8349(5)	0.8776(2)	0.4957(2)	0.0382(8)	1
N28	0.8996(4)	1.1292(2)	0.24563(19)	0.0280(7)	1
O10	0.4769(4)	0.61258(18)	0.0048(2)	0.0412(7)	1
O12	1.0021(4)	0.54371(18)	0.10187(19)	0.0402(7)	1
O17	1.5908(4)	0.66924(19)	0.2565(2)	0.0425(7)	1
O35	1.1887(5)	1.0651(2)	0.0663(2)	0.0584(10)	1
O100	0.9119(4)	0.7331(2)	0.3491(2)	0.0466(7)	1
O200	0.9018(6)	0.6908(4)	0.5387(3)	0.0906(15)	1
O300	0.5472(12)	0.3858(7)	0.3235(4)	0.175(4)	1
F6	0.3789(3)	0.93192(16)	0.04606(16)	0.0457(6)	1
Cl1	1.28290(12)	1.09337(6)	0.30739(6)	0.0342(2)	1
Ru1	1.02562(4)	1.01860(2)	0.21998(2)	0.02367(10)	1

Table 6.17. Bond lengths [Å] and angles [°] for **FL389**.

C2-N1	1.339(5)	C29-N28	1.443(4)
C2-C3	1.403(5)	C30-C31	1.391(6)
C2-C14	1.417(5)	C30-H30	0.9500
C3-N4	1.370(5)	C31-C32	1.362(8)
C3-C8	1.412(5)	C31-H31	0.9500
C5-N4	1.336(5)	C32-C33	1.362(7)
C5-C6	1.388(5)	C32-H32	0.9500
C5-H5	0.9500	C33-C34	1.388(5)
C6-C7	1.346(6)	C33-H33	0.9500
C6-F6	1.354(4)	C34-H34	0.9500
C7-C8	1.413(5)	C35-O35	1.155(5)
C7-H7	0.9500	C35-Ru1	1.841(4)
C8-C9	1.420(5)	C100-O100	1.218(5)
C9-C13	1.386(5)	C100-C101	1.486(7)
C9-C10	1.462(5)	C100-C102	1.487(7)
C10-O10	1.219(5)	C101-H10A	0.9800
C10-N11	1.389(5)	C101-H10B	0.9800
C12-O12	1.211(5)	C101-H10C	0.9800
C12-N11	1.384(5)	C102-H10D	0.9800
C12-C13	1.489(5)	C102-H10E	0.9800
C13-C14	1.405(5)	C102-H10F	0.9800
C14-C15	1.437(5)	C200-O200	1.220(8)
C15-C16	1.406(5)	C200-C202	1.459(11)
C15-C20	1.422(5)	C200-C201	1.465(9)
C16-C17	1.378(5)	C201-H20A	0.9800
C16-H16	0.9500	C201-H20B	0.9800
C17-O17	1.374(5)	C201-H20C	0.9800
C17-C18	1.407(6)	C202-H20D	0.9800
C18-C19	1.382(6)	C202-H20E	0.9800
C18-H18	0.9500	C202-H20F	0.9800
C19-C20	1.402(5)	C300-O300	1.184(9)
C19-H19	0.9500	C300-C301	1.476(12)
C20-N1	1.399(5)	C300-C302	1.492(11)
C22-N21	1.337(4)	C301-H30A	0.9800
C22-C23	1.408(5)	C301-H30B	0.9800
C22-H22	0.9500	C301-H30C	0.9800
C23-N23	1.358(5)	C302-H30D	0.9800
C23-C24	1.391(6)	C302-H30E	0.9800
C24-C25	1.375(5)	C302-H30F	0.9800
C24-H24	0.9500	N1-Ru1	2.116(3)
C25-C26	1.386(5)	N4-Ru1	2.105(3)
C25-H25	0.9500	N11-H11	0.8800
C26-N21	1.357(5)	N21-Ru1	2.138(3)
C26-C27	1.442(5)	N23-H23A	0.8020
C27-N28	1.291(5)	N23-H23B	0.8879
C27-H27	0.9500	N28-Ru1	2.071(3)
C29-C30	1.371(6)	O17-H17	0.8400
C29-C34	1.385(5)	Cl1-Ru1	2.4102(9)

N1-C2-C3	122.7(3)	C7-C6-C5	124.6(3)
N1-C2-C14	114.2(3)	F6-C6-C5	116.0(3)
C3-C2-C14	123.0(3)	C6-C7-C8	116.7(3)
N4-C3-C2	115.8(3)	C6-C7-H7	121.6
N4-C3-C8	123.8(3)	C8-C7-H7	121.6
C2-C3-C8	120.4(3)	C3-C8-C7	117.2(3)
N4-C5-C6	120.1(4)	C3-C8-C9	116.3(3)
N4-C5-H5	120.0	C7-C8-C9	126.5(3)
C6-C5-H5	120.0	C13-C9-C8	122.7(3)
C7-C6-F6	119.4(3)	C13-C9-C10	108.3(3)

C8-C9-C10	128.9(3)	C32-C33-C34	120.2(4)
O10-C10-N11	124.9(4)	C32-C33-H33	119.9
O10-C10-C9	128.8(4)	C34-C33-H33	119.9
N11-C10-C9	106.3(3)	C29-C34-C33	119.5(4)
O12-C12-N11	125.5(4)	C29-C34-H34	120.2
O12-C12-C13	129.0(3)	C33-C34-H34	120.2
N11-C12-C13	105.5(3)	O35-C35-Ru1	175.7(4)
C9-C13-C14	121.7(3)	O100-C100-C101	120.7(5)
C9-C13-C12	107.8(3)	O100-C100-C102	120.9(4)
C14-C13-C12	130.5(3)	C101-C100-C102	118.5(5)
C13-C14-C2	115.8(3)	C100-C101-H10A	109.5
C13-C14-C15	140.2(3)	C100-C101-H10B	109.5
C2-C14-C15	104.0(3)	H10A-C101-H10B	109.5
C16-C15-C20	120.9(3)	C100-C101-H10C	109.5
C16-C15-C14	133.1(3)	H10A-C101-H10C	109.5
C20-C15-C14	106.1(3)	H10B-C101-H10C	109.5
C17-C16-C15	118.0(4)	C100-C102-H10D	109.5
C17-C16-H16	121.0	C100-C102-H10E	109.5
C15-C16-H16	121.0	H10D-C102-H10E	109.5
O17-C17-C16	117.6(4)	C100-C102-H10F	109.5
O17-C17-C18	121.4(3)	H10D-C102-H10F	109.5
C16-C17-C18	121.0(4)	H10E-C102-H10F	109.5
C19-C18-C17	122.0(3)	O200-C200-C202	122.3(7)
C19-C18-H18	119.0	O200-C200-C201	120.3(7)
C17-C18-H18	119.0	C202-C200-C201	117.4(7)
C18-C19-C20	117.8(4)	C200-C201-H20A	109.5
C18-C19-H19	121.1	C200-C201-H20B	109.5
C20-C19-H19	121.1	H20A-C201-H20B	109.5
N1-C20-C19	129.1(3)	C200-C201-H20C	109.5
N1-C20-C15	110.7(3)	H20A-C201-H20C	109.5
C19-C20-C15	120.3(3)	H20B-C201-H20C	109.5
N21-C22-C23	121.9(4)	C200-C202-H20D	109.5
N21-C22-H22	119.1	C200-C202-H20E	109.5
C23-C22-H22	119.1	H20D-C202-H20E	109.5
N23-C23-C24	122.0(4)	C200-C202-H20F	109.5
N23-C23-C22	119.5(4)	H20D-C202-H20F	109.5
C24-C23-C22	118.5(3)	H20E-C202-H20F	109.5
C25-C24-C23	118.8(3)	O300-C300-C301	121.1(10)
C25-C24-H24	120.6	O300-C300-C302	123.8(10)
C23-C24-H24	120.6	C301-C300-C302	115.1(7)
C24-C25-C26	120.5(4)	C300-C301-H30A	109.5
C24-C25-H25	119.7	C300-C301-H30B	109.5
C26-C25-H25	119.7	H30A-C301-H30B	109.5
N21-C26-C25	120.8(3)	C300-C301-H30C	109.5
N21-C26-C27	114.5(3)	H30A-C301-H30C	109.5
C25-C26-C27	124.6(4)	H30B-C301-H30C	109.5
N28-C27-C26	119.1(4)	C300-C302-H30D	109.5
N28-C27-H27	120.5	C300-C302-H30E	109.5
C26-C27-H27	120.5	H30D-C302-H30E	109.5
C30-C29-C34	120.5(4)	C300-C302-H30F	109.5
C30-C29-N28	120.2(3)	H30D-C302-H30F	109.5
C34-C29-N28	119.3(3)	H30E-C302-H30F	109.5
C29-C30-C31	118.5(4)	C2-N1-C20	105.1(3)
C29-C30-H30	120.7	C2-N1-Ru1	109.1(2)
C31-C30-H30	120.7	C20-N1-Ru1	145.8(2)
C32-C31-C30	121.4(5)	C5-N4-C3	117.6(3)
C32-C31-H31	119.3	C5-N4-Ru1	130.5(3)
C30-C31-H31	119.3	C3-N4-Ru1	111.9(2)
C31-C32-C33	119.8(4)	C12-N11-C10	112.1(3)
C31-C32-H32	120.1	C12-N11-H11	124.0
C33-C32-H32	120.1	C10-N11-H11	124.0

C22-N21-C26	119.5(3)	C35-Ru1-N1	95.05(15)
C22-N21-Ru1	127.2(3)	N28-Ru1-N1	168.31(11)
C26-N21-Ru1	113.3(2)	N4-Ru1-N1	80.42(11)
C23-N23-H23A	119.1	C35-Ru1-N21	172.58(15)
C23-N23-H23B	116.0	N28-Ru1-N21	77.43(12)
H23A-N23-H23B	124.9	N4-Ru1-N21	88.25(11)
C27-N28-C29	117.1(3)	N1-Ru1-N21	92.34(11)
C27-N28-Ru1	115.7(2)	C35-Ru1-Cl1	89.47(13)
C29-N28-Ru1	127.1(2)	N28-Ru1-Cl1	90.89(9)
C17-O17-H17	109.5	N4-Ru1-Cl1	174.35(8)
C35-Ru1-N28	95.29(15)	N1-Ru1-Cl1	94.65(8)
C35-Ru1-N4	93.70(15)	N21-Ru1-Cl1	89.21(8)
N28-Ru1-N4	93.47(12)		

Symmetry transformations used to generate equivalent atoms:

Table 6.18. Anisotropic displacement parameters ($Å^2$) for **FL389**.
The anisotropicdisplacement factor exponent takes the form: $-2\pi^2[h^2a^{*2}U^{11} + ... + 2 h k a^* b^* U^{12}]$

	U^{11}	U^{22}	U^{33}	U^{23}	U^{13}	U^{12}
C2	0.0272(19)	0.0242(19)	0.0271(18)	0.0050(15)	-0.0007(14)	-0.0006(15)
C3	0.0296(19)	0.0217(18)	0.0271(18)	0.0071(15)	0.0013(14)	0.0007(15)
C5	0.031(2)	0.030(2)	0.0314(19)	0.0076(16)	0.0012(15)	0.0068(16)
C6	0.0236(18)	0.034(2)	0.035(2)	0.0059(17)	-0.0018(15)	0.0076(15)
C7	0.0251(18)	0.031(2)	0.0309(19)	0.0040(16)	-0.0038(14)	0.0005(15)
C8	0.0250(18)	0.0262(19)	0.0276(18)	0.0033(15)	-0.0001(14)	0.0003(15)
C9	0.0270(19)	0.0263(19)	0.0300(19)	0.0037(15)	-0.0025(14)	0.0011(15)
C10	0.034(2)	0.026(2)	0.036(2)	0.0023(16)	-0.0050(16)	-0.0017(16)
C12	0.033(2)	0.0245(19)	0.0311(19)	0.0045(16)	-0.0026(15)	0.0012(16)
C13	0.0283(19)	0.0226(19)	0.0297(18)	0.0032(15)	0.0001(14)	0.0013(15)
C14	0.0250(18)	0.0226(18)	0.0261(17)	0.0025(14)	-0.0010(14)	0.0021(14)
C15	0.0238(18)	0.0236(18)	0.0270(18)	0.0060(15)	-0.0013(14)	-0.0002(14)
C16	0.0250(18)	0.0250(19)	0.036(2)	0.0049(16)	-0.0020(15)	0.0005(15)
C17	0.0264(19)	0.031(2)	0.038(2)	0.0085(17)	-0.0019(15)	0.0021(16)
C18	0.0244(19)	0.036(2)	0.037(2)	0.0056(17)	-0.0060(15)	-0.0046(16)
C19	0.0255(18)	0.027(2)	0.0322(19)	0.0026(16)	-0.0034(14)	-0.0022(15)
C20	0.0275(18)	0.0236(18)	0.0254(17)	0.0043(15)	0.0007(14)	0.0011(15)
C22	0.0304(19)	0.0266(19)	0.0244(18)	0.0080(15)	-0.0019(14)	-0.0023(15)
C23	0.0290(19)	0.030(2)	0.0297(19)	0.0064(16)	-0.0042(15)	-0.0079(16)
C24	0.028(2)	0.042(2)	0.0281(19)	0.0048(17)	0.0034(15)	-0.0027(17)
C25	0.0283(19)	0.039(2)	0.0313(19)	0.0038(17)	0.0012(15)	0.0034(17)
C26	0.0273(19)	0.029(2)	0.0312(19)	0.0036(16)	-0.0025(15)	0.0024(15)
C27	0.0310(19)	0.0260(19)	0.0314(19)	0.0042(16)	-0.0009(15)	0.0032(15)
C29	0.034(2)	0.0237(19)	0.0326(19)	0.0075(16)	0.0033(15)	0.0035(15)
C30	0.055(3)	0.027(2)	0.050(3)	0.0053(19)	0.006(2)	0.0029(19)
C31	0.079(4)	0.022(2)	0.074(4)	0.010(2)	0.016(3)	0.006(2)
C32	0.065(3)	0.036(3)	0.072(3)	0.029(3)	0.013(3)	0.012(2)
C33	0.044(2)	0.046(3)	0.045(2)	0.024(2)	0.0071(19)	0.013(2)
C34	0.032(2)	0.030(2)	0.041(2)	0.0100(18)	0.0012(16)	0.0035(16)
C35	0.041(2)	0.025(2)	0.043(2)	0.0027(18)	0.0045(18)	0.0093(17)
C100	0.037(2)	0.045(3)	0.036(2)	0.0077(19)	0.0042(17)	0.007(2)
C101	0.042(3)	0.098(5)	0.054(3)	0.011(3)	-0.002(2)	0.009(3)
C102	0.076(4)	0.039(3)	0.065(3)	0.007(2)	0.006(3)	0.016(3)
C200	0.060(4)	0.112(5)	0.057(3)	0.034(4)	0.010(3)	0.009(4)
C201	0.059(4)	0.126(7)	0.156(8)	0.085(6)	0.003(4)	0.004(4)
C202	0.129(8)	0.141(9)	0.163(9)	0.094(8)	0.060(7)	0.056(7)
C300	0.089(5)	0.123(7)	0.068(4)	0.026(4)	0.030(4)	-0.007(4)
C301	0.153(8)	0.084(6)	0.101(6)	0.007(5)	0.022(6)	-0.023(5)
C302	0.087(5)	0.080(5)	0.130(7)	0.033(5)	0.028(5)	0.014(4)
N1	0.0248(15)	0.0224(16)	0.0260(15)	0.0034(12)	0.0007(11)	-0.0010(12)
N4	0.0295(16)	0.0249(16)	0.0271(15)	0.0066(13)	0.0030(12)	0.0057(13)
N11	0.0328(18)	0.0197(16)	0.0480(19)	-0.0005(14)	-0.0072(14)	-0.0034(13)
N21	0.0224(15)	0.0246(16)	0.0276(15)	0.0017(13)	-0.0014(12)	-0.0035(12)
N23	0.047(2)	0.0354(19)	0.0321(17)	0.0107(15)	0.0040(14)	-0.0031(15)
N28	0.0310(16)	0.0229(16)	0.0278(16)	0.0032(13)	-0.0020(13)	-0.0006(13)
O10	0.0329(16)	0.0285(15)	0.0564(18)	0.0018(13)	-0.0125(13)	-0.0027(12)
O12	0.0411(16)	0.0235(14)	0.0526(17)	0.0039(13)	-0.0132(13)	0.0034(12)
O17	0.0307(15)	0.0361(16)	0.0591(19)	0.0086(14)	-0.0123(13)	0.0066(12)
O35	0.079(2)	0.059(2)	0.056(2)	0.0341(18)	0.0395(18)	0.0349(19)
O100	0.0412(17)	0.0410(18)	0.0551(19)	0.0056(15)	-0.0040(14)	0.0063(14)
O200	0.062(3)	0.142(5)	0.071(3)	0.035(3)	0.004(2)	0.004(3)
O300	0.185(8)	0.263(11)	0.072(4)	0.034(5)	0.015(4)	-0.003(7)
F6	0.0336(13)	0.0417(14)	0.0595(15)	0.0037(12)	-0.0123(11)	0.0142(11)
Cl1	0.0325(5)	0.0293(5)	0.0362(5)	0.0018(4)	-0.0014(4)	-0.0062(4)
Ru1	0.02657(16)	0.01878(15)	0.02449(15)	0.00348(11)	0.00129(10)	-0.00018(10)

Table 6.19. Hydrogen coordinates and isotropic displacement parameters ($Å^2$)for **FL389**.

	x	y	z	U(eq)	Occupancy
H5	0.6332	1.0245	0.1333	0.036	1
H7	0.4486	0.7765	0.0224	0.036	1
H16	1.2909	0.6376	0.1754	0.035	1
H18	1.6313	0.8368	0.3134	0.040	1
H19	1.4403	0.9377	0.2960	0.035	1
H22	0.9767	0.8977	0.3578	0.033	1
H24	0.6659	1.0135	0.5346	0.041	1
H25	0.6450	1.1201	0.4548	0.040	1
H27	0.7462	1.1864	0.3276	0.036	1
H30	0.9737	1.2964	0.3060	0.053	1
H31	0.9875	1.4085	0.2304	0.070	1
H32	0.9435	1.3790	0.0834	0.065	1
H33	0.8766	1.2372	0.0086	0.051	1
H34	0.8595	1.1233	0.0818	0.041	1
H10A	1.2143	0.7750	0.4131	0.098	1
H10B	1.2810	0.6835	0.3756	0.098	1
H10C	1.1830	0.6973	0.4628	0.098	1
H10D	0.9957	0.5540	0.3612	0.090	1
H10E	1.0467	0.5721	0.2700	0.090	1
H10F	0.8488	0.5759	0.2973	0.090	1
H20A	0.6276	0.7202	0.4745	0.160	1
H20B	0.5276	0.6780	0.5446	0.160	1
H20C	0.5410	0.6211	0.4507	0.160	1
H20D	0.7276	0.5109	0.4788	0.196	1
H20E	0.6806	0.5387	0.5763	0.196	1
H20F	0.8818	0.5399	0.5534	0.196	1
H30A	0.4923	0.5013	0.2516	0.175	1
H30B	0.3368	0.4412	0.1900	0.175	1
H30C	0.5345	0.4451	0.1614	0.175	1
H30D	0.4396	0.2416	0.2304	0.145	1
H30E	0.5382	0.2747	0.1549	0.145	1
H30F	0.3330	0.2824	0.1632	0.145	1
H11	0.6904	0.5012	0.0249	0.042	1
H23A	0.8804	0.8364	0.4734	0.046	1
H23B	0.7923	0.8846	0.5470	0.046	1
H17	1.6827	0.6951	0.2852	0.064	1

Table 6.20. Torsion angles [°] for **FL389**.

N1-C2-C3-N4	-0.9(5)	C23-C24-C25-C26	-1.4(6)
C14-C2-C3-N4	179.7(3)	C24-C25-C26-N21	1.2(6)
N1-C2-C3-C8	-179.7(3)	C24-C25-C26-C27	-175.8(3)
C14-C2-C3-C8	0.9(5)	N21-C26-C27-N28	0.7(5)
N4-C5-C6-C7	1.6(6)	C25-C26-C27-N28	178.0(4)
N4-C5-C6-F6	-178.0(3)	C34-C29-C30-C31	1.3(7)
F6-C6-C7-C8	179.1(3)	N28-C29-C30-C31	-179.3(4)
C5-C6-C7-C8	-0.5(6)	C29-C30-C31-C32	-1.2(8)
N4-C3-C8-C7	1.2(5)	C30-C31-C32-C33	0.8(8)
C2-C3-C8-C7	179.9(3)	C31-C32-C33-C34	-0.5(7)
N4-C3-C8-C9	-177.6(3)	C30-C29-C34-C33	-1.1(6)
C2-C3-C8-C9	1.1(5)	N28-C29-C34-C33	179.6(4)
C6-C7-C8-C3	-0.8(5)	C32-C33-C34-C29	0.7(6)
C6-C7-C8-C9	177.8(4)	C3-C2-N1-C20	-179.6(3)
C3-C8-C9-C13	-1.7(5)	C14-C2-N1-C20	-0.1(4)
C7-C8-C9-C13	179.6(3)	C3-C2-N1-Ru1	0.8(4)
C3-C8-C9-C10	174.3(4)	C14-C2-N1-Ru1	-179.6(2)
C7-C8-C9-C10	-4.4(6)	C19-C20-N1-C2	-178.6(4)
C13-C9-C10-O10	177.2(4)	C15-C20-N1-C2	0.7(4)
C8-C9-C10-O10	0.8(7)	C19-C20-N1-Ru1	0.7(7)
C13-C9-C10-N11	-1.5(4)	C15-C20-N1-Ru1	179.9(3)
C8-C9-C10-N11	-178.0(4)	C6-C5-N4-C3	-1.2(5)
C8-C9-C13-C14	0.2(6)	C6-C5-N4-Ru1	179.7(3)
C10-C9-C13-C14	-176.5(3)	C2-C3-N4-C5	-179.0(3)
C8-C9-C13-C12	177.8(3)	C8-C3-N4-C5	-0.2(5)
C10-C9-C13-C12	1.1(4)	C2-C3-N4-Ru1	0.4(4)
O12-C12-C13-C9	-179.4(4)	C8-C3-N4-Ru1	179.1(3)
N11-C12-C13-C9	-0.3(4)	O12-C12-N11-C10	178.4(4)
O12-C12-C13-C14	-2.0(7)	C13-C12-N11-C10	-0.7(4)
N11-C12-C13-C14	177.1(4)	O10-C10-N11-C12	-177.4(4)
C9-C13-C14-C2	1.7(5)	C9-C10-N11-C12	1.4(4)
C12-C13-C14-C2	-175.3(4)	C23-C22-N21-C26	0.1(5)
C9-C13-C14-C15	179.8(4)	C23-C22-N21-Ru1	178.2(3)
C12-C13-C14-C15	2.8(8)	C25-C26-N21-C22	-0.6(5)
N1-C2-C14-C13	178.2(3)	C27-C26-N21-C22	176.8(3)
C3-C2-C14-C13	-2.3(5)	C25-C26-N21-Ru1	-178.9(3)
N1-C2-C14-C15	-0.5(4)	C27-C26-N21-Ru1	-1.5(4)
C3-C2-C14-C15	179.0(3)	C26-C27-N28-C29	-175.6(3)
C13-C14-C15-C16	2.5(8)	C26-C27-N28-Ru1	0.5(4)
C2-C14-C15-C16	-179.3(4)	C30-C29-N28-C27	47.4(5)
C13-C14-C15-C20	-177.3(4)	C34-C29-N28-C27	-133.2(4)
C2-C14-C15-C20	0.9(4)	C30-C29-N28-Ru1	-128.1(4)
C20-C15-C16-C17	1.5(5)	C34-C29-N28-Ru1	51.2(5)
C14-C15-C16-C17	-178.3(4)	O35-C35-Ru1-N28	12(5)
C15-C16-C17-O17	179.0(3)	O35-C35-Ru1-N4	106(5)
C15-C16-C17-C18	-0.6(6)	O35-C35-Ru1-N1	-173(5)
O17-C17-C18-C19	-179.9(4)	O35-C35-Ru1-N21	1(6)
C16-C17-C18-C19	-0.3(6)	O35-C35-Ru1-Cl1	-79(5)
C17-C18-C19-C20	0.3(6)	C27-N28-Ru1-C35	-179.5(3)
C18-C19-C20-N1	179.8(3)	C29-N28-Ru1-C35	-3.9(3)
C18-C19-C20-C15	0.6(5)	C27-N28-Ru1-N4	86.4(3)
C16-C15-C20-N1	179.1(3)	C29-N28-Ru1-N4	-98.0(3)
C14-C15-C20-N1	-1.0(4)	C27-N28-Ru1-N1	28.4(7)
C16-C15-C20-C19	-1.5(5)	C29-N28-Ru1-N1	-156.0(5)
C14-C15-C20-C19	178.3(3)	C27-N28-Ru1-N21	-1.0(3)
N21-C22-C23-N23	178.8(3)	C29-N28-Ru1-N21	174.6(3)
N21-C22-C23-C24	-0.3(5)	C27-N28-Ru1-Cl1	-90.0(3)
N23-C23-C24-C25	-178.2(3)	C29-N28-Ru1-Cl1	85.6(3)
C22-C23-C24-C25	0.9(5)	C5-N4-Ru1-C35	-86.2(3)

C3-N4-Ru1-C35	94.6(3)	C20-N1-Ru1-N4	-179.7(4)
C5-N4-Ru1-N28	9.3(3)	C2-N1-Ru1-N21	87.4(2)
C3-N4-Ru1-N28	-169.9(2)	C20-N1-Ru1-N21	-91.8(4)
C5-N4-Ru1-N1	179.3(3)	C2-N1-Ru1-Cl1	176.8(2)
C3-N4-Ru1-N1	0.0(2)	C20-N1-Ru1-Cl1	-2.4(4)
C5-N4-Ru1-N21	86.6(3)	C22-N21-Ru1-C35	-165.4(11)
C3-N4-Ru1-N21	-92.6(2)	C26-N21-Ru1-C35	12.7(13)
C5-N4-Ru1-Cl1	149.8(8)	C22-N21-Ru1-N28	-176.8(3)
C3-N4-Ru1-Cl1	-29.4(11)	C26-N21-Ru1-N28	1.4(2)
C2-N1-Ru1-C35	-93.4(3)	C22-N21-Ru1-N4	89.2(3)
C20-N1-Ru1-C35	87.4(4)	C26-N21-Ru1-N4	-92.6(3)
C2-N1-Ru1-N28	58.7(7)	C22-N21-Ru1-N1	8.9(3)
C20-N1-Ru1-N28	-120.5(6)	C26-N21-Ru1-N1	-172.9(2)
C2-N1-Ru1-N4	-0.4(2)	C22-N21-Ru1-Cl1	-85.7(3)
C26-N21-Ru1-Cl1	92.4(2)		

Symmetry transformations used to generate equivalent atoms:

Table 6.21. Hydrogen bonds for **FL389** [Å and °].

D-H...A	d(D-H)	d(H...A)	d(D...A)	<(DHA)
N11-H11...O10#1	0.88	2.05	2.894(4)	159.6
O17-H17...O100#2	0.84	1.96	2.790(4)	169.0
N23-H23A...O100	0.80	2.34	3.054(5)	148.1
N23-H23B...Cl1#3	0.89	2.39	3.271(3)	172.5

Symmetry transformations used to generate equivalent atoms:
#1 -x+1,-y+1,-z #2 x+1,y,z #3 -x+2,-y+2,-z+1

Crystal structure of FL1359.

Table 6.22. Crystal data and structure refinement for **FL1359**.

Identification code	fl1359	
Habitus, colour	prism, red	
Crystal size	0.22 x 0.10 x 0.04 mm^3	
Crystal system	Triclinic	
Space group	P -1	Z = 2
Unit cell dimensions	a = 7.8921(6) Å	α= 103.536(5)°.
	b = 12.7358(8) Å	β= 91.381(6)°.
	c = 17.8734(12) Å	γ = 98.699(6)°.
Volume	1723.2(2) $Å^3$	
Cell determination	7424 peaks with Theta 25 to 1.7°.	
Empirical formula	C_{32} H_{38} N_6 O_5 Ru S_3	
Formula weight	783.93	
Density (calculated)	1.511 Mg/m^3	
Absorption coefficient	0.686 mm^{-1}	
F(000)	808	

Data collection:

Diffractometer type	STOE IPDS2
Wavelength	0.71073 Å
Temperature	100(2) K
Theta range for data collection	1.67 to 25.00°.
Index ranges	-9<=h<=9, -15<=k<=14, -17<=l<=21
Data collection software	STOE X-AREA
Cell refinement software	STOE X-AREA
Data reduction software	STOE X-AREA

Solution and refinement:

Reflections collected	12554
Independent reflections	6038 [R(int) = 0.0656]
Completeness to theta = 25.00°	99.5 %
Observed reflections	3295[I>2(I)]
Reflections used for refinement	6038
Absorption correction	Semi-empirical from equivalents
Max. and min. transmission	0.9645 and 0.9005
Largest diff. peak and hole	0.511 and -0.328 $e.Å^{-3}$
Solution	Direct methods
Refinement	Full-matrix least-squares on F^2
Treatment of hydrogen atoms	C-H geom, N-H located, C-H riding, N-H isotr. ref.
Programs used	SUPERFLIP (Palatinus & Chapuis, 2007)
	SHELXL-97 (Sheldrick, 2008)
	Daimond 3.2 (Crystal Impact)
	STOE IPDS2 software
Data / restraints / parameters	6038 / 0 / 472
Goodness-of-fit on F^2	0.731
R index (all data)	wR2 = 0.0781
R index conventional [I>2sigma(I)]	R1 = 0.0406

Table 6.23. Atomic coordinates and equivalent isotropic displacement parameters ($Å^2$) for **FL1359**. U(eq) is defined as one third of the trace of the orthogonalized U^{ij} tensor.

	x	y	z	U(eq)	Occupancy
C2	0.8809(6)	0.5071(4)	0.1440(3)	0.0372(12)	1
C3	0.8670(6)	0.5930(4)	0.2063(3)	0.0349(12)	1
C5	0.8868(6)	0.6919(4)	0.3234(3)	0.0388(13)	1
C6	0.9170(6)	0.7352(4)	0.4019(3)	0.0455(14)	1
C7	0.8664(7)	0.8327(4)	0.4353(3)	0.0475(14)	1
C8	0.7810(7)	0.8905(4)	0.3916(3)	0.0458(13)	1
C9	0.7443(6)	0.8478(4)	0.3131(3)	0.0418(13)	1
C10	0.7958(6)	0.7496(4)	0.2783(3)	0.0385(12)	1
C11	0.7813(6)	0.6832(4)	0.2015(3)	0.0367(12)	1
C12	0.7156(6)	0.6797(4)	0.1275(3)	0.0387(13)	1
C13	0.6236(6)	0.7610(4)	0.1013(3)	0.0428(13)	1
C15	0.6447(6)	0.6175(5)	-0.0032(3)	0.0446(13)	1
C16	0.7260(6)	0.5949(4)	0.0653(3)	0.0379(13)	1
C17	0.8077(6)	0.5037(4)	0.0698(3)	0.0373(12)	1
C18	0.8264(6)	0.4128(4)	0.0096(3)	0.0451(13)	1
C19	0.9085(6)	0.3328(4)	0.0247(3)	0.0468(14)	1
C20	0.9768(6)	0.3429(4)	0.0989(3)	0.0427(13)	1
C21	0.6814(8)	1.0626(5)	0.3952(3)	0.0614(17)	1
C22	0.8379(9)	1.1187(5)	0.3646(4)	0.083(2)	1
C23	0.6017(10)	1.1406(5)	0.4552(4)	0.089(2)	1
C24	1.3840(6)	0.6440(4)	0.3475(3)	0.0410(12)	1
C25	1.3600(6)	0.5848(4)	0.4117(3)	0.0383(12)	1
C26	1.1761(6)	0.3827(4)	0.4257(3)	0.0402(12)	1
C27	1.2681(7)	0.3143(4)	0.3643(3)	0.0423(14)	1
C28	1.3840(6)	0.3428(4)	0.2188(3)	0.0429(13)	1
C29	1.4668(6)	0.4609(4)	0.2427(3)	0.0413(13)	1
N1	0.9659(5)	0.4270(3)	0.1582(2)	0.0366(11)	1
N4	0.9307(5)	0.5969(3)	0.2781(2)	0.0369(10)	1
N5	0.8212(5)	0.3685(3)	0.2963(3)	0.0442(11)	1
N6	0.7558(5)	0.3957(3)	0.3550(3)	0.0365(10)	1
N7	0.6834(5)	0.4192(4)	0.4119(3)	0.0510(12)	1
N14	0.5883(6)	0.7180(4)	0.0231(3)	0.0493(13)	1
O8	0.7314(5)	0.9845(3)	0.4342(2)	0.0571(10)	1
O13	0.5843(4)	0.8455(3)	0.1383(2)	0.0522(10)	1
O15	0.6266(4)	0.5626(3)	-0.0695(2)	0.0527(10)	1
S1	1.14083(16)	0.51131(11)	0.40486(7)	0.0375(3)	1
S2	1.18563(16)	0.31027(11)	0.26573(7)	0.0394(3)	1
S3	1.31211(16)	0.55703(10)	0.25260(7)	0.0383(3)	1
Ru1	1.05772(6)	0.46219(4)	0.27637(3)	0.03495(13)	1
O100	0.4320(6)	0.8271(4)	-0.0805(3)	0.0845(14)	1
C101	0.3299(8)	0.8855(5)	-0.0891(4)	0.0683(18)	1
C102	0.2635(12)	0.8890(6)	-0.1657(4)	0.118(3)	1
C103	0.2580(12)	0.9563(7)	-0.0232(5)	0.135(3)	1
O200	0.9429(13)	0.1063(7)	0.8658(6)	0.085(4)	0.545(12)
C200	0.855(3)	0.0961(16)	0.8171(10)	0.071(5)	0.545(12)
C20A	0.806(4)	0.068(5)	0.807(3)	0.32(4)	0.455(12)
C201	0.8016(17)	0.1900(11)	0.7935(11)	0.082(5)	0.545(12)
C202	0.770(3)	-0.0162(18)	0.7759(15)	0.160(12)	0.545(12)
O201	0.685(2)	-0.0580(14)	0.7232(10)	0.125(6)	0.455(12)
C203	0.751(2)	0.0339(19)	0.7409(13)	0.089(7)	0.455(12)
C204	0.749(2)	0.099(2)	0.693(2)	0.20(2)	0.455(12)

Table 6.24. Bond lengths [Å] and angles [°] for **FL1359**.

C2-N1	1.370(6)	C26-C27	1.508(6)
C2-C3	1.386(6)	C26-S1	1.822(5)
C2-C17	1.422(6)	C26-H26A	0.9900
C3-N4	1.352(6)	C26-H26B	0.9900
C3-C11	1.437(6)	C27-S2	1.849(5)
C5-C6	1.382(7)	C27-H27A	0.9900
C5-N4	1.387(6)	C27-H27B	0.9900
C5-C10	1.454(6)	C28-C29	1.504(6)
C6-C7	1.367(6)	C28-S2	1.832(5)
C6-H6	0.9500	C28-H28A	0.9900
C7-C8	1.414(6)	C28-H28B	0.9900
C7-H7	0.9500	C29-S3	1.839(4)
C8-O8	1.376(6)	C29-H29A	0.9900
C8-C9	1.386(7)	C29-H29B	0.9900
C9-C10	1.384(6)	N1-Ru1	2.137(4)
C9-H9	0.9500	N4-Ru1	2.109(4)
C10-C11	1.426(6)	N5-N6	1.183(6)
C11-C12	1.397(6)	N5-Ru1	2.143(5)
C12-C16	1.370(6)	N6-N7	1.177(6)
C12-C13	1.503(7)	N14-H14	0.79(5)
C13-O13	1.213(6)	S1-Ru1	2.2863(14)
C13-N14	1.381(6)	S2-Ru1	2.2861(13)
C15-O15	1.219(6)	S3-Ru1	2.2843(15)
C15-N14	1.399(7)	O100-C101	1.206(6)
C15-C16	1.475(7)	C101-C102	1.467(9)
C16-C17	1.428(6)	C101-C103	1.488(9)
C17-C18	1.413(6)	C102-H10A	0.9800
C18-C19	1.360(6)	C102-H10B	0.9800
C18-H18	0.9500	C102-H10C	0.9800
C19-C20	1.391(7)	C103-H10D	0.9800
C19-H19	0.9500	C103-H10E	0.9800
C20-N1	1.334(6)	C103-H10F	0.9800
C20-H20	0.9500	O200-C200	1.072(16)
C21-O8	1.435(6)	C200-C201	1.47(2)
C21-C23	1.502(8)	C200-C202	1.49(3)
C21-C22	1.511(8)	C20A-C203	1.21(4)
C21-H21	1.0000	C20A-H201	0.9800
C22-H22A	0.9800	C20A-H202	0.9800
C22-H22B	0.9800	C20A-H202	0.9800
C22-H22C	0.9800	C201-H20A	0.9800
C23-H23A	0.9800	C201-H20B	0.9800
C23-H23B	0.9800	C201-H20C	0.9800
C23-H23C	0.9800	C202-H20D	0.9800
C24-C25	1.514(6)	C202-H20E	0.9800
C24-S3	1.820(5)	C202-H20F	0.9800
C24-H24A	0.9900	O201-C203	1.17(2)
C24-H24B	0.9900	C203-C204	1.32(3)
C25-S1	1.825(5)	C204-H20G	0.9800
C25-H25A	0.9900	C204-H20H	0.9800
C25-H25B	0.9900	C204-H20I	0.9800
N1-C2-C3	116.6(4)	C6-C5-C10	118.9(4)
N1-C2-C17	122.8(4)	N4-C5-C10	111.8(4)
C3-C2-C17	120.6(4)	C7-C6-C5	119.9(5)
N4-C3-C2	122.1(4)	C7-C6-H6	120.1
N4-C3-C11	114.2(4)	C5-C6-H6	120.1
C2-C3-C11	123.7(5)	C6-C7-C8	121.6(5)
C6-C5-N4	129.3(5)	C6-C7-H7	119.2

C8-C7-H7	119.2	C24-C25-S1	110.1(3)
O8-C8-C9	125.3(4)	C24-C25-H25A	109.6
O8-C8-C7	114.6(5)	S1-C25-H25A	109.6
C9-C8-C7	119.9(5)	C24-C25-H25B	109.6
C10-C9-C8	119.1(4)	S1-C25-H25B	109.6
C10-C9-H9	120.4	H25A-C25-H25B	108.2
C8-C9-H9	120.4	C27-C26-S1	113.4(3)
C9-C10-C11	134.5(5)	C27-C26-H26A	108.9
C9-C10-C5	120.5(5)	S1-C26-H26A	108.9
C11-C10-C5	105.1(4)	C27-C26-H26B	108.9
C12-C11-C10	141.0(4)	S1-C26-H26B	108.9
C12-C11-C3	114.5(4)	H26A-C26-H26B	107.7
C10-C11-C3	104.5(4)	C26-C27-S2	112.5(3)
C16-C12-C11	122.7(4)	C26-C27-H27A	109.1
C16-C12-C13	108.6(4)	S2-C27-H27A	109.1
C11-C12-C13	128.7(5)	C26-C27-H27B	109.1
O13-C13-N14	125.7(5)	S2-C27-H27B	109.1
O13-C13-C12	129.6(5)	H27A-C27-H27B	107.8
N14-C13-C12	104.6(5)	C29-C28-S2	114.5(3)
O15-C15-N14	125.3(5)	C29-C28-H28A	108.6
O15-C15-C16	129.2(5)	S2-C28-H28A	108.6
N14-C15-C16	105.5(5)	C29-C28-H28B	108.6
C12-C16-C17	123.2(4)	S2-C28-H28B	108.6
C12-C16-C15	108.5(4)	H28A-C28-H28B	107.6
C17-C16-C15	128.3(5)	C28-C29-S3	113.5(3)
C18-C17-C2	116.9(4)	C28-C29-H29A	108.9
C18-C17-C16	127.9(5)	S3-C29-H29A	108.9
C2-C17-C16	115.2(4)	C28-C29-H29B	108.9
C19-C18-C17	119.8(5)	S3-C29-H29B	108.9
C19-C18-H18	120.1	H29A-C29-H29B	107.7
C17-C18-H18	120.1	C20-N1-C2	117.0(4)
C18-C19-C20	119.5(5)	C20-N1-Ru1	131.5(3)
C18-C19-H19	120.2	C2-N1-Ru1	111.5(3)
C20-C19-H19	120.2	C3-N4-C5	104.4(4)
N1-C20-C19	124.0(5)	C3-N4-Ru1	110.2(3)
N1-C20-H20	118.0	C5-N4-Ru1	145.4(4)
C19-C20-H20	118.0	N6-N5-Ru1	119.4(3)
O8-C21-C23	104.9(5)	N7-N6-N5	176.7(5)
O8-C21-C22	109.4(5)	C13-N14-C15	112.8(4)
C23-C21-C22	112.4(6)	C13-N14-H14	125(4)
O8-C21-H21	110.0	C15-N14-H14	122(4)
C23-C21-H21	110.0	C8-O8-C21	119.2(4)
C22-C21-H21	110.0	C26-S1-C25	101.6(2)
C21-C22-H22A	109.5	C26-S1-Ru1	103.24(16)
C21-C22-H22B	109.5	C25-S1-Ru1	105.65(16)
H22A-C22-H22B	109.5	C28-S2-C27	102.0(2)
C21-C22-H22C	109.5	C28-S2-Ru1	103.81(15)
H22A-C22-H22C	109.5	C27-S2-Ru1	106.01(16)
H22B-C22-H22C	109.5	C24-S3-C29	99.9(2)
C21-C23-H23A	109.5	C24-S3-Ru1	102.10(17)
C21-C23-H23B	109.5	C29-S3-Ru1	105.83(17)
H23A-C23-H23B	109.5	N4-Ru1-N1	79.61(16)
C21-C23-H23C	109.5	N4-Ru1-N5	89.81(16)
H23A-C23-H23C	109.5	N1-Ru1-N5	87.03(17)
H23B-C23-H23C	109.5	N4-Ru1-S3	91.67(12)
C25-C24-S3	113.4(3)	N1-Ru1-S3	92.16(12)
C25-C24-H24A	108.9	N5-Ru1-S3	178.16(13)
S3-C24-H24A	108.9	N4-Ru1-S2	175.77(13)
C25-C24-H24B	108.9	N1-Ru1-S2	96.27(11)
S3-C24-H24B	108.9	N5-Ru1-S2	89.04(11)
H24A-C24-H24B	107.7	S3-Ru1-S2	89.40(5)

N4-Ru1-S1	95.50(12)	H10E-C103-H10F	109.5
N1-Ru1-S1	175.01(12)	O200-C200-C201	122.0(19)
N5-Ru1-S1	92.00(13)	O200-C200-C202	119.5(18)
S3-Ru1-S1	88.95(5)	C201-C200-C202	118.2(16)
S2-Ru1-S1	88.61(5)	C203-C20A-H201	109.5
O100-C101-C102	122.1(7)	C203-C20A-H202	109.5
O100-C101-C103	122.7(7)	H201-C20A-H202	109.5
C102-C101-C103	115.2(7)	C203-C20A-H202	109.5
C101-C102-H10A	109.5	H201-C20A-H202	109.5
C101-C102-H10B	109.5	H202-C20A-H202	109.5
H10A-C102-H10B	109.5	O201-C203-C20A	116(4)
C101-C102-H10C	109.5	O201-C203-C204	121(3)
H10A-C102-H10C	109.5	C20A-C203-C204	122(4)
H10B-C102-H10C	109.5	C203-C204-H20G	109.5
C101-C103-H10D	109.5	C203-C204-H20H	109.5
C101-C103-H10E	109.5	H20G-C204-H20H	109.5
H10D-C103-H10E	109.5	C203-C204-H20I	109.5
C101-C103-H10F	109.5	H20G-C204-H20I	109.5
H10D-C103-H10F	109.5	H20H-C204-H20I	109.5

Symmetry transformations used to generate equivalent atoms:

Table 6.25. Anisotropic displacement parameters ($Å^2$) for **FL1359**.
The anisotropicdisplacement factor exponent takes the form: $-2\pi^2[h^2a^{*2}U^{11} + ... + 2 h k a^* b^* U^{12}]$

	U^{11}	U^{22}	U^{33}	U^{23}	U^{13}	U^{12}
C2	0.039(3)	0.039(3)	0.037(3)	0.014(3)	0.003(2)	0.008(2)
C3	0.034(3)	0.039(3)	0.036(3)	0.016(3)	0.009(2)	0.008(2)
C5	0.047(3)	0.030(3)	0.039(3)	0.006(2)	0.009(2)	0.006(2)
C6	0.053(3)	0.045(3)	0.043(3)	0.015(3)	0.005(3)	0.015(3)
C7	0.070(4)	0.041(3)	0.036(3)	0.015(3)	0.010(3)	0.014(3)
C8	0.059(3)	0.035(3)	0.046(4)	0.013(3)	0.006(3)	0.012(3)
C9	0.052(3)	0.034(3)	0.044(3)	0.020(3)	0.002(3)	0.007(2)
C10	0.039(3)	0.035(3)	0.046(3)	0.019(3)	0.008(2)	0.008(2)
C11	0.040(3)	0.028(3)	0.044(3)	0.011(3)	0.002(2)	0.008(2)
C12	0.038(3)	0.041(3)	0.042(3)	0.017(3)	0.005(2)	0.006(2)
C13	0.044(3)	0.040(3)	0.046(4)	0.015(3)	-0.002(3)	0.004(3)
C15	0.039(3)	0.052(4)	0.045(4)	0.017(3)	0.000(3)	0.007(3)
C16	0.039(3)	0.044(3)	0.032(3)	0.012(3)	-0.002(2)	0.003(2)
C17	0.032(3)	0.039(3)	0.041(3)	0.012(3)	0.002(2)	0.004(2)
C18	0.040(3)	0.048(3)	0.046(3)	0.011(3)	0.001(2)	0.004(3)
C19	0.051(3)	0.044(3)	0.041(3)	0.002(3)	0.002(3)	0.006(3)
C20	0.039(3)	0.049(3)	0.039(3)	0.006(3)	0.002(2)	0.008(3)
C21	0.084(5)	0.040(3)	0.062(4)	0.009(3)	-0.015(3)	0.025(3)
C22	0.119(6)	0.053(4)	0.076(5)	0.027(4)	-0.015(4)	-0.001(4)
C23	0.134(6)	0.061(4)	0.074(5)	-0.002(4)	-0.014(4)	0.054(4)
C24	0.044(3)	0.038(3)	0.039(3)	0.009(2)	0.001(2)	0.001(2)
C25	0.044(3)	0.037(3)	0.035(3)	0.007(2)	-0.005(2)	0.009(2)
C26	0.045(3)	0.043(3)	0.034(3)	0.012(2)	-0.001(2)	0.006(2)
C27	0.048(3)	0.038(3)	0.043(3)	0.013(3)	-0.009(3)	0.009(3)
C28	0.045(3)	0.047(3)	0.042(3)	0.010(3)	0.004(2)	0.022(3)
C29	0.041(3)	0.045(3)	0.040(3)	0.010(3)	0.003(2)	0.012(3)
N1	0.036(2)	0.035(3)	0.041(3)	0.010(2)	0.005(2)	0.010(2)
N4	0.038(2)	0.035(3)	0.037(3)	0.007(2)	0.005(2)	0.005(2)
N5	0.049(3)	0.035(3)	0.047(3)	0.007(2)	-0.006(2)	0.009(2)
N6	0.036(2)	0.039(3)	0.035(3)	0.012(2)	-0.007(2)	0.0065(19)
N7	0.050(3)	0.065(3)	0.039(3)	0.013(2)	0.002(2)	0.009(2)
N14	0.059(3)	0.052(3)	0.044(3)	0.023(3)	-0.007(2)	0.015(2)
O8	0.089(3)	0.043(2)	0.046(2)	0.0119(19)	0.006(2)	0.030(2)
O13	0.060(2)	0.044(2)	0.056(2)	0.015(2)	-0.0051(19)	0.0153(19)
O15	0.061(2)	0.064(3)	0.034(2)	0.014(2)	-0.0073(18)	0.0095(19)
S1	0.0415(8)	0.0375(8)	0.0356(8)	0.0120(7)	0.0018(6)	0.0080(6)
S2	0.0418(8)	0.0388(8)	0.0384(8)	0.0083(7)	-0.0008(6)	0.0112(6)
S3	0.0419(8)	0.0386(8)	0.0363(8)	0.0112(6)	0.0024(6)	0.0087(6)
Ru1	0.0381(3)	0.0352(3)	0.0333(3)	0.0097(2)	0.00177(19)	0.0090(2)
O100	0.087(3)	0.092(3)	0.087(3)	0.038(3)	-0.011(3)	0.030(3)
C101	0.069(4)	0.056(4)	0.079(5)	0.020(4)	-0.011(4)	0.005(3)
C102	0.191(9)	0.074(5)	0.090(6)	0.029(5)	-0.053(6)	0.021(5)
C103	0.169(9)	0.093(6)	0.121(8)	-0.013(6)	0.060(6)	0.002(6)
O200	0.093(8)	0.090(7)	0.073(7)	0.025(5)	0.024(6)	0.011(5)
C200	0.053(11)	0.112(14)	0.033(8)	-0.001(9)	-0.017(7)	-0.006(9)
C20A	0.057(18)	0.40(7)	0.30(6)	-0.26(5)	-0.07(2)	-0.01(3)
C201	0.053(8)	0.057(8)	0.158(15)	0.054(9)	0.049(9)	0.028(7)
C202	0.21(2)	0.064(12)	0.18(2)	-0.007(14)	-0.13(2)	0.038(13)
O201	0.150(15)	0.109(13)	0.147(16)	0.059(11)	0.022(11)	0.071(11)
C203	0.075(12)	0.084(16)	0.087(15)	-0.025(14)	-0.028(10)	0.026(12)
C204	0.032(9)	0.20(3)	0.46(6)	0.28(4)	0.004(18)	-0.001(12)

Table 6.26. Hydrogen coordinates and isotropic displacement parameters ($Å^2$)for **FL1359**.

	x	y	z	U(eq)	Occupancy
H6	0.9727	0.6974	0.4325	0.055	1
H7	0.8892	0.8622	0.4891	0.057	1
H9	0.6846	0.8853	0.2837	0.050	1
H18	0.7818	0.4076	-0.0412	0.054	1
H19	0.9190	0.2706	-0.0153	0.056	1
H20	1.0348	0.2864	0.1079	0.051	1
H21	0.5947	1.0250	0.3518	0.074	1
H22A	0.9226	1.1546	0.4074	0.124	1
H22B	0.8044	1.1734	0.3392	0.124	1
H22C	0.8881	1.0643	0.3273	0.124	1
H23A	0.5011	1.1007	0.4733	0.133	1
H23B	0.5664	1.1977	0.4328	0.133	1
H23C	0.6856	1.1742	0.4987	0.133	1
H24A	1.5072	0.6740	0.3473	0.049	1
H24B	1.3198	0.7064	0.3581	0.049	1
H25A	1.3834	0.6383	0.4622	0.046	1
H25B	1.4422	0.5326	0.4079	0.046	1
H26A	1.2441	0.3987	0.4755	0.048	1
H26B	1.0636	0.3398	0.4315	0.048	1
H27A	1.2549	0.2387	0.3713	0.051	1
H27B	1.3922	0.3445	0.3703	0.051	1
H28A	1.4672	0.2970	0.2305	0.051	1
H28B	1.3584	0.3229	0.1623	0.051	1
H29A	1.5487	0.4762	0.2041	0.050	1
H29B	1.5331	0.4736	0.2927	0.050	1
H10A	0.3553	0.8822	-0.2016	0.177	1
H10B	0.2225	0.9587	-0.1626	0.177	1
H10C	0.1684	0.8285	-0.1840	0.177	1
H10D	0.2982	0.9420	0.0252	0.203	1
H10E	0.1323	0.9403	-0.0286	0.203	1
H10F	0.2961	1.0334	-0.0227	0.203	1
H201	0.7233	0.0406	0.8410	0.474	0.455(12)
H202	0.8232	0.1482	0.8203	0.474	0.455(12)
H202	0.9154	0.0431	0.8139	0.474	0.455(12)
H20A	0.8524	0.2579	0.8304	0.123	0.545(12)
H20B	0.6762	0.1830	0.7921	0.123	0.545(12)
H20C	0.8408	0.1916	0.7421	0.123	0.545(12)
H20D	0.8318	-0.0423	0.7300	0.241	0.545(12)
H20E	0.6509	-0.0143	0.7604	0.241	0.545(12)
H20F	0.7720	-0.0658	0.8103	0.241	0.545(12)
H20G	0.6669	0.0627	0.6490	0.304	0.455(12)
H20H	0.8638	0.1132	0.6743	0.304	0.455(12)
H20I	0.7143	0.1677	0.7197	0.304	0.455(12)
H14	0.549(6)	0.748(4)	-0.006(3)	0.039(16)	1

Table 6.27. Torsion angles [°] for **FL1359**.

N1-C2-C3-N4	-1.3(7)	C17-C2-N1-C20	-0.6(7)
C17-C2-C3-N4	178.0(5)	C3-C2-N1-Ru1	-1.0(5)
N1-C2-C3-C11	-179.6(5)	C17-C2-N1-Ru1	179.8(4)
C17-C2-C3-C11	-0.4(8)	C2-C3-N4-C5	-178.2(5)
N4-C5-C6-C7	178.2(5)	C11-C3-N4-C5	0.2(6)
C10-C5-C6-C7	-2.2(8)	C2-C3-N4-Ru1	2.9(6)
C5-C6-C7-C8	0.9(8)	C11-C3-N4-Ru1	-178.7(3)
C6-C7-C8-O8	177.1(5)	C6-C5-N4-C3	178.6(5)
C6-C7-C8-C9	1.0(8)	C10-C5-N4-C3	-1.0(5)
O8-C8-C9-C10	-177.1(5)	C6-C5-N4-Ru1	-3.2(10)
C7-C8-C9-C10	-1.5(8)	C10-C5-N4-Ru1	177.2(5)
C8-C9-C10-C11	-179.9(5)	Ru1-N5-N6-N7	166(8)
C8-C9-C10-C5	0.2(7)	O13-C13-N14-C15	-178.0(5)
C6-C5-C10-C9	1.7(7)	C12-C13-N14-C15	1.1(6)
N4-C5-C10-C9	-178.6(5)	O15-C15-N14-C13	178.9(5)
C6-C5-C10-C11	-178.3(5)	C16-C15-N14-C13	-0.7(6)
N4-C5-C10-C11	1.4(5)	C9-C8-O8-C21	-18.8(8)
C9-C10-C11-C12	0.1(11)	C7-C8-O8-C21	165.3(5)
C5-C10-C11-C12	-180.0(6)	C23-C21-O8-C8	168.5(5)
C9-C10-C11-C3	178.9(6)	C22-C21-O8-C8	-70.7(6)
C5-C10-C11-C3	-1.2(5)	C27-C26-S1-C25	-67.1(4)
N4-C3-C11-C12	179.8(4)	C27-C26-S1-Ru1	42.2(4)
C2-C3-C11-C12	-1.7(7)	C24-C25-S1-C26	138.6(3)
N4-C3-C11-C10	0.6(6)	C24-C25-S1-Ru1	31.1(3)
C2-C3-C11-C10	179.1(5)	C29-C28-S2-C27	-74.0(4)
C10-C11-C12-C16	-178.7(6)	C29-C28-S2-Ru1	36.0(4)
C3-C11-C12-C16	2.6(7)	C26-C27-S2-C28	130.8(4)
C10-C11-C12-C13	0.5(10)	C26-C27-S2-Ru1	22.4(4)
C3-C11-C12-C13	-178.3(5)	C25-C24-S3-C29	-65.4(4)
C16-C12-C13-O13	178.0(6)	C25-C24-S3-Ru1	43.3(3)
C11-C12-C13-O13	-1.3(9)	C28-C29-S3-C24	130.2(4)
C16-C12-C13-N14	-1.1(6)	C28-C29-S3-Ru1	24.5(4)
C11-C12-C13-N14	179.7(5)	C3-N4-Ru1-N1	-2.4(3)
C11-C12-C16-C17	-1.4(8)	C5-N4-Ru1-N1	179.5(6)
C13-C12-C16-C17	179.3(5)	C3-N4-Ru1-N5	-89.4(3)
C11-C12-C16-C15	-180.0(5)	C5-N4-Ru1-N5	92.4(6)
C13-C12-C16-C15	0.7(5)	C3-N4-Ru1-S3	89.5(3)
O15-C15-C16-C12	-179.7(6)	C5-N4-Ru1-S3	-88.7(6)
N14-C15-C16-C12	-0.1(5)	C3-N4-Ru1-S2	-15(2)
O15-C15-C16-C17	1.8(9)	C5-N4-Ru1-S2	166.7(14)
N14-C15-C16-C17	-178.6(5)	C3-N4-Ru1-S1	178.6(3)
N1-C2-C17-C18	-0.2(7)	C5-N4-Ru1-S1	0.4(6)
C3-C2-C17-C18	-179.4(5)	C20-N1-Ru1-N4	-177.7(5)
N1-C2-C17-C16	-179.2(5)	C2-N1-Ru1-N4	1.9(3)
C3-C2-C17-C16	1.6(7)	C20-N1-Ru1-N5	-87.4(5)
C12-C16-C17-C18	-179.6(5)	C2-N1-Ru1-N5	92.2(3)
C15-C16-C17-C18	-1.3(9)	C20-N1-Ru1-S3	91.0(5)
C12-C16-C17-C2	-0.8(7)	C2-N1-Ru1-S3	-89.4(3)
C15-C16-C17-C2	177.5(5)	C20-N1-Ru1-S2	1.3(5)
C2-C17-C18-C19	1.3(7)	C2-N1-Ru1-S2	-179.1(3)
C16-C17-C18-C19	-179.9(5)	C20-N1-Ru1-S1	-166.3(12)
C17-C18-C19-C20	-1.6(8)	C2-N1-Ru1-S1	13.3(18)
C18-C19-C20-N1	0.8(8)	N6-N5-Ru1-N4	-64.8(4)
S3-C24-C25-S1	-50.2(4)	N6-N5-Ru1-N1	-144.4(4)
S1-C26-C27-S2	-43.3(5)	N6-N5-Ru1-S3	152(4)
S2-C28-C29-S3	-40.8(5)	N6-N5-Ru1-S2	119.3(4)
C19-C20-N1-C2	0.3(7)	N6-N5-Ru1-S1	30.7(4)
C19-C20-N1-Ru1	179.9(4)	C24-S3-Ru1-N4	78.0(2)
C3-C2-N1-C20	178.7(5)	C29-S3-Ru1-N4	-177.9(2)

C24-S3-Ru1-N1	157.68(19)	C28-S2-Ru1-S3	-15.65(17)
C29-S3-Ru1-N1	-98.2(2)	C27-S2-Ru1-S3	91.38(19)
C24-S3-Ru1-N5	-139(4)	C28-S2-Ru1-S1	-104.61(17)
C29-S3-Ru1-N5	-34(4)	C27-S2-Ru1-S1	2.41(19)
C24-S3-Ru1-S2	-106.07(16)	C26-S1-Ru1-N4	157.7(2)
C29-S3-Ru1-S2	-1.95(17)	C25-S1-Ru1-N4	-96.0(2)
C24-S3-Ru1-S1	-17.45(16)	C26-S1-Ru1-N1	146.4(15)
C29-S3-Ru1-S1	86.68(17)	C25-S1-Ru1-N1	-107.3(15)
C28-S2-Ru1-N4	89.0(18)	C26-S1-Ru1-N5	67.7(2)
C27-S2-Ru1-N4	-163.9(18)	C25-S1-Ru1-N5	174.01(19)
C28-S2-Ru1-N1	76.5(2)	C26-S1-Ru1-S3	-110.72(17)
C27-S2-Ru1-N1	-176.5(2)	C25-S1-Ru1-S3	-4.42(16)
C28-S2-Ru1-N5	163.4(2)	C26-S1-Ru1-S2	-21.30(17)
C27-S2-Ru1-N5	-89.6(2)	C25-S1-Ru1-S2	85.01(16)

Symmetry transformations used to generate equivalent atoms:

Table 6.28. Hydrogen bonds for **FL1359** [Å and °].

D-H...A	d(D-H)	d(H...A)	d(D...A)	<(DHA)
N14-H14...O100	0.79(5)	2.12(5)	2.915(6)	177(5)

Symmetry transformations used to generate equivalent atoms:

Crystal structure of FL626-1.

Table 6.29. Crystal data and structure refinement for **FL626-1**.

Identification code	fl626-1	
Habitus, colour	prism, red	
Crystal size	0.09 x 0.06 x 0.06 mm^3	
Crystal system	Monoclinic	
Space group	P $2_1/n$	Z = 4
Unit cell dimensions	a = 9.2402(8) Å	α= 90°.
	b = 26.2854(16) Å	β= 106.154(7)°.
	c = 15.8451(17) Å	γ = 90°.
Volume	3696.5(6) $Å^3$	
Cell determination	2729 peaks with Theta 1.6 to 22°.	
Empirical formula	C_{33} H_{35} Cl_3 F N_5 O_6 Ru S_3	
Formula weight	920.26	
Density (calculated)	1.654 Mg/m^3	
Absorption coefficient	0.867 mm^{-1}	
F(000)	1872	

Data collection:

Diffractometer type	IPDS2
Wavelength	0.71073 Å
Temperature	100(2) K
Theta range for data collection	1.55 to 25.00°.
Index ranges	-8<=h<=10, -31<=k<=30, -18<=l<=18
Data collection software	STOE WinXpose (X-Area)
Cell refinement software	STOE WinCell (X-Area)
Data reduction software	STOE WinIntegrate (X-Area)

Solution and refinement:

Reflections collected	18101
Independent reflections	6489 [R(int) = 0.2282]
Completeness to theta = 25.00°	99.8 %
Observed reflections	1531[I>2(I)]
Reflections used for refinement	6489
Absorption correction	Semi-empirical from equivalents
Max. and min. transmission	0.9544 and 0.9263
Largest diff. peak and hole	0.389 and -0.315 $e.Å^{-3}$
Solution	Direct methods
Refinement	Full-matrix least-squares on F^2
Treatment of hydrogen atoms	Calculated positions, riding model
Programs used	SIR92 (Giacovazzo et al, 1993)
	SHELXL-97 (Sheldrick, 2008)
	Diamond 3.1, STOE IPDS2 software
Data / restraints / parameters	6489 / 0 / 474
Goodness-of-fit on F^2	0.581
R index (all data)	wR2 = 0.1197
R index conventional [I>2sigma(I)]	R1 = 0.0539

Table 6.30. Atomic coordinates and equivalent isotropic displacement parameters ($Å^2$) for **FL626-1**. U(eq) is defined as one third of the trace of the orthogonalized U^{ij} tensor.

	x	y	z	U(eq)	Occupancy
C1	0.2177(16)	-0.0392(5)	0.7611(9)	0.046(4)	1
C2	0.3246(13)	-0.0039(5)	0.8082(8)	0.039(3)	1
C3	0.4348(16)	0.0680(6)	0.8507(8)	0.052(4)	1
C4	0.4756(16)	0.1181(5)	0.8632(8)	0.054(4)	1
C5	0.6204(15)	0.1296(5)	0.9242(7)	0.041(3)	1
C6	0.7119(13)	0.0921(5)	0.9675(8)	0.041(4)	1
C7	0.6730(16)	0.0420(5)	0.9508(8)	0.046(4)	1
C8	0.5384(15)	0.0292(5)	0.8976(8)	0.045(4)	1
C9	0.4613(16)	-0.0167(5)	0.8668(9)	0.050(4)	1
C10	0.4862(15)	-0.0698(5)	0.8828(8)	0.049(4)	1
C11	0.6144(19)	-0.0964(6)	0.9390(10)	0.057(4)	1
C12	0.439(2)	-0.1554(5)	0.8711(9)	0.061(4)	1
C13	0.3799(17)	-0.1044(5)	0.8398(9)	0.046(4)	1
C14	0.2445(16)	-0.0919(5)	0.7766(10)	0.048(4)	1
C15	0.1362(16)	-0.1247(5)	0.7282(8)	0.049(4)	1
C16	0.0096(15)	-0.1031(5)	0.6663(9)	0.053(4)	1
C17	-0.0105(17)	-0.0534(5)	0.6523(9)	0.054(4)	1
C18	0.9515(14)	0.0687(5)	1.0647(8)	0.059(4)	1
C19	-0.2306(15)	0.0619(6)	0.7456(9)	0.074(4)	1
C20	-0.2729(14)	0.0787(5)	0.6592(9)	0.064(4)	1
C21	-0.1486(14)	0.1190(5)	0.5267(8)	0.050(4)	1
C22	-0.1127(14)	0.1707(4)	0.5707(8)	0.046(4)	1
C23	0.0472(15)	0.1819(5)	0.6224(8)	0.057(4)	1
C24	0.0018(15)	0.1684(4)	0.7868(7)	0.047(4)	1
C25	-0.0086(14)	0.1259(4)	0.8526(8)	0.045(3)	1
C26	-0.0967(15)	0.2284(4)	0.4483(8)	0.050(4)	1
C27	-0.2967(16)	0.2402(5)	0.5187(8)	0.045(3)	1
C28	-0.4940(17)	0.2473(5)	0.5918(9)	0.055(4)	1
C29	-0.6266(17)	0.2484(5)	0.5156(11)	0.084(5)	1
C30	-0.5238(19)	0.2112(5)	0.6622(11)	0.085(5)	1
C31	-0.437(2)	0.2964(6)	0.6362(10)	0.096(6)	1
C100	0.5864(15)	-0.0961(6)	0.6544(9)	0.081(5)	1
C201	0.273(2)	0.0686(9)	0.5714(11)	0.058(6)	1
N1	0.0933(15)	-0.0195(4)	0.7002(8)	0.053(3)	1
N2	0.3044(13)	0.0475(4)	0.7974(7)	0.055(3)	1
N3	0.5809(14)	-0.1477(4)	0.9273(7)	0.053(3)	1
N4	-0.1753(13)	0.2129(4)	0.5125(7)	0.048(3)	1
N200	0.2154(18)	0.0626(7)	0.6084(9)	0.067(5)	1
O1	-0.3353(11)	0.2794(3)	0.4748(6)	0.060(3)	1
O2	-0.3661(11)	0.2201(3)	0.5740(6)	0.060(3)	1
O4	0.8450(10)	0.1099(3)	1.0234(6)	0.066(3)	1
O5	0.7303(12)	-0.0792(3)	0.9881(6)	0.060(3)	1
O6	0.3821(11)	-0.1984(4)	0.8484(6)	0.069(3)	1
O200	0.3721(14)	0.0776(6)	0.5206(8)	0.142(6)	1
F1	-0.0965(8)	-0.1341(2)	0.6178(5)	0.063(2)	1
S1	-0.0322(4)	0.06281(15)	0.8073(2)	0.0497(9)	1
S2	-0.1294(4)	0.06492(14)	0.5979(2)	0.0549(9)	1
S3	0.1259(4)	0.14796(12)	0.7220(2)	0.0503(10)	1
Ru1	0.09698(13)	0.06189(4)	0.70318(7)	0.0426(3)	1
Cl1	0.4499(5)	-0.04729(13)	0.6293(3)	0.0745(12)	1
Cl2	0.4928(5)	-0.15697(14)	0.6581(3)	0.0756(11)	1
Cl3	0.7187(4)	-0.08713(15)	0.7524(2)	0.0720(12)	1

Table 6.31. Bond lengths [Å] and angles [°] for **FL626-1**.

C1-N1	1.380(15)	C21-H21B	0.9900
C1-C2	1.410(16)	C22-N4	1.456(13)
C1-C14	1.416(15)	C22-C23	1.505(15)
C2-N2	1.368(14)	C22-H22	1.0000
C2-C9	1.386(16)	C23-S3	1.782(12)
C3-C4	1.369(17)	C23-H23A	0.9900
C3-N2	1.374(15)	C23-H23B	0.9900
C3-C8	1.453(17)	C24-C25	1.549(14)
C4-C5	1.447(16)	C24-S3	1.820(13)
C4-H4	0.9500	C24-H24A	0.9900
C5-C6	1.354(16)	C24-H24B	0.9900
C5-H5	0.9500	C25-S1	1.797(11)
C6-C7	1.373(15)	C25-H25A	0.9900
C6-O4	1.382(13)	C25-H25B	0.9900
C7-C8	1.337(17)	C26-N4	1.463(15)
C7-H7	0.9500	C26-H26A	0.9800
C8-C9	1.416(17)	C26-H26B	0.9800
C9-C10	1.426(17)	C26-H26C	0.9800
C10-C13	1.373(18)	C27-O1	1.239(14)
C10-C11	1.448(19)	C27-O2	1.332(14)
C11-O5	1.222(14)	C27-N4	1.358(16)
C11-N3	1.383(17)	C28-C29	1.462(18)
C12-O6	1.257(15)	C28-O2	1.475(16)
C12-N3	1.378(17)	C28-C31	1.494(18)
C12-C13	1.480(18)	C28-C30	1.547(18)
C13-C14	1.406(18)	C29-H29A	0.9800
C14-C15	1.380(17)	C29-H29B	0.9800
C15-C16	1.419(16)	C29-H29C	0.9800
C15-H15	0.9500	C30-H30A	0.9800
C16-C17	1.329(16)	C30-H30B	0.9800
C16-F1	1.339(13)	C30-H30C	0.9800
C17-N1	1.374(16)	C31-H31A	0.9800
C17-H17	0.9500	C31-H31B	0.9800
C18-O4	1.486(13)	C31-H31C	0.9800
C18-H18A	0.9800	C100-Cl3	1.704(14)
C18-H18B	0.9800	C100-Cl1	1.766(14)
C18-H18C	0.9800	C100-Cl2	1.827(16)
C19-C20	1.388(15)	C100-H100	1.0000
C19-S1	1.822(13)	C201-N200	0.910(18)
C19-H19A	0.9900	C201-O200	1.395(19)
C19-H19B	0.9900	N1-Ru1	2.140(10)
C20-S2	1.884(13)	N2-Ru1	2.110(11)
C20-H20A	0.9900	N3-H3	0.8800
C20-H20B	0.9900	N200-Ru1	2.090(15)
C21-C22	1.521(15)	S1-Ru1	2.290(4)
C21-S2	1.793(12)	S2-Ru1	2.285(3)
C21-H21A	0.9900	S3-Ru1	2.288(3)
C21-H21B	0.9900		

N1-C1-C2	116.5(11)	C5-C4-H4	121.2
N1-C1-C14	124.1(13)	C6-C5-C4	121.1(12)
C2-C1-C14	119.3(13)	C6-C5-H5	119.4
N2-C2-C9	113.0(12)	C4-C5-H5	119.4
N2-C2-C1	122.3(11)	C5-C6-C7	120.5(12)
C9-C2-C1	124.7(12)	C5-C6-O4	113.5(12)
C4-C3-N2	128.6(13)	C7-C6-O4	125.9(13)
C4-C3-C8	119.0(13)	C8-C7-C6	120.7(13)
N2-C3-C8	112.4(13)	C8-C7-H7	119.6
C3-C4-C5	117.6(12)	C6-C7-H7	119.6
C3-C4-H4	121.2	C7-C8-C9	136.2(13)

C7-C8-C3	120.7(14)	S3-C23-H23A	107.6
C9-C8-C3	103.0(11)	C22-C23-H23B	107.6
C2-C9-C8	107.5(11)	S3-C23-H23B	107.6
C2-C9-C10	115.4(12)	H23A-C23-H23B	107.0
C8-C9-C10	137.0(13)	C25-C24-S3	109.5(8)
C13-C10-C9	120.2(13)	C25-C24-H24A	109.8
C13-C10-C11	109.6(13)	S3-C24-H24A	109.8
C9-C10-C11	130.2(14)	C25-C24-H24B	109.8
O5-C11-N3	124.7(16)	S3-C24-H24B	109.8
O5-C11-C10	129.4(15)	H24A-C24-H24B	108.2
N3-C11-C10	105.9(14)	C24-C25-S1	114.9(8)
O6-C12-N3	124.4(14)	C24-C25-H25A	108.5
O6-C12-C13	129.1(16)	S1-C25-H25A	108.5
N3-C12-C13	106.3(13)	C24-C25-H25B	108.5
C10-C13-C14	124.8(13)	S1-C25-H25B	108.5
C10-C13-C12	106.6(13)	H25A-C25-H25B	107.5
C14-C13-C12	128.6(14)	N4-C26-H26A	109.5
C15-C14-C13	127.9(13)	N4-C26-H26B	109.5
C15-C14-C1	116.7(14)	H26A-C26-H26B	109.5
C13-C14-C1	115.5(13)	N4-C26-H26C	109.5
C14-C15-C16	117.8(12)	H26A-C26-H26C	109.5
C14-C15-H15	121.1	H26B-C26-H26C	109.5
C16-C15-H15	121.1	O1-C27-O2	125.7(15)
C17-C16-F1	117.0(13)	O1-C27-N4	120.9(14)
C17-C16-C15	123.9(13)	O2-C27-N4	113.3(12)
F1-C16-C15	119.0(12)	C29-C28-O2	112.5(12)
C16-C17-N1	120.1(14)	C29-C28-C31	118.4(13)
C16-C17-H17	119.9	O2-C28-C31	108.3(12)
N1-C17-H17	119.9	C29-C28-C30	109.4(13)
O4-C18-H18A	109.5	O2-C28-C30	98.8(11)
O4-C18-H18B	109.5	C31-C28-C30	107.5(13)
H18A-C18-H18B	109.5	C28-C29-H29A	109.5
O4-C18-H18C	109.5	C28-C29-H29B	109.5
H18A-C18-H18C	109.5	H29A-C29-H29B	109.5
H18B-C18-H18C	109.5	C28-C29-H29C	109.5
C20-C19-S1	119.3(10)	H29A-C29-H29C	109.5
C20-C19-H19A	107.5	H29B-C29-H29C	109.5
S1-C19-H19A	107.5	C28-C30-H30A	109.5
C20-C19-H19B	107.5	C28-C30-H30B	109.5
S1-C19-H19B	107.5	H30A-C30-H30B	109.5
H19A-C19-H19B	107.0	C28-C30-H30C	109.5
C19-C20-S2	113.7(9)	H30A-C30-H30C	109.5
C19-C20-H20A	108.8	H30B-C30-H30C	109.5
S2-C20-H20A	108.8	C28-C31-H31A	109.5
C19-C20-H20B	108.8	C28-C31-H31B	109.5
S2-C20-H20B	108.8	H31A-C31-H31B	109.5
H20A-C20-H20B	107.7	C28-C31-H31C	109.5
C22-C21-S2	116.7(8)	H31A-C31-H31C	109.5
C22-C21-H21A	108.1	H31B-C31-H31C	109.5
S2-C21-H21A	108.1	Cl3-C100-Cl1	113.0(9)
C22-C21-H21B	108.1	Cl3-C100-Cl2	108.6(8)
S2-C21-H21B	108.1	Cl1-C100-Cl2	109.2(7)
H21A-C21-H21B	107.3	Cl3-C100-H100	108.7
N4-C22-C23	110.7(10)	Cl1-C100-H100	108.7
N4-C22-C21	113.1(10)	Cl2-C100-H100	108.7
C23-C22-C21	118.6(10)	N200-C201-O200	175(3)
N4-C22-H22	104.2	C17-N1-C1	117.4(11)
C23-C22-H22	104.2	C17-N1-Ru1	131.7(9)
C21-C22-H22	104.2	C1-N1-Ru1	110.8(9)
C22-C23-S3	118.8(10)	C2-N2-C3	104.1(11)
C22-C23-H23A	107.6	C2-N2-Ru1	109.3(8)

C3-N2-Ru1	146.5(9)	C23-S3-Ru1	112.0(4)
C12-N3-C11	111.5(12)	C24-S3-Ru1	107.3(4)
C12-N3-H3	124.3	N200-Ru1-N2	87.5(5)
C11-N3-H3	124.3	N200-Ru1-N1	90.1(6)
C27-N4-C22	123.2(12)	N2-Ru1-N1	80.9(4)
C27-N4-C26	118.9(11)	N200-Ru1-S2	91.8(4)
C22-N4-C26	117.8(11)	N2-Ru1-S2	171.6(3)
C201-N200-Ru1	169(3)	N1-Ru1-S2	90.7(4)
C27-O2-C28	119.5(11)	N200-Ru1-S3	91.1(5)
C6-O4-C18	113.5(10)	N2-Ru1-S3	92.0(3)
C25-S1-C19	102.7(7)	N1-Ru1-S3	172.8(4)
C25-S1-Ru1	105.5(4)	S2-Ru1-S3	96.36(14)
C19-S1-Ru1	105.2(5)	N200-Ru1-S1	178.9(5)
C21-S2-C20	102.2(6)	N2-Ru1-S1	92.6(3)
C21-S2-Ru1	113.4(4)	N1-Ru1-S1	91.0(4)
C20-S2-Ru1	105.2(4)	S2-Ru1-S1	88.34(14)
C23-S3-C24	100.7(6)	S3-Ru1-S1	87.77(16)

Symmetry transformations used to generate equivalent atoms:

Table 6.32. Anisotropic displacement parameters ($Å^2$) for **FL626-1**.
The anisotropicdisplacement factor exponent takes the form: $-2\pi^2[h^2a^{*2}U^{11} + ... + 2 h k a^* b^* U^{12}]$

	U^{11}	U^{22}	U^{33}	U^{23}	U^{13}	U^{12}
C1	0.037(9)	0.036(8)	0.059(9)	0.016(7)	0.001(7)	0.000(7)
C2	0.017(8)	0.051(8)	0.049(8)	0.015(7)	0.011(6)	0.018(7)
C3	0.042(9)	0.061(10)	0.052(8)	-0.007(9)	0.013(7)	-0.004(9)
C4	0.042(10)	0.059(10)	0.056(9)	0.013(8)	0.005(7)	-0.002(8)
C5	0.054(10)	0.037(7)	0.044(8)	-0.001(6)	0.035(7)	0.009(7)
C6	0.010(7)	0.064(10)	0.045(8)	-0.014(7)	0.002(6)	-0.018(7)
C7	0.040(9)	0.044(8)	0.046(8)	-0.009(7)	-0.001(7)	-0.004(7)
C8	0.028(8)	0.073(10)	0.034(8)	0.006(7)	0.007(6)	0.010(8)
C9	0.049(10)	0.037(8)	0.068(10)	0.001(7)	0.024(8)	0.013(7)
C10	0.035(8)	0.055(10)	0.055(8)	0.011(8)	0.012(7)	0.009(8)
C11	0.065(12)	0.061(11)	0.054(10)	-0.016(8)	0.033(9)	-0.002(9)
C12	0.105(15)	0.043(9)	0.052(10)	0.001(8)	0.049(10)	-0.003(10)
C13	0.047(10)	0.041(8)	0.062(9)	0.004(8)	0.032(8)	0.011(8)
C14	0.028(9)	0.031(8)	0.091(11)	0.000(8)	0.025(8)	-0.002(7)
C15	0.050(10)	0.046(8)	0.062(10)	0.011(7)	0.036(8)	0.012(8)
C16	0.034(9)	0.047(8)	0.070(10)	-0.020(8)	0.004(7)	-0.003(8)
C17	0.069(10)	0.034(8)	0.070(9)	0.001(8)	0.037(8)	0.006(8)
C18	0.050(9)	0.048(8)	0.062(8)	0.005(8)	-0.014(7)	0.019(8)
C19	0.056(10)	0.066(9)	0.099(12)	-0.021(11)	0.022(9)	-0.017(10)
C20	0.036(9)	0.065(10)	0.089(11)	0.044(8)	0.015(8)	0.013(7)
C21	0.033(9)	0.081(11)	0.037(7)	-0.005(7)	0.009(6)	0.002(7)
C22	0.027(8)	0.040(7)	0.061(9)	0.013(7)	-0.009(7)	0.007(6)
C23	0.049(10)	0.050(8)	0.075(10)	-0.005(7)	0.022(8)	0.004(8)
C24	0.055(10)	0.037(7)	0.046(8)	0.013(6)	0.009(7)	0.003(7)
C25	0.031(8)	0.063(8)	0.043(8)	-0.015(7)	0.014(6)	0.012(7)
C26	0.066(11)	0.035(7)	0.053(9)	0.011(6)	0.022(8)	0.007(7)
C27	0.032(9)	0.048(9)	0.046(9)	0.001(7)	-0.003(7)	-0.008(8)
C28	0.050(11)	0.052(9)	0.065(10)	0.003(8)	0.020(8)	-0.002(8)
C29	0.056(12)	0.064(10)	0.128(14)	0.015(10)	0.021(10)	0.014(9)
C30	0.058(11)	0.077(11)	0.135(15)	0.019(11)	0.048(11)	0.002(10)
C31	0.105(16)	0.096(14)	0.102(14)	-0.003(11)	0.055(12)	0.007(12)
C100	0.039(10)	0.123(14)	0.083(11)	0.006(10)	0.022(9)	0.020(10)
C201	0.070(15)	0.062(12)	0.037(11)	0.008(10)	0.007(8)	0.024(12)
N1	0.043(8)	0.050(7)	0.065(8)	0.000(7)	0.010(6)	0.003(7)
N2	0.048(8)	0.027(6)	0.089(9)	0.004(6)	0.016(7)	0.007(5)
N3	0.056(9)	0.043(7)	0.059(8)	0.021(6)	0.012(6)	0.023(7)
N4	0.043(8)	0.036(7)	0.053(8)	0.005(5)	-0.006(6)	0.004(6)
N200	0.066(12)	0.037(7)	0.080(12)	0.002(10)	-0.009(8)	0.007(9)
O1	0.051(7)	0.025(5)	0.088(7)	-0.001(5)	-0.010(5)	0.011(5)
O2	0.041(6)	0.044(6)	0.097(8)	-0.004(5)	0.024(6)	0.001(5)
O4	0.040(7)	0.058(6)	0.092(7)	0.007(6)	0.004(5)	-0.011(6)
O5	0.069(7)	0.062(7)	0.055(6)	0.019(5)	0.026(5)	0.029(6)
O6	0.071(8)	0.051(6)	0.089(7)	0.014(6)	0.029(6)	0.004(6)
O200	0.076(10)	0.225(18)	0.118(10)	0.051(11)	0.017(8)	0.052(11)
F1	0.053(5)	0.040(4)	0.082(5)	-0.009(4)	-0.005(4)	-0.006(4)
S1	0.038(2)	0.0402(19)	0.073(2)	-0.008(2)	0.0179(18)	0.0028(19)
S2	0.046(2)	0.0364(18)	0.073(2)	0.003(2)	0.0006(18)	-0.001(2)
S3	0.037(2)	0.0347(18)	0.068(3)	0.0039(18)	-0.0037(19)	-0.0014(17)
Ru1	0.0347(7)	0.0330(6)	0.0573(7)	0.0057(7)	0.0082(5)	0.0034(7)
Cl1	0.061(3)	0.056(2)	0.098(3)	-0.005(2)	0.008(2)	0.0010(19)
Cl2	0.061(3)	0.068(2)	0.095(3)	-0.007(2)	0.017(2)	-0.004(2)
Cl3	0.053(3)	0.092(3)	0.071(3)	-0.009(2)	0.016(2)	-0.007(2)

Table 6.33. Hydrogen coordinates and isotropic displacement parameters ($Å^2$)for **FL626-1**.

	x	y	z	U(eq)	Occupancy
H4	0.4112	0.1444	0.8330	0.065	1
H5	0.6517	0.1640	0.9339	0.049	1
H7	0.7426	0.0161	0.9773	0.055	1
H15	0.1460	-0.1605	0.7361	0.058	1
H17	-0.0968	-0.0414	0.6090	0.065	1
H18A	0.9132	0.0509	1.1084	0.089	1
H18B	1.0503	0.0834	1.0934	0.089	1
H18C	0.9611	0.0446	1.0194	0.089	1
H19A	-0.2666	0.0264	0.7458	0.089	1
H19B	-0.2860	0.0826	0.7786	0.089	1
H20A	-0.2903	0.1159	0.6588	0.077	1
H20B	-0.3693	0.0623	0.6279	0.077	1
H21A	-0.0820	0.1139	0.4881	0.060	1
H21B	-0.2535	0.1199	0.4885	0.060	1
H22	-0.1702	0.1712	0.6156	0.056	1
H23A	0.0538	0.2186	0.6366	0.069	1
H23B	0.1123	0.1757	0.5833	0.069	1
H24A	0.0416	0.1999	0.8192	0.056	1
H24B	-0.0997	0.1758	0.7475	0.056	1
H25A	-0.0944	0.1336	0.8765	0.054	1
H25B	0.0843	0.1267	0.9022	0.054	1
H26A	-0.1689	0.2436	0.3971	0.075	1
H26B	-0.0495	0.1986	0.4298	0.075	1
H26C	-0.0189	0.2535	0.4750	0.075	1
H29A	-0.6064	0.2703	0.4700	0.125	1
H29B	-0.7128	0.2619	0.5331	0.125	1
H29C	-0.6494	0.2139	0.4925	0.125	1
H30A	-0.5362	0.1763	0.6394	0.128	1
H30B	-0.6157	0.2218	0.6767	0.128	1
H30C	-0.4384	0.2125	0.7152	0.128	1
H31A	-0.3320	0.2923	0.6711	0.143	1
H31B	-0.4987	0.3063	0.6748	0.143	1
H31C	-0.4431	0.3229	0.5917	0.143	1
H100	0.6382	-0.0976	0.6068	0.097	1
H3	0.6424	-0.1723	0.9526	0.064	1

Table 6.34. Torsion angles [°] for **FL626-1**.

N1-C1-C2-N2	3(2)	C21-C22-C23-S3	-68.0(15)
C14-C1-C2-N2	-178.8(13)	S3-C24-C25-S1	-44.3(11)
N1-C1-C2-C9	-174.9(14)	C16-C17-N1-C1	1(2)
C14-C1-C2-C9	4(2)	C16-C17-N1-Ru1	-176.1(11)
N2-C3-C4-C5	179.5(13)	C2-C1-N1-C17	178.6(12)
C8-C3-C4-C5	-0.9(19)	C14-C1-N1-C17	0(2)
C3-C4-C5-C6	-0.3(19)	C2-C1-N1-Ru1	-3.7(16)
C4-C5-C6-C7	4(2)	C14-C1-N1-Ru1	177.9(12)
C4-C5-C6-O4	-179.6(11)	C9-C2-N2-C3	0.7(16)
C5-C6-C7-C8	-6(2)	C1-C2-N2-C3	-177.0(13)
O4-C6-C7-C8	177.6(12)	C9-C2-N2-Ru1	177.7(9)
C6-C7-C8-C9	-179.4(15)	C1-C2-N2-Ru1	-0.1(16)
C6-C7-C8-C3	5(2)	C4-C3-N2-C2	178.3(14)
C4-C3-C8-C7	-1.5(19)	C8-C3-N2-C2	-1.3(15)
N2-C3-C8-C7	178.2(13)	C4-C3-N2-Ru1	4(3)
C4-C3-C8-C9	-178.4(13)	C8-C3-N2-Ru1	-176.1(13)
N2-C3-C8-C9	1.3(14)	O6-C12-N3-C11	179.0(13)
N2-C2-C9-C8	0.0(16)	C13-C12-N3-C11	3.5(15)
C1-C2-C9-C8	177.7(13)	O5-C11-N3-C12	177.2(13)
N2-C2-C9-C10	178.0(12)	C10-C11-N3-C12	-2.5(15)
C1-C2-C9-C10	-4(2)	O1-C27-N4-C22	171.3(11)
C7-C8-C9-C2	-176.9(16)	O2-C27-N4-C22	-9.5(17)
C3-C8-C9-C2	-0.8(14)	O1-C27-N4-C26	-4.4(18)
C7-C8-C9-C10	6(3)	O2-C27-N4-C26	174.8(10)
C3-C8-C9-C10	-178.0(16)	C23-C22-N4-C27	-118.2(14)
C2-C9-C10-C13	1.5(19)	C21-C22-N4-C27	106.0(14)
C8-C9-C10-C13	178.6(16)	C23-C22-N4-C26	57.6(15)
C2-C9-C10-C11	179.8(13)	C21-C22-N4-C26	-78.3(14)
C8-C9-C10-C11	-3(3)	O200-C201-N200-Ru1	63(49)
C13-C10-C11-O5	-179.3(14)	O1-C27-O2-C28	-4.8(19)
C9-C10-C11-O5	2(2)	N4-C27-O2-C28	176.1(10)
C13-C10-C11-N3	0.4(15)	C29-C28-O2-C27	68.5(15)
C9-C10-C11-N3	-178.0(13)	C31-C28-O2-C27	-64.2(15)
C9-C10-C13-C14	2(2)	C30-C28-O2-C27	-176.1(11)
C11-C10-C13-C14	-176.6(13)	C5-C6-O4-C18	-174.6(11)
C9-C10-C13-C12	-179.8(12)	C7-C6-O4-C18	1.8(19)
C11-C10-C13-C12	1.7(15)	C24-C25-S1-C19	-76.8(10)
O6-C12-C13-C10	-178.3(15)	C24-C25-S1-Ru1	33.1(10)
N3-C12-C13-C10	-3.1(15)	C20-C19-S1-C25	87.4(13)
O6-C12-C13-C14	0(2)	C20-C19-S1-Ru1	-22.8(14)
N3-C12-C13-C14	175.0(14)	C22-C21-S2-C20	62.1(11)
C10-C13-C14-C15	176.9(14)	C22-C21-S2-Ru1	-50.6(10)
C12-C13-C14-C15	-1(2)	C19-C20-S2-C21	-145.8(11)
C10-C13-C14-C1	-3(2)	C19-C20-S2-Ru1	-27.1(12)
C12-C13-C14-C1	179.4(13)	C22-C23-S3-C24	-62.2(11)
N1-C1-C14-C15	-1(2)	C22-C23-S3-Ru1	51.5(11)
C2-C1-C14-C15	-179.7(12)	C25-C24-S3-C23	150.7(9)
N1-C1-C14-C13	178.4(13)	C25-C24-S3-Ru1	33.5(9)
C2-C1-C14-C13	0(2)	C201-N200-Ru1-N2	-73(13)
C13-C14-C15-C16	-178.4(14)	C201-N200-Ru1-N1	-154(13)
C1-C14-C15-C16	1(2)	C201-N200-Ru1-S2	115(13)
C14-C15-C16-C17	0(2)	C201-N200-Ru1-S3	19(13)
C14-C15-C16-F1	179.4(12)	C201-N200-Ru1-S1	20(35)
F1-C16-C17-N1	179.4(12)	C2-N2-Ru1-N200	-92.0(10)
C15-C16-C17-N1	-1(2)	C3-N2-Ru1-N200	82.7(18)
S1-C19-C20-S2	33.6(16)	C2-N2-Ru1-N1	-1.5(9)
S2-C21-C22-N4	-161.4(10)	C3-N2-Ru1-N1	173.2(18)
S2-C21-C22-C23	66.4(15)	C2-N2-Ru1-S2	-7(3)
N4-C22-C23-S3	158.8(9)	C3-N2-Ru1-S2	167.7(14)

C2-N2-Ru1-S3	177.0(8)	C21-S2-Ru1-S1	121.3(5)
C3-N2-Ru1-S3	-8.3(18)	C20-S2-Ru1-S1	10.4(4)
C2-N2-Ru1-S1	89.2(9)	C23-S3-Ru1-N200	58.7(7)
C3-N2-Ru1-S1	-96.2(18)	C24-S3-Ru1-N200	168.3(6)
C17-N1-Ru1-N200	-92.4(13)	C23-S3-Ru1-N2	146.2(6)
C1-N1-Ru1-N200	90.3(11)	C24-S3-Ru1-N2	-104.2(5)
C17-N1-Ru1-N2	-179.9(14)	C23-S3-Ru1-N1	158(3)
C1-N1-Ru1-N2	2.8(10)	C24-S3-Ru1-N1	-92(3)
C17-N1-Ru1-S2	-0.7(13)	C23-S3-Ru1-S2	-33.2(5)
C1-N1-Ru1-S2	-178.0(10)	C24-S3-Ru1-S2	76.4(4)
C17-N1-Ru1-S3	168(2)	C23-S3-Ru1-S1	-121.3(5)
C1-N1-Ru1-S3	-9(4)	C24-S3-Ru1-S1	-11.7(4)
C17-N1-Ru1-S1	87.7(13)	C25-S1-Ru1-N200	-11(23)
C1-N1-Ru1-S1	-89.6(10)	C19-S1-Ru1-N200	98(23)
C21-S2-Ru1-N200	-57.6(7)	C25-S1-Ru1-N2	83.2(5)
C20-S2-Ru1-N200	-168.5(6)	C19-S1-Ru1-N2	-168.7(6)
C21-S2-Ru1-N2	-142(2)	C25-S1-Ru1-N1	164.1(5)
C20-S2-Ru1-N2	107(2)	C19-S1-Ru1-N1	-87.8(7)
C21-S2-Ru1-N1	-147.7(6)	C25-S1-Ru1-S2	-105.2(4)
C20-S2-Ru1-N1	101.4(5)	C19-S1-Ru1-S2	3.0(6)
C21-S2-Ru1-S3	33.7(5)	C25-S1-Ru1-S3	-8.7(4)
C20-S2-Ru1-S3	-77.2(4)	C19-S1-Ru1-S3	99.4(6)

Symmetry transformations used to generate equivalent atoms:

Table 6.35. Hydrogen bonds for **FL626-1** [Å and °].

D-H...A	d(D-H)	d(H...A)	d(D...A)	<(DHA)
N3-H3...O1#1	0.88	2.23	3.094(14)	167.2

Symmetry transformations used to generate equivalent atoms:
#1 -x+1/2,y-1/2,-z+3/2

Crystal structure of FL1473.

Table 6.36. Crystal data and structure refinement for **FL1473**.

Identification code	fl1473	
Habitus, colour	plate, red	
Crystal size	0.30 x 0.12 x 0.03 mm^3	
Crystal system	Triclinic	
Space group	$P\bar{1}$	Z = 2
Unit cell dimensions	a = 7.8245(5) Å	α= 103.037(6)°.
	b = 12.9163(9) Å	β= 92.371(6)°.
	c = 18.1901(13) Å	γ = 98.690(5)°.
Volume	1765.0(2) $Å^3$	
Cell determination	11100 peaks with Theta 1.6 to 25°.	
Empirical formula	$C_{31.50}$ H_{39} N_7 O_5 Ru S_2	
Formula weight	760.89	
Density (calculated)	1.432 Mg/m^3	
Absorption coefficient	0.611 mm^{-1}	
F(000)	786	

Data collection:

Diffractometer type	STOE IPDS2
Wavelength	0.71073 Å
Temperature	100(2) K
Theta range for data collection	1.64 to 25.00°.
Index ranges	-9<=h<=9, -15<=k<=15, -21<=l<=21
Data collection software	STOE X-AREA
Cell refinement software	STOE X-AREA
Data reduction software	STOE X-AREA

Solution and refinement:

Reflections collected	13673
Independent reflections	6203 [R(int) = 0.0638]
Completeness to theta = 25.00°	99.7 %
Observed reflections	4022[I>2(I)]
Reflections used for refinement	6203
Absorption correction	Semi-empirical from equivalents
Max. and min. transmission	0.9876 and 0.8903
Largest diff. peak and hole	0.775 and -0.731 $e.Å^{-3}$
Solution	Direct methods
Refinement	Full-matrix least-squares on F^2
Treatment of hydrogen atoms	CH calc., riding, NH located, isotr. ref.
Programs used	SIR92 (Giacovazzo et al, 1993)
	SHELXL-97 (Sheldrick, 2008)
	DIAMOND 3.2 (Crystal Impcat)
STOE IPDS2 software	
Data / restraints / parameters	6203 / 25 / 461
Goodness-of-fit on F^2	0.862
R index (all data)	wR2 = 0.1043
R index conventional [I>2sigma(I)]	R1 = 0.0459

Table 6.37. Atomic coordinates and equivalent isotropic displacement parameters ($Å^2$) for **FL1473**. U(eq) is defined as one third of the trace of the orthogonalized U^{ij} tensor.

	x	y	z	U(eq)	Occupancy
C2	0.3795(6)	0.5145(4)	0.6495(3)	0.0323(11)	1
C3	0.3665(6)	0.6007(4)	0.7122(3)	0.0301(11)	1
C5	0.3845(6)	0.6971(4)	0.8274(3)	0.0334(11)	1
C6	0.4143(6)	0.7372(4)	0.9052(3)	0.0377(12)	1
C7	0.3598(7)	0.8333(4)	0.9371(3)	0.0452(13)	1
C8	0.2765(7)	0.8902(4)	0.8933(3)	0.0431(13)	1
C9	0.2441(6)	0.8515(4)	0.8155(3)	0.0378(12)	1
C10	0.2971(6)	0.7542(4)	0.7825(3)	0.0308(11)	1
C11	0.2847(6)	0.6900(4)	0.7059(3)	0.0307(11)	1
C12	0.2176(6)	0.6888(4)	0.6333(3)	0.0324(11)	1
C13	0.1245(6)	0.7664(4)	0.6067(3)	0.0387(12)	1
C15	0.1430(6)	0.6263(4)	0.5041(3)	0.0413(12)	1
C16	0.2277(6)	0.6046(4)	0.5719(3)	0.0344(11)	1
C17	0.3077(6)	0.5147(4)	0.5773(3)	0.0341(11)	1
C18	0.3232(6)	0.4239(4)	0.5176(3)	0.0418(13)	1
C19	0.4063(6)	0.3457(4)	0.5341(3)	0.0414(13)	1
C20	0.4733(6)	0.3535(4)	0.6077(3)	0.0376(12)	1
C21	0.1805(9)	1.0612(5)	0.8950(4)	0.0636(17)	1
C22	0.3421(10)	1.1186(5)	0.8640(5)	0.086(2)	1
C23	0.1045(10)	1.1396(5)	0.9535(4)	0.077(2)	1
C24	0.7650(6)	0.3189(4)	0.8657(3)	0.0395(13)	1
C25	0.6717(6)	0.3821(4)	0.9272(3)	0.0372(12)	1
C26	0.8433(6)	0.5885(4)	0.9152(3)	0.0344(11)	1
C27	0.8580(6)	0.6374(4)	0.8471(3)	0.0364(11)	1
C29	0.9446(6)	0.4813(4)	0.7621(3)	0.0375(12)	1
C30	0.8694(6)	0.3635(4)	0.7269(3)	0.0395(12)	1
C31	0.8058(6)	0.6099(4)	0.7127(3)	0.0411(12)	1
N1	0.4653(5)	0.4366(3)	0.6660(2)	0.0329(10)	1
N4	0.4284(5)	0.6029(3)	0.7825(2)	0.0311(10)	1
N5	0.3067(5)	0.3786(3)	0.7955(2)	0.0369(10)	1
N6	0.2456(5)	0.3991(3)	0.8555(3)	0.0359(10)	1
N7	0.1798(5)	0.4168(4)	0.9126(2)	0.0455(11)	1
N14	0.0846(6)	0.7259(4)	0.5293(3)	0.0441(11)	1
N28	0.8061(5)	0.5544(3)	0.7721(2)	0.0330(9)	1
O1	0.0851(5)	0.8504(3)	0.6433(2)	0.0498(9)	1
O2	0.1227(5)	0.5746(3)	0.4395(2)	0.0484(9)	1
O3	0.2304(5)	0.9846(3)	0.9342(2)	0.0525(10)	1
S1	0.67704(16)	0.31788(11)	0.77051(8)	0.0381(3)	1
S2	0.62603(15)	0.50928(10)	0.90970(7)	0.0329(3)	1
Ru1	0.55005(5)	0.46766(4)	0.78292(3)	0.02997(13)	1
O100	-0.0548(15)	0.8326(7)	0.4251(6)	0.147(5)	0.75
C100	-0.124(2)	0.8779(7)	0.3974(6)	0.109(5)	0.75
C101	-0.236(3)	0.9267(14)	0.4492(13)	0.266(16)	0.75
C102	-0.1464(18)	0.8802(7)	0.3226(6)	0.102(4)	0.75
O200	-0.2305(17)	1.0662(8)	0.7744(7)	0.166(5)	0.75
C201	-0.3400(13)	0.8967(9)	0.6837(8)	0.102(4)	0.75
C200	-0.2741(15)	0.9682(10)	0.7630(9)	0.104(4)	0.75
C202	-0.2544(14)	0.9216(9)	0.8272(9)	0.112(5)	0.75
O300	-0.525(4)	0.895(2)	0.574(2)	0.176(16)	0.25
O400	-0.660(4)	0.888(3)	0.3957(17)	0.149(11)	0.25

Table 6.38. Bond lengths [Å] and angles [°] for **FL1473**.

C2-N1	1.369(6)	C25-H25A	0.9900
C2-C17	1.409(7)	C25-H25B	0.9900
C2-C3	1.422(7)	C26-C27	1.513(7)
C3-N4	1.341(6)	C26-S2	1.834(5)
C3-C11	1.425(6)	C26-H26A	0.9900
C5-C6	1.390(7)	C26-H26B	0.9900
C5-N4	1.402(6)	C27-N28	1.529(6)
C5-C10	1.433(7)	C27-H27A	0.9900
C6-C7	1.384(7)	C27-H27B	0.9900
C6-H6	0.9500	C29-C30	1.526(7)
C7-C8	1.401(7)	C29-N28	1.533(6)
C7-H7	0.9500	C29-H29A	0.9900
C8-O3	1.385(6)	C29-H29B	0.9900
C8-C9	1.389(7)	C30-S1	1.812(5)
C9-C10	1.396(6)	C30-H30A	0.9900
C9-H9	0.9500	C30-H30B	0.9900
C10-C11	1.443(7)	C31-N28	1.424(6)
C11-C12	1.395(7)	C31-H31A	0.9800
C12-C16	1.386(7)	C31-H31B	0.9800
C12-C13	1.477(7)	C31-H31C	0.9800
C13-O1	1.228(6)	N1-Ru1	2.132(4)
C13-N14	1.392(7)	N4-Ru1	2.113(4)
C15-O2	1.204(6)	N5-N6	1.200(6)
C15-N14	1.416(7)	N5-Ru1	2.120(4)
C15-C16	1.478(7)	N6-N7	1.170(6)
C16-C17	1.420(7)	N14-H14	1.07(7)
C17-C18	1.430(7)	N28-Ru1	2.183(4)
C18-C19	1.362(7)	S1-Ru1	2.2767(14)
C18-H18	0.9500	S2-Ru1	2.2785(14)
C19-C20	1.395(7)	O100-C100	1.048(13)
C19-H19	0.9500	C100-C102	1.371(12)
C20-N1	1.338(6)	C100-C101	1.423(17)
C20-H20	0.9500	C101-H10A	0.9800
C21-O3	1.432(7)	C101-H10B	0.9800
C21-C23	1.504(8)	C101-H10C	0.9800
C21-C22	1.558(10)	C102-H10D	0.9800
C21-H21	1.0000	C102-H10E	0.9800
C22-H22A	0.9800	C102-H10F	0.9800
C22-H22B	0.9800	O200-C200	1.228(14)
C22-H22C	0.9800	C201-C200	1.548(18)
C23-H23A	0.9800	C201-H20A	0.9800
C23-H23B	0.9800	C201-H20B	0.9800
C23-H23C	0.9800	C201-H20C	0.9800
C24-C25	1.513(7)	C200-C202	1.441(17)
C24-S1	1.833(5)	C202-H20D	0.9800
C24-H24A	0.9900	C202-H20E	0.9800
C24-H24B	0.9900	C202-H20F	0.9800
C25-S2	1.825(5)		

N1-C2-C17	125.2(4)	C7-C6-H6	120.9
N1-C2-C3	115.0(5)	C5-C6-H6	120.9
C17-C2-C3	119.7(4)	C6-C7-C8	122.0(5)
N4-C3-C2	122.1(4)	C6-C7-H7	119.0
N4-C3-C11	114.8(4)	C8-C7-H7	119.0
C2-C3-C11	123.1(5)	O3-C8-C9	124.6(5)
C6-C5-N4	128.7(5)	O3-C8-C7	114.5(5)
C6-C5-C10	120.0(4)	C9-C8-C7	120.9(5)
N4-C5-C10	111.3(4)	C8-C9-C10	117.9(5)
C7-C6-C5	118.2(5)	C8-C9-H9	121.1

C10-C9-H9	121.1	C27-C26-S2	108.8(3)
C9-C10-C5	121.0(5)	C27-C26-H26A	109.9
C9-C10-C11	133.5(5)	S2-C26-H26A	109.9
C5-C10-C11	105.6(4)	C27-C26-H26B	109.9
C12-C11-C3	115.8(4)	S2-C26-H26B	109.9
C12-C11-C10	140.3(4)	H26A-C26-H26B	108.3
C3-C11-C10	103.8(4)	C26-C27-N28	113.1(4)
C16-C12-C11	121.7(4)	C26-C27-H27A	109.0
C16-C12-C13	108.1(4)	N28-C27-H27A	109.0
C11-C12-C13	130.2(4)	C26-C27-H27B	109.0
O1-C13-N14	124.4(5)	N28-C27-H27B	109.0
O1-C13-C12	129.0(5)	H27A-C27-H27B	107.8
N14-C13-C12	106.6(4)	C30-C29-N28	112.8(4)
O2-C15-N14	123.9(5)	C30-C29-H29A	109.0
O2-C15-C16	130.5(5)	N28-C29-H29A	109.0
N14-C15-C16	105.6(4)	C30-C29-H29B	109.0
C12-C16-C17	123.3(5)	N28-C29-H29B	109.0
C12-C16-C15	108.5(4)	H29A-C29-H29B	107.8
C17-C16-C15	128.2(5)	C29-C30-S1	112.2(3)
C2-C17-C16	116.4(4)	C29-C30-H30A	109.2
C2-C17-C18	116.2(4)	S1-C30-H30A	109.2
C16-C17-C18	127.4(5)	C29-C30-H30B	109.2
C19-C18-C17	118.6(5)	S1-C30-H30B	109.2
C19-C18-H18	120.7	H30A-C30-H30B	107.9
C17-C18-H18	120.7	N28-C31-H31A	109.5
C18-C19-C20	120.6(5)	N28-C31-H31B	109.5
C18-C19-H19	119.7	H31A-C31-H31B	109.5
C20-C19-H19	119.7	N28-C31-H31C	109.5
N1-C20-C19	124.0(5)	H31A-C31-H31C	109.5
N1-C20-H20	118.0	H31B-C31-H31C	109.5
C19-C20-H20	118.0	C20-N1-C2	115.4(5)
O3-C21-C23	104.7(5)	C20-N1-Ru1	131.9(4)
O3-C21-C22	110.1(5)	C2-N1-Ru1	112.7(3)
C23-C21-C22	111.2(6)	C3-N4-C5	104.4(4)
O3-C21-H21	110.2	C3-N4-Ru1	110.6(3)
C23-C21-H21	110.2	C5-N4-Ru1	144.9(3)
C22-C21-H21	110.2	N6-N5-Ru1	118.4(3)
C21-C22-H22A	109.5	N7-N6-N5	177.3(5)
C21-C22-H22B	109.5	C13-N14-C15	111.1(5)
H22A-C22-H22B	109.5	C13-N14-H14	124(3)
C21-C22-H22C	109.5	C15-N14-H14	124(3)
H22A-C22-H22C	109.5	C31-N28-C27	108.6(4)
H22B-C22-H22C	109.5	C31-N28-C29	110.2(4)
C21-C23-H23A	109.5	C27-N28-C29	106.4(4)
C21-C23-H23B	109.5	C31-N28-Ru1	112.5(3)
H23A-C23-H23B	109.5	C27-N28-Ru1	106.4(3)
C21-C23-H23C	109.5	C29-N28-Ru1	112.5(3)
H23A-C23-H23C	109.5	C8-O3-C21	119.4(4)
H23B-C23-H23C	109.5	C30-S1-C24	102.3(2)
C25-C24-S1	112.5(4)	C30-S1-Ru1	98.60(16)
C25-C24-H24A	109.1	C24-S1-Ru1	106.10(17)
S1-C24-H24A	109.1	C25-S2-C26	102.7(2)
C25-C24-H24B	109.1	C25-S2-Ru1	103.31(17)
S1-C24-H24B	109.1	C26-S2-Ru1	101.79(16)
H24A-C24-H24B	107.8	N4-Ru1-N5	89.30(16)
C24-C25-S2	113.9(4)	N4-Ru1-N1	79.55(16)
C24-C25-H25A	108.8	N5-Ru1-N1	86.02(16)
S2-C25-H25A	108.8	N4-Ru1-N28	93.00(15)
C24-C25-H25B	108.8	N5-Ru1-N28	177.50(17)
S2-C25-H25B	108.8	N1-Ru1-N28	95.35(15)
H25A-C25-H25B	107.7	N4-Ru1-S1	174.27(13)

N5-Ru1-S1	91.06(12)	C102-C100-C101	118.9(18)
N1-Ru1-S1	94.77(12)	C100-C101-H10A	109.5
N28-Ru1-S1	86.75(10)	C100-C101-H10B	109.5
N4-Ru1-S2	96.44(12)	H10A-C101-H10B	109.5
N5-Ru1-S2	92.58(12)	C100-C101-H10C	109.5
N1-Ru1-S2	175.76(12)	H10A-C101-H10C	109.5
N28-Ru1-S2	86.21(11)	H10B-C101-H10C	109.5
S1-Ru1-S2	89.25(5)	O200-C200-C202	116.5(15)
O100-C100-C102	132.3(16)	O200-C200-C201	122.4(14)
O100-C100-C101	107.4(16)	C202-C200-C201	121.1(11)

Symmetry transformations used to generate equivalent atoms:

Table 6.39. Anisotropic displacement parameters ($Å^2$) for **FL1473**.
The anisotropicdisplacement factor exponent takes the form: $-2\pi^2[h^2a^{*2}U^{11} + ... + 2 h k a^* b^* U^{12}]$

	U^{11}	U^{22}	U^{33}	U^{23}	U^{13}	U^{12}
C2	0.026(3)	0.040(3)	0.034(3)	0.012(2)	0.008(2)	0.008(2)
C3	0.025(2)	0.038(3)	0.030(3)	0.013(2)	0.004(2)	0.007(2)
C5	0.030(3)	0.031(3)	0.038(3)	0.006(2)	0.005(2)	0.003(2)
C6	0.041(3)	0.048(3)	0.026(3)	0.008(2)	0.002(2)	0.017(2)
C7	0.057(3)	0.047(3)	0.036(3)	0.010(3)	0.002(3)	0.020(3)
C8	0.056(3)	0.036(3)	0.038(3)	0.004(2)	0.006(3)	0.016(2)
C9	0.035(3)	0.040(3)	0.042(3)	0.015(2)	0.004(2)	0.011(2)
C10	0.027(2)	0.036(3)	0.034(3)	0.013(2)	0.007(2)	0.008(2)
C11	0.027(2)	0.034(3)	0.036(3)	0.013(2)	0.005(2)	0.010(2)
C12	0.031(3)	0.039(3)	0.030(3)	0.011(2)	0.004(2)	0.009(2)
C13	0.038(3)	0.040(3)	0.039(3)	0.013(3)	-0.001(2)	0.005(2)
C15	0.036(3)	0.049(3)	0.040(3)	0.010(3)	0.006(2)	0.008(2)
C16	0.029(2)	0.046(3)	0.030(3)	0.012(2)	0.003(2)	0.008(2)
C17	0.029(2)	0.039(3)	0.035(3)	0.008(2)	0.006(2)	0.007(2)
C18	0.037(3)	0.056(3)	0.031(3)	0.008(3)	0.002(2)	0.006(2)
C19	0.037(3)	0.043(3)	0.042(3)	0.001(3)	0.005(2)	0.010(2)
C20	0.033(3)	0.042(3)	0.038(3)	0.004(2)	0.004(2)	0.013(2)
C21	0.088(5)	0.051(3)	0.056(4)	0.008(3)	-0.011(3)	0.033(3)
C22	0.105(6)	0.054(4)	0.094(6)	0.027(4)	-0.028(5)	-0.007(4)
C23	0.112(6)	0.056(4)	0.059(4)	-0.015(3)	-0.022(4)	0.050(4)
C24	0.030(3)	0.044(3)	0.043(3)	0.007(3)	-0.004(2)	0.009(2)
C25	0.036(3)	0.039(3)	0.038(3)	0.012(2)	0.003(2)	0.007(2)
C26	0.036(3)	0.033(2)	0.035(3)	0.008(2)	0.002(2)	0.009(2)
C27	0.031(3)	0.043(3)	0.036(3)	0.008(2)	0.006(2)	0.010(2)
C29	0.028(2)	0.048(3)	0.041(3)	0.013(2)	0.004(2)	0.015(2)
C30	0.037(3)	0.050(3)	0.038(3)	0.013(2)	0.011(2)	0.020(2)
C31	0.038(3)	0.049(3)	0.038(3)	0.009(3)	0.007(2)	0.014(2)
N1	0.028(2)	0.041(2)	0.032(2)	0.009(2)	0.0031(18)	0.0110(19)
N4	0.032(2)	0.034(2)	0.029(2)	0.0078(19)	0.0053(18)	0.0082(18)
N5	0.033(2)	0.040(2)	0.038(3)	0.007(2)	0.0021(19)	0.0069(18)
N6	0.026(2)	0.037(2)	0.046(3)	0.015(2)	-0.006(2)	0.0031(17)
N7	0.035(2)	0.071(3)	0.031(2)	0.016(2)	0.002(2)	0.006(2)
N14	0.051(3)	0.050(3)	0.035(3)	0.015(2)	-0.006(2)	0.014(2)
N28	0.027(2)	0.033(2)	0.037(2)	0.0001(19)	0.0007(17)	0.0110(17)
O1	0.064(3)	0.045(2)	0.043(2)	0.0122(19)	-0.0056(19)	0.0175(19)
O2	0.050(2)	0.061(2)	0.031(2)	0.0033(18)	0.0000(17)	0.0124(18)
O3	0.078(3)	0.042(2)	0.041(2)	0.0038(17)	0.0015(19)	0.034(2)
S1	0.0344(7)	0.0410(7)	0.0402(8)	0.0082(6)	0.0014(6)	0.0126(6)
S2	0.0297(6)	0.0378(7)	0.0332(7)	0.0098(6)	0.0035(5)	0.0095(5)
Ru1	0.0256(2)	0.0347(2)	0.0305(2)	0.00634(17)	0.00306(15)	0.00935(15)
O100	0.229(11)	0.085(5)	0.130(8)	0.059(6)	-0.111(8)	0.017(6)
C100	0.226(15)	0.027(5)	0.053(6)	0.013(5)	-0.058(8)	-0.031(7)
C101	0.35(3)	0.137(16)	0.23(2)	-0.025(16)	0.14(2)	-0.15(2)
C102	0.195(13)	0.039(5)	0.071(7)	0.016(5)	-0.008(8)	0.019(6)
O200	0.255(13)	0.091(6)	0.181(11)	0.050(7)	0.075(10)	0.071(7)
C201	0.062(6)	0.090(8)	0.140(11)	0.006(8)	0.035(7)	-0.003(6)
C200	0.089(8)	0.072(7)	0.171(14)	0.047(9)	0.046(8)	0.038(6)
C202	0.067(7)	0.073(7)	0.209(15)	0.066(9)	0.013(8)	0.007(5)
O300	0.17(2)	0.16(2)	0.31(4)	0.19(3)	0.20(3)	0.14(2)
O400	0.17(3)	0.17(3)	0.11(2)	0.006(19)	0.001(19)	0.10(2)

Table 6.40. Hydrogen coordinates and isotropic displacement parameters ($Å^2$)for **FL1473**.

	x	y	z	U(eq)	Occupancy
H6	0.4705	0.6996	0.9357	0.045	1
H7	0.3794	0.8615	0.9902	0.054	1
H9	0.1877	0.8899	0.7858	0.045	1
H18	0.2764	0.4184	0.4676	0.050	1
H19	0.4188	0.2852	0.4950	0.050	1
H20	0.5280	0.2964	0.6172	0.045	1
H21	0.0911	1.0245	0.8525	0.076	1
H22A	0.4267	1.1566	0.9063	0.129	1
H22B	0.3064	1.1703	0.8370	0.129	1
H22C	0.3949	1.0649	0.8294	0.129	1
H23A	0.0024	1.1017	0.9715	0.116	1
H23B	0.0705	1.1964	0.9310	0.116	1
H23C	0.1911	1.1719	0.9962	0.116	1
H24A	0.7556	0.2438	0.8713	0.047	1
H24B	0.8895	0.3508	0.8719	0.047	1
H25A	0.7432	0.3973	0.9758	0.045	1
H25B	0.5609	0.3370	0.9326	0.045	1
H26A	0.8629	0.6463	0.9623	0.041	1
H26B	0.9322	0.5416	0.9160	0.041	1
H27A	0.9791	0.6729	0.8467	0.044	1
H27B	0.7829	0.6934	0.8518	0.044	1
H29A	1.0317	0.5069	0.7295	0.045	1
H29B	1.0047	0.4866	0.8121	0.045	1
H30A	0.9582	0.3182	0.7325	0.047	1
H30B	0.8401	0.3545	0.6721	0.047	1
H31A	0.7099	0.6511	0.7169	0.062	1
H31B	0.7914	0.5575	0.6637	0.062	1
H31C	0.9159	0.6590	0.7165	0.062	1
H10A	-0.2811	0.8766	0.4797	0.399	0.75
H10B	-0.3330	0.9443	0.4211	0.399	0.75
H10C	-0.1717	0.9927	0.4825	0.399	0.75
H10D	-0.0348	0.8800	0.3001	0.153	0.75
H10E	-0.1919	0.9455	0.3187	0.153	0.75
H10F	-0.2286	0.8166	0.2957	0.153	0.75
H20A	-0.3785	0.9415	0.6515	0.153	0.75
H20B	-0.4373	0.8417	0.6884	0.153	0.75
H20C	-0.2459	0.8615	0.6609	0.153	0.75
H20D	-0.1789	0.8670	0.8156	0.168	0.75
H20E	-0.3683	0.8881	0.8383	0.168	0.75
H20F	-0.2025	0.9782	0.8713	0.168	0.75
H14	0.040(8)	0.771(5)	0.492(4)	0.07(2)	1

Table 6.41. Torsion angles [°] for **FL1473**.

N1-C2-C3-N4	-2.3(6)	C3-C2-N1-C20	178.0(4)
C17-C2-C3-N4	178.2(4)	C17-C2-N1-Ru1	-179.4(3)
N1-C2-C3-C11	178.8(4)	C3-C2-N1-Ru1	1.1(5)
C17-C2-C3-C11	-0.7(6)	C2-C3-N4-C5	-177.7(4)
N4-C5-C6-C7	179.5(5)	C11-C3-N4-C5	1.2(5)
C10-C5-C6-C7	-1.0(7)	C2-C3-N4-Ru1	2.2(5)
C5-C6-C7-C8	0.0(8)	C11-C3-N4-Ru1	-178.8(3)
C6-C7-C8-O3	179.9(5)	C6-C5-N4-C3	178.3(5)
C6-C7-C8-C9	0.5(8)	C10-C5-N4-C3	-1.3(5)
O3-C8-C9-C10	-179.4(5)	C6-C5-N4-Ru1	-1.6(9)
C7-C8-C9-C10	0.0(7)	C10-C5-N4-Ru1	178.8(4)
C8-C9-C10-C5	-0.9(7)	Ru1-N5-N6-N7	165(11)
C8-C9-C10-C11	179.3(5)	O1-C13-N14-C15	-178.3(5)
C6-C5-C10-C9	1.4(7)	C12-C13-N14-C15	1.0(5)
N4-C5-C10-C9	-178.9(4)	O2-C15-N14-C13	179.3(5)
C6-C5-C10-C11	-178.8(4)	C16-C15-N14-C13	-0.7(5)
N4-C5-C10-C11	0.9(5)	C26-C27-N28-C31	173.6(4)
N4-C3-C11-C12	-179.3(4)	C26-C27-N28-C29	-67.8(5)
C2-C3-C11-C12	-0.3(6)	C26-C27-N28-Ru1	52.3(4)
N4-C3-C11-C10	-0.7(5)	C30-C29-N28-C31	-100.3(5)
C2-C3-C11-C10	178.3(4)	C30-C29-N28-C27	142.2(4)
C9-C10-C11-C12	-2.3(10)	C30-C29-N28-Ru1	26.0(5)
C5-C10-C11-C12	177.9(6)	C9-C8-O3-C21	-14.5(8)
C9-C10-C11-C3	179.7(5)	C7-C8-O3-C21	166.2(5)
C5-C10-C11-C3	-0.1(5)	C23-C21-O3-C8	168.4(5)
C3-C11-C12-C16	1.1(6)	C22-C21-O3-C8	-72.0(7)
C10-C11-C12-C16	-176.8(5)	C29-C30-S1-C24	-68.2(4)
C3-C11-C12-C13	179.3(4)	C29-C30-S1-Ru1	40.5(4)
C10-C11-C12-C13	1.4(9)	C25-C24-S1-C30	127.3(4)
C16-C12-C13-O1	178.3(5)	C25-C24-S1-Ru1	24.5(4)
C11-C12-C13-O1	-0.1(9)	C24-C25-S2-C26	-66.4(4)
C16-C12-C13-N14	-0.9(5)	C24-C25-S2-Ru1	39.2(4)
C11-C12-C13-N14	-179.3(5)	C27-C26-S2-C25	131.5(3)
C11-C12-C16-C17	-0.7(7)	C27-C26-S2-Ru1	24.7(3)
C13-C12-C16-C17	-179.3(4)	C3-N4-Ru1-N5	-87.2(3)
C11-C12-C16-C15	179.1(4)	C5-N4-Ru1-N5	92.7(5)
C13-C12-C16-C15	0.5(5)	C3-N4-Ru1-N1	-1.1(3)
O2-C15-C16-C12	-179.9(5)	C5-N4-Ru1-N1	178.8(5)
N14-C15-C16-C12	0.1(5)	C3-N4-Ru1-N28	93.8(3)
O2-C15-C16-C17	-0.1(9)	C5-N4-Ru1-N28	-86.3(5)
N14-C15-C16-C17	179.9(4)	C3-N4-Ru1-S1	6.4(14)
N1-C2-C17-C16	-178.4(4)	C5-N4-Ru1-S1	-173.7(9)
C3-C2-C17-C16	1.1(6)	C3-N4-Ru1-S2	-179.7(3)
N1-C2-C17-C18	1.8(7)	C5-N4-Ru1-S2	0.2(5)
C3-C2-C17-C18	-178.7(4)	N6-N5-Ru1-N4	-72.5(4)
C12-C16-C17-C2	-0.4(7)	N6-N5-Ru1-N1	-152.1(4)
C15-C16-C17-C2	179.8(4)	N6-N5-Ru1-N28	85(4)
C12-C16-C17-C18	179.4(4)	N6-N5-Ru1-S1	113.2(4)
C15-C16-C17-C18	-0.4(8)	N6-N5-Ru1-S2	23.9(4)
C2-C17-C18-C19	-0.8(6)	C20-N1-Ru1-N4	-176.3(4)
C16-C17-C18-C19	179.5(5)	C2-N1-Ru1-N4	0.0(3)
C17-C18-C19-C20	0.7(7)	C20-N1-Ru1-N5	-86.2(4)
C18-C19-C20-N1	-1.5(8)	C2-N1-Ru1-N5	90.0(3)
S1-C24-C25-S2	-42.8(5)	C20-N1-Ru1-N28	91.7(4)
S2-C26-C27-N28	-52.0(4)	C2-N1-Ru1-N28	-92.1(3)
N28-C29-C30-S1	-46.0(5)	C20-N1-Ru1-S1	4.5(4)
C19-C20-N1-C2	2.3(7)	C2-N1-Ru1-S1	-179.3(3)
C19-C20-N1-Ru1	178.4(4)	C20-N1-Ru1-S2	-157.0(14)
C17-C2-N1-C20	-2.5(7)	C2-N1-Ru1-S2	19.2(19)

C31-N28-Ru1-N4	-49.3(3)	C24-S1-Ru1-N5	-93.2(2)
C27-N28-Ru1-N4	69.4(3)	C30-S1-Ru1-N1	75.2(2)
C29-N28-Ru1-N4	-174.4(3)	C24-S1-Ru1-N1	-179.3(2)
C31-N28-Ru1-N5	153(4)	C30-S1-Ru1-N28	-19.9(2)
C27-N28-Ru1-N5	-88(4)	C24-S1-Ru1-N28	85.6(2)
C29-N28-Ru1-N5	28(4)	C30-S1-Ru1-S2	-106.14(18)
C31-N28-Ru1-N1	30.4(3)	C24-S1-Ru1-S2	-0.63(18)
C27-N28-Ru1-N1	149.2(3)	C25-S2-Ru1-N4	162.57(19)
C29-N28-Ru1-N1	-94.7(3)	C26-S2-Ru1-N4	-91.17(19)
C31-N28-Ru1-S1	124.9(3)	C25-S2-Ru1-N5	72.99(19)
C27-N28-Ru1-S1	-116.3(3)	C26-S2-Ru1-N5	179.24(19)
C29-N28-Ru1-S1	-0.2(3)	C25-S2-Ru1-N1	143.5(16)
C31-N28-Ru1-S2	-145.6(3)	C26-S2-Ru1-N1	-110.2(16)
C27-N28-Ru1-S2	-26.8(3)	C25-S2-Ru1-N28	-104.83(19)
C29-N28-Ru1-S2	89.3(3)	C26-S2-Ru1-N28	1.43(19)
C30-S1-Ru1-N4	67.8(12)	C25-S2-Ru1-S1	-18.04(16)
C24-S1-Ru1-N4	173.3(12)	C26-S2-Ru1-S1	88.22(16)
C30-S1-Ru1-N5	161.3(2)		

Symmetry transformations used to generate equivalent atoms:

Table 6.42. Hydrogen bonds for **FL1473** [Å and °].

D-H...A	d(D-H)	d(H...A)	d(D...A)	<(DHA)
N14-H14...O100	1.07(7)	1.79(7)	2.852(9)	173(5)

Symmetry transformations used to generate equivalent atoms:

Crystal structure of FL1528-1.

Table 6.43. Crystal data and structure refinement for **FL1528-1**.

Identification code	fl1528-1	
Habitus, colour	prism, colourless	
Crystal size	0.33 x 0.06 x 0.04 mm^3	
Crystal system	Triclinic	
Space group	$P\bar{1}$	Z = 2
Unit cell dimensions	a = 7.9971(19) Å	α= 74.807(19)°.
	b = 13.072(3) Å	β= 89.225(19)°.
	c = 17.991(4) Å	γ = 78.37(2)°.
Volume	1776.1(7) $Å^3$	
Cell determination	3421 peaks with Theta 1.6 to 23°.	
Empirical formula	C_{32} H_{39} N_8 O_6 Ru S_3	
Formula weight	828.96	
Density (calculated)	1.550 Mg/m^3	
Absorption coefficient	0.673 mm^{-1}	
F(000)	854	

Data collection:

Diffractometer type	STOE IPDS 2
Wavelength	0.71073 Å
Temperature	100(2) K
Theta range for data collection	1.65 to 25.00°.
Index ranges	-9<=h<=9, -15<=k<=15, -21<=l<=18
Data collection software	STOE X-AREA
Cell refinement software	STOE X-AREA
Data reduction software	STOE X-AREA

Solution and refinement:

Reflections collected	12663
Independent reflections	6223 [R(int) = 0.2069]
Completeness to theta = 25.00°	99.4 %
Observed reflections	1513[I>2(I)]
Reflections used for refinement	6223
Absorption correction	Integration
Max. and min. transmission	0.9855 and 0.8708
Largest diff. peak and hole	0.635 and -0.720 e.$Å^{-3}$
Solution	Direct methods
Refinement	Full-matrix least-squares on F^2
Treatment of hydrogen atoms	Calculated positions, riding model
Programs used	SIR2008 (Giacovazzo et al, 2008)
	SHELXL-97 (Sheldrick, 2008)
	DIAMOND 3.2 (Crystal Impcat)
	STOE IPDS2 software
Data / restraints / parameters	6223 / 149 / 457
Goodness-of-fit on F^2	0.650
R index (all data)	wR2 = 0.1423
R index conventional [I>2sigma(I)]	R1 = 0.0650

Table 6.44. Atomic coordinates and equivalent isotropic displacement parameters ($Å^2$) for **FL1528-1**. U(eq) is defined as one third of the trace of the orthogonalized U^{ij} tensor.

	x	y	z	U(eq)	Occupancy
C2	0.6157(16)	0.5051(13)	0.3510(8)	0.041(3)	1
C3	0.6238(16)	0.5911(12)	0.2898(7)	0.038(3)	1
C5	0.6005(14)	0.6910(12)	0.1707(7)	0.036(3)	1
C6	0.5722(16)	0.7417(13)	0.0929(8)	0.052(4)	1
C7	0.6195(16)	0.8366(12)	0.0591(8)	0.049(4)	1
C8	0.6988(16)	0.8903(12)	0.1051(8)	0.044(4)	1
C9	0.7345(16)	0.8449(13)	0.1839(7)	0.048(4)	1
C10	0.6824(14)	0.7499(11)	0.2158(7)	0.036(3)	1
C11	0.6982(15)	0.6805(12)	0.2907(8)	0.042(4)	1
C12	0.7586(16)	0.6740(13)	0.3687(8)	0.044(4)	1
C13	0.8479(17)	0.7523(13)	0.3930(8)	0.049(4)	1
C15	0.8314(17)	0.6103(13)	0.4985(8)	0.049(4)	1
C16	0.7559(17)	0.5864(13)	0.4291(8)	0.047(4)	1
C17	0.6863(15)	0.4980(12)	0.4238(7)	0.043(4)	1
C18	0.6682(15)	0.4069(12)	0.4865(8)	0.046(4)	1
C19	0.5917(16)	0.3258(13)	0.4730(7)	0.047(4)	1
C20	0.5283(16)	0.3345(12)	0.3991(7)	0.041(4)	1
C21	0.8115(19)	1.0542(13)	0.0998(9)	0.066(4)	1
C22	0.668(2)	1.1135(15)	0.1396(9)	0.087(6)	1
C23	0.892(2)	1.1271(15)	0.0404(9)	0.087(6)	1
C24	0.0344(14)	0.4702(12)	0.2628(8)	0.049(4)	1
C25	0.1258(14)	0.3510(11)	0.2847(7)	0.042(3)	1
C26	0.1126(15)	0.6551(12)	0.1514(7)	0.051(3)	1
C27	0.1360(15)	0.5945(11)	0.0892(7)	0.050(3)	1
C28	0.2433(19)	0.3275(14)	0.1364(7)	0.057(4)	1
C29	0.3306(16)	0.3908(12)	0.0747(7)	0.044(3)	1
C300	0.607(2)	0.0611(17)	0.6763(11)	0.099(7)	1
C301	0.7370(18)	0.1846(14)	0.7188(11)	0.078(5)	1
C302	0.719(2)	0.0141(17)	0.8040(10)	0.118(9)	1
N1	0.5341(14)	0.4242(11)	0.3404(6)	0.048(3)	1
N4	0.5606(14)	0.5969(11)	0.2153(6)	0.044(3)	1
N14	0.8783(13)	0.7074(10)	0.4714(6)	0.052(3)	1
N101	0.6868(14)	0.3733(10)	0.2002(7)	0.051(3)	1
N102	0.7543(12)	0.4004(10)	0.1433(6)	0.040(3)	1
N103	0.8321(14)	0.4263(12)	0.0872(7)	0.070(4)	1
N300	0.6906(18)	0.0828(13)	0.7311(9)	0.090(5)	1
O8	0.7427(11)	0.9864(8)	0.0613(5)	0.055(3)	1
O13	0.8760(11)	0.8380(9)	0.3540(5)	0.061(3)	1
O15	0.8471(10)	0.5492(9)	0.5659(5)	0.053(3)	1
O19	0.3998(11)	0.2117(8)	0.2715(5)	0.057(3)	1
O300	0.5657(19)	0.1217(13)	0.6094(7)	0.123(5)	1
S1	0.1852(5)	0.5617(3)	0.2480(2)	0.0503(11)	1
S2	0.3200(5)	0.3248(4)	0.2347(2)	0.0471(11)	1
S3	0.3622(5)	0.5169(3)	0.0919(2)	0.0452(11)	1
Ru1	0.44363(17)	0.46305(13)	0.22152(8)	0.0433(4)	1
C200	1.0962(18)	0.8679(12)	0.5434(9)	0.064(5)	1
C201	1.146(3)	0.8947(18)	0.6691(9)	0.118(8)	1
C202	1.3234(18)	0.9670(13)	0.5539(10)	0.077(5)	1
N200	1.1827(14)	0.9127(11)	0.5870(7)	0.062(4)	1
O200	0.9807(12)	0.8228(9)	0.5656(5)	0.064(3)	1

Table 6.45. Bond lengths [Å] and angles [°] for **FL1528-1**.

C2-C3	1.363(18)	C25-H25B	0.9900
C2-N1	1.403(16)	C26-C27	1.521(18)
C2-C17	1.406(15)	C26-S1	1.866(13)
C3-N4	1.417(15)	C26-H26A	0.9900
C3-C11	1.418(17)	C26-H26B	0.9900
C5-N4	1.375(16)	C27-S3	1.882(13)
C5-C6	1.383(16)	C27-H27A	0.9900
C5-C10	1.492(16)	C27-H27B	0.9900
C6-C7	1.356(18)	C28-C29	1.461(17)
C6-H6	0.9500	C28-S2	1.869(12)
C7-C8	1.442(17)	C28-H28A	0.9900
C7-H7	0.9500	C28-H28B	0.9900
C8-C9	1.395(17)	C29-S3	1.821(14)
C8-O8	1.404(15)	C29-H29A	0.9900
C9-C10	1.370(18)	C29-H29B	0.9900
C10-C11	1.404(17)	C300-O300	1.262(19)
C11-C12	1.467(16)	C300-N300	1.32(2)
C12-C16	1.360(19)	C300-H300	0.9500
C12-C13	1.512(18)	C301-N300	1.41(2)
C13-O13	1.217(15)	C301-H30A	0.9800
C13-N14	1.383(16)	C301-H30B	0.9800
C15-O15	1.256(15)	C301-H30C	0.9800
C15-N14	1.361(18)	C302-N300	1.374(19)
C15-C16	1.525(17)	C302-H30D	0.9800
C16-C17	1.405(18)	C302-H30E	0.9800
C17-C18	1.439(18)	C302-H30F	0.9800
C18-C19	1.399(18)	N1-Ru1	2.163(11)
C18-H18	0.9500	N4-Ru1	2.122(13)
C19-C20	1.397(15)	N14-H14	0.8800
C19-H19	0.9500	N101-N102	1.156(14)
C20-N1	1.365(16)	N101-Ru1	2.145(13)
C20-H20	0.9500	N102-N103	1.188(14)
C21-O8	1.448(15)	O19-S2	1.467(10)
C21-C23	1.47(2)	S1-Ru1	2.320(5)
C21-C22	1.53(2)	S2-Ru1	2.188(4)
C21-H21	1.0000	S3-Ru1	2.313(4)
C22-H22A	0.9800	C200-O200	1.203(15)
C22-H22B	0.9800	C200-N200	1.362(16)
C22-H22C	0.9800	C200-H200	0.9500
C23-H23A	0.9800	C201-N200	1.469(19)
C23-H23B	0.9800	C201-H20A	0.9800
C23-H23C	0.9800	C201-H20B	0.9800
C24-C25	1.531(18)	C201-H20C	0.9800
C24-S1	1.833(12)	C202-N200	1.485(18)
C24-H24A	0.9900	C202-H20D	0.9800
C24-H24B	0.9900	C202-H20E	0.9800
C25-S2	1.801(13)	C202-H20F	0.9800
C25-H25A	0.9900		

C3-C2-N1	118.9(12)	C7-C6-H6	118.6
C3-C2-C17	120.7(13)	C5-C6-H6	118.6
N1-C2-C17	120.4(12)	C6-C7-C8	120.0(13)
C2-C3-N4	121.4(13)	C6-C7-H7	120.0
C2-C3-C11	126.3(12)	C8-C7-H7	120.0
N4-C3-C11	112.3(12)	C9-C8-O8	125.5(12)
N4-C5-C6	131.4(12)	C9-C8-C7	121.5(13)
N4-C5-C10	113.3(11)	O8-C8-C7	112.9(12)
C6-C5-C10	115.2(13)	C10-C9-C8	116.5(12)
C7-C6-C5	122.8(13)	C9-C10-C11	132.9(12)

C9-C10-C5	123.9(12)	S1-C26-H26A	109.4
C11-C10-C5	103.0(11)	C27-C26-H26B	109.4
C10-C11-C3	108.2(11)	S1-C26-H26B	109.4
C10-C11-C12	140.4(12)	H26A-C26-H26B	108.0
C3-C11-C12	111.3(12)	C26-C27-S3	110.9(8)
C16-C12-C11	122.1(13)	C26-C27-H27A	109.5
C16-C12-C13	110.3(12)	S3-C27-H27A	109.5
C11-C12-C13	127.3(13)	C26-C27-H27B	109.5
O13-C13-N14	128.2(13)	S3-C27-H27B	109.5
O13-C13-C12	128.3(12)	H27A-C27-H27B	108.1
N14-C13-C12	103.3(13)	C29-C28-S2	113.0(9)
O15-C15-N14	128.9(12)	C29-C28-H28A	109.0
O15-C15-C16	125.1(14)	S2-C28-H28A	109.0
N14-C15-C16	105.9(13)	C29-C28-H28B	109.0
C12-C16-C17	123.6(12)	S2-C28-H28B	109.0
C12-C16-C15	105.9(13)	H28A-C28-H28B	107.8
C17-C16-C15	130.4(14)	C28-C29-S3	113.4(10)
C16-C17-C2	115.7(13)	C28-C29-H29A	108.9
C16-C17-C18	126.3(12)	S3-C29-H29A	108.9
C2-C17-C18	117.8(12)	C28-C29-H29B	108.9
C19-C18-C17	120.0(12)	S3-C29-H29B	108.9
C19-C18-H18	120.0	H29A-C29-H29B	107.7
C17-C18-H18	120.0	O300-C300-N300	126.7(19)
C20-C19-C18	120.1(14)	O300-C300-H300	116.7
C20-C19-H19	119.9	N300-C300-H300	116.7
C18-C19-H19	119.9	N300-C301-H30A	109.5
N1-C20-C19	120.3(13)	N300-C301-H30B	109.5
N1-C20-H20	119.9	H30A-C301-H30B	109.5
C19-C20-H20	119.9	N300-C301-H30C	109.5
O8-C21-C23	106.4(13)	H30A-C301-H30C	109.5
O8-C21-C22	109.4(11)	H30B-C301-H30C	109.5
C23-C21-C22	113.6(15)	N300-C302-H30D	109.5
O8-C21-H21	109.1	N300-C302-H30E	109.5
C23-C21-H21	109.1	H30D-C302-H30E	109.5
C22-C21-H21	109.1	N300-C302-H30F	109.5
C21-C22-H22A	109.5	H30D-C302-H30F	109.5
C21-C22-H22B	109.5	H30E-C302-H30F	109.5
H22A-C22-H22B	109.5	C20-N1-C2	121.1(11)
C21-C22-H22C	109.5	C20-N1-Ru1	129.2(9)
H22A-C22-H22C	109.5	C2-N1-Ru1	109.6(9)
H22B-C22-H22C	109.5	C5-N4-C3	103.0(11)
C21-C23-H23A	109.5	C5-N4-Ru1	147.8(9)
C21-C23-H23B	109.5	C3-N4-Ru1	109.1(9)
H23A-C23-H23B	109.5	C15-N14-C13	114.3(11)
C21-C23-H23C	109.5	C15-N14-H14	122.8
H23A-C23-H23C	109.5	C13-N14-H14	122.8
H23B-C23-H23C	109.5	N102-N101-Ru1	121.2(11)
C25-C24-S1	112.1(8)	N101-N102-N103	176.3(12)
C25-C24-H24A	109.2	C300-N300-C302	122.0(16)
S1-C24-H24A	109.2	C300-N300-C301	120.2(17)
C25-C24-H24B	109.2	C302-N300-C301	117.3(16)
S1-C24-H24B	109.2	C8-O8-C21	119.7(10)
H24A-C24-H24B	107.9	C24-S1-C26	102.2(6)
C24-C25-S2	113.6(9)	C24-S1-Ru1	106.2(5)
C24-C25-H25A	108.8	C26-S1-Ru1	101.9(4)
S2-C25-H25A	108.8	O19-S2-C25	105.2(6)
C24-C25-H25B	108.8	O19-S2-C28	106.0(7)
S2-C25-H25B	108.8	C25-S2-C28	103.7(6)
H25A-C25-H25B	107.7	O19-S2-Ru1	125.2(4)
C27-C26-S1	111.0(10)	C25-S2-Ru1	107.9(4)
C27-C26-H26A	109.4	C28-S2-Ru1	107.0(5)

C29-S3-C27	101.8(6)	O200-C200-N200	124.6(16)
C29-S3-Ru1	101.9(5)	O200-C200-H200	117.7
C27-S3-Ru1	103.9(4)	N200-C200-H200	117.7
N4-Ru1-N101	88.4(5)	N200-C201-H20A	109.5
N4-Ru1-N1	80.9(4)	N200-C201-H20B	109.5
N101-Ru1-N1	86.8(5)	H20A-C201-H20B	109.5
N4-Ru1-S2	176.8(4)	N200-C201-H20C	109.5
N101-Ru1-S2	93.1(3)	H20A-C201-H20C	109.5
N1-Ru1-S2	96.3(3)	H20B-C201-H20C	109.5
N4-Ru1-S3	93.8(3)	N200-C202-H20D	109.5
N101-Ru1-S3	92.1(3)	N200-C202-H20E	109.5
N1-Ru1-S3	174.6(4)	H20D-C202-H20E	109.5
S2-Ru1-S3	88.98(14)	N200-C202-H20F	109.5
N4-Ru1-S1	90.3(4)	H20D-C202-H20F	109.5
N101-Ru1-S1	178.0(3)	H20E-C202-H20F	109.5
N1-Ru1-S1	91.4(4)	C200-N200-C201	117.8(14)
S2-Ru1-S1	88.14(16)	C200-N200-C202	120.3(13)
S3-Ru1-S1	89.58(15)	C201-N200-C202	121.5(12)

Symmetry transformations used to generate equivalent atoms:

Table 6.46. Anisotropic displacement parameters ($Å^2$) for **FL1528-1**.
The anisotropicdisplacement factor exponent takes the form: $-2\pi^2[h^2a^{*2}U^{11} + ... + 2 h k a^* b^* U^{12}]$

	U^{11}	U^{22}	U^{33}	U^{23}	U^{13}	U^{12}
C2	0.042(8)	0.051(9)	0.034(6)	-0.007(5)	-0.007(6)	-0.026(7)
C3	0.038(7)	0.050(9)	0.029(6)	-0.012(5)	0.005(6)	-0.016(7)
C5	0.022(7)	0.049(9)	0.033(6)	-0.006(5)	-0.001(6)	-0.007(6)
C6	0.050(8)	0.067(10)	0.039(6)	0.002(7)	-0.005(7)	-0.037(8)
C7	0.057(9)	0.058(10)	0.035(7)	-0.008(6)	-0.007(7)	-0.027(8)
C8	0.043(8)	0.050(9)	0.045(7)	-0.010(6)	0.006(7)	-0.025(7)
C9	0.042(8)	0.069(10)	0.033(6)	-0.005(6)	-0.002(6)	-0.023(8)
C10	0.021(7)	0.042(8)	0.046(6)	-0.014(5)	0.002(6)	-0.007(6)
C11	0.038(7)	0.063(9)	0.040(6)	-0.018(6)	0.002(6)	-0.034(8)
C12	0.038(8)	0.064(9)	0.040(6)	-0.018(6)	-0.003(7)	-0.028(8)
C13	0.053(9)	0.057(10)	0.041(7)	-0.010(6)	-0.017(7)	-0.024(8)
C15	0.053(9)	0.057(10)	0.041(6)	-0.015(6)	-0.010(7)	-0.019(8)
C16	0.048(8)	0.059(9)	0.039(6)	-0.014(6)	-0.013(7)	-0.020(8)
C17	0.033(7)	0.063(9)	0.036(6)	-0.010(6)	-0.018(6)	-0.022(7)
C18	0.036(8)	0.068(10)	0.036(7)	-0.011(6)	-0.007(6)	-0.020(8)
C19	0.046(8)	0.066(10)	0.029(6)	-0.009(7)	-0.009(6)	-0.016(7)
C20	0.052(8)	0.042(9)	0.027(6)	0.000(6)	-0.009(6)	-0.017(7)
C21	0.070(10)	0.061(11)	0.070(11)	-0.002(8)	-0.030(7)	-0.040(8)
C22	0.114(13)	0.114(17)	0.059(11)	-0.047(10)	-0.025(8)	-0.048(12)
C23	0.113(13)	0.098(15)	0.063(11)	-0.007(10)	-0.020(8)	-0.069(11)
C24	0.024(6)	0.064(8)	0.057(9)	-0.001(7)	-0.010(6)	-0.020(5)
C25	0.049(6)	0.053(7)	0.028(7)	-0.005(7)	-0.017(5)	-0.030(5)
C26	0.035(7)	0.063(10)	0.045(7)	-0.002(6)	0.019(6)	-0.007(5)
C27	0.059(7)	0.044(9)	0.039(7)	0.006(7)	-0.012(6)	-0.015(6)
C28	0.074(10)	0.073(11)	0.035(6)	-0.017(7)	-0.009(6)	-0.040(9)
C29	0.036(7)	0.055(8)	0.044(6)	-0.014(7)	-0.005(6)	-0.019(6)
C300	0.123(15)	0.114(18)	0.064(10)	0.013(11)	-0.010(11)	-0.078(14)
C301	0.057(10)	0.067(11)	0.120(15)	-0.036(10)	0.032(10)	-0.020(9)
C302	0.116(15)	0.121(18)	0.096(12)	0.034(12)	-0.053(13)	-0.055(14)
N1	0.057(7)	0.059(8)	0.031(5)	-0.006(5)	-0.019(5)	-0.031(6)
N4	0.050(6)	0.064(7)	0.026(5)	-0.010(5)	0.004(5)	-0.030(6)
N14	0.056(7)	0.069(8)	0.044(6)	-0.028(5)	-0.005(6)	-0.030(7)
N101	0.058(5)	0.062(8)	0.053(6)	-0.024(7)	-0.003(4)	-0.045(5)
N102	0.028(6)	0.062(9)	0.030(6)	-0.006(6)	-0.010(4)	-0.020(6)
N103	0.040(7)	0.121(13)	0.050(7)	-0.015(9)	-0.011(5)	-0.030(8)
N300	0.098(11)	0.085(12)	0.085(9)	0.011(9)	-0.015(8)	-0.057(10)
O8	0.067(6)	0.047(7)	0.053(6)	-0.010(5)	-0.006(5)	-0.024(5)
O13	0.062(6)	0.079(8)	0.048(6)	-0.006(5)	-0.016(5)	-0.041(6)
O15	0.043(5)	0.086(8)	0.035(5)	-0.017(5)	-0.007(4)	-0.021(5)
O19	0.059(6)	0.052(6)	0.060(6)	-0.023(5)	-0.025(5)	0.001(5)
O300	0.186(14)	0.124(14)	0.069(8)	-0.009(9)	0.005(8)	-0.077(11)
S1	0.058(2)	0.059(3)	0.040(2)	-0.009(2)	-0.0074(18)	-0.033(2)
S2	0.047(2)	0.060(3)	0.038(2)	-0.007(2)	-0.0133(18)	-0.025(2)
S3	0.046(2)	0.054(3)	0.039(2)	-0.013(2)	-0.0100(18)	-0.016(2)
Ru1	0.0440(7)	0.0594(10)	0.0302(7)	-0.0065(7)	-0.0115(6)	-0.0251(7)
C200	0.060(10)	0.046(11)	0.083(11)	-0.006(9)	-0.036(8)	-0.019(8)
C201	0.18(2)	0.12(2)	0.038(8)	0.023(11)	-0.034(9)	-0.062(16)
C202	0.078(11)	0.067(13)	0.100(12)	-0.028(11)	-0.011(9)	-0.037(9)
N200	0.060(8)	0.069(10)	0.060(7)	-0.019(8)	-0.022(6)	-0.018(6)
O200	0.071(7)	0.089(9)	0.047(6)	-0.022(6)	-0.001(5)	-0.045(6)

Table 6.47. Hydrogen coordinates and isotropic displacement parameters ($Å^2$)for **FL1528-1**.

	x	y	z	U(eq)	Occupancy
H6	0.5174	0.7086	0.0617	0.062	1
H7	0.6005	0.8676	0.0051	0.058	1
H18	0.7083	0.4018	0.5371	0.055	1
H19	0.5828	0.2647	0.5142	0.056	1
H20	0.4809	0.2778	0.3897	0.049	1
H21	0.9008	1.0076	0.1394	0.079	1
H22A	0.7091	1.1693	0.1573	0.130	1
H22B	0.6332	1.0616	0.1840	0.130	1
H22C	0.5703	1.1475	0.1032	0.130	1
H23A	0.8123	1.1603	-0.0043	0.130	1
H23B	0.9961	1.0857	0.0247	0.130	1
H23C	0.9204	1.1838	0.0613	0.130	1
H24A	-0.0427	0.4840	0.3042	0.059	1
H24B	-0.0364	0.4856	0.2149	0.059	1
H25A	0.0472	0.3069	0.2734	0.050	1
H25B	0.1531	0.3275	0.3409	0.050	1
H26A	-0.0095	0.6892	0.1523	0.061	1
H26B	0.1789	0.7133	0.1392	0.061	1
H27A	0.1077	0.6468	0.0380	0.060	1
H27B	0.0568	0.5438	0.0970	0.060	1
H28A	0.2610	0.2523	0.1318	0.068	1
H28B	0.1191	0.3585	0.1302	0.068	1
H29A	0.2630	0.4076	0.0257	0.052	1
H29B	0.4433	0.3464	0.0687	0.052	1
H300	0.5744	-0.0072	0.6885	0.119	1
H30A	0.6742	0.2352	0.6730	0.118	1
H30B	0.8600	0.1763	0.7111	0.118	1
H30C	0.7089	0.2128	0.7638	0.118	1
H30D	0.6214	-0.0213	0.8175	0.178	1
H30E	0.7319	0.0556	0.8410	0.178	1
H30F	0.8229	-0.0409	0.8057	0.178	1
H14	0.9240	0.7389	0.5013	0.062	1
H200	1.1294	0.8727	0.4919	0.076	1
H20A	1.0317	0.8778	0.6771	0.177	1
H20B	1.1494	0.9602	0.6853	0.177	1
H20C	1.2311	0.8340	0.6995	0.177	1
H20D	1.3339	0.9664	0.4996	0.116	1
H20E	1.4308	0.9284	0.5826	0.116	1
H20F	1.2982	1.0420	0.5575	0.116	1

Table 6.48. Torsion angles [°] for **FL1528-1**.

N1-C2-C3-N4	-4(2)	C17-C2-N1-C20	-3(2)
C17-C2-C3-N4	176.9(14)	C3-C2-N1-Ru1	0.8(17)
N1-C2-C3-C11	178.7(14)	C17-C2-N1-Ru1	-179.8(11)
C17-C2-C3-C11	-1(2)	C6-C5-N4-C3	-179.8(15)
N4-C5-C6-C7	178.9(14)	C10-C5-N4-C3	-2.6(14)
C10-C5-C6-C7	2(2)	C6-C5-N4-Ru1	-2(3)
C5-C6-C7-C8	-2(2)	C10-C5-N4-Ru1	174.9(15)
C6-C7-C8-C9	2(2)	C2-C3-N4-C5	-177.0(14)
C6-C7-C8-O8	178.9(13)	C11-C3-N4-C5	0.9(16)
O8-C8-C9-C10	-179.3(12)	C2-C3-N4-Ru1	4.4(17)
C7-C8-C9-C10	-3(2)	C11-C3-N4-Ru1	-177.7(10)
C8-C9-C10-C11	178.4(14)	O15-C15-N14-C13	177.9(15)
C8-C9-C10-C5	4(2)	C16-C15-N14-C13	-1.0(17)
N4-C5-C10-C9	179.5(14)	O13-C13-N14-C15	179.5(15)
C6-C5-C10-C9	-2.8(19)	C12-C13-N14-C15	3.9(17)
N4-C5-C10-C11	3.4(14)	Ru1-N101-N102-N103	145(25)
C6-C5-C10-C11	-179.0(12)	O300-C300-N300-C302	175(2)
C9-C10-C11-C3	-178.2(15)	O300-C300-N300-C301	3(3)
C5-C10-C11-C3	-2.6(14)	C9-C8-O8-C21	-8(2)
C9-C10-C11-C12	6(3)	C7-C8-O8-C21	175.3(13)
C5-C10-C11-C12	-178.7(18)	C23-C21-O8-C8	163.1(14)
C2-C3-C11-C10	179.0(14)	C22-C21-O8-C8	-73.9(16)
N4-C3-C11-C10	1.2(17)	C25-C24-S1-C26	128.4(10)
C2-C3-C11-C12	-4(2)	C25-C24-S1-Ru1	22.0(11)
N4-C3-C11-C12	178.6(12)	C27-C26-S1-C24	-64.5(10)
C10-C11-C12-C16	-178.1(17)	C27-C26-S1-Ru1	45.3(9)
C3-C11-C12-C16	6(2)	C24-C25-S2-O19	171.8(8)
C10-C11-C12-C13	-5(3)	C24-C25-S2-C28	-77.1(10)
C3-C11-C12-C13	178.7(14)	C24-C25-S2-Ru1	36.2(9)
C16-C12-C13-O13	178.8(16)	C29-C28-S2-O19	-115.4(12)
C11-C12-C13-O13	5(3)	C29-C28-S2-C25	134.1(12)
C16-C12-C13-N14	-5.6(17)	C29-C28-S2-Ru1	20.2(13)
C11-C12-C13-N14	-179.1(14)	C28-C29-S3-C27	-65.3(11)
C11-C12-C16-C17	-4(2)	C28-C29-S3-Ru1	41.8(10)
C13-C12-C16-C17	-177.9(14)	C26-C27-S3-C29	139.7(10)
C11-C12-C16-C15	178.9(14)	C26-C27-S3-Ru1	34.1(10)
C13-C12-C16-C15	5.1(15)	C5-N4-Ru1-N101	92.8(19)
O15-C15-C16-C12	178.3(15)	C3-N4-Ru1-N101	-89.8(10)
N14-C15-C16-C12	-2.7(15)	C5-N4-Ru1-N1	179.8(19)
O15-C15-C16-C17	2(3)	C3-N4-Ru1-N1	-2.8(10)
N14-C15-C16-C17	-179.4(15)	C5-N4-Ru1-S2	-150(6)
C12-C16-C17-C2	-1(2)	C3-N4-Ru1-S2	27(8)
C15-C16-C17-C2	175.5(14)	C5-N4-Ru1-S3	0.8(19)
C12-C16-C17-C18	-175.1(14)	C3-N4-Ru1-S3	178.2(9)
C15-C16-C17-C18	1(3)	C5-N4-Ru1-S1	-88.8(19)
C3-C2-C17-C16	3(2)	C3-N4-Ru1-S1	88.6(9)
N1-C2-C17-C16	-176.3(14)	N102-N101-Ru1-N4	-62.5(10)
C3-C2-C17-C18	178.0(14)	N102-N101-Ru1-N1	-143.4(10)
N1-C2-C17-C18	-1(2)	N102-N101-Ru1-S2	120.4(10)
C16-C17-C18-C19	178.1(14)	N102-N101-Ru1-S3	31.3(10)
C2-C17-C18-C19	4(2)	N102-N101-Ru1-S1	-114(11)
C17-C18-C19-C20	-2(2)	C20-N1-Ru1-N4	-175.1(13)
C18-C19-C20-N1	-3(2)	C2-N1-Ru1-N4	1.2(10)
S1-C24-C25-S2	-37.9(12)	C20-N1-Ru1-N101	-86.2(13)
S1-C26-C27-S3	-53.4(11)	C2-N1-Ru1-N101	90.1(10)
S2-C28-C29-S3	-41.7(14)	C20-N1-Ru1-S2	6.5(13)
C19-C20-N1-C2	5(2)	C2-N1-Ru1-S2	-177.2(9)
C19-C20-N1-Ru1	-178.8(11)	C20-N1-Ru1-S3	-165(4)
C3-C2-N1-C20	177.5(14)	C2-N1-Ru1-S3	12(5)

C20-N1-Ru1-S1	94.8(13)	C27-S3-Ru1-N101	176.3(6)
C2-N1-Ru1-S1	-88.9(10)	C29-S3-Ru1-N1	149(4)
O19-S2-Ru1-N4	-80(7)	C27-S3-Ru1-N1	-106(5)
C25-S2-Ru1-N4	44(7)	C29-S3-Ru1-S2	-22.2(5)
C28-S2-Ru1-N4	155(7)	C27-S3-Ru1-S2	83.3(5)
O19-S2-Ru1-N101	37.1(6)	C29-S3-Ru1-S1	-110.4(4)
C25-S2-Ru1-N101	161.4(5)	C27-S3-Ru1-S1	-4.8(5)
C28-S2-Ru1-N101	-87.6(7)	C24-S1-Ru1-N4	-177.8(6)
O19-S2-Ru1-N1	-50.0(7)	C26-S1-Ru1-N4	75.6(6)
C25-S2-Ru1-N1	74.2(5)	C24-S1-Ru1-N101	-127(11)
C28-S2-Ru1-N1	-174.7(7)	C26-S1-Ru1-N101	127(11)
O19-S2-Ru1-S3	129.1(6)	C24-S1-Ru1-N1	-96.9(6)
C25-S2-Ru1-S3	-106.6(4)	C26-S1-Ru1-N1	156.4(6)
C28-S2-Ru1-S3	4.5(6)	C24-S1-Ru1-S2	-0.6(5)
O19-S2-Ru1-S1	-141.3(6)	C26-S1-Ru1-S2	-107.3(5)
C25-S2-Ru1-S1	-17.0(4)	C24-S1-Ru1-S3	88.4(5)
C28-S2-Ru1-S1	94.1(6)	C26-S1-Ru1-S3	-18.3(5)
C29-S3-Ru1-N4	159.3(6)	O200-C200-N200-C201	7(2)
C27-S3-Ru1-N4	-95.1(6)	O200-C200-N200-C202	-179.8(15)
C29-S3-Ru1-N101	70.8(5)		

Symmetry transformations used to generate equivalent atoms:

Table 6.49. Hydrogen bonds for **FL1528-1** [Å and °].

D-H...A	d(D-H)	d(H...A)	d(D...A)	<(DHA)
N14-H14...O200	0.88	1.90	2.773(14)	169.2

Symmetry transformations used to generate equivalent atoms:

Crystal structure of FL1370-1.

Table 6.50. Crystal data and structure refinement for **FL1370-1**.

Identification code	fl1370-1	
Habitus, colour	plate, dark red	
Crystal size	0.18 x 0.12 x 0.08 mm^3	
Crystal system	Orthorhombic	
Space group	P b c n	Z = 8
Unit cell dimensions	a = 17.5344(12) Å	α= 90°.
	b = 14.0596(7) Å	β= 90°.
	c = 23.5300(11) Å	γ = 90°.
Volume	5800.8(6) $Å^3$	
Cell determination	7607 peaks with Theta 1.7 to 25°.	
Empirical formula	C_{28} H_{30} N_4 O_4 Ru S_4	
Formula weight	715.87	
Density (calculated)	1.639 Mg/m^3	
Absorption coefficient	0.871 mm^{-1}	
F(000)	2928	

Data collection:

Diffractometer type	STOE IPDS2
Wavelength	0.71073 Å
Temperature	100(2) K
Theta range for data collection	1.86 to 25.00°.
Index ranges	-20<=h<=18, -16<=k<=16, -27<=l<=27
Data collection software	STOE X-AREA
Cell refinement software	STOE X-AREA
Data reduction software	STOE X-AREA

Solution and refinement:

Reflections collected	21516
Independent reflections	5117 [R(int) = 0.1483]
Completeness to theta = 25.00°	100.0 %
Observed reflections	2225[I>2(I)]
Reflections used for refinement	5117
Absorption correction	Semi-empirical from equivalents
Max. and min. transmission	1.0016 and 0.8295
Largest diff. peak and hole	0.570 and -0.458 $e.Å^{-3}$
Solution	Direct methods
Refinement	Full-matrix least-squares on F^2
Treatment of hydrogen atoms	CH, OH calc., riding model, NH located, isotr. ref.
Programs used	SIR92 (Giacovazzo et al, 1993)
	SHELXL-97 (Sheldrick, 2008)
	DIAMOND 3.2 (Crystal Impact)
	STOE X-AREA
Data / restraints / parameters	5117 / 0 / 377
Goodness-of-fit on F^2	0.774
R index (all data)	wR2 = 0.0827
R index conventional [I>2sigma(I)]	R1 = 0.0495

Table 6.51. Atomic coordinates and equivalent isotropic displacement parameters ($Å^2$) for **FL1370-1**. U(eq) is defined as one third of the trace of the orthogonalized U^{ij} tensor.

	x	y	z	U(eq)	Occupancy
C2	0.3706(4)	-0.2370(5)	0.4276(2)	0.041(2)	1
C3	0.3618(4)	-0.1422(5)	0.4092(2)	0.0402(19)	1
C5	0.3375(5)	0.0095(5)	0.4109(2)	0.0385(18)	1
C6	0.3151(4)	0.1002(5)	0.4254(2)	0.047(2)	1
C7	0.3117(4)	0.1710(5)	0.3847(2)	0.047(2)	1
C8	0.3289(5)	0.1485(5)	0.3270(2)	0.0424(18)	1
C9	0.3493(4)	0.0583(5)	0.3115(2)	0.045(2)	1
C10	0.3534(4)	-0.0127(5)	0.3520(2)	0.041(2)	1
C11	0.3696(4)	-0.1128(5)	0.3513(2)	0.0419(19)	1
C12	0.3856(4)	-0.1871(5)	0.3130(2)	0.0394(19)	1
C13	0.4002(5)	-0.1845(6)	0.2498(2)	0.047(2)	1
C15	0.4031(5)	-0.3408(6)	0.2792(3)	0.052(2)	1
C16	0.3918(4)	-0.2797(5)	0.3298(2)	0.042(2)	1
C17	0.3839(4)	-0.3094(5)	0.3880(2)	0.043(2)	1
C18	0.3864(4)	-0.4033(5)	0.4098(3)	0.054(2)	1
C19	0.3778(5)	-0.4176(5)	0.4668(3)	0.053(2)	1
C20	0.3665(4)	-0.3417(5)	0.5025(3)	0.048(2)	1
C21	0.4519(5)	0.0310(5)	0.5886(2)	0.055(2)	1
C22	0.3815(5)	0.0885(5)	0.5740(3)	0.054(2)	1
C23	0.2810(5)	-0.0115(6)	0.6461(2)	0.058(2)	1
C24	0.2621(4)	-0.1149(7)	0.6554(2)	0.055(2)	1
C25	0.4166(4)	-0.1736(6)	0.6506(2)	0.054(2)	1
C26	0.4794(4)	-0.1625(5)	0.6077(2)	0.050(2)	1
C27	0.3273(5)	0.3140(5)	0.2981(2)	0.054(2)	1
C28	0.3060(4)	0.3679(5)	0.2449(2)	0.057(2)	1
C29	0.4054(5)	0.3406(6)	0.3179(3)	0.071(3)	1
C100	0.4311(5)	-0.4823(6)	0.1284(3)	0.077(3)	1
C101	0.1621(6)	-0.1670(6)	0.5048(3)	0.047(3)	1
N1	0.3613(3)	-0.2507(4)	0.48491(16)	0.0427(16)	1
N4	0.3431(4)	-0.0692(4)	0.44479(17)	0.0378(15)	1
N14	0.4079(4)	-0.2765(5)	0.2334(2)	0.053(2)	1
N100	0.2178(4)	-0.1575(4)	0.5093(2)	0.0353(18)	1
O8	0.3235(3)	0.2151(3)	0.28375(14)	0.0545(15)	1
O13	0.4025(3)	-0.1152(4)	0.21900(15)	0.0512(14)	1
O15	0.4079(4)	-0.4274(4)	0.27535(18)	0.0637(17)	1
O100	0.4320(4)	-0.3740(5)	0.12939(18)	0.0808(19)	1
S1	0.45607(13)	-0.08303(14)	0.54961(6)	0.0490(6)	1
S2	0.29446(12)	0.01553(14)	0.57040(6)	0.0493(5)	1
S3	0.32405(13)	-0.19578(15)	0.61571(6)	0.0531(6)	1
S4	0.06211(15)	-0.18106(16)	0.49794(8)	0.0674(7)	1
Ru01	0.33227(4)	-0.12346(4)	0.52848(2)	0.04400(17)	1

Table 6.52. Bond lengths [Å] and angles [°] for **FL1370-1**.

C2-N1	1.372(7)	C22-H22B	0.9900
C2-C17	1.399(9)	C23-C24	1.506(11)
C2-C3	1.410(9)	C23-S2	1.837(6)
C3-N4	1.364(7)	C23-H23A	0.9900
C3-C11	1.430(7)	C23-H23B	0.9900
C5-N4	1.368(7)	C24-S3	1.829(8)
C5-C6	1.378(8)	C24-H24A	0.9900
C5-C10	1.446(7)	C24-H24B	0.9900
C6-C7	1.381(8)	C25-C26	1.503(8)
C6-H6	0.9500	C25-S3	1.845(7)
C7-C8	1.427(8)	C25-H25A	0.9900
C7-H7	0.9500	C25-H25B	0.9900
C8-C9	1.367(8)	C26-S1	1.811(6)
C8-O8	1.386(6)	C26-H26A	0.9900
C9-C10	1.382(8)	C26-H26B	0.9900
C9-H9	0.9500	C27-O8	1.433(8)
C10-C11	1.435(9)	C27-C29	1.494(11)
C11-C12	1.408(8)	C27-C28	1.509(8)
C12-C16	1.367(9)	C27-H27	1.0000
C12-C13	1.509(7)	C28-H28A	0.9800
C13-O13	1.215(8)	C28-H28B	0.9800
C13-N14	1.357(8)	C28-H28C	0.9800
C15-O15	1.224(8)	C29-H29A	0.9800
C15-N14	1.410(9)	C29-H29B	0.9800
C15-C16	1.482(9)	C29-H29C	0.9800
C16-C17	1.437(8)	C100-O100	1.523(9)
C17-C18	1.417(9)	C100-H10A	0.9800
C18-C19	1.363(8)	C100-H10B	0.9800
C18-H18	0.9500	C100-H10C	0.9800
C19-C20	1.373(8)	C101-N100	0.991(9)
C19-H19	0.9500	C101-S4	1.772(10)
C20-N1	1.349(7)	N1-Ru01	2.123(6)
C20-H20	0.9500	N4-Ru01	2.120(4)
C21-C22	1.514(10)	N14-H14	0.89(6)
C21-S1	1.848(7)	N100-Ru01	2.112(7)
C21-H21A	0.9900	O100-H100	0.8400
C21-H21B	0.9900	S1-Ru01	2.298(2)
C22-S2	1.841(8)	S2-Ru01	2.287(2)
C22-H22A	0.9900	S3-Ru01	2.2951(15)

N1-C2-C17	124.9(6)	C8-C9-H9	120.0
N1-C2-C3	114.9(6)	C10-C9-H9	120.0
C17-C2-C3	120.1(5)	C9-C10-C11	135.3(5)
N4-C3-C2	123.3(5)	C9-C10-C5	119.6(6)
N4-C3-C11	113.0(6)	C11-C10-C5	105.1(5)
C2-C3-C11	123.7(6)	C12-C11-C3	114.5(6)
N4-C5-C6	128.7(5)	C12-C11-C10	140.7(5)
N4-C5-C10	111.7(5)	C3-C11-C10	104.7(5)
C6-C5-C10	119.5(6)	C16-C12-C11	122.5(5)
C5-C6-C7	120.5(5)	C16-C12-C13	107.1(6)
C5-C6-H6	119.7	C11-C12-C13	130.3(6)
C7-C6-H6	119.7	O13-C13-N14	126.2(6)
C6-C7-C8	119.3(6)	O13-C13-C12	127.8(7)
C6-C7-H7	120.3	N14-C13-C12	106.0(6)
C8-C7-H7	120.3	O15-C15-N14	125.2(7)
C9-C8-O8	116.7(5)	O15-C15-C16	130.2(7)
C9-C8-C7	121.0(5)	N14-C15-C16	104.5(7)
O8-C8-C7	122.3(6)	C12-C16-C17	123.0(6)
C8-C9-C10	120.0(5)	C12-C16-C15	109.3(6)

C17-C16-C15	127.6(7)	C27-C28-H28A	109.5
C2-C17-C18	116.2(6)	C27-C28-H28B	109.5
C2-C17-C16	116.0(6)	H28A-C28-H28B	109.5
C18-C17-C16	127.7(7)	C27-C28-H28C	109.5
C19-C18-C17	119.3(7)	H28A-C28-H28C	109.5
C19-C18-H18	120.3	H28B-C28-H28C	109.5
C17-C18-H18	120.3	C27-C29-H29A	109.5
C18-C19-C20	120.3(7)	C27-C29-H29B	109.5
C18-C19-H19	119.9	H29A-C29-H29B	109.5
C20-C19-H19	119.9	C27-C29-H29C	109.5
N1-C20-C19	124.0(6)	H29A-C29-H29C	109.5
N1-C20-H20	118.0	H29B-C29-H29C	109.5
C19-C20-H20	118.0	O100-C100-H10A	109.5
C22-C21-S1	112.6(5)	O100-C100-H10B	109.5
C22-C21-H21A	109.1	H10A-C100-H10B	109.5
S1-C21-H21A	109.1	O100-C100-H10C	109.5
C22-C21-H21B	109.1	H10A-C100-H10C	109.5
S1-C21-H21B	109.1	H10B-C100-H10C	109.5
H21A-C21-H21B	107.8	N100-C101-S4	178.3(9)
C21-C22-S2	112.9(5)	C20-N1-C2	115.3(6)
C21-C22-H22A	109.0	C20-N1-Ru01	131.9(4)
S2-C22-H22A	109.0	C2-N1-Ru01	112.7(4)
C21-C22-H22B	109.0	C3-N4-C5	105.5(5)
S2-C22-H22B	109.0	C3-N4-Ru01	108.7(4)
H22A-C22-H22B	107.8	C5-N4-Ru01	145.7(4)
C24-C23-S2	111.7(5)	C13-N14-C15	112.8(6)
C24-C23-H23A	109.3	C13-N14-H14	134(4)
S2-C23-H23A	109.3	C15-N14-H14	114(4)
C24-C23-H23B	109.3	C101-N100-Ru01	171.8(8)
S2-C23-H23B	109.3	C8-O8-C27	118.7(4)
H23A-C23-H23B	107.9	C100-O100-H100	109.5
C23-C24-S3	113.3(5)	C26-S1-C21	99.8(3)
C23-C24-H24A	108.9	C26-S1-Ru01	102.9(2)
S3-C24-H24A	108.9	C21-S1-Ru01	106.5(3)
C23-C24-H24B	108.9	C23-S2-C22	100.2(3)
S3-C24-H24B	108.9	C23-S2-Ru01	106.2(3)
H24A-C24-H24B	107.7	C22-S2-Ru01	104.8(3)
C26-C25-S3	111.3(4)	C24-S3-C25	100.9(3)
C26-C25-H25A	109.4	C24-S3-Ru01	102.7(2)
S3-C25-H25A	109.4	C25-S3-Ru01	105.6(2)
C26-C25-H25B	109.4	N100-Ru01-N4	88.2(2)
S3-C25-H25B	109.4	N100-Ru01-N1	86.2(2)
H25A-C25-H25B	108.0	N4-Ru01-N1	80.39(18)
C25-C26-S1	113.9(5)	N100-Ru01-S2	90.58(18)
C25-C26-H26A	108.8	N4-Ru01-S2	96.85(15)
S1-C26-H26A	108.8	N1-Ru01-S2	175.84(15)
C25-C26-H26B	108.8	N100-Ru01-S3	91.76(16)
S1-C26-H26B	108.8	N4-Ru01-S3	174.61(15)
H26A-C26-H26B	107.7	N1-Ru01-S3	94.23(13)
O8-C27-C29	111.0(7)	S2-Ru01-S3	88.54(7)
O8-C27-C28	106.3(5)	N100-Ru01-S1	178.76(18)
C29-C27-C28	111.1(7)	N4-Ru01-S1	91.59(17)
O8-C27-H27	109.5	N1-Ru01-S1	94.93(16)
C29-C27-H27	109.5	S2-Ru01-S1	88.23(8)
C28-C27-H27	109.5	S3-Ru01-S1	88.59(7)

Symmetry transformations used to generate equivalent atoms:

Table 6.53. Anisotropic displacement parameters ($Å^2$) for **FL1370-1**.
The anisotropicdisplacement factor exponent takes the form: $-2\pi^2[h^2a^{*2}U^{11} + ... + 2 h k a^* b^* U^{12}]$

	U^{11}	U^{22}	U^{33}	U^{23}	U^{13}	U^{12}
C2	0.054(5)	0.046(5)	0.025(3)	-0.010(3)	0.001(3)	0.000(4)
C3	0.046(5)	0.041(5)	0.033(3)	0.004(3)	-0.002(3)	-0.002(4)
C5	0.052(5)	0.035(4)	0.028(3)	0.002(3)	-0.006(3)	0.007(5)
C6	0.053(6)	0.058(5)	0.029(3)	0.002(3)	-0.004(3)	-0.002(5)
C7	0.062(6)	0.045(5)	0.034(3)	-0.003(3)	-0.006(3)	0.008(4)
C8	0.061(5)	0.035(5)	0.031(3)	0.003(3)	-0.010(4)	-0.002(5)
C9	0.060(6)	0.054(5)	0.020(3)	-0.002(3)	-0.002(3)	-0.006(5)
C10	0.052(6)	0.048(5)	0.025(3)	-0.005(3)	-0.005(3)	-0.002(4)
C11	0.062(5)	0.044(5)	0.020(3)	0.003(3)	0.000(3)	-0.006(5)
C12	0.063(6)	0.039(5)	0.016(3)	-0.002(3)	0.002(3)	0.001(4)
C13	0.062(6)	0.056(6)	0.025(3)	-0.002(4)	-0.002(3)	-0.002(5)
C15	0.059(6)	0.053(6)	0.045(4)	-0.003(4)	0.005(4)	-0.009(5)
C16	0.055(5)	0.041(5)	0.032(3)	-0.005(3)	0.003(3)	-0.002(4)
C17	0.053(6)	0.041(5)	0.036(3)	0.005(3)	-0.001(3)	-0.004(4)
C18	0.053(6)	0.049(6)	0.058(4)	0.008(4)	0.001(4)	-0.002(4)
C19	0.081(7)	0.031(4)	0.046(4)	0.006(4)	0.003(4)	-0.001(4)
C20	0.052(5)	0.051(6)	0.041(3)	0.011(4)	-0.008(4)	0.003(4)
C21	0.068(6)	0.071(6)	0.026(3)	-0.013(3)	-0.006(4)	-0.007(5)
C22	0.071(6)	0.056(6)	0.035(3)	-0.008(3)	-0.002(4)	-0.003(5)
C23	0.056(6)	0.094(7)	0.025(3)	-0.013(4)	0.005(4)	0.000(6)
C24	0.054(5)	0.085(7)	0.028(3)	0.018(4)	0.008(3)	0.005(6)
C25	0.054(6)	0.077(6)	0.032(3)	0.013(4)	-0.010(4)	0.012(5)
C26	0.056(6)	0.063(6)	0.031(3)	0.003(3)	0.004(3)	-0.005(5)
C27	0.073(6)	0.052(5)	0.037(3)	0.005(3)	-0.006(4)	0.010(6)
C28	0.072(6)	0.045(5)	0.056(4)	0.015(4)	-0.016(4)	0.002(5)
C29	0.103(8)	0.062(7)	0.049(4)	0.011(4)	-0.026(5)	-0.014(6)
C100	0.097(8)	0.065(7)	0.067(5)	-0.016(5)	0.007(5)	0.003(7)
C101	0.091(8)	0.038(5)	0.012(3)	-0.004(3)	-0.009(5)	0.020(6)
N1	0.055(4)	0.050(4)	0.023(3)	0.017(2)	0.000(2)	-0.009(3)
N4	0.052(4)	0.033(3)	0.028(2)	0.001(2)	0.001(3)	0.005(3)
N14	0.070(5)	0.059(5)	0.032(3)	-0.016(3)	0.005(3)	-0.003(4)
N100	0.046(5)	0.037(4)	0.023(3)	0.000(2)	0.004(3)	0.003(4)
O8	0.094(4)	0.037(3)	0.032(2)	0.0059(19)	-0.012(3)	-0.004(4)
O13	0.075(4)	0.058(3)	0.021(2)	-0.002(2)	0.001(2)	0.000(3)
O15	0.096(5)	0.047(4)	0.048(3)	-0.009(3)	0.008(3)	-0.002(4)
O100	0.098(5)	0.099(5)	0.046(3)	-0.014(3)	0.003(3)	-0.007(5)
S1	0.0600(15)	0.0613(14)	0.0256(7)	0.0015(8)	-0.0014(9)	0.0003(12)
S2	0.0619(14)	0.0617(14)	0.0242(7)	-0.0034(8)	0.0003(9)	-0.0002(13)
S3	0.0605(15)	0.0698(14)	0.0289(8)	0.0115(8)	0.0014(10)	0.0012(14)
S4	0.0771(18)	0.0746(16)	0.0504(10)	-0.0036(10)	-0.0041(12)	-0.0053(15)
Ru01	0.0571(4)	0.0540(4)	0.02093(19)	0.0028(3)	-0.0003(3)	-0.0018(4)

Table 6.54. Hydrogen coordinates and isotropic displacement parameters ($Å^2$) for **FL1370-1**.

	x	y	z	U(eq)	Occupancy
H6	0.3018	0.1142	0.4636	0.056	1
H7	0.2980	0.2340	0.3951	0.057	1
H9	0.3606	0.0444	0.2729	0.053	1
H18	0.3940	-0.4558	0.3850	0.064	1
H19	0.3797	-0.4803	0.4818	0.063	1
H20	0.3621	-0.3541	0.5421	0.058	1
H21A	0.4523	0.0180	0.6299	0.066	1
H21B	0.4978	0.0689	0.5794	0.066	1
H22A	0.3894	0.1202	0.5369	0.065	1
H22B	0.3745	0.1386	0.6031	0.065	1
H23A	0.3282	0.0045	0.6672	0.070	1
H23B	0.2393	0.0283	0.6614	0.070	1
H24A	0.2086	-0.1262	0.6440	0.067	1
H24B	0.2665	-0.1295	0.6965	0.067	1
H25A	0.4131	-0.1152	0.6739	0.065	1
H25B	0.4287	-0.2273	0.6763	0.065	1
H26A	0.4920	-0.2259	0.5918	0.060	1
H26B	0.5255	-0.1382	0.6272	0.060	1
H27	0.2895	0.3283	0.3287	0.065	1
H28A	0.2545	0.3493	0.2329	0.086	1
H28B	0.3424	0.3528	0.2146	0.086	1
H28C	0.3071	0.4363	0.2526	0.086	1
H29A	0.4173	0.3059	0.3529	0.107	1
H29B	0.4073	0.4092	0.3253	0.107	1
H29C	0.4427	0.3242	0.2884	0.107	1
H10A	0.4771	-0.5057	0.1093	0.115	1
H10B	0.3859	-0.5044	0.1078	0.115	1
H10C	0.4297	-0.5065	0.1674	0.115	1
H100	0.4165	-0.3531	0.0980	0.121	1
H14	0.415(4)	-0.305(5)	0.200(2)	0.05(2)	1

Table 6.55. Torsion angles [°] for **FL1370-1**.

N1-C2-C3-N4	-2.1(11)	C3-C2-N1-C20	177.4(6)
C17-C2-C3-N4	174.9(7)	C17-C2-N1-Ru01	-174.8(6)
N1-C2-C3-C11	179.6(7)	C3-C2-N1-Ru01	2.1(8)
C17-C2-C3-C11	-3.4(11)	C2-C3-N4-C5	-178.0(7)
N4-C5-C6-C7	-178.8(8)	C11-C3-N4-C5	0.5(9)
C10-C5-C6-C7	-3.6(11)	C2-C3-N4-Ru01	0.9(9)
C5-C6-C7-C8	2.3(11)	C11-C3-N4-Ru01	179.4(5)
C6-C7-C8-C9	-0.5(12)	C6-C5-N4-C3	175.2(8)
C6-C7-C8-O8	177.2(7)	C10-C5-N4-C3	-0.3(9)
O8-C8-C9-C10	-177.9(7)	C6-C5-N4-Ru01	-2.8(16)
C7-C8-C9-C10	0.0(12)	C10-C5-N4-Ru01	-178.4(7)
C8-C9-C10-C11	177.4(8)	O13-C13-N14-C15	179.6(8)
C8-C9-C10-C5	-1.2(11)	C12-C13-N14-C15	-2.4(9)
N4-C5-C10-C9	179.0(7)	O15-C15-N14-C13	179.6(9)
C6-C5-C10-C9	3.0(11)	C16-C15-N14-C13	-0.6(9)
N4-C5-C10-C11	0.0(9)	S4-C101-N100-Ru01	10(39)
C6-C5-C10-C11	-176.0(7)	C9-C8-O8-C27	-159.9(8)
N4-C3-C11-C12	-177.3(6)	C7-C8-O8-C27	22.3(11)
C2-C3-C11-C12	1.2(11)	C29-C27-O8-C8	68.9(9)
N4-C3-C11-C10	-0.5(8)	C28-C27-O8-C8	-170.1(7)
C2-C3-C11-C10	178.0(7)	C25-C26-S1-C21	67.7(6)
C9-C10-C11-C12	-3.1(17)	C25-C26-S1-Ru01	-41.9(5)
C5-C10-C11-C12	175.7(10)	C22-C21-S1-C26	-132.8(5)
C9-C10-C11-C3	-178.5(9)	C22-C21-S1-Ru01	-26.1(5)
C5-C10-C11-C3	0.3(8)	C24-C23-S2-C22	-135.1(6)
C3-C11-C12-C16	1.0(11)	C24-C23-S2-Ru01	-26.3(6)
C10-C11-C12-C16	-174.1(9)	C21-C22-S2-C23	71.1(5)
C3-C11-C12-C13	-177.7(7)	C21-C22-S2-Ru01	-38.8(5)
C10-C11-C12-C13	7.2(16)	C23-C24-S3-C25	66.1(5)
C16-C12-C13-O13	-177.3(9)	C23-C24-S3-Ru01	-42.8(5)
C11-C12-C13-O13	1.5(14)	C26-C25-S3-C24	-134.8(6)
C16-C12-C13-N14	4.7(9)	C26-C25-S3-Ru01	-28.3(6)
C11-C12-C13-N14	-176.4(8)	C101-N100-Ru01-N4	-118(6)
C11-C12-C16-C17	-1.1(12)	C101-N100-Ru01-N1	162(6)
C13-C12-C16-C17	177.9(7)	C101-N100-Ru01-S2	-21(6)
C11-C12-C16-C15	175.8(7)	C101-N100-Ru01-S3	68(6)
C13-C12-C16-C15	-5.2(9)	C101-N100-Ru01-S1	-38(11)
O15-C15-C16-C12	-176.4(10)	C3-N4-Ru01-N100	-86.2(5)
N14-C15-C16-C12	3.8(9)	C5-N4-Ru01-N100	91.8(10)
O15-C15-C16-C17	0.3(16)	C3-N4-Ru01-N1	0.3(5)
N14-C15-C16-C17	-179.5(8)	C5-N4-Ru01-N1	178.3(10)
N1-C2-C17-C18	1.2(11)	C3-N4-Ru01-S2	-176.6(4)
C3-C2-C17-C18	-175.5(7)	C5-N4-Ru01-S2	1.5(10)
N1-C2-C17-C16	179.9(7)	C3-N4-Ru01-S3	3(2)
C3-C2-C17-C16	3.2(11)	C5-N4-Ru01-S3	-179(54)
C12-C16-C17-C2	-1.1(12)	C3-N4-Ru01-S1	95.0(5)
C15-C16-C17-C2	-177.4(8)	C5-N4-Ru01-S1	-87.0(10)
C12-C16-C17-C18	177.5(8)	C20-N1-Ru01-N100	-86.8(6)
C15-C16-C17-C18	1.1(14)	C2-N1-Ru01-N100	87.5(5)
C2-C17-C18-C19	-1.5(11)	C20-N1-Ru01-N4	-175.6(7)
C16-C17-C18-C19	179.9(8)	C2-N1-Ru01-N4	-1.3(5)
C17-C18-C19-C20	0.3(12)	C20-N1-Ru01-S2	-126.9(18)
C18-C19-C20-N1	1.6(12)	C2-N1-Ru01-S2	47(2)
S1-C21-C22-S2	43.0(6)	C20-N1-Ru01-S3	4.7(6)
S2-C23-C24-S3	46.4(7)	C2-N1-Ru01-S3	178.9(5)
S3-C25-C26-S1	47.3(7)	C20-N1-Ru01-S1	93.7(6)
C19-C20-N1-C2	-1.9(11)	C2-N1-Ru01-S1	-92.1(5)
C19-C20-N1-Ru01	172.2(6)	C23-S2-Ru01-N100	92.1(3)
C17-C2-N1-C20	0.5(11)	C22-S2-Ru01-N100	-162.4(3)

C23-S2-Ru01-N4	-179.7(3)	C24-S3-Ru01-S2	19.7(3)
C22-S2-Ru01-N4	-74.2(3)	C25-S3-Ru01-S2	-85.6(3)
C23-S2-Ru01-N1	132(2)	C24-S3-Ru01-S1	108.0(3)
C22-S2-Ru01-N1	-122(2)	C25-S3-Ru01-S1	2.7(3)
C23-S2-Ru01-S3	0.4(3)	C26-S1-Ru01-N100	124(7)
C22-S2-Ru01-S3	105.8(2)	C21-S1-Ru01-N100	19(7)
C23-S2-Ru01-S1	-88.3(3)	C26-S1-Ru01-N4	-156.8(3)
C22-S2-Ru01-S1	17.2(2)	C21-S1-Ru01-N4	98.7(3)
C24-S3-Ru01-N100	-70.8(3)	C26-S1-Ru01-N1	-76.4(3)
C25-S3-Ru01-N100	-176.1(3)	C21-S1-Ru01-N1	179.1(2)
C24-S3-Ru01-N4	-160.0(19)	C26-S1-Ru01-S2	106.4(2)
C25-S3-Ru01-N4	94.7(19)	C21-S1-Ru01-S2	1.9(2)
C24-S3-Ru01-N1	-157.1(3)	C26-S1-Ru01-S3	17.8(2)
C25-S3-Ru01-N1	97.5(3)		
C21-S1-Ru01-S3	-86.7(2)		

Symmetry transformations used to generate equivalent atoms:

Table 6.56. Hydrogen bonds for **FL1370-1** [Å and °].

D-H...A	d(D-H)	d(H...A)	d(D...A)	<(DHA)
O100-H100...S4#1	0.84	2.43	3.190(5)	150.5
N14-H14...O100	0.89(6)	1.94(6)	2.836(7)	176(6)

Symmetry transformations used to generate equivalent atoms:
#1 -x+1/2,-y-1/2,z-1/2

B. ^{1}H NMR, ^{13}C NMR Spectra

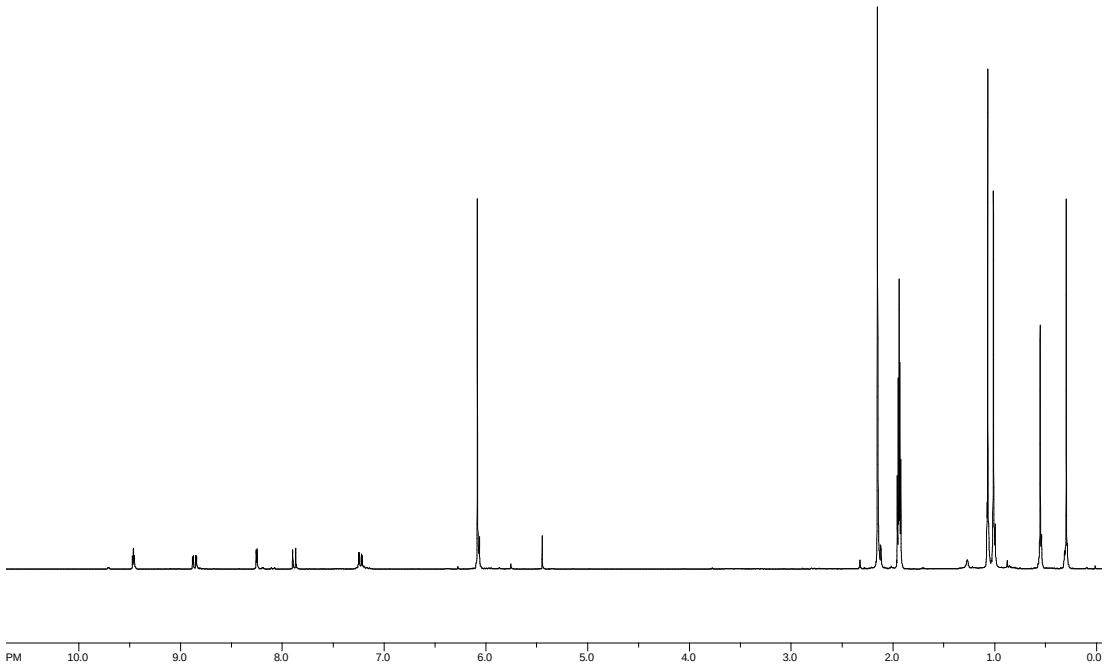

Figure 6.1.1. ^{1}H NMR of complex 2.2 ($CDCl_3$).

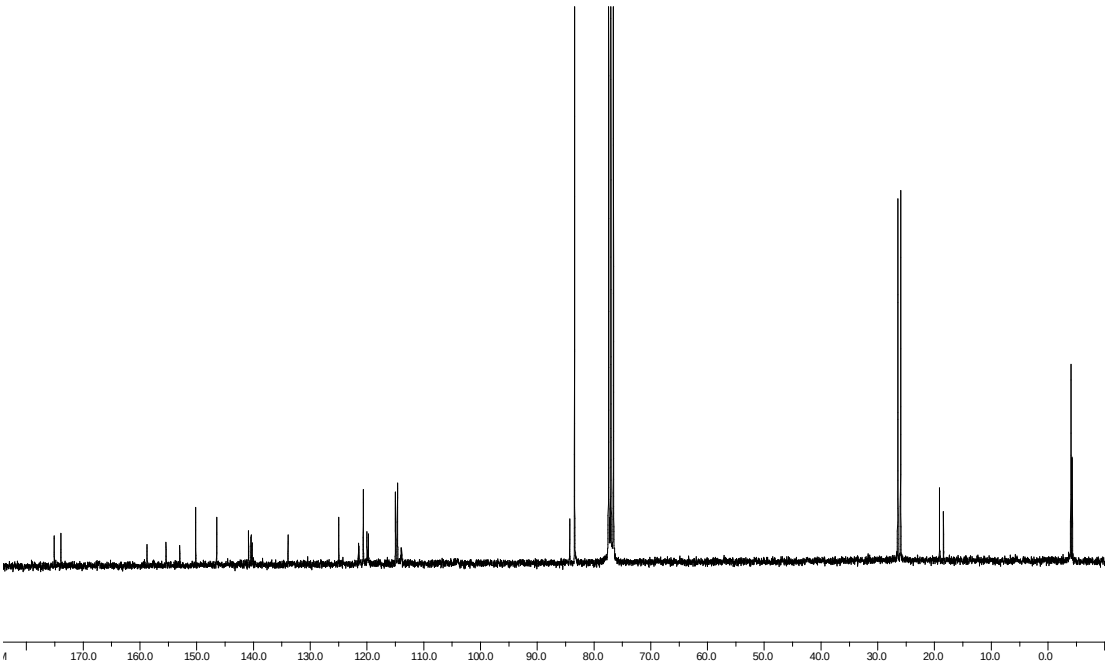

Figure 6.1.2. ^{13}C NMR of complex 2.2 ($CDCl_3$).

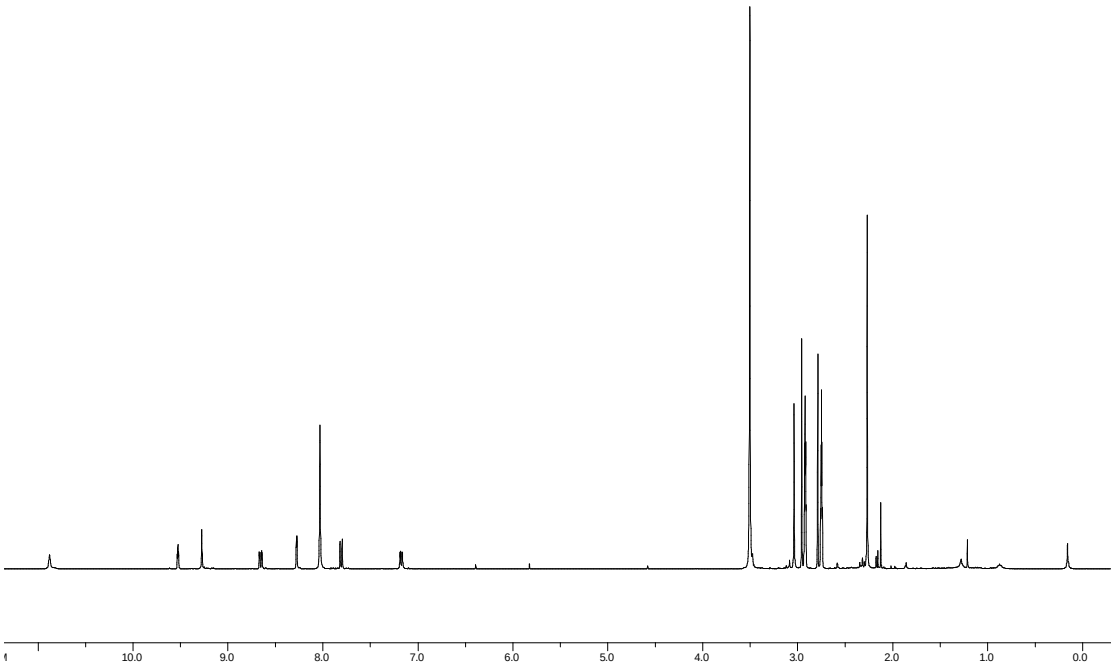

Figure 6.2.1. ^{1}H NMR of complex 2.3 (DMF-d_7).

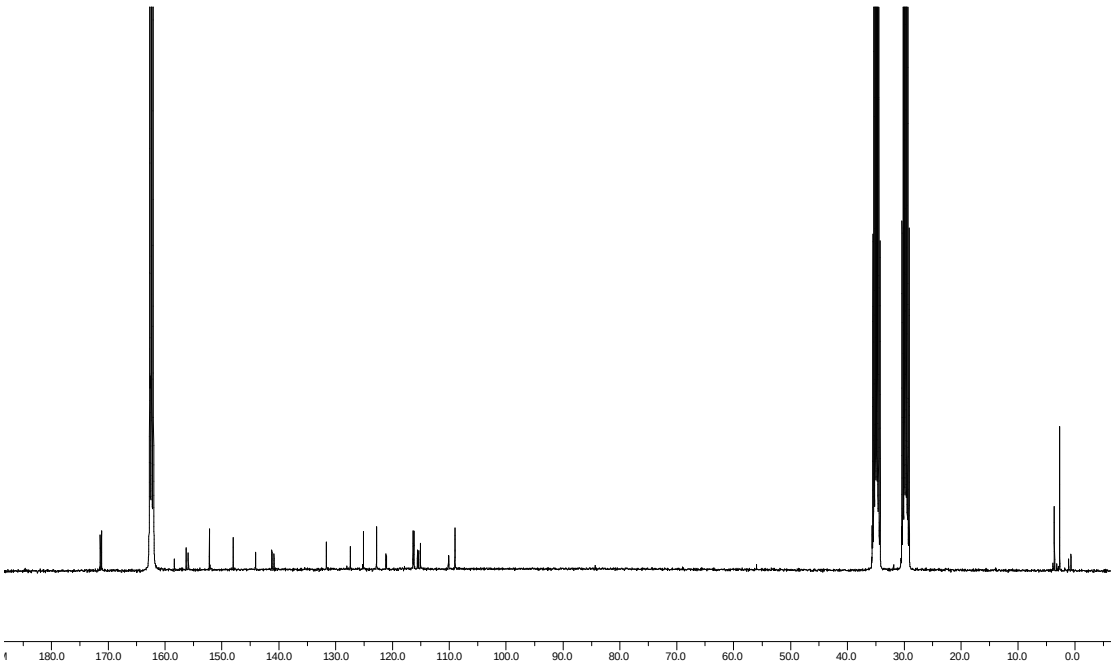

Figure 6.2.2. ^{13}C NMR of complex 2.3 (DMF-d_7).

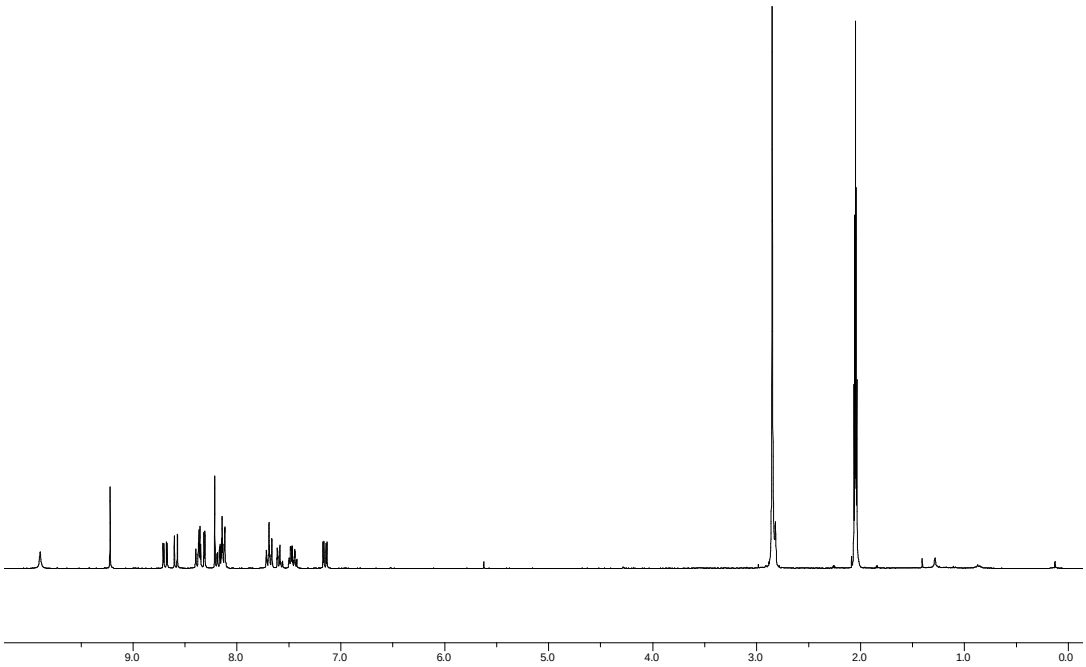

Figure 6.3.1. ^{1}H NMR of complex FL172 (Acetone-d_6).

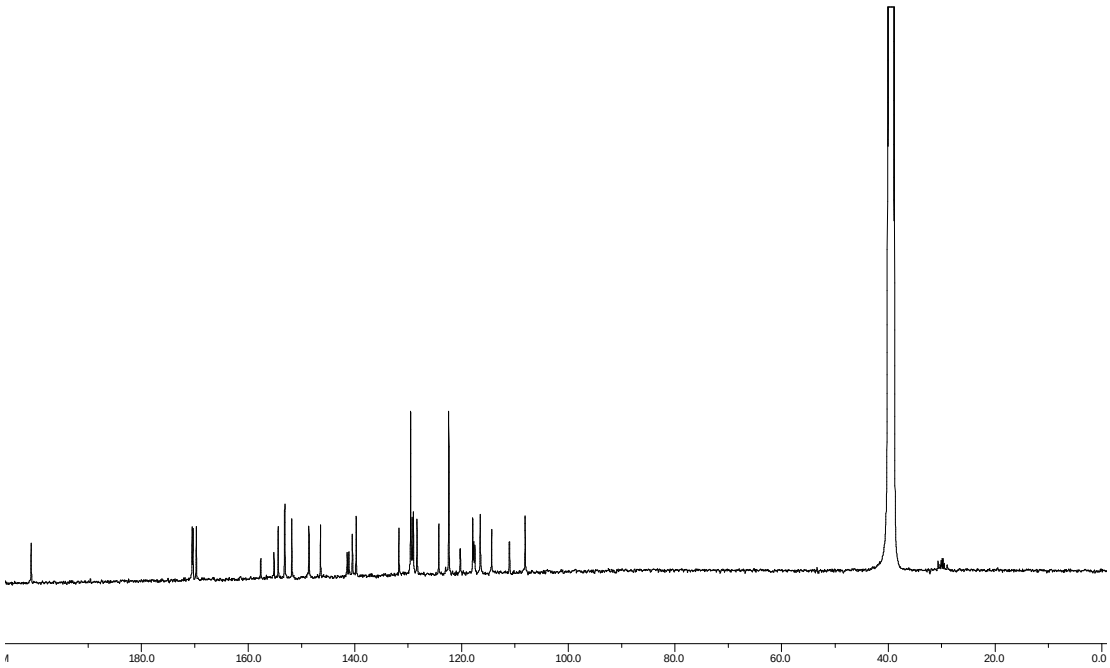

Figure 6.3.2. ^{13}C NMR of complex FL172 (DMSO-d_6).

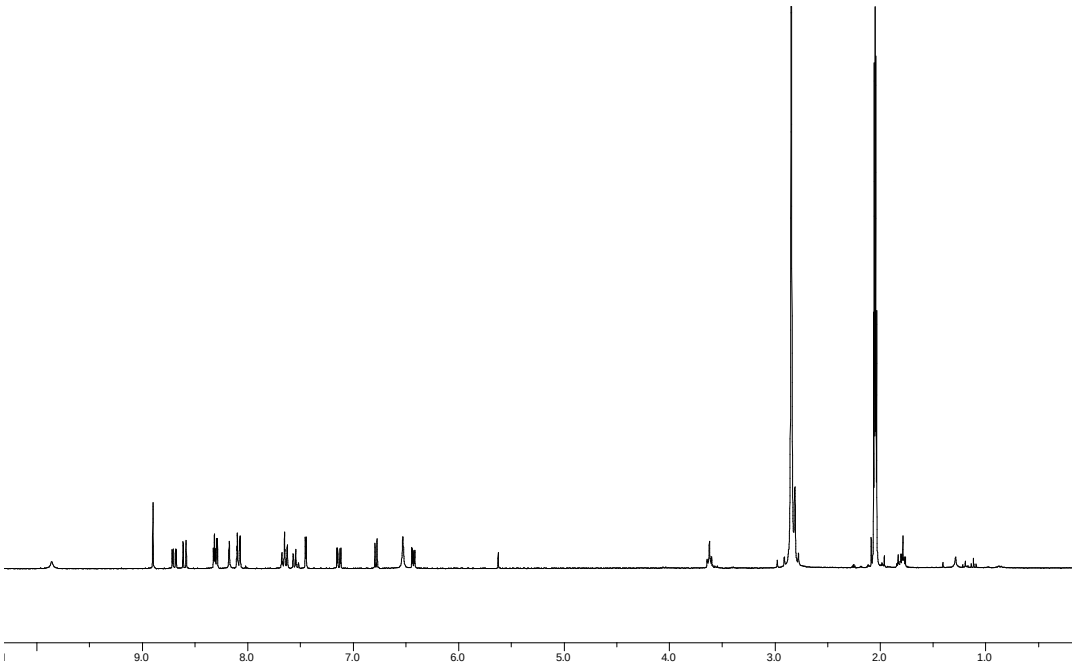

Figure 6.4.1. ^{1}H NMR of complex FL411 (Acetone-d_6).

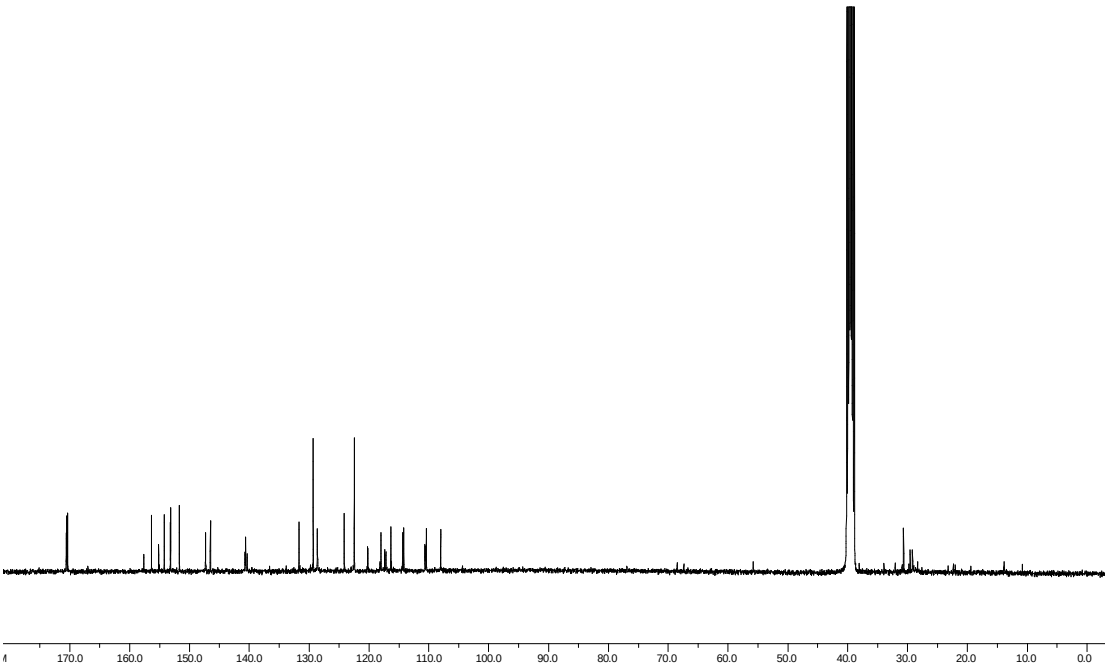

Figure 6.4.2. ^{13}C NMR of complex FL411 (DMSO-d_6).

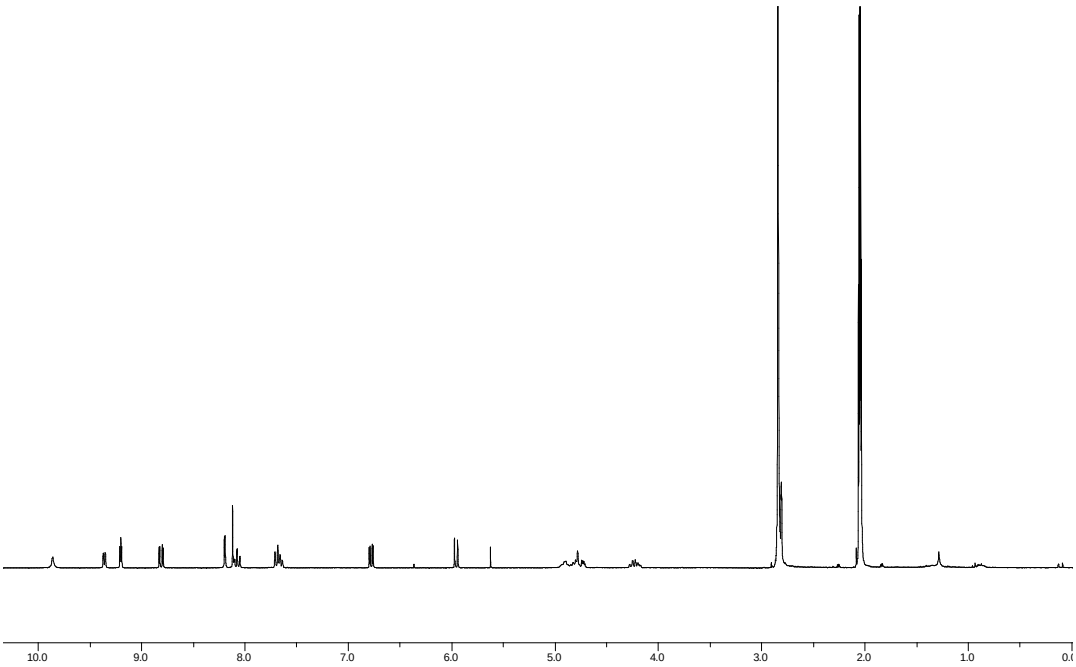

Figure 6.5.1. ^{1}H NMR of complex FL115-1 (Acetone-d_6).

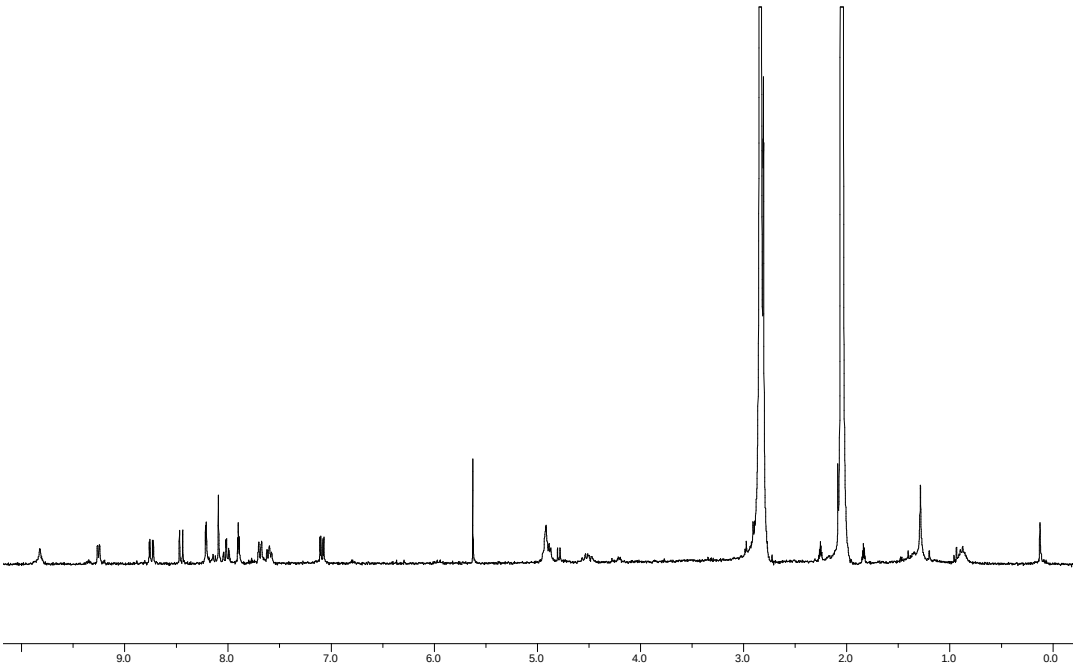

Figure 6.6.1. ^{1}H NMR of complex FL115-2 (Acetone-d_6).

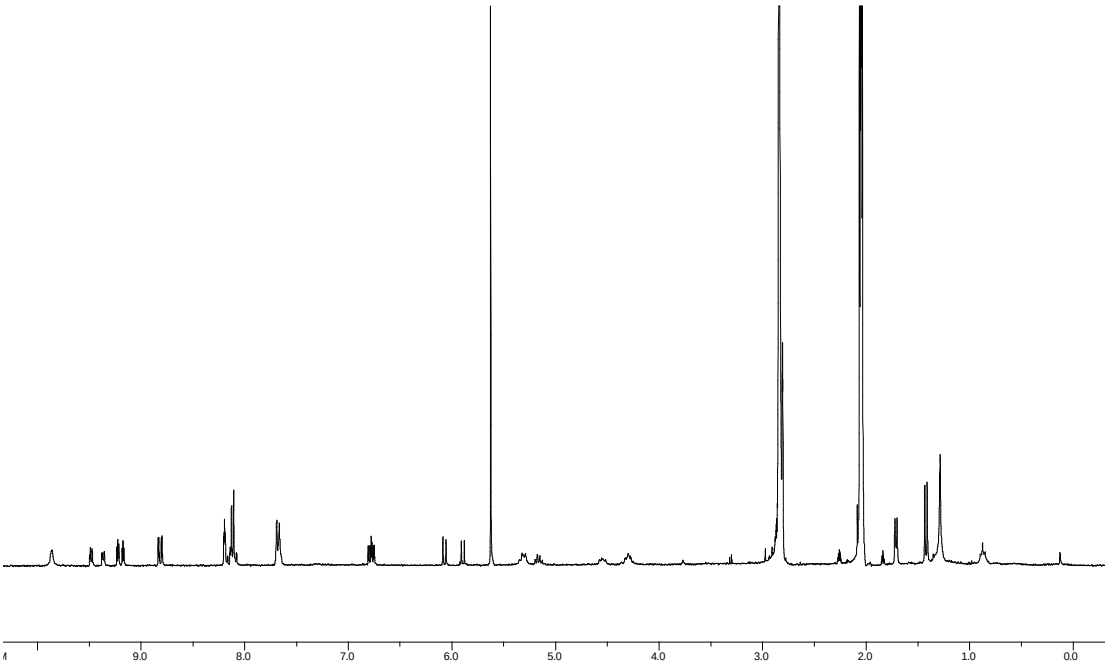

Figure 6.7.1. ^{1}H NMR of complex FL114-1 (Acetone-d_6).

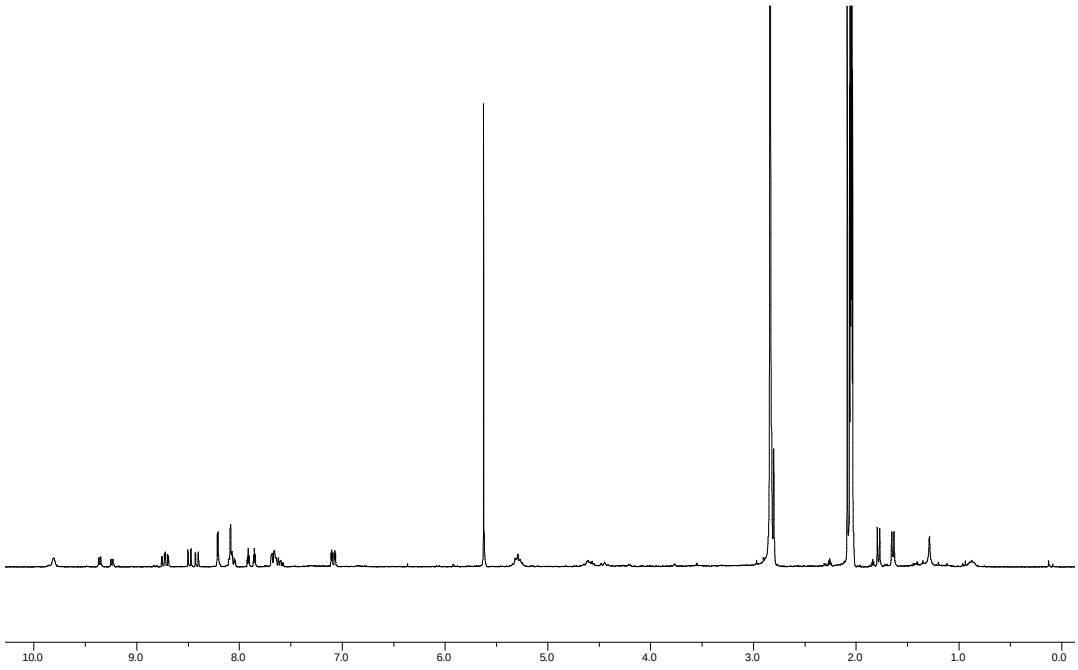

Figure 6.8.1. ^{1}H NMR of complex FL114-2 (Acetone-d_6).

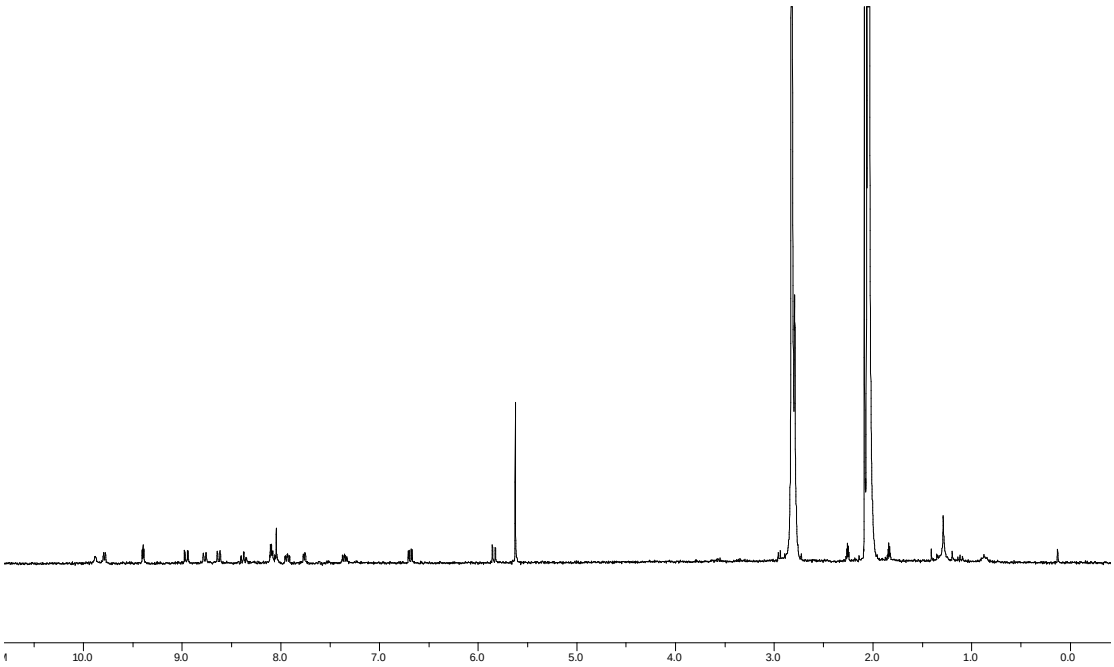

Figure 6.9.1. ^{1}H NMR of complex FL111-1 (Acetone-d_6).

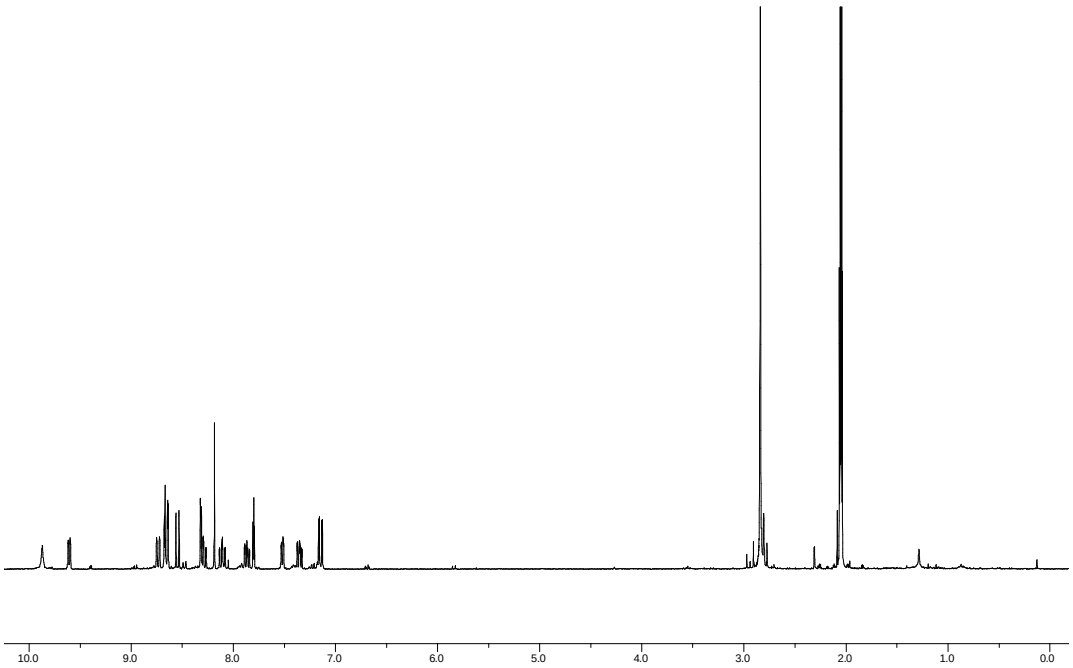

Figure 6.10.1. ^{1}H NMR of complex FL111-2 (Acetone-d_6).

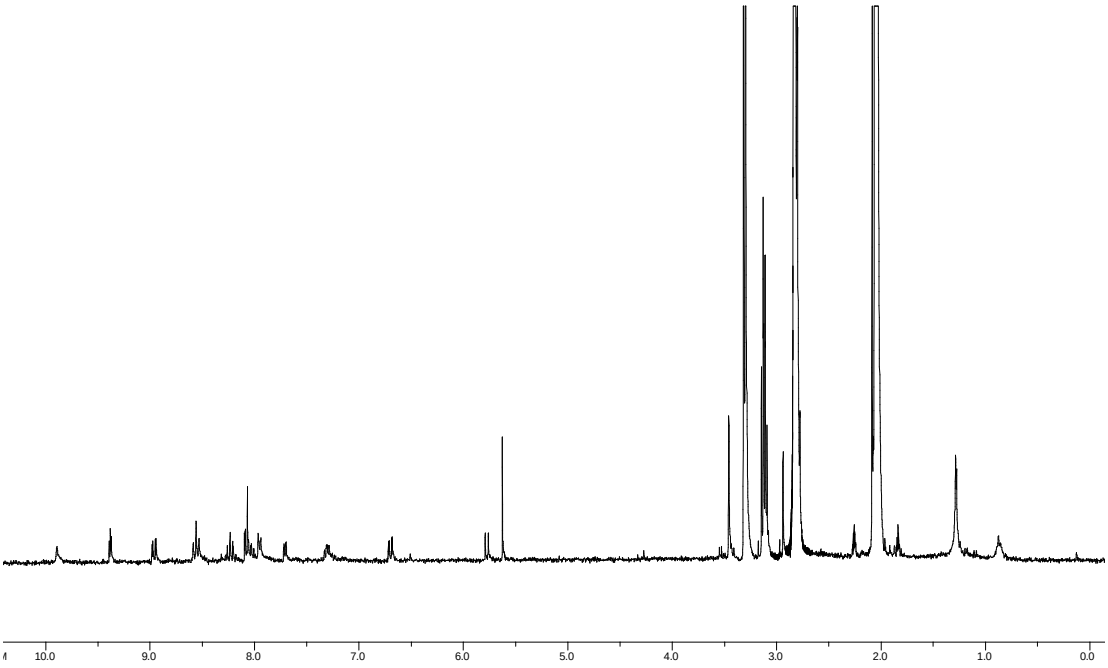

Figure 6.11.1. ^{1}H NMR of complex FL161-1 (Acetone-d_6).

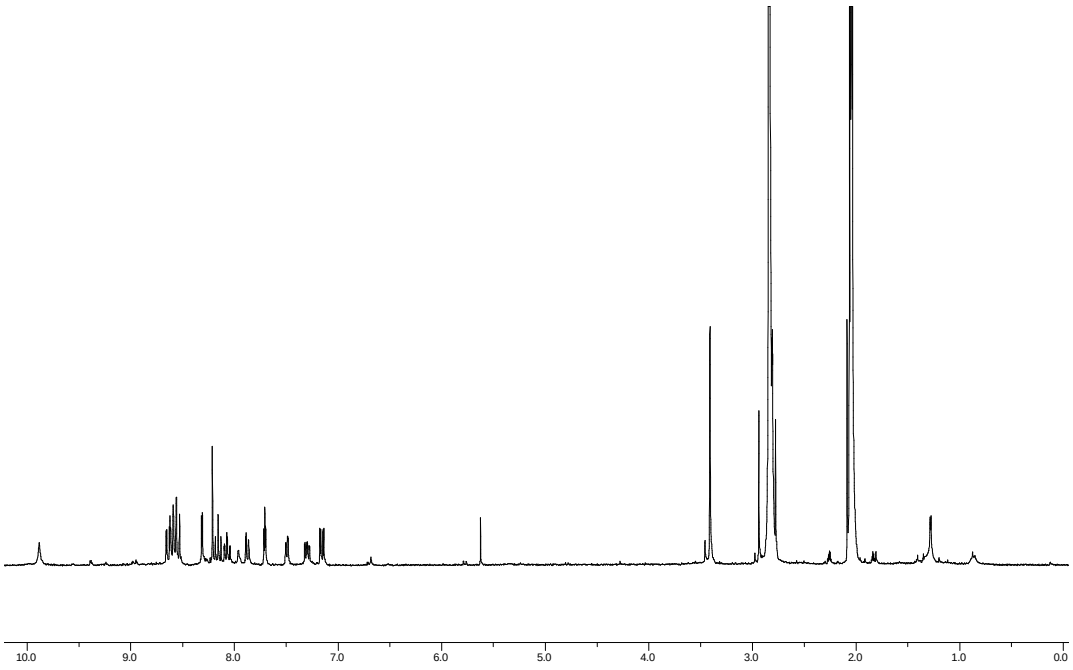

Figure 6.12.1. ^{1}H NMR of complex FL161-2 (Acetone-d_6).

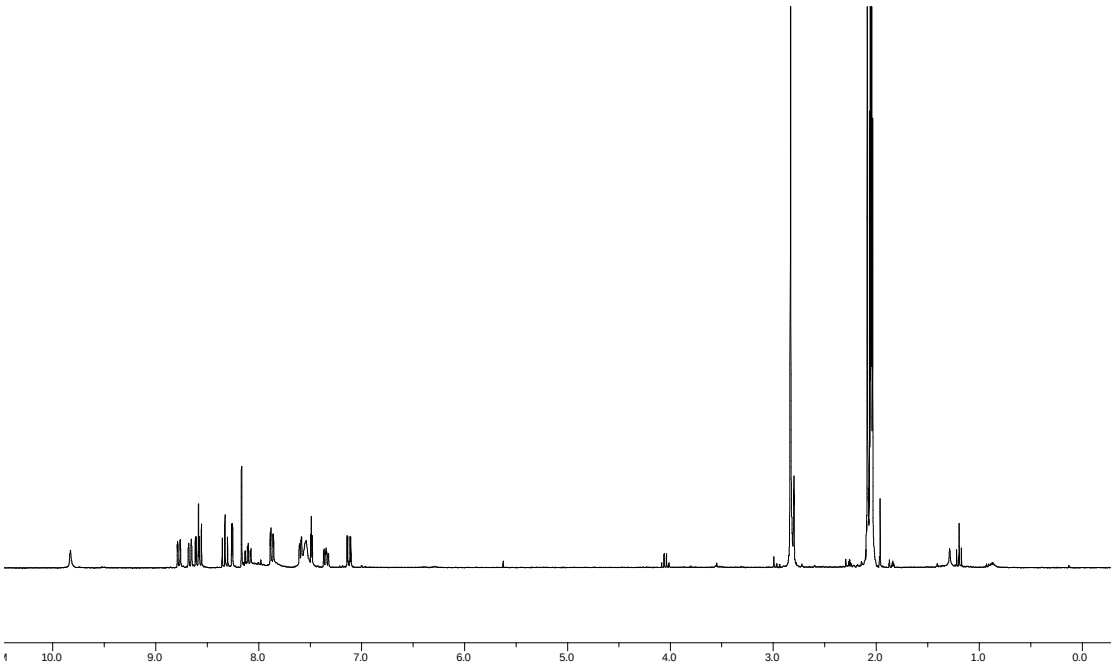

Figure 6.13.1. ^{1}H NMR of complex FL174-2 (Acetone-d_6).

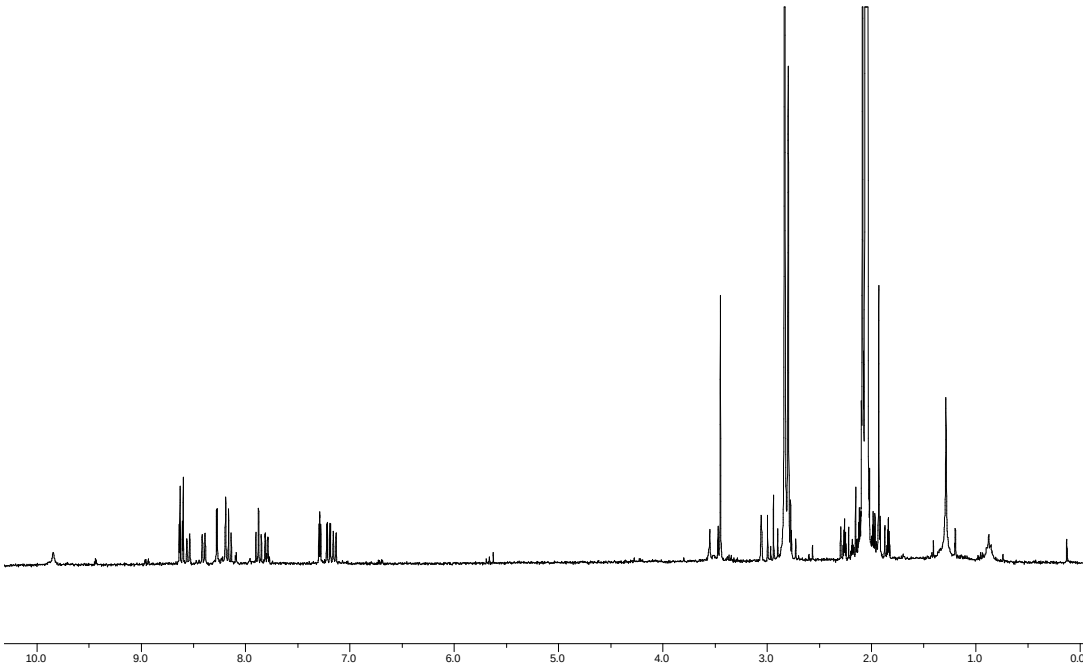

Figure 6.14.1. ^{1}H NMR of complex FL178 (Acetone-d_6).

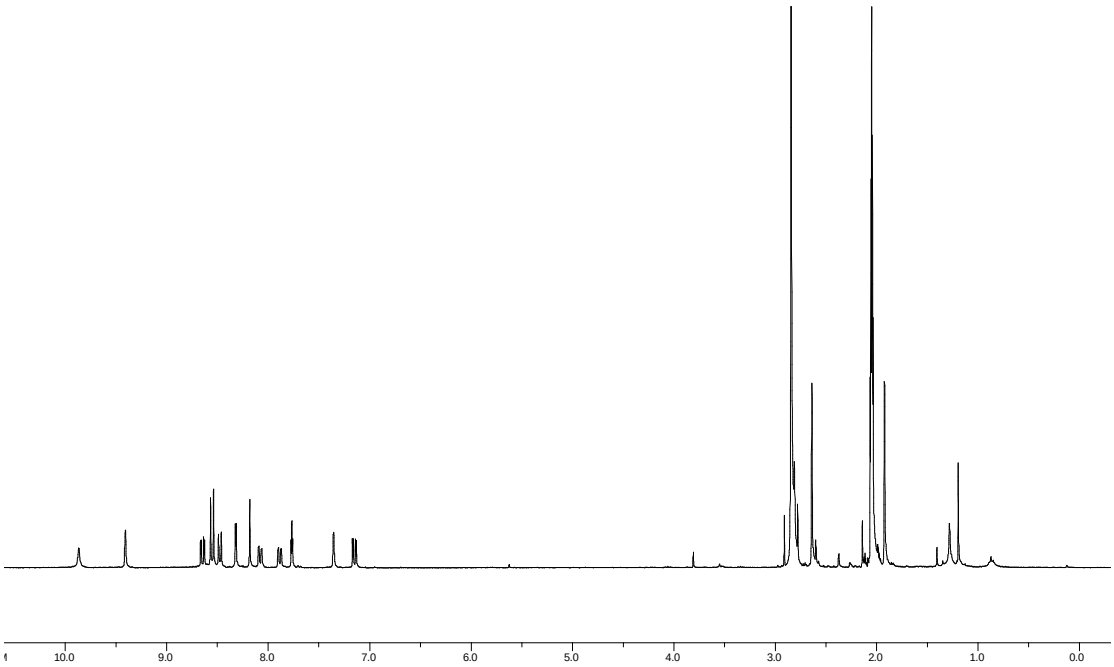

Figure 6.15.1. ^{1}H NMR of complex FL134 (Acetone-d_6).

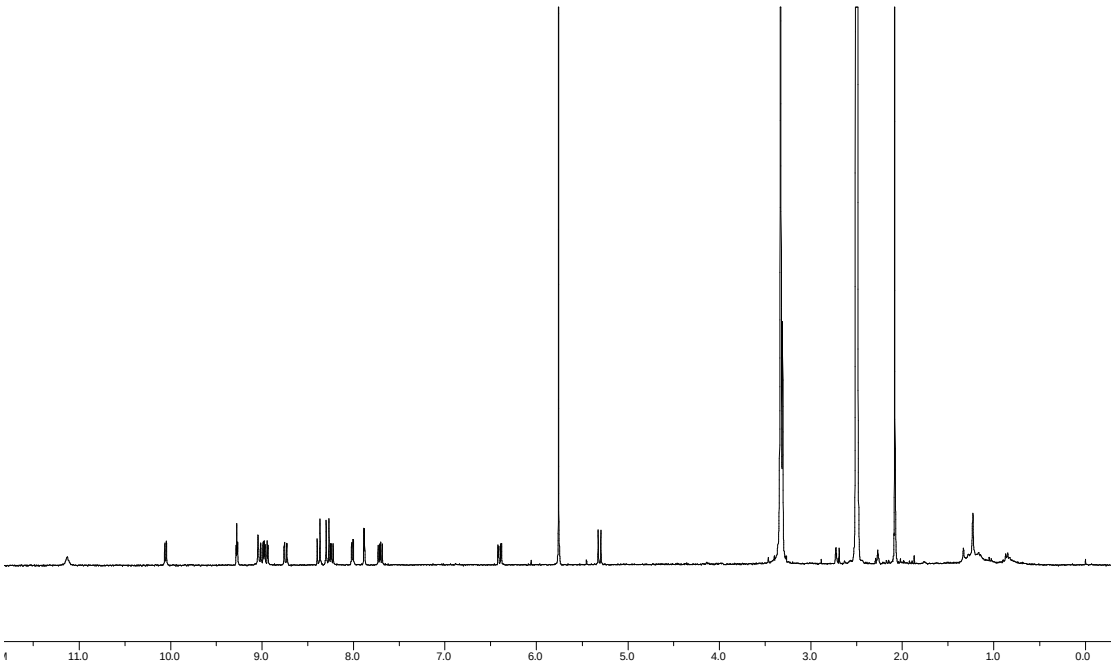

Figure 6.16.1. ^{1}H NMR of complex FL151-1 (Acetone-d_6).

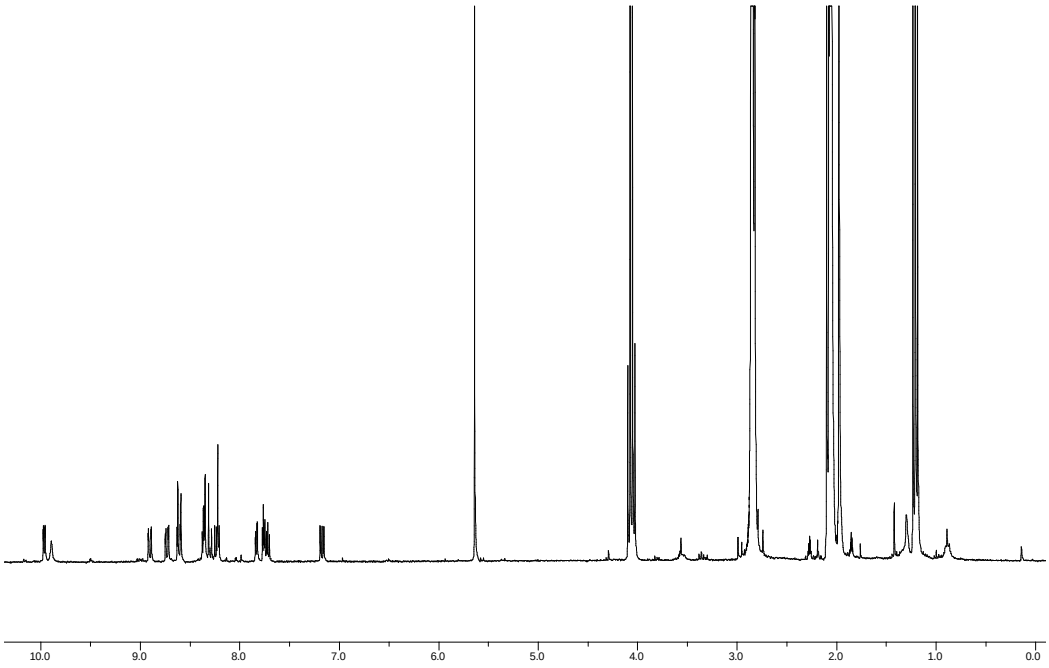

Figure 6.17.1. ^{1}H NMR of complex FL151-2 (Acetone-d_6).

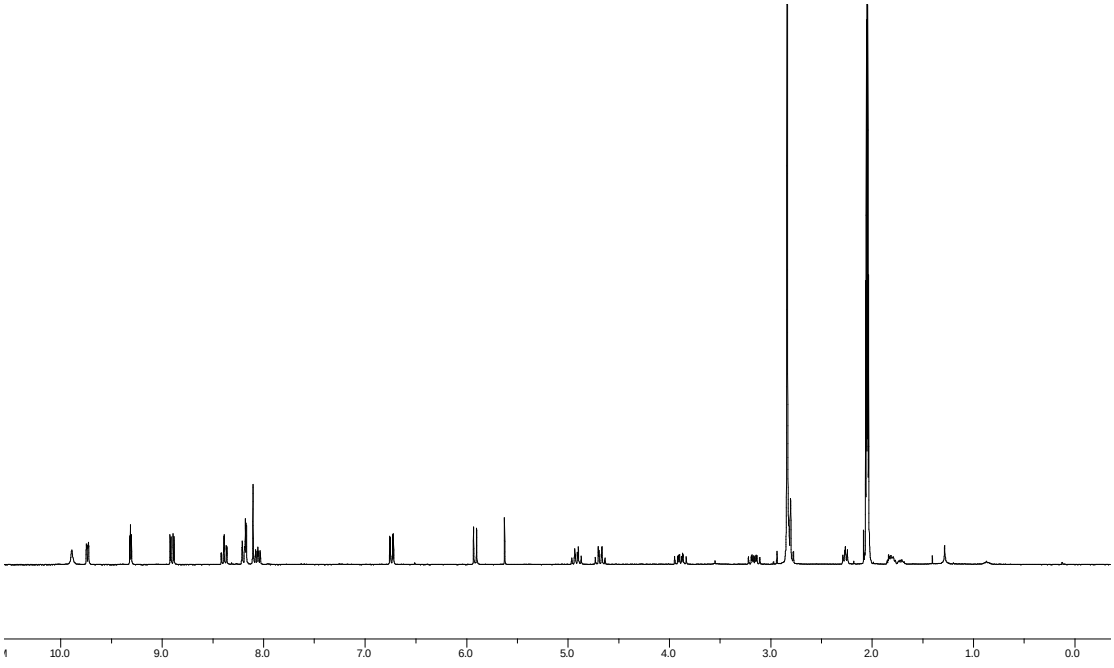

Figure 6.18.1. ^{1}H NMR of complex FL182-1 (Acetone-d_6).

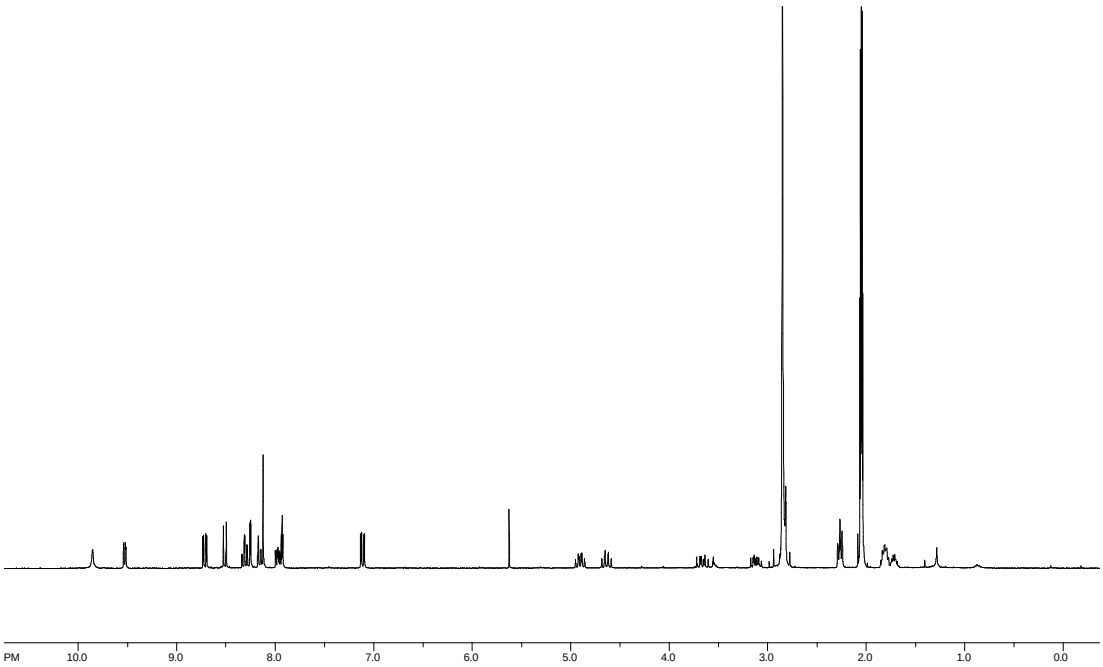

Figure 6.19.1. ^{1}H NMR of complex FL182-2 (Acetone-d_6).

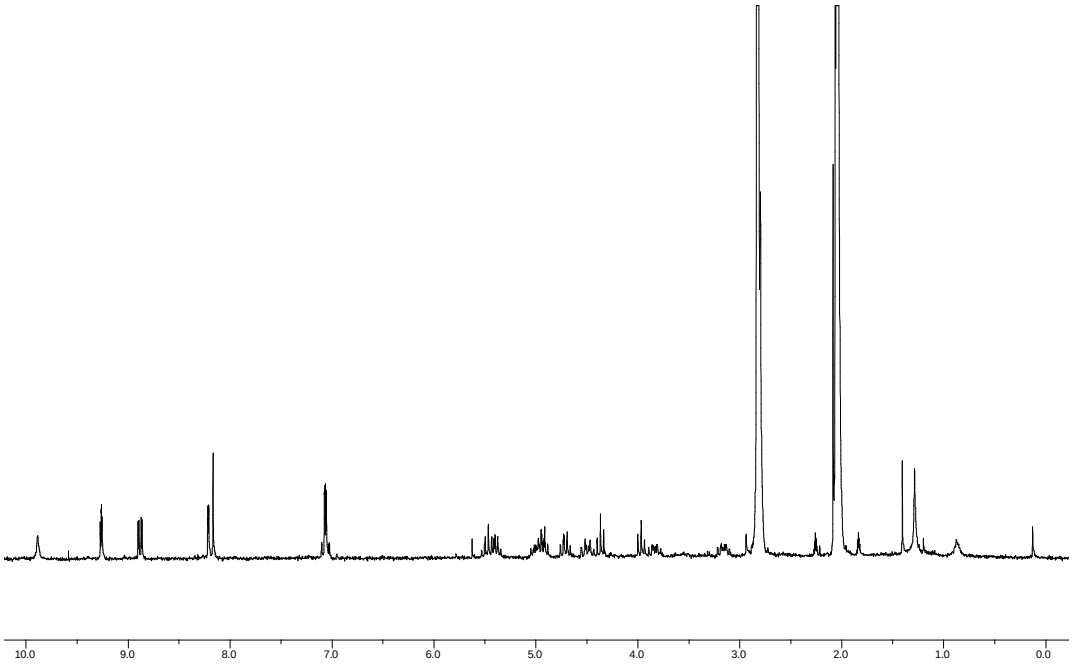

Figure 6.20.1. ^{1}H NMR of complex FL162-1 (Acetone-d_6).

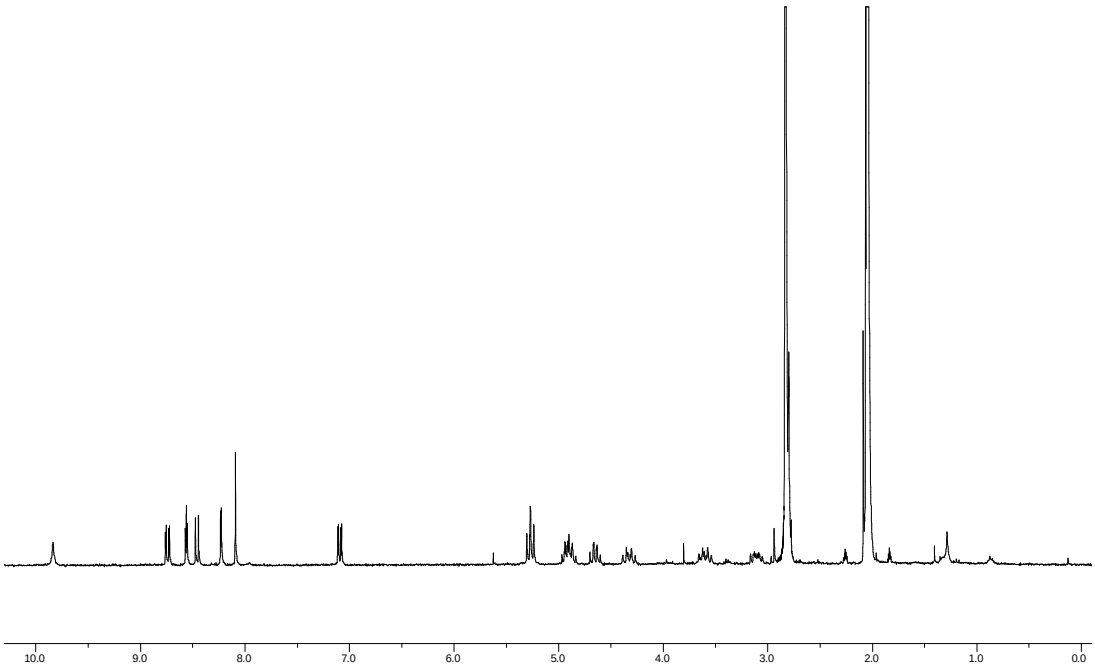

Figure 6.21.1. ^{1}H NMR of complex FL162-2 (Acetone-d_6).

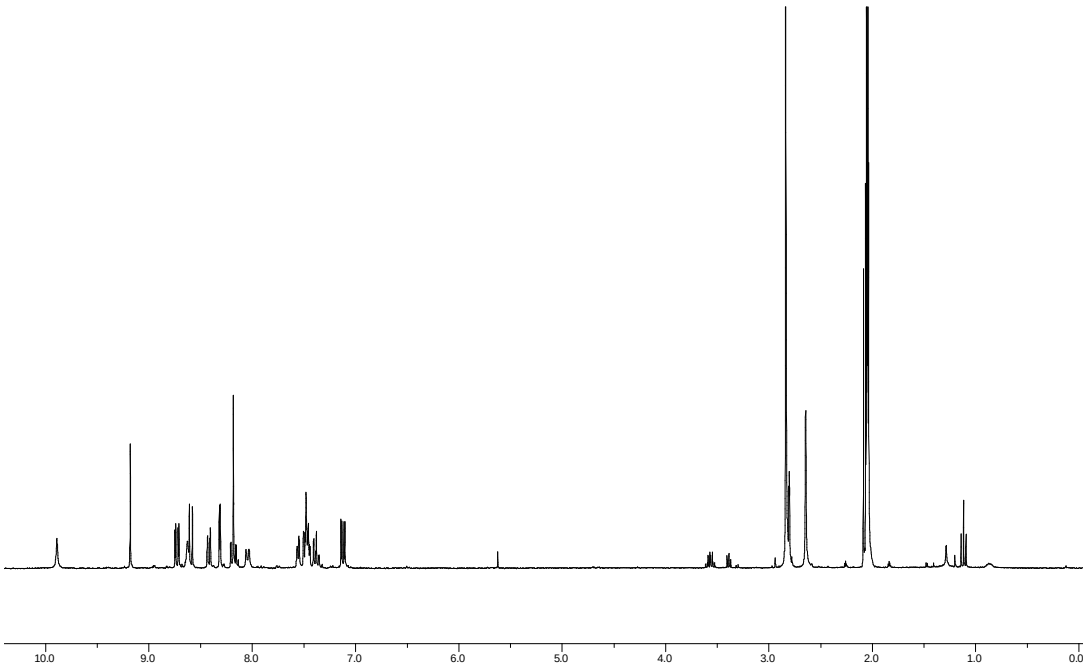

Figure 6.22.1. ^{1}H NMR of complex FL227 (Acetone-d_6).

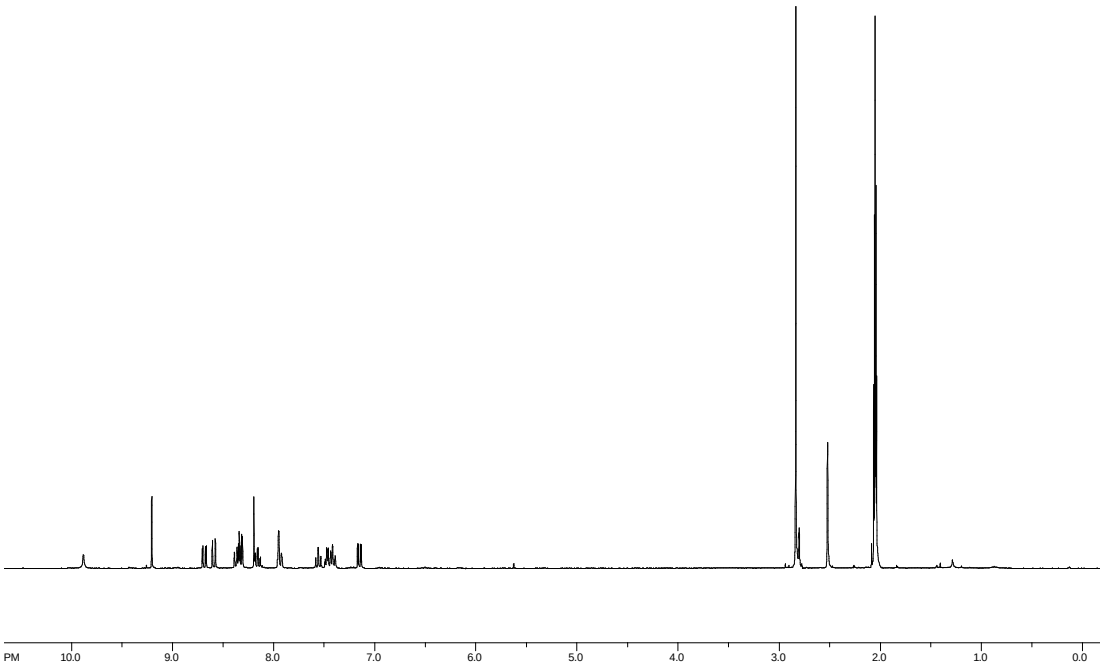

Figure 6.23.1. ^{1}H NMR of complex FL226 (Acetone-d_6).

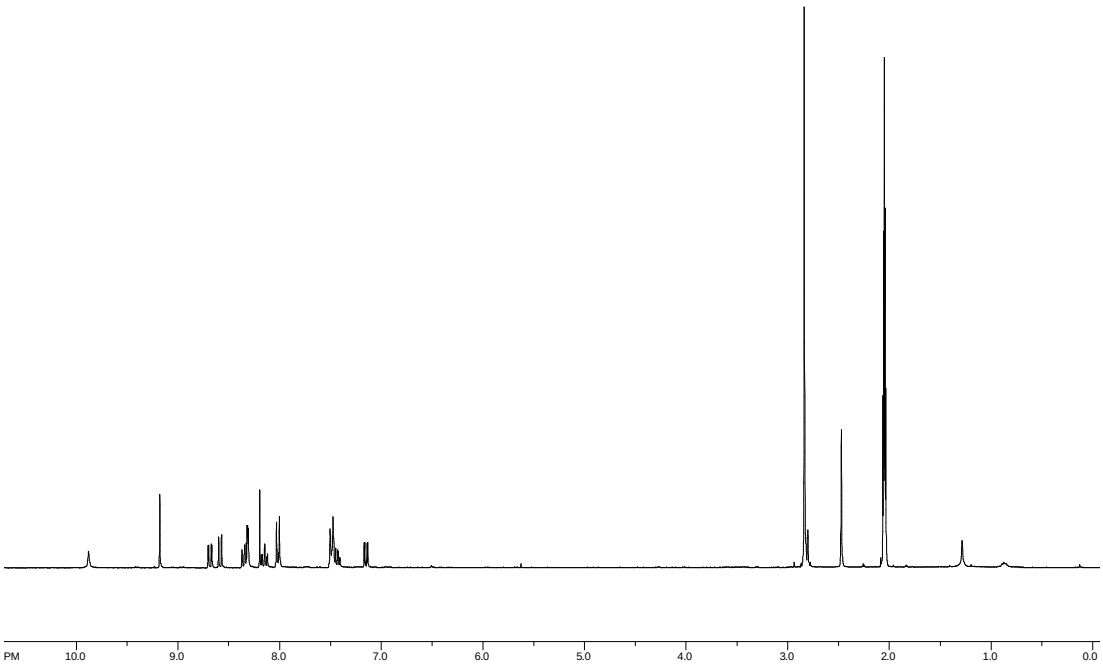

Figure 6.24.1. ^{1}H NMR of complex FL224 (Acetone-d_6).

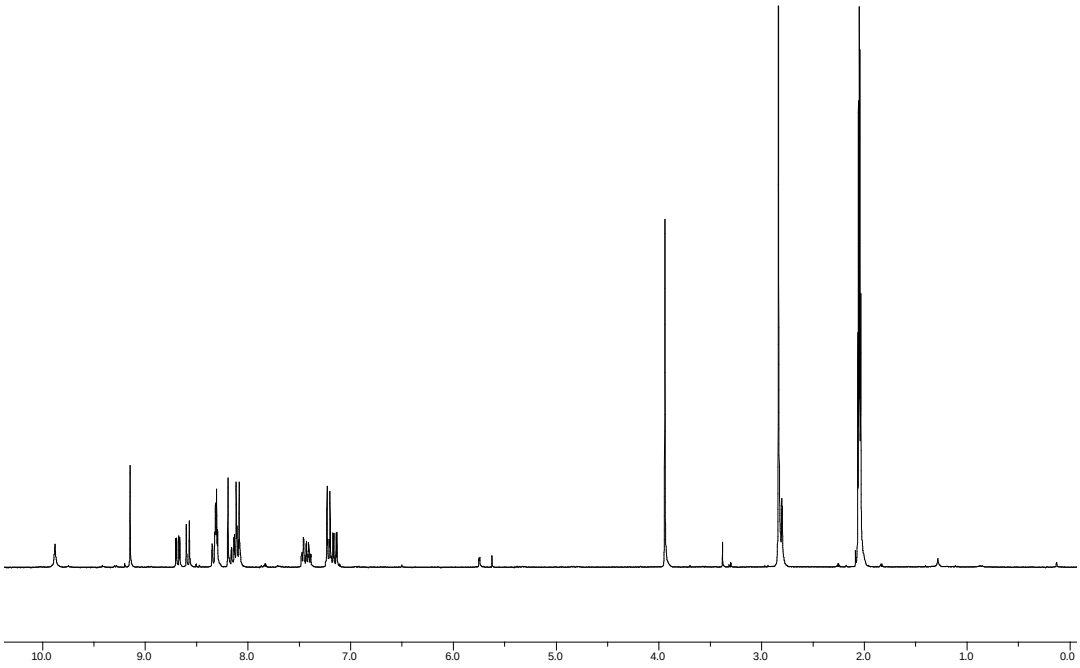

Figure 6.25.1. ^{1}H NMR of complex FL237 (Acetone-d_6).

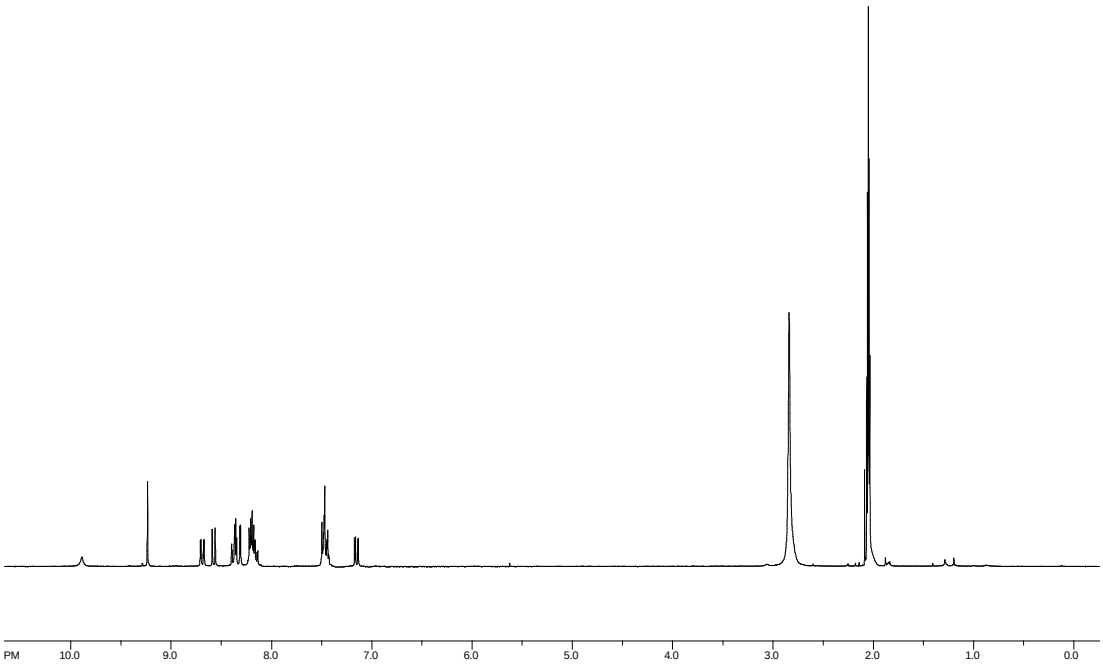

Figure 6.26.1. ^{1}H NMR of complex FL252 (Acetone-d_6).

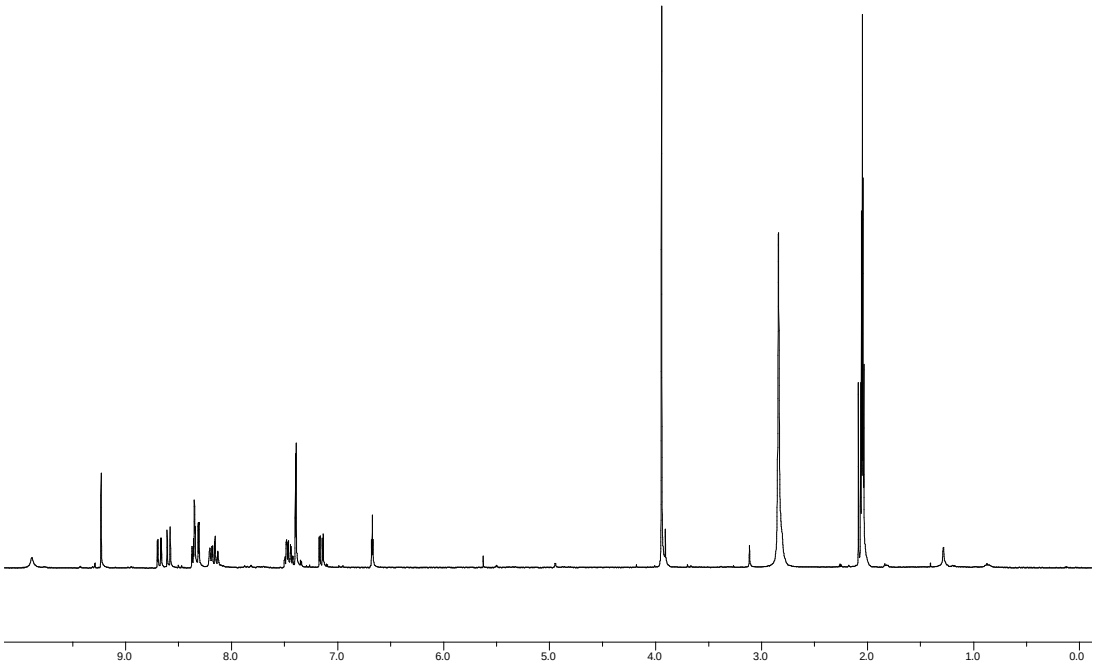

Figure 6.27.1. ^{1}H NMR of complex FL254 (Acetone-d_6).

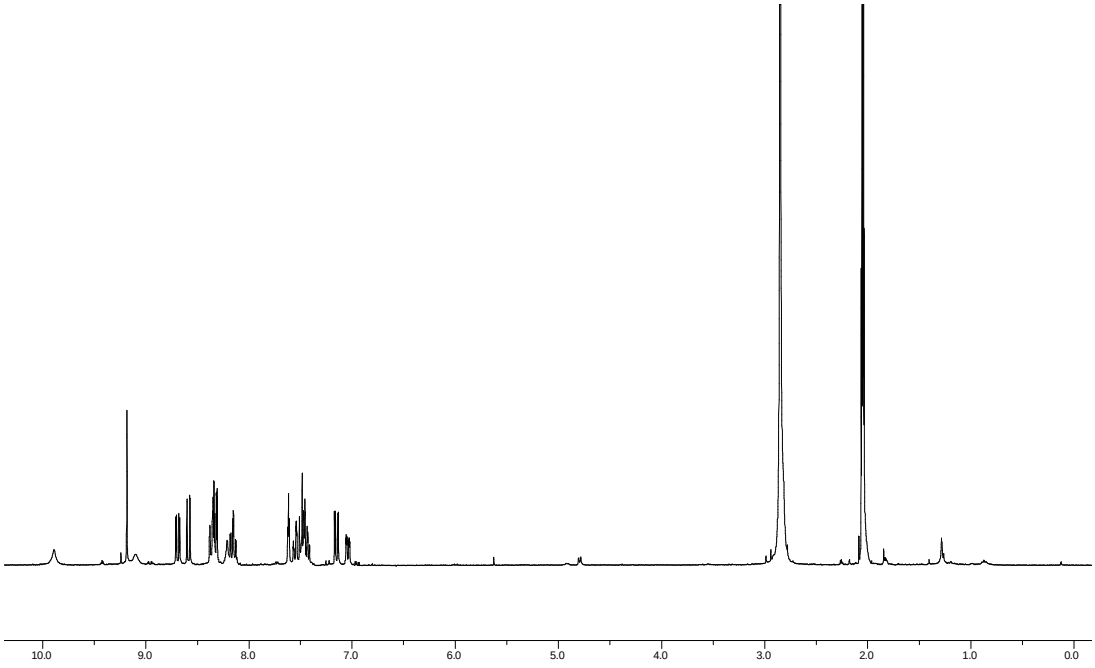

Figure 6.28.1. ^{1}H NMR of complex FL256 (Acetone-d_6).

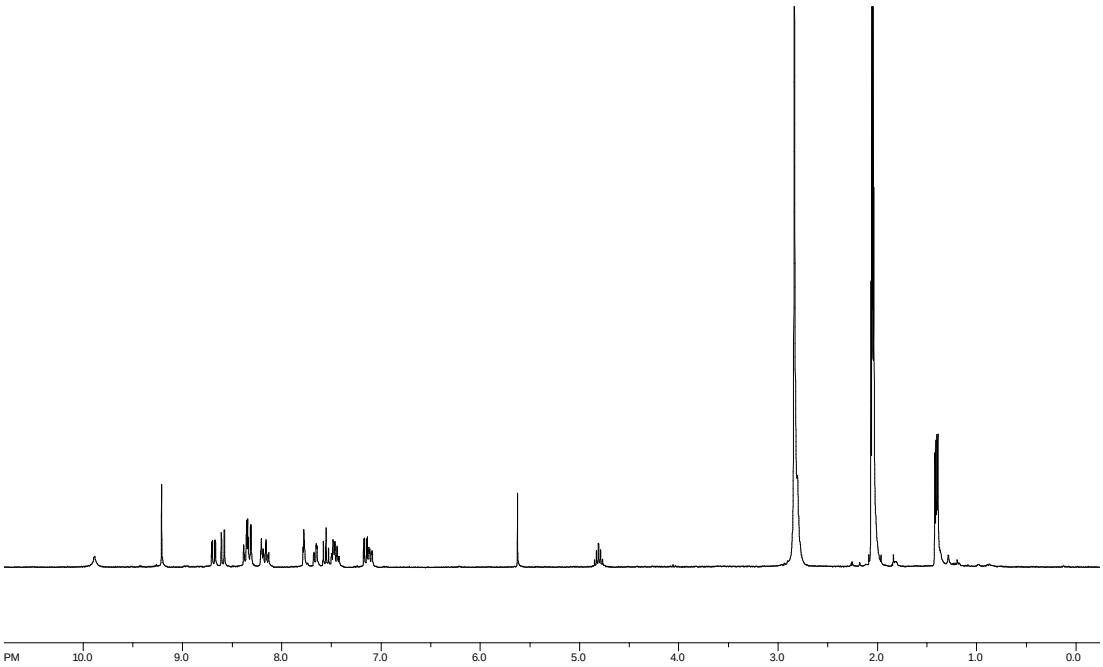

Figure 6.29.1. ^{1}H NMR of complex FL258 (Acetone-d_6).

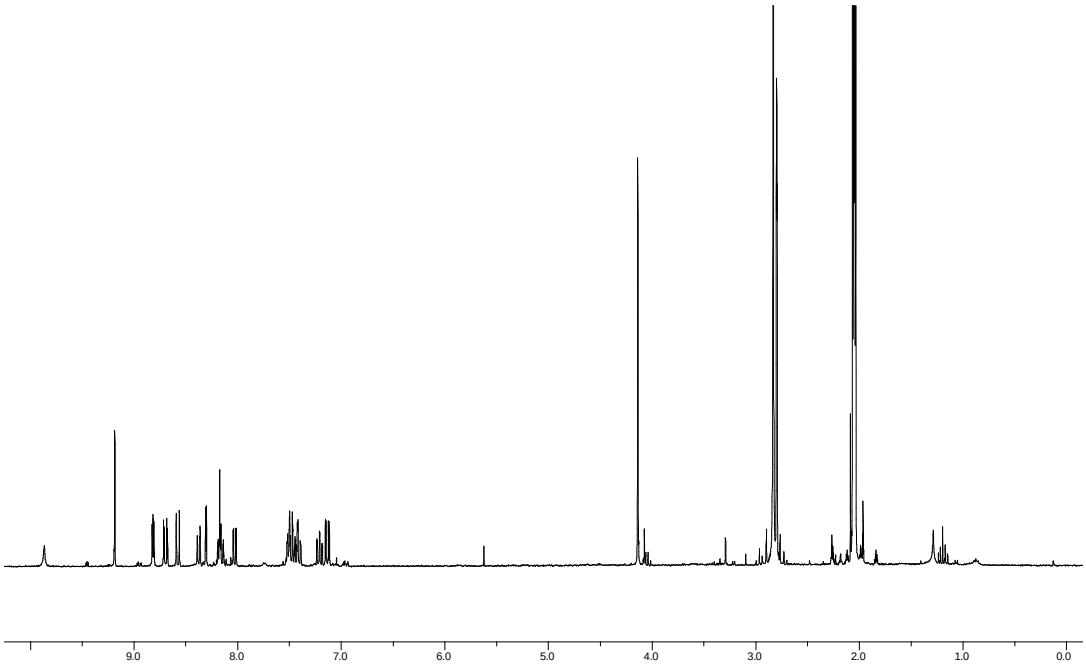

Figure 6.30.1. ^{1}H NMR of complex FL262-3 (Acetone-d_6).

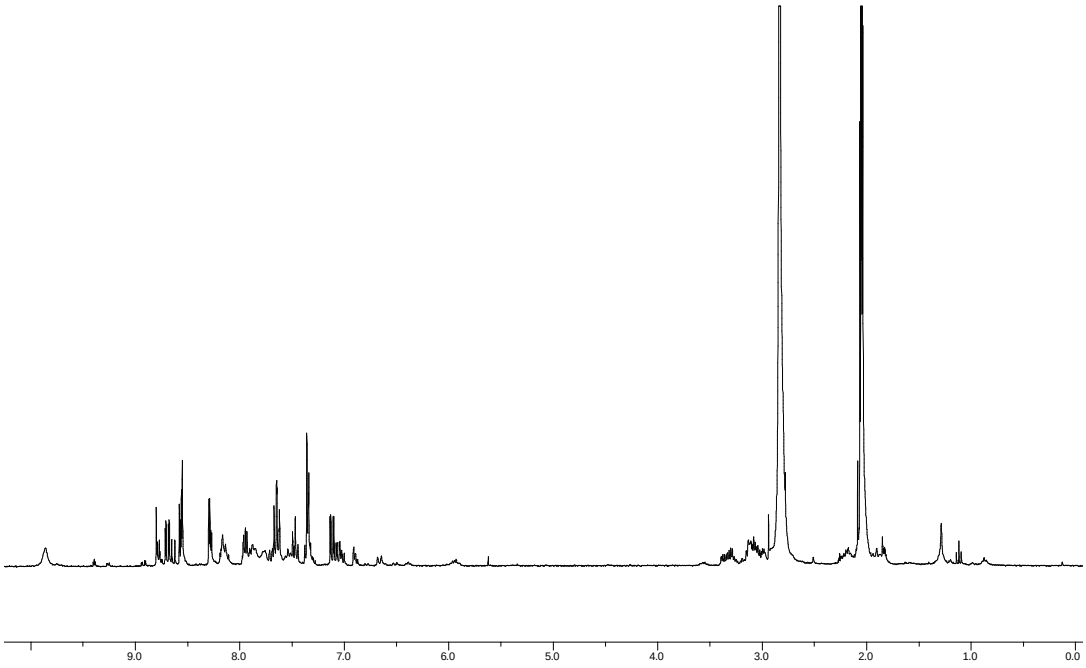

Figure 6.31.1. ^{1}H NMR of complex FL355 (Acetone-d_6).

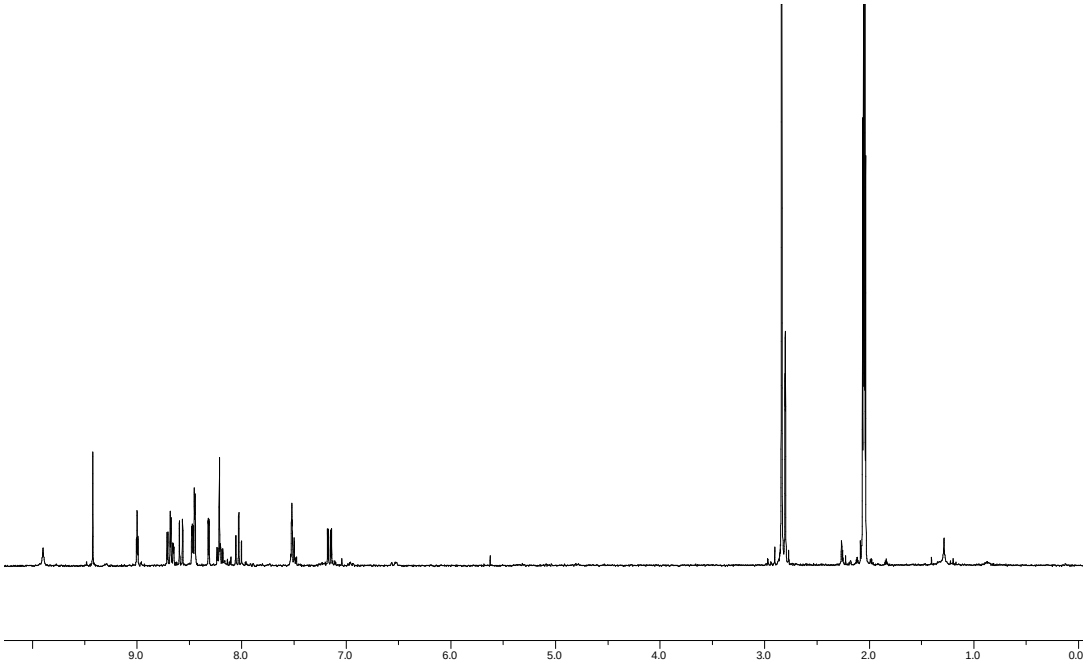

Figure 6.32.1. ^{1}H NMR of complex FL262-9 (Acetone-d_6).

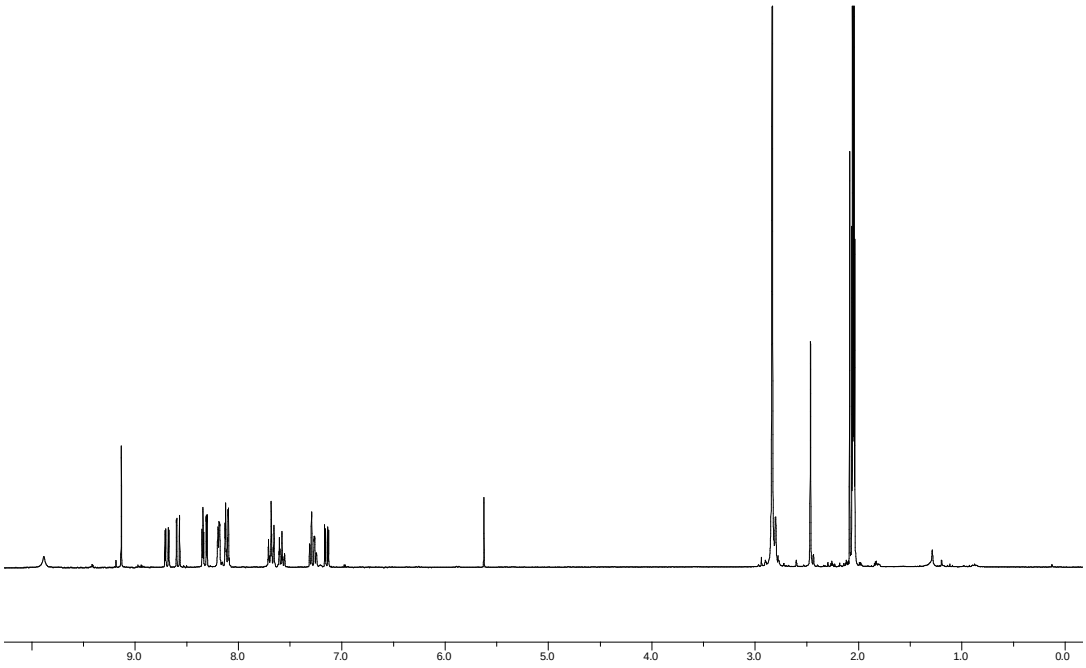

Figure 6.33.1. ^{1}H NMR of complex FL343 (Acetone-d_6).

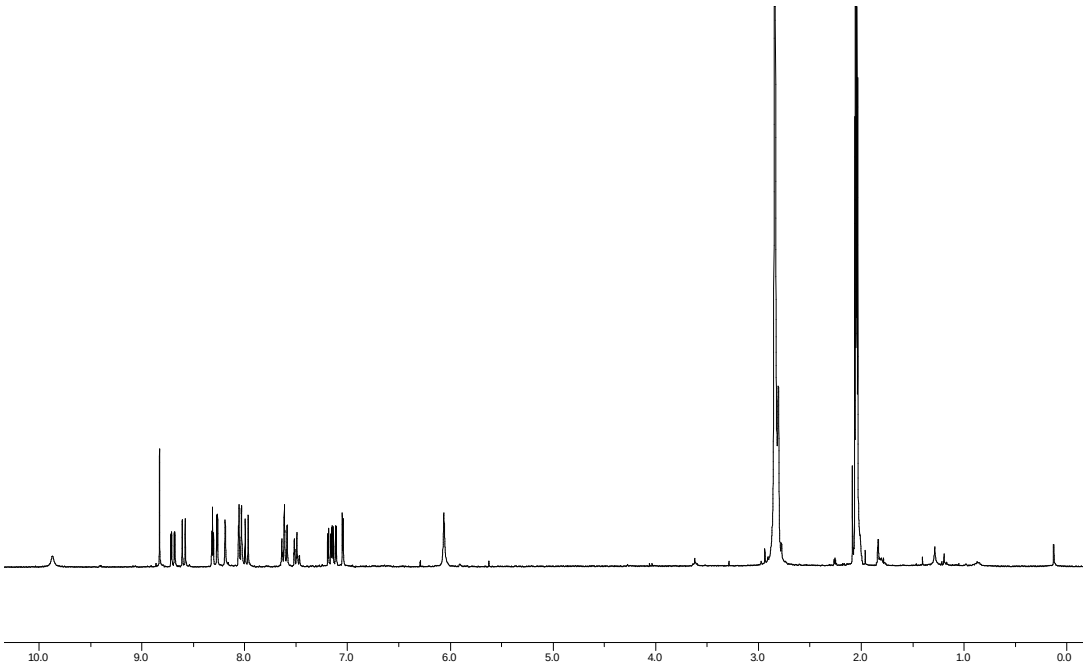

Figure 6.34.1. ^{1}H NMR of complex FL389 (Acetone-d_6).

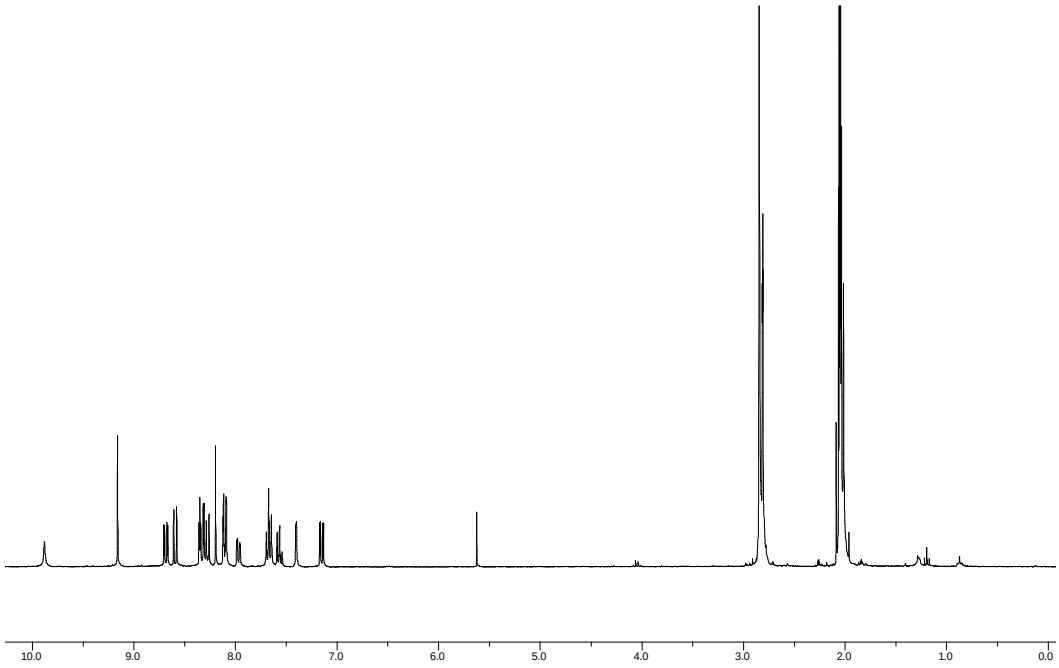

Figure 6.35.1. ^{1}H NMR of complex FL327 (Acetone-d_6).

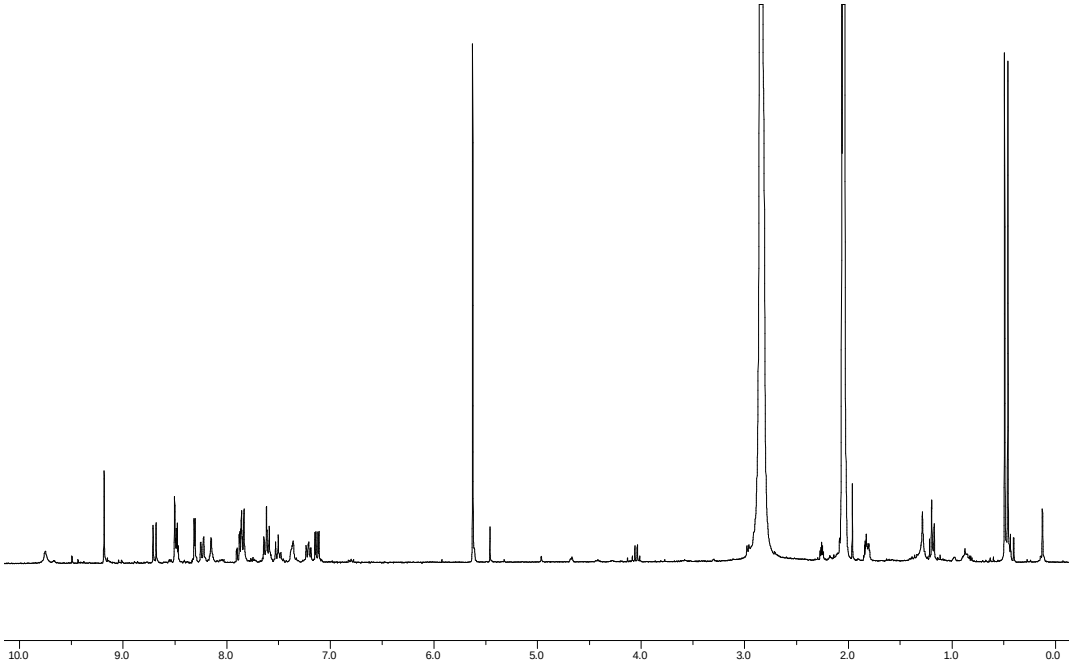

Figure 6.36.1. ^{1}H NMR of complex FL637 (Acetone-d_6).

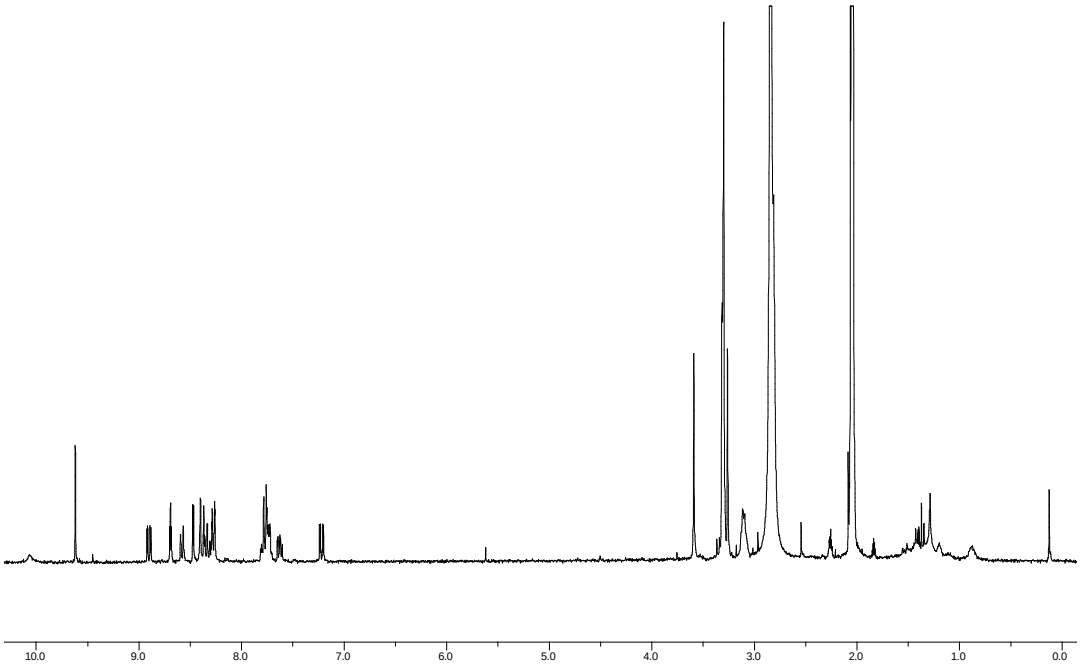

Figure 6.37.1. ^{1}H NMR of complex FL866 (Acetone-d_6).

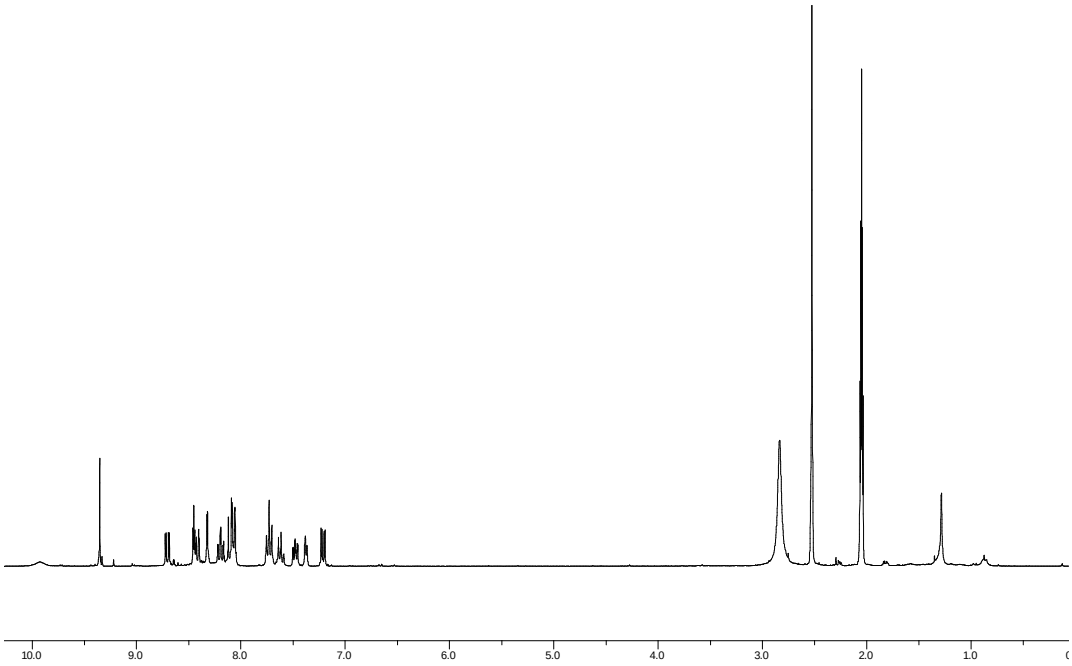

Figure 6.38.1. ^{1}H NMR of complex FL922 (Acetone-d_6).

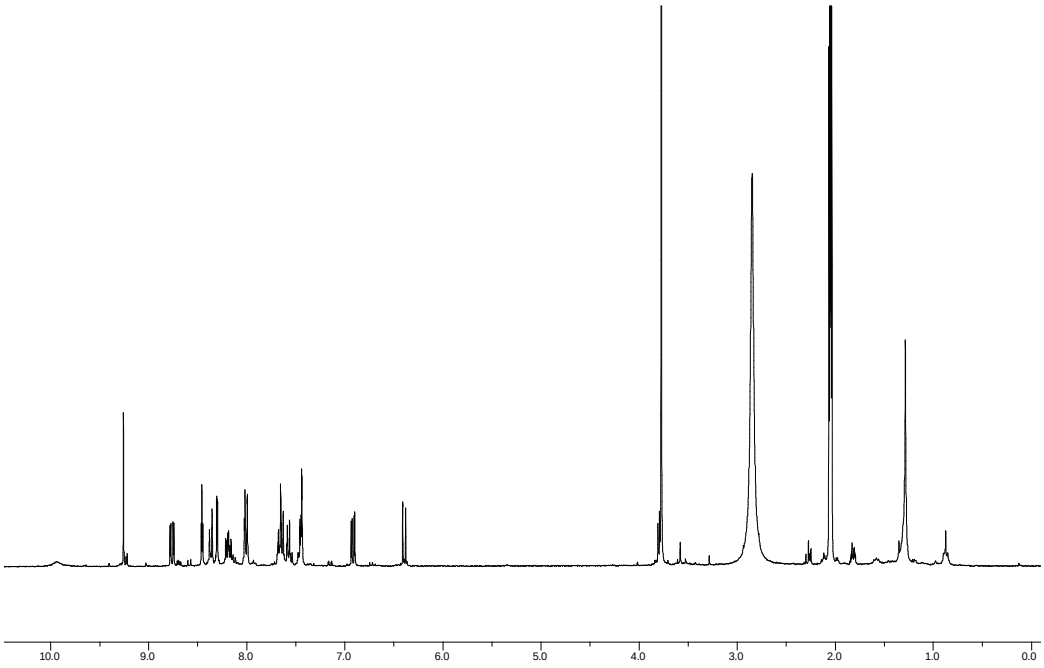

Figure 6.39.1. ^{1}H NMR of complex FL931 (Acetone-d_6).

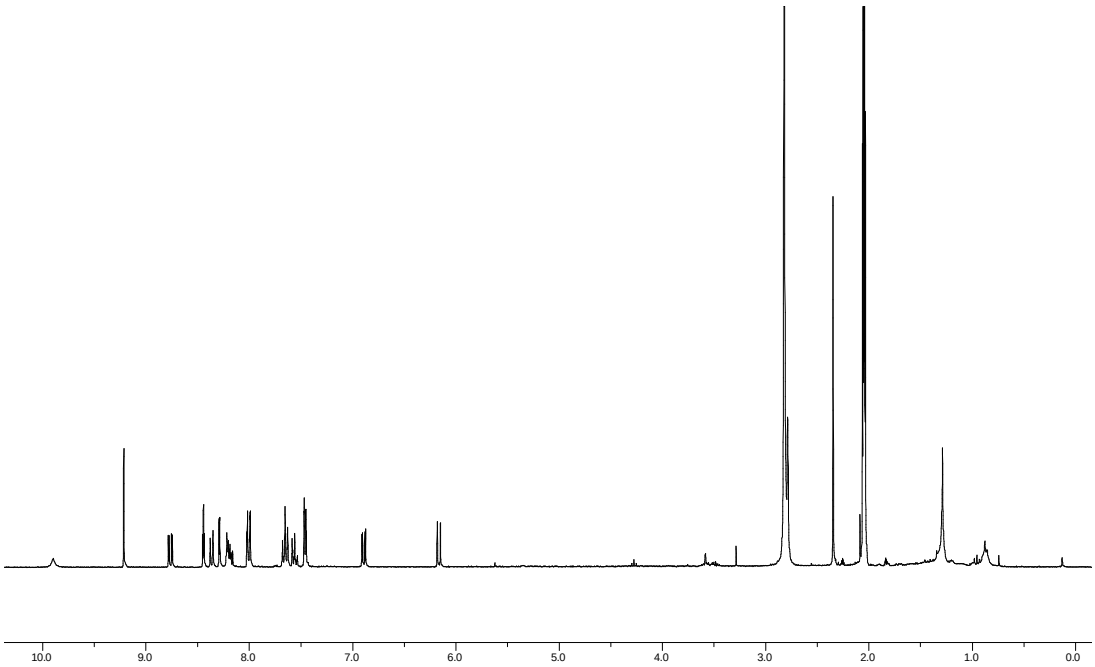

Figure 6.40.1. ^{1}H NMR of complex FL864 (Acetone-d_6).

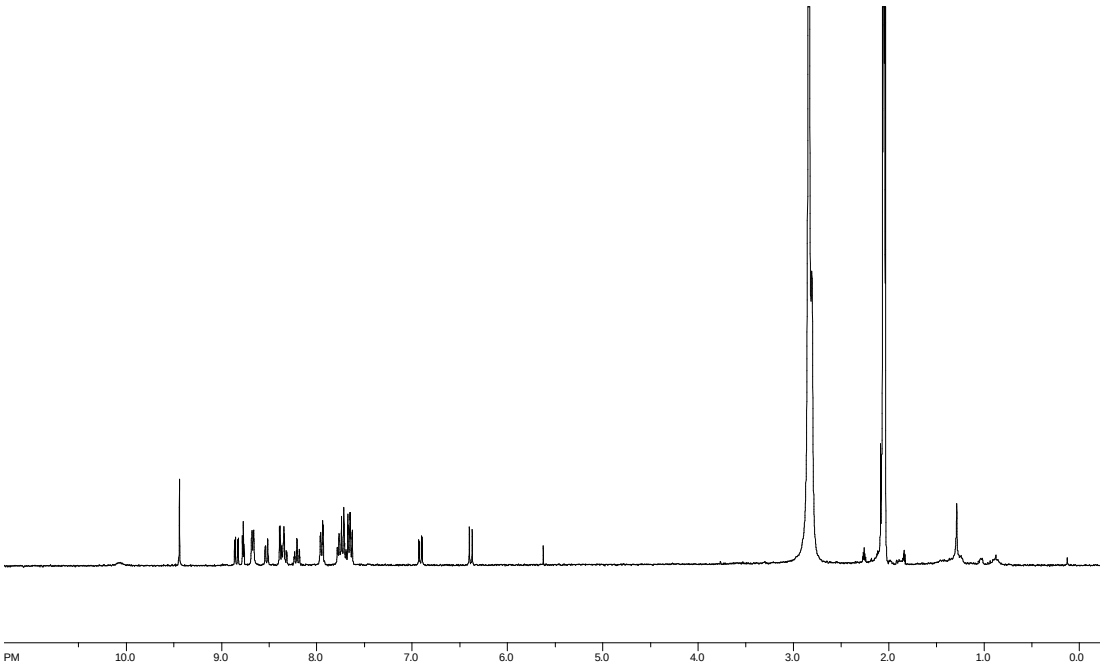

Figure 6.41.1. ^{1}H NMR of complex FL889 (Acetone-d_6).

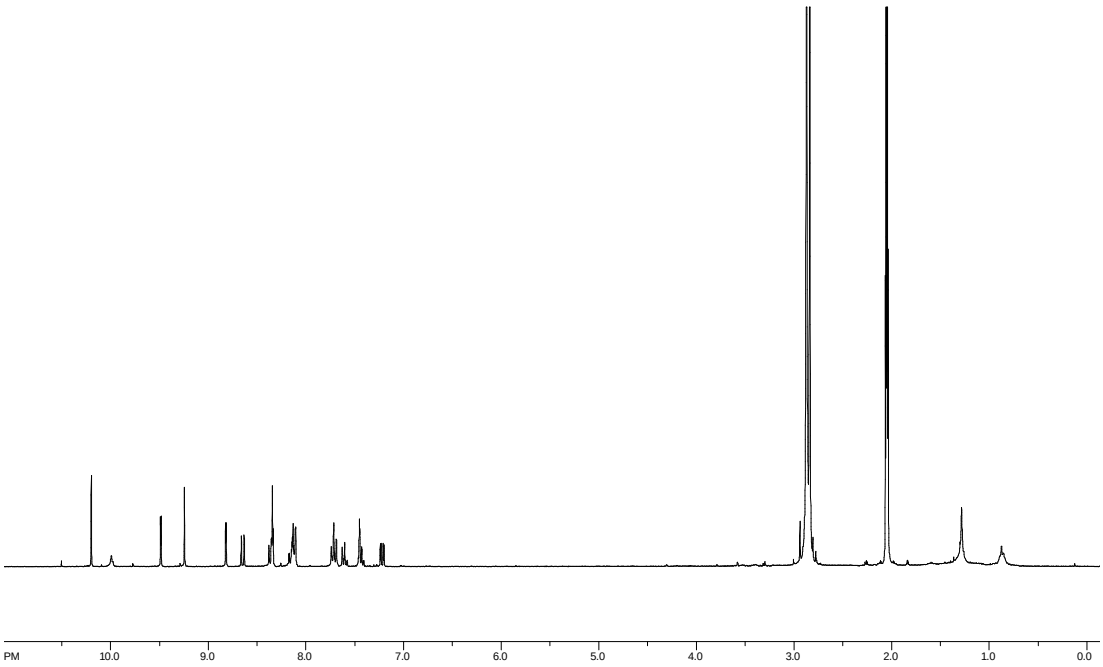

Figure 6.42.1. ^{1}H NMR of complex FL1088 (Acetone-d_6).

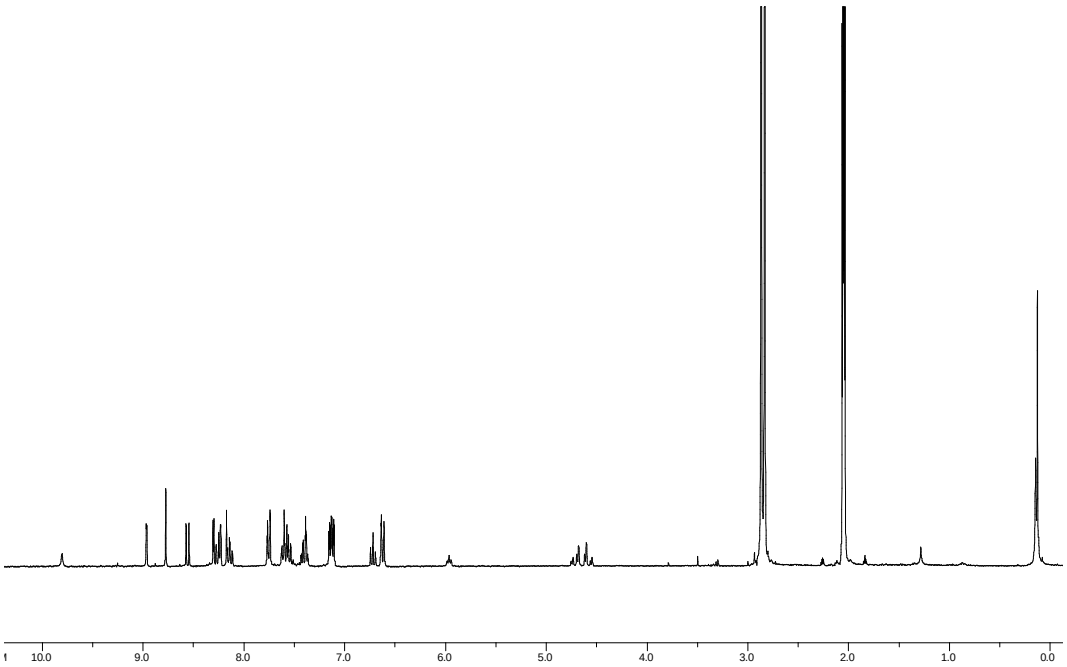

Figure 6.43.1. ^{1}H NMR of complex FL1103 (Acetone-d_6).

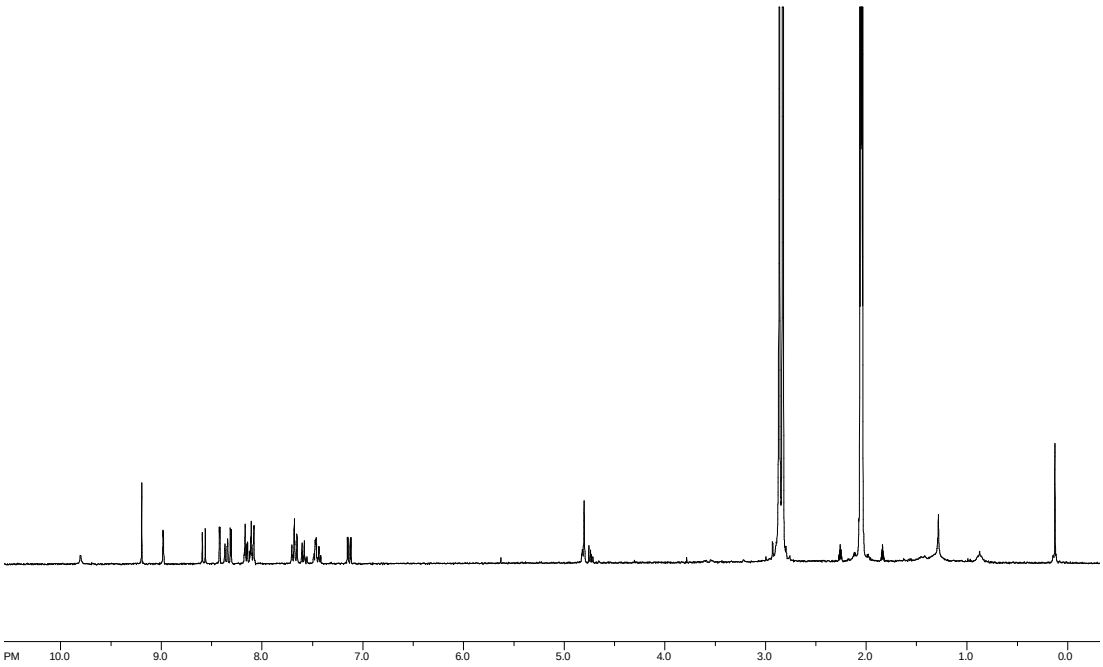

Figure 6.44.1. ^{1}H NMR of complex FL1109 (Acetone-d_6).

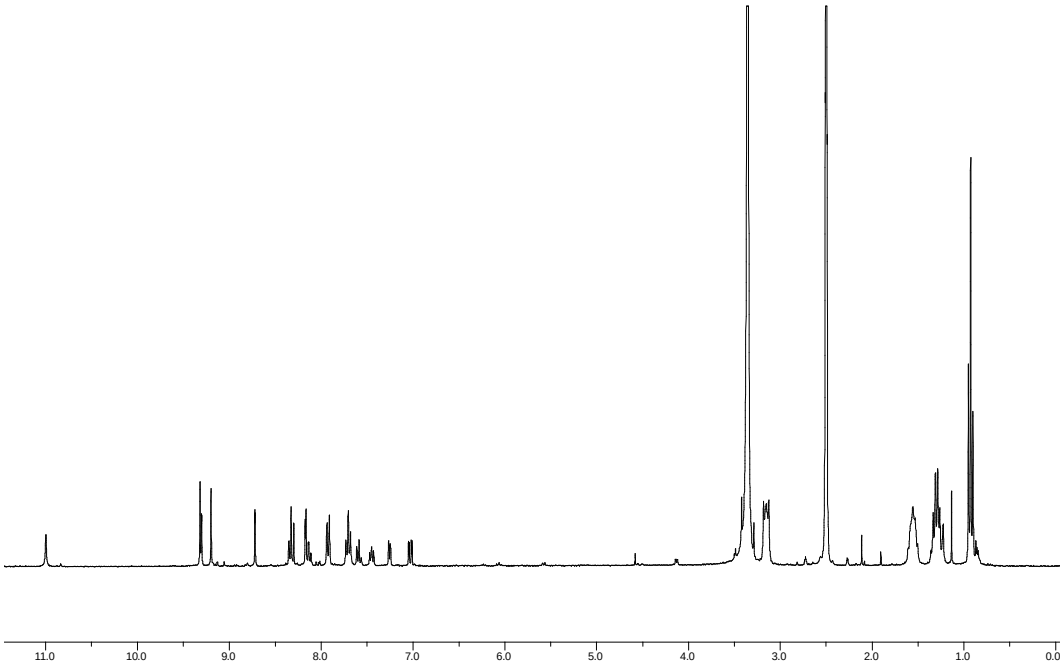

Figure 6.45.1. ^{1}H NMR of complex FL1118 (DMSO-d_6).

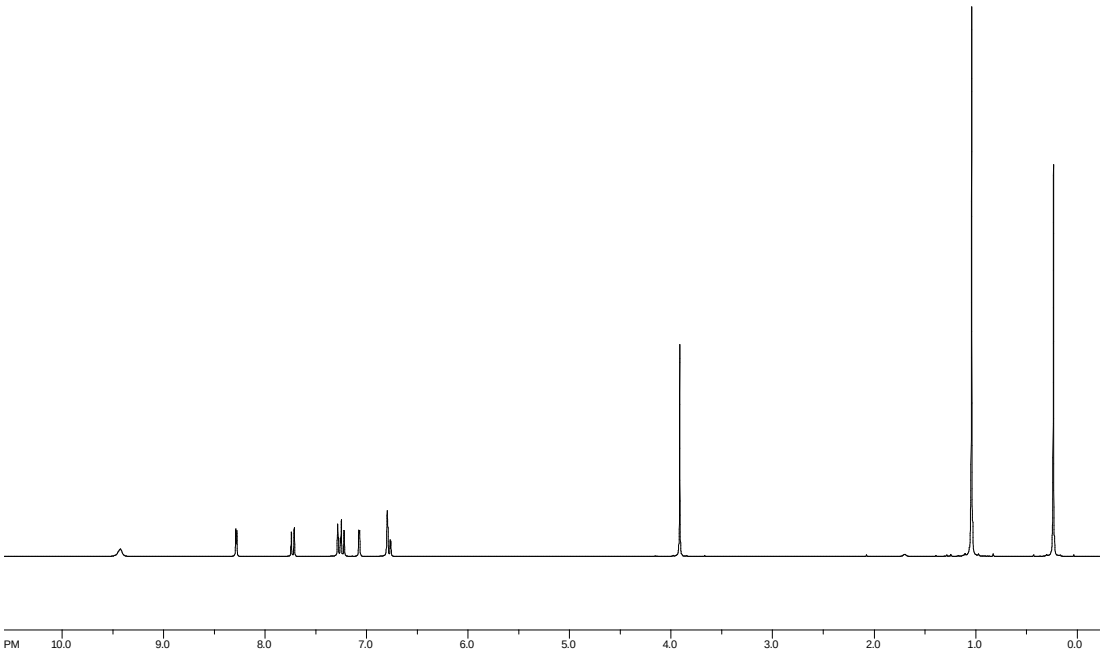

Figure 6.46.1. ^{1}H NMR of compound 2.5 ($CDCl_3$).

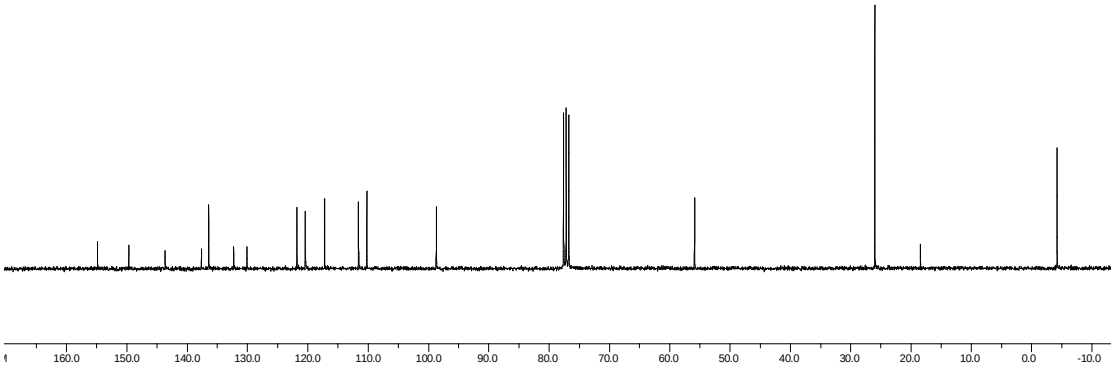

Figure 6.46.2. ^{13}C NMR of compound 2.5 ($CDCl_3$).

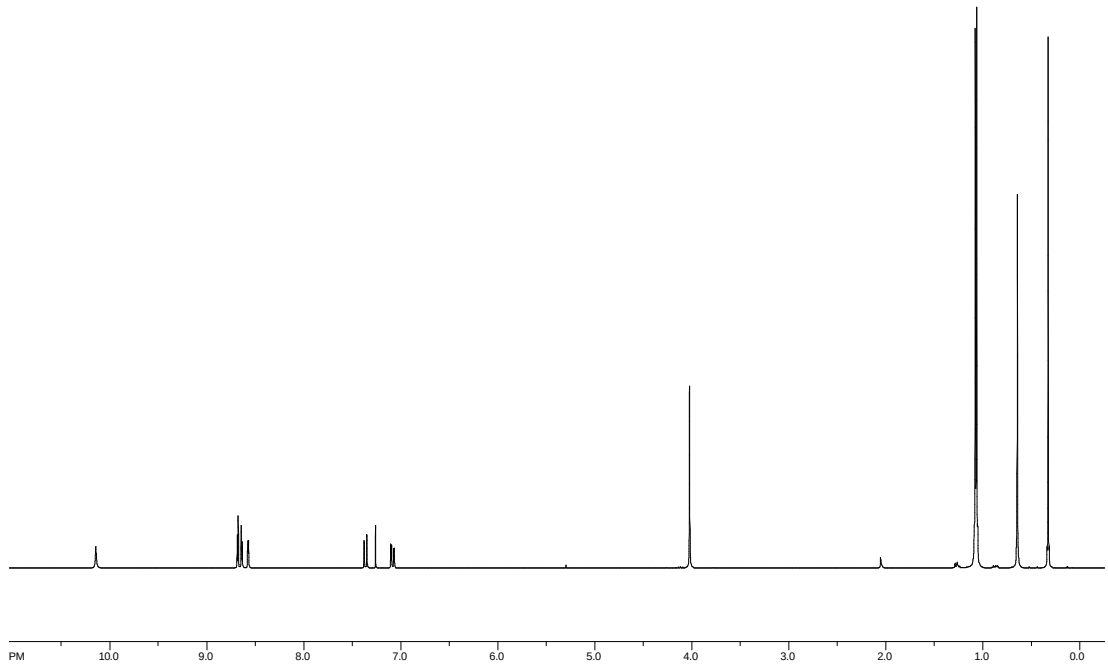

Figure 6.47.1. ^{1}H NMR of compound 2.7 ($CDCl_3$).

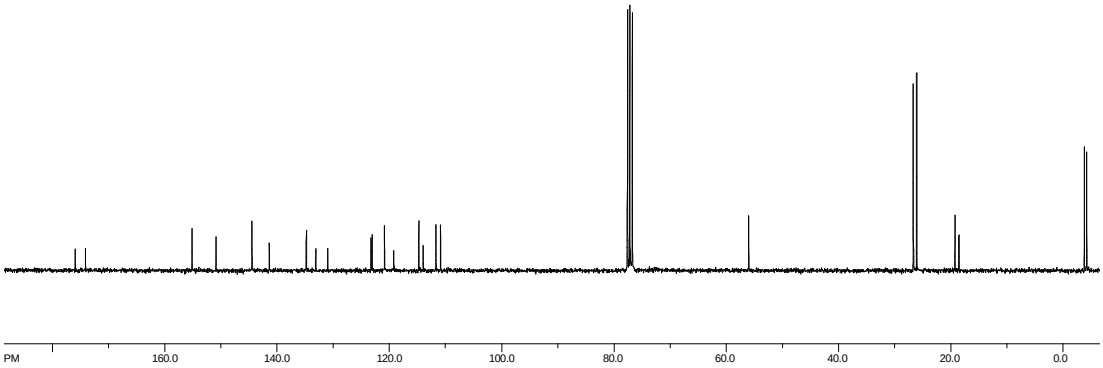

Figure 6.47.2. ^{13}C NMR of compound 2.7 ($CDCl_3$).

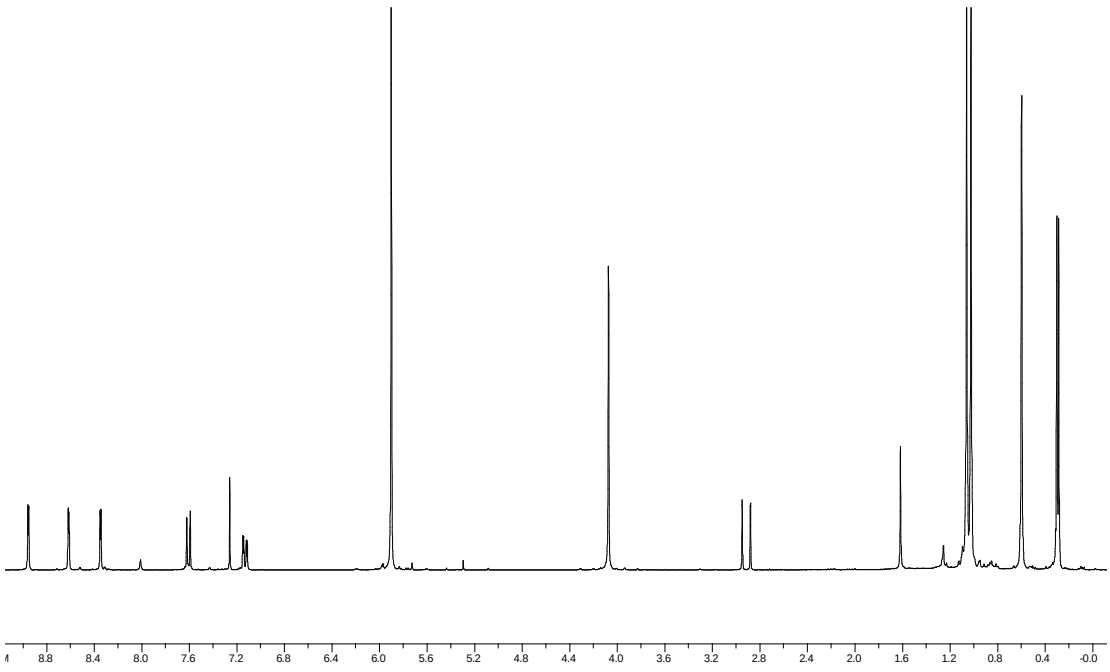

Figure 6.48.1. ^{1}H NMR of complex 2.8 ($CDCl_3$).

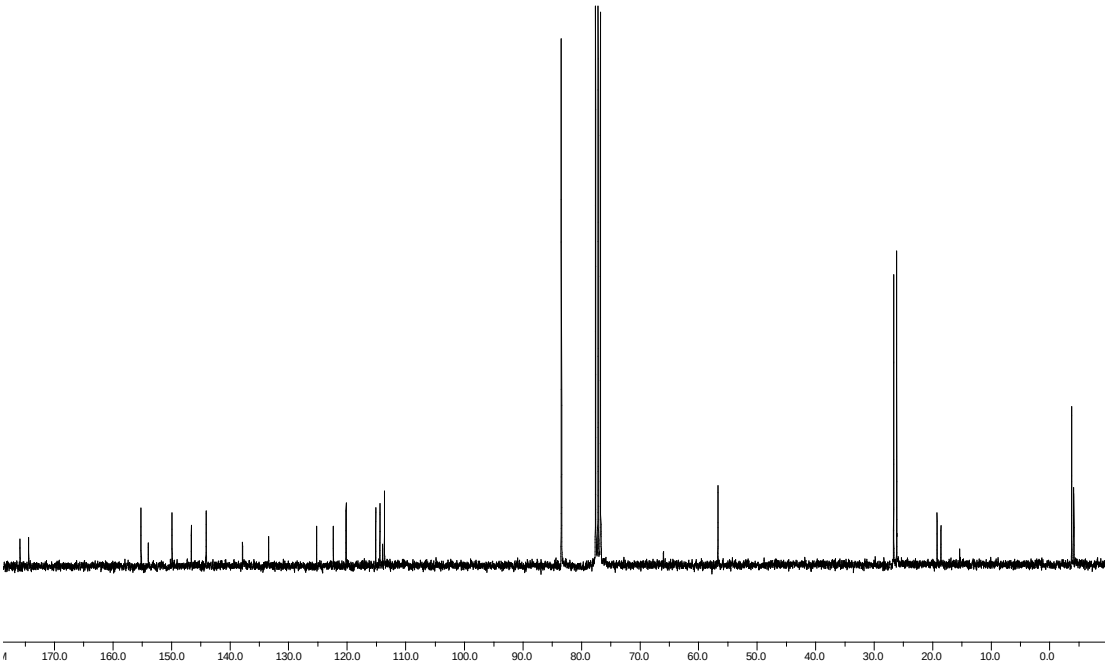

Figure 6.48.2. ^{13}C NMR of complex 2.8 ($CDCl_3$).

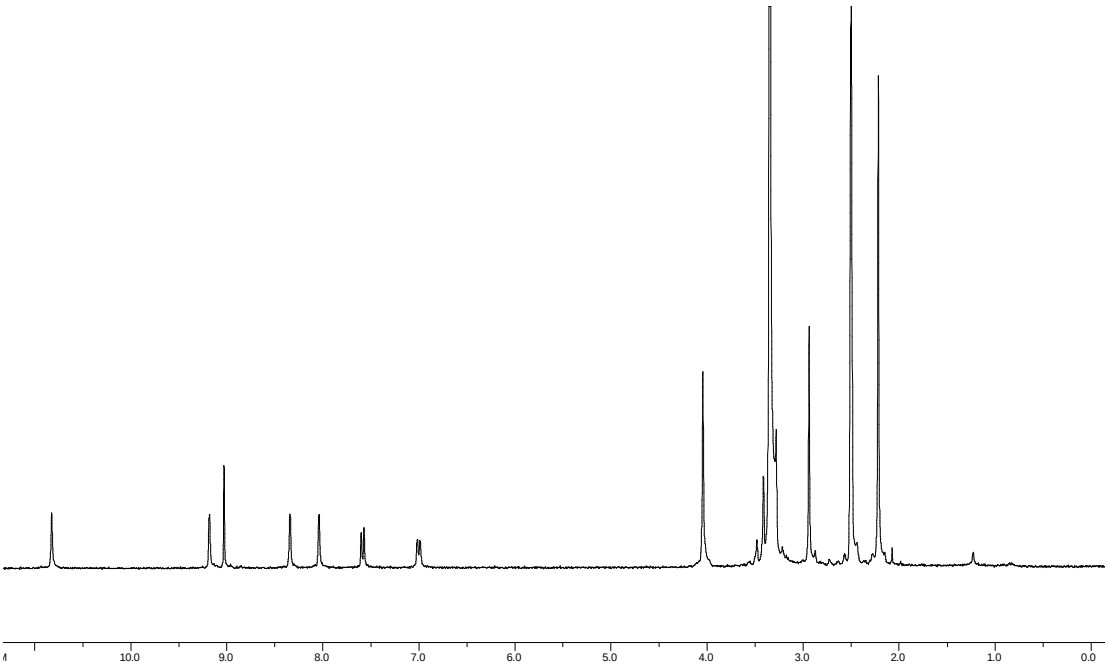

Figure 6.49.1. ^{1}H NMR of complex 2.9 (DMSO-d_6).

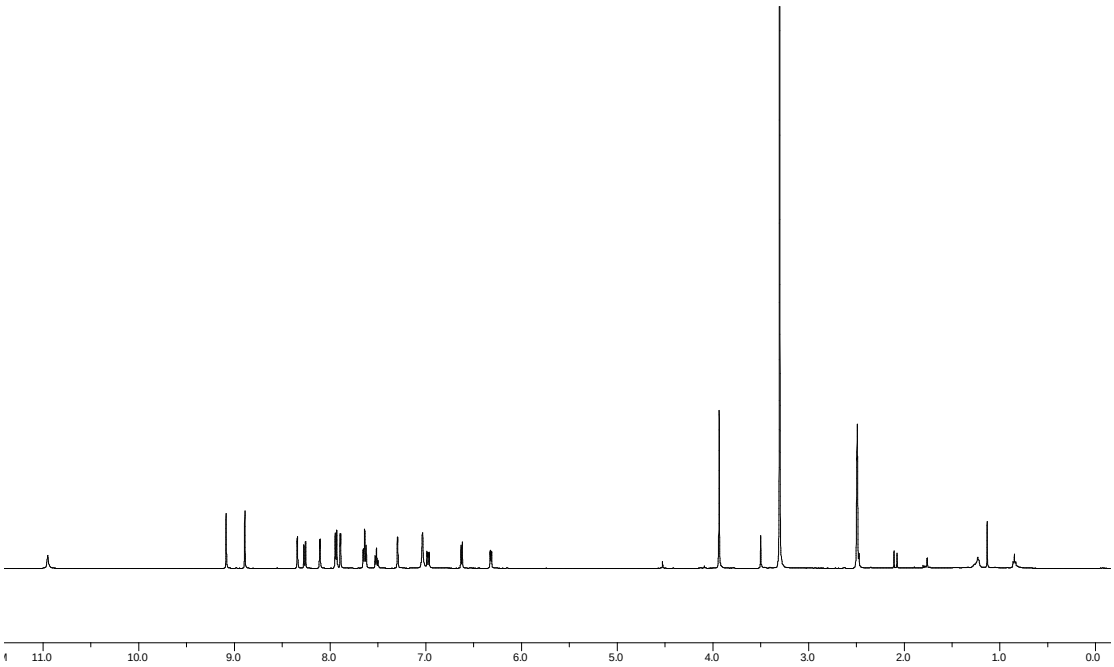

Figure 6.50.1. ^{1}H NMR of complex FL1422 (DMSO-d_6).

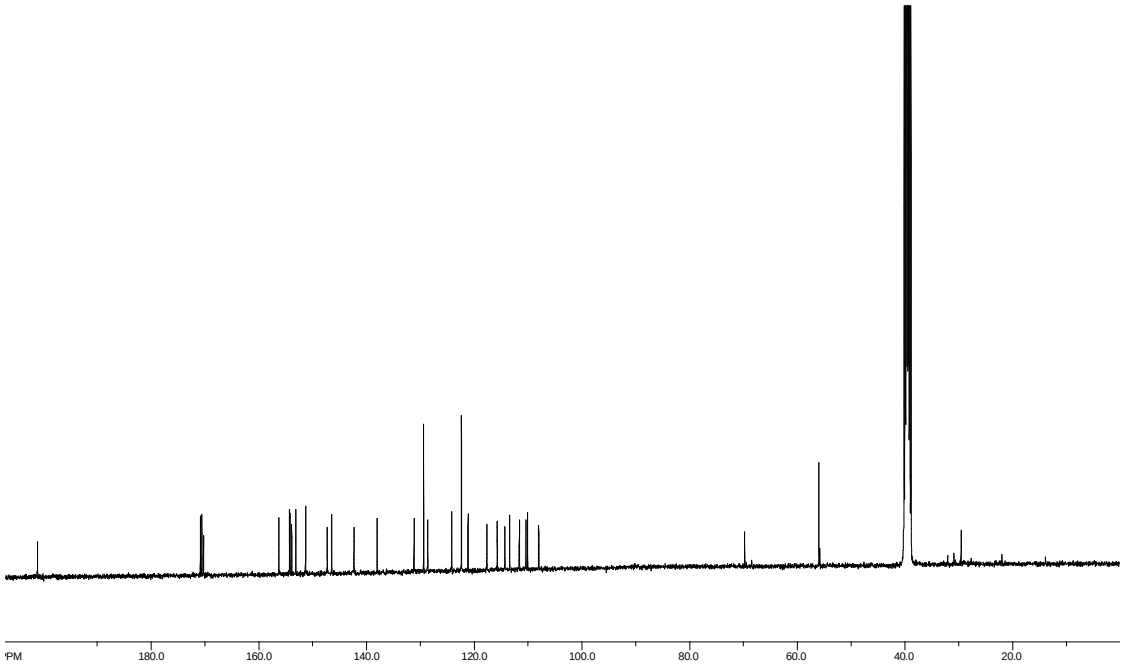

Figure 6.50.2. ^{13}C NMR of complex FL1422 (DMSO-d_6).

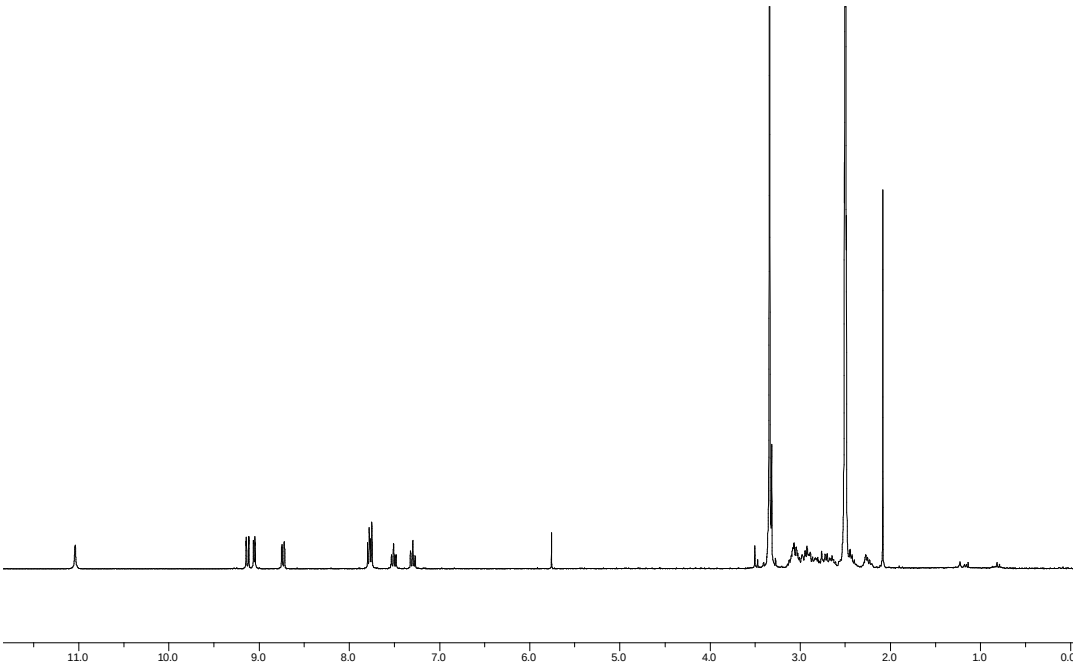

Figure 6.51.1. ^{1}H NMR of complex 3.82 (DMSO-d_6).

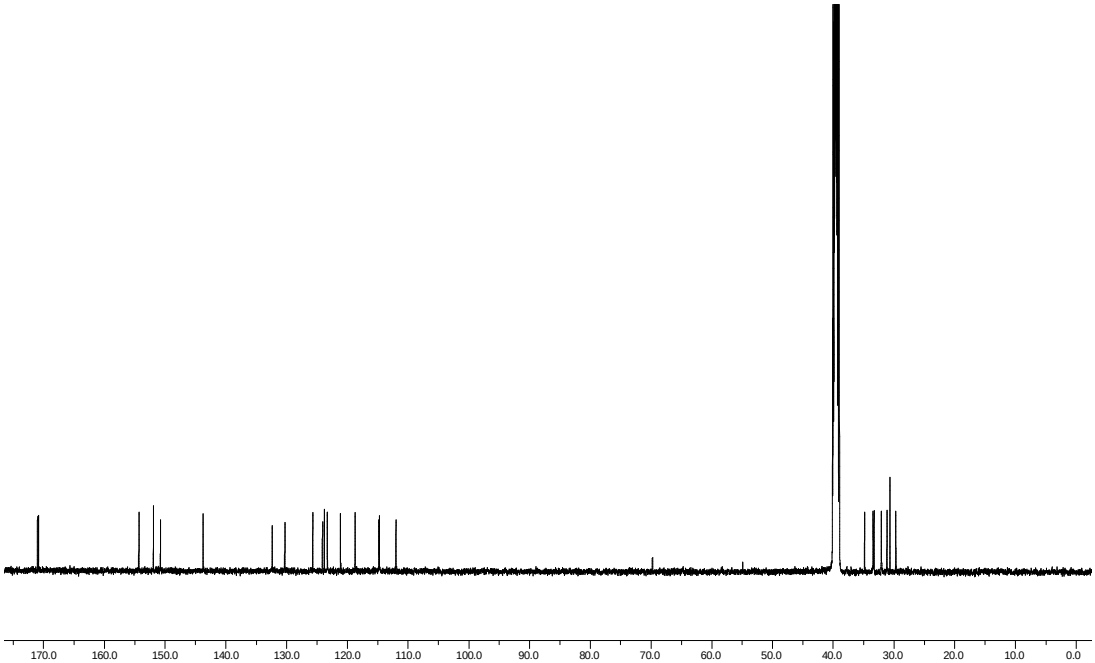

Figure 6.51.2. ^{13}C NMR of complex 3.82 (DMSO-d_6).

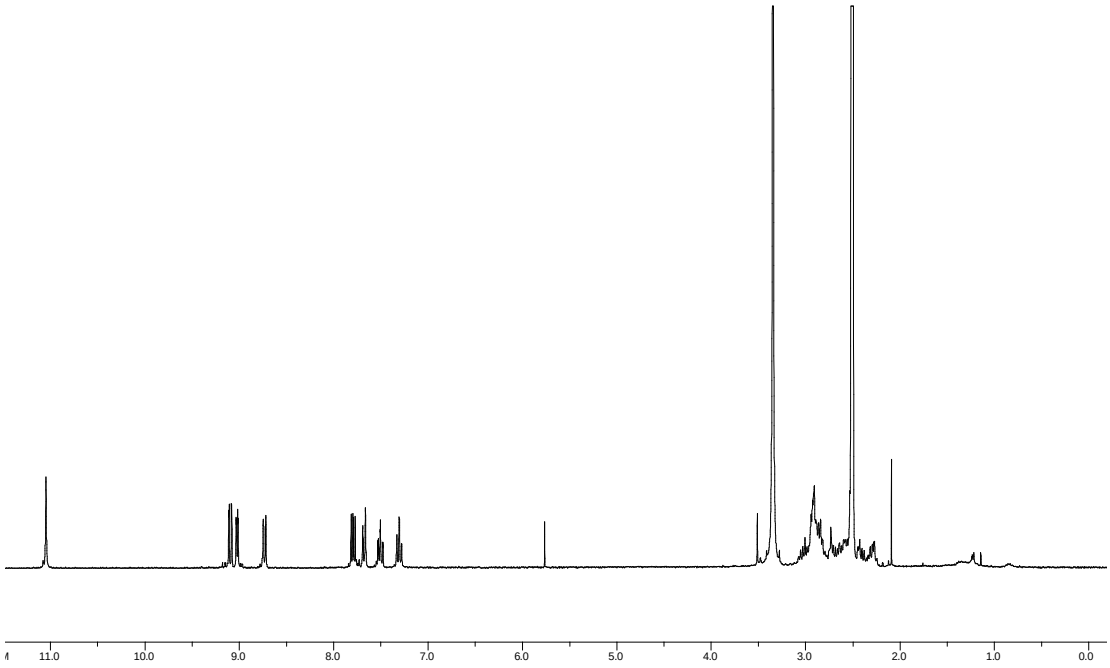

Figure 6.52.1. ^{1}H NMR of complex 3.83 (DMSO-d_6).

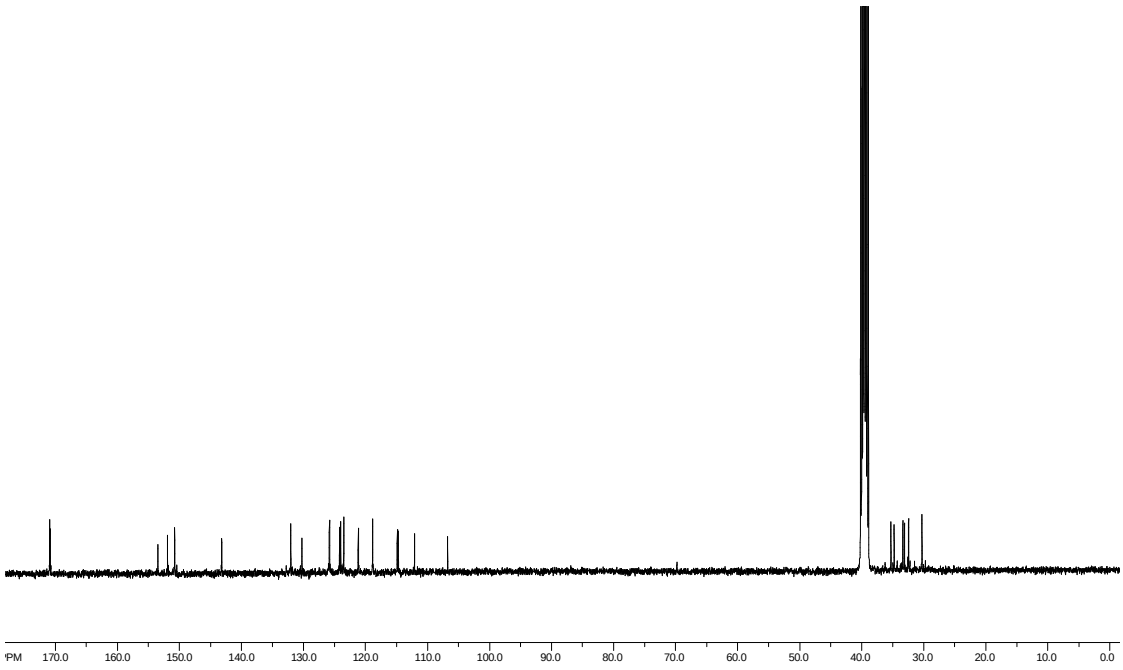

Figure 6.52.2. ^{13}C NMR of complex 3.83 (DMSO-d_6).

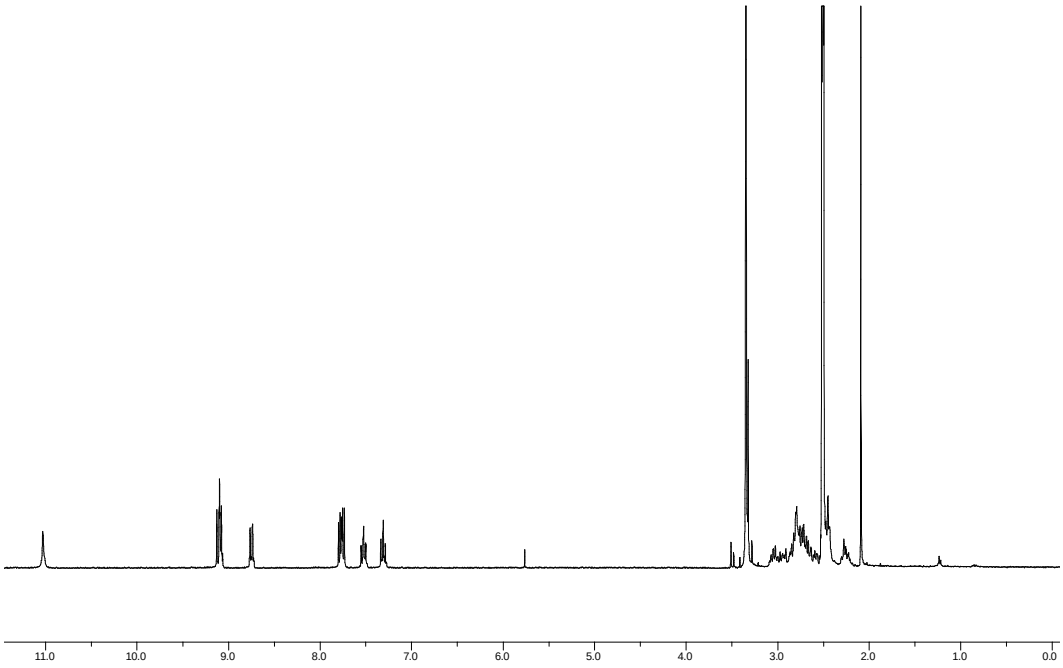

Figure 6.53.1. ^{1}H NMR of complex 3.84 (DMSO-d_6).

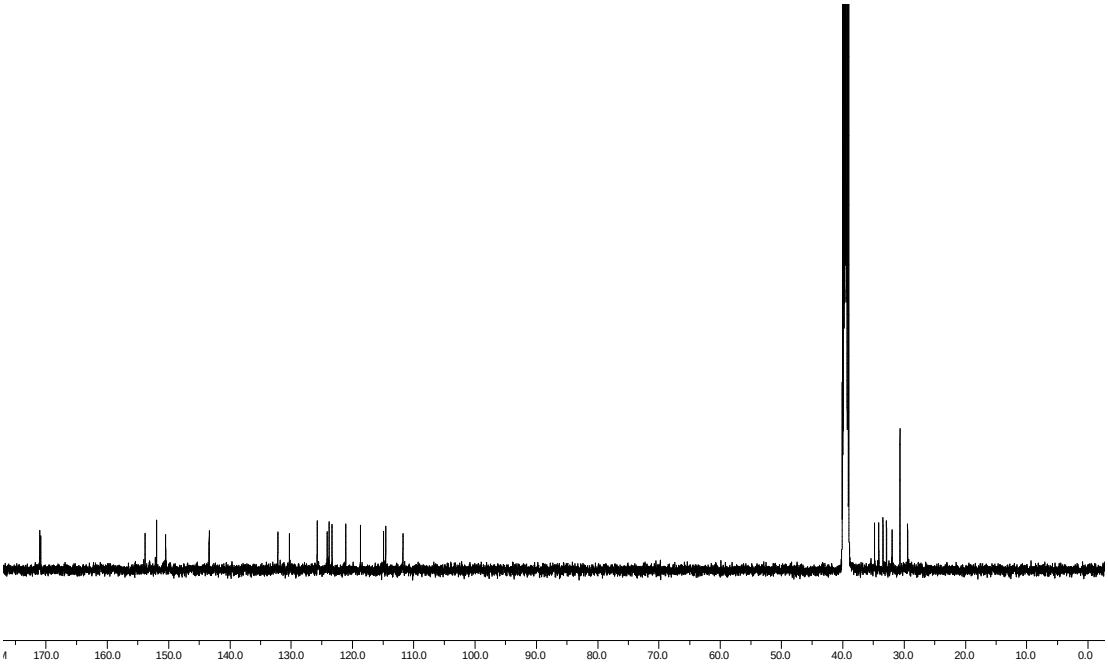

Figure 6.53.2. ^{13}C NMR of complex 3.84 (DMSO-d_6).

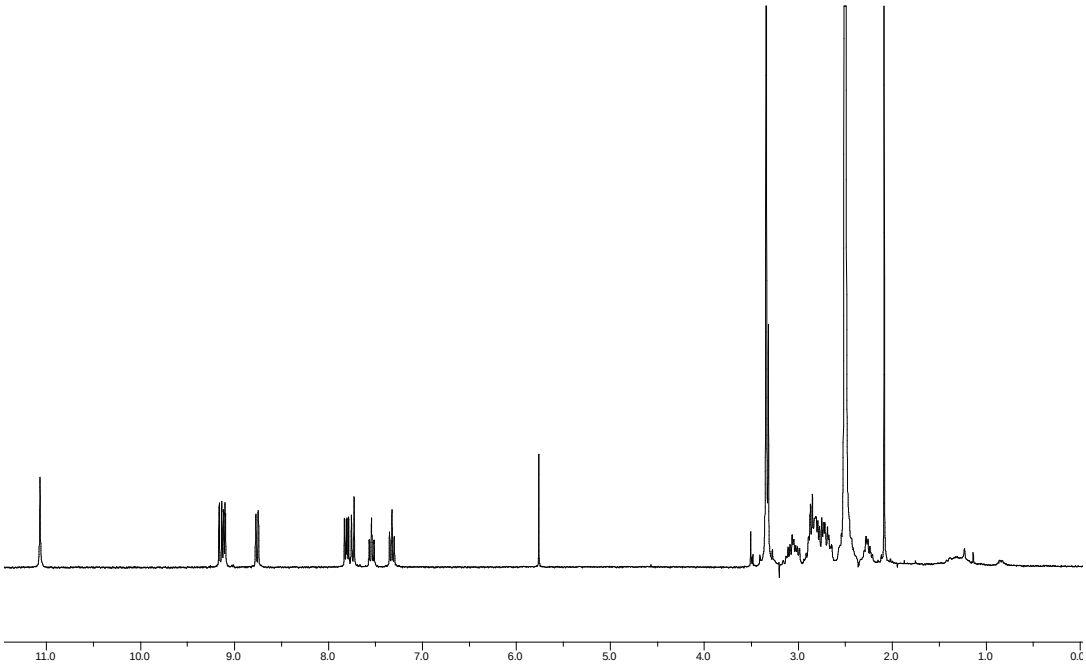

Figure 6.54.1. ^{1}H NMR of complex 3.86 (DMSO-d_6).

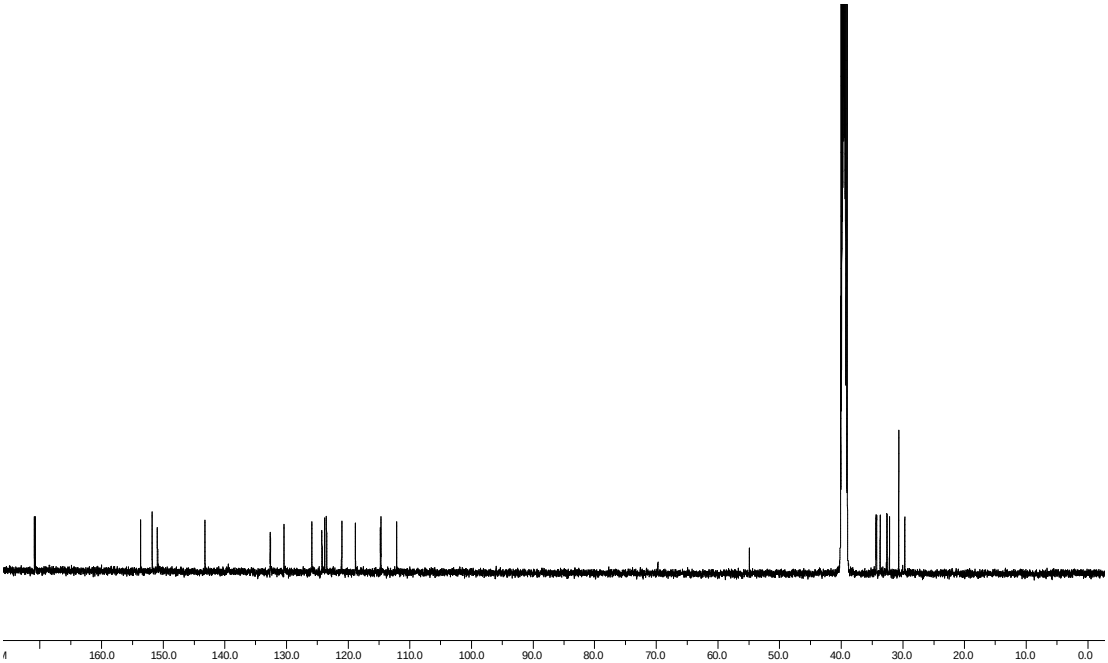

Figure 6.54.2. ^{13}C NMR of complex 3.86 (DMSO-d_6).

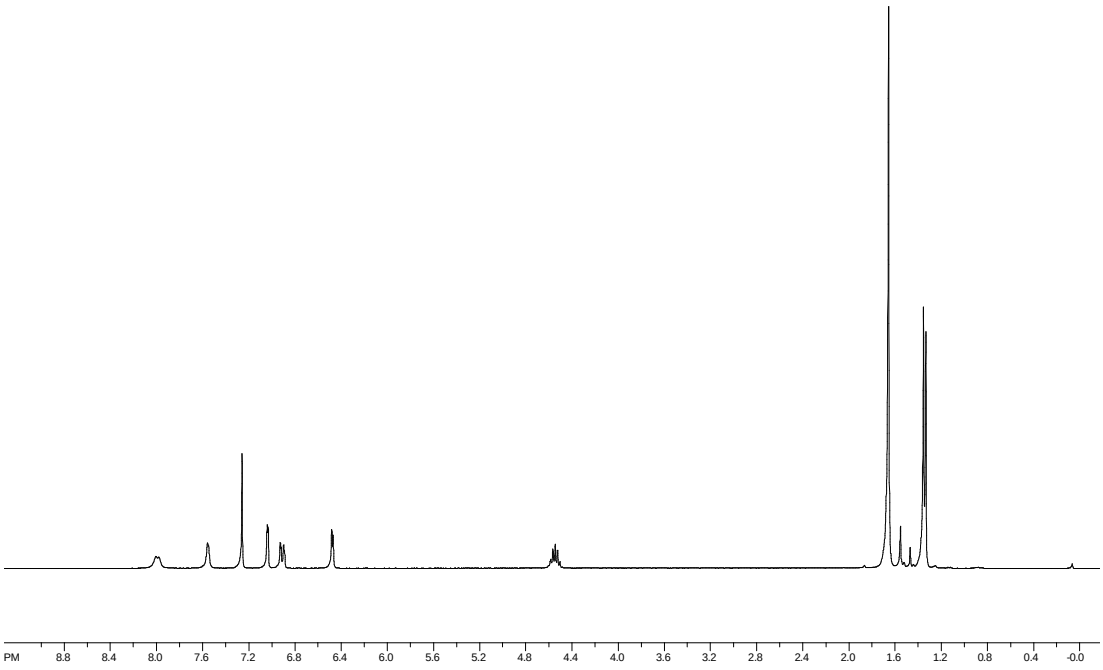

Figure 6.55.1. ^{1}H NMR of compound 3.2 ($CDCl_3$).

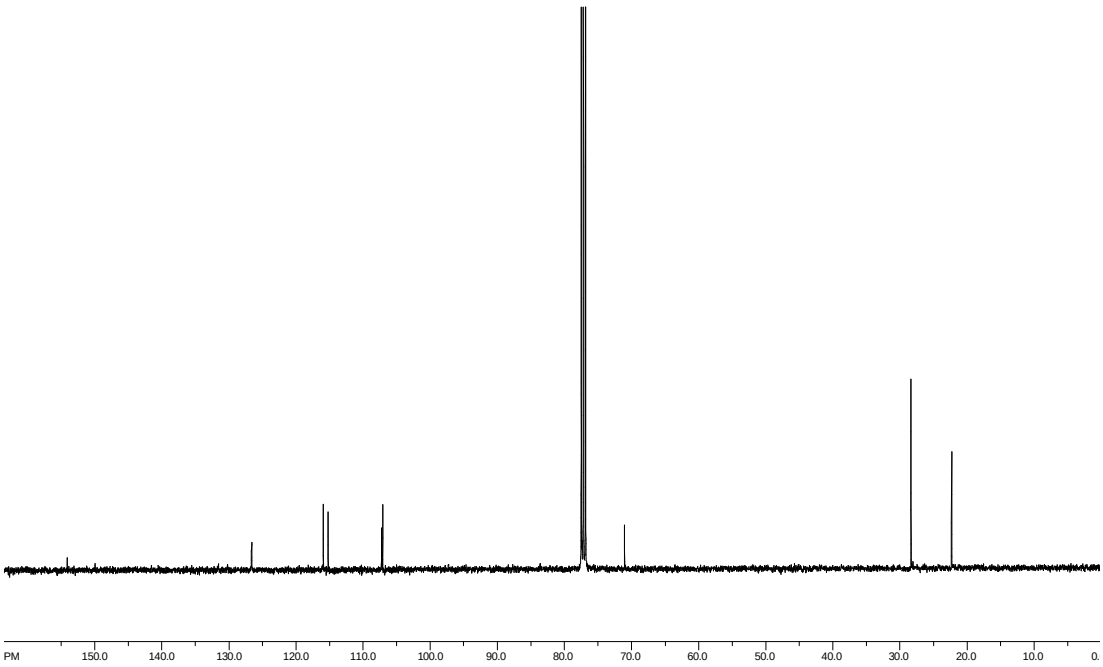

Figure 6.55.2. ^{13}C NMR of compound 3.2 ($CDCl_3$).

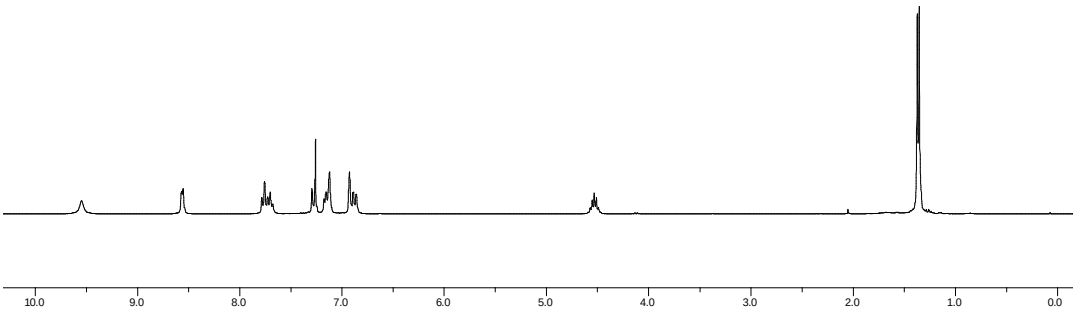

Figure 6.56.1. ^{1}H NMR of compound 3.4 ($CDCl_3$).

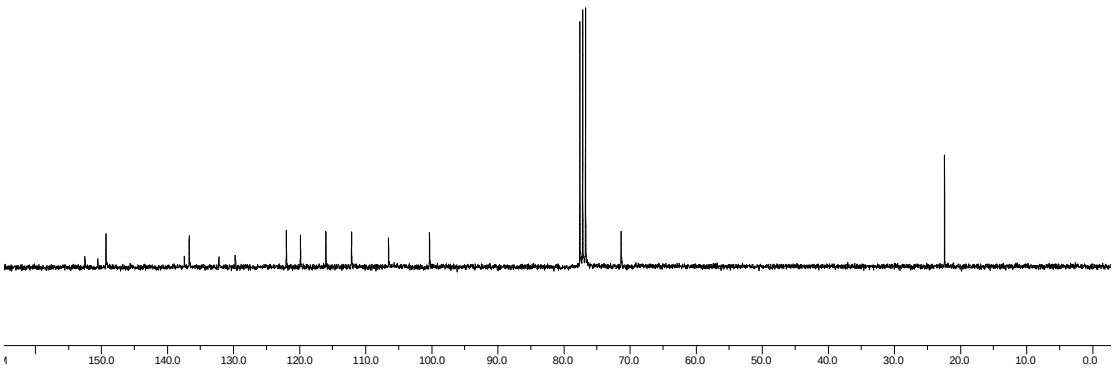

Figure 6.56.2. ^{13}C NMR of compound 3.4 ($CDCl_3$).

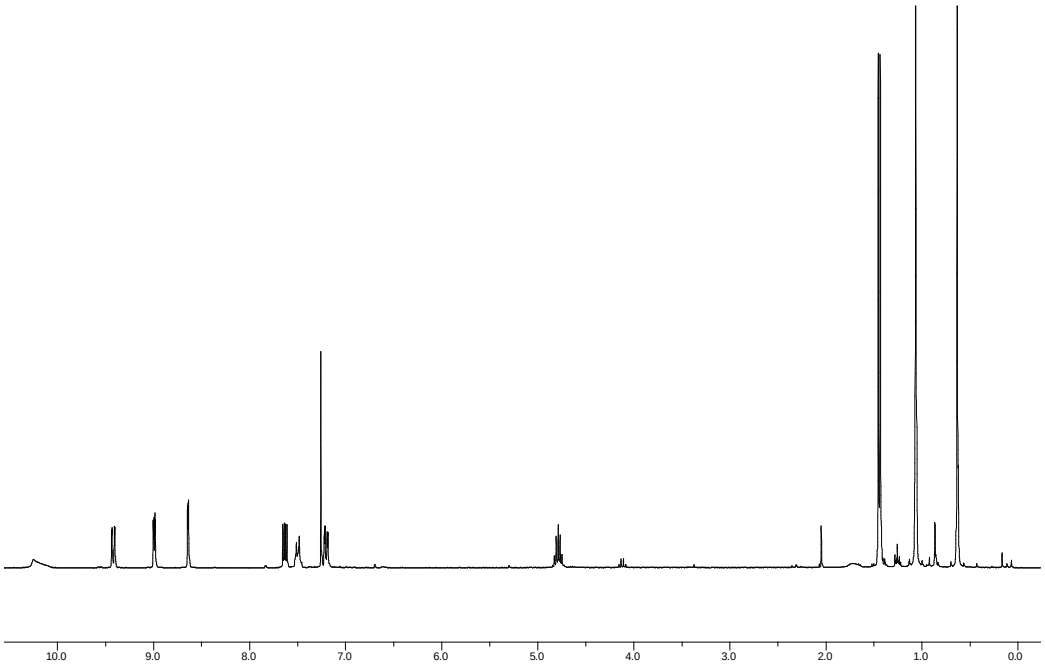

Figure 6.57.1. ^{1}H NMR of compound 3.6 ($CDCl_3$).

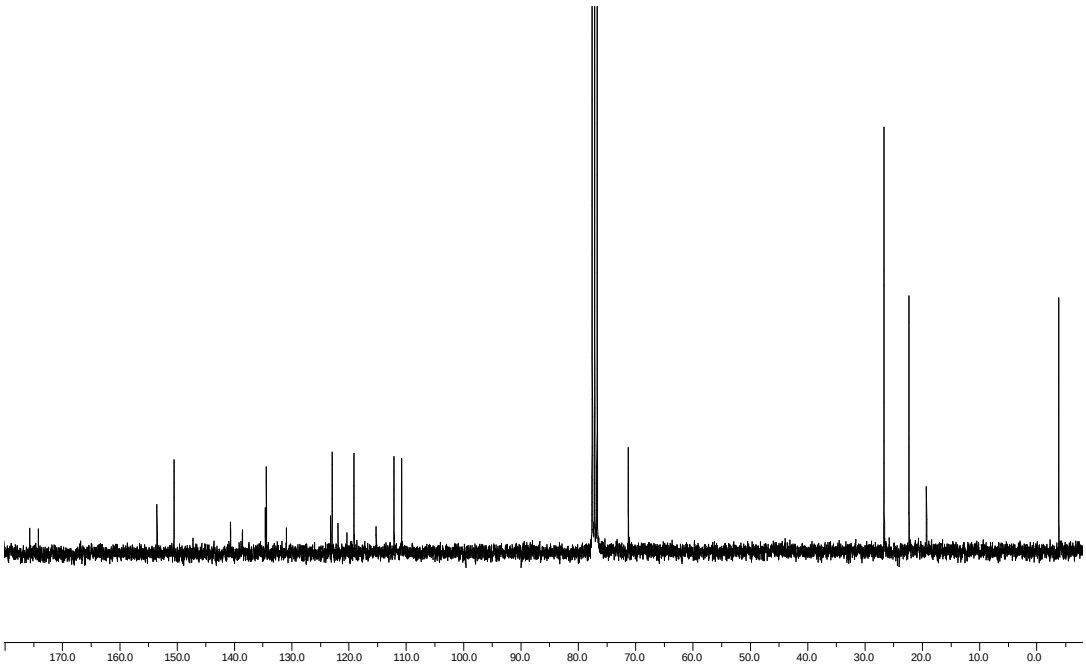

Figure 6.57.2. ^{13}C NMR of compound 3.6 ($CDCl_3$).

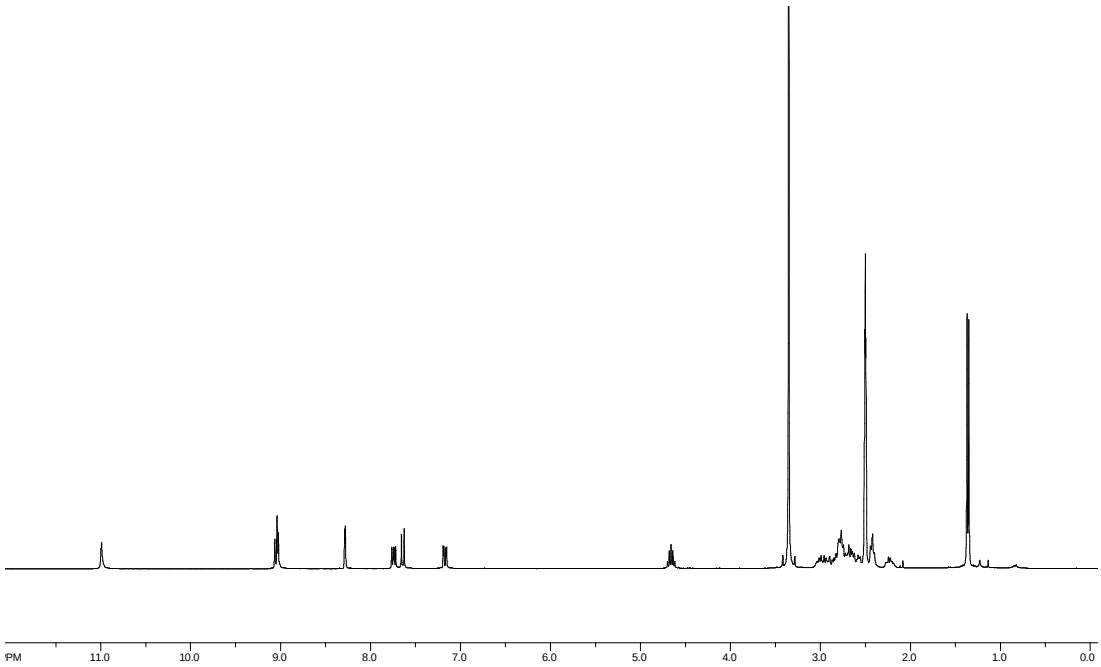

Figure 6.58.1. ^{1}H NMR of complex FL1359 (DMSO-d_6).

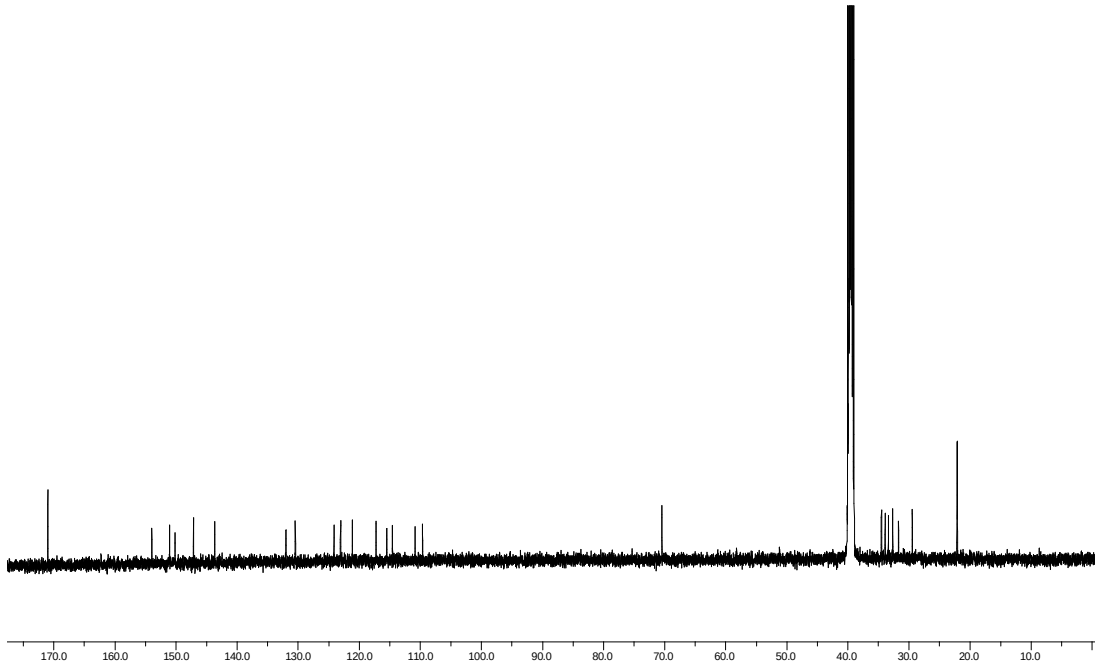

Figure 6.58.2. ^{13}C NMR of complex FL1359 (DMSO-d_6).

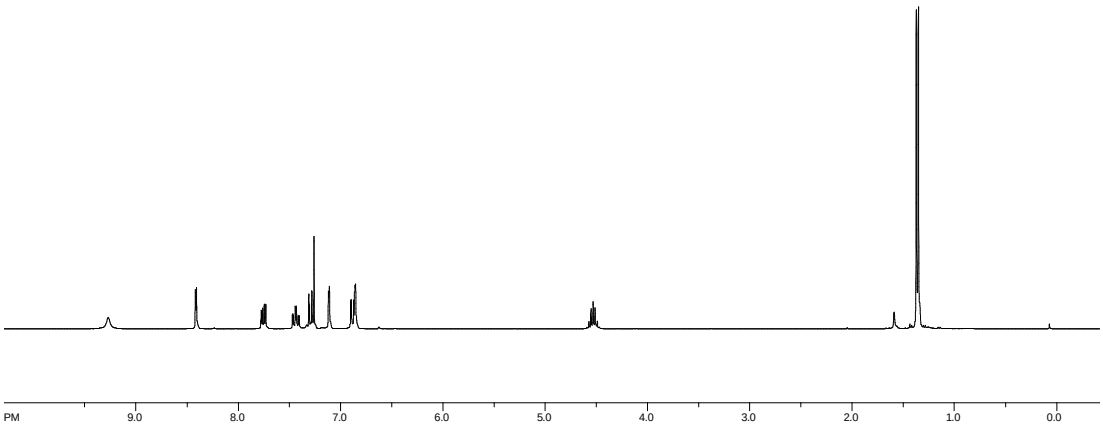

Figure 6.59.1. ^{1}H NMR of compound 3.8 ($CDCl_3$).

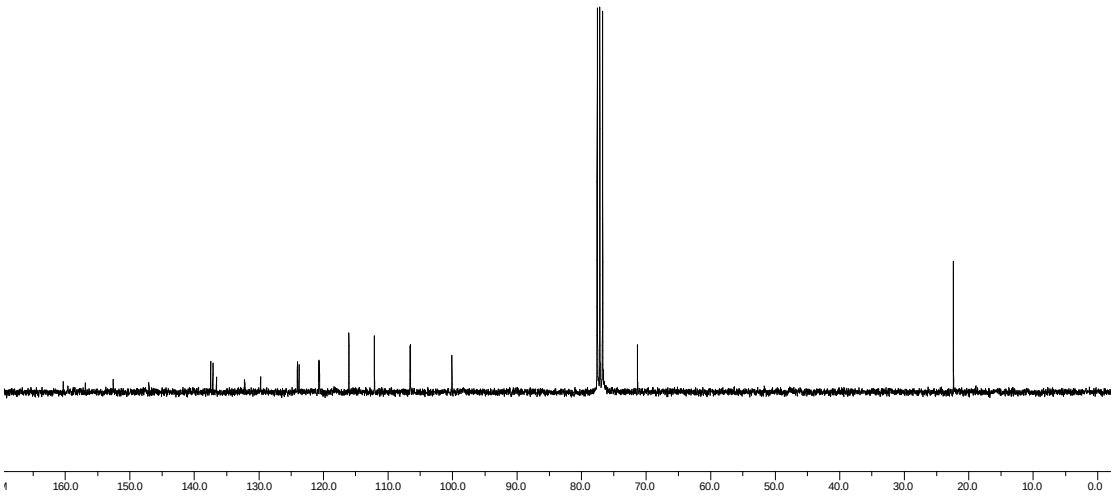

Figure 6.59.2. ^{13}C NMR of compound 3.8 ($CDCl_3$).

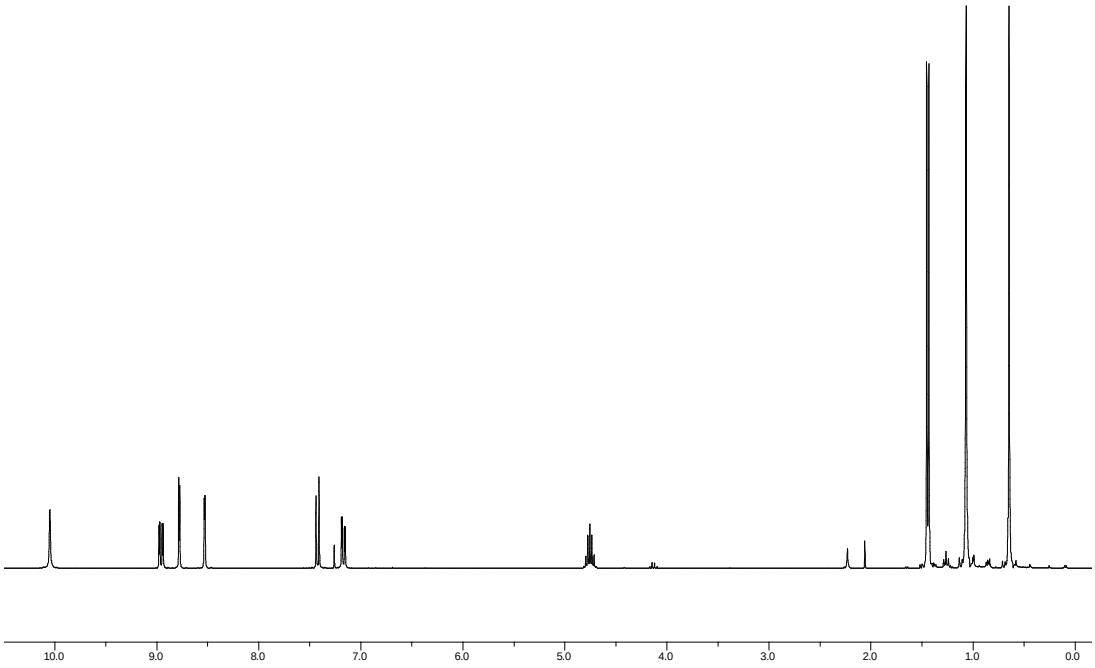

Figure 6.60.1. ^{1}H NMR of compound 3.10 ($CDCl_3$).

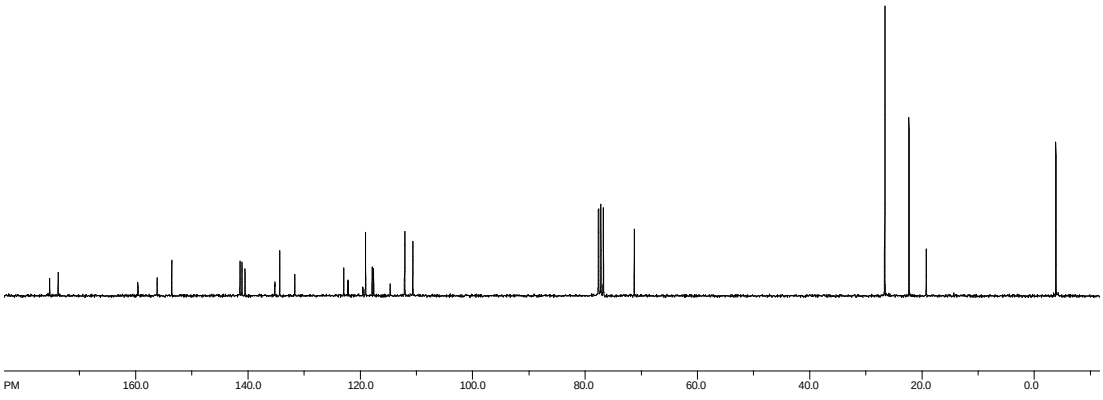

Figure 6.60.2. ^{13}C NMR of compound 3.10 ($CDCl_3$).

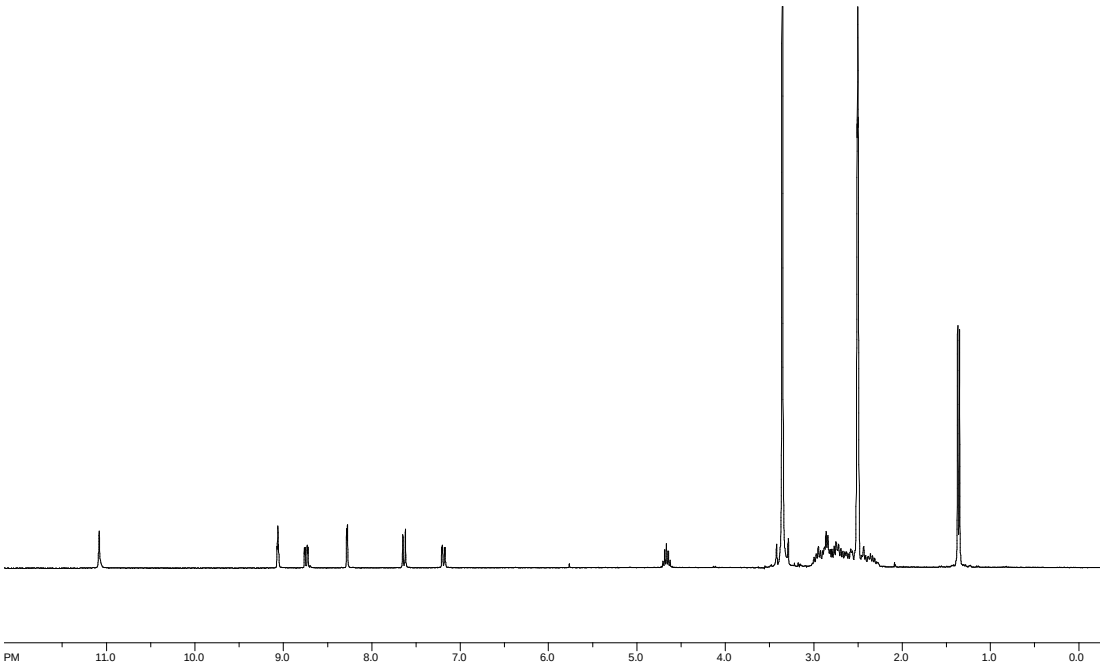

Figure 6.61.1. ^{1}H NMR of complex FL1335 (DMSO-d_6).

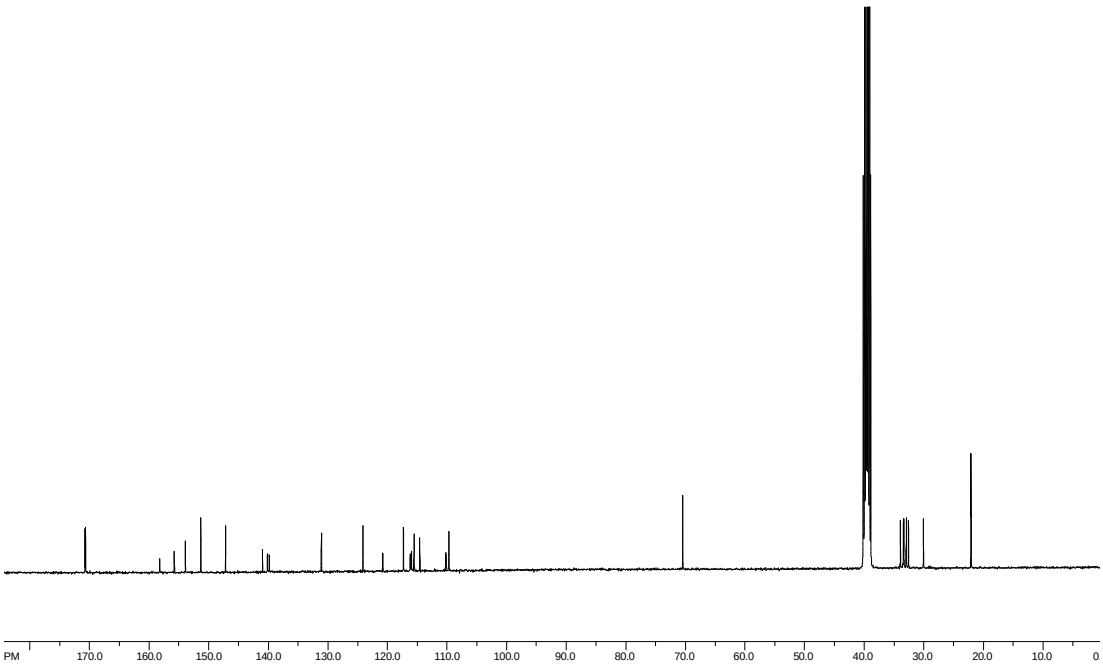

Figure 6.61.2. ^{13}C NMR of complex FL1335 (DMSO-d_6).

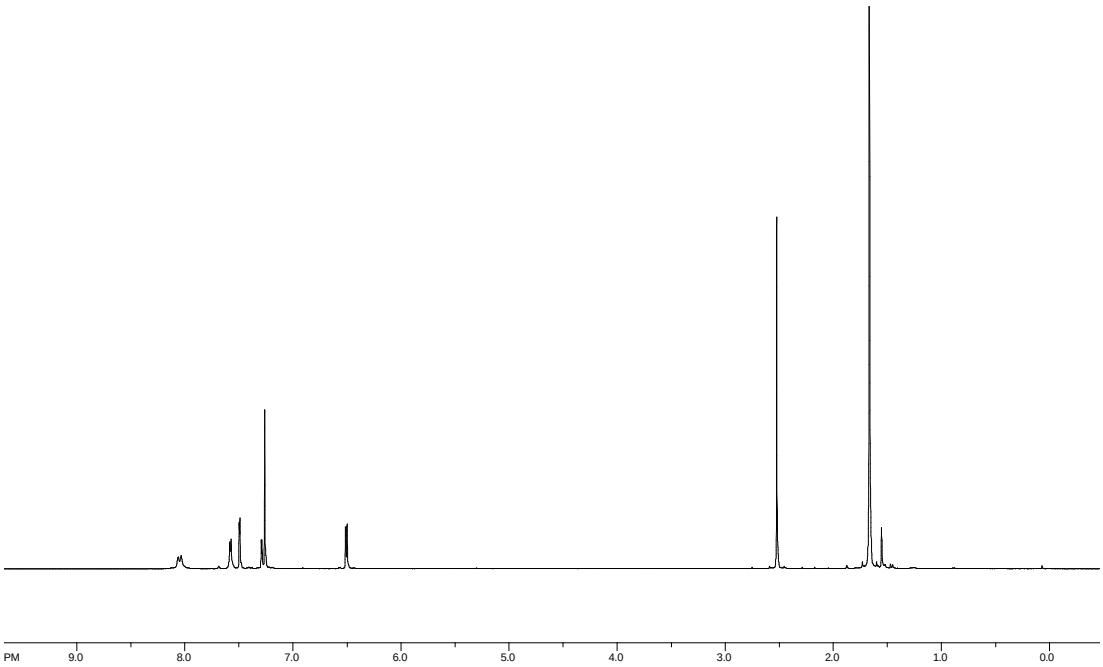

Figure 6.62.1. ^{1}H NMR of compound 3.13 ($CDCl_3$).

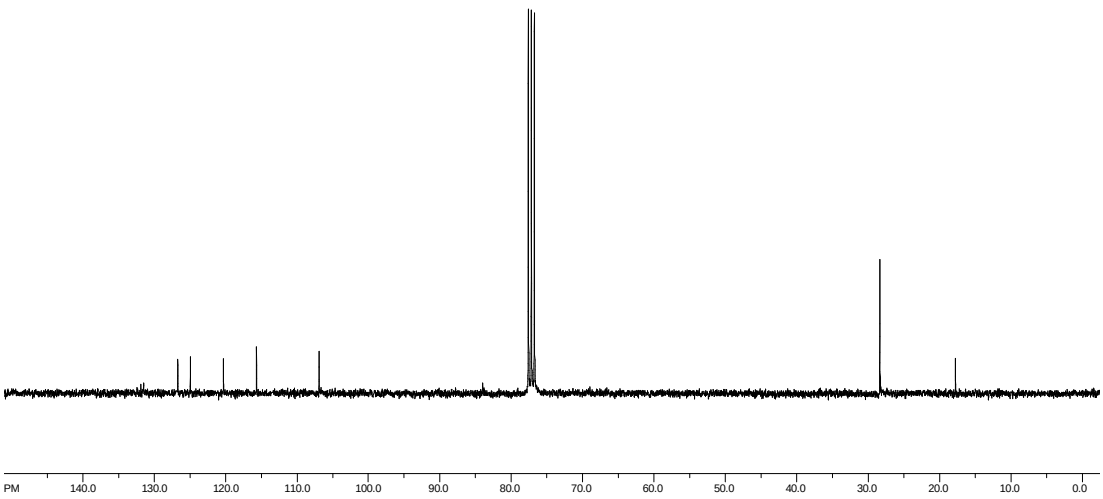

Figure 6.62.2. ^{13}C NMR of compound 3.13 ($CDCl_3$).

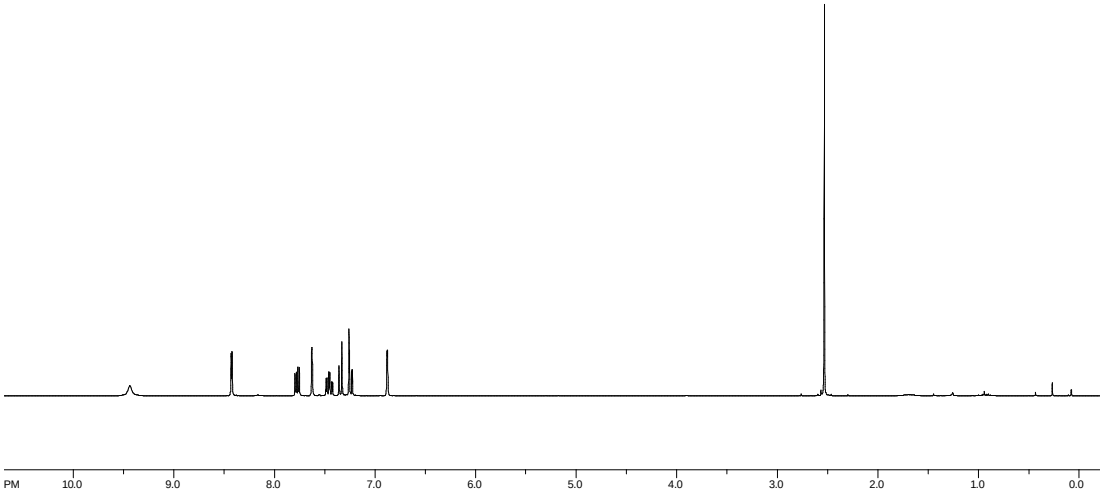

Figure 6.63.1. ^{1}H NMR of compound 3.15 ($CDCl_3$).

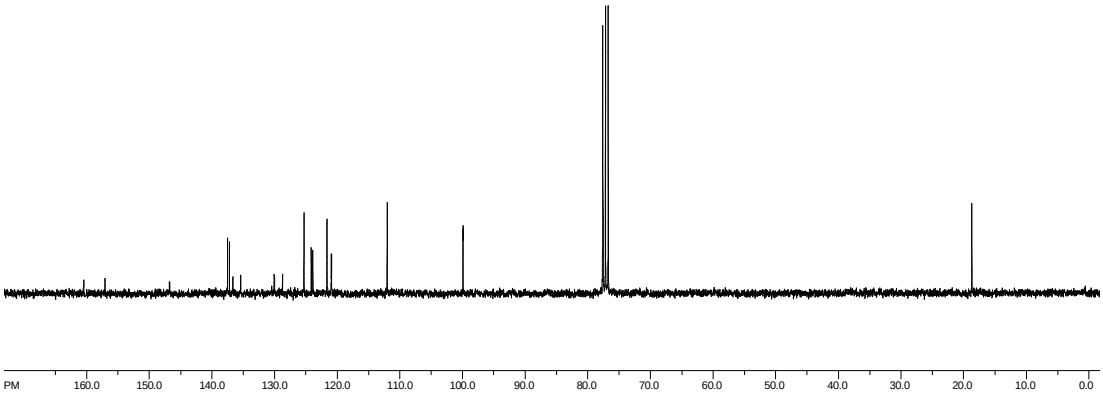

Figure 6.63.2. ^{13}C NMR of compound 3.15 ($CDCl_3$).

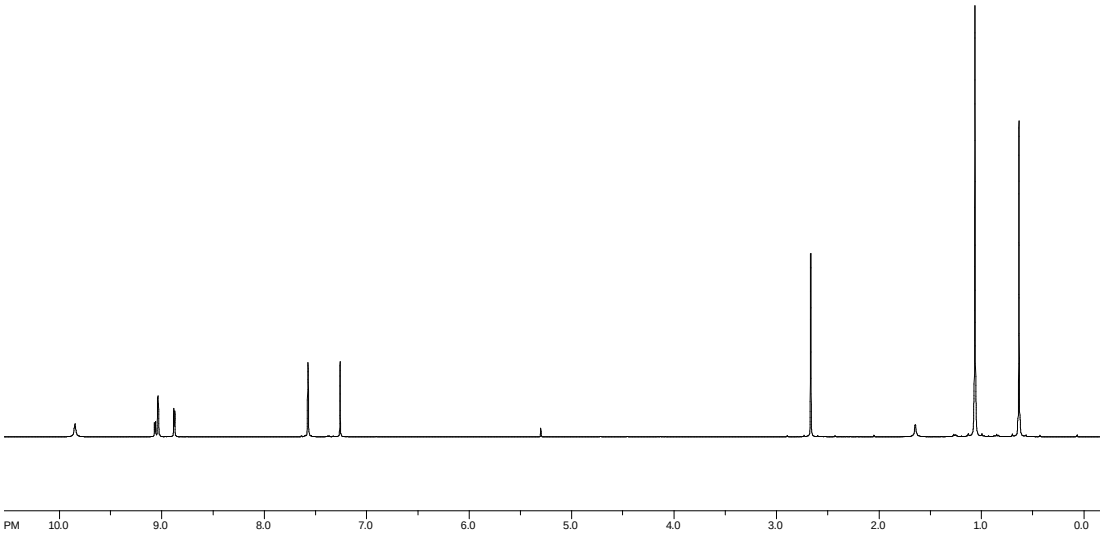

Figure 6.64.1. ^{1}H NMR of compound 3.17 ($CDCl_3$).

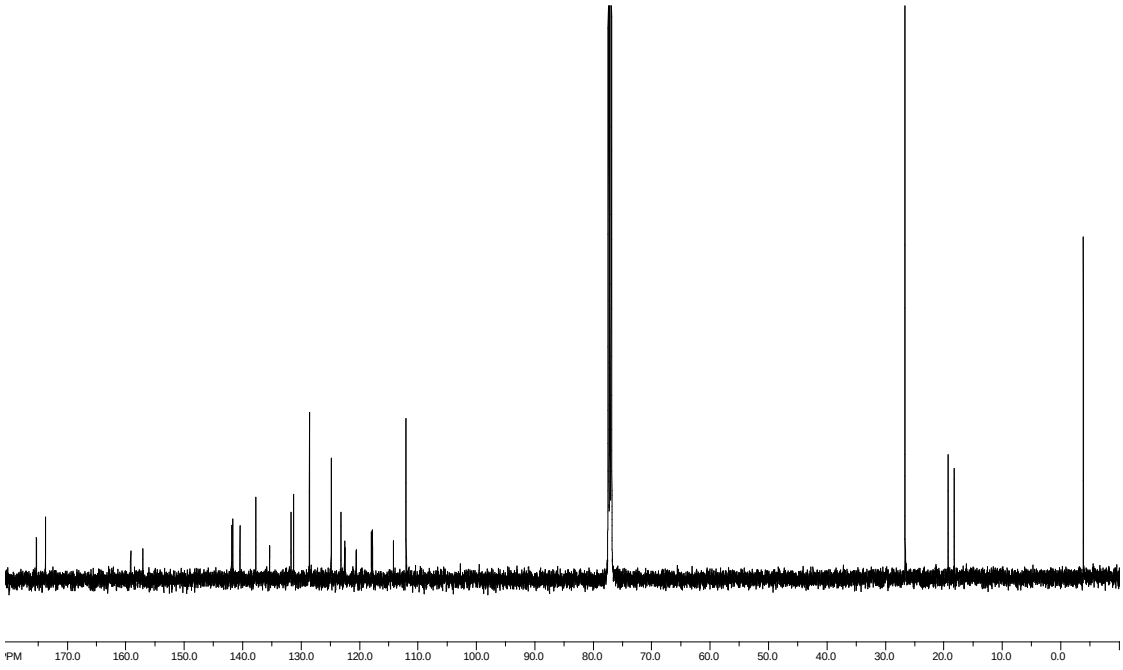

Figure 6.64.2. ^{13}C NMR of compound 3.17 ($CDCl_3$).

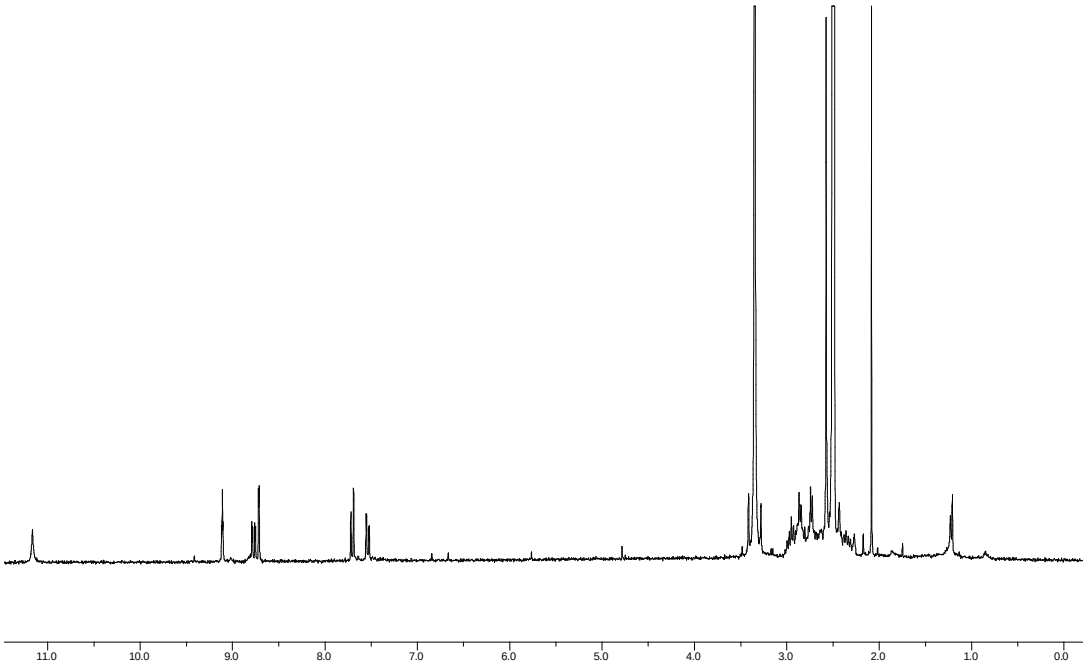

Figure 6.65.1. ^{1}H NMR of complex FL1288 (DMSO-d_6).

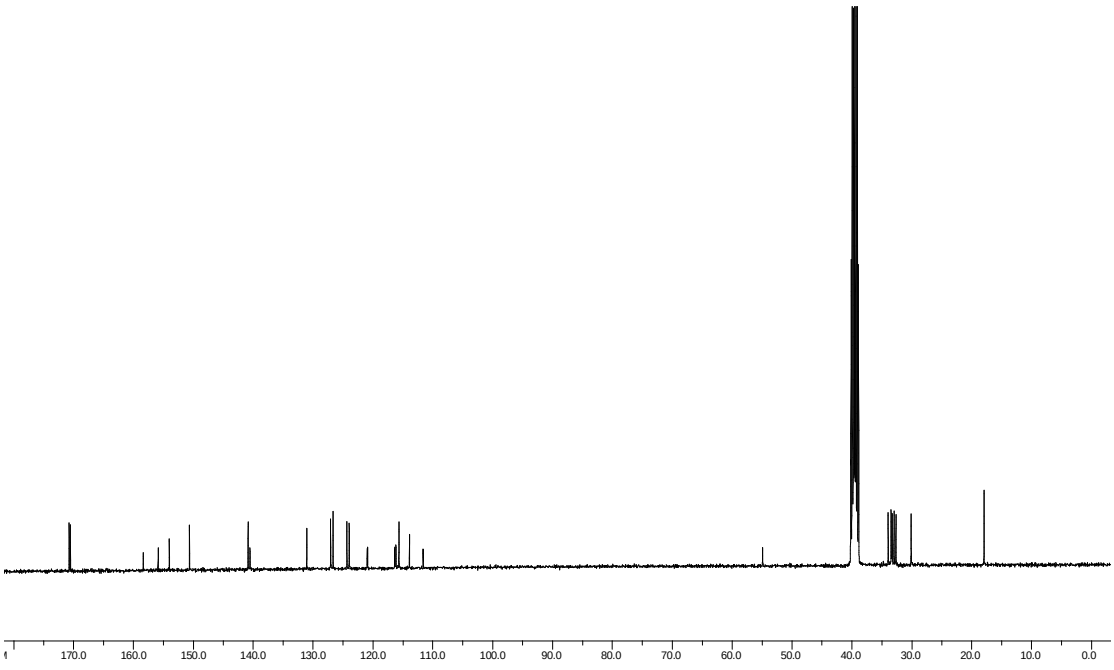

Figure 6.65.2. ^{13}C NMR of complex FL1288 (DMSO-d_6).

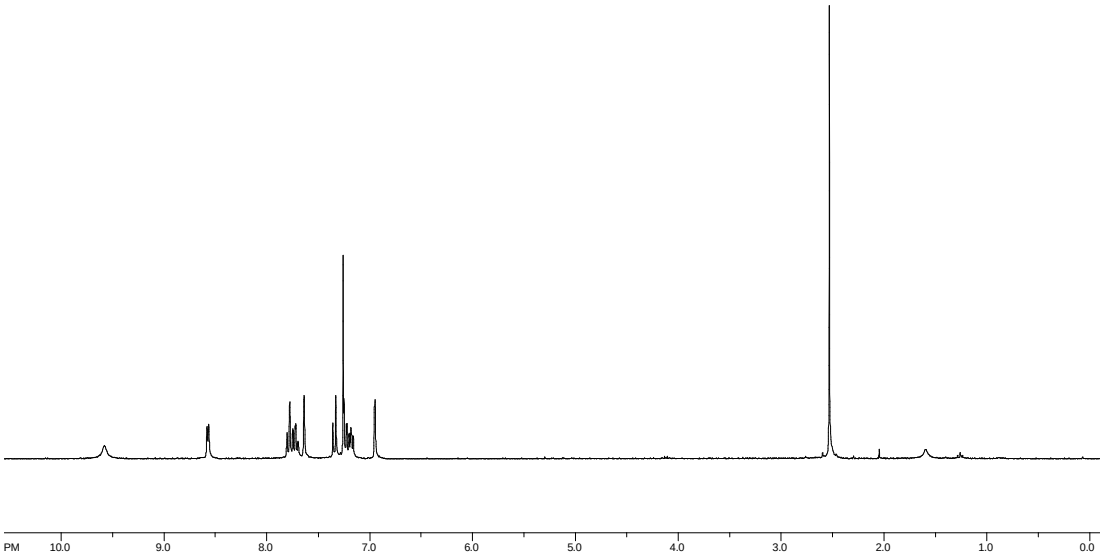

Figure 6.66.1. ^{1}H NMR of compound 3.19 ($CDCl_3$).

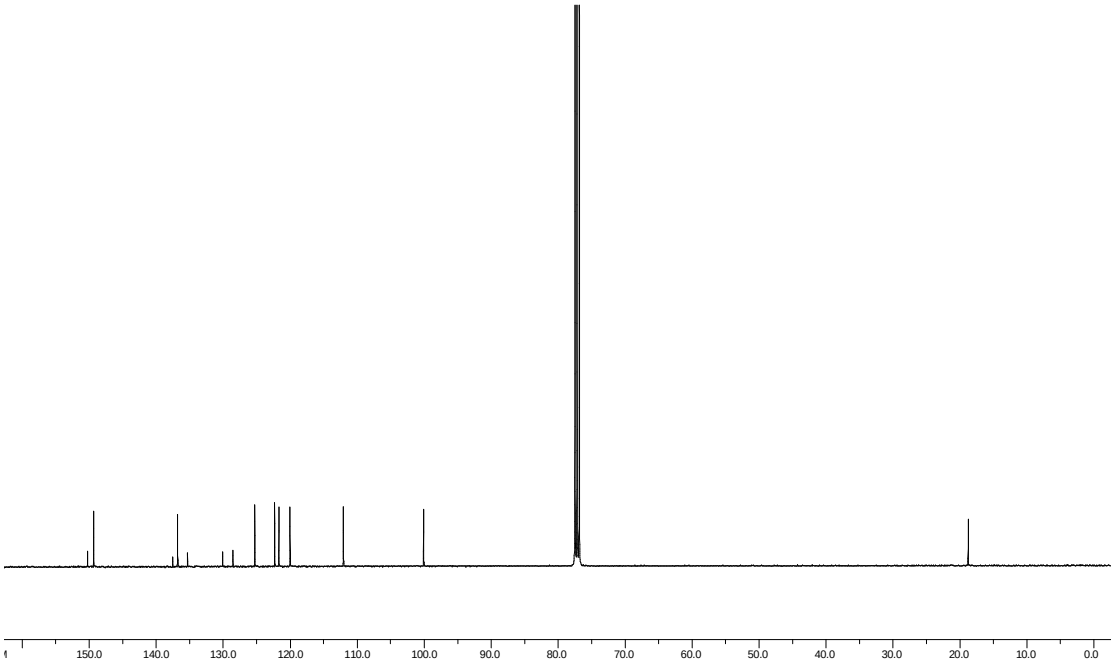

Figure 6.66.2. ^{13}C NMR of compound 3.19 ($CDCl_3$).

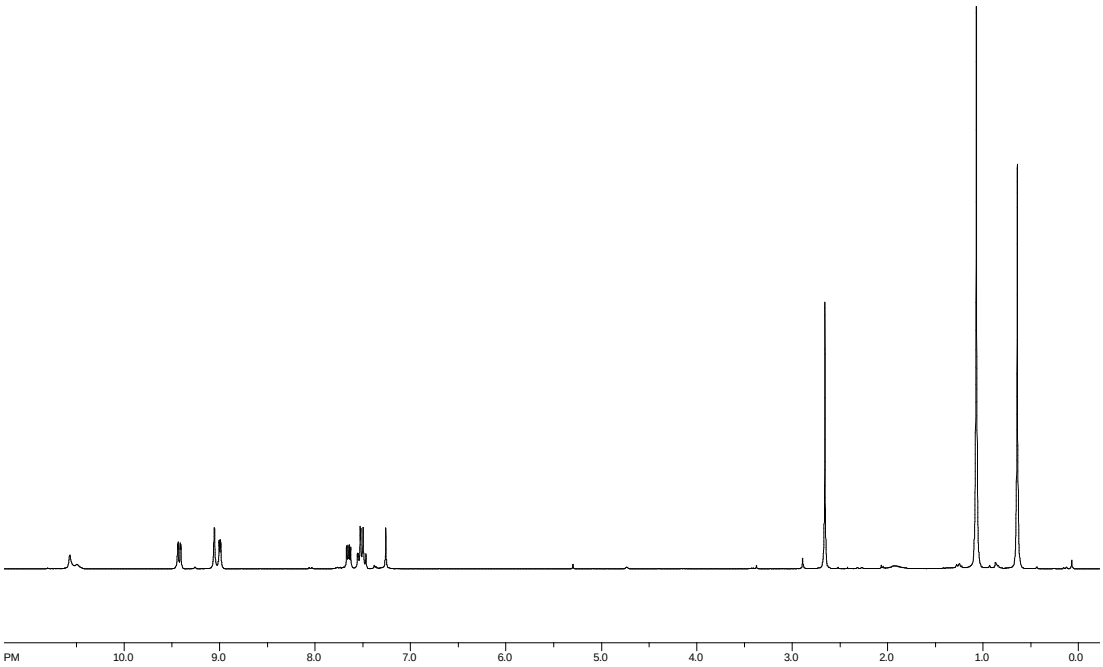

Figure 6.67.1. ^{1}H NMR of compound 3.21 ($CDCl_3$).

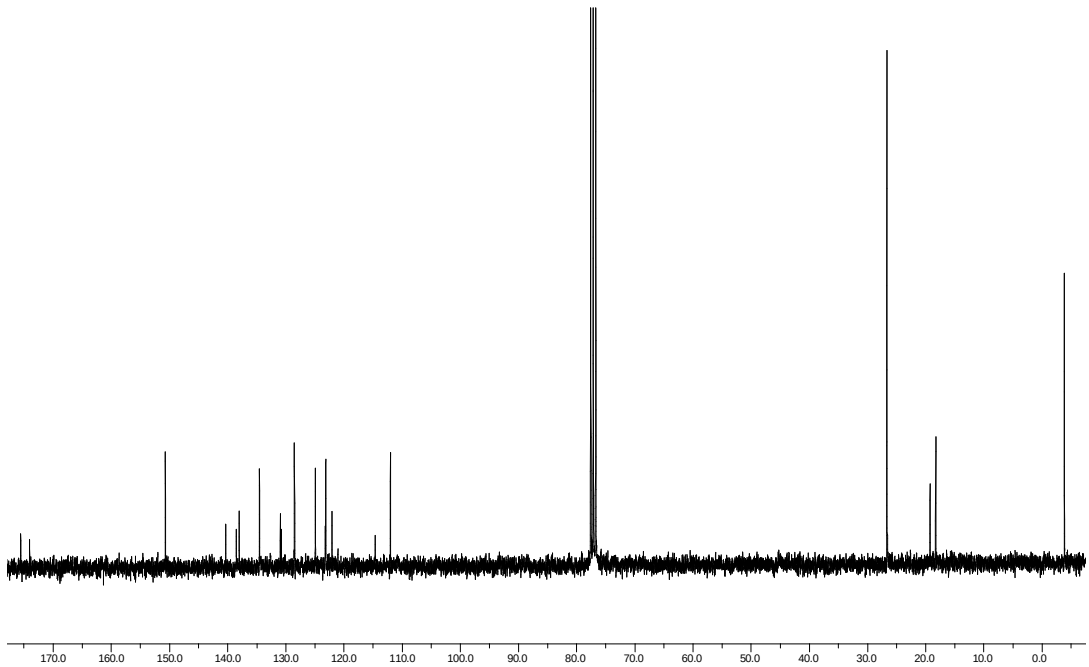

Figure 6.67.2. ^{13}C NMR of compound 3.21 ($CDCl_3$).

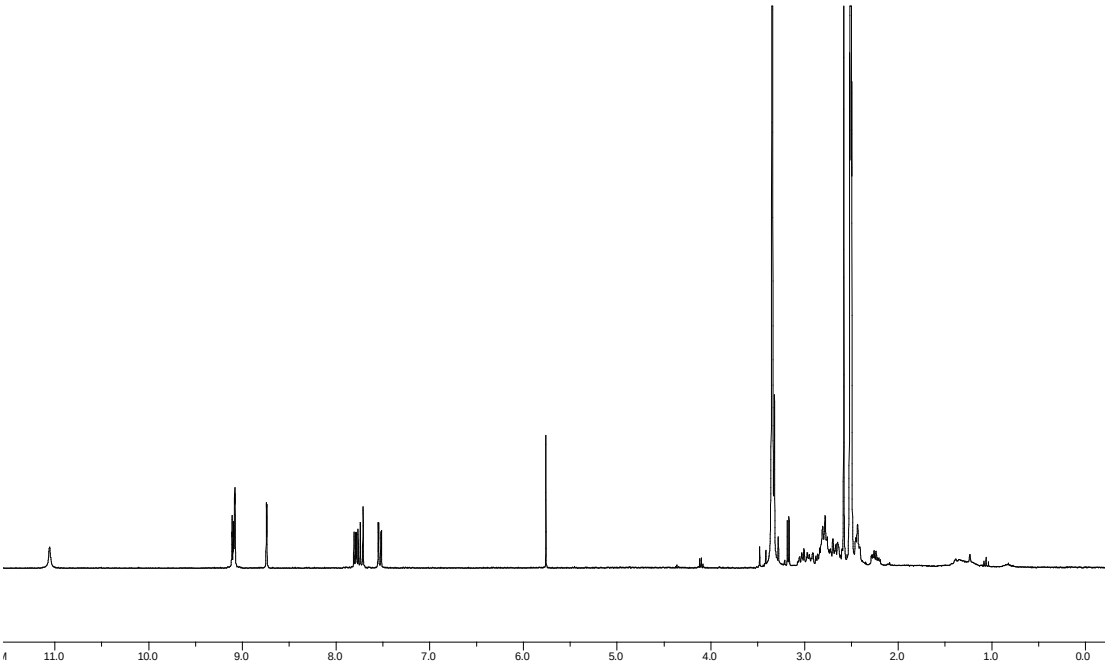

Figure 6.68.1. ^{1}H NMR of complex FL1343 (DMSO-d_6).

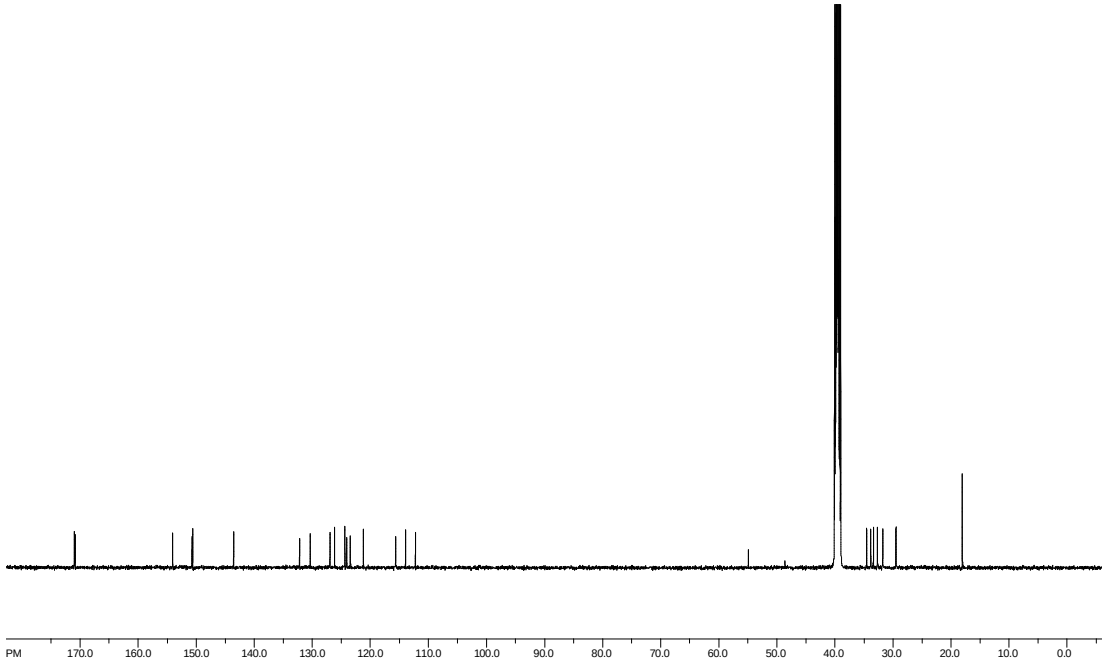

Figure 6.68.2. ^{13}C NMR of complex FL1343 (DMSO-d_6).

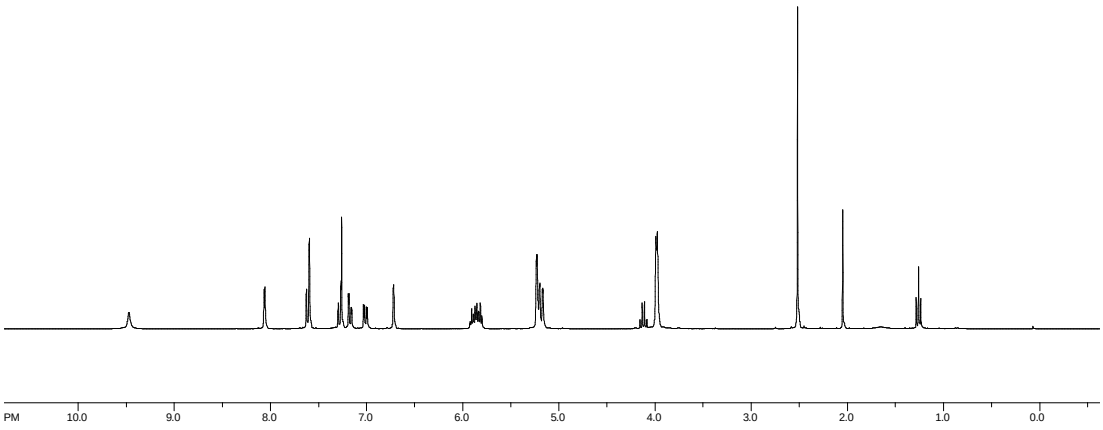

Figure 6.69.1. ^{1}H NMR of compound 3.24 ($CDCl_3$).

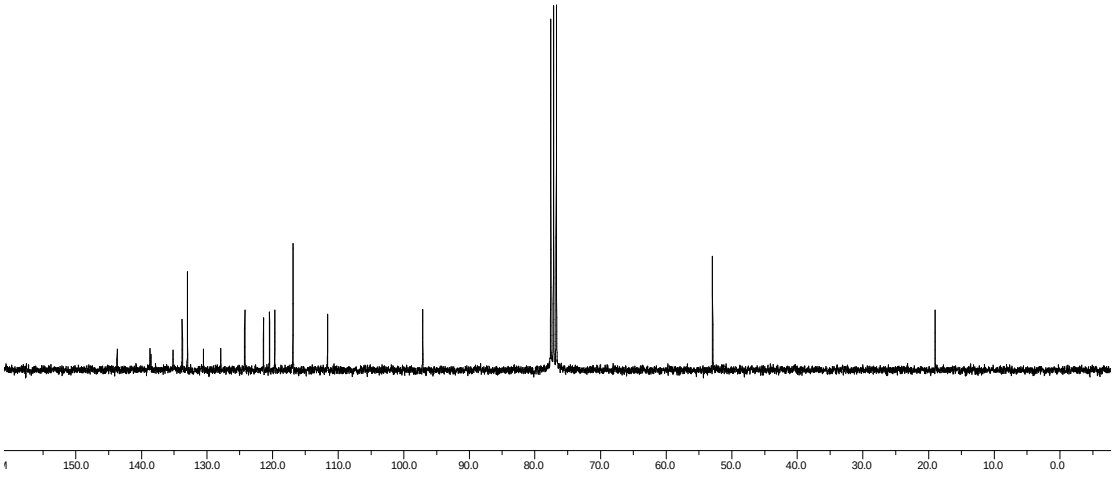

Figure 6.69.2. ^{13}C NMR of compound FL3.24 ($CDCl_3$).

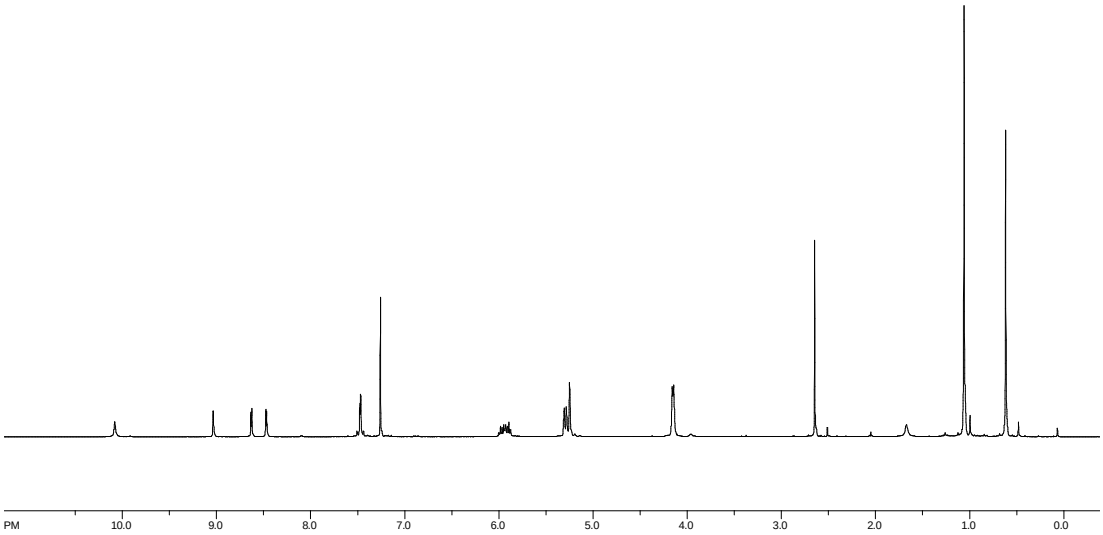

Figure 6.70.1. ^{1}H NMR of compound 3.26 ($CDCl_3$).

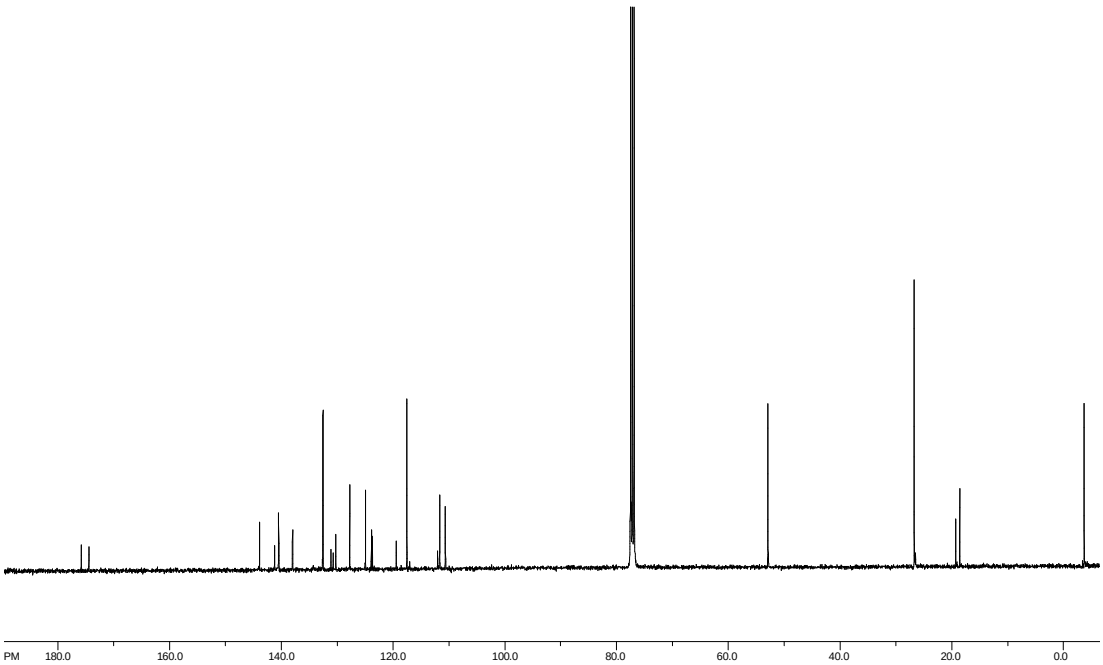

Figure 6.70.2. ^{13}C NMR of compound FL3.26 ($CDCl_3$).

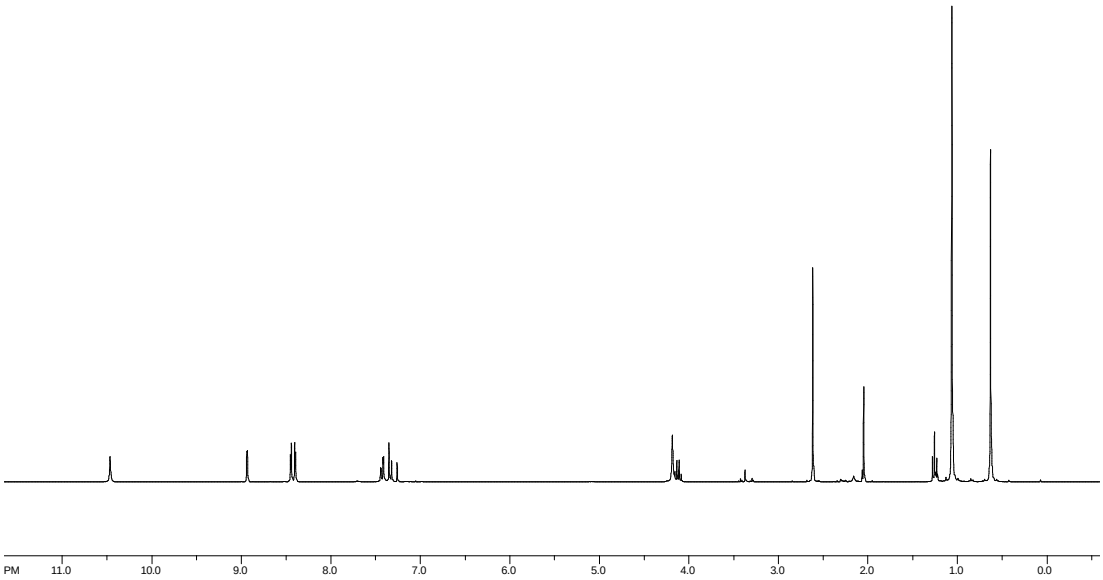

Figure 6.71.1. ^{1}H NMR of compound 3.27 ($CDCl_3$).

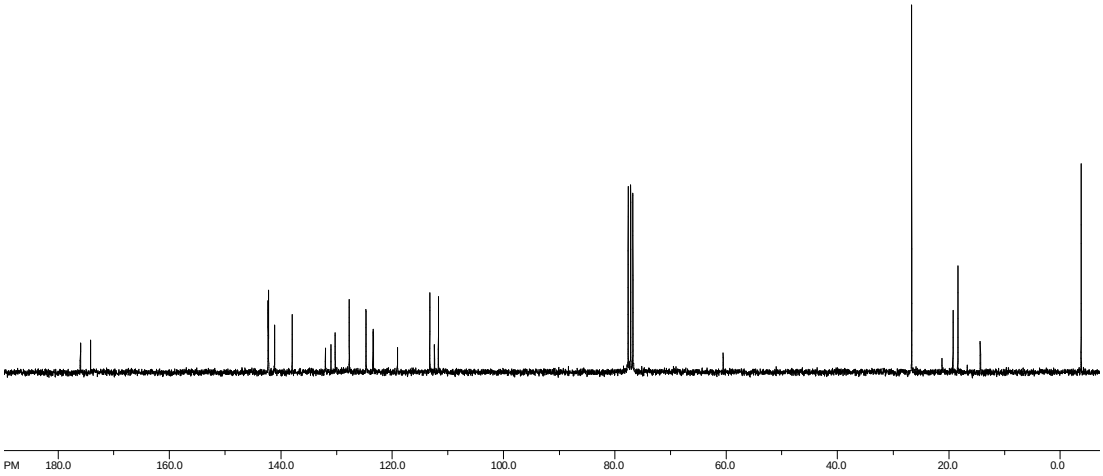

Figure 6.71.2. ^{13}C NMR of compound FL3.27 ($CDCl_3$).

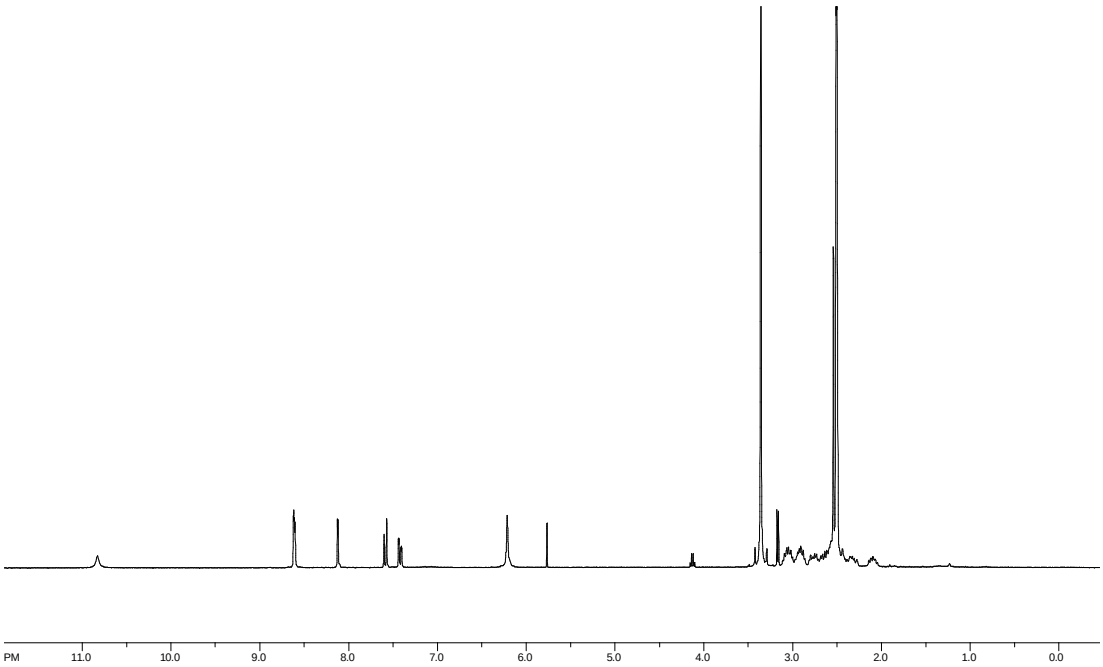

Figure 6.72.1. ^{1}H NMR of complex FL1358 (DMSO-d_6).

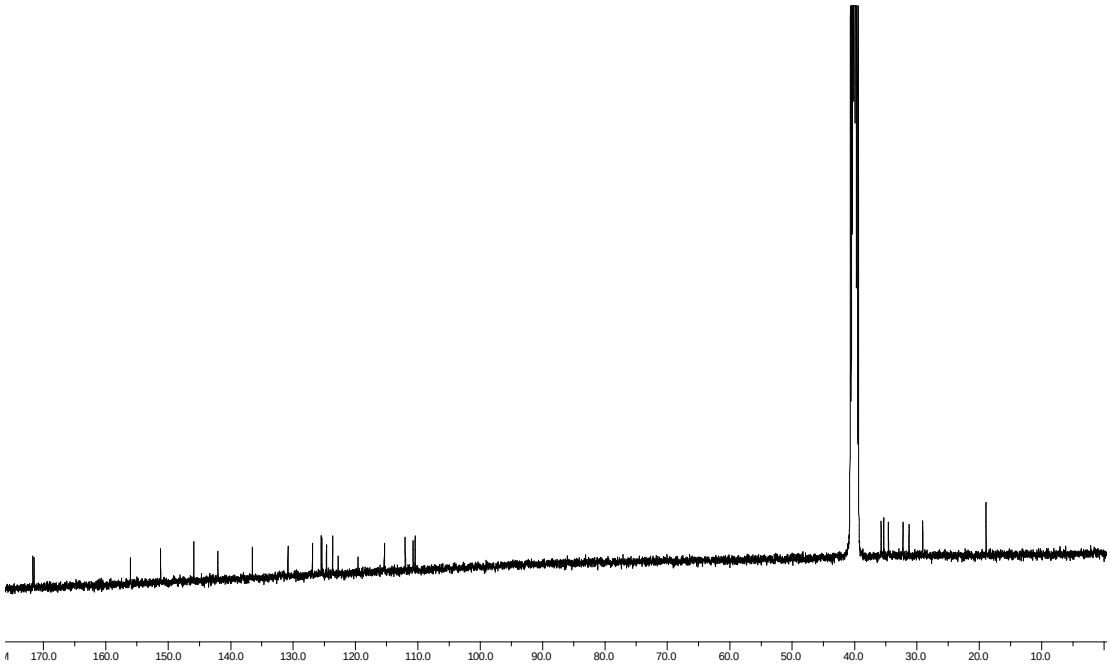

Figure 6.72.2. ^{13}C NMR of complex FL1358 (DMSO-d_6).

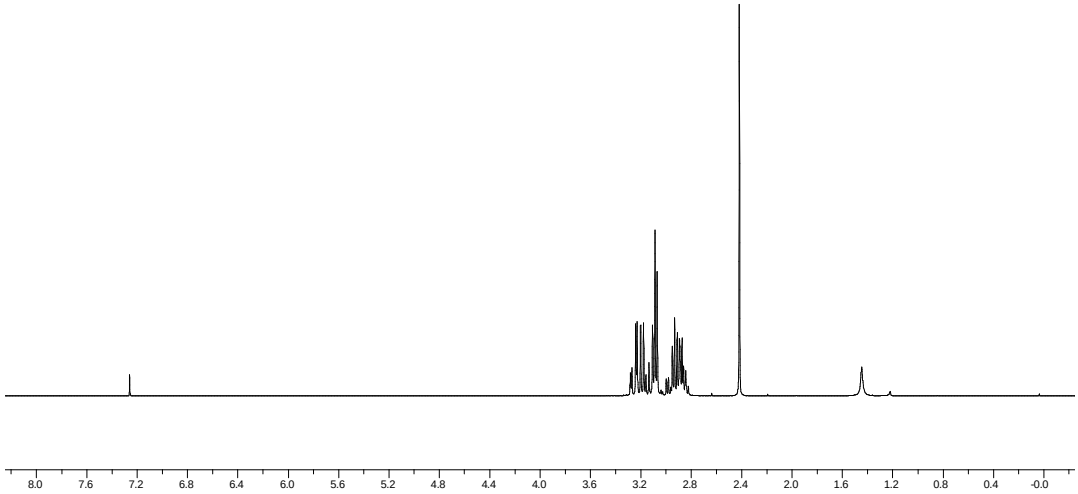

Figure 6.73.1. ^{1}H NMR of compound 3.62 ($CDCl_3$).

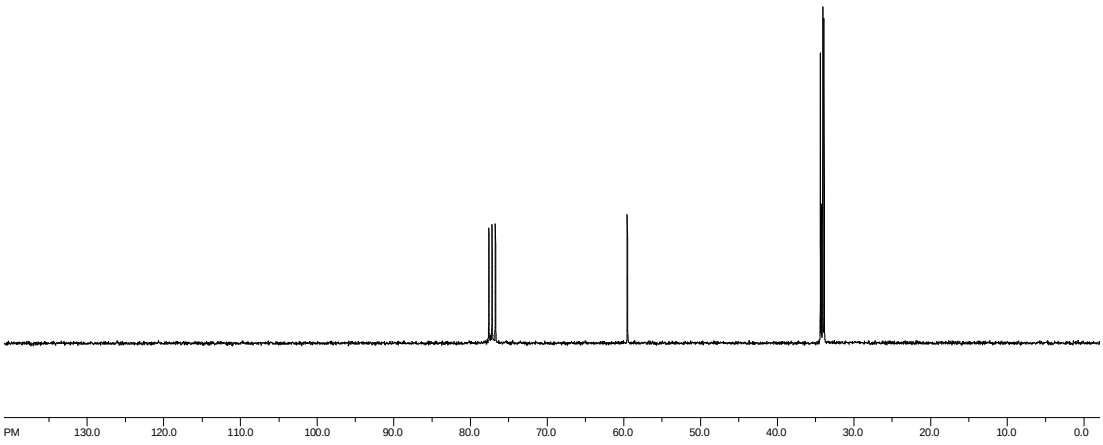

Figure 6.73.2. ^{13}C NMR of compound 3.62 ($CDCl_3$).

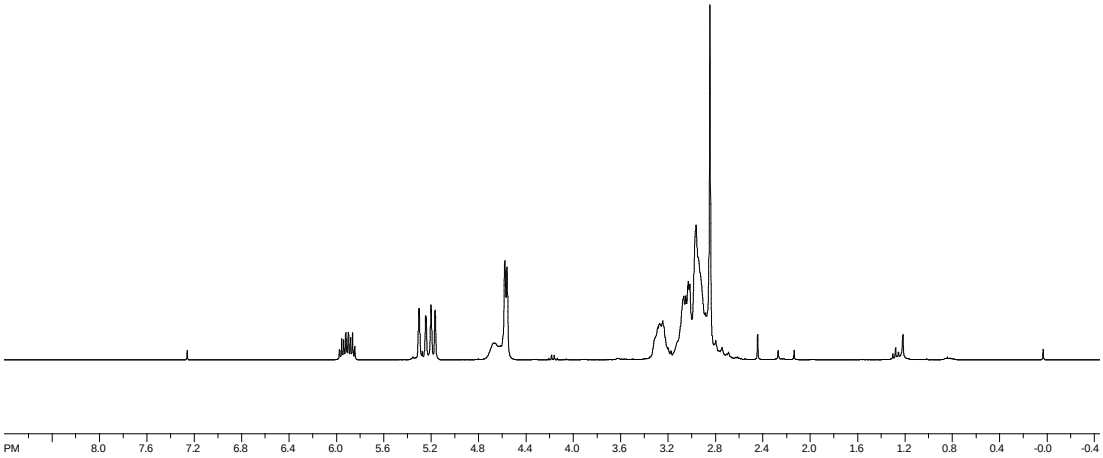

Figure 6.74.1. ^{1}H NMR of compound 3.63 ($CDCl_3$).

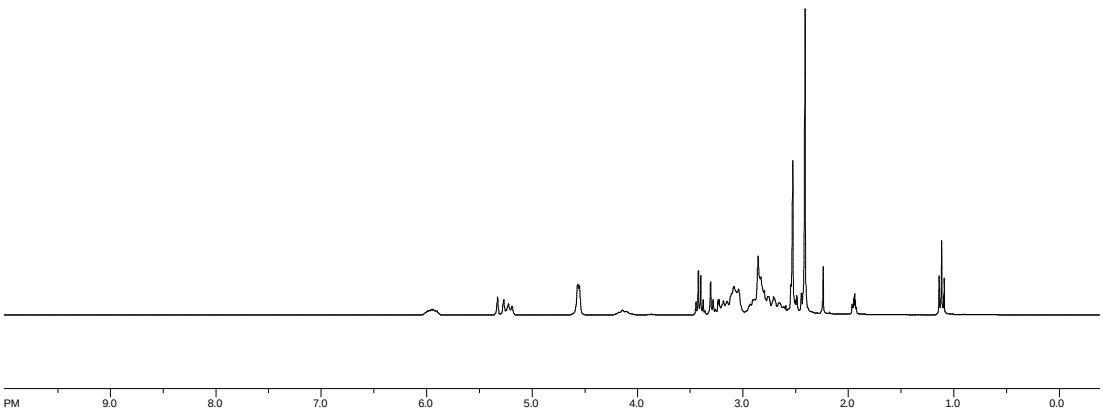

Figure 6.75.1. ^{1}H NMR of compound 3.65 (CD_3CN).

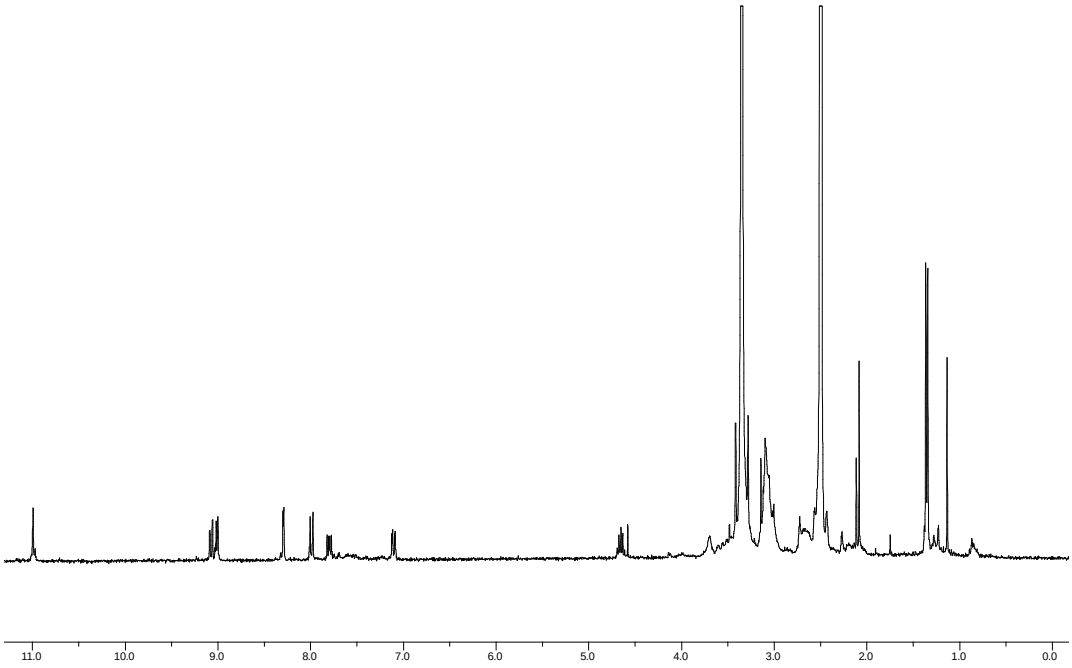

Figure 6.76.1. ^{1}H NMR of complex FL1392 (DMSO-d_6).

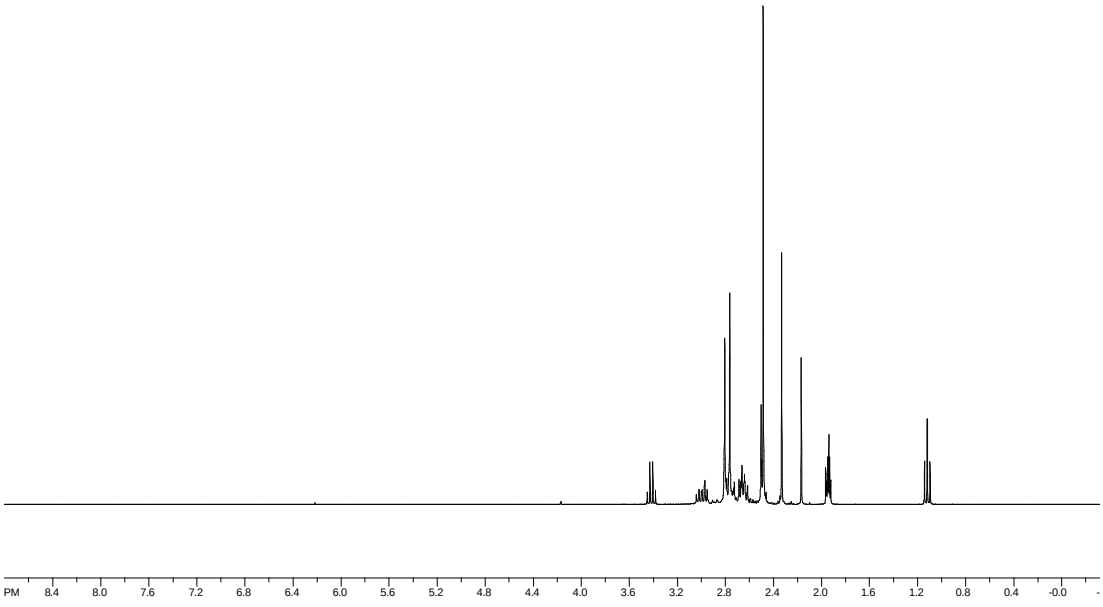

Figure 6.77.1. ^{1}H NMR of compound 3.68 (CD_3CN).

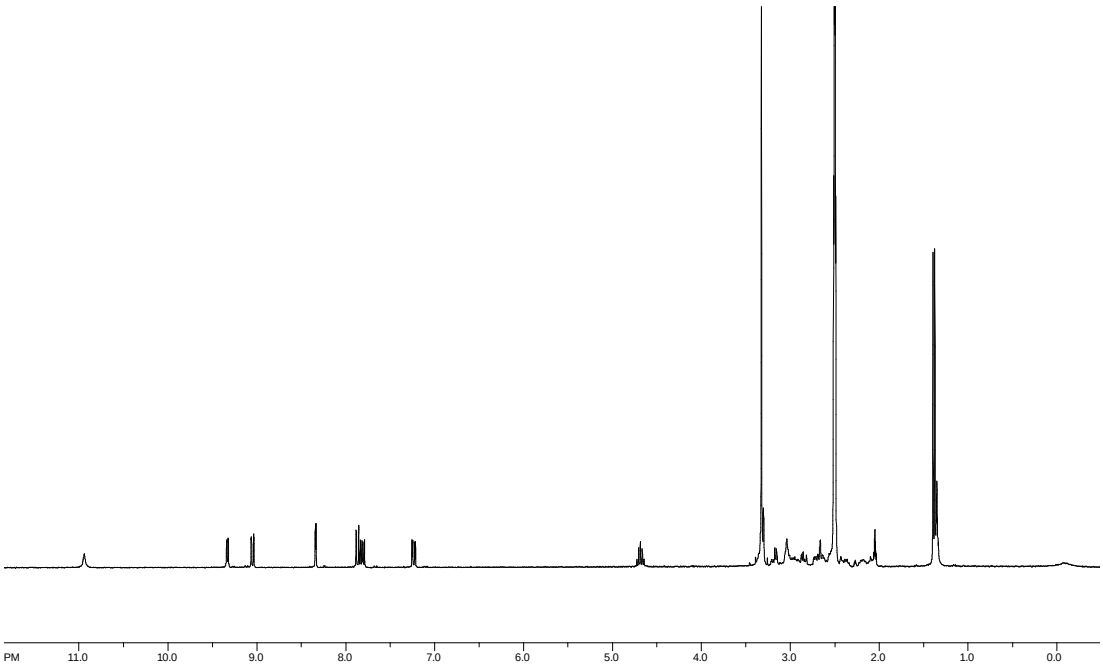

Figure 6.78.1. ^{1}H NMR of complex FL1473 (DMSO-d_6).

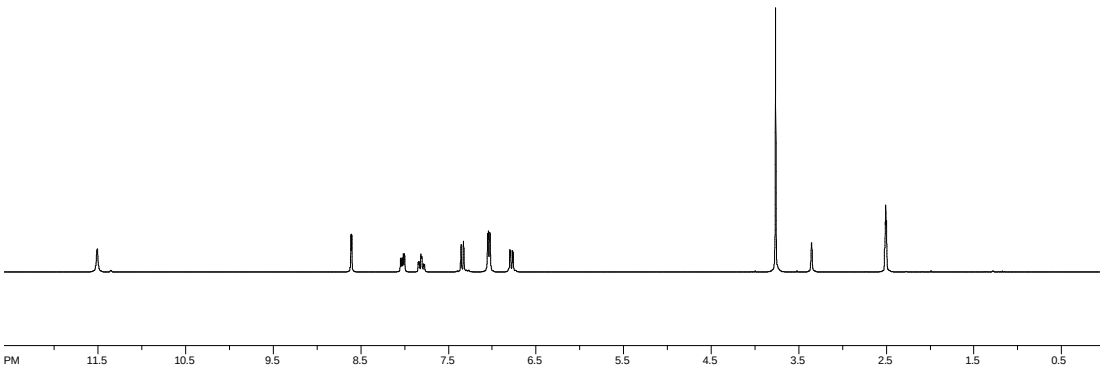

Figure 6.79.1. ^{1}H NMR of compound 3.35 (DMSO-d_6).

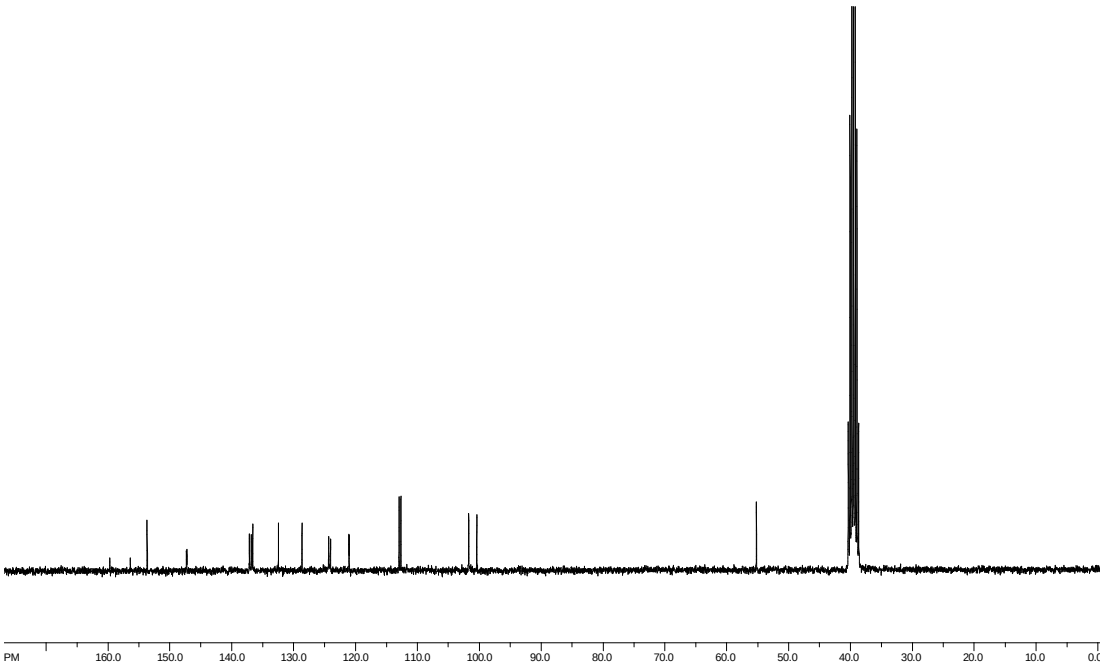

Figure 6.79.2. ^{13}C NMR of compound 3.35 (DMSO-d_6).

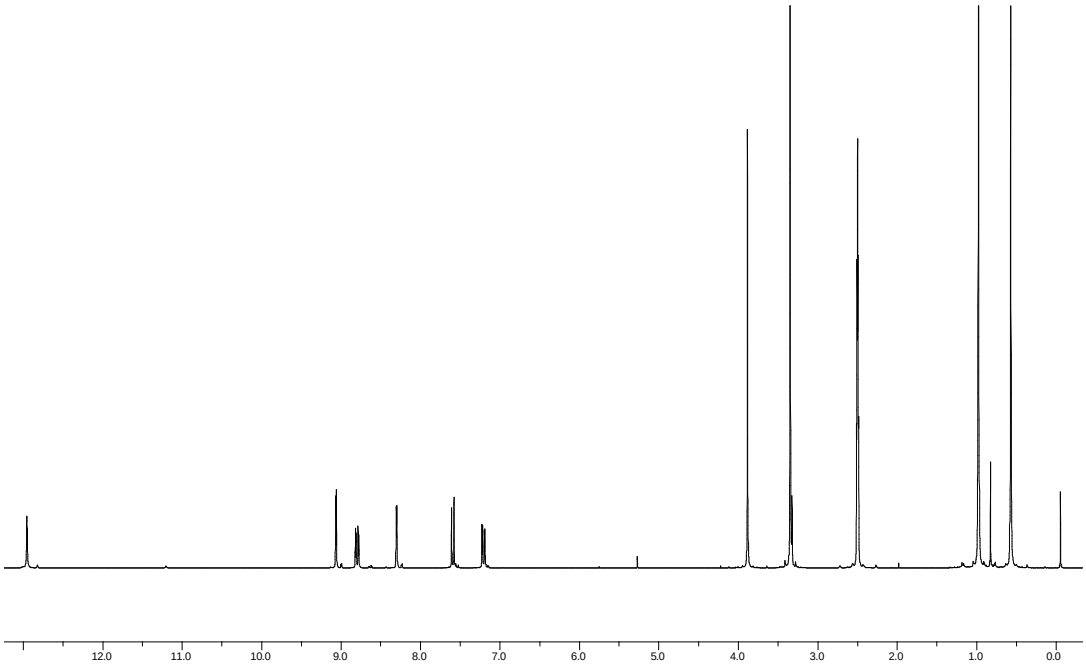

Figure 6.80.1. ^{1}H NMR of compound 3.37 (DMSO-d_6).

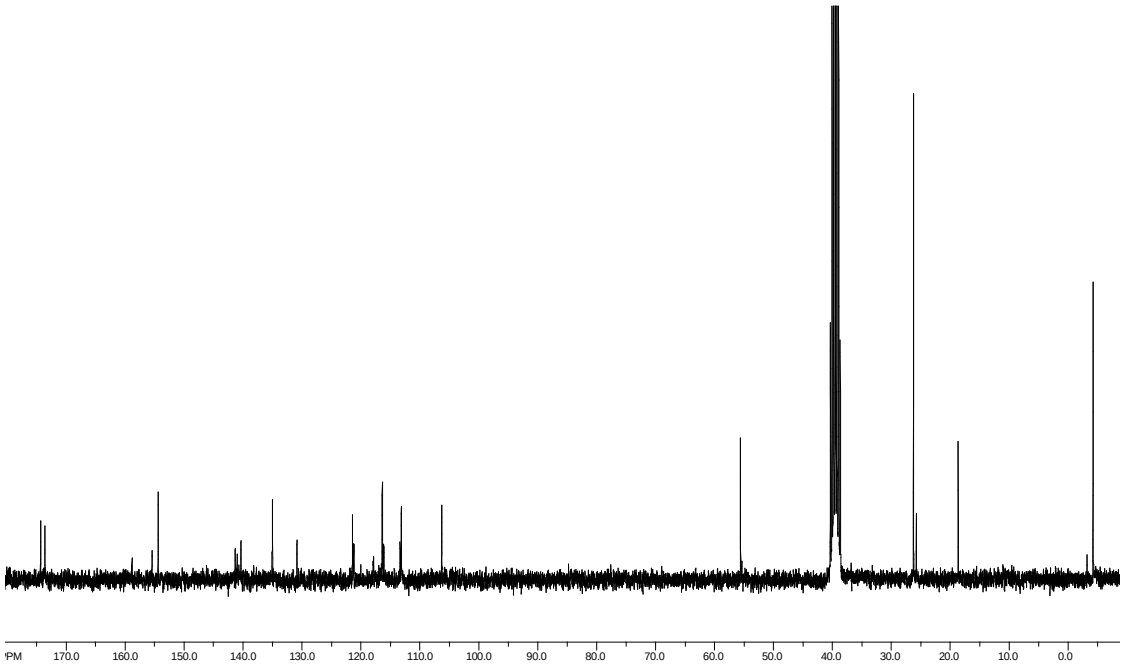

Figure 6.80.2. ^{13}C NMR of compound 3.37 (DMSO-d_6).

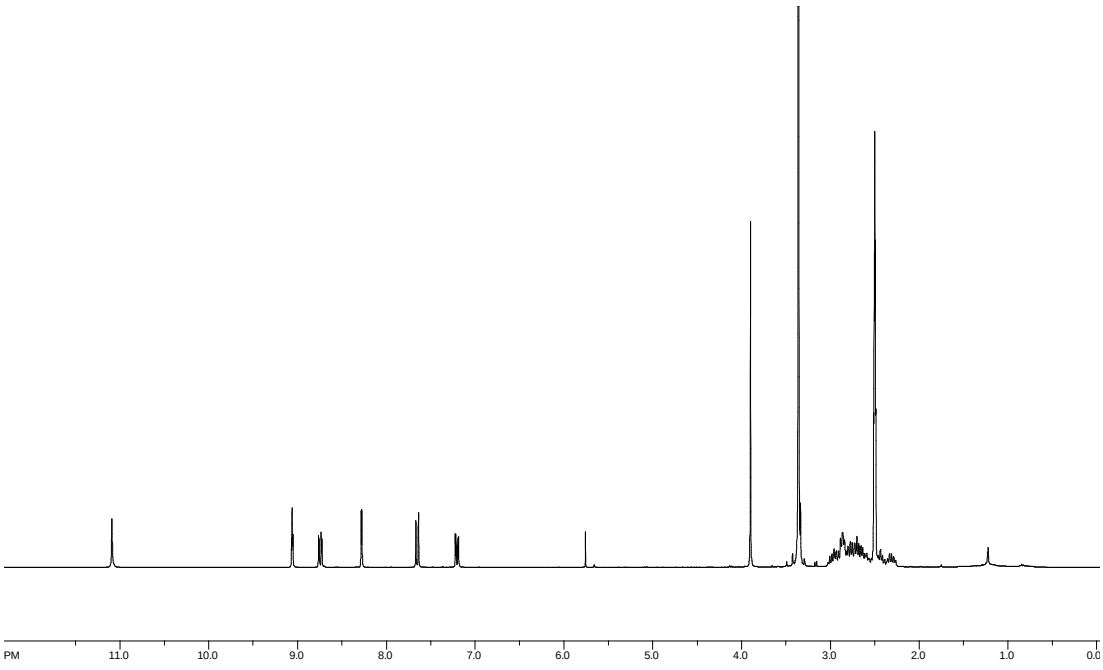

Figure 6.81.1. ^{1}H NMR of complex FL1055 (DMSO-d_6).

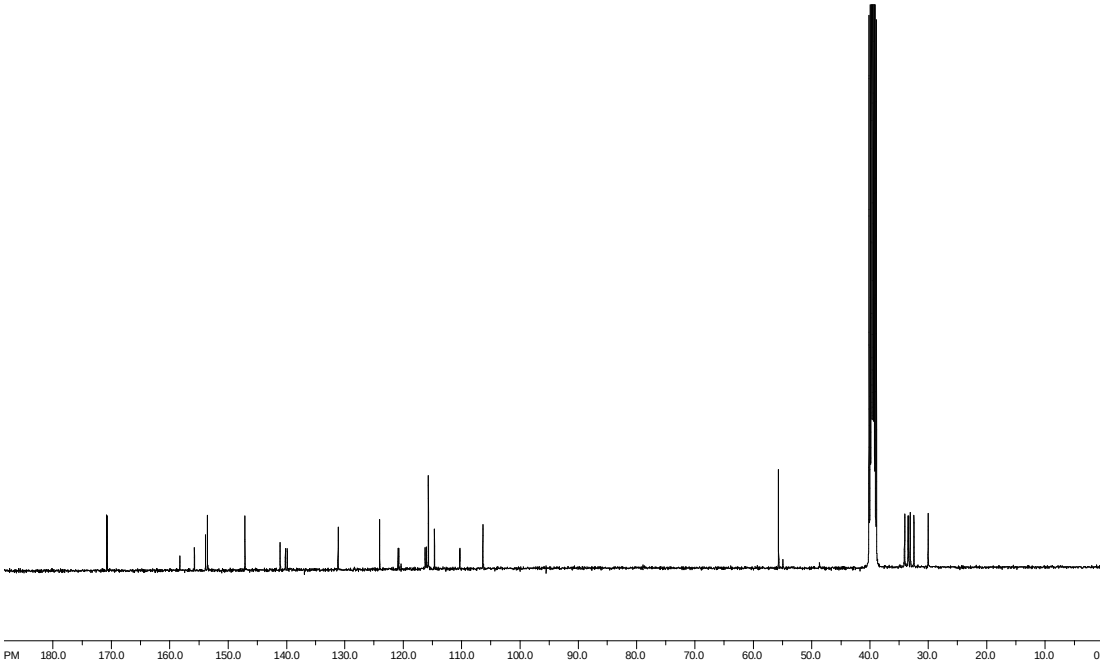

Figure 6.81.2. ^{13}C NMR of complex FL1055 (DMSO-d_6).

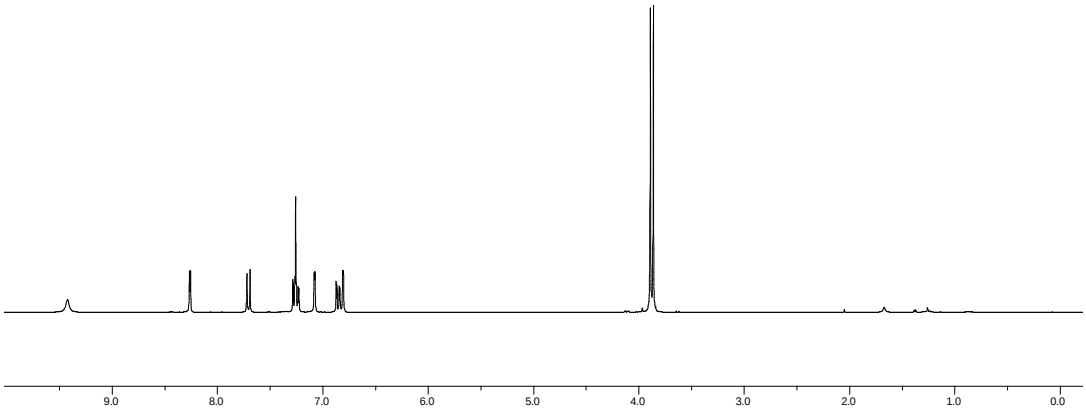

Figure 6.82.1. ^{1}H NMR of compound 3.39 ($CDCl_3$).

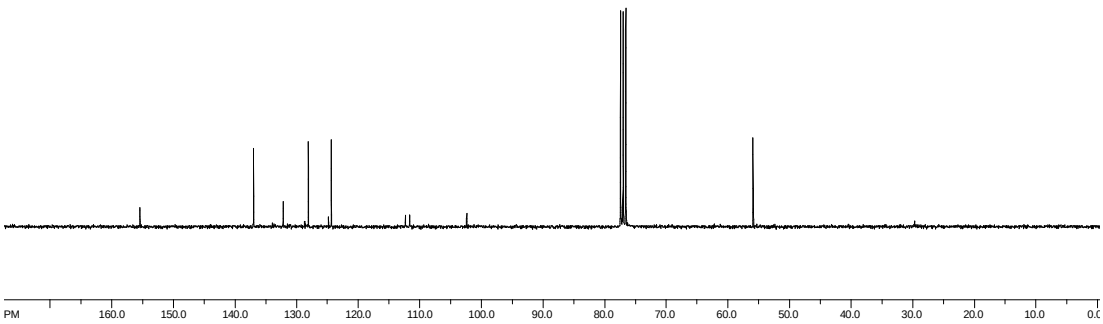

Figure 6.82.2. ^{13}C NMR of compound 3.39 ($CDCl_3$).

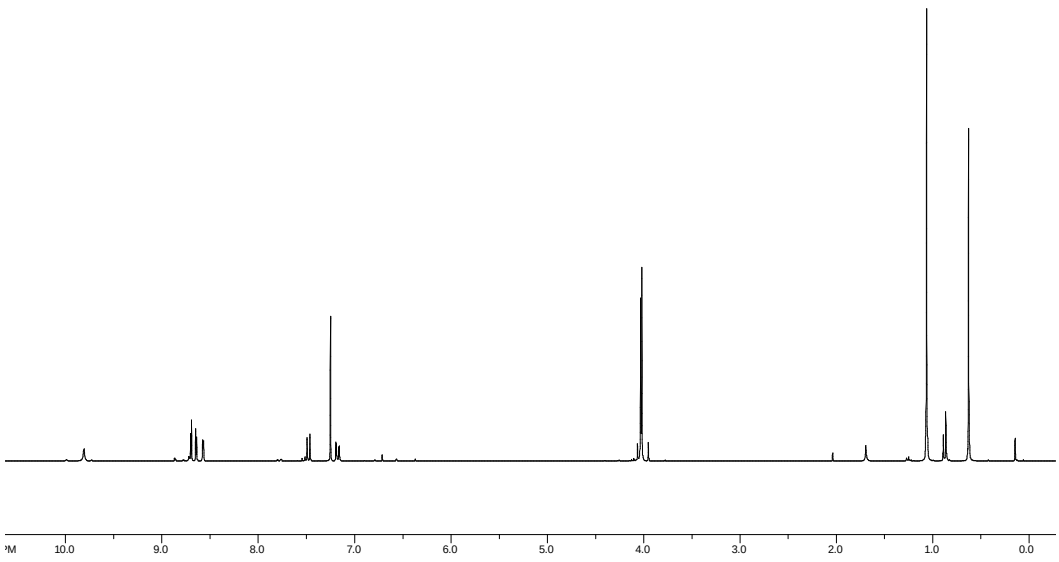

Figure 6.83.1. ^{1}H NMR of compound 3.41 ($CDCl_3$).

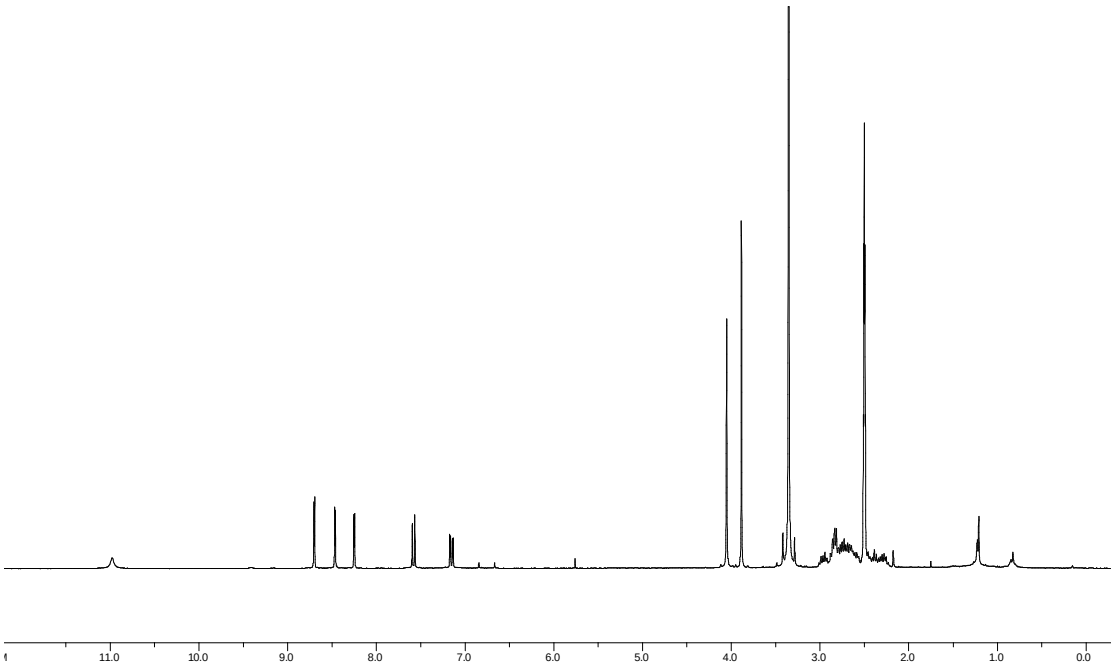

Figure 6.84.1. ^{1}H NMR of complex FL1229 (DMSO-d_6).

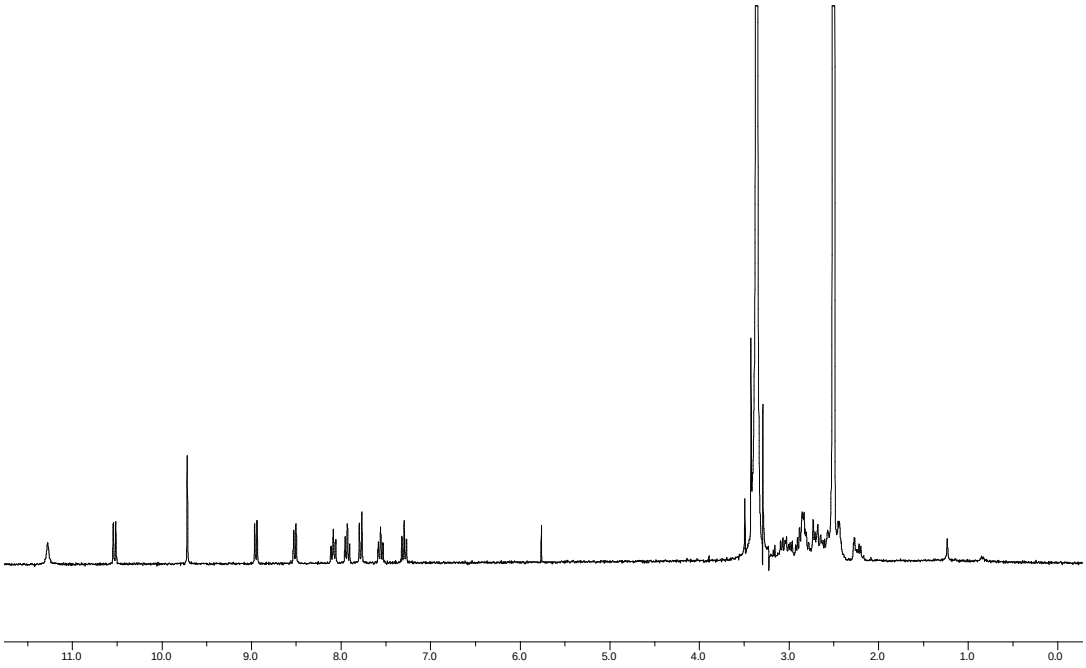

Figure 6.85.1. ^{1}H NMR of complex FL1125 (DMSO-d_6).

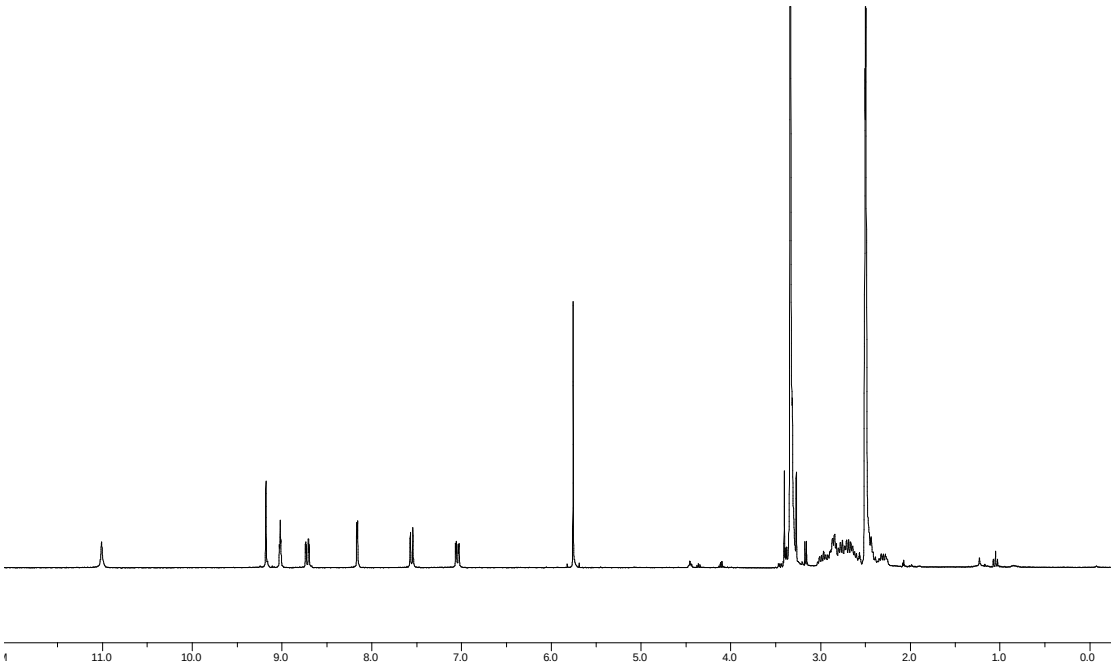

Figure 6.86.1. ^{1}H NMR of complex FL123 (DMSO-d_6).

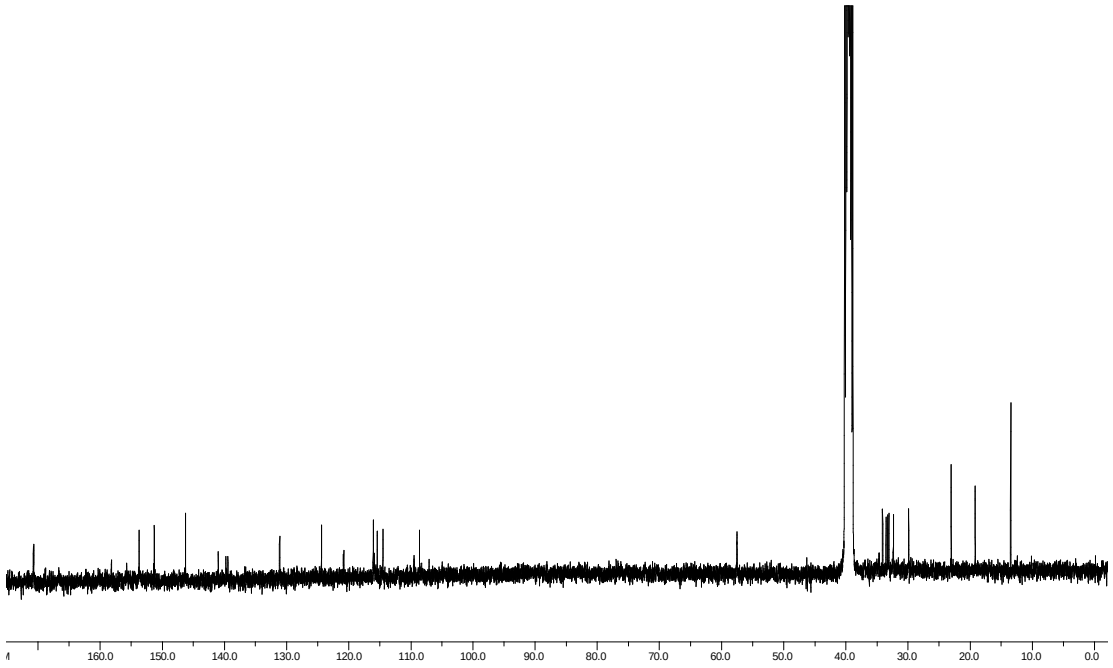

Figure 6.86.2. ^{13}C NMR of complex FL123 (DMSO-d_6).

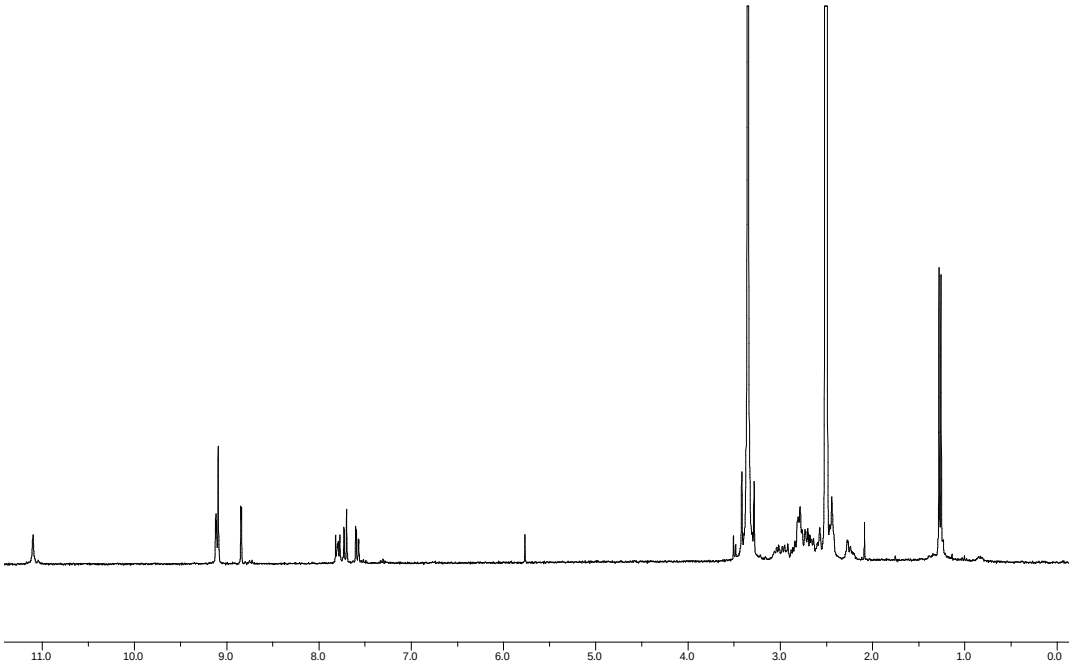

Figure 6.87.1. ^{1}H NMR of complex FL1397 (DMSO-d_6).

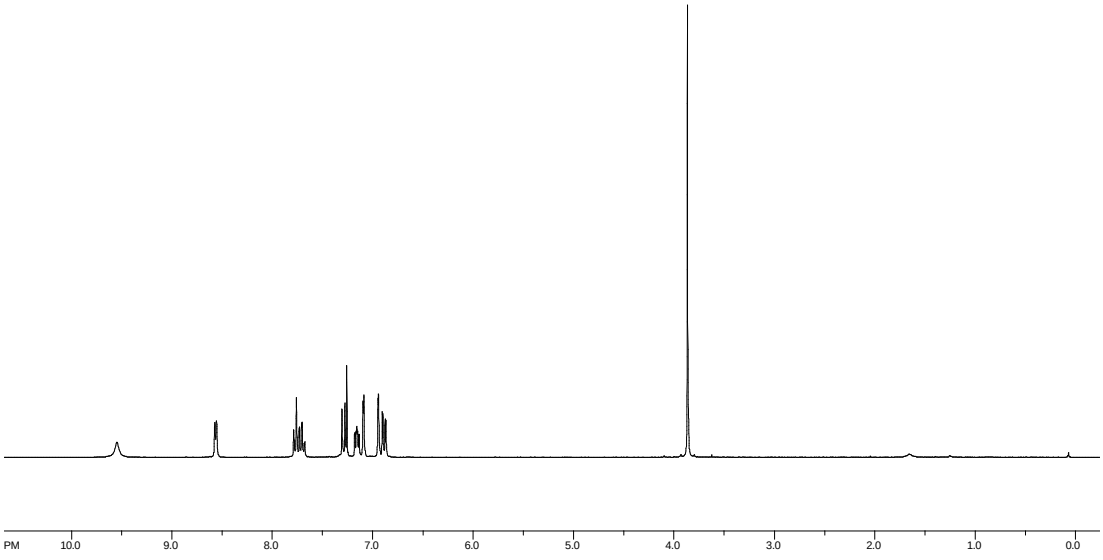

Figure 6.88.1. ^{1}H NMR of compound 3.54 ($CDCl_3$).

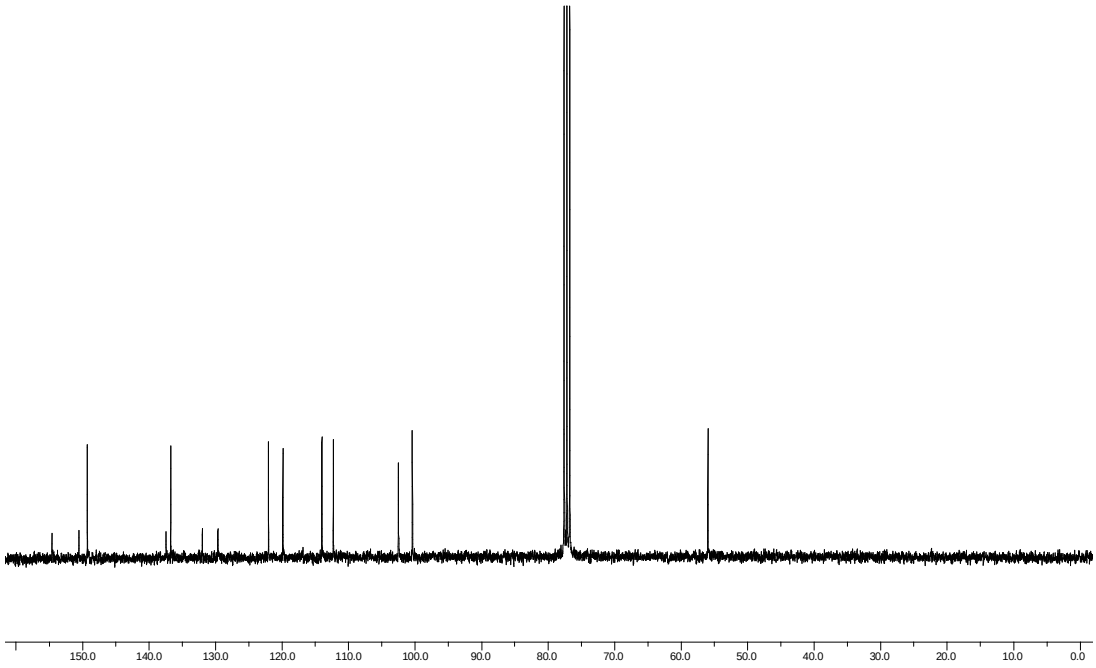

Figure 6.88.2. ^{13}C NMR of compound 3.54 ($CDCl_3$).

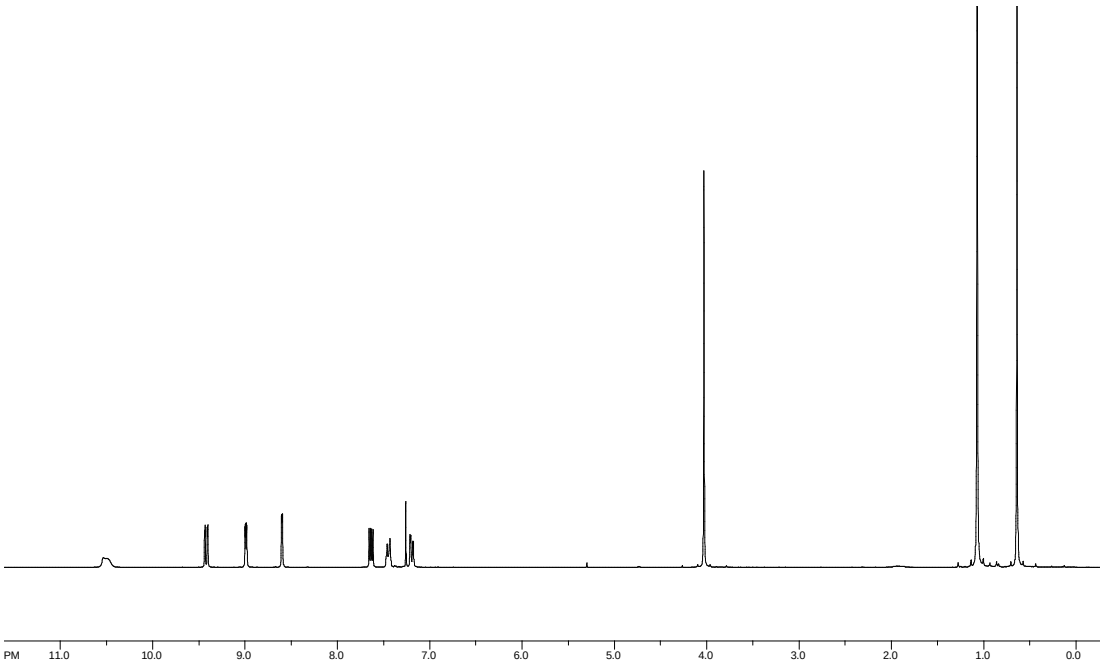

Figure 6.89.1. ^{1}H NMR of compound 3.56 ($CDCl_3$).

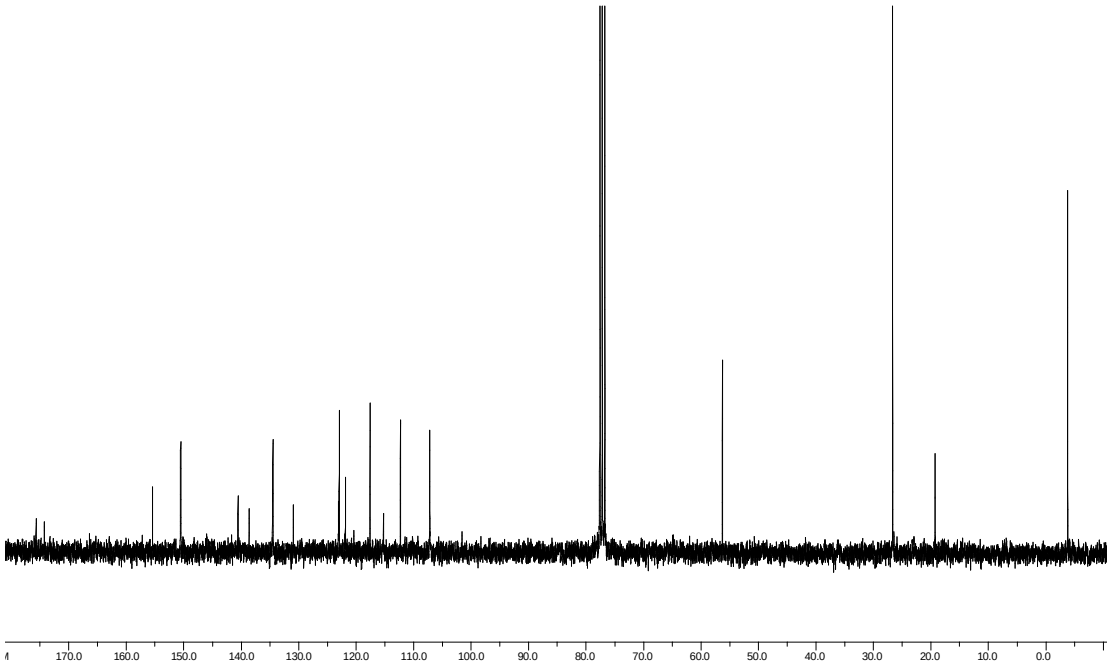

Figure 6.89.2. ^{13}C NMR of compound 3.56 ($CDCl_3$).

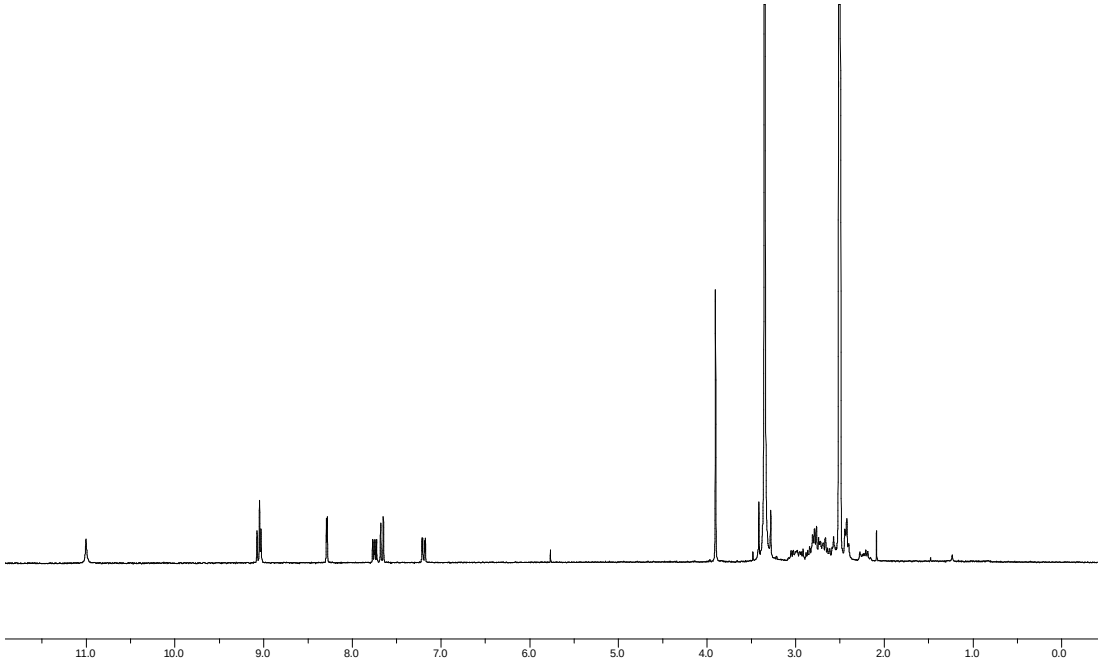

Figure 6.90.1. ^{1}H NMR of complex FL1381 (DMSO-d_6).

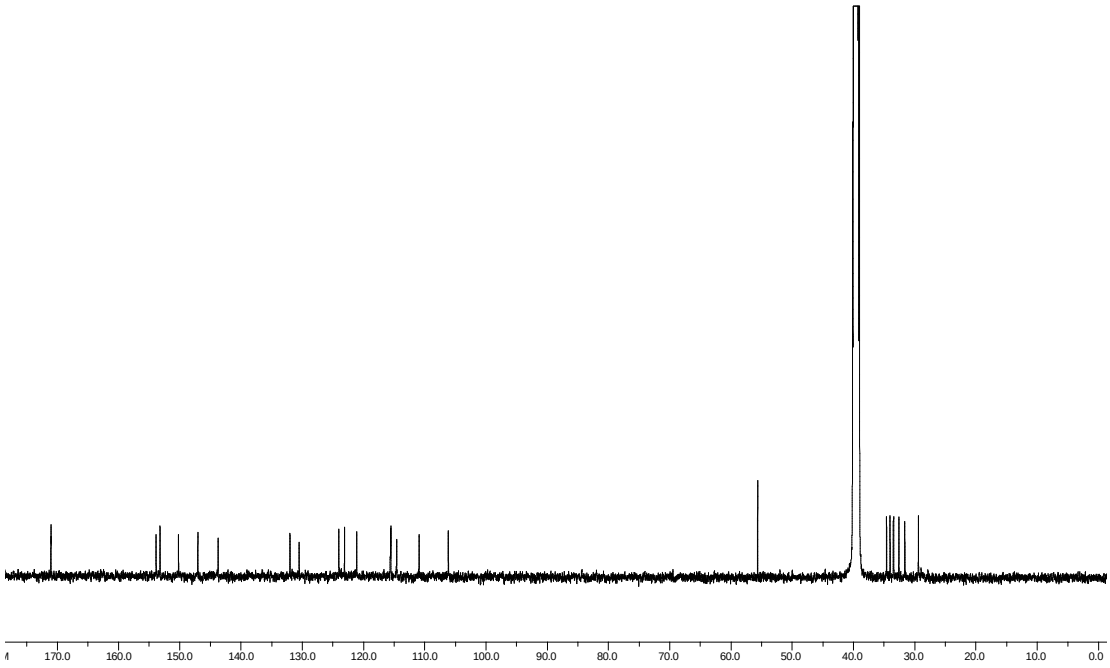

Figure 6.90.2. ^{13}C NMR of complex FL1381 (DMSO-d_6).

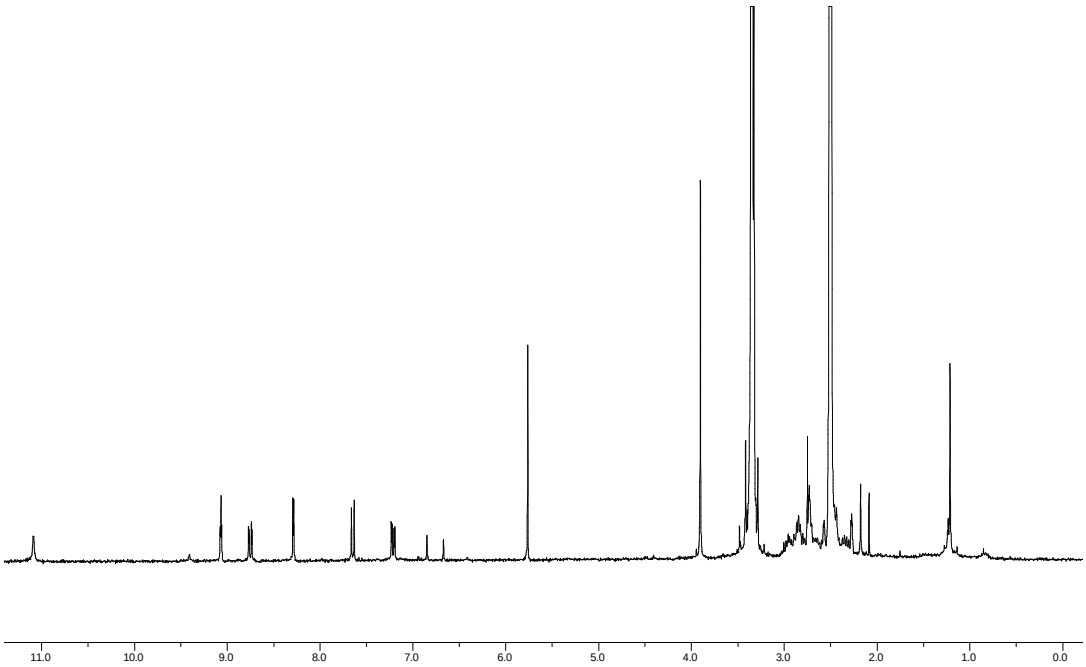

Figure 6.91.1. ^{1}H NMR of complex FL1041 (DMSO-d_6).

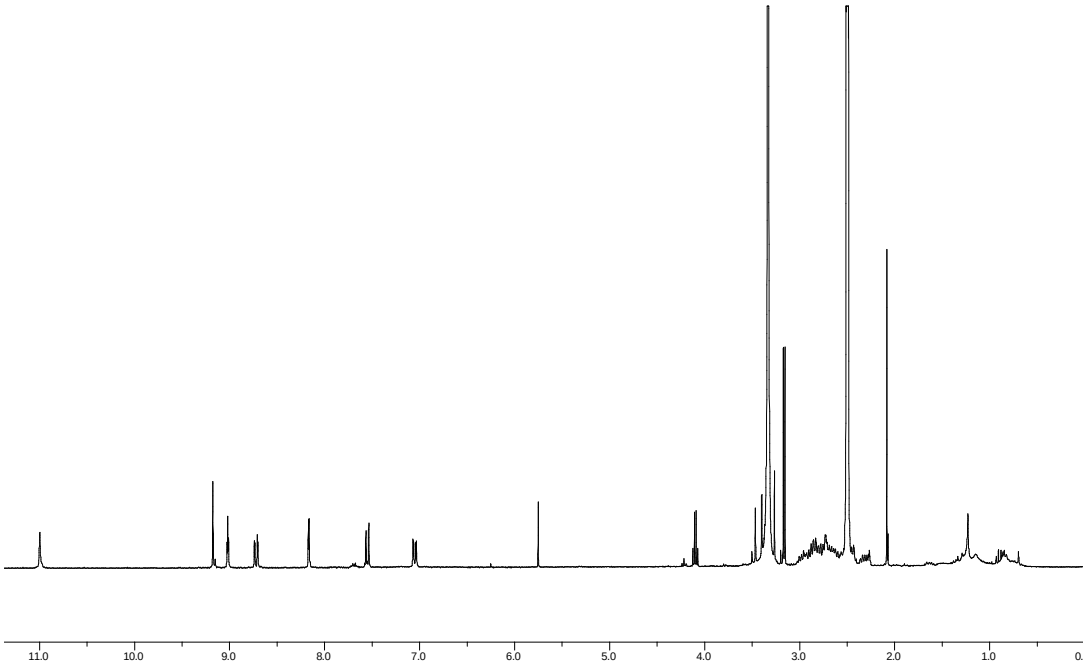

Figure 6.92.1. ^{1}H NMR of complex FL475 (DMSO-d_6).

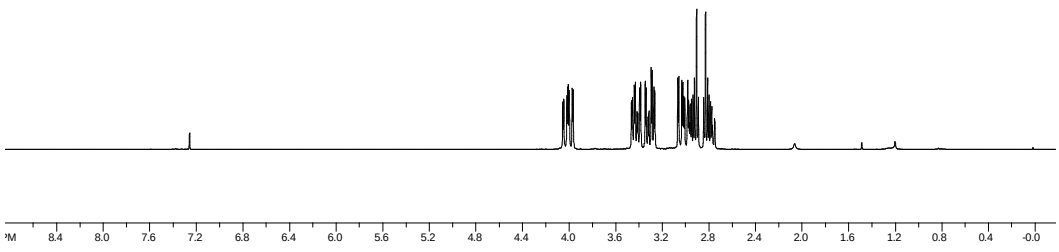

Figure 6.93.1. ^{1}H NMR of compound 3.60 ($CDCl_3$).

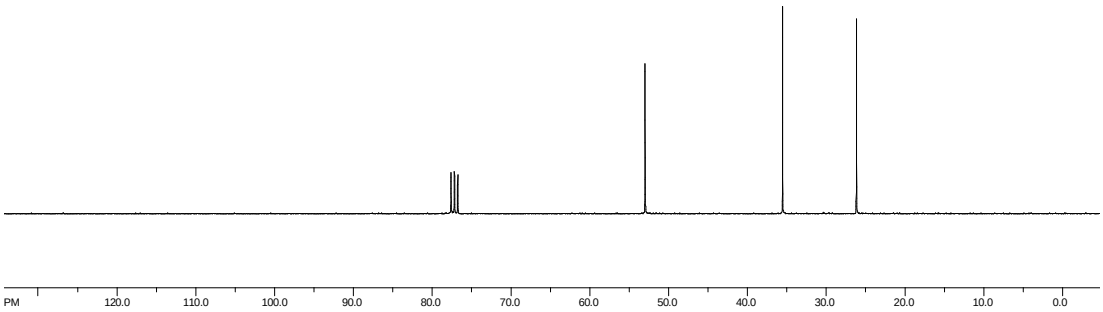

Figure 6.93.2. ^{13}C NMR of compound 3.60 ($CDCl_3$).

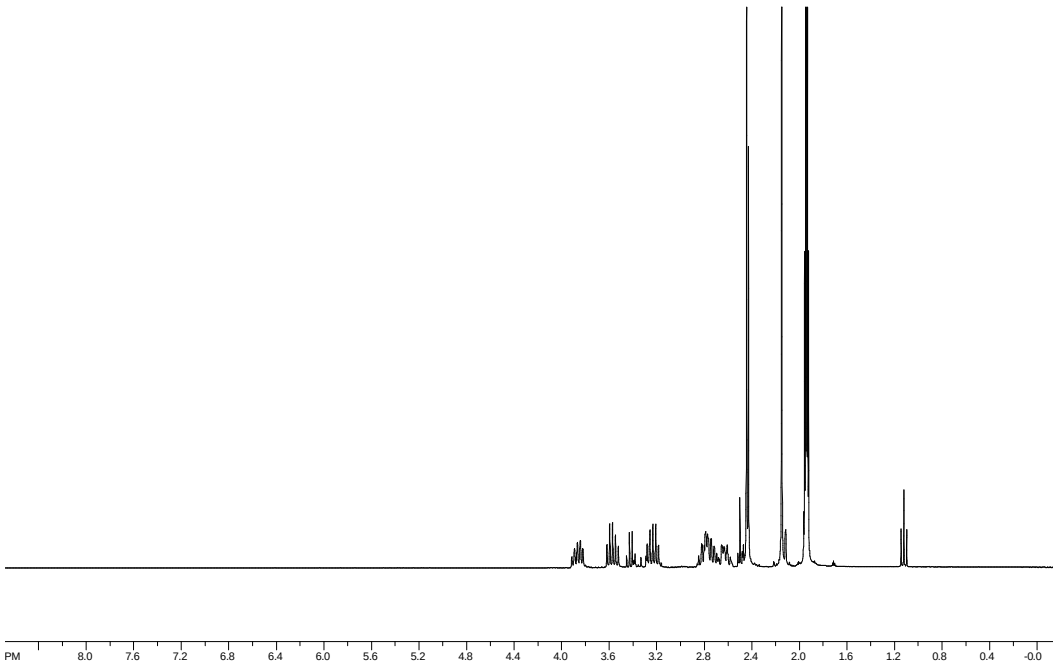

Figure 6.94.1. ^{1}H NMR of compound 3.61 (CD_3CN).

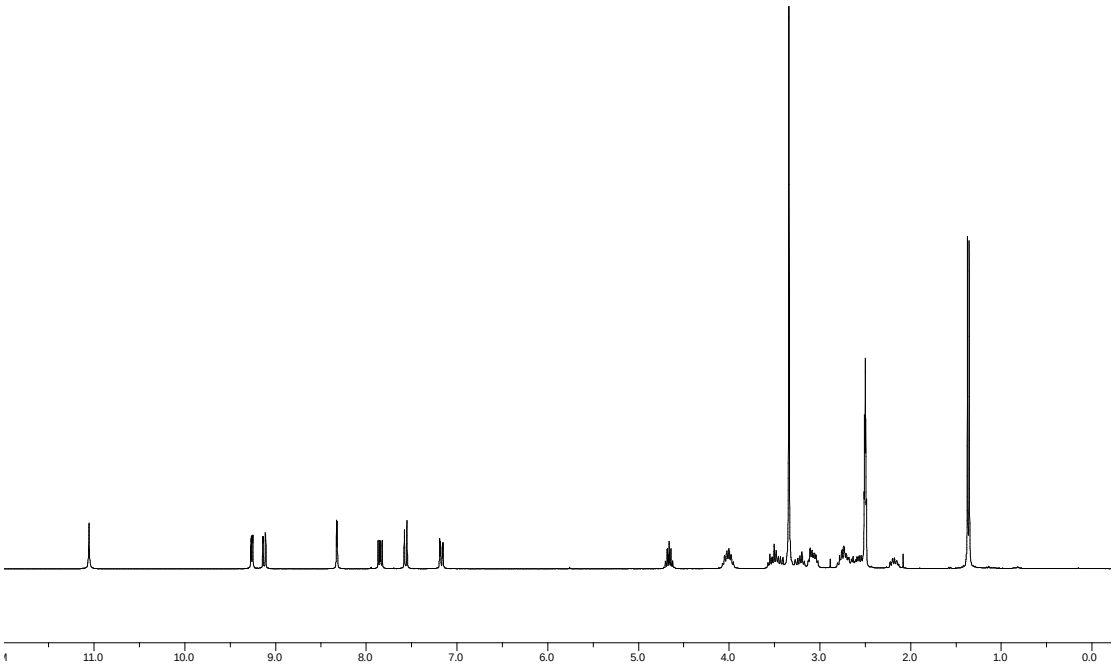

Figure 6.95.1. ^{1}H NMR of complex FL1528-1 (DMSO-d_6).

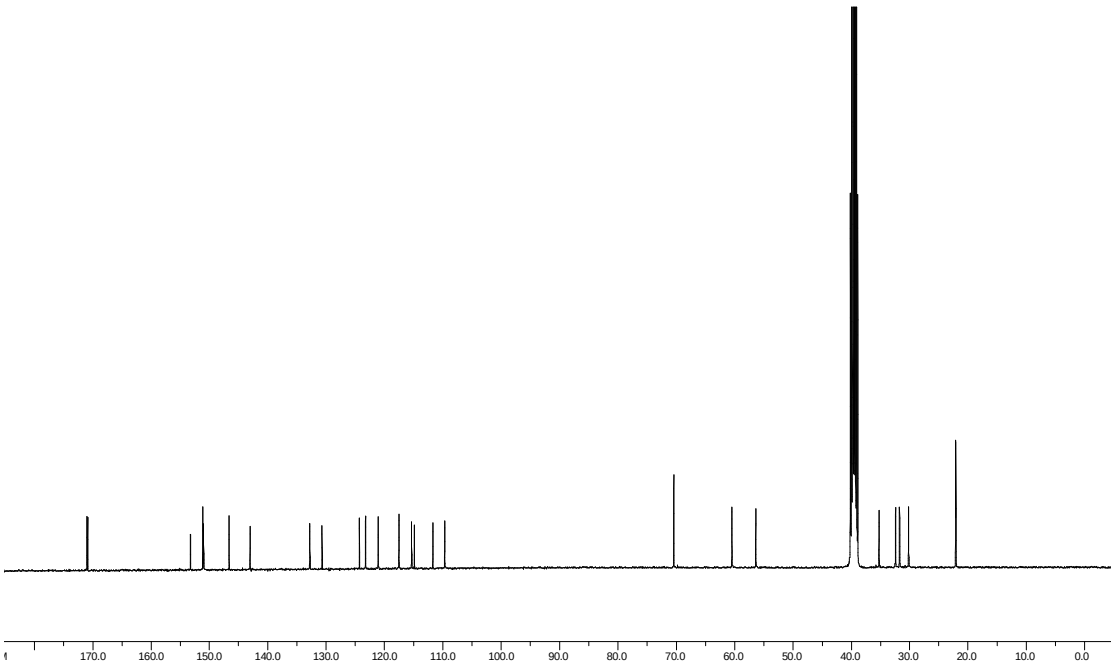

Figure 6.95.2. ^{13}C NMR of complex FL1528-1 (DMSO-d_6).

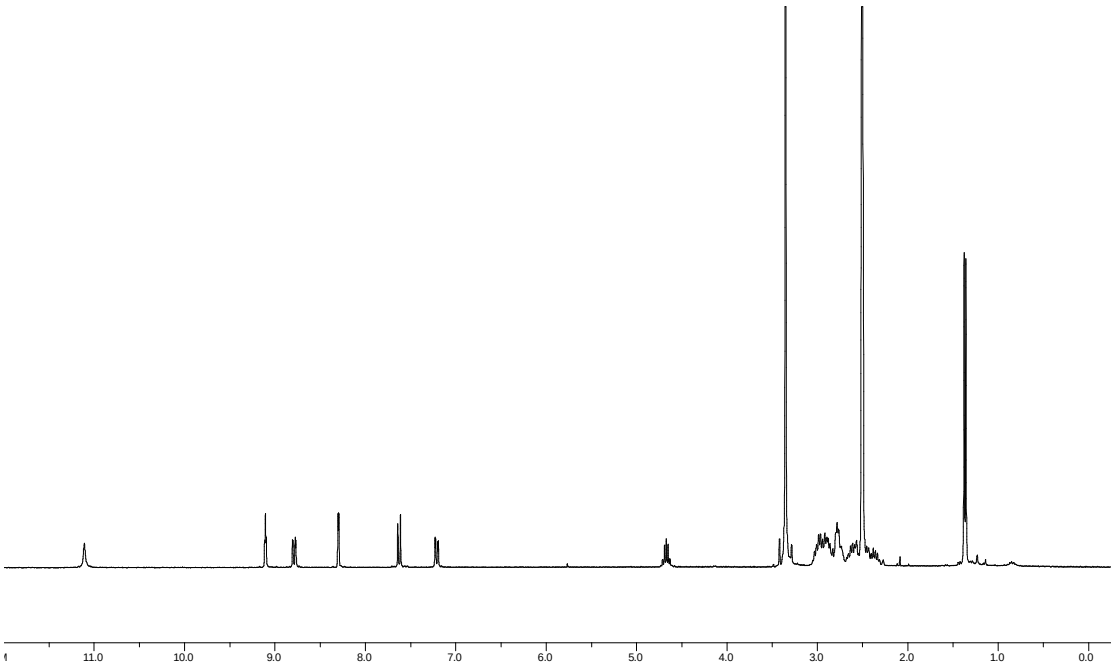

Figure 6.96.1. ^{1}H NMR of complex FL1353-1 (DMSO-d_6).

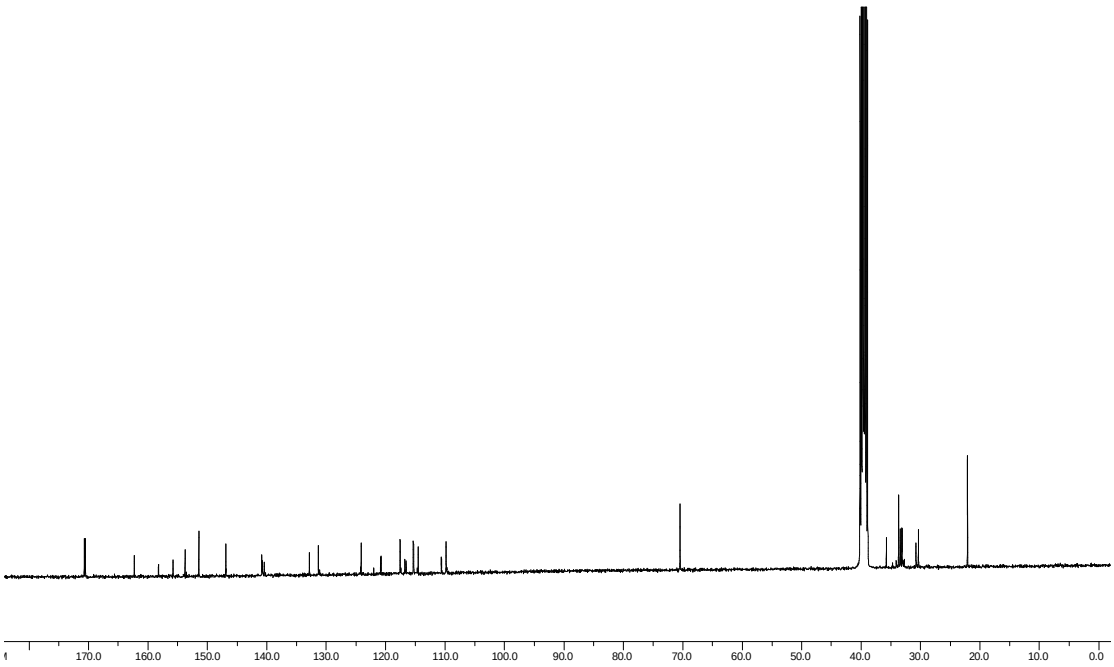

Figure 6.96.2. ^{13}C NMR of complex FL1353-1 (DMSO-d_6).

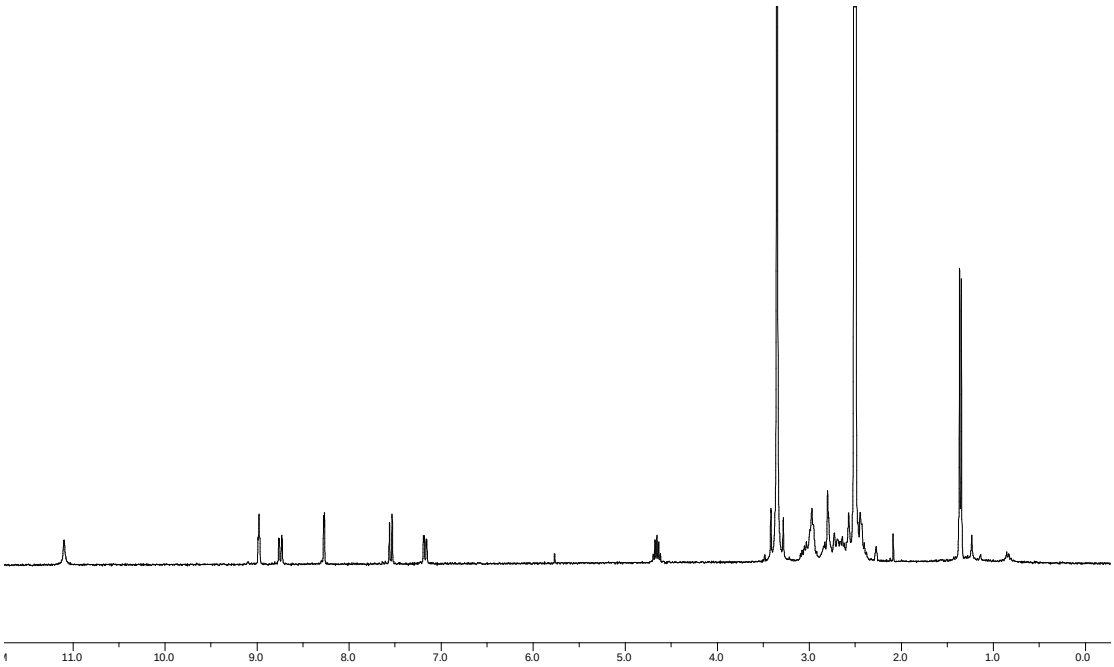

Figure 6.97.1. ^{1}H NMR of complex FL1353-2 (DMSO-d_6).

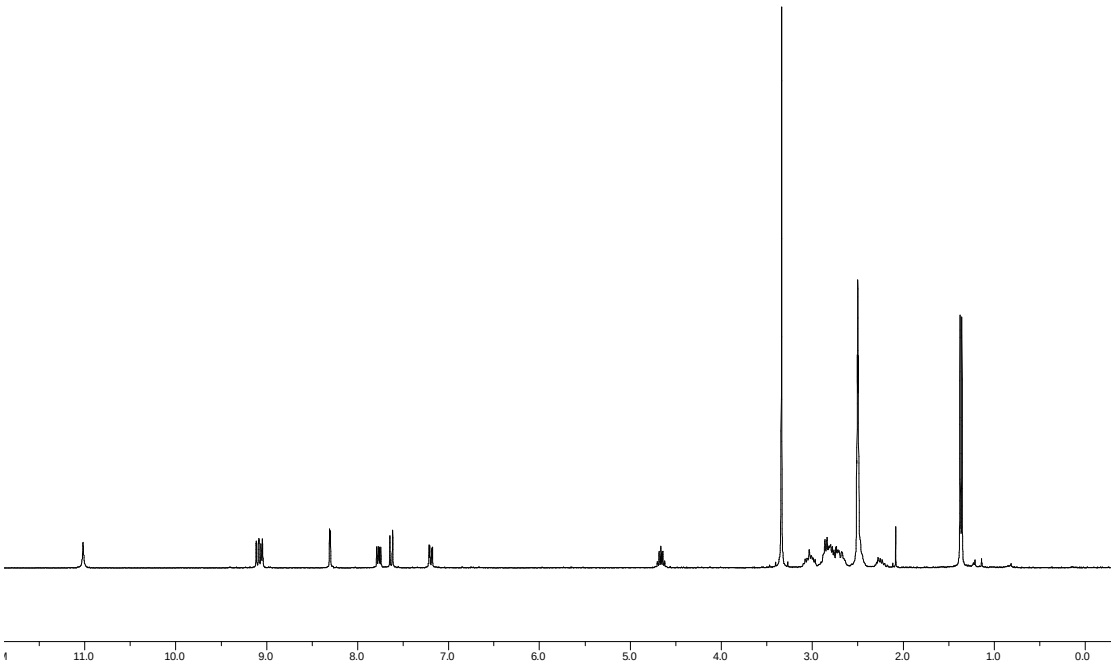

Figure 6.98.1. ^{1}H NMR of complex FL1370-1 (DMSO-d_6).

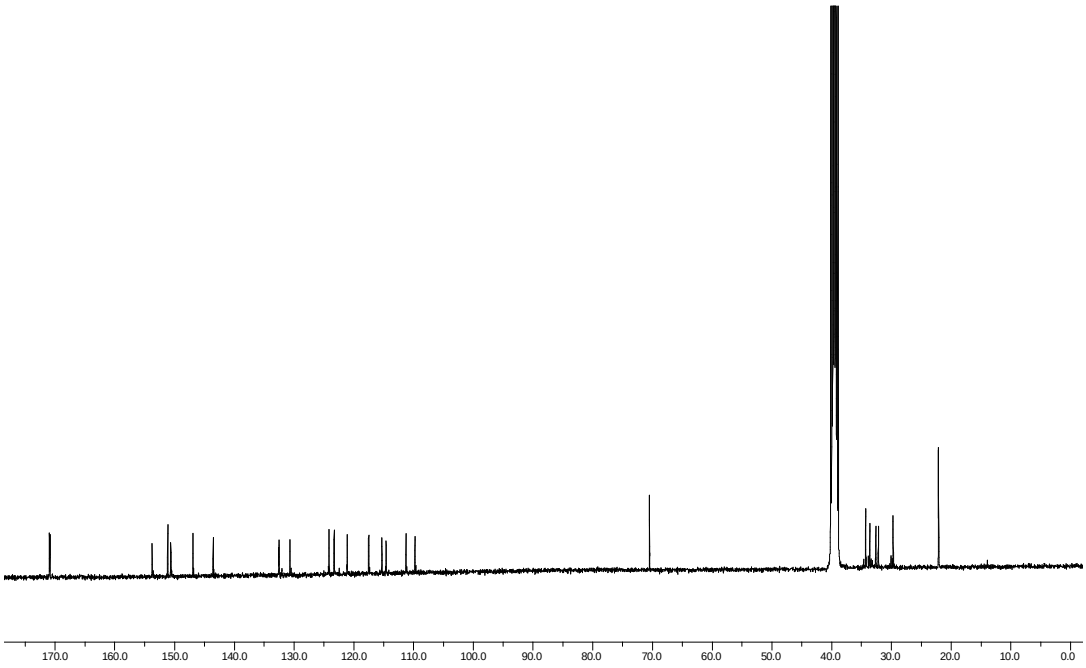

Figure 6.98.2. ^{13}C NMR of complex FL1370-1 (DMSO-d_6).

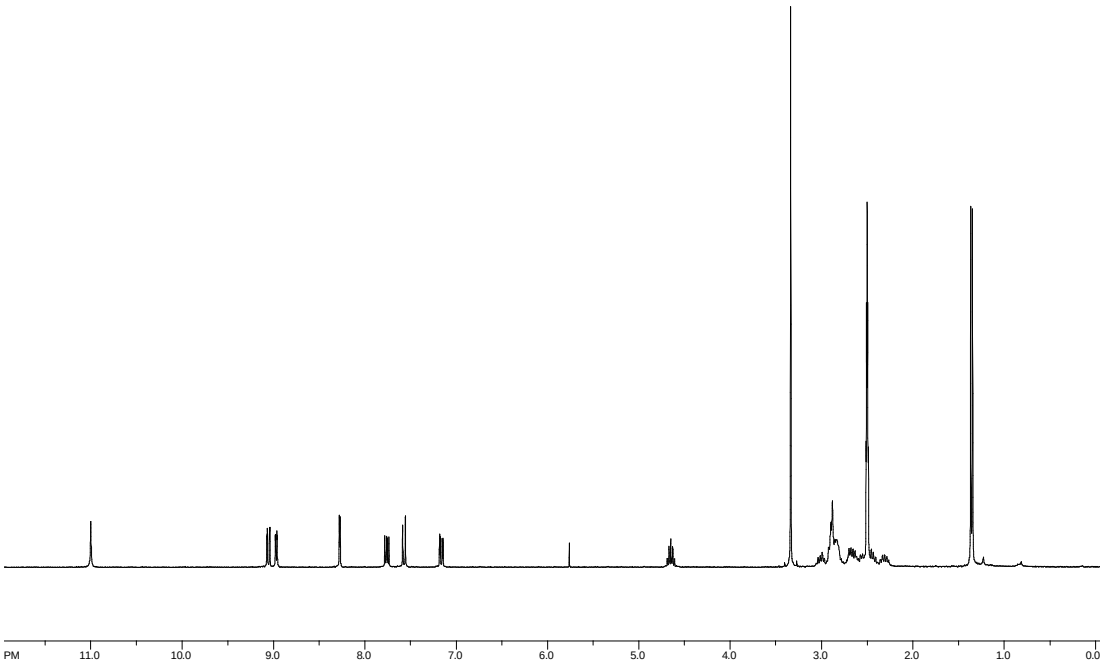

Figure 6.99.1. ^{1}H NMR of complex FL1370-2 (DMSO-d_6).

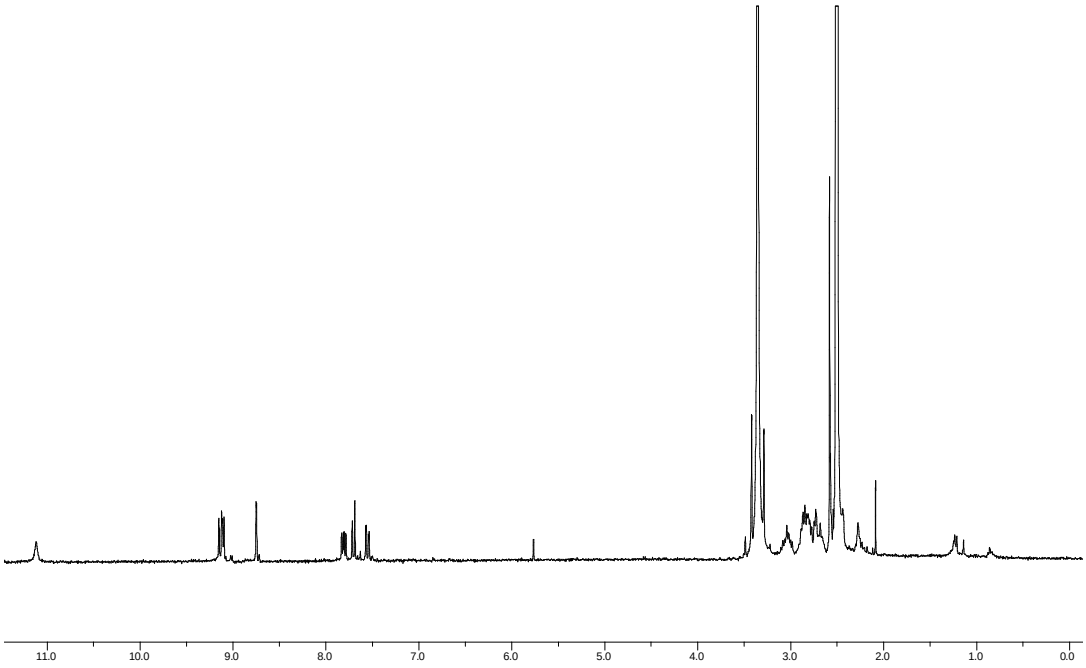

Figure 6.100.1. ^{1}H NMR of complex FL1352-1 (DMSO-d_6).

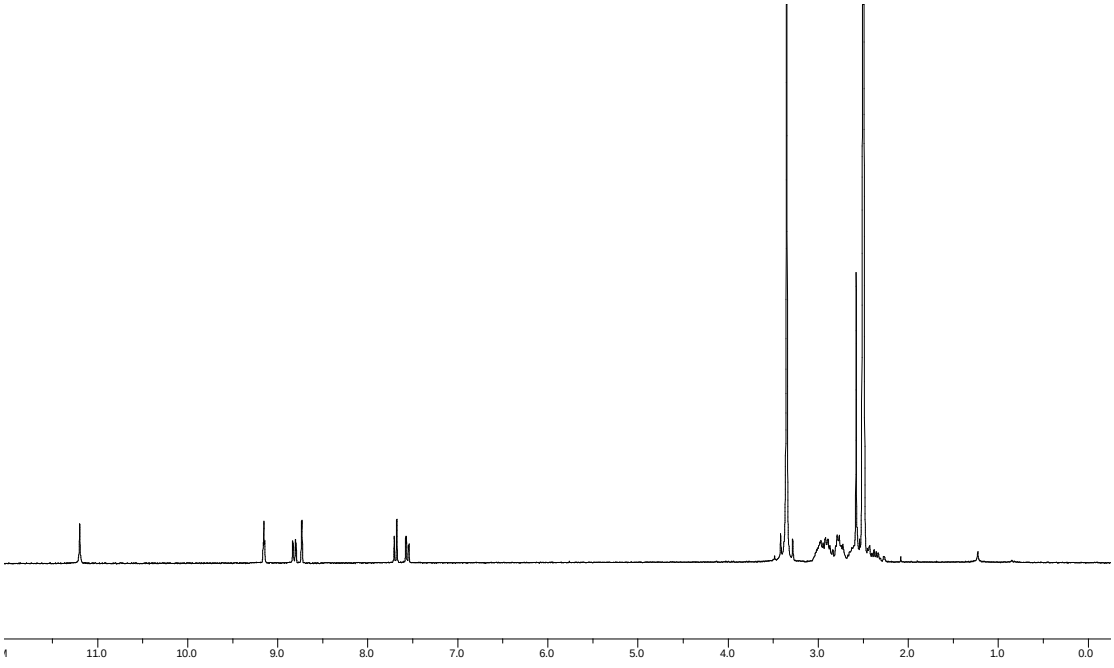

Figure 6.101.1. ^{1}H NMR of complex FL1289-1 (DMSO-d_6).

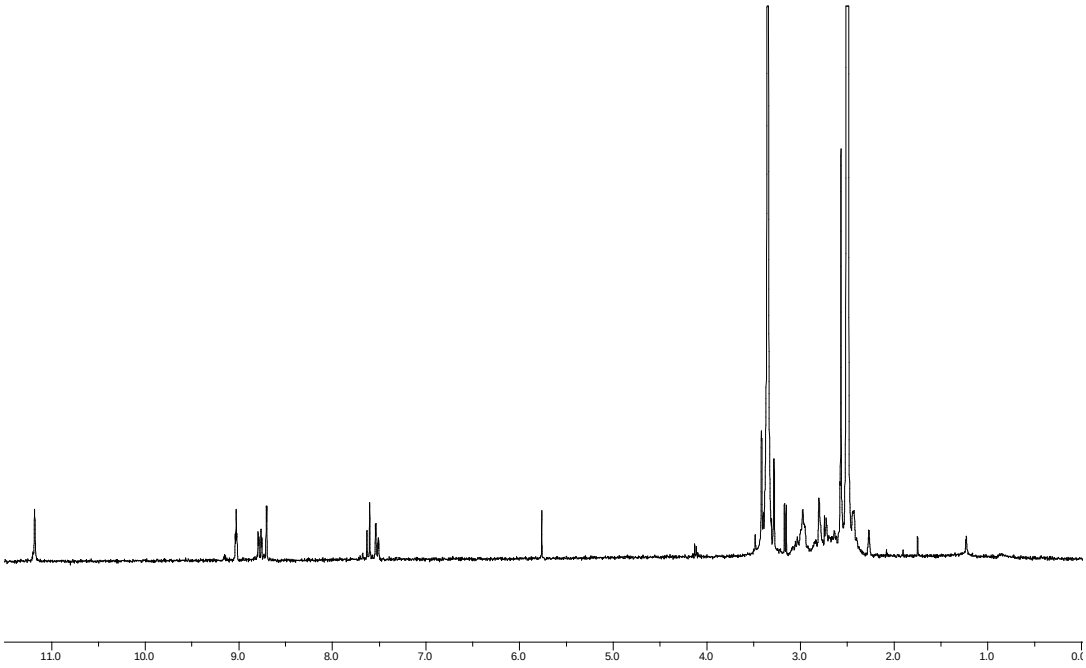

Figure 6.102.1. ^{1}H NMR of complex FL1289-2 (DMSO-d_6).

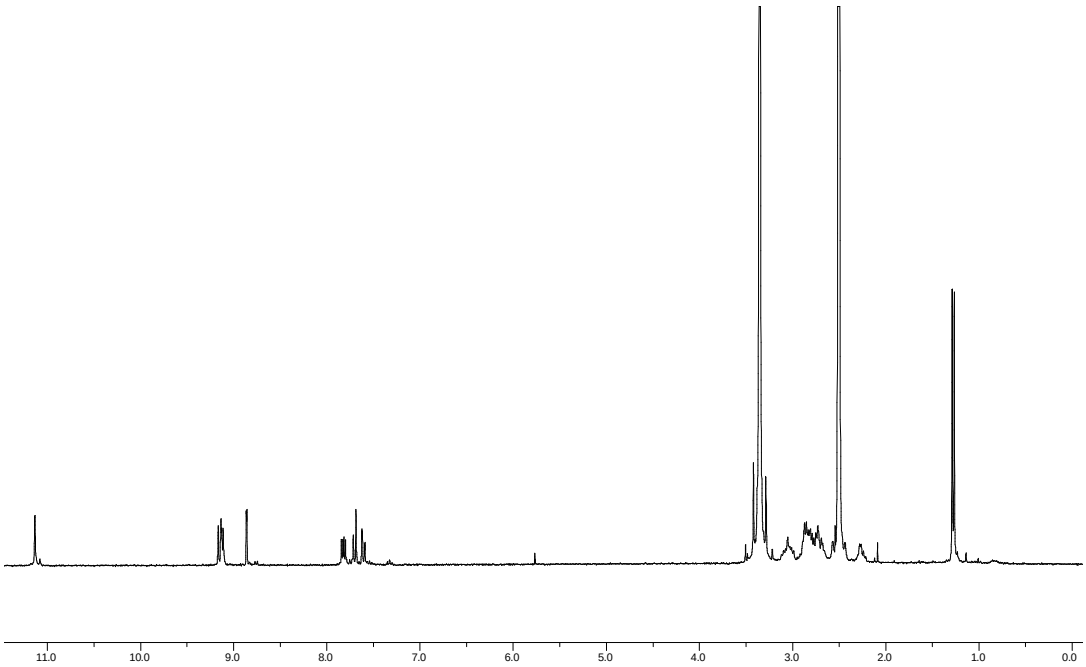

Figure 6.103.1. ^{1}H NMR of complex FL1399-1 (DMSO-d_6).

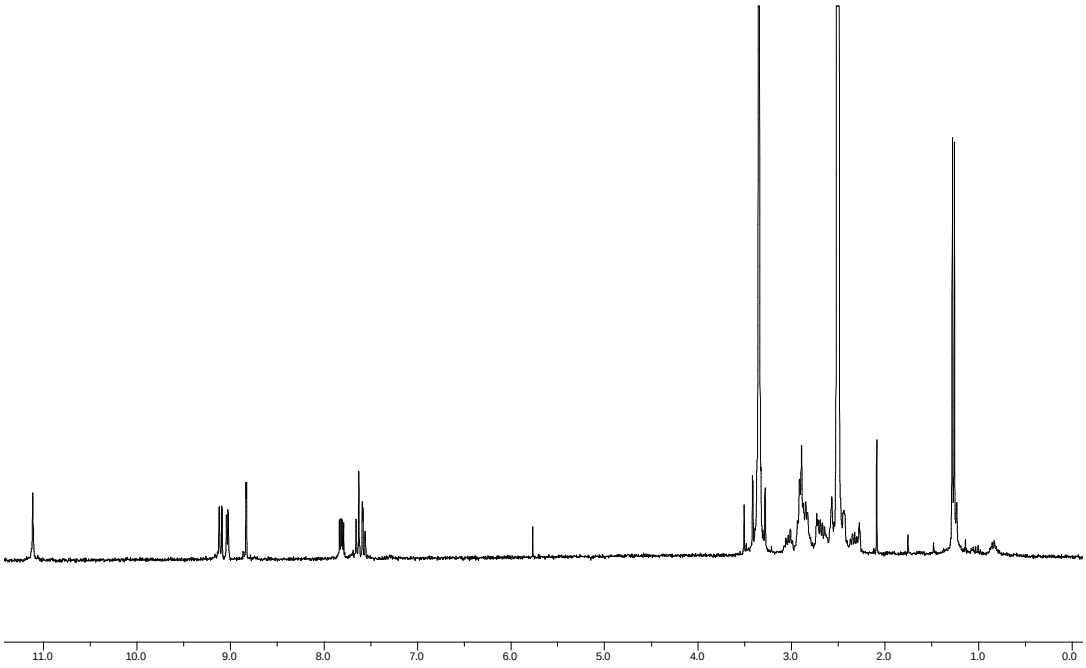

Figure 6.104.1. ^{1}H NMR of complex FL1399-2 (DMSO-d_6).

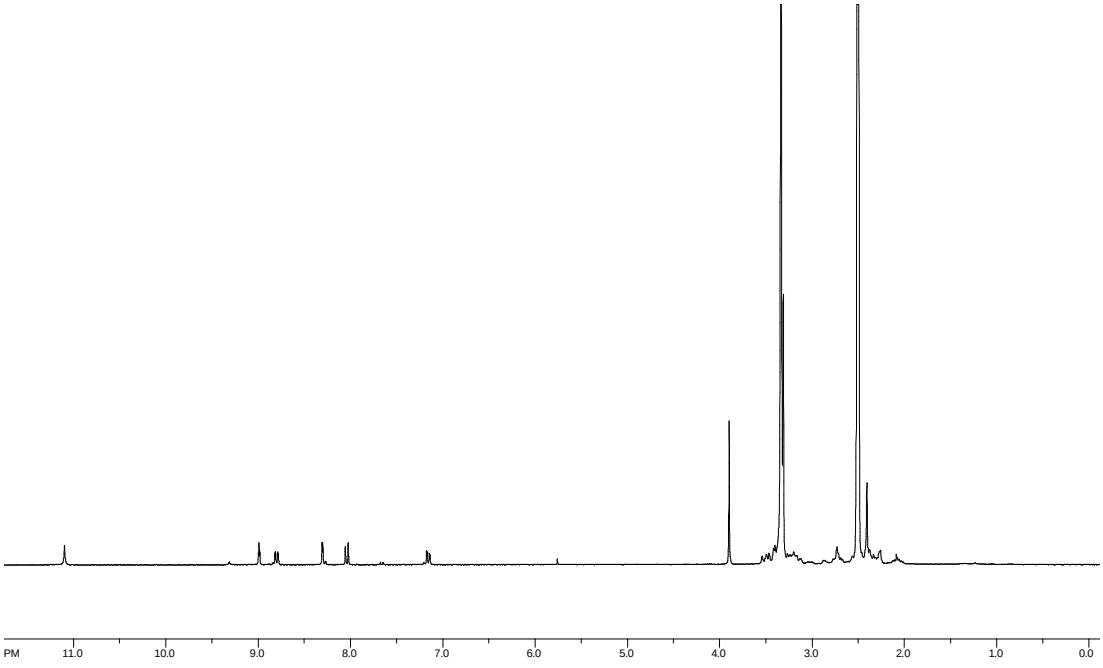

Figure 6.105.1. ^{1}H NMR of complex FL848-1 (DMSO-d_6).

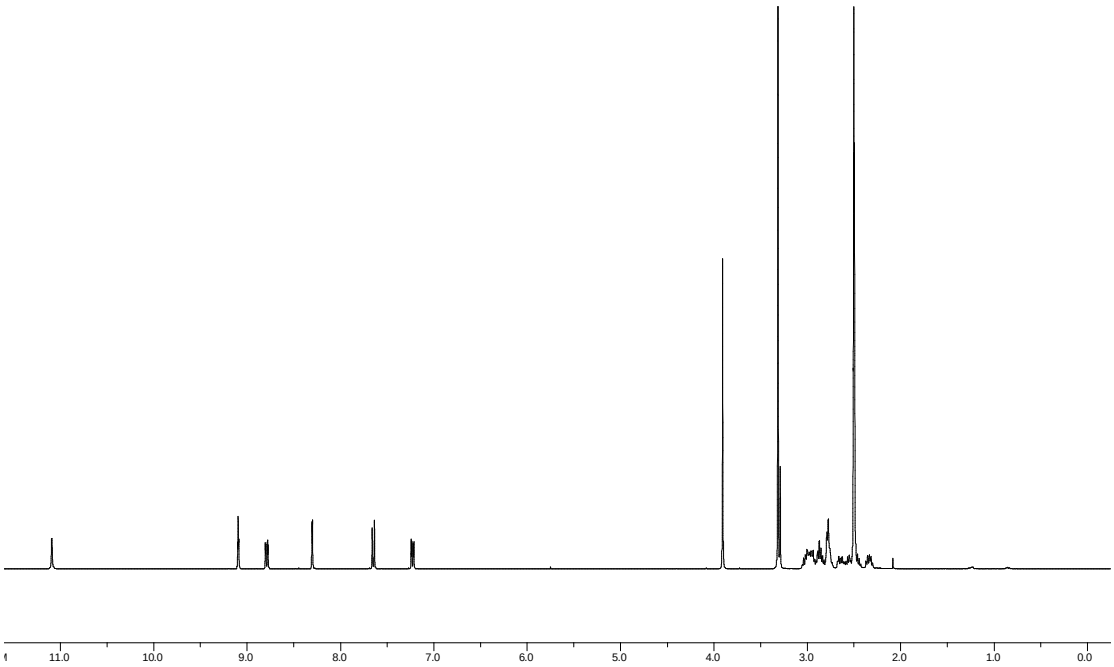

Figure 6.106.1. ^{1}H NMR of complex FL812-1 (DMSO-d_6).

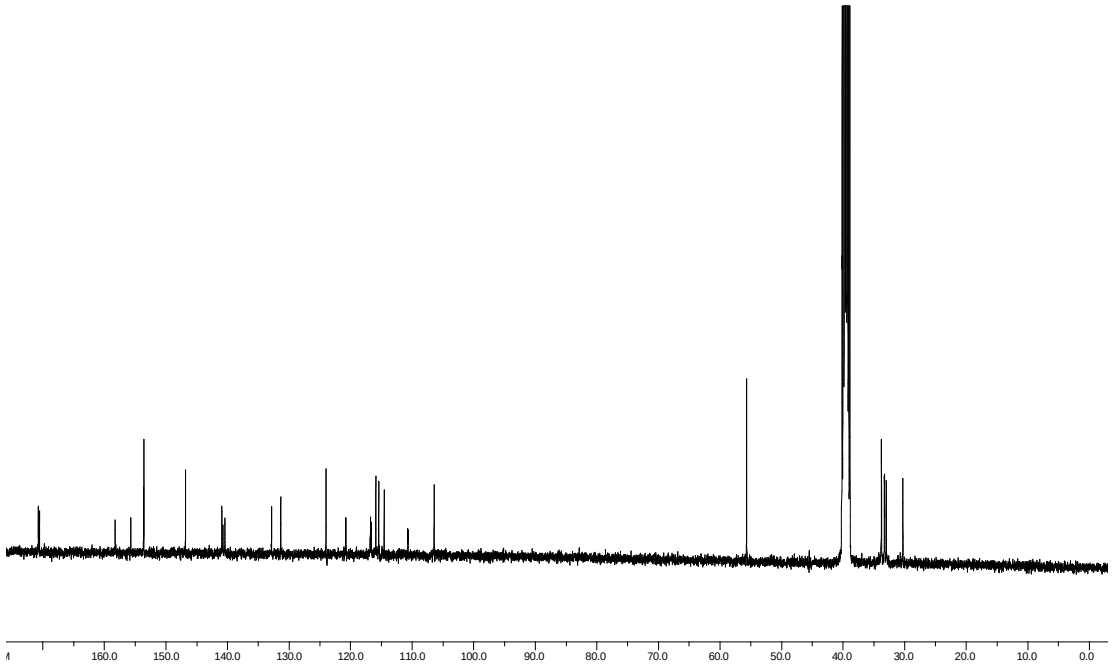

Figure 6.106.2. ^{13}C NMR of complex FL812-1 (DMSO-d_6).

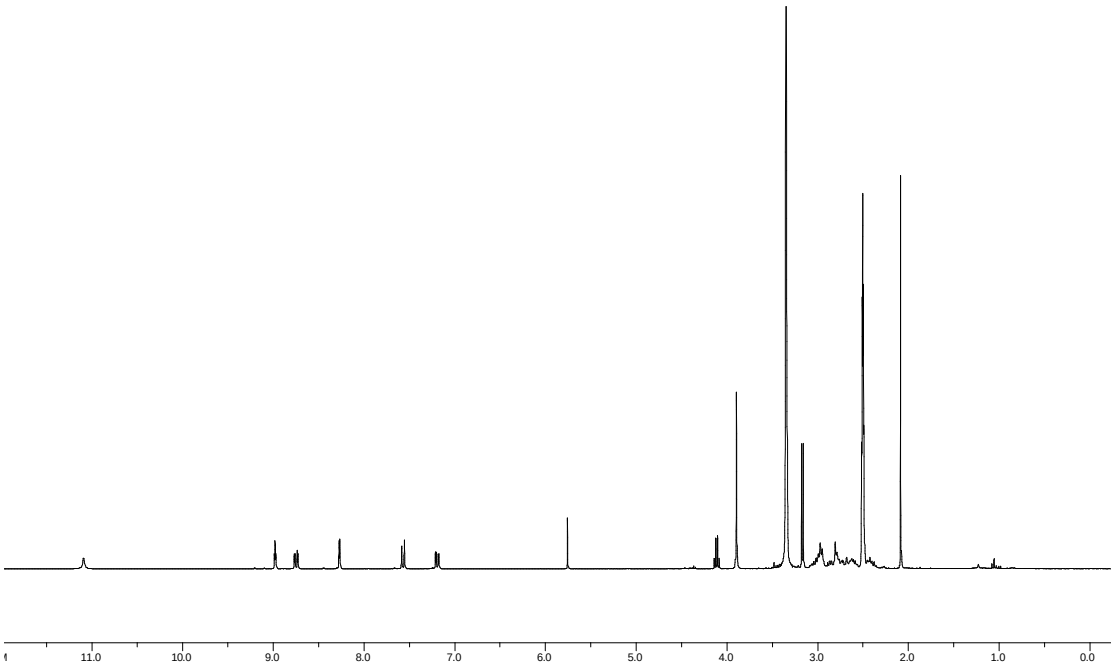

Figure 6.107.1. ^{1}H NMR of complex FL812-2 (DMSO-d_6).

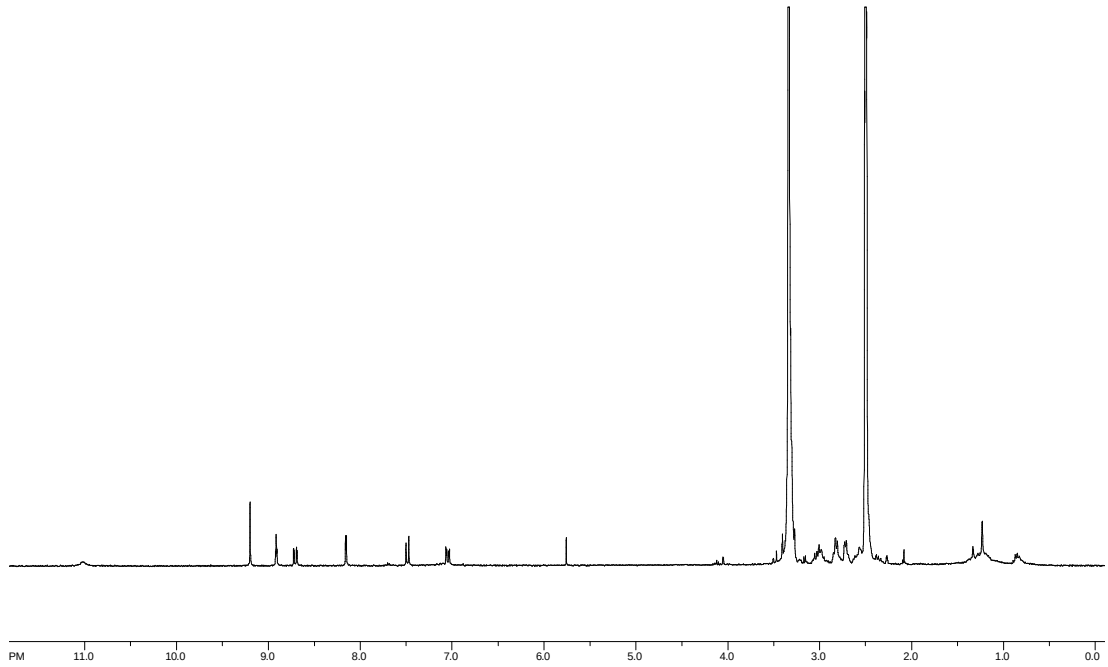

Figure 6.108.1. ^{1}H NMR of complex FL253 (DMSO-d_6).

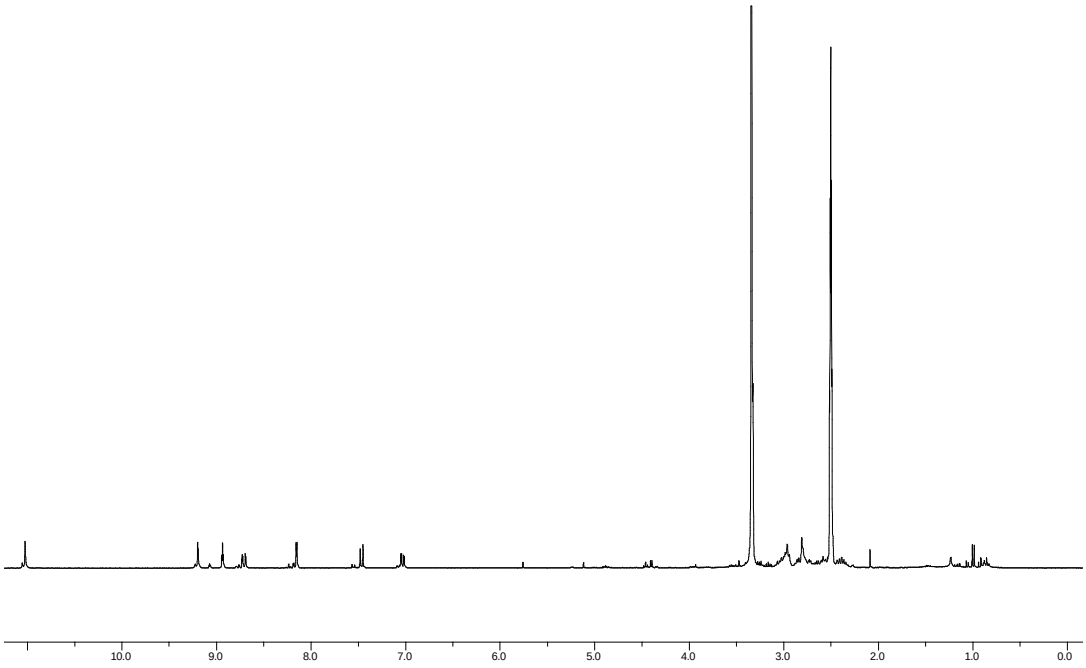

Figure 6.109.1. ^{1}H NMR of complex FL528 (DMSO-d_6).

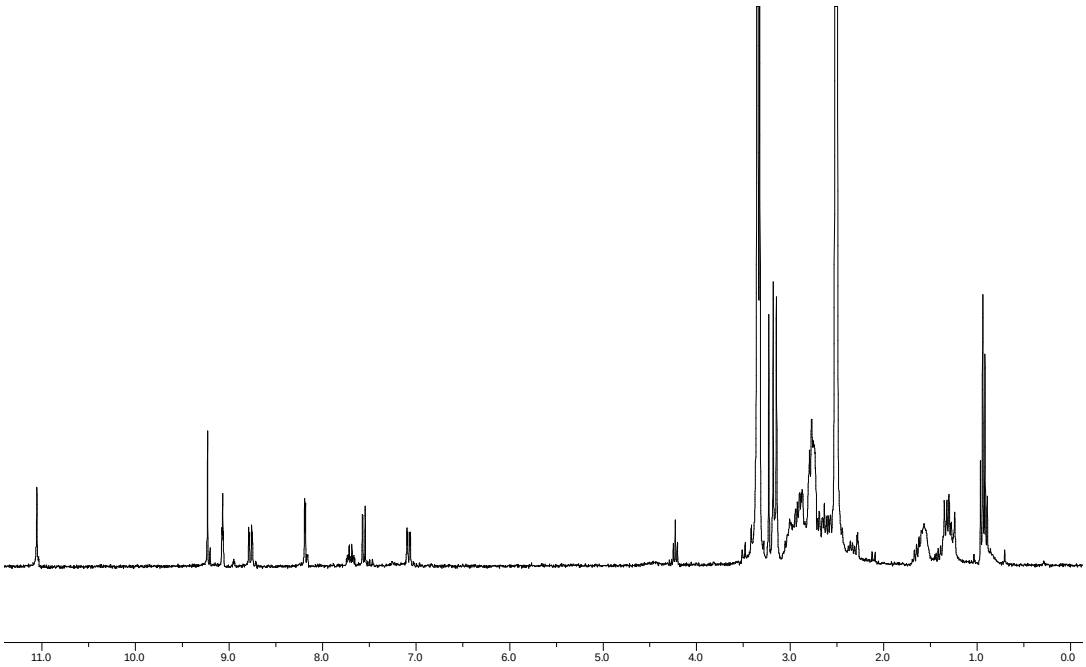

Figure 6.110.1. ^{1}H NMR of complex FL823-1 (DMSO-d_6).

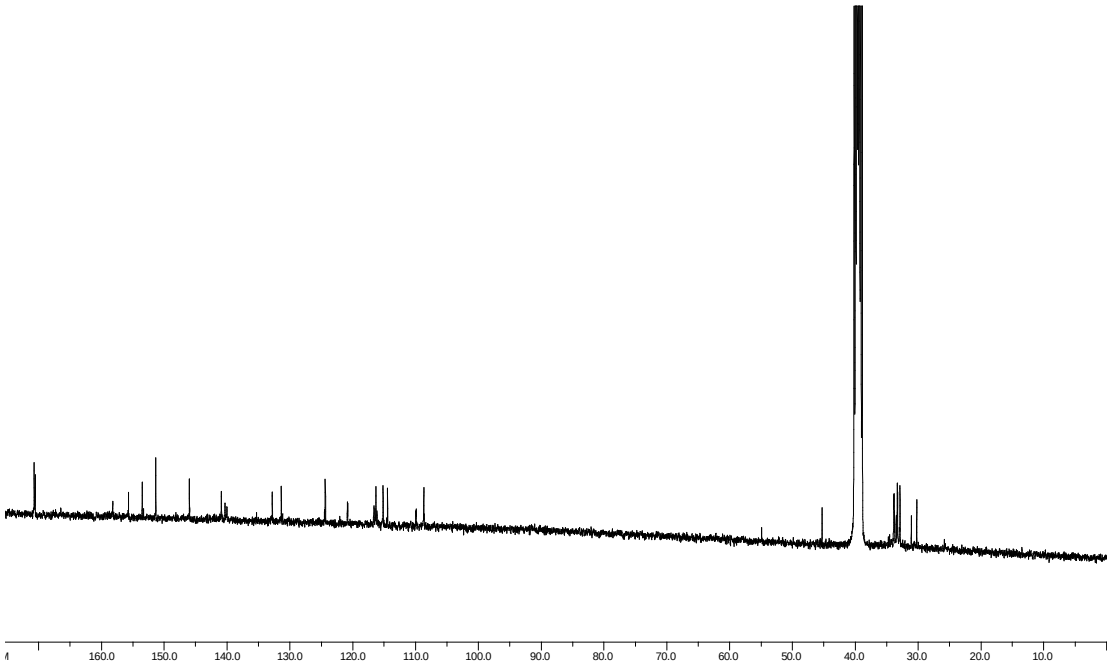

Figure 6.110.2. ^{13}C NMR of complex FL823-1 (DMSO-d_6).

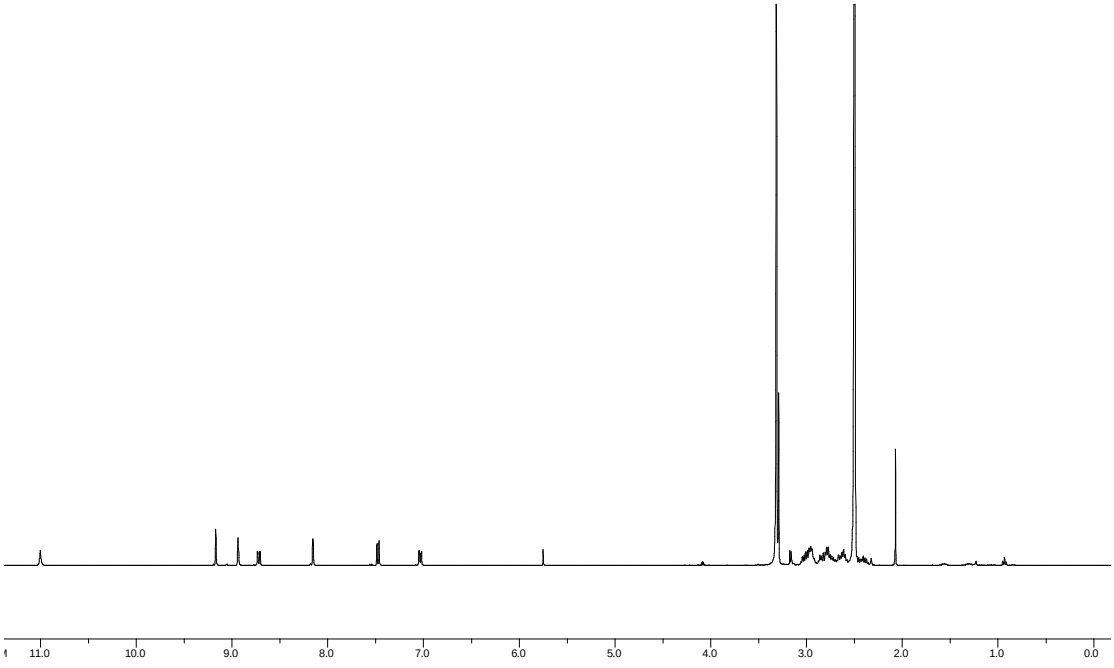

Figure 6.111.1. ^{1}H NMR of complex FL823-2 (DMSO-d_6).

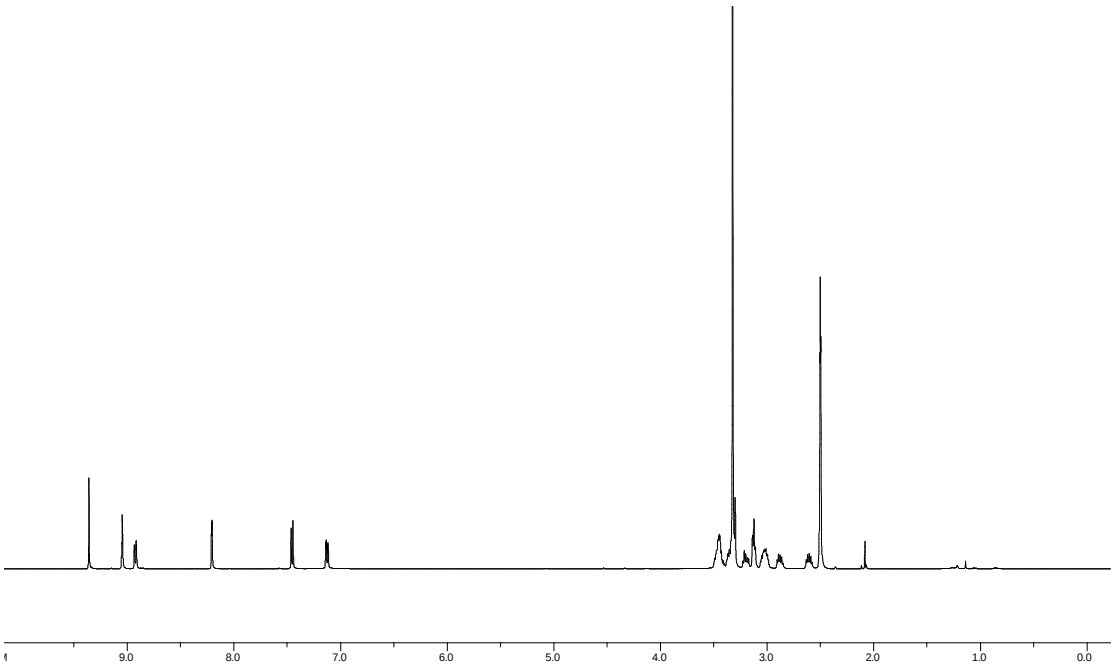

Figure 6.112.1. 1H NMR of complex FL829 (DMSO-d_6).

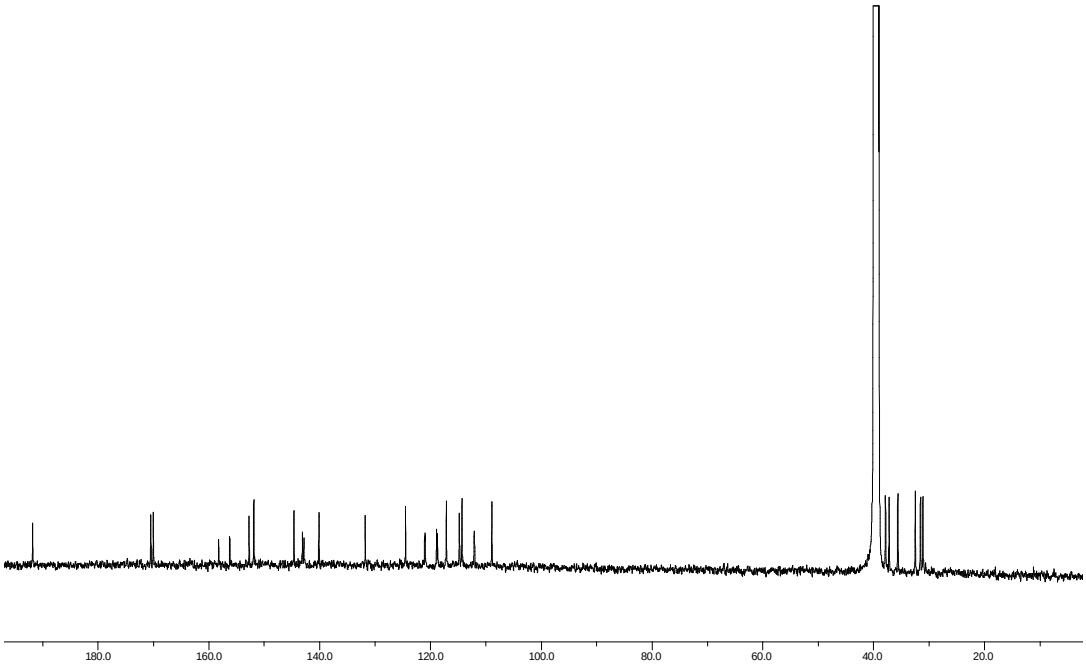

Figure 6.112.2. ^{13}C NMR of complex FL829 (DMSO-d_6).

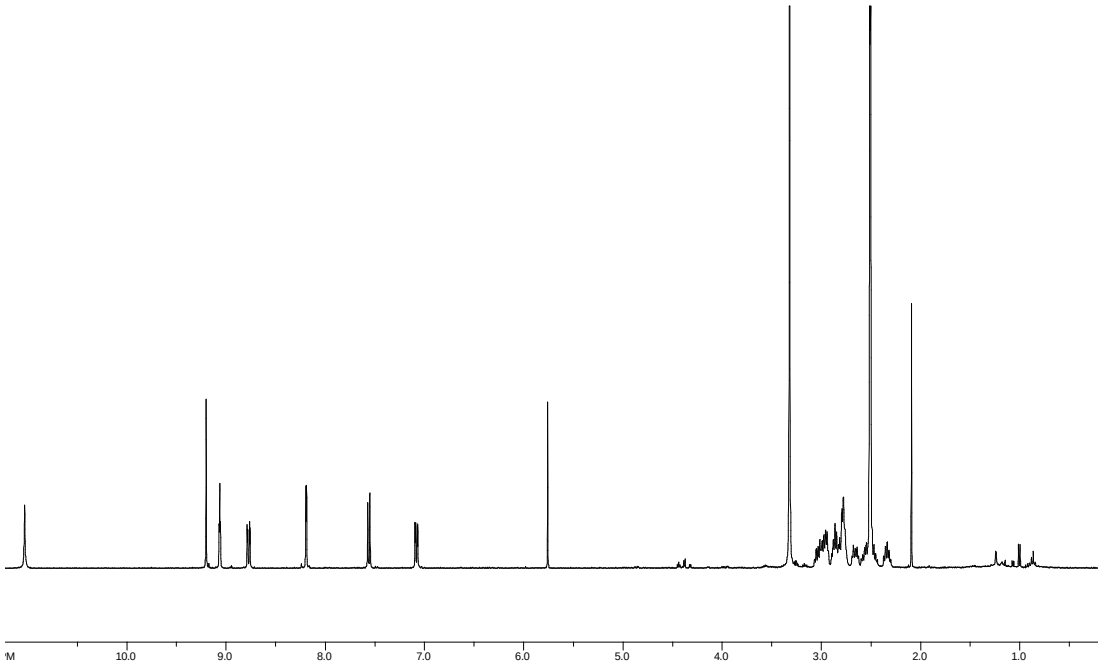

Figure 6.113.1. ^{1}H NMR of complex FL534-1 (DMSO-d_6).

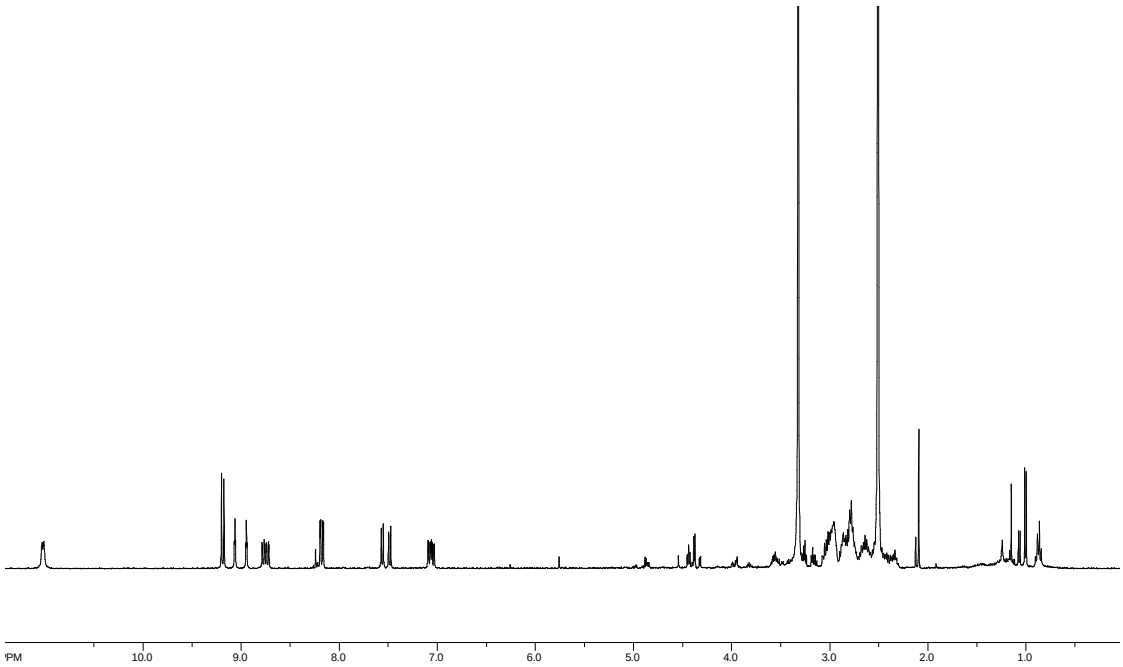

Figure 6.114.1. ^{1}H NMR of complex FL534-2 (DMSO-d_6).

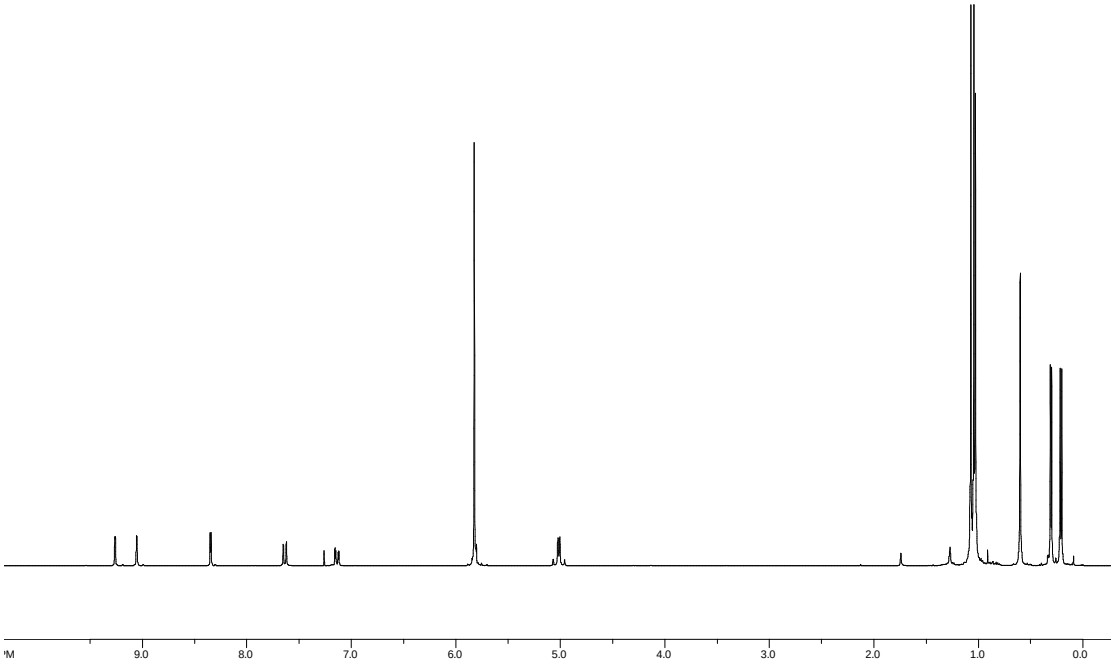

Figure 6.115.1. ^{1}H NMR of complex 3.70 ($CDCl_3$).

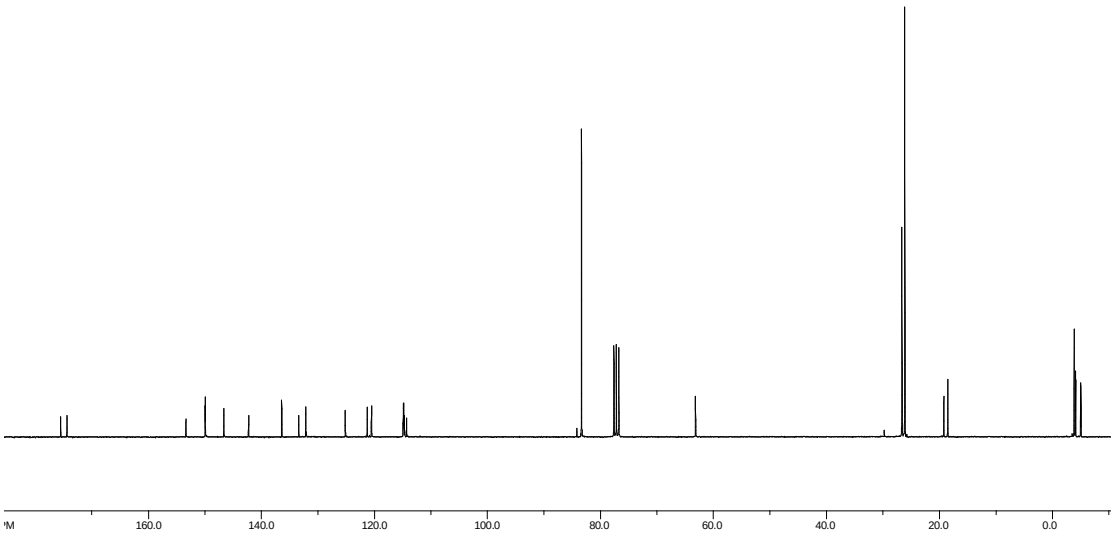

Figure 6.115.2. ^{13}C NMR of complex 3.70 ($CDCl_3$).

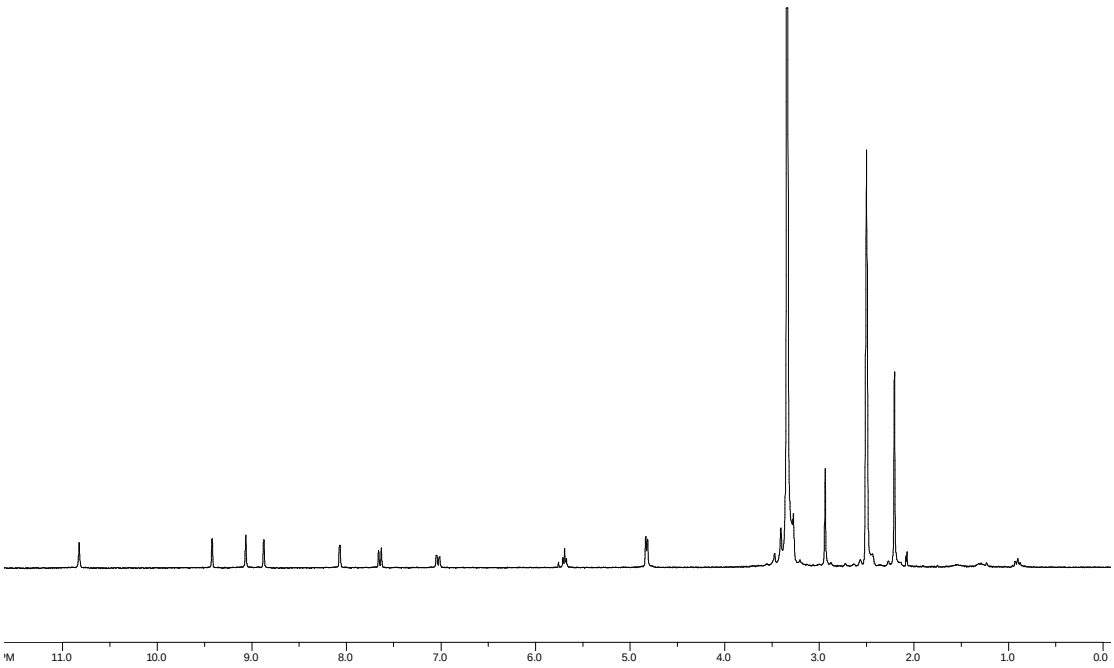

Figure 6.116.1. ^{1}H NMR of complex 3.71 (DMSO-d_6).

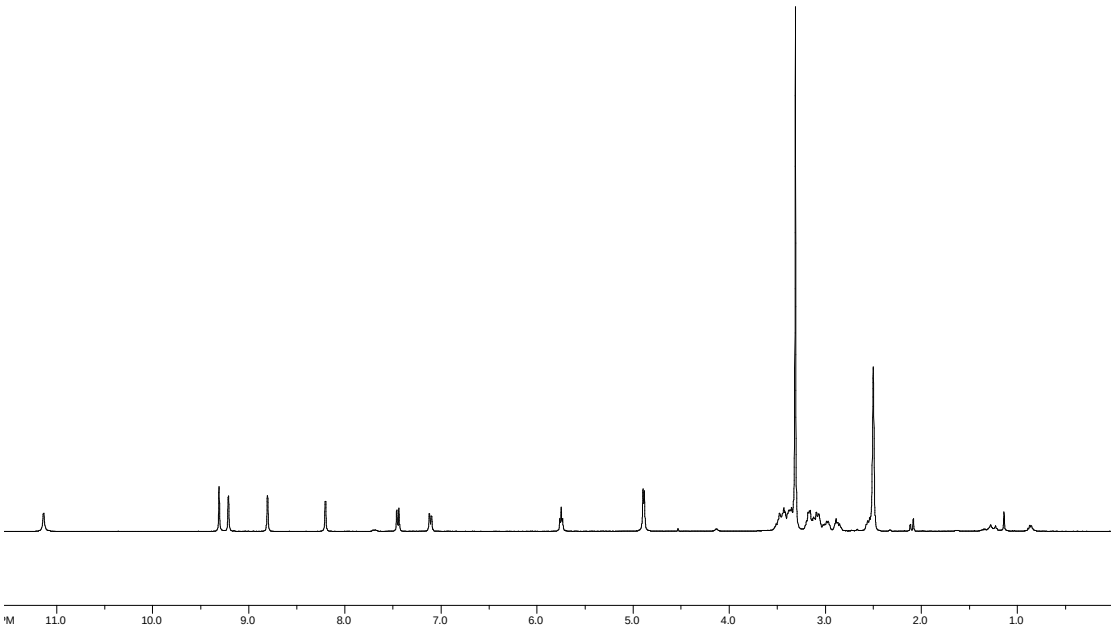

Figure 6.117.1. ^{1}H NMR of complex FL1360 (DMSO-d_6).

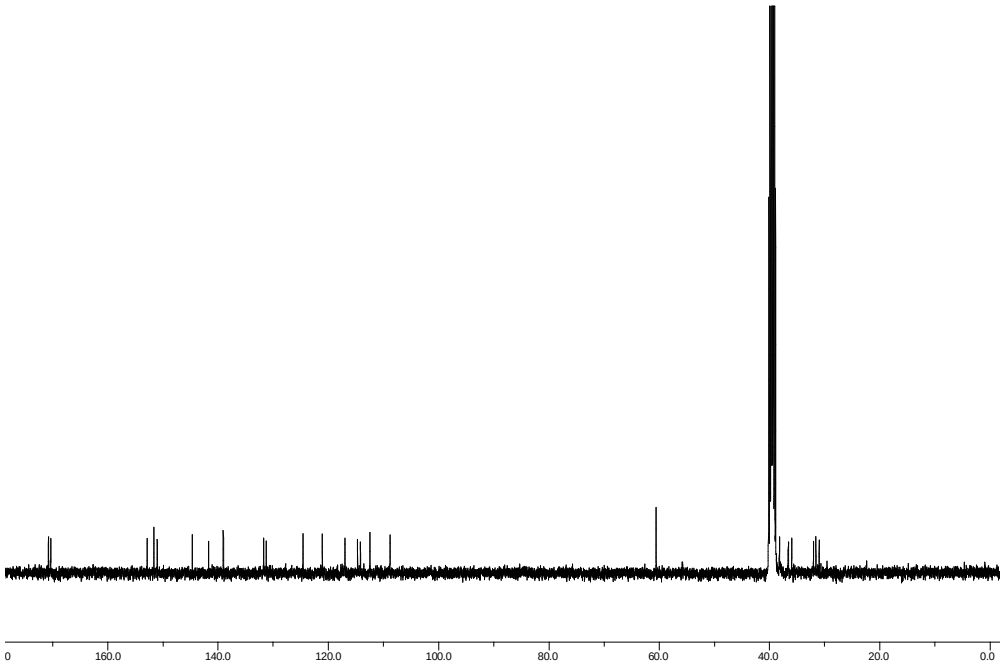

Figure 6.117.2. ^{13}C NMR of complex FL1360 (DMSO-d_6).

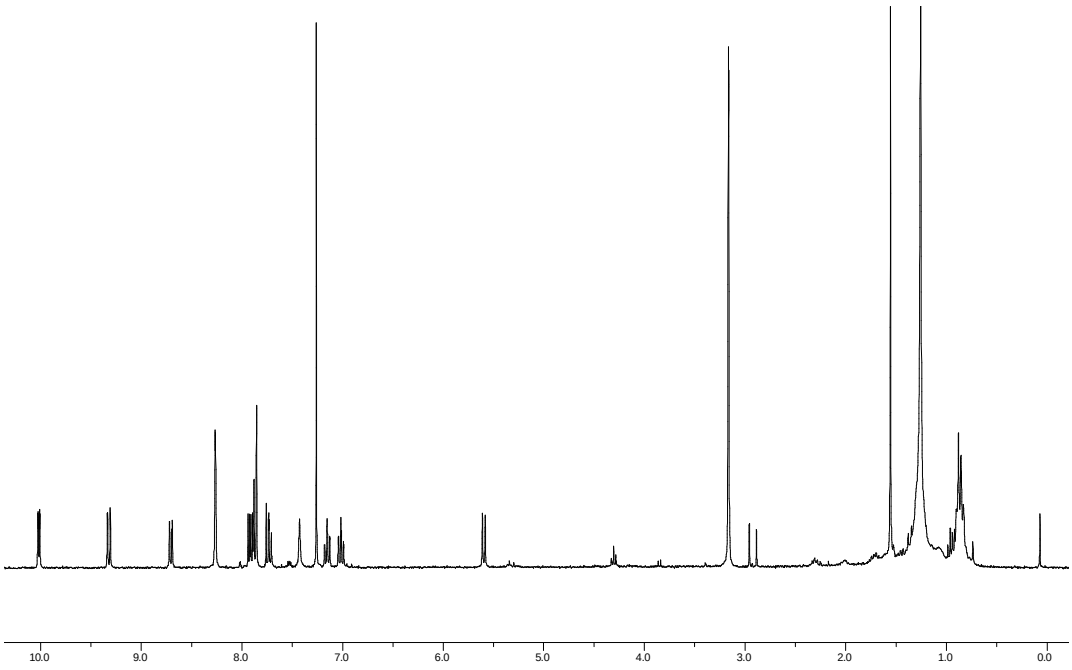

Figure 6.118.1. ^{1}H NMR of complex FL792-1 ($CDCl_3$).

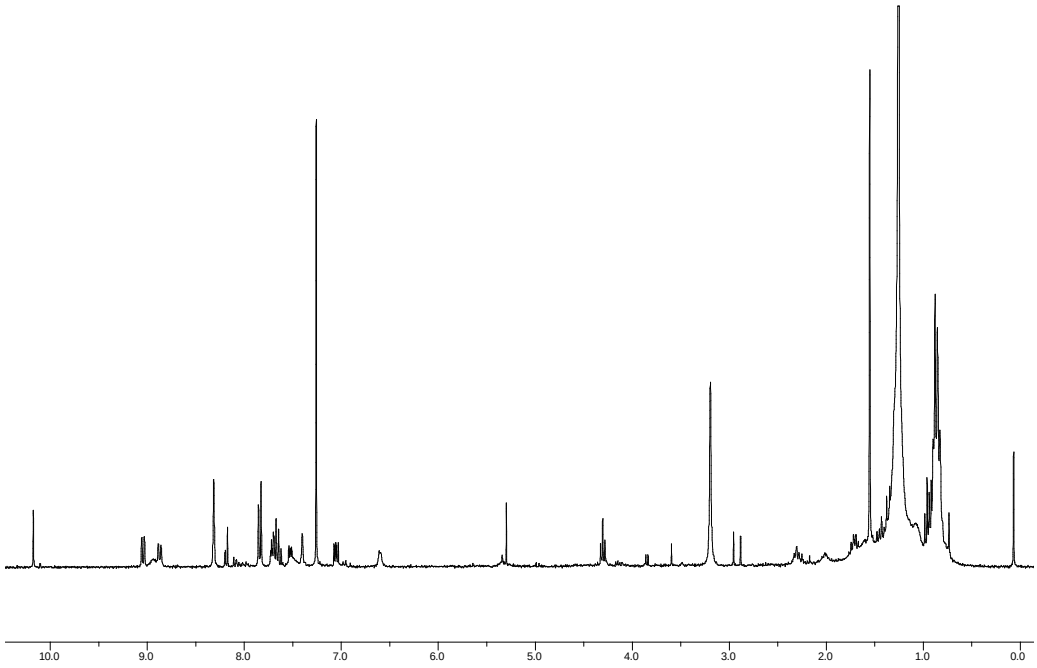

Figure 6.119.1. ^{1}H NMR of complex FL792-2 ($CDCl_3$).

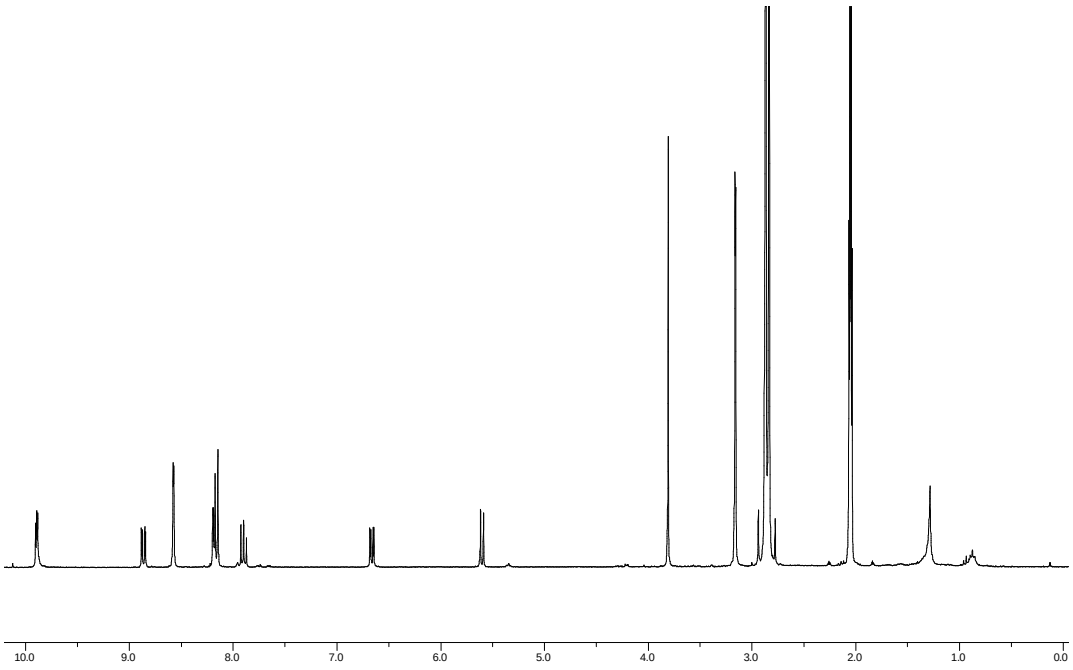

Figure 6.120.1. ^{1}H NMR of complex FL1138-1 (Acetone-d_6).

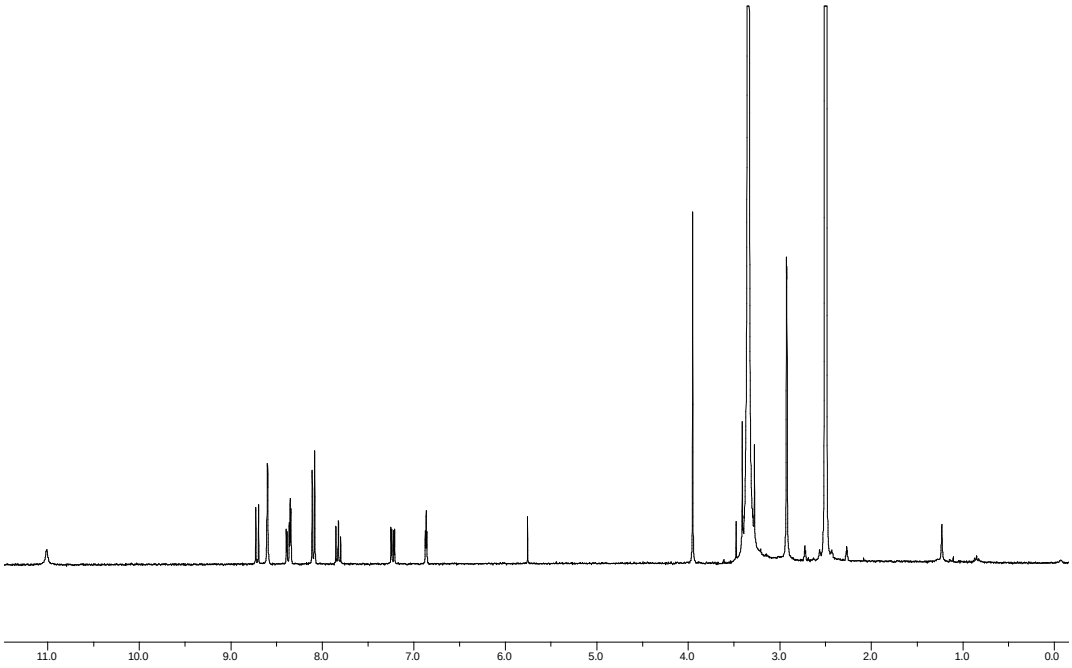

Figure 6.121.1. ^{1}H NMR of complex FL1138-2 (DMSO-d_6).

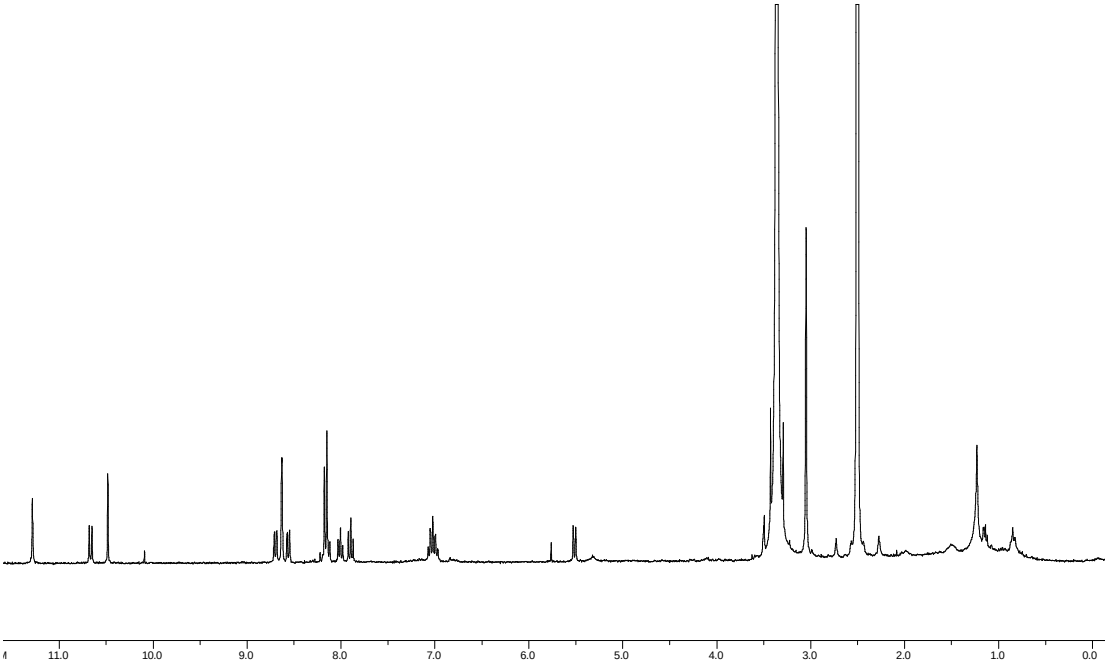

Figure 6.122.1. ^{1}H NMR of complex FL1124-1 (DMSO-d_6).

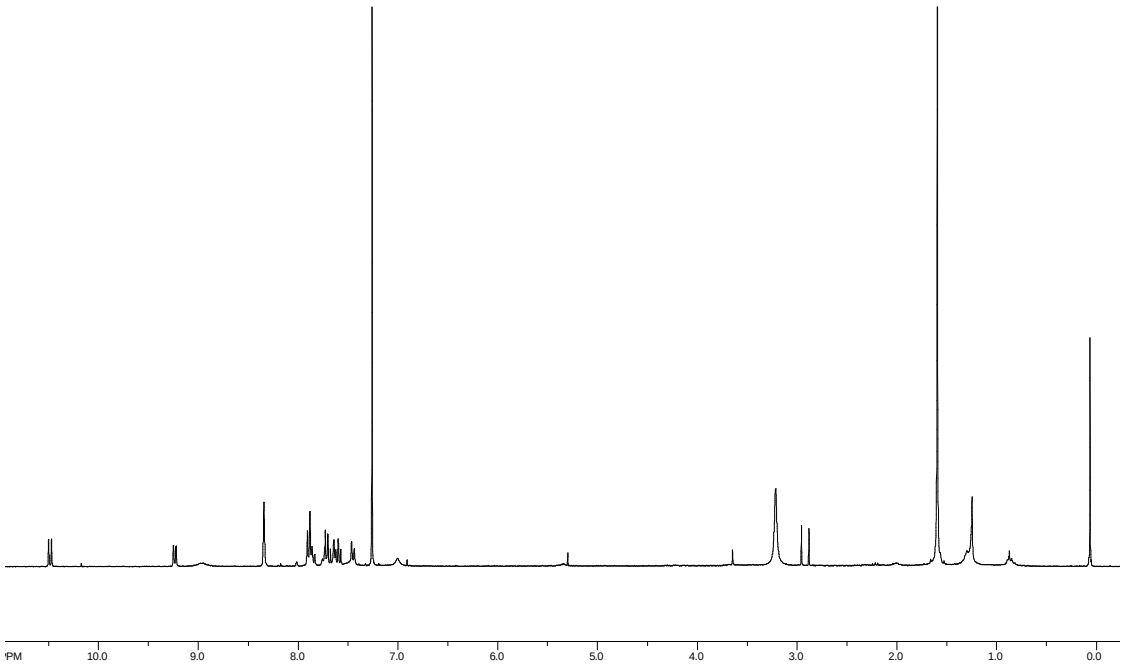

Figure 6.123.1. ^{1}H NMR of complex FL1124-2 ($CDCl_3$).

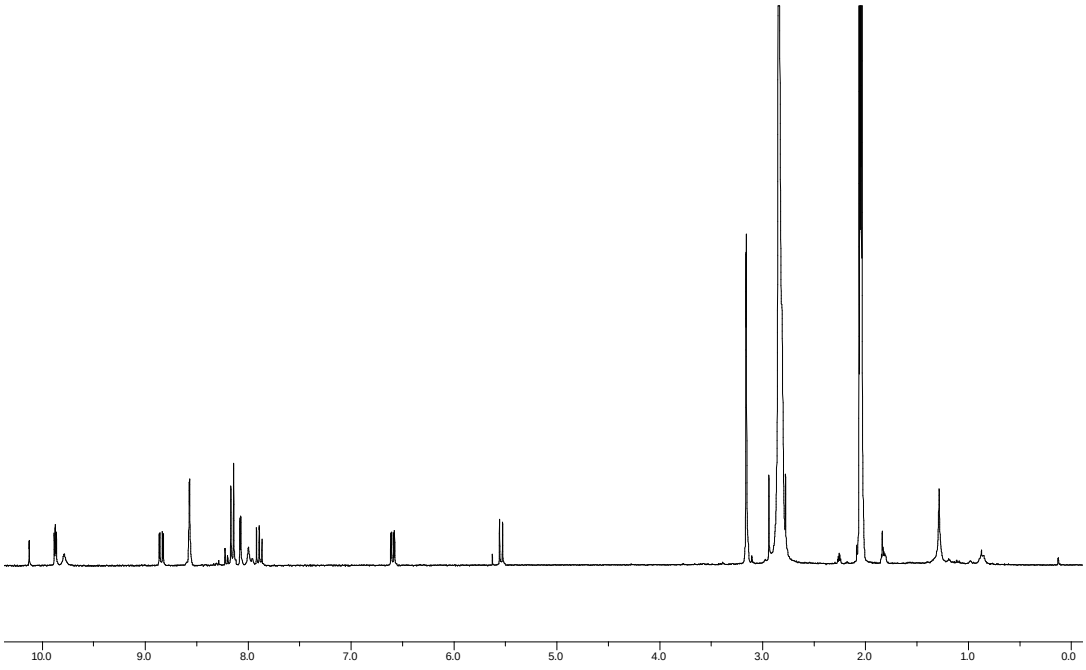

Figure 6.124.1. ^{1}H NMR of complex FL609-1 (Acetone-d_6).

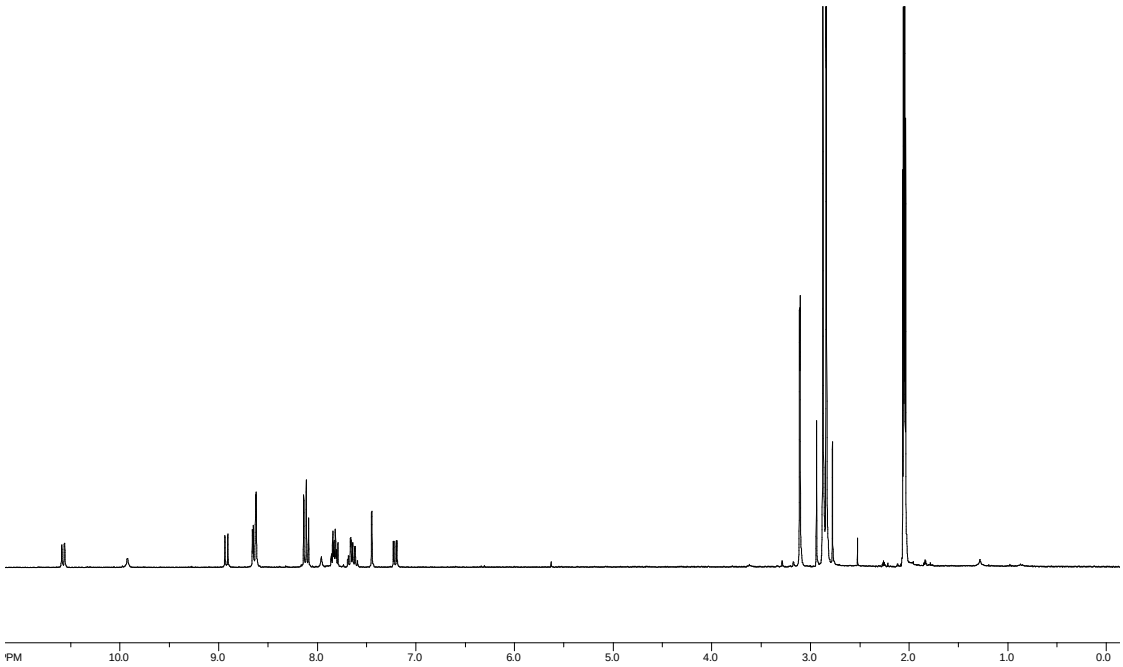

Figure 6.125.1. ^{1}H NMR of complex FL1190-2 (Acetone-d_6).

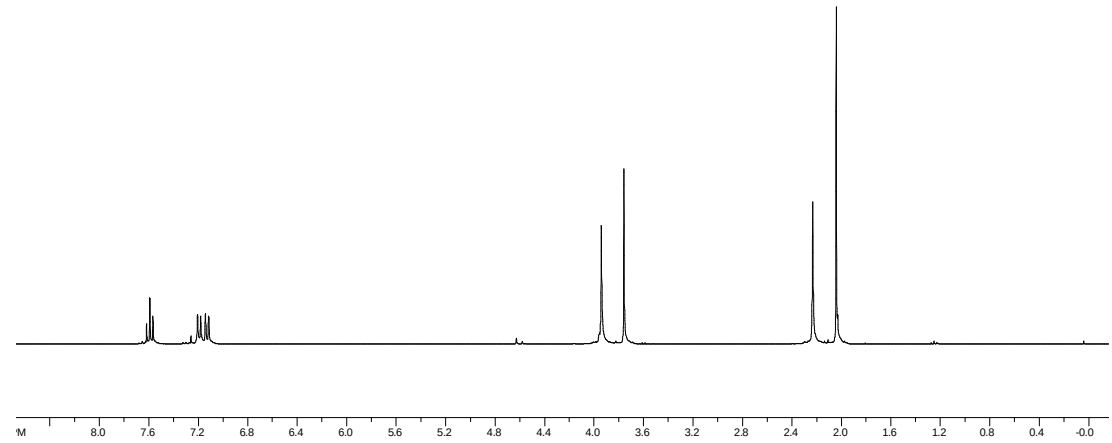

Figure 6.126.1. ^{1}H NMR of compound 4.6 ($CDCl_3$).

C. Kinase Screening Data

Selectivity of FL172 in a panel of 264 protein kinases

Kinase	Activity (%)	Kinase	Activity (%)	Kinase	Activity (%)
Abl(h)	94	FGFR2(h)	108	PDGF(842)(h)	60
Abl(m)	77	FGFR(N549H)(h)	84	PDGF(561)(h)	51
Abl(H396P)(h)	83	FGFR3(h)	97	PDGFRβ(h)	104
Abl(M351T)(h)	92	FGFR4(h)	89	PDK1(h)	92
Abl(Q252H)(h)	80	Fgr(h)	63	PhKγ2(h)	93
Abl(T315I)(h)	88	Flt1(h)	75	Pim-1(h)	1
Abl(Y253F)(h)	88	Flt3(D835Y)(h)	26	Pim-2(h)	1
ACK1(h)	91	Flt3(h)	33	Pim-3(h)	24
ALK(h)	117	Flt4(h)	30	PKA(h)	69
ALK4(h)	0	Fms(h)	28	PKBα(h)	20
Arg(h)	68	Fyn(h)	83	PKBβ(h)	54
AMPK(r)	74	GCK(h)	99	PKBγ(h)	27
Arg(m)	88	GRK5(h)	81	PKCα(h)	63
ARK5(h)	0	GRK6(h)	75	PKCβI(h)	38
ASK1(h)	0	GRK7(h)	25	PKCβII(h)	25
Aurora-A(h)	77	GSK3α(h)	2	PKCγ(h)	33
Axl(h)	50	GSK3β(h)	25	PKCδ(h)	71
Blk(m)	54	Haspin(h)	66	PKCε(h)	65
Bmx(h)	147	Hck(h)	30	PKCη(h)	97
BRK(h)	115	HIPK1(h)	83	PKCι(h)	77
BrSK1(h)	95	HIPK2(h)	64	PKCμ(h)	102
BrSK2(h)	101	HIPK3(h)	87	PKCθ(h)	15
BTK(h)	71	IGF-1R(h)	78	PKCζ(h)	73
CaMKI(h)	107	IGF (h),activated	78	PKD2(h)	98
CaMKIIβ(h)	66	IKKα(h)	123	PKG1α(h)	40
CaMKIIγ(h)	50	IKKβ(h)	93	PKG1β(h)	36
CaMKIδ(h)	80	IR(h)	103	Plk1(h)	101
CaMKIIδ(h)	45	IR(h),activated	105	Plk3(h)	108
CaMKIV(h)	81	IRR(h)	59	PRAK(h)	48
CDK1/cyclinB(h)	72	IRAK1(h)	86	PRK2(h)	32
CDK2/cyclinA(h)	78	IRAK4(h)	97	PrKX(h)	76
CDK2/cyclinE(h)	54	Itk(h)	73	PTK5(h)	68
CDK3/cyclinE(h)	108	JAK2(h)	117	Pyk2(h)	76
CDK5/p25(h)	81	JAK3(h)	92	Ret(h)	87
CDK5/p35(h)	56	JNK1α1(h)	107	Ret(I804L)(h)	89
CDK7/MAT1(h)	114	JNK2α2(h)	100	Ret(I804M)(h)	79
CDK9/T1(h)	96	JNK3(h)	68	RIPK2(h)	95

CHK1(h)	74	KDR(h)	39	ROCK-I(h)	108
CHK2(h)	52	Lck(h)	61	ROCK-II(h)	83
CHK1(I157T)(h)	67	LIMK1(h)	95	ROCK-II(r)	85
CHK2(I145W)(h)	55	LKB1(h)	100	Ron(h)	98
CK1γ1(h)	89	LOK(h)	90	Ros(h)	90
CK1γ2(h)	85	Lyn(h)	14	Rse(h)	21
CK1γ3(h)	50	Lyn(m)	12	Rsk1(h)	13
CK1δ(h)	88	MAPK1(h)	86	Rsk1(r)	22
CK1(y)	59	MAPK2(h)	103	Rsk2(h)	33
CK2(h)	109	MAPK2(m)	99	Rsk3(h)	33
CK2α2(h)	109	MAPKAP-K2(h)	100	Rsk4(h)	20
CLK2(h)	20	MAPKAP-K3(h)	112	SAPK2a(h)	103
CLK3(h)	80	MEK1(h)	106	SAPK(TM)(h)	106
cKit(h)	88	MARK1(h)	86	SAPK2b(h)	96
cKit(D816V)(h)	105	MELK(h)	23	SAPK3(h)	112
cKit(D816H)(h)	66	Mer(h)	33	SAPK4(h)	107
cKit(V560G)(h)	19	Met(h)	57	SGK(h)	84
cKit(V654A)(h)	94	MINK(h)	95	SGK2(h)	104
CSK(h)	110	MKK4(m)	117	SGK3(h)	98
c-RAF(h)	44	MKK6(h)	109	SIK(h)	59
cSRC(h)	59	MKK7β(h)	65	Snk(h)	99
DAPK1(h)	104	MLCK(h)	14	Src(1-530)h	60
DAPK2(h)	90	MLK1(h)	33	Src(T341M)h	73
DCAMKL2(h)	80	Mnk2(h)	99	SRPK1(h)	93
DDR2(h)	84	MRCKα(h)	111	SRPK2(h)	85
DMPK(h)	107	MRCKβ(h)	96	STK33(h)	50
DRAK1(h)	52	MSK1(h)	48	Syk(h)	83
DYRK2(h)	113	MSK2(h)	61	TAK1(h)	108
eEF-2K(h)	112	MSSK1(h)	100	TAO1(h)	60
EGFR(h)	94	MST1(h)	95	TAO2(h)	37
EGFR(L858R)(h)	80	MST2(h)	65	TAO3(h)	65
EGFR(L861Q)(h)	94	MST3(h)	39	TBK1(h)	81
EGFR(T790M)(h)	90	mTOR(h)	87	Tec(h)	94
EGFR(V858R)(h)	62	mTOR/FKBP (h)	100	Tie2(h)	67
EphA1(h)	97	MuSK(h)	81	Tie(I849W)(h)	61
EphA2(h)	96	NEK2(h)	86	Tie(I897S)(h)	82
EphA3(h)	109	NEK3(h)	85	TLK2(h)	100
EphA4(h)	111	NEK6(h)	112	TrkA(h)	30
EphA5(h)	119	NEK7(h)	102	TrkB(h)	7
EphA7(h)	106	NEK11(h)	49	TSSK1(h)	74
EphA8(h)	118	NLK(h)	98	TSSK2(h)	104
EphB2(h)	135	p70S6K(h)	76	Txk(h)	96
EphB1(h)	112	PAK1(h)	17	ULK2(h)	97

EphB3(h)	94	PAK2(h)	26	ULK3(h)	111
EphB4(h)	124	PAK3(h)	8	WNK2(h)	77
ErbB4(h)	93	PAK4(h)	82	WNK3(h)	81
FAK(h)	83	PAK5(h)	71	VRK2(h)	93
Fer(h)	80	PAK6(h)	92	Yes(h)	54
Fes(h)	127	PAR-1Bα(h)	42	ZAP-70(h)	126
FGFR1(h)	96	PASK(h)	109	ZIPK(h)	18

Measured by Millipore UK Ltd (Millipore Kinase Profiler^{TM}). PAK1 was purified and the PAK1 assay was measured separately by Jasna Maksimoska because it was not available in the Kinase Profiler panel. Conditions: 3 μM **FL172** at an ATP concentration of 10 μM. Measurements were performed in duplicate and the average taken. Kinases displaying less than 20% activity under these conditions were highlighted.

Screening data of FL475 against 232 human protein kinases

Kinase	Activity (%)	Kinase	Activity (%)	Kinase	Activity (%)
Abl(h)	101	Flt4(h)	55	PDK1(h)	24
ACK1(h)	96	Fms(h)	68	PhKγ2(h)	95
ALK(h)	60	Fyn(h)	77	Pim-1(h)	31
ALK4(h)	123	GCK(h)	109	Pim-2(h)	24
Arg(h)	93	GRK5(h)	65	Pim-3(h)	30
AMPK(r)	93	GRK6(h)	53	PKA(h)	72
Arg(m)	113	GRK7(h)	46	PKBα(h)	76
ARK5(h)	88	GSK3α(h)	58	PKBβ(h)	90
ASK1(h)	104	GSK3β(h)	90	PKBγ(h)	49
Aurora-A(h)	117	Haspin(h)	79	PKCα(h)	113
Axl(h)	100	Hck(h)	50	PKCβI(h)	99
Blk(m)	113	HIPK1(h)	85	PKCβII(h)	82
Bmx(h)	124	HIPK2(h)	70	PKCγ(h)	99
BRK(h)	114	HIPK3(h)	91	PKCδ(h)	88
BrSK1(h)	92	IGF-1R(h)	92	PKCε(h)	90
BrSK2(h)	80	IKKα(h)	119	PKCη(h)	106
BTK(h)	99	IKKβ(h)	97	PKCι(h)	88
CaMKI(h)	108	IR(h)	104	PKCμ(h)	100
CaMKIIβ(h)	63	IRR(h)	54	PKCθ(h)	42
CaMKIIγ(h)	29	IRAK1(h)	97	PKCζ(h)	96
CaMKIδ(h)	49	IRAK4(h)	108	PKD2(h)	103
CaMKIIδ(h)	23	Itk(h)	96	PKG1α(h)	25

CaMKIV(h)	59	JAK2(h)	108	PKG1β(h)	24
CDK1/cyclinB(h)	120	JAK3(h)	103	Plk1(h)	103
CDK2/cyclinA(h)	115	JNK1α1(h)	106	Plk3(h)	113
CDK2/cyclinE(h)	103	JNK2α2(h)	98	PRAK(h)	86
CDK3/cyclinE(h)	119	JNK3(h)	86	PRK2(h)	76
CDK5/p25(h)	106	KDR(h)	78	PrKX(h)	66
CDK5/p35(h)	98	Lck(h)	105	PTK5(h)	73
CDK7/MAT1(h)	114	LIMK1(h)	103	Pyk2(h)	62
CDK9/cyclin T1(h)	108	LKB1(h)	106	Ret(h)	45
CHK1(h)	97	LOK(h)	93	RIPK2(h)	87
CHK2(h)	89	Lyn(h)	86	ROCK-I(h)	113
CK1γ1(h)	66	Lyn(m)	72	ROCK-II(h)	99
CK1γ2(h)	44	MAPK1(h)	47	ROCK-II(r)	107
CK1γ3(h)	28	MAPK2(h)	89	Ron(h)	108
CK1δ(h)	24	MAPKAP-K2(h)	115	Ros(h)	102
CK1(y)	14	MAPKAP-K3(h)	105	Rse(h)	61
CK2(h)	113	MEK1(h)	103	Rsk1(h)	26
CK2α2(h)	107	MARK1(h)	78	Rsk1(r)	25
CLK2(h)	2	MELK(h)	4	Rsk2(h)	21
CLK3(h)	105	Mer(h)	19	Rsk3(h)	31
cKit(h)	121	Met(h)	132	Rsk4(h)	22
CSK(h)	102	MINK(h)	77	SAPK2a(h)	111
c-RAF(h)	111	MKK4(m)	103	SAPK2b(h)	106
cSRC(h)	80	MKK6(h)	115	SAPK3(h)	109
DAPK1(h)	21	MKK7β(h)	63	SAPK4(h)	91
DAPK2(h)	8	MLCK(h)	2	SGK(h)	82
DCAMKL2(h)	97	MLK1(h)	86	SGK2(h)	53
DDR2(h)	92	Mnk2(h)	95	SGK3(h)	92
DMPK(h)	110	MRCKα(h)	108	SIK(h)	69
DRAK1(h)	94	MRCKβ(h)	105	Snk(h)	96
DYRK2(h)	114	MSK1(h)	15	SRPK1(h)	35
eEF-2K(h)	107	MSK2(h)	22	SRPK2(h)	30
EGFR(h)	121	MSSK1(h)	57	STK33(h)	100
EphA1(h)	107	MST1(h)	78	Syk(h)	114
EphA2(h)	97	MST2(h)	50	TAK1(h)	107
EphA3(h)	115	MST3(h)	43	TAO1(h)	105
EphA4(h)	107	mTOR(h)	99	TAO2(h)	103
EphA5(h)	124	mTOR (h)	108	TAO3(h)	100
EphA7(h)	113	MuSK(h)	108	TBK1(h)	90
EphA8(h)	134	NEK2(h)	105	Tec(h)	102
EphB2(h)	116	NEK3(h)	97	Tie2(h)	86
EphB1(h)	146	NEK6(h)	94	TLK2(h)	108
EphB3(h)	109	NEK7(h)	83	TrkA(h)	104

EphB4(h)	113	NEK11(h)	101	TrkB(h)	75
ErbB4(h)	111	NLK(h)	104	TSSK1(h)	50
FAK(h)	98	p70S6K(h)	54	TSSK2(h)	100
Fer(h)	101	PAK2(h)	91	Txk(h)	99
Fes(h)	97	PAK3(h)	98	ULK2(h)	106
FGFR1(h)	132	PAK4(h)	104	ULK3(h)	109
FGFR2(h)	118	PAK5(h)	96	WNK2(h)	90
FGFR3(h)	100	PAK6(h)	96	WNK3(h)	99
FGFR4(h)	98	PAR-1Bα(h)	54	VRK2(h)	77
Fgr(h)	81	PASK(h)	102	ZIPK(h)	18
Flt1(h)	64	PDGFRα(h)	127		
Flt3(h)	32	PDGFRβ(h)	107		

Measured by Millipore UK Ltd (Millipore Kinase Profiler^{TM}). Conditions: 100 nM of **FL475** with an ATP concentration of 10 μM. Measurements were performed in duplicate and the average taken.

Screening data of FL1528-1 against 230 human protein kinases

Kinase	Activity (%)	Kinase	Activity (%)	Kinase	Activity (%)
Abl(h)	93	CK2α2(h)	98	MST1(h)	91
ACK1(h)	85	CLK2(h)	53	MST2(h)	85
ALK(h)	77	CLK3(h)	92	MST3(h)	41
ALK4(h)	80	cKit(h)	111	mTOR(h)	99
Arg(h)	82	CSK(h)	104	mTOR(h)	95
AMPKα1(h)	71	c-RAF(h)	87	MuSK(h)	108
AMPKα2(h)	67	cSRC(h)	105	NEK2(h)	87
ARK5(h)	90	DAPK1(h)	15	NEK3(h)	95
ASK1(h)	88	DAPK2(h)	12	NEK6(h)	90
Aurora-A(h)	74	DCAMKL2(h)	98	NEK7(h)	88
Aurora-B(h)	71	DDR2(h)	94	NEK11(h)	99
Axl(h)	77	DMPK(h)	101	NLK(h)	84
Bmx(h)	94	DRAK1(h)	80	p70S6K(h)	26
BRK(h)	96	DYRK2(h)	99	PAK2(h)	94
BrSK1(h)	77	eEF-2K(h)	78	PAK4(h)	101
BrSK2(h)	70	EGFR(h)	110	PAK3(h)	99
BTK(h)	99	EphA1(h)	99	PAK5(h)	93
CaMKI(h)	65	EphA2(h)	94	PAK6(h)	101
CaMKIIβ(h)	98	EphA3(h)	103	PAR-1Bα(h)	56
CaMKIIγ(h)	66	EphA4(h)	99	PASK(h)	98
CaMKIδ(h)	60	EphA5(h)	99	PDGFRα(h)	85
CaMKIIδ(h)	77	MAPKAP-K2(h)	98	PDGFRβ(h)	75

CaMKIV(h)	61	MAPKAP-K3(h)	107	PDK1(h)	40
CDK1/cyclinB(h)	92	MEK1(h)	105	PhKγ2(h)	94
CDK2/cyclinA(h)	101	MARK1(h)	59	Pim-1(h)	56
CDK2/cyclinE(h)	86	MELK(h)	34	Pim-2(h)	42
CDK3/cyclinE(h)	93	Mer(h)	25	Pim-3(h)	82
CDK5/p25(h)	98	Met(h)	50	PKA(h)	78
CDK5/p35(h)	99	MINK(h)	74	PKBα(h)	86
CDK6 (h)	94	MKK6(h)	94	PKBβ(h)	88
CDK7 (h)	96	MKK7β(h)	95	PKBγ(h)	63
CDK9 (h)	88	MLCK(h)	2	PKCα(h)	91
CHK1(h)	91	MLK1(h)	59	PKCβI(h)	92
CHK2(h)	43	Mnk2(h)	100	PKCβII(h)	93
CK1γ1(h)	89	MRCKα(h)	98	PKCγ(h)	97
CK1γ2(h)	83	MRCKβ(h)	102	PKCδ(h)	84
CK1γ3(h)	93	MSK1(h)	44	PKCε(h)	100
CK1δ(h)	85	MSK2(h)	33	PKCη(h)	89
CK2(h)	106	MSSK1(h)	74	PKCι(h)	89
PKCμ(h)	100	Rse(h)	86	TBK1(h)	82
PKCθ(h)	84	Rsk1(h)	20	Tec(h)	112
PKCζ(h)	82	Rsk2(h)	19	Tie2(h)	100
PKD2(h)	95	Rsk3(h)	34	TLK2(h)	96
PKG1α(h)	55	Rsk4(h)	27	TrkA(h)	94
PKG1β(h)	49	SAPK2a(h)	100	TrkB(h)	118
Plk1(h)	104	SAPK2b(h)	94	TSSK1(h)	78
Plk3(h)	93	SAPK3(h)	63	TSSK2(h)	85
PRAK(h)	79	SAPK4(h)	64	Txk(h)	83
PRK2(h)	95	SGK(h)	45	ULK2(h)	97
PrKX(h)	56	SGK3(h)	39	ULK3(h)	99
PTK5(h)	99	SIK(h)	89	WNK2(h)	87
Pyk2(h)	98	Snk(h)	85	WNK3(h)	97
Ret(h)	13	SRPK1(h)	81	VRK2(h)	84
RIPK2(h)	84	SRPK2(h)	81	Yes(h)	84
ROCK-I(h)	90	STK33(h)	76	ZAP-70(h)	99
ROCK-II(h)	101	Syk(h)	97	ZIPK(h)	5
Ron(h)	84	TAK1(h)	98		
Ros(h)	100	TAO1(h)	94		

Measured by Millipore UK Ltd (Millipore Kinase Profiler^{TM}). Conditions: 30 nM of **FL1528-1** with an ATP concentration of 10 μM. Measurements were performed in duplicate and the average taken. Kinases displaying less than 30% activity under these conditions were highlighted.

Screening data of FL1353-1 against 102 human protein kinases

Kinase	Activity (%)	Kinase	Activity (%)	Kinase	Activity (%)
Abl(h)	104	eEF-2K(h)	103	Mer(h)	74
Arg(h)	102	EGFR(h)	98	PAK2(h)	103
AMPKα1(h)	82	EphA5(h)	111	PAK3(h)	102
AMPKα2(h)	74	Fes(h)	105	PAK5(h)	96
Aurora-B(h)	107	FGFR2(h)	108	PAK6(h)	109
BrSK1(h)	83	FGFR3(h)	111	PAR-1Bα(h)	64
CaMKI(h)	76	FGFR4(h)	88	Pim-1(h)	38
CaMKIIβ(h)	92	Fgr(h)	88	Pim-3(h)	97
CaMKIIγ(h)	66	GCK(h)	117	PKA(h)	88
CaMKIδ(h)	75	GSK3α(h)	94	PKBγ(h)	77
CaMKIIδ(h)	69	GSK3β(h)	95	PKCα(h)	80
CDK1/cyclinB(h)	99	Hck(h)	100	PKCβI(h)	98
CDK2/cyclinA(h)	101	HIPK1(h)	104	PKCβII(h)	101
CDK2/cyclinE(h)	104	HIPK2(h)	107	PKCγ(h)	101
CDK3/cyclinE(h)	105	HIPK3(h)	101	PKCδ(h)	98
CDK5/p25(h)	97	IGF-1R(h)	99	PKCε(h)	101
CDK5/p35(h)	98	IR(h), activated	87	PKCη(h)	104
CHK2(h)	88	IRAK1(h)	102	PKCι(h)	103
CK1γ1(h)	102	IRAK4(h)	96	PKCμ(h)	105
CK1γ2(h)	99	JAK2(h)	99	PKCζ(h)	98
CK1γ3(h)	101	JAK3(h)	97	PKD2(h)	99
CK1δ(h)	80	Lck(h) activated	80	PKG1α(h)	99
CK2(h)	98	Lyn(h)	103	PKG1β(h)	79
CK2α2(h)	113	MAPK1(h)	107	PRAK(h)	95
CLK2(h)	67	MAPKAP-K2(h)	99	Ret(h)	67
CLK3(h)	108	MAPKAP-K3(h)	100	ROCK-II(h)	105
DAPK1(h)	12	MEK1(h)	108	Rsk1(h)	31
DCAMKL2(h)	97	MARK1(h)	77	Rsk2(h)	27
DYRK2(h)	108	MELK(h)	37	SGK(h)	94
SGK3(h)	139	TAO1(h)	98	TSSK2(h)	102
Src(1-530)(h)	92	TAO2(h)	98	Txk(h)	79
SRPK1(h)	74	Tec(h) activated	103	ULK3(h)	111
SRPK2(h)	104	TLK2(h)	103	Yes(h)	99
Syk(h)	84	TSSK1(h)	86	ZIPK(h)	22

Measured by Millipore UK Ltd (Millipore Kinase Profiler^{TM}). Conditions: 10 nM of **FL1353-1** with an ATP concentration of 10 μM. Measurements were performed in duplicate and the average taken. Kinases displaying less than 50% activity under these

conditions were highlighted.

Screening data of FL792-1 and FL792-2 against 227 human protein kinases

Kinase	Activity (%) FL792-1	Activity (%) FL792-2	Kinase	Activity (%) FL792-1	Activity (%) FL792-2
Abl(h)	102	98	cKit(h)	83	95
ACK1(h)	75	79	CSK(h)	105	101
ALK(h)	86	88	c-RAF(h)	82	93
ALK4(h)	85	91	cSRC(h)	92	88
Arg(h)	81	82	DAPK1(h)	106	100
ARK5(h)	95	96	DAPK2(h)	91	87
ASK1(h)	108	113	DDR2(h)	104	96
Aurora-A(h)	51	37	DMPK(h)	108	109
Aurora-B(h)	80	104	DRAK1(h)	126	129
Axl(h)	80	80	DYRK2(h)	111	112
Bmx(h)	86	75	eEF-2K(h)	105	103
BRK(h)	91	94	EGFR(h)	103	110
BrSK1(h)	102	103	EphA1(h)	106	108
BrSK2(h)	90	87	EphA2(h)	106	98
BTK(h)	99	84	EphA3(h)	109	103
CaMKI(h)	87	91	EphA4(h)	120	105
CaMKIIβ(h)	53	60	EphA5(h)	97	100
CaMKIIγ(h)	64	83	EphA7(h)	93	71
CaMKIδ(h)	103	103	EphA8(h)	102	110
CaMKIIδ(h)	56	86	EphB2(h)	113	97
CaMKIV(h)	101	94	EphB1(h)	88	97
CDK1/cyclinB(h)	87	97	EphB3(h)	86	83
CDK2/cyclinA(h)	97	107	EphB4(h)	111	104
CDK2/cyclinE(h)	85	95	ErbB4(h)	114	106
CDK3/cyclinE(h)	93	98	FAK(h)	76	85
CDK5/p25(h)	84	90	Fer(h)	63	69
CDK5/p35(h)	96	102	Fes(h)	88	99
CDK6/cyclinD3(h)	82	96	FGFR1(h)	40	47
CDK7/cyclinH (h)	90	94	FGFR2(h)	68	58
CDK9/cyclinT1(h)	62	29	FGFR3(h)	94	108
CHK1(h)	98	106	FGFR4(h)	101	114
CHK2(h)	89	3	Fgr(h)	91	86
CK1γ1(h)	91	84	Flt1(h)	41	34
CK1γ2(h)	72	78	Flt3(h)	46	41
CK1γ3(h)	98	113	Flt4(h)	26	28
CK1δ(h)	96	84	Fms(h)	19	17

CK2(h)	104	94	Fyn(h)	66	76
CK2α2(h)	109	108	GCK(h)	98	98
CLK2(h)	89	107	GRK5(h)	109	123
CLK3(h)	19	98	MKK6(h)	103	96
GRK7(h)	92	86	MKK7β(h)	94	44
GSK3α(h)	9	28	MLCK(h)	61	84
GSK3β(h)	22	50	MLK1(h)	63	64
Haspin(h)	122	119	Mnk2(h)	95	99
Hck(h)	65	74	MRCKα(h)	104	89
Hck(h) activated	88	87	MRCKβ(h)	102	84
HIPK1(h)	67	87	MSK1(h)	88	71
HIPK2(h)	69	95	MSK2(h)	89	70
HIPK3(h)	95	101	MSSK1(h)	112	110
IGF-1R(h)	91	77	MST1(h)	79	90
IGF-1R(h), activated	84	79	MST2(h)	73	81
IKKα(h)	107	94	MST3(h)	69	49
IKKβ(h)	103	102	mTOR(h)	103	112
IR(h)	98	86	mTOR/FKBP12(h)	94	89
IR(h), activated	89	90	MuSK(h)	72	87
IRR(h)	101	97	NEK2(h)	99	97
IRAK1(h)	109	107	NEK3(h)	89	92
IRAK4(h)	99	108	NEK6(h)	104	99
Itk(h)	101	92	NEK7(h)	97	95
JAK2(h)	110	108	NEK11(h)	92	100
JAK3(h)	106	115	NLK(h)	76	77
JNK1α1(h)	118	107	p70S6K(h)	88	80
JNK2α2(h)	94	97	PAK2(h)	91	91
JNK3(h)	78	51	PAK4(h)	82	89
KDR(h)	68	73	PAK3(h)	230	145
Lck(h)	84	91	PAK5(h)	85	90
Lck(h) activated	103	106	PAK6(h)	99	97
LIMK1(h)	97	98	PAR-1Bα(h)	96	86
LKB1(h)	100	98	PASK(h)	107	114
LOK(h)	71	93	PDGFRα(h)	119	89
Lyn(h)	68	69	PDGFRβ(h)	94	103
MAPK1(h)	101	105	PDK1(h)	91	91
MAPK2(h)	96	103	PhKγ2(h)	104	99
MAPKAP-K2(h)	105	105	Pim-1(h)	6	8
MAPKAP-K3(h)	102	108	Pim-2(h)	51	98
MEK1(h)	78	101	Pim-3(h)	77	100
MARK1(h)	79	81	PKA(h)	102	104
MELK(h)	66	88	PKBα(h)	101	106

Mer(h)	63	95	PKBβ(h)	100	111
Met(h)	93	99	PKBγ(h)	82	85
MINK(h)	87	81	SRPK1(h)	98	104
PKCα(h)	95	87	SAPK2b(h)	109	104
PKCβI(h)	106	100	SAPK3(h)	100	101
PKCβII(h)	97	94	SAPK4(h)	91	95
PKCγ(h)	95	100	SGK(h)	108	101
PKCδ(h)	93	76	SGK2(h)	105	99
PKCε(h)	97	82	SGK3(h)	102	105
PKCη(h)	104	94	SIK(h)	111	109
PKCι(h)	86	120	Snk(h)	114	103
PKCμ(h)	96	84	SRPK2(h)	88	99
PKCθ(h)	80	59	STK33(h)	105	107
PKCζ(h)	96	100	Syk(h)	86	86
PKD2(h)	102	104	TAK1(h)	100	108
PKG1α(h)	43	94	TAO1(h)	86	94
PKG1β(h)	43	91	TAO2(h)	89	91
Plk1(h)	90	96	TAO3(h)	75	76
Plk3(h)	104	106	TBK1(h)	102	96
PRAK(h)	67	69	Tec(h) activated	89	99
PRK2(h)	47	52	Tie2(h)	105	88
PrKX(h)	108	95	TLK2(h)	99	100
PTK5(h)	86	89	TrkA(h)	4	22
Pyk2(h)	66	89	TrkB(h)	17	93
Ret(h)	83	73	TSSK1(h)	102	108
RIPK2(h)	102	104	TSSK2(h)	101	104
ROCK-I(h)	109	100	Txk(h)	103	108
ROCK-II(h)	98	97	ULK2(h)	99	103
Ron(h)	97	106	ULK3(h)	92	87
Ros(h)	79	110	WNK2(h)	92	95
Rse(h)	133	132	WNK3(h)	90	95
Rsk1(h)	89	82	VRK2(h)	105	95
Rsk2(h)	94	95	Yes(h)	86	89
Rsk3(h)	104	83	ZAP-70(h)	96	106
Rsk4(h)	95	89	ZIPK(h)	113	122
SAPK2a(h)	118	109			

Measured by Millipore UK Ltd (Millipore Kinase Profiler^{TM}) Conditions: 1 μM of **FL792-1** and **FL792-2** with an ATP concentration of 10 μM. Measurements were performed in duplicate and the average taken. Kinases displaying less than 10% activity under these conditions were highlighted.

Initial screening of an organometallic library for PAK1 inhibition

A library of 48 organometallic complexes was tested for PAK1 inhibition at the concentration of 10 μM with an ATP concentration of 1 μM. The results are shown in the bar diagram below (Figure 5.127) with the corresponding molecular structures of the library members displayed in Figure 5.128. These complexes were synthesized by former lab colleagues and tested by Jasna Maksimoska.

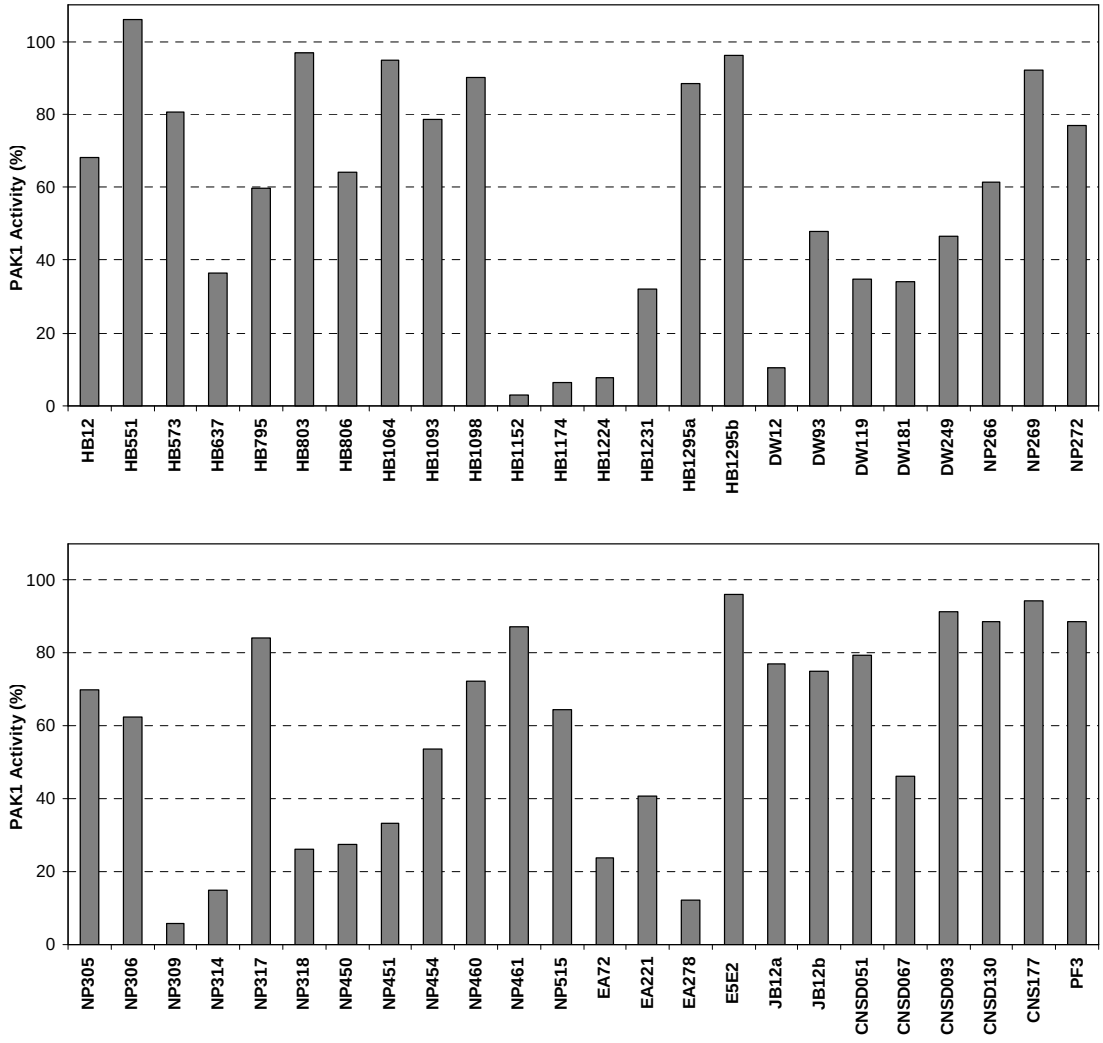

Figure 5.127. Initial screening of a 48-member organometallic library for PAK1 inhibition at a complex concentration of 10 μM with 1 μM ATP.

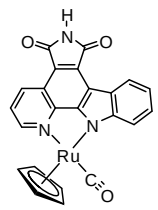

HB12

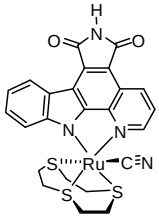

HB551

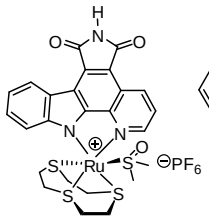

HB573

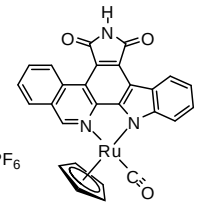

HB637

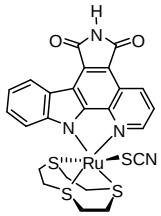

HB795

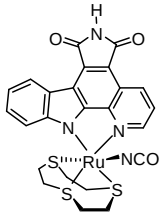

HB803

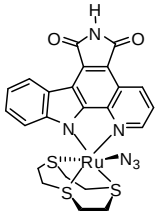

HB806

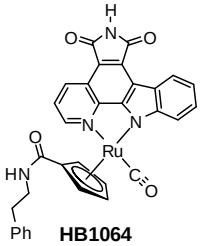

HB1064

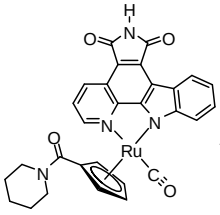

HB1093

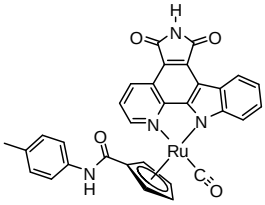

HB1098

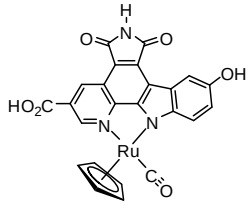

HB1152

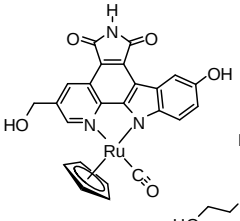

HB1174

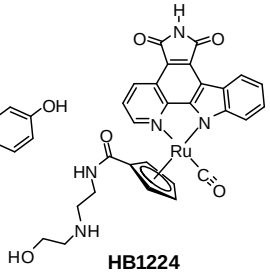

HB1224

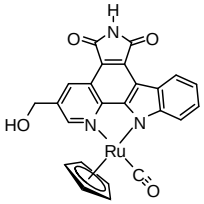

HB1231

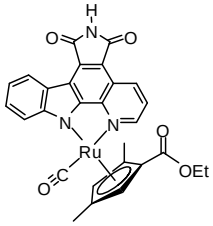

HB1295a, **HB1295b**
(individual diastereomers)

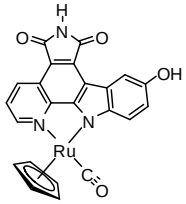

DW12

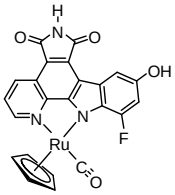

DW93

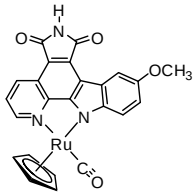

DW119

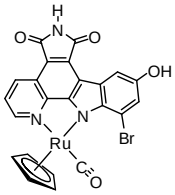

DW181

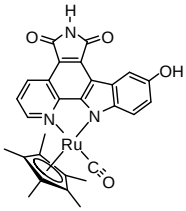

DW249

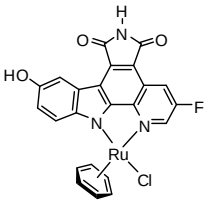

NP266

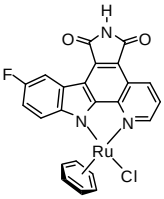

NP269

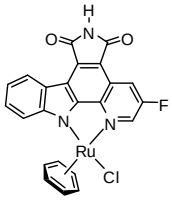

NP272

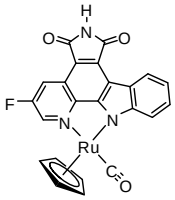

NP305

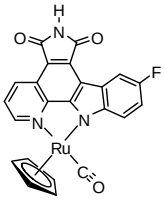

NP306

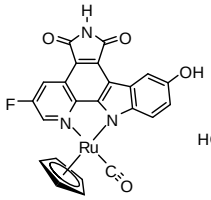

NP309

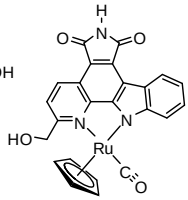

NP314

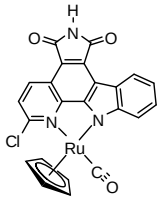

NP317

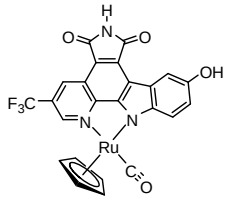

NP318

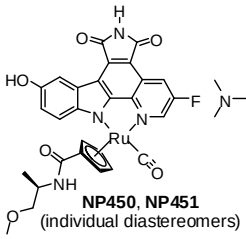

NP450, **NP451**
(individual diastereomers)

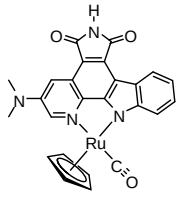

NP454

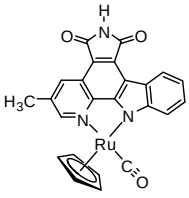

NP460

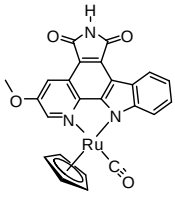

NP461

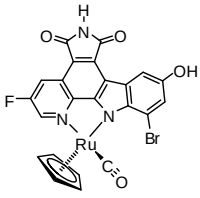

NP515

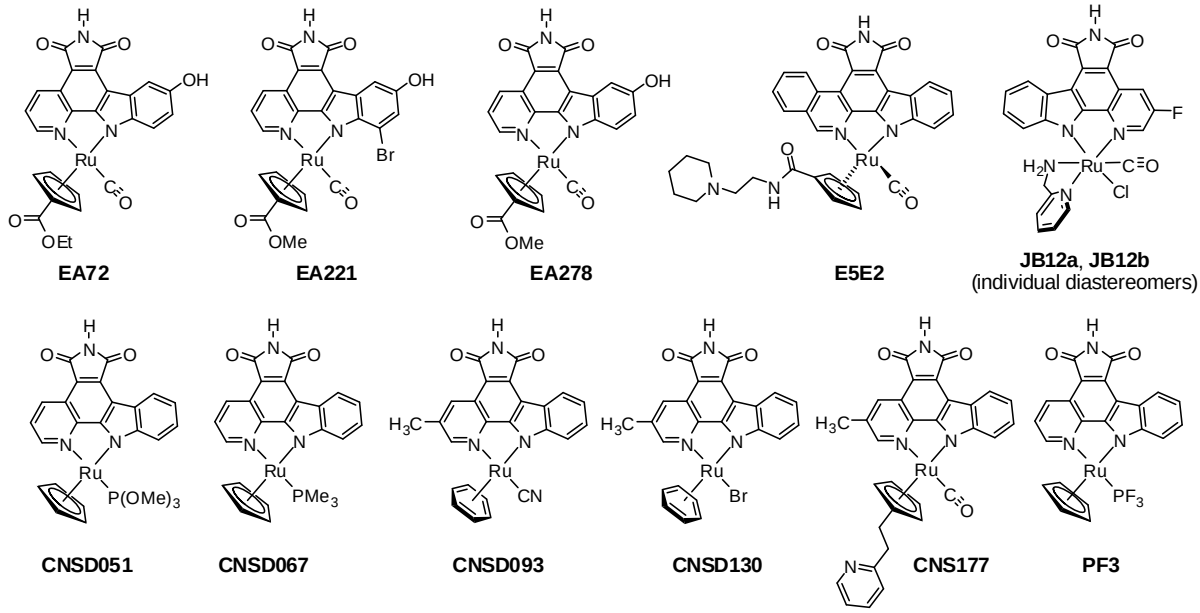

Figure 5.128. Molecular structures of the 48-member organometallic library. Complexes were racemic, except for **E5E2** for which the absolute stereochemistry is indicated.

List of Figures

Figure 1.1. Structure of the catalytic domain of cAbl according to ref. 10. 2
Figure 1.2. Kinase inhibitor binding modes. 3
Figure 1.3. MEK1 protein kinase structure and the active site are occupied by MgATP and inhibitor PD318088, and the structure of other derivatives according to ref. 35. 3
Figure 1.5. Structures of some kinase inhibitors marketed in the U.S. as of 2009 according to ref. 33. 6
Figure 1.6. Structure of inhibitor 1.1 and 1.2. 7
Figure 1.8. a) ATP in the ATP-binding site of CDK-2. b) Staurosporine in the ATP binding site of CDK-2. 9
Figure 1.9. Design of ruthenium complexes as protein kinase inhibitors by using staurosporine as lead structure. A, B, C and D represent the organic ligands coordinated to the metal center. 10
Figure 1.10. Structures of some organoruthenium inhibitors for their respective protein kinases. 10
Figure 1.11. Octahedral scaffold with well defined three-dimensional structure compare with half-sandwich geometry. 11
Figure 2.2. Cocrystal structure at 2.35 Å of (*R*)-DW12 with PAK1 (249-545, mutation Lys299Arg). 16
Figure 2.3. Crystal structure of complex 2.8. 19
Figure 2.5. Example of the assignment of the relative stereochemistry of racemic octahedral complexes in Figure 2.4 by ^{1}H NMR spectroscopy. 23
Figure 2.6. Crystal structure of complex FL151-1. 24
Figure 2.7. Remaining activities of PAK1 with 20 ruthenium complexes. 24
Figure 2.8. Circular dichroism spectra of the two enantiomers of FL172, ... 26
Figure 2.9. Individual enantiomers of FL172. 26
Figure 2.10. Kinase selectivity switched by the transformation of a small half-sandwich scaffold into rigid and bulky octahedral ruthenium complex. 27
Figure 2.11. Cocrystal structure of **Λ**-FL172 with PAK1 (amino acids 249-545, mutation Lys299Arg) at 1.65 Å 28
Figure 2.13. Inhibition of PAK1 by racemic derivatives of FL172 at a single inhibitor concentration of 100 nM and in the presence of 1 μM ATP. 31
Figure 2.14. Circular dichroism spectra of the two enantiomers of FL411, ... 31
Figure 2.15. a) Crystal structure of complex FL327. b) Crystal structure of complex FL389. 33
Figure 2.16. Circular dichroism spectra of the two enantiomers of FL1422, ... 43
Figure 3.2. Crystal structure of complex FL1359. 55
Figure 3.4. Crystal structure of complex FL626-1. 59
Figure 3.5. Crystal structure of the complex FL1473. 61
Figure 3.6. Crystal structure of complex FL1528-1. 62
Figure 3.7. Selectivity profile of racemic FL1528-1 tested against a panel of 230 human wild-type protein kinases at a single concentration of 30 nM and an ATP concentration of 10 μM. 64
Figure 3.8. Racemic complex 3.86 was identified as initial DAPK1 inhibitor. 65
Figure 3.9. IC_{50} values of racemic 3.86 and FL823-1 for DAPK1 with 100 μM ATP. 66
Figure 3.10. Synthesis of ruthenium complexes with different monodentate ligands. 67
Figure 3.11. Selectivity profile of racemic FL1353-1 tested against a panel of 102 human wild-type protein kinases at a single concentration of 10 nM and an ATP concentration of 10 μM,

.....71
Figure 3.12. Crystal structure of complex FL1370-1.....72
Figure 3.13. Structure of racemic complexes FL534-1 and FL534-2. 73
Figure 3.14. ^{15}N NMR spectra of FL534-1 and FL534-2. NH_3 liquid was used as standard, and FL534-2 was measured as a mixture of both linkage isomers. 74
Figure 3.15. Cocrystal structure of (*R*)-FL1353-1 with DAPK1 at the resolution of 2.2 Å. a) Hydrogen bonding interactions between the hinge region and (*R*)-FL1353-1. b) Hydrophobic interactions of (*R*)-FL1353-1 in the active site. 76
Figure 3.16. Potency for Pim1 was improved by the transformation of half-sandwich scaffold into octahedral scaffold. 78
Figure 4.1. Structure of TrkA inhibitor NP. 85
Figure 4.2. Structure of complex FL1220. 89
Figure 4.3. Structures of tridentate ligands used to modify TrkA inhibitors. 91
Figure 5.1. Design of ruthenium complexes as protein kinase inhibitors by using staurosporine as lead structure. A, B, C and D represent the organic ligands coordinated to the metal center. 94
Figure 5.2. Structures of Λ-FL172 and Λ-FL1422. 95
Figure 5.3. Cocrystal structure of **Λ**-FL172 with PAK1 (amino acids 249-545, mutation Lys299Arg) at 1.65 Å (by Jasna Maksimoska 95
Figure 5.4. Structure of complex FL1528-1 96
Figure 5.5. Structure of complex FL1353-1 96
Figure 5.6. Cocrystal structure of (*R*)-FL1353-1 with DAPK1 at the resolution of 2.2 Å. a) Hydrogen bonding interactions between the hinge region and (*R*)-FL1353-1. b) Hydrophobic interactions of (*R*)-FL1353-1 in the active site. (cocrystallized by Katja Kräling and the cocrystal structure was obtained by Yann Geisselbrecht from the group of Prof. Dr. Lars-Oliver Essen) 97
Figure 5.7. Potency for Pim1 was improved by the transformation of half-sandwich scaffold into octahedral scaffold. 98
Figure 5.8. Structure of complex FL1260-2 98
Figure 6.1.1. ^{1}H NMR of complex 2.2 ($CDCl_3$) 288
Figure 6.1.2. ^{13}C NMR of complex 2.2 ($CDCl_3$) 288
Figure 6.2.1. ^{1}H NMR of complex 2.3 (DMF-d_7). 289
Figure 6.2.2. ^{13}C NMR of complex 2.3 (DMF-d_7). 289
Figure 6.3.1. ^{1}H NMR of complex FL172 (Acetone-d_6). 290
Figure 6.3.2. ^{13}C NMR of complex FL172 (DMSO-d_6). 290
Figure 6.4.1. ^{1}H NMR of complex FL411 (Acetone-d_6). 291
Figure 6.4.2. ^{13}C NMR of complex FL411 (DMSO-d_6) 291
Figure 6.5.1. ^{1}H NMR of complex FL115-1 (Acetone-d_6) 292
Figure 6.6.1. ^{1}H NMR of complex FL115-2 (Acetone-d_6) 292
Figure 6.7.1. ^{1}H NMR of complex FL114-1 (Acetone-d_6) 293
Figure 6.8.1. ^{1}H NMR of complex FL114-2 (Acetone-d_6) 293
Figure 6.9.1. ^{1}H NMR of complex FL111-1 (Acetone-d_6). 294
Figure 6.10.1. ^{1}H NMR of complex FL111-2 (Acetone-d_6). 294
Figure 6.11.1. ^{1}H NMR of complex FL161-1 (Acetone-d_6) 295
Figure 6.12.1. ^{1}H NMR of complex FL161-2 (Acetone-d_6). 295
Figure 6.13.1. ^{1}H NMR of complex FL174-2 (Acetone-d_6). 296
Figure 6.14.1. ^{1}H NMR of complex FL178 (Acetone-d_6). 296

Figure 6.15.1. ^{1}H NMR of complex FL134 (Acetone-d_6).....297
Figure 6.16.1. ^{1}H NMR of complex FL151-1 (Acetone-d_6). 297
Figure 6.17.1. ^{1}H NMR of complex FL151-2 (Acetone-d_6). 298
Figure 6.18.1. ^{1}H NMR of complex FL182-1 (Acetone-d_6). 298
Figure 6.19.1. ^{1}H NMR of complex FL182-2 (Acetone-d_6). 299
Figure 6.20.1. ^{1}H NMR of complex FL162-1 (Acetone-d_6). 299
Figure 6.21.1. ^{1}H NMR of complex FL162-2 (Acetone-d_6). 300
Figure 6.22.1. ^{1}H NMR of complex FL227 (Acetone-d_6).....300
Figure 6.23.1. ^{1}H NMR of complex FL226 (Acetone-d_6).....301
Figure 6.24.1. ^{1}H NMR of complex FL224 (Acetone-d_6).....301
Figure 6.25.1. ^{1}H NMR of complex FL237 (Acetone-d_6).....302
Figure 6.26.1. ^{1}H NMR of complex FL252 (Acetone-d_6).....302
Figure 6.27.1. ^{1}H NMR of complex FL254 (Acetone-d_6).....303
Figure 6.28.1. ^{1}H NMR of complex FL256 (Acetone-d_6).....303
Figure 6.29.1. ^{1}H NMR of complex FL258 (Acetone-d_6).....304
Figure 6.30.1. ^{1}H NMR of complex FL262-3 (Acetone-d_6). 304
Figure 6.31.1. ^{1}H NMR of complex FL355 (Acetone-d_6).....305
Figure 6.32.1. ^{1}H NMR of complex FL262-9 (Acetone-d_6). 305
Figure 6.33.1. ^{1}H NMR of complex FL343 (Acetone-d_6).....306
Figure 6.34.1. ^{1}H NMR of complex FL389 (Acetone-d_6).....306
Figure 6.35.1. ^{1}H NMR of complex FL327 (Acetone-d_6).....307
Figure 6.36.1. ^{1}H NMR of complex FL637 (Acetone-d_6).....307
Figure 6.37.1. ^{1}H NMR of complex FL866 (Acetone-d_6).....308
Figure 6.38.1. ^{1}H NMR of complex FL922 (Acetone-d_6).....308
Figure 6.39.1. ^{1}H NMR of complex FL931 (Acetone-d_6).....309
Figure 6.40.1. ^{1}H NMR of complex FL864 (Acetone-d_6).....309
Figure 6.41.1. ^{1}H NMR of complex FL889 (Acetone-d_6).....310
Figure 6.42.1. ^{1}H NMR of complex FL1088 (Acetone-d_6).....310
Figure 6.43.1. ^{1}H NMR of complex FL1103 (Acetone-d_6).....311
Figure 6.44.1. ^{1}H NMR of complex FL1109 (Acetone-d_6).....311
Figure 6.45.1. ^{1}H NMR of complex FL1118 (DMSO-d_6).....312
Figure 6.46.1. ^{1}H NMR of compound 2.5 ($CDCl_3$).....312
Figure 6.46.2. ^{13}C NMR of compound 2.5 ($CDCl_3$). 313
Figure 6.47.1. ^{1}H NMR of compound 2.7 ($CDCl_3$).....313
Figure 6.47.2. ^{13}C NMR of compound 2.7 ($CDCl_3$). 314
Figure 6.48.1. ^{1}H NMR of complex 2.8 ($CDCl_3$).....314
Figure 6.48.2. ^{13}C NMR of complex 2.8 ($CDCl_3$).....315
Figure 6.49.1. ^{1}H NMR of complex 2.9 (DMSO-d_6). 315
Figure 6.50.1. ^{1}H NMR of complex FL1422 (DMSO-d_6). 316
Figure 6.50.2. ^{13}C NMR of complex FL1422 (DMSO-d_6). 316
Figure 6.51.1. ^{1}H NMR of complex 3.82 (DMSO-d_6). 317
Figure 6.51.2. ^{13}C NMR of complex 3.82 (DMSO-d_6). 317
Figure 6.52.1. ^{1}H NMR of complex 3.83 (DMSO-d_6). 318
Figure 6.52.2. ^{13}C NMR of complex 3.83 (DMSO-d_6). 318
Figure 6.53.1. ^{1}H NMR of complex 3.84 (DMSO-d_6). 319

Figure 6.53.2. ^{13}C NMR of complex 3.84 (DMSO-d_6). 319
Figure 6.54.1. ^{1}H NMR of complex 3.86 (DMSO-d_6). 320
Figure 6.54.2. ^{13}C NMR of complex 3.86 (DMSO-d_6). 320
Figure 6.55.1. ^{1}H NMR of compound 3.2 ($CDCl_3$) 321
Figure 6.55.2. ^{13}C NMR of compound 3.2 ($CDCl_3$). 321
Figure 6.56.1. ^{1}H NMR of compound 3.4 ($CDCl_3$) 322
Figure 6.56.2. ^{13}C NMR of compound 3.4 ($CDCl_3$). 322
Figure 6.57.1. ^{1}H NMR of compound 3.6 ($CDCl_3$) 323
Figure 6.57.2. ^{13}C NMR of compound 3.6 ($CDCl_3$). 323
Figure 6.58.1. ^{1}H NMR of complex FL1359 (DMSO-d_6). 324
Figure 6.58.2. ^{13}C NMR of complex FL1359 (DMSO-d_6). 324
Figure 6.59.1. ^{1}H NMR of compound 3.8 ($CDCl_3$) 325
Figure 6.59.2. ^{13}C NMR of compound 3.8 ($CDCl_3$). 325
Figure 6.60.1. ^{1}H NMR of compound 3.10 ($CDCl_3$) 326
Figure 6.60.2. ^{13}C NMR of compound 3.10 ($CDCl_3$). 326
Figure 6.61.1. ^{1}H NMR of complex FL1335 (DMSO-d_6). 327
Figure 6.61.2. ^{13}C NMR of complex FL1335 (DMSO-d_6). 327
Figure 6.62.1. ^{1}H NMR of compound 3.13 ($CDCl_3$) 328
Figure 6.62.2. ^{13}C NMR of compound 3.13 ($CDCl_3$). 328
Figure 6.63.1. ^{1}H NMR of compound 3.15 ($CDCl_3$) 329
Figure 6.63.2. ^{13}C NMR of compound 3.15 ($CDCl_3$). 329
Figure 6.64.1. ^{1}H NMR of compound 3.17 ($CDCl_3$) 330
Figure 6.64.2. ^{13}C NMR of compound 3.17 ($CDCl_3$). 330
Figure 6.65.1. ^{1}H NMR of complex FL1288 (DMSO-d_6). 331
Figure 6.65.2. ^{13}C NMR of complex FL1288 (DMSO-d_6). 331
Figure 6.66.1. ^{1}H NMR of compound 3.19 ($CDCl_3$) 332
Figure 6.66.2. ^{13}C NMR of compound 3.19 ($CDCl_3$). 332
Figure 6.67.1. ^{1}H NMR of compound 3.21 ($CDCl_3$) 333
Figure 6.67.2. ^{13}C NMR of compound 3.21 ($CDCl_3$). 333
Figure 6.68.1. ^{1}H NMR of complex FL1343 (DMSO-d_6). 334
Figure 6.68.2. ^{13}C NMR of complex FL1343 (DMSO-d_6). 334
Figure 6.69.1. ^{1}H NMR of compound 3.24 ($CDCl_3$) 335
Figure 6.69.2. ^{13}C NMR of compound FL3.24 ($CDCl_3$). 335
Figure 6.70.1. ^{1}H NMR of compound 3.26 ($CDCl_3$) 336
Figure 6.70.2. ^{13}C NMR of compound FL3.26 ($CDCl_3$). 336
Figure 6.71.1. ^{1}H NMR of compound 3.27 ($CDCl_3$) 337
Figure 6.71.2. ^{13}C NMR of compound FL3.27 ($CDCl_3$). 337
Figure 6.72.1. ^{1}H NMR of complex FL1358 (DMSO-d_6). 338
Figure 6.72.2. ^{13}C NMR of complex FL1358 (DMSO-d_6). 338
Figure 6.73.1. ^{1}H NMR of compound 3.62 ($CDCl_3$) 339
Figure 6.73.2. ^{13}C NMR of compound 3.62 ($CDCl_3$). 339
Figure 6.74.1. ^{1}H NMR of compound 3.63 ($CDCl_3$) 340
Figure 6.75.1. ^{1}H NMR of compound 3.65 (CD_3CN). 340
Figure 6.76.1. ^{1}H NMR of complex FL1392 (DMSO-d_6). 341
Figure 6.77.1. ^{1}H NMR of compound 3.68 (CD_3CN). 341

Figure 6.78.1. ^{1}H NMR of complex FL1473 (DMSO-d_6). 342
Figure 6.79.1. ^{1}H NMR of compound 3.35 (DMSO-d_6). 342
Figure 6.79.2. ^{13}C NMR of compound 3.35 (DMSO-d_6). 343
Figure 6.80.1. ^{1}H NMR of compound 3.37 (DMSO-d_6). 343
Figure 6.80.2. ^{13}C NMR of compound 3.37 (DMSO-d_6). 344
Figure 6.81.1. ^{1}H NMR of complex FL1055 (DMSO-d_6). 344
Figure 6.81.2. ^{13}C NMR of complex FL1055 (DMSO-d_6). 345
Figure 6.82.1. ^{1}H NMR of compound 3.39 ($CDCl_3$). 345
Figure 6.82.2. ^{13}C NMR of compound 3.39 ($CDCl_3$). 346
Figure 6.83.1. ^{1}H NMR of compound 3.41 ($CDCl_3$). 346
Figure 6.84.1. ^{1}H NMR of complex FL1229 (DMSO-d_6). 347
Figure 6.85.1. ^{1}H NMR of complex FL1125 (DMSO-d_6). 347
Figure 6.86.1. ^{1}H NMR of complex FL123 (DMSO-d_6). 348
Figure 6.86.2. ^{13}C NMR of complex FL123 (DMSO-d_6). 348
Figure 6.87.1. ^{1}H NMR of complex FL1397 (DMSO-d_6). 349
Figure 6.88.1. ^{1}H NMR of compound 3.54 ($CDCl_3$). 349
Figure 6.88.2. ^{13}C NMR of compound 3.54 ($CDCl_3$). 350
Figure 6.89.1. ^{1}H NMR of compound 3.56 ($CDCl_3$). 350
Figure 6.89.2. ^{13}C NMR of compound 3.56 ($CDCl_3$). 351
Figure 6.90.1. ^{1}H NMR of complex FL1381 (DMSO-d_6). 351
Figure 6.90.2. ^{13}C NMR of complex FL1381 (DMSO-d_6). 352
Figure 6.91.1. ^{1}H NMR of complex FL1041 (DMSO-d_6). 352
Figure 6.92.1. ^{1}H NMR of complex FL475 (DMSO-d_6). 353
Figure 6.93.1. ^{1}H NMR of compound 3.60 ($CDCl_3$). 353
Figure 6.93.2. ^{13}C NMR of compound 3.60 ($CDCl_3$). 354
Figure 6.94.1. ^{1}H NMR of compound 3.61 (CD_3CN). 354
Figure 6.95.1. ^{1}H NMR of complex FL1528-1 (DMSO-d_6). 355
Figure 6.95.2. ^{13}C NMR of complex FL1528-1 (DMSO-d_6). 355
Figure 6.96.1. ^{1}H NMR of complex FL1353-1 (DMSO-d_6). 356
Figure 6.96.2. ^{13}C NMR of complex FL1353-1 (DMSO-d_6). 356
Figure 6.97.1. ^{1}H NMR of complex FL1353-2 (DMSO-d_6). 357
Figure 6.98.1. ^{1}H NMR of complex FL1370-1 (DMSO-d_6). 357
Figure 6.98.2. ^{13}C NMR of complex FL1370-1 (DMSO-d_6). 358
Figure 6.99.1. ^{1}H NMR of complex FL1370-2 (DMSO-d_6). 358
Figure 6.100.1. ^{1}H NMR of complex FL1352-1 (DMSO-d_6). 359
Figure 6.101.1. ^{1}H NMR of complex FL1289-1 (DMSO-d_6). 359
Figure 6.102.1. ^{1}H NMR of complex FL1289-2 (DMSO-d_6). 360
Figure 6.103.1. ^{1}H NMR of complex FL1399-1 (DMSO-d_6). 360
Figure 6.104.1. ^{1}H NMR of complex FL1399-2 (DMSO-d_6). 361
Figure 6.105.1. ^{1}H NMR of complex FL848-1 (DMSO-d_6). 361
Figure 6.106.1. ^{1}H NMR of complex FL812-1 (DMSO-d_6). 362
Figure 6.106.2. ^{13}C NMR of complex FL812-1 (DMSO-d_6). 362
Figure 6.107.1. ^{1}H NMR of complex FL812-2 (DMSO-d_6). 363
Figure 6.108.1. ^{1}H NMR of complex FL253 (DMSO-d_6). 363
Figure 6.109.1. ^{1}H NMR of complex FL528 (DMSO-d_6). 364

Figure 6.110.1. ^{1}H NMR of complex FL823-1 (DMSO-d_6). 364
Figure 6.110.2. ^{13}C NMR of complex FL823-1 (DMSO-d_6). 365
Figure 6.111.1. ^{1}H NMR of complex FL823-2 (DMSO-d_6). 365
Figure 6.112.1. 1H NMR of complex FL829 (DMSO-d_6). 366
Figure 6.112.2. ^{13}C NMR of complex FL829 (DMSO-d_6). 366
Figure 6.113.1. ^{1}H NMR of complex FL534-1 (DMSO-d_6). 367
Figure 6.114.1. ^{1}H NMR of complex FL534-2 (DMSO-d_6). 367
Figure 6.115.1. ^{1}H NMR of complex 3.70 ($CDCl_3$). 368
Figure 6.115.2. ^{13}C NMR of complex 3.70 ($CDCl_3$). 368
Figure 6.116.1. ^{1}H NMR of complex 3.71 (DMSO-d_6). 369
Figure 6.117.1. ^{1}H NMR of complex FL1360 (DMSO-d_6). 369
Figure 6.117.2. ^{13}C NMR of complex FL1360 (DMSO-d_6). 370
Figure 6.118.1. ^{1}H NMR of complex FL792-1 ($CDCl_3$). 370
Figure 6.119.1. ^{1}H NMR of complex FL792-2 ($CDCl_3$). 371
Figure 6.120.1. ^{1}H NMR of complex FL1138-1 (Acetone-d_6). 371
Figure 6.121.1. ^{1}H NMR of complex FL1138-2 (DMSO-d_6). 372
Figure 6.122.1. ^{1}H NMR of complex FL1124-1 (DMSO-d_6). 372
Figure 6.123.1. ^{1}H NMR of complex FL1124-2 ($CDCl_3$). 373
Figure 6.124.1. ^{1}H NMR of complex FL609-1 (Acetone-d_6). 373
Figure 6.125.1. ^{1}H NMR of complex FL1190-2 (Acetone-d_6). 374
Figure 6.126.1. ^{1}H NMR of compound 4.6 ($CDCl_3$). 374
Figure 5.127. Initial screening of a 48-member organometallic library for PAK1 inhibition at a complex concentration of 10 μM with 1 μM ATP. 385

List of Tables

Table 2.1. IC_{50} values in nM of DW12, NP309 and FL172 against GSK3β, Pim1 and PAK1 in the presence of 1 µM ATP. 27
Table 2.2. Activities in % of PAK1 and Pim1 with individual enantiomers of FL256, FL411 and FL172 at a concentration of 0.1 µM and in the presence of 1 µM ATP. 32
Table 2.3. IC_{50} values in nM of individual enantiomers of FL411 against GSK3β, Pim1 and PAK1 in the presence of 1 µM ATP. 32
Table 2.4. Activities in % of PAK1 with racemic FL637 and FL172. Measured at concentrations of 3 µM, 1 µM and 0.3 µM of the inhibitors and in the presence of 1 µM ATP. 35
Table 2.5. IC_{50} values of the racmic derivatives of FL172 with 1 µM ATP. 37
Table 2.6. IC_{50} values of the racemic derivatives of FL172 with modified pyridocarbazole in the presence of 1 µM ATP. 42
Table 2.7. IC_{50} values of **Λ**-FL1422 against GSK3β, Pim1 and PAK1 in the presence of 1 µM ATP. 44
Table 3.1. IC_{50} values of the racemic ruthenium complexes for MLCK, Pim1 and GSK3α in the presence of 100 µM ATP. 51
Table 3.2. Pyridylindole synthesis by Suzuki coupling. 52
Table 3.3. Synthesis of pyridocarbazoles from pyridylindoles. 53
Table 3.4. Racemic ruthenium complexes synthesized with microwave irradiation. 54
Table 3.5. IC_{50} values in nM of racemic complexes against MLCK and Pim1 in the presence of 100 µM ATP. 56
Table 3.6. IC_{50} values of racemic FL1528-1 against MLCK, PAK1, DAPK1, GSK3α, Flt4 and Pim1 in the presence of 100 µM ATP. 63
Table 3.7. IC_{50} values of racemic ruthenium complexes with different monodentate ligands on the axial position in the presence of 100 µM ATP. 67
Table 3.8. Ruthenium complexes with different substituents on the pyridocarbazole. 69
Table3.9. IC_{50} values in nM of racemic derivatives with different pyridocarbazoles for DAPK1 and Pim1 in the presence of 100 µM ATP. 70
Table 3.10. IC_{50} values of racemic FL1353-1 against DAPK1, Pim1, PAK1, MLCK, GSK3α and Flt4 in the presence of 100 µM ATP. 71
Table 3.11. Ratio of Ru-N bonding isomer and Ru-S bonding isomer. 74
Table 3.12. IC_{50} values of racemic FL1360 against protein kinases of Pim1, DAPK1, PAK1, MLCK, GSK3α and Flt4 in the presence of 100 µM ATP. 79
Table 4.1. IC_{50} values of the derivatives for TrkA in the presence of 100 µM ATP. 88
Table 4.2. IC_{50} values of ruthenium complexes with different tridentate ligands for TrkA in the presence of 100 µM ATP. 92
Table 6.1. Crystal data and structure refinement for FL151-1. 209
Table 6.2. Atomic coordinates and equivalent isotropic displacement parameters ($Å^2$) for FL151-1. 210
Table 6.3. Bond lengths [Å] and angles [°] for FL151-1. 211
Table 6.4. Anisotropic displacement parameters ($Å^2$) for FL151-1. 214
Table 6.5. Hydrogen coordinates and isotropic displacement parameters ($Å^2$)for FL151-1. 215
Table 6.6. Torsion angles [°] for FL151-1 216
Table 6.7. Hydrogen bonds for FL151-1 [Å and °]. 218

Table 6.8. Crystal data and structure refinement for FL327. 219
Table 6.9. Atomic coordinates and equivalent isotropic displacement parameters (Å^2) for FL327. 220
Table 6.10. Bond lengths [Å] and angles [°] for FL327. 221
Table 6.11. Anisotropic displacement parameters (Å^2) for FL327. 224
Table 6.12. Hydrogen coordinates and isotropic displacement parameters (Å^2)for FL327. 225
Table 6.13. Torsion angles [°] for FL327. 226
Table 6.14. Hydrogen bonds for FL327 [Å and °]. 228
Table 6.15. Crystal data and structure refinement for FL389. 229
Table 6.16. Atomic coordinates and equivalent isotropic displacement parameters (Å^2) for FL389. 230
Table 6.17. Bond lengths [Å] and angles [°] for FL389. 231
Table 6.18. Anisotropic displacement parameters (Å^2) for FL389. 234
Table 6.19. Hydrogen coordinates and isotropic displacement parameters (Å^2)for FL389. 235
Table 6.20. Torsion angles [°] for FL389. 236
Table 6.21. Hydrogen bonds for FL389 [Å and °]. 238
Table 6.22. Crystal data and structure refinement for FL1359. 239
Table 6.23. Atomic coordinates and equivalent isotropic displacement parameters (Å^2) for FL1359. 240
Table 6.24. Bond lengths [Å] and angles [°] for FL1359. 241
Table 6.25. Anisotropic displacement parameters (Å^2) for FL1359. 244
Table 6.26. Hydrogen coordinates and isotropic displacement parameters (Å^2)for FL1359. 245
Table 6.27. Torsion angles [°] for FL1359. 246
Table 6.28. Hydrogen bonds for FL1359 [Å and °]. 248
Table 6.29. Crystal data and structure refinement for FL626-1. 249
Table 6.30. Atomic coordinates and equivalent isotropic displacement parameters (Å^2) for FL626-1. 250
Table 6.31. Bond lengths [Å] and angles [°] for FL626-1. 251
Table 6.32. Anisotropic displacement parameters (Å^2) for FL626-1. 254
Table 6.33. Hydrogen coordinates and isotropic displacement parameters (Å^2)for FL626-1. 255
Table 6.34. Torsion angles [°] for FL626-1. 256
Table 6.35. Hydrogen bonds for FL626-1 [Å and °]. 258
Table 6.36. Crystal data and structure refinement for FL1473. 259
Table 6.37. Atomic coordinates and equivalent isotropic displacement parameters (Å^2) for FL1473. 260
Table 6.38. Bond lengths [Å] and angles [°] for FL1473. 261
Table 6.39. Anisotropic displacement parameters (Å^2) for FL1473. 264
Table 6.40. Hydrogen coordinates and isotropic displacement parameters (Å^2)for FL1473. 265
Table 6.41. Torsion angles [°] for FL1473. 266
Table 6.42. Hydrogen bonds for FL1473 [Å and °]. 268
Table 6.43. Crystal data and structure refinement for FL1528-1. 269
Table 6.44. Atomic coordinates and equivalent isotropic displacement parameters (Å^2) for FL1528-1. 270
Table 6.45. Bond lengths [Å] and angles [°] for FL1528-1. 271
Table 6.46. Anisotropic displacement parameters (Å^2) for FL1528-1. 274

Table 6.47. Hydrogen coordinates and isotropic displacement parameters ($Å^2$)for FL1528-1. ... 275
Table 6.48. Torsion angles [°] for FL1528-1. ... 276
Table 6.49. Hydrogen bonds for FL1528-1 [Å and °]. ... 278
Table 6.50. Crystal data and structure refinement for FL1370-1. ... 279
Table 6.51. Atomic coordinates and equivalent isotropic displacement parameters ($Å^2$) for FL1370-1. ... 280
Table 6.52. Bond lengths [Å] and angles [°] for FL1370-1. ... 281
Table 6.53. Anisotropic displacement parameters ($Å^2$) for FL1370-1. ... 283
Table 6.54. Hydrogen coordinates and isotropic displacement parameters ($Å^2$) for FL1370-1. .. 284
Table 6.55. Torsion angles [°] for FL1370-1. ... 285
Table 6.56. Hydrogen bonds for FL1370-1 [Å and °]. ... 287